**Aus dem C. und O. Vogt Institut für Hirnforschung**
**der Heinrich-Heine-Universität Düsseldorf**

**Direktor: Univ.-Prof. Dr. med. Dr. h.c. Karl Zilles**

# Struktur-Funktionsbeziehungen in Assoziationsgebieten des Gehirns am Beispiel des unteren Parietallappens

Habilitationsschrift
zur Erlangung der Venia Legendi für das Fach Neurowissenschaften
der Hohen Medizinischen Fakultät
der Heinrich-Heine-Universität Düsseldorf

**vorgelegt von**
**Dr. med. Dr. rer. pol. Svenja Inga Verena Caspers**

2012

Meinen Eltern gewidmet:
Prof. h.c. Dr. h.c. Dr. med. Hans-Peter Caspers
Monika Caspers, geb. van Heemskerk

## INHALTSVERZEICHNIS

# I EINLEITUNG

Das menschliche Gehirn setzt sich aus einer Vielzahl strukturell und funktionell unterschiedlicher Einheiten zusammen. Im Bereich der Hirnrinde resultiert daraus eine Untergliederung in Areale, die sich aufgrund ihrer Verarbeitungsmodalitäten hierarchisch ordnen lassen. Zum einen existieren primäre und sekundäre Areale, die sich mit der Verarbeitung einer Sinnesmodalität, wie z.B. Sehen, Hören oder Fühlen, befassen. Zum anderen gibt es einen gerade im menschlichen Gehirn sehr großen Bereich, der als multi- oder supramodaler Assoziationskortex bezeichnet wird. Dazu gehören große Teile des Frontal-, Parietal- und Temporallappens. Regionen des Assoziationskortex ist gemeinsam, dass sie Informationen verschiedener Sinnesmodalitäten erhalten und diese nutzen, um daraus einen Gesamteindruck zu generieren. Funktionell stehen in diesen Regionen somit insbesondere die höhere Verarbeitung von Sinneseindrücken sowie Planungs- und Entscheidungsaufgaben im Vordergrund.

Besonders für die Bereiche des Assoziationskortex sind die zwei in den Neurowissenschaften etablierten Grundprinzipien über die Organisation des Gehirns von besonderer Bedeutung: funktionelle Integration vs. funktionelle Segregation. Diese beiden Konzepte beschreiben sich scheinbar widersprechende Phänomene der Funktionsweise des Gehirns.

Mit funktioneller Segregation wird die Aufteilung der Hirnrinde in einzelne funktionelle Areale bezeichnet. Jedes dieser Areale erfüllt seine spezifische Funktion, die von keinem anderen Areal in dieser Form erfüllt wird. Besonders leicht ersichtlich wird dieses Prinzip in den primären und sekundären Hirnrindenregionen, die für die direkte und unmittelbare Verarbeitung der Informationen aus den verschiedenen Sinnesorganen zuständig sind. Beispielsweise werden in der primären Sehrinde V1 die hereinkommenden Informationen aus den Retinae beider Augen in spezialisierter Weise verarbeitet, um diese für die weitere Prozessierung in anderen Hirnrindenarealen aufzubereiten. In gleicher Weise gibt es solche Spezialisierungen auch in Arealen des Assoziationskortex, nur der Begriff „Funktion“ muss hier anders verwendet werden. Es gibt beispielsweise im Bereich der visuellen Verarbeitung höher geordnete Areale, von denen eines sehr spezifisch auf Gesichter reagiert („fusiform face area“), während ein anderes benachbartes Areal sehr spezifisch auf Wörter reagiert („visual word form area“). Anhand dieser Beispiele wird allerdings auch ein Problem dieses Spezialisierungskonzeptes deutlich, das insbesondere für Areale des Assoziationskortex zutrifft. Es ist auch nach Jahrzehnten neurowissenschaftlicher Forschung für viele Areale des Assoziationskortex noch in der Diskussion, welche „Funktion“ sie tatsächlich erfüllen bzw., anders formuliert, wie die „Funktion“ des Areals richtig beschrieben werden kann. Auf der einen Seite erfolgt die Erforschung von Hirnfunktionen anhand funktioneller

Bildgebungsexperimente. Diese nutzen psychologische Konstrukte zur Beschreibung der Funktionen, die mit Hilfe geeigneter funktioneller Paradigmen untersucht werden sollen. Gleichzeitig werden Blutfluss- oder Stoffwechselveränderungen in Gehirnregionen gemessen und statistisch ausgewertet, so dass Aussagen über die Beteiligung bestimmter Hirnregionen an einer gestellten Aufgabe getroffen werden können. Diese Beschreibung der Funktion eines Areals deckt eine Meta-Ebene ab: Es wird mit den möglichen Begriffen versucht, die „Funktion“ zu benennen und so exakt wie möglich zu beschreiben (Bandettini 2009; Logothetis 2008). Auf der anderen Seite existieren funktionelle elektrophysiologische Studien, die sehr gezielt Aussagen zur Aktivität einzelner Nervenzellen treffen können und sich somit auf einer ganz anderen Betrachtungsebene befinden. Daraus resultieren wiederum andere Bezeichnungen für deren „Funktion“, die häufig eher mechanistisch geprägt sind und beschreiben, dass Aktionspotenziale in Nervenzellen auf bestimmte Reize hin entstehen. Das passiert prinzipiell in jeder Nervenzelle des Gehirns in gleicher Art und Weise, nur in verschiedenen Regionen des Gehirns nicht gleichförmig auf jeden Reiz. Es ist zum jetzigen Zeitpunkt nicht möglich, beide Betrachtungsweisen abschließend sinnvoll zu vereinen. Beide Ansätze liefern essentielle Beiträge zum Verständnis der Funktionsweise des Gehirns und seiner einzelnen funktionellen Einheiten, aber auf verschiedenen Ebenen, die durch Verwendung geeigneter Methoden zumindest angenähert werden können. Dazu gehören neuere neuroinformatische und computerbasierte neurowissenschaftliche Modellierungsmethoden, die versuchen, Teile der Hirnrinde aus einzelnen modellierten Nervenzellen nachzubauen, um dadurch Rückschlüsse auf das Zusammenspiel der Nervenzellen bei der Erfüllung bestimmter Funktionen ziehen zu können (Peters et al. 2012; Plaut und Behrmann 2011; Wagatsuma et al. 2011).

Das zweite Grundkonzept, die funktionelle Integration, beschreibt das Zusammenspiel verschiedener Areale des Gehirns bei der Erfüllung einer Funktion. Dieses Konzept scheint auf den ersten Blick im Widerspruch zu dem zuvor erläuterten Konzept der funktionellen Segregation zu stehen: Wie kann eine Funktion gleichzeitig in einem Areal lokalisiert und von einem Netzwerk verschiedener Hirnrindenareale erfüllt werden? Diese vermeintliche Widersprüchlichkeit führt wiederum zu der Betrachtung des Begriffs „Funktion“. Eine so komplexe „Funktion“ wie beispielsweise räumliche Aufmerksamkeit ist letztlich eigentlich eine zusammengesetzte „Funktion“ auf einer Meta-Ebene, die aus vielen einzelnen, sehr viel basaleren Teilfunktionen besteht. Dazu müssen die eingehenden visuellen Reize aufgenommen und in ihren Einzelteilen verarbeitet werden, der Bezug zum eigenen Körper muss hergestellt werden, die Augen müssen im Raum bewegt und gezielt auf einen Gegenstand oder Punkt im Raum gerichtet werden. Schließlich müssen die Ergebnisse dieser Einzelanalysen zu dem Gesamteindruck räumliche Aufmerksamkeit zusammengesetzt werden. Anhand dieses Beispiels wird wiederum deutlich, wie schwierig

der Begriff „Funktion“ zu fassen ist und dass die psychologischen Konstrukte uns nur einen Eindruck von der Arbeitsweise des Gehirns vermitteln. Um die beiden Konzepte funktionelle Segregation und Integration zu vereinen, ist deswegen die möglichst exakte Benennung jeder einzelnen Komponente einer komplexen psychologischen „Funktion“ von entscheidender Bedeutung. Sehr prominente Bespiele wurden bereits früh aus der Untersuchung von Patienten gewonnen, bei denen beispielsweise durch Schlaganfälle Teile des Gehirns ausfallen. So konnten für die Funktion „Sprache“ zwei unterschiedliche Regionen des Gehirns mit verschiedenen Teilaufgaben in Verbindung gebracht werden: Während die Broca-Region im kaudalen Bereich des linken Gyrus frontalis inferior eher für motorische Sprachproduktion verantwortlich schien, wurde durch den Ausfall des linken Gyrus angularis am Übergang zum Gyrus temporalis superior eine Störung des Sprachverständnisses bei Erhalt der Fähigkeit zur motorischen Sprachproduktion bewirkt. Diese wegweisenden Erkenntnisse aus den Arbeiten von Paul Broca und Carl Wernicke aus dem 19. Jahrhundert konnten zwischenzeitlich deutlich erweitert werden. Es konnte gezeigt werden, dass die beiden Regionen auch noch in viele andere Aufgaben involviert sind und somit die „Funktion“ dieser Areale weiterhin nicht vollständig geklärt ist.

Ein Bereich des Assoziationskortex, der trotz intensiver Forschung auch heute zu den immer noch rätselhaften Gebieten des menschlichen Gehirns zählt, ist der untere Parietallappen (IPL). Der IPL umfasst den unteren Anteil des posterioren Parietallappens kaudal des Sulcus postcentralis und ventral des Sulcus intraparietalis (Abb. 1).

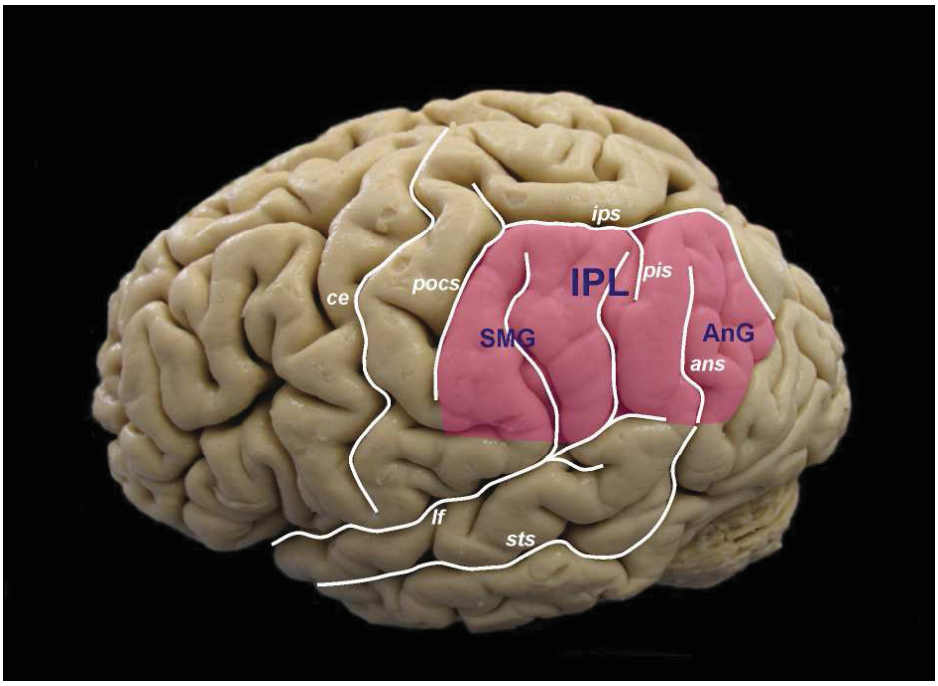


**Abbildung 1:** Linke Lateralansicht einer post-mortem Hemisphäre. Hervorhebung des Bereichs des IPL (pink) sowie der relevanten Sulci. SMG: Gyrus supramarginalis, AnG: Gyrus angularis, ans: Sulcus angularis, ce: Sulcus centralis, ips: Sulcus intraparietalis, lf: Fissura lateralis Sylvii, pis: Sulcus intermedius primus, pocs: Sulcus postcentralis, sts: Sulcus temporalis superior.

Innerhalb des IPL lassen sich zwei größere Hirnwindungen voneinander unterscheiden: der Gyrus supramarginalis im rostralen und der Gyrus angularis im kaudalen Bereich (Abb. 1). Getrennt werden diese beiden Gyri durch den Sulcus intermedius primus (Jenssen), einem Abgang des Sulcus intraparietalis, der allerdings sehr variabel ausgestaltet ist (**Caspers** et al. 2011a; Ono et al. 1990). Alle weiteren Unterteilungen der Gyri durch zusätzliche Sulci zeigen eine deutlich stärkere interindividuelle Variabilität (Rademacher et al. 1993), da sich diese Bereiche des Gehirns ontogenetisch erst vergleichsweise spät entwickeln. Sie zählen somit zu den tertiären und höheren Sulci, im Gegensatz zum Sulcus centralis oder der Fissura lateralis. Somit ist der IPL bereits von seinem makroskopischen Aufbau her betrachtet sehr komplex und kann von Mensch zu Mensch deutlich variieren.

Neben der Makroskopie gibt insbesondere auch die Mikroskopie Aufschlüsse über die Struktur der Hirnrinde. Mit deren Hilfe lässt sich die Zytoarchitektonik der Hirnrinde untersuchen. Unterschiede im Zellverteilungsmuster und der Zellpackungsdichte in den Schichten des Kortex erlauben die Abgrenzung von zytoarchitektonischen Hirnrindenarealen und damit die Kartierung des Gehirns. Eine der ersten und auch heute noch am weitesten verbreiteten Hirnkarten ist die von Korbinian Brodmann (1909). Er unterteilte den IPL in zwei zytoarchitektonische Areale BA40 und BA39, die weitestgehend der makroskopischen Unterteilung in Gyrus supramarginalis und Gyrus angularis entsprachen (Abb. 2A).

Danach folgten weitere zyto- und myeloarchitektonische Untersuchungen (Bartsch 1952; Gerhardt 1940; Sarkissov et al. 1955; Vogt und Vogt 1919; von Economo und Koskinas 1925), die weitere Unterteilungen der beiden Hauptgebiete des IPL nach Brodmann postulierten, zum Teil als eigenständige Gebiete, zum Teil als Unterformen von Hauptgebieten. Allerdings beruhten alle diese Untersuchungen auf einem oder zwei Gehirnen, teilweise sogar nur auf einer Hemisphäre. Dadurch konnte der Anteil der interindividuellen Variabilität, der insbesondere in Bereichen höher geordneter Kortizes auch auf mikroskopischer Ebene vorhanden ist (Fischl et al. 2008), nicht ausreichend berücksichtigt werden. Zusätzlich existieren diese früheren Karten lediglich als zweidimensionale schematische Karten, die keine Aussage über die Ausdehnung der Areale in den Sulci des Gehirns erlauben. Da sich der menschliche Kortex zu ca. 2/3 in der Tiefe der Sulci befindet, kommt es zu einer deutlichen Unterschätzung der Ausdehnung und des Volumens eines Areals (Zilles et al. 1988). Ein dritter und für die vorliegenden Untersuchungen sehr wesentlicher Aspekt ist, dass diese früheren Karten nicht unmittelbar mit Ergebnisse funktioneller Bildgebungsstudien, z.B. mittels funktioneller Magnetresonanztomographie (fMRT), Positronen-Emissions-Tomographie (PET), Magnet- oder Elektroenzephalographie (MEG/EEG) genutzt werden können. Das beruht zum einen ebenfalls auf ihrer Zweidimensionalität, zum anderen aber auch auf dem Fehlen eines gemeinsamen Bezugsraums mit funktionellen Bildgebungsstudien. Eine genaue

anatomische Lokalisation funktioneller Hirnforschungsergebnisse ist somit anhand dieser älteren Karten nur bedingt möglich.

Diese Problematik konnte in einer neueren zytoarchitektonischen Untersuchung (**Caspers** et al. 2006, 2008) angegangen werden, indem an einer Stichprobe von 10 post-mortem Gehirnen unter Verwendung eines untersucher-unabhängigen statistischen Analyse-Algorithmus (Schleicher et al. 1999, 2005; Zilles et al. 2002) zytoarchitektonische Areale des IPL abgegrenzt werden konnten. Insgesamt wurden sieben unterschiedliche Areale gefunden, fünf im Bereich von BA40 (PFt, PFop, PF, PFm, PFcm) und zwei im Bereich von BA39 (PGa, PGp) (**Caspers** et al. 2006, Abb. 2B).

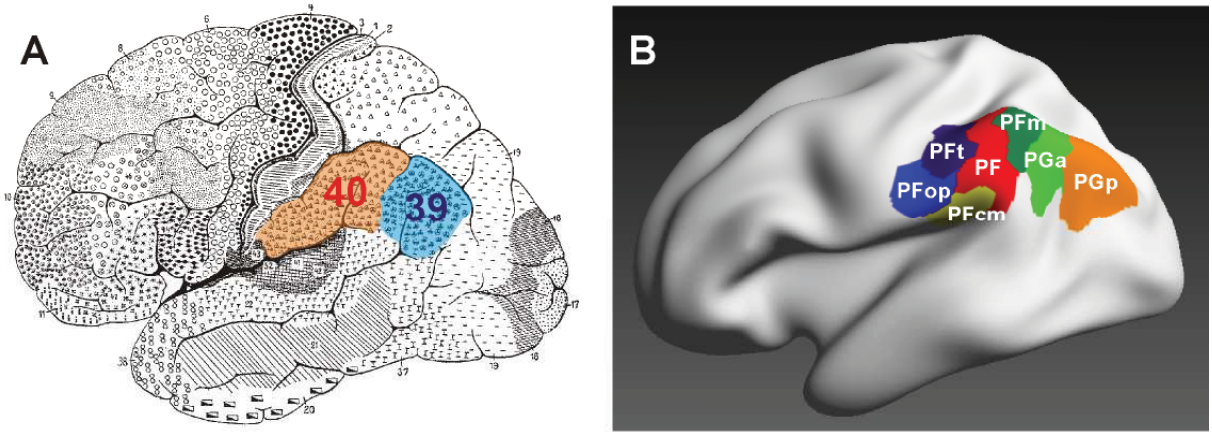


**Abbildung 2:** Karten des IPL, basierend auf zytoarchitektonischen Untersuchungen. (A) Brodmann (1909), (B) **Caspers** et al. (2006, 2008).
Abbildungsteil B aus: **Caspers** et al. 2012, Cereb Cortex, im Druck.

Die Einzelergebnisse aller zehn untersuchten Gehirne wurden in einem gemeinsamen Referenzraum, dem Montreal Neurological Institute (MNI)-Raum, überlagert. Daraus entstand für jedes der sieben IPL-Areale eine Wahrscheinlichkeitskarte, die für jeden Bildpunkt im Gehirn angibt, mit welcher Wahrscheinlichkeit das Areal an dieser Stelle im Gehirn gefunden werden kann (**Caspers** et al. 2008). Da die interindividuelle Variabilität im Bereich des IPL sehr groß ist, überlappen sich die einzelnen Wahrscheinlichkeitskarten der IPL-Areale unterschiedlich stark. Um eine kontinuierliche Repräsentation der IPL-Areale ohne Überlappung zu erhalten, wurden somit anschließend maximale Wahrscheinlichkeitskarten (Maximum Probability Maps, MPM) berechnet, die jeden Voxel des Kortex dem Areal mit der höchsten Wahrscheinlichkeit zuordnen (Eickhoff et al. 2006). Diese dreidimensionalen Karten des IPL befinden sich im gemeinsamen MNI-Referenzraum und lassen sich in diesem mit den Ergebnissen funktioneller Studien überlagern. Damit existiert eine strukturelle Grundlage, aufgrund derer sich funktionelle Ergebnisse anatomisch präzise zuordnen und interpretieren lassen (Zilles und Amunts 2010).

Dieser Aspekt ist besonders wichtig, um einzelne Funktionen voneinander abgrenzen zu können. Beispielsweise würde die Beschreibung „IPL“ für einen sehr großen Teil von

Aktivierungen funktioneller Bildgebungsstudien zutreffen. Das liegt in der großen funktionellen Heterogenität des IPL als Teil des Assoziationskortex begründet. Der rostrale IPL beidseits wurde z.B. wiederholt in Studien zu höherer motorischer Verarbeitung gefunden, wozu insbesondere das potentielle menschliche Spiegelneuronensystem zu zählen ist (**Caspers** et al. 2010 ***[Publikation 4]***; Iacoboni 2005, 2009; Iacoboni und Dapretto 2006; Keysers and Gazzola 2009; Rizzolatti und Craighero 2004). Für den kaudalen IPL wurden eher lateralisierte Funktionen gefunden: Während die rechte Seite in räumliche und nicht-räumliche Aufmerksamkeitsfunktionen involviert zu sein scheint und damit als Teil des ventralen Aufmerksamkeitsnetzwerks gesehen wird (Corbetta und Shulman 2002; Corbetta et al. 2008; Fink et al. 2001; Jakobs et al. 2012 ***[Publikation 6]***), ist der linke kaudale IPL eher in die Verarbeitung sprachrelevanter Aufgaben wie semantische oder phonologische Verarbeitung involviert (Gernsbacher und Kaschak 2003; Geschwind 1970; Price 2000; Shalom und Poeppel 2008; Vigneau et al. 2006). Zusätzlich wurden Aktivierungen im kaudalen IPL auch wiederholt im Zusammenhang mit der Bearbeitung mathematischer Aufgaben (Grabner et al. 2007; Ischebeck et al. 2007; Wu et al. 2009 ***[Publikation 7]***) und moralischer Entscheidungsfindung (Moll et al. 2002; Greene et al. 2004; Raine und Yang 2006) gefunden.

Eine ähnliche funktionelle Heterogenität wurde auch bei Makaken gefunden. Es konnte gezeigt werden, dass der rostrale IPL in das bei Makaken erstmals entdeckte Spiegelneuronensystem sowie in sensomotorische Verarbeitung involviert ist, während der kaudale IPL eher bei Aufgaben zu räumlicher Aufmerksamkeit, auditorisch-sensorischer Integration und visuo-motorischer Koordination, wie z.B. Greifen, beteiligt ist (Gallese et al. 1996; Fogassi et al. 2005; Hyvärinen 1982; Mountcastle et al. 1975; Pandya und Seltzer 1982; Rozzi et al. 2008; Seltzer und Pandya 1984). Vor dem Hintergrund eines ähnlichen strukturellen Aufbaus des IPL bei Makaken, mit einer rostro-kaudalen Anordnung von vier Arealen auf der lateralen Oberfläche (Gregoriou et al. 2006; Pandya and Seltzer 1984), ist diese ähnliche funktionelle Heterogenität besonders interessant. Zusammen genommen deutet das verstärkt auf Homologien zwischen den beiden verwandten Spezies Affe und Mensch hin. Es muss dabei allerdings berücksichtigt werden, dass die bisherigen Affen-Studien fast ausschließlich an Makaken und Rhesus-Affen durchgeführt wurden. Die Menschenaffen als dem Menschen näher verwandte Tierart wurden bislang noch nicht eingehend untersucht.

Die Untersuchung an Affen erlaubte zudem bislang die einzige weitergehende Aussage über mögliche Verbindungen zwischen den Arealen des IPL und anderen Gebieten der Hirnrinde. Erst mit der Entwicklung und verbreiteten Nutzung der diffusions-gewichteten MRT (Le Bihan et al. 2003) werden auch beim Menschen verstärkt die Faserbahnen zwischen Arealen eines Netzwerks untersucht. Tracer-Studien am Affen deuten darauf hin, dass der vordere IPL

insbesondere mit Arealen des sensomotorischen, prämotorischen und inferior frontalen Kortex verbunden ist, während der kaudale IPL stark ausgeprägte Verbindungen zu höheren visuellen Arealen und zum Temporallappen hat (Andersen et al. 1990; Cavada and Goldman-Rakic 1989a,b; Gregoriou et al. 2006; Neal et al. 1990a,b; Rozzi et al. 2006). Diese unterschiedlichen Verbindungen der rostralen und kaudalen IPL-Areale zusammen mit der stark ausgeprägten funktionellen Heterogenität deuten darauf hin, dass die verschiedenen IPL-Areale in unterschiedliche funktionelle Netzwerke mit unterschiedlichen anderen kortikalen Arealen eingebunden sind.

Ein ähnlicher Zusammenhang lässt sich für den menschlichen IPL vermuten. Basierend auf einer Vielzahl funktioneller Studien lässt sich eine noch deutlich stärkere funktionelle Diversität postulieren. Strukturell ist der menschliche IPL ebenfalls deutlich heterogener als früher gedacht. Die beiden Entitäten „Struktur“ und „Funktion“ stellen allerdings keine einzelnen Aspekte dar, sondern spiegeln zwei Seiten des Gehirnaufbaus wider. Für das Verständnis der Rolle des IPL im Gesamtsystem „Gehirn“ ist somit von entscheidender Bedeutung, beide für den Aufbau des IPL so relevanten Komponenten Struktur und Funktion und deren Verknüpfung in einem ganzheitlichen Ansatz zu betrachten.

# II ZIELSETZUNG UND AUFBAU DER ARBEIT

Die vorliegende Arbeit beschäftigt sich mit Struktur und Funktion des IPL des menschlichen Gehirns. Die bislang größtenteils getrennt betrachteten Aspekte der funktionellen und strukturellen Heterogenität innerhalb dieses Hirngebietes legten die Vermutung nahe, dass dem ein gemeinsames Bauprinzip zugrunde liegen müsste. Für das Verständnis der Rolle des IPL ist es unerlässlich, diese beiden Aspekte in einem Modell zu vereinen. Nur so wird es möglich sein, die Rolle einzelner Areale des IPL zu definieren. Ziel dieser Arbeit war es somit, ein Modell der Organisationsprinzipien des IPL und seiner Beziehungen zu anderen Hirnarealen zu erstellen, das den strukturellen Aufbau des IPL funktionell relevant widerspiegelt.

Dazu wurde in der vorliegenden Arbeit eine multimodale Herangehensweise gewählt: Es wurden Studien zu verschiedenen Aspekten der Struktur und Funktion des IPL durchgeführt, um daraus ein Modell über die Organisation des IPL zu erstellen. Aufbauend auf den zytoarchitektonischen Karten wurde die Struktur des IPL auf zwei zusätzlichen Ebenen charakterisiert: zum einen im Hinblick auf die strukturelle Einbindung der Areale in kortikale Netzwerke mittels Untersuchungen zur strukturellen Konnektivität und zum anderen bezogen auf den funktionell relevanten Aufbau der Hirnrinde des IPL anhand von Untersuchungen zur Verteilung von Neurotransmitter-Rezeptoren.

Zur Erfassung funktionell relevanter Aspekte wurden Meta-Analysen funktioneller Bildgebungsexperimente zur Verarbeitung von Handlungskontrolle und Aufmerksamkeitsprozessen sowie funktionelle Studien zur mathematischen Kognition und zur Entscheidungsfindung durchgeführt. Des Weiteren wurde die funktionelle Konnektivität der verschiedenen Bereiche des IPL untersucht, die Auskunft darüber gibt, mit welchen anderen Hirnregionen die verschiedenen Anteile des IPL in funktionellen Netzwerken verbunden sind. Das wurde anhand des generellen Ko-Aktivierungsmusters in einem großen Pool von Bildgebungsstudien ermittelt.

Basierend auf den Ergebnissen zum strukturellen und funktionellen Aufbau des IPL wurde abschließend ein Organisationsmodell des IPL entworfen, das die verschiedenen Bereiche des IPL und deren Bezug zu anderen kortikalen Arealen darstellt. Dieses Modell zeigt die Einbettung des IPL in das Gesamtsystem Gehirn und ermöglicht ein Verständnis der konsekutiven Entwicklung verschiedener funktioneller Netzwerke.

# III ERGEBNISSE UND DISKUSSION

## III.1 STRUKTURELLE UNTERSUCHUNGEN

### Strukturelle Konnektivität

Neben der Untersuchung des Kortex des Gehirns, in dem sich die funktionell relevanten Neurone befinden und der aufgrund seiner Einteilung in einzelne Areale mit unterschiedlicher funktioneller Relevanz starke Aufmerksamkeit erfahren hat, ist insbesondere in den letzten Jahren durch die Entwicklung neuer Techniken die weiße Substanz des Gehirns vermehrt in den Fokus des Interesses gerückt. In der weißen Substanz verlaufen die Faserbahnen, die verschiedene Hirnrindenareale miteinander verbinden. Ausgehend von zahlreichen invasiven Tracer-Studien beim Affen (s. Einleitung) stellte sich somit auch beim Menschen die Frage, durch welche Faserbahnen die verschiedenen Areale des IPL mit anderen kortikalen Arealen verbunden sind. Dadurch lässt sich die Frage beantworten, wie die IPL-Areale strukturell in verschiedene Netzwerke eingebunden sind.

Diese strukturelle Konnektivität lässt sich mittels diffusionsgewichteter MRT (DW-MRT) in-vivo untersuchen. Dieses Verfahren stellt eine indirekte Untersuchung von Faserbündeln dar und beruht auf dem Prinzip der gerichteten Wasserdiffusion im Gehirn (Henkelman et al. 1994; Moseley et al. 1990, 1991; Tanner und Stejskal 1968). In einer strukturierten Umgebung wie der weißen Substanz des Gehirns, in der Faserbahnen verlaufen, haben Wassermoleküle, die zwischen den Fasern liegen, eine bevorzugte Diffusionsrichtung entlang der Myelinscheiden der Fasern, was durch verschiedene Komponenten und Moleküle der Zellmembran und des Zytoskeletts beeinflusst wird (Beaulieu und Allen 1994a,b; Le Bihan et al. 1993). Diese bevorzugte Diffusionsrichtung kann mittels DW-MRT untersucht werden (Pierpaoli and Basser 1996). Mit Hilfe von Traktographie-Algorithmen (Behrens et al. 2003a, 2007) ist es anschließend möglich, den Verlauf der Faserbahnen zu rekonstruieren. Es ist anzumerken, dass diese Art der Untersuchung keine unmittelbare Aussage über die Konnektivität sensu stricto erlaubt. Dazu bedarf es invasiver Techniken, bei denen fluoreszierende Tracer direkt in ein Hirnareal injiziert werden und deren Verteilung entlang der Axone der Neurone untersucht wird. Da dieses Verfahren aus ethischen Gründen am Menschen nicht einsetzbar ist, stellt die DW-MRT das zum jetzigen Zeitpunkt bestmögliche Verfahren zur Untersuchung der Konnektivität dar.

Erste Traktographie-Studien zu Verbindungen der Sprachregionen des Gehirns deuteten darauf hin, dass der IPL möglicherweise unterschiedlich mit verschiedenen Regionen des Frontal- und Temporallappens verbunden sein könnte (Catani et al. 2005; Makris et al. 2005; Rushworth et al. 2006; Saur et al. 2008). Eine aktuelle Studie (Mars et al. 2011) konnte zeigen, dass sich der rechte IPL anhand seines generellen strukturellen

Konnektivitätsmusters in ähnliche rostro-kaudal angeordnete Areale unterteilen ließ wie anhand der Zytoarchitektonik (**Caspers** et al. 2006, 2008).

In der vorliegenden Arbeit wurde eine systematische Untersuchung der strukturellen Konnektivität der fünf auf der freien Oberfläche des IPL liegenden Areale (PFt, PF, PFm, PGa, PGp) in einer Stichprobe von 40 gesunden Probanden untersucht. Die Faserbahnen wurden mittels probabilistischer Traktographie rekonstruiert. Dieses Verfahren berechnet Wahrscheinlichkeitsverläufe der Fasern anhand der zugrunde liegenden Daten zur Wasserdiffusion (Behrens et al. 2003a,b). Stellen kreuzender Fasern werden gesondert modelliert, indem nicht nur die Hauptrichtung der Wasserdiffusion, sondern auch Nebenrichtungen berücksichtigt werden (Behrens et al. 2007). Die IPL-Areale dienten hierbei als Start-Region, in denen der probabilistische Traktographie-Algorithmus beginnt und sich konsekutiv den wahrscheinlichsten Weg durch das Diffusions-Tensor-Feld innerhalb der weißen Substanz sucht. Alle anderen Regionen des Kortex wurden als mögliche Zielregionen genutzt. Zur Auswertung wurde neben einer qualitativen Analyse der Faserbahnen (Abb. 3) eine neue statistische Auswertemethode genutzt, um die Verbindungen zu einzelnen Zielregionen zu quantifizieren und dadurch vergleichbar zu machen: Durch einen Vergleich der Anzahl der rekonstruierten Fasern, die ausgehend von einer IPL-Startregion in einer bestimmten Zielregion endeten, mit der Anzahl der Fasern, die generell in dieser Entfernung von der IPL-Startregion endeten, konnte erfasst werden, ob eine Zielregion signifikant häufiger erreicht wurde als in der Entfernung von der Startregion zu erwarten gewesen wäre. Eine solche entfernungsabhängige Korrektur war nötig, da aufgrund des relativ hohen Rauschanteils diffusionsgewichteter MR-Bilder die Reliabilität der Rekonstruktion der Faserbahnen mit steigender Entfernung von der Startregion abnimmt. Die quantitative Auswertung bestätigte die qualitative Analyse und erlaubte detaillierte Aussagen über die wahrscheinliche Existenz von Faserverbindungen zu einzelnen Hirnrindenarealen.

In dieser Analyse zeigte sich, dass der Verlauf der Faserbahnen der IPL-Areale einen rostro-kaudalen Shift aufwies: Die rostralen IPL-Areale hatten bevorzugte Konnektivität mit Arealen des primären und sekundären somatosensorischen Kortex, des rostralen superioren Parietallappens, des prämotorischen Kortex und des kaudalen Anteils des Gyrus frontalis inferior. Je weiter kaudal die IPL-Areale gelegen waren, desto mehr veränderte sich die Konnektivität hin zu lateralen und medialen präfrontalen Arealen, zu kaudalen Anteilen des superioren Parietallappens sowie zu Arealen des inferioren und rostralen Temporallappens (**Caspers** et al. 2011b ***[Publikation 1]***) (Abb. 3).

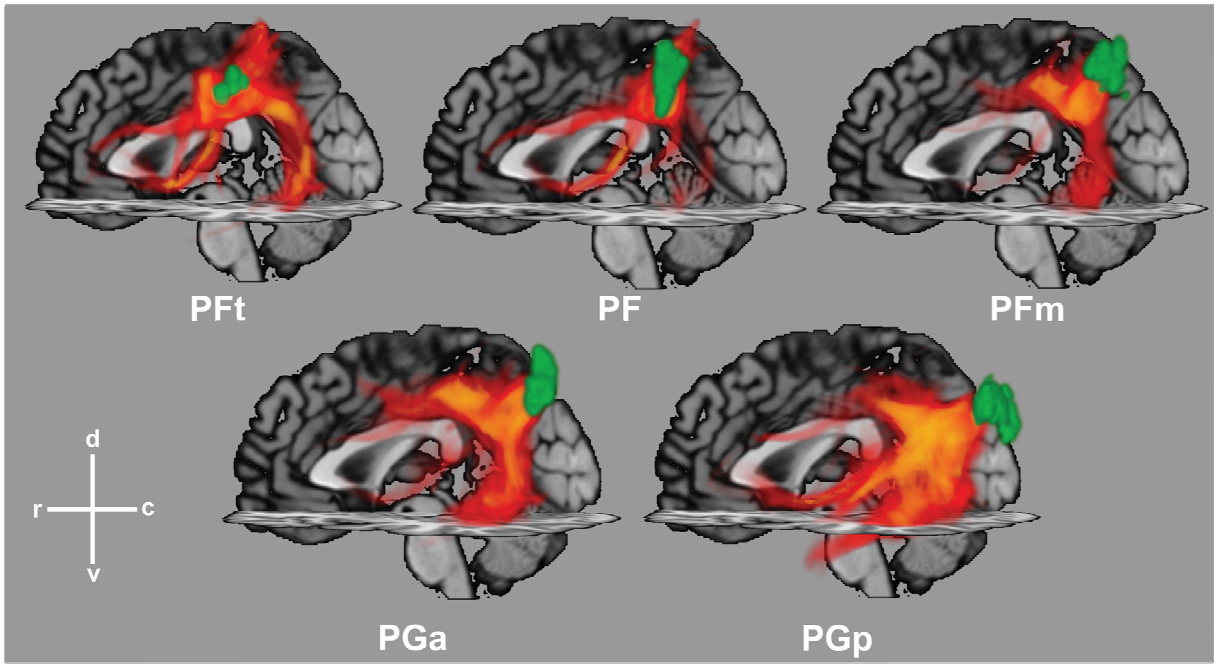


**Abbildung 3:** Faserbahnverläufe fünf verschiedener IPL-Areale von rostral nach kaudal (PFt, PF, PFm, PGa, PGp), ermittelt durch probabilistische Traktographie auf DW-MRT-Daten. Es ist ein Shift der Faserbahnverläufe von rostralen zu kaudalen IPL-Arealen zu erkennen.
Abbildung aus: **Caspers** et al. 2011b, NeuroImage 58 (2): 362-380.

In einer zweiten Studie zur strukturellen Konnektivität wurden die Faserverbindungen zweier Areale des parietalen Operculums ebenfalls mittels probabilistischer Traktographie untersucht. Die möglichen Zielregionen wurden hierbei mittels einer Meta-Analyse über funktionelle Bildgebungsstudien ermittelt, um die kortikalen Regionen zu finden, die konsistent über Studien hinweg mit den Arealen des parietalen Operculums ko-aktiviert waren. Es zeigte sich, dass von diesen verschiedenen Zielregionen der vordere IPL besonders stark mit den Arealen des parietalen Operculums verbunden war. Die funktionelle Definition der Zielregionen in Verbindung mit den behaviouralen Daten der in der Meta-Analyse verwendeten funktionellen Studien erlaubte darüber hinaus eine mögliche funktionelle Charakterisierung dieses Netzwerks: Studien zur Bewegungssteuerung und -verarbeitung waren besonders häufig vertreten. Damit konnte in dieser Studie insbesondere gezeigt werden, dass die rostralen IPL-Areale am ehesten sowohl strukturell als auch funktionell in ein Netzwerk aus Hirnrindenarealen eingeordnet sind, das der Verarbeitung von Bewegungsabläufen dient (Eickhoff, Jbabdi, **Caspers** et al. 2010 ***[Publikation 2]***).

## Molekulare Organisation

Die funktionell relevante Organisation eines Hirnrindenareals lässt sich durch Analyse der Rezeptorarchitektur ermitteln (Zilles und Amunts 2009; Zilles et al. 2002). Die Rezeptorarchitektur beschreibt die Verteilung von Rezeptoren aller klassischen

Neurotransmittersysteme in der Hirnrinde des IPL. Neurotransmitterrezeptoren dienen der Signalübertragung zwischen Neuronen. Durch ein charakteristisches Verteilungsmuster der verschiedenen Rezeptortypen wird die Funktion eines kortikalen Areals maßgeblich beeinflusst und zu großen Teilen determiniert. Insbesondere das Zusammenspiel der verschiedenen Neurotransmittersysteme ist hier von entscheidender Bedeutung (Zilles und Amunts 2009). Somit wird derzeit davon ausgegangen, dass Hirnareale mit einem ähnlichen Verteilungsmuster der Rezeptoren auch in gemeinsamen funktionellen Netzwerken verbunden sind.

Die Studie in der vorliegenden Arbeit baut auf diesem Konzept auf, indem sie das Verteilungsmuster der Rezeptoren in den IPL-Arealen bestimmte und einen Vergleich mit dem Verteilungsmuster in anderen Hirnregionen ermöglichte. Dazu wurde in einer Stichprobe von neun post-mortem Hemisphären das Verfahren der in-vitro Rezeptorautoradiographie verwendet. Hierbei wurden tiefgefrorene Hirnschnitte mit 15 verschiedenen Tritium-markierten Liganden aller klassischen Neurotransmittersysteme (glutamaterg, GABAerg, cholinerg, adrenerg, serotoninerg, dopaminerg) inkubiert. Durch die Untersuchung der laminären Verteilung der Rezeptoren konnten innerhalb des IPL zunächst verschiedene Gebiete mit unterschiedlichen Rezeptorverteilungen voneinander und von den umgebenden Gebieten des Sulcus intraparietalis, des parietalen Operculums und des okzipito-temporalen Kortex abgegrenzt werden. Ein Vergleich mit entsprechenden zytoarchitektonischen Schnitten in den gleichen Gehirnen zeigte, dass die Abgrenzungen in den Rezeptorschnitten mit den Abgrenzungen in den zytoarchitektonischen Schnitten übereinstimmten und dadurch die gleichen sieben IPL-Areale identifiziert werden konnten, die bereits in der zytoarchitektonischen Studie (**Caspers** et al. 2006, 2008) gefunden wurden.

Da nicht jeder Rezeptor jede Grenze zwischen Arealen zeigt und die Funktion eines Areals insbesondere durch das Zusammenspiel verschiedener Rezeptoren bestimmt wird (Zilles et al. 2004), wurden insgesamt die Konzentrationen von 15 verschiedenen Rezeptoren in jedem der sieben IPL-Gebiete bestimmt. Die charakteristische Ausstattung eines IPL-Areals mit allen untersuchten Rezeptoren wurde dann für die weitere Analyse in einem Rezeptor-Fingerprint dargestellt. Die vergleichende Untersuchung der Rezeptor-Fingerprints erlaubte schließlich eine Aussage über Ähnlichkeiten und Unterschiede in der Rezeptor-Ausstattung der IPL-Areale. In einer Cluster-Analyse über die Rezeptor-Fingerprints der sieben IPL-Areale zeigte sich, dass diese aufgrund ihrer Ähnlichkeiten in der Rezeptorverteilung in drei Gruppen eingeteilt werden konnten: eine rostrale Gruppe, bestehend aus den Arealen PFt, PFop und PFcm; eine mittlere Gruppe mit den Arealen PF und PFm; sowie eine kaudale Gruppe aus den Arealen PGa und PGp. Ein Vergleich mit der Rezeptorverteilung in anderen Hirnregionen zeigte, dass alle IPL-Areale, besonders aber die mittlere und kaudale Gruppe

Ähnlichkeiten mit der Broca-Region im Gyrus frontalis inferior aufwiesen. Die mittlere Gruppe hatte zusätzliche Ähnlichkeiten mit dem kaudalen superioren Parietallappen, während die kaudale Gruppe sehr ähnliche Rezeptormuster aufwies wie höhere extrastriäre Areale des ventralen visuellen Kortex. Besonders der letztgenannte Befund weist darauf hin, dass die kaudalen IPL-Areale in höhere visuelle Verarbeitung eingebunden sein könnten, was bereits bei funktionellen Studien und Tracer-Experimenten zur Darstellung der Faserverbindungen im Makaken nachgewiesen werden konnte (Hyvärinen 1982; Mountcastle et al. 1975; Felleman und van Essen 1991).

Der IPL ist somit durch die Expression multipler Transmitterrezeptoren in drei organisatorische Einheiten gegliedert. Die Ähnlichkeiten zu verschiedenen anderen kortikalen Arealen deuten zusätzlich darauf hin, dass die drei funktionell relevanten organisatorischen Einheiten des IPL in unterschiedliche kortikale Netzwerke eingebunden sind und somit unterschiedliche Aufgaben im Gesamtsystem Gehirn wahrnehmen. Es ist zu betonen, dass die drei organisatorischen Einheiten, wie sie durch die rezeptorarchitektonischen Analysen ermittelt werden konnten, eine neue Betrachtungsebene im Vergleich zu den zytoarchitektonischen Analysen erlauben. Die Zytoarchitektonik zeigte sieben unterschiedliche IPL-Areale, die auch in gleicher Form durch die Rezeptorarchitektonik identifiziert werden konnten. Die Rezeptorarchitektonik gibt darüber hinaus Informationen über funktionell relevante Einheiten. Die einzelnen Areale innerhalb dieser Einheiten könnten dabei mögliche Subfunktionen der in der Einheit vornehmlich durchgeführten Aufgabe erfüllen (**Caspers** et al. 2012 ***[Publikation 3]***).

## III.2 FUNKTIONELLE UNTERSUCHUNGEN

In Zusammenschau mit den Ergebnissen zur strukturellen Konnektivität ist diese funktionell relevante Dreiteilung des IPL besonders interessant. Die Ähnlichkeiten der IPL-Areale mit den Arealen des Frontallappens, insbesondere der Broca-Region, korrespondieren mit den Erkenntnissen zu entsprechenden Faserverbindungen. Zusammen deuten diese Ergebnisse somit darauf hin, dass der IPL zumindest in drei unterschiedliche funktionelle Netzwerke des Gehirns eingebunden sein könnte.

Dieser Frage wurde in der vorliegenden Arbeit zum einen durch mehrere einzelne funktionelle Studien und Meta-Analysen zu verschiedenen funktionellen Aspekten des IPL nachgegangen. Zum anderen wurde eine Untersuchung zur allgemeinen funktionellen Konnektivität (d.h. über eine große Anzahl funktioneller Studien hinweg) der drei IPL-Cluster durchgeführt.

**Bewegungssteuerung**

Aufbauend auf einer Literaturrecherche zur möglichen Involvierung der sieben IPL-Areale bzw. der drei IPL-Cluster in unterschiedliche kognitive Netzwerke wurde eine Meta-Analyse zum potentiellen menschlichen Spiegelneuronensystem durchgeführt. Dieses System wurde ausgewählt, weil hierfür eine sehr selektive Beteiligung des rostralen Anteils des IPL vermutet wurde (z.B. Rozzi et al. 2008) und somit die Hypothese bestand, dass das in der zytoarchitektonischen Analyse identifizierte rostrale Areal PFt am ehesten als anatomisches Korrelat im IPL in Frage käme. Eine solche spezifische Vorannahme über die Zuordnung einzelner Funktionen zu bestimmten Arealen ist auf Basis des derzeitigen Forschungsstandes für solche höher geordneten Hirnregionen wie den Parietallappen häufig diffizil. Das liegt vornehmlich an der Schwierigkeit, die wirkliche „Funktion“ des Areals adäquat mittels neuropsychologischer Konstrukte abbilden zu können. In funktionellen Bildgebungsstudien wird versucht, sich mit Hilfe einzelner funktioneller Aufgaben, die von den Probanden im Magnetresonanztomographen (MRT) durchgeführt werden, den neuronalen Korrelaten dieser Funktionen anzunähern. Jede funktionelle MRT-Studie bildet dabei, abhängig von den eingesetzten Bedingungen, einen möglichen kleinen Ausschnitt des übergeordneten psychologischen Konstruktes ab. Durch die Bündelung vieler verschiedener fMRT-Studien zu einem übergeordneten Thema können Meta-Analysen dazu beitragen, die Netzwerke des Gehirns, die generell und über Studien hinweg an einer bestimmten Funktion beteiligt sind, näher zu charakterisieren.

Das Ziel dieser Meta-Analyse der vorliegenden Arbeit war, neben der Identifikation des im IPL relevanten Areals, die Charakterisierung des gesamten potentiellen menschlichen Spiegelneuronen-Systems bzw. der damit verbundenen Konstrukte Handlungsbeobachtung und Handlungsimitation. Dazu wurden alle relevanten Publikationen über fMRT-Studien zu diesen Themen mittels einer Datenbankrecherche identifiziert. Alle dort berichteten Aktivierungsfoki im gesamten Gehirn wurden mittels eines etablierten Meta-Analyse-Algorithmus (Activation Likelihood Estimation (ALE); Eickhoff et al. 2009, Laird et al. 2005) daraufhin untersucht, ob sie über Studien hinweg eine räumliche Konvergenz zeigten. Sowohl die neuronalen Korrelate für Bewegungsbeobachtung als auch die für Bewegungsimitation zeigten ein ausgedehntes Netzwerk frontaler, parietaler und temporaler Areale, wobei die Aktivierungen im Bewegungsbeobachtungsnetzwerk etwas ausgedehnter waren als im Bewegungsimitationsnetzwerk. Es zeigten sich zudem Unterschiede der Involvierung des prämotorischen Kortex für die Verarbeitung unterschiedlicher Effektoren, mit Aktivierungen des ventralen prämotorischen Kortex bei der Verarbeitung von Mund- und Gesichtsbewegungen und Aktivierungen des dorsalen prämotorischen Kortex bei der Verarbeitung von Handbewegungen. Eine solche Unterscheidung fand sich nicht im Parietallappen. Allerdings konnte im IPL die Hypothese, dass hauptsächlich das Areal PFt in

das Spiegelneuronensystem involviert ist, bestätigt werden: sowohl in den Einzelanalysen zur Bewegungsbeobachtung und –imitation als auch in der Konjunktionsanalyse über beide zeigte sich insbesondere das Areal PFt innerhalb des rostralen IPL bevorzugt involviert. Es interagiert in diesem funktionellen Netzwerk mit Arealen in der Broca-Region (kaudaler Anteil des Gyrus frontalis inferior), des prämotorischen Kortex, des superioren Parietallappens sowie des temporo-okzipitalen Kortex (Caspers et al. 2010 ***[Publikation 4]***).

### Aufmerksamkeit

Als weiteren Einzelaspekt der funktionellen Segregation des IPL wurden zwei Studien zur Aufmerksamkeit durchgeführt

In einer fMRT-Studie wurde die Entscheidungsfindung in Abhängigkeit von der übergeordneten Wertepräferenz einer Person untersucht. In bisherigen Studien zu moralischen Dilemmata zeigte sich eine Involvierung des kaudalen Anteils des IPL (Gyrus angularis). Dabei wurden allerdings konkrete, moralisch relevante Situationen gezeigt. Die Idee der vorliegenden Studie war es vielmehr, davon zu abstrahieren und das allgemeine Wertemuster einer Person zugrunde zu legen. Dazu wurde mit 38 Probanden eine Entscheidungsaufgabe durchgeführt, in der sich die Probanden zwischen je zwei Begriffen, die Wertvorstellungen beschrieben, entscheiden sollten. Anhand des Entscheidungsverhaltens konnten die Probanden in Personen mit vorzugsweise individualistischem Wertemuster und solche mit präferentiell kollektivistischem Wertemuster unterteilt werden. Die Untersuchung der neuronalen Korrelate während der Entscheidungsaufgabe zeigte unterschiedliche Verarbeitungsstrategien in Abhängigkeit vom dominierenden Wertemuster einer Person: Während individualistische Personen verstärkte Aktivierung in der Amygdala zeigten, war bei den kollektivistischen Personen eine Aktivierung in einem kortikalen Netzwerk, bestehend aus linkem anteriorem lateralem präfrontalem Kortex, rechtem Gyrus frontalis medius und linkem rostralen Anteil des IPL (Areal PFt) zu finden. Bezogen auf die Aktivierung des linksseitigen rostralen IPL ist bekannt, dass Aktivierungen in diesem Bereich gehäuft bei selektiven Aufmerksamkeitsprozessen gefunden wurden. Der IPL scheint hierbei insbesondere für die Auswahl nicht-salienter Stimuli vonnöten zu sein, eine Interpretation, die auch im Zusammenhang der vorliegenden Studie sinnvoll erschien: Die Kollektivisten waren in der Lage, beide präsentierten Begriffe gegeneinander abzuwägen und zu bewerten, so dass sie sich leichter auch für den Begriff entscheiden konnten, der nicht unmittelbar präferiert wurde, was wiederum zu dem ihnen zugeschriebenen Verhalten (Ausrichtung an einer Gruppe, Zurückstellen eigener Interessen, Berücksichtigung aller Möglichkeiten) passte (**Caspers** et al. 2011 ***[Publikation 5]***).

Zusammen mit der Aktivierung des Areals PFt in der Meta-Analyse zum potentiellen Spiegelneuronensystem des Menschen deuten diese Befunde darauf hin, dass das Areal PFt eine über beide Aufgabentypen hinweg gehende, übergeordnete Funktion zu haben scheint. Möglicherweise spielt die Unterdrückung nicht-salienter Stimuli ebenfalls bei der Handlungsbeobachtung und -imitation eine Rolle, so dass das Areal PFt in beiden Arten der hier untersuchten Aufgaben diese Funktion übernimmt.

In einer zweiten Studie wurde ein Teil des Areals PFm, das zum mittleren IPL gehört, mit Hilfe einer Meta-Analyse und der Untersuchung seiner Rolle in Resting-State-Netzwerken hinsichtlich seiner möglichen Funktion untersucht. Mittels Meta-Analyse wird hierbei die aufgabenbezogene funktionelle Konnektivität untersucht, während die Untersuchung mittels Resting-State-MRT erlaubt, die aufgabenfreie funktionelle Konnektivität einer Hirnregion zu untersuchen. Der „resting state“ des Gehirns beschreibt die funktionelle Grundaktivität, die im Gehirn zu jedem wachen Tageszeitpunkt ohne gezielten Input von außen gemessen werden kann (Gusnard and Raichle 2001; Raichle et al. 2001). Durch die Kombination beider Techniken wird somit die funktionelle Konnektivität umfassend beschrieben. Dabei sind insbesondere Netzwerke, die durch beide Arten funktioneller Konnektivität miteinander verbunden sind, als besonders relevant für das System Gehirn zu sehen.

Für die vorliegende Analyse wurde die Region, deren funktionelle Konnektivität charakterisiert werden sollte, funktionell definiert, basierend auf drei vorherigen fMRT-Studien zu sensomotorischer Integration, räumlicher Aufmerksamkeit und Stimulus-Response-Mapping (Cieslik et al. 2010; Eickhoff et al. 2011; Jakobs et al. 2009). Diese Region nahm den ventralen Anteil des Areals PFm rechts ein. Die Untersuchung der funktionellen Konnektivität dieses Areals mittels Meta-Analyse, d.h. das Ko-Aktivierungs-Muster über verschiedene funktionelle Bildgebungsstudien, sowie mittels Resting-State-Analyse zeigte, dass dieser ventrale Anteil von PFm, der funktionell auch häufig als temporoparietale Übergangszone (TPJ) bezeichnet wird, in ein Netzwerk aus ventralem prämotorischem Kortex, Arealen 44 und 45 des Gyrus frontalis inferior sowie anteriorer Inselrinde involviert ist. Dieses Netzwerk entspricht dem so genannten ventralen Aufmerksamkeitsnetzwerk (Corbetta and Shulman 2002; Corbetta et al. 2008). Dieses Netzwerk ist für die Umorientierung von Aufmerksamkeit zuständig: Wenn unerwartete Stimuli auftauchen, wird die bestehende Daueraufmerksamkeit unterbrochen und auf den neuen Stimulus umgelenkt. Besonders interessant in der vorliegenden Studie war allerdings, dass dieses funktionelle Netzwerk unter Einbeziehung des IPL-Areals PFm über verschiedene Studien hinweg und nicht nur spezifisch bei Aufmerksamkeitsstudien gefunden wurde und dass sich das gleiche Muster in Abwesenheit einer spezifischen Aufgabe (Resting-state) zeigte. Das deutet darauf hin, dass dieses mittlere IPL-Netzwerk zwar grundsätzlich in dieses Aufmerksamkeitsnetzwerk involviert ist, darin aber möglicherweise

eine Funktion übernimmt, die auch für eine Vielzahl anderer Aufgaben relevant ist (Jakobs, Langner, **Caspers** et al. 2012 ***[Publikation 6]***).

### Mathematische Kognition

Um auch den Bereich des kaudalen IPL und damit vornehmlich den Gyrus angularis funktionell näher zu untersuchen, wurde eine fMRT-Studie zur Verarbeitung von Rechenaufgaben durchgeführt.

Den Probanden wurden Rechenaufgaben mit je drei Operanden und jeweils einem Additions- und einem Subtraktionsteil präsentiert. Als ein relevanter Einflussfaktor auf die Rechenleistung (Schnelligkeit und Genauigkeit) wurden diese Rechenaufgaben einerseits in arabischen Ziffern (leichte Bedingung, eher automatisiert) und andererseits mit römischen Zahlen (schwere Bedingung, weniger automatisiert) wiedergegeben. Vor dem Hintergrund bekannter Aktivierungsunterschiede innerhalb des Gyrus angularis in Abhängigkeit von der Aufgabenschwierigkeit bzw. der möglichen Automatisierung der Verarbeitung bei leichteren Aufgaben (Dehaene et al. 2003; Grabner et al. 2007; Krueger et al. 2008) wurden die Aktivierungen dieser Studie mit Hilfe der zytoarchitektonischen Karten des IPL gezielt analysiert. Dadurch konnten die möglichen Aktivierungsunterschiede sehr deutlich voneinander abgegrenzt und einzelnen IPL-Arealen zugeordnet werden.

Sowohl in der leichten als auch in der schweren Rechen-Bedingung wurden ausgeprägte Deaktivierungen in beiden Arealen PGa und PGp des Gyrus angularis gefunden. Die Deaktivierung war allerdings deutlicher in der schweren Bedingung. Deaktivierungen im IPL bei Rechenaufgaben wurden wiederholt beobachtet. Die unterschiedlichen Deaktivierungslevel in Abhängigkeit von der Aufgabenschwierigkeit unterstützen die Hypothese, dass eine stärkere Automatisierung einer Rechenaufgabe weniger Deaktivierung im kaudalen IPL erfordert. In der vorliegenden Studie wurde das durch die leichtere Verarbeitung arabischer relativ zu römischen Zahlen hervorgerufen, es zeigte sich aber auch in Studien zu Trainingseffekten (Delazer et al. 2003; Ischebeck et al. 2006). Um die Bedeutung dieser Deaktivierungen zu verstehen, ist insbesondere räumliche Koinzidenz der Befunde dieser Studie mit Studien zum ‚Default Mode Network' interessant. Dieses Netzwerk wurde wiederholt stark deaktiviert gefunden, wenn kognitiv anspruchsvolle Aufgaben gelöst werden mussten (z.B. Seeley et al. 2007), um eine bessere Verarbeitung komplexer visueller Stimuli zu ermöglichen. Diese Interpretation wurde zusätzlich durch die Analyse der individuellen Performance der Probanden in der vorliegenden Studie unterstützt. Die Analyse zeigte, dass die Antwortgenauigkeit mit stärkerer Deaktivierung in den Arealen PGa und PGp zunahm oder anders ausgedrückt: Je stärker die kaudalen IPL-Areale involviert wurden, desto schlechter war die Performance der Probanden. Das deutete darauf hin, dass es für

die akkurate Durchführung einer kognitiv anspruchsvollen Aufgabe wie Rechnen notwendig ist, den kaudalen Anteil des IPL weniger stark zu involvieren als z.B. frontale Areale.
Die Befunde dieser Studie zeigen somit, dass die funktionelle Rolle der IPL-Areale nicht nur im Hinblick auf Aktivierungen, sondern auch unter Berücksichtigung möglicher Deaktivierungen eruiert werden muss. Dies stellt nach dem derzeitigen Stand der Forschung eine besondere Herausforderung dar, da derzeit die Bedeutung einer reduzierten Blutantwort (BOLD) im Rahmen funktioneller Bildgebungsexperimente noch nicht abschließend geklärt ist. Es ist zum einen möglich, dass eine reduzierte BOLD-Antwort tatsächlich die aktive Inhibition von Neuronengruppen widerspiegelt und somit tatsächlich einzelne Hirnareale für die Erfüllung bestimmter Aufgaben gezielt unterdrückt werden. Zum anderen ist aber auch denkbar, dass es sich lediglich um eine geringere Aktivierung relativ zu Aktivierungen in anderen Arealen handelt (Bandettini 2009; Devor et al. 2007; Logothetis 2008).
In Zusammenschau mit anderen Befunden funktioneller Bildgebungsstudien zur Involvierung des kaudalen IPL, insbesondere bei Sprach- oder moralischen Entscheidungsaufgaben, stellt sich somit die Frage, was die genaue Funktion dieses Teils des IPL ist. Die Funktion muss bei einigen Aufgaben zu einer Aktivierung in dieser Region und bei anderen Aufgaben, wie der in der vorliegenden Studie, zu einer Deaktivierung der gleichen Region führen (Wu, Chang, Majid, **Caspers** et al. 2009 ***[Publikation 7]***).

### Funktionelle Konnektivität

Betrachtet man diese Befunde der einzelnen funktionellen Studien bzw. Meta-Analysen zu einem speziellen Thema von der Perspektive des gesamten IPL, zeigt sich, dass verschiedene Bereiche des IPL in verschiedene funktionelle Systeme eingebunden zu sein scheinen. Unterstützt werden diese funktionellen Einzelbefunde durch die Ergebnisse der Rezeptorautoradiographie des IPL, die eine Einteilung des IPL in drei organisatorische Einheiten gezeigt hat. Bereits die grobe Zuordnung der Befunde der einzelnen funktionellen Studien zu den drei Einheiten des IPL deutet darauf hin, dass der rostrale IPL eher in Bewegungssteuerung und direkte Kontrolle von Handlungen involviert ist, während der mittlere IPL eher in Aufmerksamkeitsprozesse und der kaudale IPL in höhere Zahlenverarbeitung involviert ist. Die Ergebnisse der Faserbahn-Traktographie des IPL zeigte zudem, dass sich die Erkenntnisse zur strukturellen Konnektivität und zur funktionellen Netzwerkcharakterisierung des rostralen IPL komplementär ergänzen: Die Areale, die in einem gemeinsamen funktionellen Netzwerk zu Handlungsbeobachtung und -imitation interagieren, weisen beispielsweise auch strukturelle anatomische Verbindungen auf. Ähnliches gilt für die Faserbahnen des mittleren und kaudalen IPL. Daraus lässt sich bereits eine erste Hypothese über ein mögliches Organisationsmodell des IPL generieren,

dass sich aus strukturellen und spezifischen funktionellen Daten herleitet: Während die rostralen Areale des IPL in ein Netzwerk von Arealen, die in enger Nachbarschaft zum Sulcus centralis stehen, eingebunden zu sein scheinen, interagieren die kaudalen IPL-Areale eher mit weiter entfernt liegenden Regionen des rostralen Bereichs des Frontal- und Temporallappens.

Da die einzelnen funktionellen Studien nur einen sehr selektiven Ausschnitt aus dem breiten Spektrum möglicher Paradigmen und damit Funktionen, in die der IPL involviert ist, repräsentieren, wurde in einer weiteren Studie die generelle funktionelle Konnektivität des IPL untersucht. Dazu wurde die Methode des Meta-Analytic Connectivity Modelling (MACM) verwendet (Eickhoff et al. 2009, 2012). Aus der Brainmap-Datenbank (www.brainmap.org; Laird et al. 2005, 2009), einer Datenbank über publizierte fMRT-Studien, wurden alle Studien, die zumindest einen Aktivierungsfokus im IPL hatten, auf ihre Ko-Aktivierungsmuster hin untersucht. Der IPL wurde hierzu anhand der rezeptorautoradiographischen Studie in ein rostrales, ein mittleres und ein kaudales Cluster eingeteilt. Dadurch konnten funktionell unterschiedliche Organisationseinheiten bestmöglich voneinander abgegrenzt werden.

Die Ko-Aktivierungen aller einzelnen Studien wurden auf Konsistenz über Studien hinweg getestet (gleiches Verfahren wie für die Studie zum potentiellen menschlichen Spiegelneuronensystem beschrieben (**Caspers** et al. 2010 ***[Publikation 4]***: Activation Likelihood Estimation (ALE) Methode; Eickhoff et al. 2009; Turkeltaub et al. 2011). Im Unterschied zur vorherigen Analyse zum menschlichen Spiegelneuronensystem wurde bei dieser Untersuchung keine Vorauswahl von Studien basierend auf inhaltlichen Kriterien getroffen wurde. Stattdessen wurden alle in der Datenbank verfügbaren Studien als Basis genommen, wodurch Aussagen über die generelle, über verschiedene funktionelle Domänen hinweg bestehende funktionelle Konnektivität getroffen werden konnte.

Dabei zeigte sich folgendes Muster der Ko-Aktivierungen und damit der funktionellen Konnektivität der drei IPL-Cluster: die rostrale Gruppe hatte starke funktionelle Konnektivität mit dem kaudalen Anteil des Gyrus frontalis inferior und des frontalen Operculums, dem prämotorischen Kortex, dem primären somatosensorischen Kortex am Übergang zum Sulcus intraparietalis, sowie dem medial gelegenen supplementär-motorischen Kortex (Abb. 4, blaue Blobs). Das kaudale Cluster zeigte starke funktionelle Konnektivität mit den rostralen Anteilen des Gyrus frontalis inferior und des frontalen Operculums, mit lateralen und medialen präfrontalen Arealen, rostralen temporalen Arealen sowie dem posterioren cingulären Kortex (Abb. 4, grüne Blobs). Das mittlere IPL-Cluster hatte Ko-Aktivierungen, die sich zwischen die des rostralen und kaudalen Clusters einordneten (Abb. 4, rote Blobs).

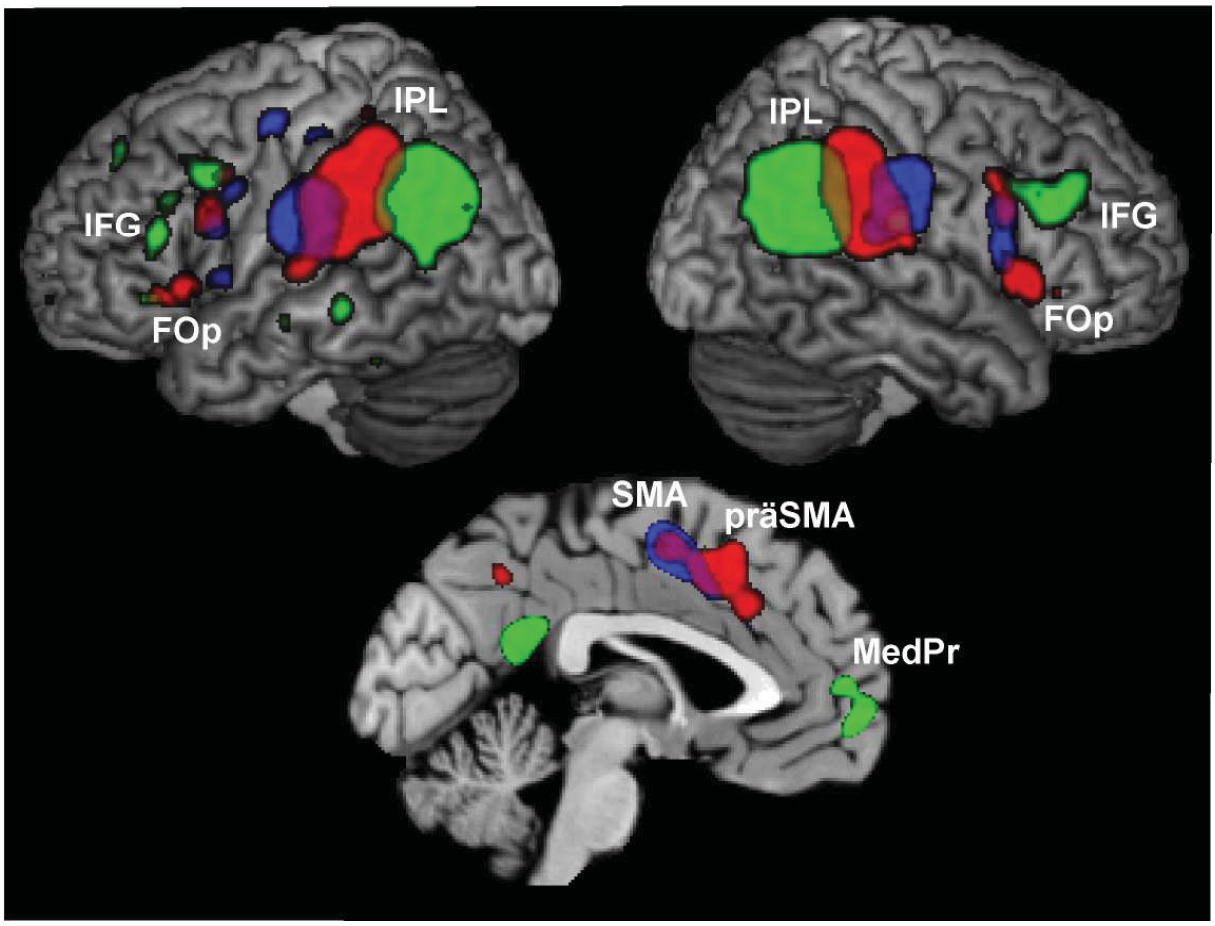


**Abbildung 4:** Funktionelle Konnektivität der drei IPL-Cluster (rostrales: blau; mittleres: rot; kaudales: grün), dargestellt auf dem Standardgehirn des Montreal Neurological Institute (MNI)-Raums. FOp: frontales Operculum; IFG: Gyrus frontalis inferior; IPL: Lobulus parietalis inferior; MedPr: medialer präfrontaler Kortex; (prä-)SMA: (prä-) supplementär motorischer Kortex

Zusätzlich existierten zu jeder funktionellen Studie aus der Brainmap-Datenbank, die in diese Analyse eingegangen ist, Meta-Daten, wie z.B. die Art des verwendeten funktionellen Paradigmas sowie die relevante funktionelle Domäne oder der verwendete Stimulus-Typ. Dadurch konnten die drei IPL-Cluster und die über Ko-Aktivierung mit ihnen verbundenen Netzwerkpartner funktionell charakterisiert werden (Abb. 5).

Es zeigte sich insbesondere, dass der rostrale IPL in Handlungs- und Bewegungssteuerung involviert war, wie es auch bereits in der Meta-Analyse zum menschlichen Spiegelneuronensystem gefunden werden konnte (**Caspers** et al. 2010 ***[Publikation 4]***). Je weiter man im IPL nach kaudal gelangt, desto mehr verschiebt sich das funktionelle Profil hin zu mehr kognitiven Aufgaben wie Aufmerksamkeits- und Sprachverarbeitung. In ähnlicher Weise lässt sich diese Verschiebung auch anhand der verwendeten Stimuli beschreiben: Je weiter kaudal im IPL, desto eher sind komplexere Verarbeitungsmuster notwendig, z.B. zur Verarbeitung von Wörtern im Gegensatz zu einzelnen Buchstaben (mittlerer IPL) oder zur Verarbeitung von Bildern im Gegensatz zu einzelnen Objekten oder Formen (rostraler IPL). Dabei ist zu beachten, dass diese Beschreibungen psychologische Konstrukte darstellen, die

die tatsächliche mechanistisch zugrunde liegende „Funktion“ einzelner Hirnareale nur bedingt beschreiben können. Sie dienen einer grundsätzlichen Kategorisierung, um Hinweise darauf zu bekommen, welche Auswirkungen der unterschiedliche mirkostrukturelle und neurochemische Aufbau der Hirnrinde für das Verhalten des Menschen haben könnte. Die Verbindung dieser unterschiedlichen Ebenen ist bis heute noch weitgehend unklar (Laird et al. 2009; Poldrack 2006).

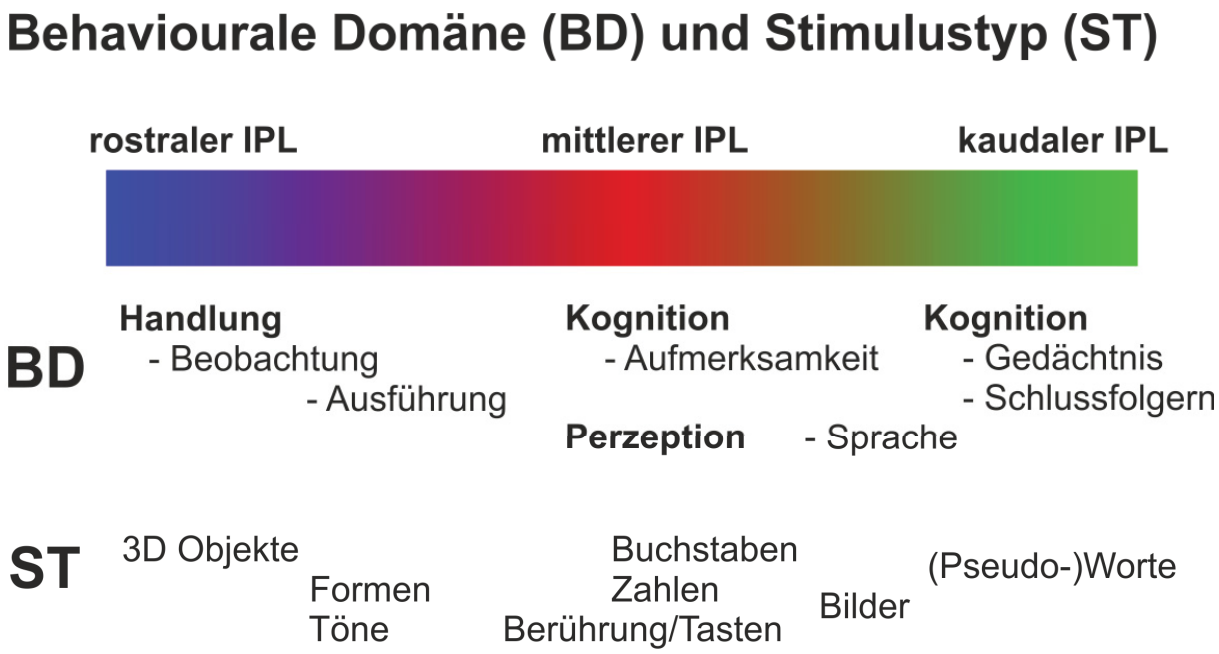


**Abbildung 5:** Schematische Darstellung der relevanten Meta-Daten der Analyse zur funktionellen Konnektivität des IPL. Der Farbbalken markiert den Verlauf von rostralem zu kaudalem IPL (gleiche Farbgebung wie in Abb. 4). Darunter der Zuordnung der getesteten funktionellen Domänen (behaviourale Domäne, BD) und des verwendeten Stimulustyps (ST) zu den drei Bereichen rostraler, mittlerer und kaudaler IPL.

Diese Befunde zur funktionellen Konnektivität komplettieren die Erkenntnisse einzelner funktioneller Studien in Zusammenschau mit den Erkenntnissen zur strukturellen Konnektivität und Rezeptorarchitektur des IPL. Diese verschiedenen Entitäten tragen durch unterschiedliche Informationen dazu bei, den IPL in seiner strukturell-funktionellen Organisation eingehender zu verstehen. Besonders die Bestätigung der funktionellen Architektur des IPL auf Basis einer großen Anzahl unselektierter funktioneller Bildgebungsstudien, wie in der Analyse zur generellen funktionellen Konnektivität des IPL ermittelt, gibt zusätzliche Hinweise auf ein allgemeines Organisationsprinzip innerhalb des IPL. Dieses funktionell motivierte Modell wird durch die Befunde zur Struktur vervollständigt.

## III.3 STRUKTURELL-FUNKTIONELLES ORGANISATIONSMODELL DES IPL

Auf Grundlage der in der vorliegenden Arbeit berichteten Studien lässt sich nun ein multimodal motiviertes Modell der strukturellen und funktionellen Organisation des IPL postulieren. Dieses Modell berücksichtigt somit sowohl die Informationen zur Struktur des IPL (Zyto- und Rezeptorarchitektonik, anatomischen Konnektivität) als auch zur Funktion (einzelne fMRT-Studien zu spezifischen funktionellen Paradigmen, Meta-Analysen und generelle funktionelle Konnektivität).

Der IPL scheint sowohl strukturell als auch funktionell so in das Gesamtsystem Gehirn eingebettet zu sein, dass die resultierenden Netzwerke um den Sulcus centralis als Referenzstruktur symmetrisch in Form von sich umschließenden Schalen angeordnet sind. Ein solches Modell ließe sich somit als „Zwiebelschalen-Modell“ der Organisation des IPL bezeichnen (Abb. 6).

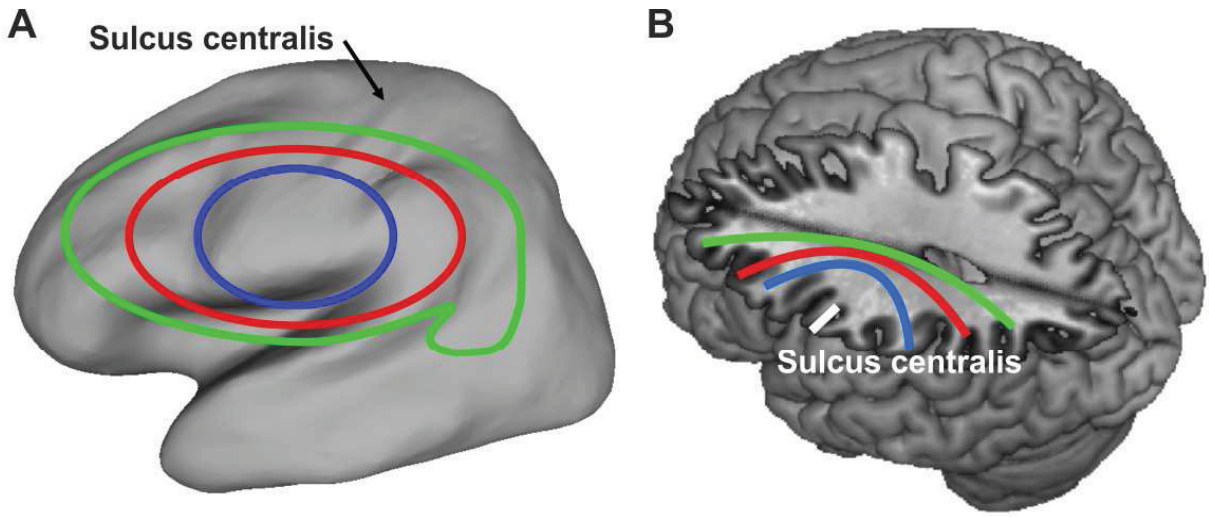


**Abbildung 6:** Schalenmodell der Organisation des IPL. (A) Ansicht von lateral, dargestellt auf inflated-Ansicht des Gehirns, Netzwerke der IPL-Areale farbig auf der Oberfläche dargestellt. (B) Aufsicht auf schematischen Verlauf der Faserbahnen auf den verschiedenen Schalen in 3D-Ansicht des Gehirns mit herausgenommenen Anteilen des oberen Parietal- und Frontallappens.

Die innere Schale wird gebildet durch den rostralen IPL und der mit ihm verbundenen, direkt um den Sulcus centralis gelegenen Hirnregionen (kaudaler Gyrus frontalis inferior, prämotorischer Kortex, supplementär-motorischer Kortex, primärer und sekundärer somatosensorischer Kortex). Erweitert man den Radius, gelangt man zur zweiten Schale, die den mittleren Bereich des IPL und die damit verbundenen Areale umfasst (Broca-Region, mittlerer Bereich des frontalen Operculums, prä-supplementär-motorischer Kortex, medialer superiorer Parietallappen / Präcuneus). Eine erneute Erweiterung des Schalenradius führt auf die dritte und damit äußerste Schale, die den kaudalen IPL und alle mit diesem Gebiet verbundenen Hirnareale enthält (rostraler Anteil des Gyrus frontalis inferior und des frontalen

Operculums, lateraler und medialer präfrontaler Kortex, posteriorer cingulärer Kortex, rostraler Gyrus temporalis medius).

Die Schalen repräsentieren zusätzlich den ungefähren Verlauf der in diesen Netzwerken verlaufenden Faserbahnen, die sich insbesondere um den Sulcus centralis schichtweise herumlagern müssen (Abb. 6B). Die Faserbahnen des rostralen Netzwerks verlaufen in der Capsula interna relativ weit lateral, nah am Boden des Sulcus centralis, um direkt rostral davon die Verbindung zum kaudalen Gyrus frontalis inferior herzustellen, während die im kaudalen Netzwerk relevanten Fasern sich medial davon anordnen, um die langen Verbindungen zu den weiter entfernt liegenden Arealen zu ermöglichen. Da der Sulcus centralis ontogenetisch als einer der ersten Sulci entsteht und aus diesem Grund sehr invariant über Personen hinweg ist, ist ein solcher Verlauf der Faserbahnen in den Netzwerken des IPL auch entwicklungsgeschichtlich plausibel: Die später enstehenden Areale und deren Verbindungen lagern sich um den Sulcus centralis herum.

Die anhand dieses multimodal generierten Schalen-Modells gezeigte Einordnung des IPL in das Gesamtsystem Gehirn leistet einen neuen Beitrag zur Diskussion um die grundsätzliche Organisation des Gehirns. Für den Frontallappen beispielsweise wurde ein prinzipielles Entwicklungsschema aufgestellt, das in der so genannten Gradationshypothese seinen Ausdruck fand (Brockhaus 1940; Sanides 1964; Vogt 1910): Der frontale Neocortex entwickelt sich in Gradationswellen, in denen von zentralen Startpunkten im Gehirn, vornehmlich aus der Insel, schrittweise die verschiedenen Areale und deren Verbindungen entstehen und sich dadurch umeinander lagern. Das zeigt sich im zytoarchitektonischen Aufbau sowie der genetischen Topographie (Chen et al. 2012; Zilles und Amunts 2012). Der schalenartige Aufbau der IPL-Netzwerke, wie er anhand strukturell-funktioneller Korrelationen in der vorliegenden Arbeit gezeigt werden konnte, spiegelt wahrscheinlich diese Entwicklungshypothesen auf einer anderen Betrachtungsebene wider. Zudem wurde beispielsweise innerhalb der Insel eine ähnliche graduelle funktionelle Anordnung gefunden, wie sie anhand des Schalenmodells des IPL zu erwarten wäre, mit Handlungskontrolle im kaudalen Bereich der Insel und eher kognitiver Verarbeitung im rostralen Anteil (Cauda et al. 2011; Chang et al. 2012; Kurth et al. 2010). Ähnliche Anordnungen ko-aktivierter Regionen des IPL fanden sich auch bereits in Analysen von Resting-State MRT-Daten, d.h. von Daten zur Aktivität des Gehirns ohne eine strukturierte Aufgabe von außen. Yeo et al. (2011) konnten u.a. zeigen, dass die Resting-State Aktivität des rostralen IPL mit der entsprechenden Aktivität im kaudalen Bereich des Gyrus frontalis inferior korrelierte, während die Aktivität des kaudalen IPL mit der Aktivität im ventro- und dorsolateralen präfrontalen Kortex korrelierte. Zusätzlich konnte in einer fMRT-Analyse mit einer einzelnen strukturierten Aufgabe, nämlich zum sprachlichen Verständnis von Aussagen, in denen Quantoren benutzt werden (Beispiele für die Verwendung von Quantoren sind: „7 ist größer

als 5“, „in dem Korb sind mindestens 3 Äpfel“), gezeigt werden, dass hier für verschiedene Teilfunktionen ebenfalls Areale des rostralen IPL und angrenzenden IPS mit kaudalen Bereichen des Gyrus frontalis inferior bzw. des kaudalen IPL mit rostralen Anteilen des Gyrus frontalis inferior ko-aktivierten und zwei, umeinander geschachtelte Netzwerke bildeten (Heim et al. 2012). Die Befunde über die allgemeine Korrelation der IPL-Areale mit frontalen Arealen im Resting-State als auch innerhalb einer Studie mit einem speziellen funktionellen Paradigma unterstützen zusätzlich die Idee, dass die Involvierung der IPL-Areale in funktionelle Netzwerke schalenförmig erfolgt, was durch eine entsprechende strukturelle Einbettung unterstützt wird.

Eine mögliche ursächliche Erklärung für eine solche Organisation des IPL-Systems und seiner Netzwerkpartner könnte die notwendige Schnelligkeit der Informationsübertragung für die verschiedenen Funktionen sein: Das rostrale IPL-Netzwerk scheint vornehmlich in Handlungskontrolle und -verarbeitung involviert zu sein. Dafür sind häufig sehr schnelle Reaktionen notwendig, die durch eine schnelle Abstimmung der beteiligten Hirnareale innerhalb dieses Netzwerks zustande kommen. Für höhere kognitive Aufgaben, wie sie bevorzugt im kaudalen IPL-Netzwerk, insbesondere in Zusammenarbeit mit Arealen des präfrontalen Kortex durchgeführt werden, ist eine solche Schnelligkeit nicht unbedingt erforderlich. Beispielsweise können Entscheidungen und damit verbundene Planungen weiterer Aktivitäten langsamer vonstatten gehen, weil alle relevanten Informationen integriert werden müssen. Der Informationsaustausch muss dann nicht auf Basis einer Reaktionsschnelligkeit (im Bereich von Millisekunden bis zu wenigen Sekunden) wie im motorisch dominierten Netzwerk zur Handlungsverarbeitung vonstatten gehen, weswegen die Länge der Faserbahnen und die damit verbundene längere Dauer des Informationsaustausches weniger wichtig werden.

Auf Basis des hier postulierten Modells können solche Annahmen und mögliche ursächliche Erklärungen überprüft werden. Anhand des Modells können die relevanten Netzwerke für die verschiedenen Bereiche des IPL und deren Verbindungen untereinander identifiziert werden. Dazu können anschließend gezielte Experimente zu spezifischen Funktionen durchgeführt werden. Dadurch würde es möglich, die tatsächliche „Funktion“ des IPL, d.h. seine Rolle in der Verarbeitung von Informationen, exakter und damit wahrscheinlich von psychologischen Konstrukten abstrahiert zu beschreiben.

# IV ZUSAMMENFASSENDE BETRACHTUNG

Der menschliche inferiore Parietallappen ist eine strukturell und funktionell sehr heterogene Hirnregion. Die im Rahmen dieser kumulativen Habilitationsschrift vorgestellten Arbeiten leisten Beiträge zum Verständnis dieser beiden Aspekte des Aufbaus des IPL und ihrer Beziehung zueinander.

Aufbauend auf vorherigen Untersuchungen zum zytoarchitektonischen Aufbau des IPL konnte anhand der Rezeptorarchitektur zunächst die zytoarchitektonische Einteilung in sieben unterschiedliche Areale bestätigt werden. Zusätzlich konnte durch rezeptorarchitektonische Ähnlichkeiten innerhalb der IPL-Areale eine funktionell relevante, zuvor nicht bekannte Unterteilung des IPL in drei Organisationseinheiten identifiziert werden. Diese drei rostro-kaudal angeordneten Organisationseinheiten des IPL konnten durch die Untersuchung der anatomischen Konnektivität strukturell in das Gesamtsystem Gehirn eingeordnet werden, indem ihre Faserverbindungen zu anderen Hirnregionen charakterisiert wurden. Diese zeigen eine graduelle Anordnung: Von rostral nach kaudal im IPL verschieben sich die Zielregionen der Faserverbindungen von sensomotorischen Regionen für den rostralen IPL über Areale des superioren Parietallappens für den mittleren IPL zu Regionen des Temporallappens für den kaudalen IPL.

Zudem konnte in verschiedenen einzelnen funktionellen Bildgebungsstudien und Meta-Analysen die rostralen, mittleren und kaudalen Anteile des IPL funktionell unterschiedlichen Netzwerken zugeordnet werden. Diese umfassten das menschliche Spiegelneuronensystem (rostraler IPL), selektive Aufmerksamkeitsprozesse (rostraler und mittlerer IPL) sowie die Verarbeitung von Rechenprozessen (kaudaler IPL). In Ergänzung dazu konnte die allgemeine funktionelle Konnektivität des rostralen, mittleren und kaudalen IPL auf einer breiten Basis funktioneller Bildgebungsstudien zeigen, dass die Topographie der ko-aktivierten Gehirnregionen im Frontallappen sich umgekehrt zur Topographie innerhalb des IPL verhielt: Je weiter kaudal im IPL, desto weiter rostral im Frontallappen lagen die Netzwerkpartner der verschiedenen funktionellen Entitäten. Von rostral nach kaudal zeigte sich der IPL graduell involviert in Handlungsverarbeitung (rostral) bzw. kognitive Verarbeitung wie Aufmerksamkeits- und Sprachprozesse (kaudal).

Aus diesen Befunden konnte ein strukturell-funktionelles Organisationsmodell des IPL und seiner verbundenen Netzwerkpartner erstellt werden. Dieses Schalenmodell mit umeinander angeordneten Schalen von verbundenen Hirnregionen, die sich in einem funktionellen und strukturellen Netzwerk befinden, zeigt eine grundsätzliche Organisation und Entwicklung des IPL innerhalb des Gehirns.

Zusammenfassend konnte durch diese Arbeiten der IPL strukturell und funktionell in einem einheitlichen Modell in das Gesamtsystem Gehirn eingebettet werden, wodurch die Bedeutung dieses Assoziationsgebiets für die Funktion des Gehirns ersichtlich wird.

# V LITERATURVERZEICHNIS

Andersen RA, Asanuma C, Essick G, Siegel RM. 1990. Corticocortical connections of anatomically and physiologically defined subdivisions within the inferior parietal lobule. J Comp Neurol 296: 65-113.

Bandettini PA. 2009. What's new in neuroimaging methods? Ann N Y Acad Sci 1156: 260-293.

Batsch EG. 1956. Die myeloarchitektonische Untergliederung des Isocortex parietalis beim Menschen. J Hirnforsch 2: 225-258.

Beaulieu C, Allen PS. 1994a. Determinants of anisotropic water diffusion in nerves. Magn Reson Med 31 (4): 394-400.

Beaulieu C, Allen PS. 1994b. Water diffusion in the giant axon of the squid: implications for diffusion-weighted MRI of nervous system. Magn Reson Med 32 (5): 579-583.

Behrens TE, Johansen-Berg H, Woolrich MW, Smith SM, Wheeler-Kingshott CAM, Boulby PA, Barker GJ, Sillery EL, Sheehan K, Ciccarelli O, Thompson AJ, Brady JM, Matthews PM. 2003a. Non-invasive mapping of connections between human thalamus and cortex using diffusion imaging. Nat Neurosci 6 (7): 750-757.

Behrens TE, Woolrich MW, Jenkinson M, Johansen-Berg H, Nunes RG, Clare S, Matthews PM, Brady JM, Smith SM. 2003b. Charaterization and propagation of uncertainty in diffusion-weighted MR imaging. Magn Reson Med 50: 1077-1088.

Behrens TE, Johansen-Berg H, Jbabdi S, Rushworth MF, Woolrich MW. 2007. Probabilistic diffusion tractography with multiple fibre orientations: What can we gain? NeuroImage 34 (1): 144-155.

Brockhaus H. 1940. Die Cyto- und Myeloarchitektonik des Cortex claustralis und des Claustrum beim Menschen. J Psychol Neurol 49: 249-348.

Brodmann K. 1909. Vergleichende Lokalisationslehre der Großhirnrinde. Barth, Leipzig.

**Caspers S**, Amunts K, Zilles K. 2011a. Posterior parietal cortex: multimodal association cortex. In: The Human Nervous System, 3rd edition (Hrsg.: Mai JH, Paxinos G). Elsevier, S. 1027-1045.

**Caspers S**, Eickhoff SB, Geyer S, Scheperjans F, Mohlberg H, Zilles K, Amunts K. 2008. The human inferior parietal lobule in stereotaxic space. Brain Struct Funct 212: 481-495.

**Caspers S**, Eickhoff SB, Rick T, von Kapri A, Kuhlen T, Huang R, Shah NJ, Zilles K. 2011b. Probabilistic fibre tract analysis of cytoarchitectonically defined human inferior parietal lobule areas reveals similarities to macaques. NeuroImage 58 (2): 360-382.

**Caspers S**, Geyer S, Schleicher A, Mohlberg H, Amunts K, Zilles K. 2006. The human inferior parietal cortex: Cytoarchitectonic parcellation and interindividual variability. NeuroImage 33: 430-448.

**Caspers S**, Zilles K, Laird AR, Eickhoff SB. 2010. ALE meta-analysis of action observation and imitation in the human brain. NeuroImage 50: 1148-1167.

Catani M, Jones DK, ffytche DH. 2005. Perisylvian language networks of the human brain. Ann Neurol 57: 8-16.

Cauda F, D'Agata F, Sacco K, Duca S, Geminiani G, Vercelli A. 2011. Functional connectivity of the insula in the restino brain. NeuroImage 55 (1): 8-23.

Cavada C, Goldman-Rakic PS. 1989a. Posterior parietal cortex in rhesus monkey: I. Parcellation of areas based on distinctive limbic and sensory corticocortical connections. J Comp Neurol 287: 393-421.

Cavada C, Goldman-Rakic PS. 1989b. Posterior parietal cortex in rhesus monkey: II. Evidence of segregated corticocortical networks linking sensory and limbic areas with the frontal lobe. J Comp Neurol 287: 422-445.

Chang LJ, Yarkoni T, Khaw MW, Sanfey AG. 2012. Decoding the role of the insula in human cognition: functional parcellation and large-scale reverse inference. Cereb Cortex, in press. DOI: 10.1093/cercor/bhs065.

Cieslik EC, Zilles K, Kurth F, Eickhoff SB. 2010. Dissociating bottom-up and top-down processes in a manual stimulus-response compatibility task. J Neurophysiol 104 (3): 1472-1483.

Corbetta M, Shulman GL. 2002. Control of goal-directed and stimulus-driven attention in the brain. Nat Rev Neurosci 3 (3): 201-215.

Corbetta M, Patel G, Shulman GL. 2008. The reorienting system of the human brain: from environment to theory of mind. Neuron 58: 306-324.

Dehaene S, Piazza M, Pinel P, Cohen L. 2003. Three parietal circuits for number processing. Cogn Neuropsychol 20: 487-506.

Delazer M, Domahs F, Bartha L, Brenneis C, Lochy A, Trieb T, Benke T. 2003. Learning complex arithmetic – an fMRI study. Brain Res Cogn Brain Res 18: 76-88.

Devor A, Tian P, Nishimura N, Teng IC, Hillman EM, Narayanan SN, Ulbert I, Boas DA, Kleinfeld D, Dale AM. 2007. Suppressed neuronal activity and concurrent arteriolar vasoconstriction may explain negative blood oxygenation level-dependent signal. J Neurosci 27 (16): 4452-4459.

Eickhoff SB, Bzdok D, Laird AR, Kurth F, Fox PT. 2012. Activation likelihood estimation meta-analysis revisited. NeuroImage 59 (3): 2349-2361.

Eickhoff SB, Heim S, Zilles K, Amunts K. 2006. Testing anatomically specified hypotheses in functional imaging studies using cytoarchitectonic maps. NeuroImage 32: 570-582.

Eickhoff SB, Jbabdi S, **Caspers S**, Laird AR, Fox PT, Zilles K, Behrens TEJ. 2010. Anatomical and functional connectivity of cytoarchitectonic areas within the human parietal operculum. J Neurosci 30 (18): 6409-6421.

Eickhoff SB, Laird AR, Grefkes C, Wang LE, Zilles K, Fox PT. 2009. Coordinate-based activation likelihood estimation meta-analysis of neuroimaging data: a random-effects approach based on empirical estimates of spatial uncertainty. Hum Brain Mapp 30 (9): 2907-2926.

Eickhoff SB, Pomjanski W, Jakobs O, Zilles K, Langner R. 2011. Neural correlates of developing and adapting behavioral biases in speeded choice reactions – an fMRI study on predictive motor coding. Cereb Cortex 21 (5): 1178-1191.

Felleman DJ, van Essen DC. 1991. Distributed hierarchical processing in the primate cerebral cortex. Cereb Cortex 1: 1-47.

Fink GR, Marshall JC, Weiss PH, Zilles K. 2001. The neural basis of vertical and horizontal line bisection judgments: an fMRI study of normal volunteers. NeuroImage 14: 59-67.

Fischl B, Rajendran N, Busa E, Augustinack J, Hinds O, Yeo BT, Mohlberg H, Amunts K, Zilles K. 2008. Cortical folding patterns and predicting cytoarchitecture. Cereb Cortex 18 (8): 1973-1980.

Fogassi L, Ferrari PF, Gesierich B, Rozzi S, Chersi F, Rizzolatti G. 2005. Parietal lobe: from action organization to intentino understanding. Science 308: 662-667.

Gallese V, Fadiga L, Fogassi L, Rizzolatti G. 1996. Action recognition in the premotor cortex. Brain 119 (Pt 2): 593-609.

Gerhardt E. 1940. Die Cytoarchitektonik des Isocortex parietalis beim Menschen. J Psychol Neurol 49: 367-419.

Gernsbacher MA, Kaschak MP. 2003. Neuroimaging studies of language production and comprehension. Annu Rev Psychol 54: 91-114.

Geschwind N. 1970. The organization of language and the brain. Science 170: 940-944.

Grabner RH, Ansari D, Reishofer G, Stern E, Ebner F, Neuper C. 2007. Individual differences in mathematical competence predict parietal brain activation during mental calculation. NeuroImage 38: 346-356.

Greene JD, Nystrom LE, Engell AD, Darley JM, Cohen JD. 2004. The neural bases of cognitive conflict and control in moral judgment. Neuron 44: 389-400.

Gregoriou GG, Borra E, Matelli M, Luppino G. 2006. Architectonic organization of the inferior parietal convexity of the macaque monkey. J Comp Neurol 496 (3): 422-451.

Gusnard DA, Raichle ME. 2001. Searching for a baseline: functional imaging and the resting human brain. Nat Rev Neurosci 2 (10): 685-694.

Heim S, Amunts K, Drai D, Eickhoff SB, Hautvast S, Grodzinsky Y. 2012. The language-number interface in the brain: a complex parametric study of quantifiers and quantities. Front Evol Neurosci 4: 4.

Hyvärinen J. 1982. Posterior parietal lobe of the primate brain. Physiol Rev 62: 1060-1129.

Iacoboni M. 2005. Neural mechanisms of imitation. Curr Opin Neurobiol 15: 632-637.

Iacoboni M. 2009. Imitation, empathy, and mirror neurons. Annu Rev Psychol 60: 653-670.

Iacoboni M, Dapretto M. 2006. The mirror neuron system and the consequences of its dysfunction. Nat Rev Neurosci 7: 942-951.

Ischebeck A, Zamarian L, Egger K, Schocke M, Delazer M. 2007. Imaging early practice effects in arithmetic. NeuroImage 36: 993-1003.

Jakobs O, Langner R, **Caspers S**, Roski C, Cieslik EC, Zilles K, Laird AR, Fox PT, Eickhoff SB. 2012. Across-study and within-subject functional connectivity of a right temporo-parietal junction subregion involved in stimulus-context integration. NeuroImage 60: 2389-2398.

Jakobs O, Wang LE, Dafotakis M, Grefkes C, Zilles K, Eickhoff SB. 2009. Effects of timing and movement uncertainty implicate the temporo-parietal junction in the prediction of forthcoming motor actions. NeuroImage 47 (2): 667-677.

Keysers C, Gazzola V. 2009. Expanding the mirror: vicarious activity for actions, emotions, and sensations. Curr Opin Neurobiol 19: 666-671.

Krueger F, Spampinato MV, Pardini M, Pajevic S, Wood NJ, Weiss GH, Landgraf S, Grafman J. 2008. Integral calculus problem solving: an fMRI investigation. Neuroreport 19: 1095-1099.

Kurth F, Zilles K, Fox PT, Laird AR, Eickhoff SB. 2010. A link between the systems: functional differentiation and integration within the human insula revealed by meta-analysis. Brain Struct Funct 214 (5-6): 519-534.

Laird AR, Eickhoff SB, Kurth F, Fox PM, Uecker AM, Turner JA, Robinson JL, Lancaster JL, Fox PT. 2009. ALE meta-analysis workflows via the Brainmap database: progress towards a probabilistic functional brain atlas. Front Neuroinform 3: 23.

Laird AR, Lancaster JL, Fox PT. 2005. BrainMap: the social evolution of a human brain mapping database. Neuroinformatics 3 (1): 65-78.

Le Bihan D. 2003. Looking into the functional architecture of the brain with diffusion MRI. Nat Rev Neurosci 4: 469-480.

Le Bihan D, Turner R, Douek P. 1993. Is water diffusion restricted in human brain white matter? An echo-planar NMR imaging study. Neuroreport 4 (7): 887-890.

Logothetis NK. 2008. What we can do and what we cannot do with fMRI. Nature 453 (7197): 869-878.

Makris N, Kennedy DN, McInerney S, Sorensen AG, Wang R, Caviness Jr VS, Pandya DN. 2005. Segmentation of subcomponents within the superior longitudinal fascicle in humans: a quantitative, in vivo, DT-MRI study. Cereb Cortex 15 (6): 854-869.

Mars RB, Jbabdi S, Sallet J, O'Reilly JX, Croxson PL, Olivier E, Noonan MP, Bergmann C, Mitchell AS, Baxter MG, Behrens TEJ. 2011. Diffusion-weighted imaging tractography-based parcellation of the human parietal cortex and comparison with human and macaque resting-state functional connectivity. J Neurosci 31 (11): 4087-4100.

Moll J, Oliveira-Souza R, Bramati IE, Grafman J. 2002. Functional networks in emotional moral and nonmoral social judgments. NeuroImage 16: 696-703.

Moseley ME, Cohen Y, Kucharczyk J, Mintorovitch J, Asgari HS, Wendland MF, Tsurunda J, Norman D. 1990. Diffusion-weighted MR imaging of anisotropic water diffusion in cat central nervous system. Radiology 176 (2): 439-445.

Moseley ME, Kucharczyk J, Asgari HS, Norman D. 1991. Anisotropy in diffusion-weighted MRI. Magn Reson Med 19 (2): 321-326.

Mountcastle VB, Lynch JC, Georgopoulos A, Sakata H, Acuna C. 1975. Posterior parietal association cortex of the monkey: command functions for operations within extrapersonal space. J Neurophysiol 38: 871-908.

Neal JW, Pearson RCA, Powell TPS. 1990a. The ipsilateral cortico-cortical connections of area 7b, PF, in the parietal and temporal lobes of the monkey. Brain Res 524: 119-132.

Neal JW, Pearson RCA, Powell TPS. 1990b. The connections of area PG, 7a, with cortex in the parietal, occipital, and temporal lobes of the monkey. Brain Res 532: 249-264.

Ono M, Kubik S, Abernathey CD. 1990. Atlas of the Cerebral Sulci. Thieme, Stuttgart / New York.

Pandya DN, Seltzer B. 1982. Intrinsic connections and architectonics of posterior parietal cortex in the rhesus monkey. J Comp Neurol 204: 196-210.

Peters JC, Reithler J, Goebel R. 2012. Modelling invariant object processing based on tight integration of simulated and empirical data in a common brain space. Front Comput Neurosci 6:12.

Pierpaoli C, Basser PJ. 1996. Toward a quantitative assessment of diffusion anisotropy. Magn Reson Med 36 (6): 893-906.

Plaut DC, Behrmann M. 2011. Complementary neural representations for faces and words: a computational exploration. Cogn Neuropsychol 28 (3-4): 251-275.

Poldrack RA. 2006. Can cognitive processes be inferred from neuroimaging data? Trends Cogn Sci 10 (2): 59-63.

Price CJ. 2000. The anatomy of language: contributions from functional neuroimaging. J Anat 197: 335-359.

Rademacher J, Caviness J, Steinmetz H, Galaburda AM. 1993. Topographical variation of the human primary cortices: implications for neuroimaging, brain mapping, and neurobiology. Cereb Cortex 3 (4): 313-319.

Raichle ME, MacLeod AM, Snyder AZ, Powers WJ, Gusnard DA, Shulman GL. 2001. A default mode of brain function. Proc Natl Acad Sci U S A 98 (2): 676-682.

Raine A, Yang Y. 2006. Neural foundations to moral reasoning and antisocial behavior. SCAN 1, 203-213.

Rizzolatti G, Craighero L. 2004. The mirror-neuron system. Annu Rev Neurosci 27: 169-192.

Rozzi S, Calzavara R, Belmalih A, Borra E, Gregoriou GG, Matelli M, Luppino G. 2006. Cortical connections of the inferior parietal cortical convexity of the macaque monkey. Cereb Cortex 16 (10): 1389-1417.

Rozzi S, Ferrari PF, Bonini L, Rizzolatti G, Fogassi L. 2008. Functional organization of inferior parietal lobule convexity in the macaque monkey: electrophysiological characterization of motor, sensory and mirror responses and their correlation with cytoarchitectonic areas. Eur J Neurosci 28 (8): 1569-1588.

Rushworth MFS, Behrens TEJ, Johansen-Berg H. 2006. Connection patterns distinguish 3 regions of human parietal cortex. Cereb Cortex 16: 1418-1430.

Sanides F. 1964. The cyto-myeloarchitecture of the human frontal lobe and its relation of phylogenetic differentiation of the cerebral cortex. J Hirnforsch 6: 269-282.

Sarkissov SA, Filimonoff IN, Preobrashenskaya NS. 1949. Cytoarchitecture of the human cortex cerebri (russ.). Medgiz, Moskau.

Saur D, Kreher BW, Schnell S, Kümmerer D, Kellmeyer P, Vry MS, Umarova R, Musso M, Glauche V, Abel S, Huber W, Rijntjes M, Hennig J, Weiller C. 2008. Ventral and dorsal pathways for language. Proc Natl Acad Sci U S A 105 (46): 18035-18040.

Schleicher A, Amunts K, Geyer S, Morosan P, Zilles K. 1999. Oberver-independent method for microstrutural parcellation of cerebral cortex: A quantitative approach to cytoarchitectonics. NeuroImage 9: 165-177.

Schleicher A, Palomero-Gallagher N, Morosan P, Eickhoff SB, Kowalski T, de Vos K, Amunts K, Zilles K. 2005. Quantitative architectural analysis: a new approach to cortical mapping. Anat. Embryol 210 (5-6): 373-386.

Seeley WW, Menon V, Schatzberg AF, Keller J, Glover GH, Kenna H, Reiss AL, Greicius MD. 2007. Dissociable intrinsic connectivity networks for salience processing and executive control. J Neurosci 27: 2349-2356.

Seltzer B, Pandya DN. 1984. Further observations on parieto-temporal connections in the rhesus monkey. Exp Brain Res 55: 301-312

Shalom DB, Poeppel D. 2008. Functional anatomic models of language: assembling the pieces. Neuroscientist 14 (1): 119-127.

Tanner JE, Stejskal EO. 1968. Restricted self-diffusion of protons in colloidal systems by the pulsed-gradient, spin-echo method. J Chem Phys 49 (4): 1768-1777.

Turkeltaub PE, Eickhoff SB, Laird AR, Fox M, Wiener M, Fox P. 2012. Minimizing within-experiment and within-group effects in Activation Likelihood Estimation meta-analyses. Hum Brain Mapp 33 (1): 1-13.

Vigneau M, Beaucousin V, Hervé PY, Duffau H, Crivello F, Houdé O, Mazoyer B, Tzourio-Mazoyer N. 2006. Meta-analyzing left hemisphere language areas: phonology, semantics, and sentence processing. NeuroImage 30: 1414-1432.

Vogt C, Vogt O. 1919. Allgemeinere Ergebnisse unserer Hirnforschung. J Psychol Neurol 25: 279-461.

Vogt O. 1910. Die myeloarchitektonische Felderung des menschlichen Stirnhirns. J Psychol Neurol 15: 221-232.

Vogt O. 1911. Die Myeloarchitektonik des Isocortex parietalis. J Psychol Neurol 18: 107-118.

von Economo K, Koskinas G. 1925. Die Cytoarchitektonik der Hirnrinde des erwachsenen Menschen. Springer, Wien.

Wagatsuma N, Potjans TC, Diesmann M, Fukai T. 2011. Layer-dependent attentional processing by top-down signals in a visual cortical microcircuit model. Front Comput Neurosci 5: 31.

Wu SS, Chang TT, Majid A, **Caspers S**, Eickhoff SB, Menon V. 2009. Functional heterogeneity of inferior parietal cortex during mathematical cognition assessed with cytoarchitectonic probability maps. Cereb Cortex 19: 2930-2945.

Yeo BT, Krienen FM, Sepulcre J, Sabuncu MR, Lashkari D, Hollinshead M, Roffman JL, Smoller JW, Zollei L, Polimeni JR, Fischl B, Liu H, Buckner RL. 2011. The organization of the human cerebral cortex estimated by intrinsic functional connectivity. J Neurophysiol 106: 1125-1165.

Zilles K, Amunts K. 2009. Receptor mapping: architecture of the human cerebral cortex. Curr Opin Neurol 22 (4): 331-339.

Zilles K, Amunts K. 2010. Centenary of Brodmann's map – conception and fate. Nat Rev Neurosci 11 (2): 139-145.

Zilles K, Amunts K. 2012. Segregation and wiring in the brain. Science 335: 1582-1584.

Zilles K, Armstrong E, Schleicher A, Kretschmann HJ. 1988. The human pattern of gyrification in the cerebral cortex. Anat Embryol 179 (2): 173-179.

Zilles K, Palomero-Gallagher N, Schleicher A. 2004. Transmitter receptors and functional anatomy of the cerebral cortex. J Anat 205: 417-432.

Zilles K, Schleicher A, Palomero-Gallagher N, Amunts K. 2002. Quantitative analysis of cyto- and receptorarchitecture of the human brain. In: Brain Mapping: The Methods, 2nd edition (Hrsg.: Toga AW, Mazziotta JC). Academic Press, San Diego. S. 573-602.

# VI DANKSAGUNG

Auf dem Weg zu dieser Habilitation habe ich vielseitige Unterstützung erfahren.

Mein besonders herzlicher Dank gilt meinem langjährigen wissenschaftlichen Lehrer und Mentor, Herrn Universitätsprofessor Dr. med. Dr. h. c. Karl Zilles. In den vielen Jahren der Zusammenarbeit in den von ihm geleiteten Instituten C. und O. Vogt Institut für Hirnforschung der Universität Düsseldorf und dem Institut für Neurowissenschaften und Medizin (INM-2) des Forschungszentrum Jülich hat er mir ermöglicht, meinen Weg in der Wissenschaft zu finden und zu festigen. Seine Begeisterung für die Forschung und sein umfangreiches Wissen, auch über neurowissenschaftliche Fragestellungen hinaus, haben mir in vielen Diskussionen immer wieder neue Wege und Möglichkeiten für meine eigene Forschung aufgezeigt. Für seine vielfältige und sehr auf die verschiedenen Abschnitte meiner wissenschaftlichen Laufbahn zugeschnittene Unterstützung bin ich ihm zu großem Dank verpflichtet.

Ebenfalls sehr herzlich danken möchte ich Frau Universitätsprofessorin Dr. med. Katrin Amunts. In der über die Jahre immer intensiveren Zusammenarbeit im Institut für Neurowissenschaften und Medizin, Forschungszentrum Jülich, hat sie mich stets uneingeschränkt unterstützt und mir durch ihr großes, in mich gesetztes Vertrauen die Möglichkeit gegeben, mich selbständig zu entwickeln und an den Aufgaben zu wachsen. Durch ihre stets freundliche und offene Art und ihre Leidenschaft für die wissenschaftliche Arbeit konnte sie mich immer wieder ermutigen, den für mich richtigen Weg zu gehen.

Darüber hinaus möchte ich mich bei allen Kollegen, nicht nur der eigenen Arbeitsgruppe, sondern auch in den vielen anderen Arbeitsgruppen und Institutsbereichen im Forschungszentrum Jülich bedanken. In einem offenen und durch gegenseitiges Interesse geprägten Arbeitsumfeld war es jederzeit möglich, auch interdisziplinäre Fragestellungen zielgerichtet zu besprechen.

Mein größter und zutiefst empfundener Dank gilt meinen Eltern Frau Monika Caspers und Herrn Prof. h. c. Dr. h. c. Dr. med. Hans-Peter Caspers. Ihre in allen Phasen meines Lebens konstant liebevolle und unermüdliche Unterstützung, nicht zuletzt während der Entstehung dieser Habilitation, ist für mich von unermesslichem Wert. Ihnen, meinem Bruder Julian, mit dem ich meine Leidenschaft für die Neurowissenschaften teile und viele sehr bereichernde und anregende Gespräche genießen durfte, sowie meinen Großeltern bin ich für ihren bedingungslosen Rückhalt unendlich dankbar.

# VII LEBENSLAUF

| | |
|---|---|
| Name: | Dr. med. Dr. rer. pol. Svenja Inga Verena Caspers |
| Geburtstag/-ort: | 16.09.1982 in Krefeld |
| Familienstand: | ledig |
| Staatsangehörigkeit: | deutsch |

## Beruflicher Werdegang:

| | |
|---|---|
| 02/2008 – heute | Wissenschaftliche Mitarbeiterin, Institut für Neurowissenschaften und Medizin, INM-2, Forschungszentrum Jülich |
| 10/2011 – 11/2011 | Lehrauftrag Anatomie, Heinrich-Heine-Universität Düsseldorf |
| 05/2011 – 07/2011 | Lehrauftrag Neuroanatomie, Heinrich-Heine-Universität Düsseldorf |
| 11/2010 – 02/2011 | Lehrauftrag Anatomie, Heinrich-Heine-Universität Düsseldorf |
| 10/2008 – 11/2008 | Lehrauftrag Anatomie, Heinrich-Heine-Universität Düsseldorf |

## Weitere Tätigkeiten:

| | |
|---|---|
| 05/2009 – heute | Mitglied des Wissenschaftlich-Technischen Rates, Forschungszentrum Jülich |

## Hochschulausbildung:

| | |
|---|---|
| 02/2012 | Promotion Betriebswirtschaftslehre (Dr. rer. pol.), *„magna cum laude“* Institut für Wirtschafts- und Sozialpsychologie, Wirtschafts- und Sozialwissenschaftliche Fakultät, Universität zu Köln, *Thema:* „Kognitive Verarbeitung wertbasierter Entscheidungen bei Führungskräften – eine neuropsychoökonomische Studie“ |
| 11/2008 | Promotion Medizin (Dr. med.), *“summa cum laude”*“ C. &. O. Vogt Institut für Hirnforschung, Heinrich-Heine-Universität Düsseldorf, *Thema*: “Zytoarchitektonische und rezeptorautoradiographische Kartierung des inferioren Parietallappens des Menschen”, *Veröffentlichung Zusammenfassung in:* „Medizin – summa cum laude 2008“, Roter Fleck Verlag, Darmstadt, S. 56-57 (2009). |
| 12/2007 | Ärztliche Approbation |
| 12/2007 | Staatsexamen Medizin, *Note “sehr gut”* |
| 10/2007 | Diplom Betriebswirtschaftslehre, *Note 2,9* |
| 09/2008 | Diplom Volkswirtschaftslehre, *Note 2,7* |
| 10/2001 – 09/2007 | Studium der Humanmedizin, Heinrich-Heine-Universität Düsseldorf |

| | |
|---|---|
| 04/2003 – 09/2007 | Studium der Betriebswirtschaftslehre, FernUniversität in Hagen |
| 04/2003 – 09/2008 | Studium der Volkswirtschaftslehre, FernUniversität in Hagen |
| 06/2001 | Abitur, *Note: 1,0*, Erasmus-von-Rotterdam-Gymnasium Viersen |

## Auszeichnungen

| | |
|---|---|
| 2010 | Promotionspreis der medizinischen Fakultät der Heinrich-Heine-Universität Düsseldorf, "Beste Dissertation des Jahres 2009" |
| 2009 | Posterpreis der "Faculty of 1000"<br>Kongress: „Annual Meeting of the Society for Neuroscience 2009"<br>*Videodreh am Poster und Veröffentlichung unter:*<br>http://www.youtube.com/user/Facultyof1000#p/a/u/0/9zrVNl62ysw (Teil 1)<br>http://www.youtube.com/watch?v=VVIQ_T0eCVU&feature=related (Teil 2)<br>*Bewertung durch die „Faculty of 1000":* Faculty of 1000 Medicine: evaluations for Caspers S et al. Neuroscience 2009 Conference, 2009 Oct 17-21: 260.9, http://f1000medicine.com/article/id/1556024/evaluation |
| 2001 | "Bester Chemie-Abiturient", Unternehmerschaft Chemie Niederrhein, Erasmus-von-Rotterdam-Gymnasium, Viersen |

## Stipendien:

| | |
|---|---|
| 08/2011 – 04/2013 | Trainee der Helmholtz-Akademie für Führungskräfte |
| 2009-2010 | Mentee Mentoring-Programm „In Führung gehen", Helmholtz-Gemeinschaft |
| 2009 | JARA Seed Fund zur Forschungsförderung, Exzellenzinitiative RWTH Aachen |
| 2008 | ESP-Stipendium National Institute of Health Sciences, Niederlande |
| 2005, 2007 | Trainee Abstract Award, Organization for Human Brain Mapping (OHBM) |

## Review-Tätigkeit für wissenschaftliche Journale

Annals of the New York Academy of Sciences, Brain Imaging and Behavior, Brain Research Bulletin, Brain Structure and Function, Cortex, Frontiers in Integrative Neuroscience, Human Brain Mapping, Journal of Magnetic Resonance Imaging, Journal of Neurophysiology, Journal of Neuroscience, Journal of Neuroscience Methods, NeuroImage, Neuroinformatics, Neuroscience and Biobehavioural Reviews, Neuroscience Letters, Neuroscientist, PLoS One, Recent Patents on Signal Processing

# VIII PUBLIKATIONEN

## Originalarbeiten

**Caspers S**, Heim S, Lucas MG, Stephan E, Fischer L, Amunts K, Zilles K
Dissociated neural processing for decisions in managers and non-managers.
***PLoS One**, im Druck (2012)*

**Caspers S**, Schleicher A, Bacha-Trams M, Palomero-Gallagher N, Amunts K, Zilles K
Organization of the human inferior parietal lobule based on receptor architectonics.
***Cereb Cortex***, im Druck (2012)

Cieslik EC, Zilles K, **Caspers S**, Roski C, Kellermann TS, Jakobs O, Langner R, Laird AR, Fox PT, Eickhoff SB. Is there “one” DLPFC in cognitive action control? Evidence for heterogeneity from co-activation-based parcellation.
***Cereb Cortex***, im Druck (2012)

Jakobs O, Langner R, **Caspers S**, Roski C, Cieslik EC, Zilles K, Fox PT, Eickhoff SB
Across-study and within-subject functional connectivity of a right temporo-parietal junction subregion.
***NeuroImage*** 60 (4): 2389-2398 (2012)

zu Eulenburg P, **Caspers S**, Roski C, Eickhoff SB
Meta-analytic definition and functional connectivity of the human vestibular cortex.
***NeuroImage*** 60 (1): 162-169 (2012)

**Caspers S**, Eickhoff SB, Rick T, von Kapri A, Kuhlen T, Huang R, Shah NJ, Zilles K
Probabilistic fibre tract analysis of cytoarchitectonically defined human inferior parietal lobule areas reveals similarities to macaques.
***NeuroImage*** 58 (2): 362-380 (2011)

Eickhoff SB, Bzdok D, Laird AR, Roski C, **Caspers S**, Zilles K, Fox PT
Co-activation patterns distinguish cortical modules, their connectivity and functional differentiation.
***NeuroImage*** 57 (3): 938-949 (2011)

**Caspers S**, Heim S, Lucas MG, Stephan E, Fischer L, Amunts K, Zilles K
Moral concepts set decision strategies to abstract values.
***PLoS One*** 6 (4): e18451 (2011)

Rick T, von Kapri A, **Caspers S**, Amunts K, Zilles K, Kuhlen T
Visualization of probabilistic fiber tracts in virtual reality.
***Stud Health Technol Inform*** 163: 486-492 (2011)

Bzdok D, Langner R, **Caspers S**, Kurth F, Habel U, Zilles K, Laird AR, Eickhoff SB
ALE meta-analysis on facial judgements of trustworthiness and attractiveness.
***Brain Struct Funct*** 215 (3-4): 209-233 (2011)

**Caspers S**, Zilles K, Laird AR, Eickhoff SB
ALE meta-analysis of action observation and imitation in the human brain.
***NeuroImage*** 50 (3): 1148-1167 (2010)

Eickhoff SB, Jbabdi S, **Caspers S**, Laird AR, Fox PT, Zilles K, Behrens TEJ
Anatomical and functional connectivity of cytoarchitectonic areas within the human secondary somatosensory cortex.
***J Neurosci*** 30 (18): 6409-6421 (2010)

von Kapri A, Rick T, **Caspers S**, Eickhoff SB, Zilles K, Kuhlen T
Evaluating a visualization of uncertainty in probabilistic tractography.
***Proceedings of SPIE – The International Society for Optical Engineering*** 7625: 762534 (2009)

Wu SS, Chang TT, Majid A, **Caspers S**, Eickhoff SB, Menon V
Functional heterogeneity of inferior parietal cortex during mathematical cognition assessed with cytoarchitectonic probability maps.
***Cereb Cortex*** 19 (12): 2930-2945 (2009)

**Caspers S**, Eickhoff SB, Geyer S, Scheperjans F, Mohlberg H, Zilles K, Amunts K
The human inferior parietal lobule in stereotaxic space.
***Brain Struct Funct*** 212 (3-4): 481-495 (2008)

Eickhoff SB, Paus T, **Caspers S**, Grosbras MH, Evans AC, Zilles K, Amunts K
Assignment of functional activations to probabilistic cytoarchitectonic areas revisited.
***NeuroImage*** 36 (3): 511-521 (2007)

**Caspers S**, Geyer S, Schleicher A, Mohlberg H, Amunts K, Zilles K
The human inferior parietal cortex: cytoarchitectonic parcellation and interindividual variability.
***NeuroImage*** 33 (2): 430-448 (2006)

## Buchkapitel

Eickhoff SB, Rottschy C, **Caspers S**
Ein Tool zur integrierten Analyse von Struktur, Funktion und Konnektivität: Die SPM Anatomy Toolbox.
In: Funktionelle MRT in Psychiatrie und Neurologie, 2. Auflage (Hrsg.: Schneider F, Fink GR). Springer, im Druck (2012)

**Caspers S**, Amunts K, Zilles K
Posterior parietal cortex: Multimodal association cortex.
In: The Human Nervous System, 3rd edition (Hrsg.: Mai JH, Paxinos G). Elsevier, S. 1027-1045 (2011)

# IX ORIGINALARBEITEN ALS GRUNDLAGE DER KUMULATIVEN HABILITATIONSSCHRIFT

Im Folgenden sind sieben Originalarbeiten als Sonderdrucke angefügt, die in einem engen inhaltlichen Zusammenhang stehen und dieser kumulativen Habilitationsschrift zugrunde liegen.

1. **Caspers S**, Eickhoff SB, Rick T, von Kapri A, Kuhlen T, Huang R, Shah NJ, Zilles K
   Probabilistic fibre tract analysis of cytoarchitectonically defined human inferior parietal lobule areas reveals similarities to macaques.
   *NeuroImage* 58 (2): 362-380 (2011)
2. Eickhoff SB, Jbabdi S, **Caspers S**, Laird AR, Fox PT, Zilles K, Behrens TEJ
   Anatomical and functional connectivity of cytoarchitectonic areas within the human secondary somatosensory cortex.
   *J Neurosci* 30 (18): 6409-6421 (2010)
3. **Caspers S**, Schleicher A, Bacha-Trams M, Palomero-Gallagher N, Amunts K, Zilles K
   Organization of the human inferior parietal lobule based on receptor architectonics.
   *Cereb Cortex*, im Druck (2012)
4. **Caspers S**, Zilles K, Laird AR, Eickhoff SB
   ALE meta-analysis of action observation and imitation in the human brain.
   *NeuroImage* 50 (3): 1148-1167 (2010)
5. **Caspers S**, Heim S, Lucas MG, Stephan E, Fischer L, Amunts K, Zilles K
   Moral concepts set decision strategies to abstract values.
   *PLoS One* 6 (4): e18451 (2011)
6. Jakobs O, Langner R, **Caspers S**, Roski C, Cieslik EC, Zilles K, Fox PT, Eickhoff SB
   Across-study and within-subject functional connectivity of a right temporo-parietal junction subregion.
   *NeuroImage* 60 (4): 2389-2398 (2012)
7. Wu SS, Chang TT, Majid A, **Caspers S**, Eickhoff SB, Menon V
   Functional heterogeneity of inferior parietal cortex during mathematical cognition assessed with cytoarchitectonic probability maps.
   *Cereb Cortex* 19 (12): 2930-2945 (2009)

NeuroImage 58 (2011) 362–380

Contents lists available at ScienceDirect

NeuroImage

journal homepage: www.elsevier.com/locate/ynimg

# Probabilistic fibre tract analysis of cytoarchitectonically defined human inferior parietal lobule areas reveals similarities to macaques

Svenja Caspers [a,*,1], Simon B. Eickhoff [a,b,c,1], Tobias Rick [b,d], Anette von Kapri [b,d], Torsten Kuhlen [b,d], Ruiwang Huang [e], Nadim J. Shah [a,b,f], Karl Zilles [a,b,g]

[a] Institute of Neuroscience and Medicine (INM-2, INM-4), Research Centre Jülich, 52425 Jülich, Germany
[b] Jülich-Aachen Research Alliance (JARA-BRAIN, JARA-HPC), 52425 Jülich, Germany
[c] Department of Psychiatry, Psychotherapy and Psychosomatics, RWTH Aachen University, 52074 Aachen, Germany
[d] Institute for Scientific Computing, Virtual Reality Group, RWTH Aachen University, 52074 Aachen, Germany
[e] Center for the Study of Applied Psychology and Imaging Center for Brain Research, South China Normal University, Guangzhou 510631, PR China
[f] Department of Neurology, RWTH Aachen University, 52074 Aachen, Germany
[g] C. and O. Vogt Institute for Brain Research, Heinrich-Heine-University Düsseldorf, 40001 Düsseldorf, Germany

ARTICLE INFO

*Article history:*
Received 18 April 2011
Revised 7 June 2011
Accepted 9 June 2011
Available online 21 June 2011

*Keywords:*
Diffusion tensor imaging
DTI
Probabilistic tractography
Inferior parietal
Fibre tract
Cytoarchitecture

ABSTRACT

The human inferior parietal lobule (IPL) is a multimodal brain region, subdivided in several cytoarchitectonic areas which are involved in neural networks related to spatial attention, language, and higher motor processing. Tracer studies in macaques revealed differential connectivity patterns of IPL areas as the respective structural basis. Evidence for comparable differential fibre tracts of human IPL is lacking. Here, anatomical connectivity of five cytoarchitectonic human IPL areas to 64 cortical targets was investigated using probabilistic tractography. Connection likelihood was assessed by evaluating the number of traces between seed and target against the distribution of traces from that seed to voxels in the same distance as the target. The main fibre tract pattern shifted gradually from rostral to caudal IPL: Rostral areas were predominantly connected to somatosensory and superior parietal areas while caudal areas more strongly connected with auditory, anterior temporal and higher visual cortices. All IPL areas were strongly connected with inferior frontal, insular and posterior temporal areas. These results showed striking similarities with connectivity patterns in macaques, providing further evidence for possible homologies between these two species. This shift in fibre tract pattern supports a differential functional involvement of rostral (higher motor functions) and caudal IPL (spatial attention), with probable overlapping language involvement. The differential functional involvement of IPL areas was further supported by hemispheric asymmetries of connection patterns which showed left–right differences especially with regard to connections to sensorimotor, inferior frontal and temporal areas.



## Introduction

The human inferior parietal lobule (IPL) is a heterogeneous, multimodal brain region as demonstrated by functional neuroimaging and lesion mapping studies. Thus, different parts of human IPL seem to be involved in different functional brain networks, where they interact with different other cortical regions within frontal, occipital, and temporal lobe.

Rostral IPL areas bilaterally seem to be involved in higher motor functions, potentially including parts of a human mirror neuron system (Rizzolatti and Craighero, 2004; Iacoboni, 2005; Keysers and Gazzola, 2009; Caspers et al., 2010). The caudal IPL, in contrast, was shown to feature hemisphere-specific functionality. The right IPL is recruited during spatial and non-spatial attention and motor preparation tasks and conceptualised as part of the "ventral attention network" (Fink et al., 2001; Corbetta and Shulman, 2002; Corbetta et al., 2008; Jakobs et al., 2009). Contrastingly, its left counter-part is thought to form Geschwind's area in the language network, being mainly involved in semantic and phonological processing (Geschwind, 1970; Price, 2000; Gernsbacher and Kaschak, 2003; Vigneau et al., 2006).

In macaque monkeys, electrophysiological recordings have shown evidence of a comparable functional segregation of the IPL as in humans (apart from language processing). Rostral IPL areas in this species have been shown to contain mirror neurons and participate in sensorimotor processing, whereas caudal areas are mainly involved in functions such as spatial attention, auditory-sensory integration, and visuo-motor coordination, e.g., grasping (Hyvärinen, 1982; Pandya and Seltzer, 1982; Seltzer and Pandya, 1984; Rozzi et al., 2006).

* Corresponding author at: Institute of Neuroscience and Medicine, INM-2, Research Center Jülich 52425 Jülich, Germany. Fax: +49 2461 612990.
*E-mail address:* s.caspers@fz-juelich.de (S. Caspers).
[1] These authors contributed equally to the present study.

1053-8119/$ – see front matter © 2011 Elsevier Inc. All rights reserved.
doi:10.1016/j.neuroimage.2011.06.027

In both species, this functional heterogeneity is reflected on a cytoarchitectonic level. In humans, a recent study delineated seven cytoarchitectonically distinct areas within the IPL (Caspers et al., 2006, 2008). Five of these cover the lateral surface of the IPL in a rostro-caudal sequence (Fig. 1A). The remaining two are located in the Sylvian fissure. Comparably, the macaque IPL has been reported to consist of six main areas (Pandya and Seltzer, 1982; Gregoriou et al., 2006). Of these, four are located on the lateral surface in a rostro-caudal sequence (Fig. 1B), the other two in the Sylvian fissure.

Tracer studies of axonal connectivity in macaques have provided a potential link between structural heterogeneity and functional diversity of the IPL by revealing a differentiated connectivity pattern of the cortical areas in this region. Rostral areas (PF, PFG) show strong reciprocal connections to (pre-) motor, somatosensory and superior parietal areas. In contrast, caudal areas are mainly connected to higher visual areas within occipital and inferior temporal cortex (Cavada and Goldman-Rakic, 1989a,b; Felleman and Van Essen, 1991; Gregoriou et al., 2006).

In humans, the anatomical connectivity of individual IPL areas is largely unknown, although macroanatomical fibre preparations and studies on disconnection syndromes such as apraxia (Freund, 2003; Culham and Valyear, 2006), spatial neglect (Karnath, 2001; Hillis, 2006; Husain and Nachev, 2007) or aphasia (Dronkers et al., 2004) support the idea of a similar connection pattern for humans as in macaques. Diffusion tensor imaging (DTI) studies in healthy humans were indeed able to show partly different connectivity of different aspects of the IPL. Makris et al. (2005) found a partition of one of the two main fibre pathways connecting the IPL with mainly frontal regions, i.e. the superior longitudinal fascicle (SLF) which they could subdivide into four distinct parts, two of which running into the rostral and caudal aspect of the IPL, respectively. Catani et al. (2005) found a comparable partition for the other main pathway, i.e. the arcuate fascicle. They demonstrated that different parts of the arcuate fascicle reach either the rostral or the caudal aspect of the IPL, comparable to the SLF as reported by Makris et al. (2005). Focusing on a possible subdivision of the parietal cortex by means of connectivity based parcellation, Rushworth et al. (2006) showed that rostral IPL is more likely to connect to ventral premotor cortex whereas caudal IPL was more likely to connect with the parahippocampal gyrus. A recent study by Mars et al. (2011) used connectivity-based parcellation of the IPL, resulting in a comparable subdivision of this region as found by cytoarchitectonic parcellation (Caspers et al., 2006, 2008). Consecutive resting-state functional connectivity analyses showed how the IPL areas were differentially connected to premotor, prefrontal and parahippocampal areas (Mars et al., 2011). These studies provide first hints that the fibre tract pattern of human IPL is different in its many parts, at least in rostral and caudal IPL.

But it can be assumed that the functional and cytoarchitectonic heterogeneity of the IPL is also reflected by a more differentiated fibre tract pattern than a bipartition. In order to provide a precise identification of areal-specific fibre tract pattern as structural basis for the involvement in different functional networks, we assessed the fibre tracts related to five cytoarchitectonic areas of the lateral IPL using probabilistic tractography based on DTI data.

## Material and methods

### *Data acquisition*

We acquired diffusion-weighted data from 40 healthy, right-handed human subjects (20 males, mean age ± SD = 28.65 ± 5.73, range 21–42; 20 females, mean age ± SD = 28.75 ± 6.20, range 21–42) on a 3.0 T Tim-Trio Siemens whole-body scanner (Siemens, Erlangen, Germany) with a maximum gradient strength of 40 mT $m^{-1}$, using a 12-channel phased-array head coil for signal reception. Subjects had no history of neurological or psychiatric disease, or head injury. All subjects gave informed, written consent to participate in the study which was approved by the local Ethics Committee of the RWTH Aachen University.

Diffusion-weighted images were acquired using a twice-refocused spin-echo sequence (axial slices, slice thickness: 1.8 mm, number of slices: 75, matrix = 128 × 128, field of view = 230 × 230 $mm^2$, bandwidth = 1502 Hz/pixel, reconstruction using an iPAT GRAPPA-scheme, final voxel resolution of 1.8 × 1.8 × 1.8 $mm^3$). The diffusion sensitive gradients were distributed along 60 directions in an icosahedral scheme (Jones et al., 1999). For each set of diffusion-weighted data, 60 volumes with b-value = 800 s/$mm^2$ and 7 volumes with b-value = 0 s/$mm^2$ were obtained. For each subject, the entire diffusion measurement was repeated four times in successive sessions for subsequent averaging. The total scan time for the diffusion-weighted imaging protocol was about 50 min. A scanning protocol with special focus on quality protection of the data was applied, in particular with respect to the prevention of head motion. The four data sets for each subject were obtained in two 6-minute runs each which minimised motion within a scan session as subjects could relax in-between. Head fixation was carried out using foam paddles at

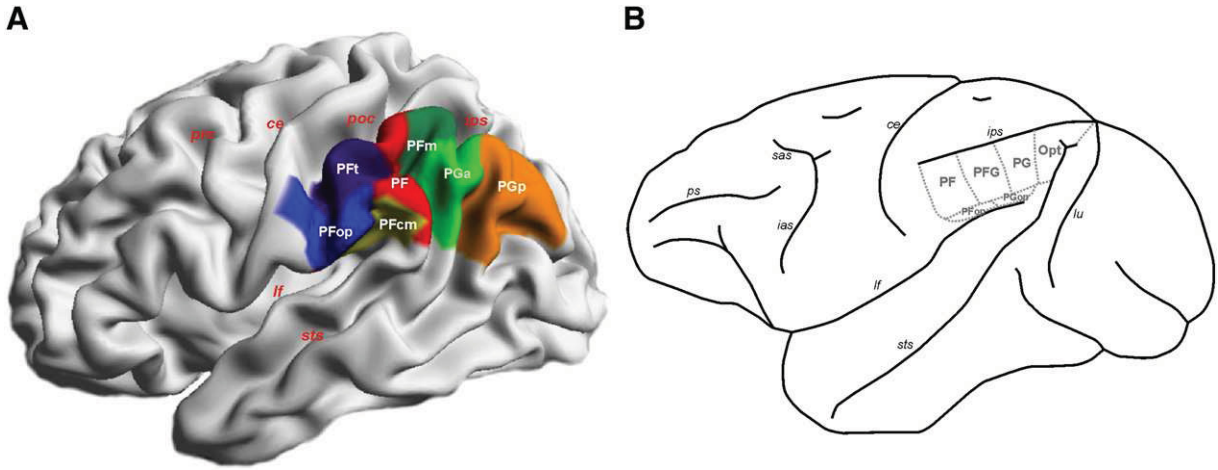


**Fig. 1.** (A) 3D reconstruction of maximum probability maps (MPM; Eickhoff et al., 2006a) of the cytoarchitectonic areas (PFop, PFt, PF, PFm, PFcm, PGa, PGp) defined within the human IPL (Caspers et al., 2006, 2008), displayed on a lateral surface view of the MNI single subject template. (B) Schematic depiction of the six areas (PF, PFG, PG, Opt, PFop, PGop) of the macaque IPL, adopted from Pandya and Seltzer (1982) and Gregoriou et al. (2006). ce central sulucs, ias inferior arcuate sulcus, ips intraparietal sulcus, lf lateral fissure, lu lunate sulcus, poc postcentral sulcus, prc precentral sulcus, ps principal sulcus, sas superior arcuate sulcus, sts superior temporal sulcus.

either side of the subjects' head. Light in the scanner room was dimmed to avoid visual distraction of the subjects during scanning. Quality of scanning in general was checked by routinely applied phantom measurements with retrieval of signal and noise change measures within the acquired images and the background to assure stability of the scanning protocol over time.

*Definition of seed and target areas*

The five cytoarchitectonic areas on the lateral surface of the IPL (in rostro-caudal sequence: PFt, PF, PFm, PGa, PGp; Caspers et al., 2006, 2008) were used as seed areas. Definition of the seed volumes was based on probabilistic cytoarchitectonic maps (Caspers et al., 2008) as

**Table 1**
Target areas for connectivity analysis of IPL seed areas.

| | Target area | Atlas | Labelling |
|---|---|---|---|
| Frontal lobe | Broca's speech region, BA 44 | JHA | BA 44 |
| | Broca's speech region, BA 45 | JHA | BA 45 |
| | Primary motor area 4a | JHA | 4a |
| | Primary motor area 4p | JHA | 4p |
| | Premotor cortex, BA 6 | JHA | BA 6 |
| | Frontal medial cortex | HOCSA | FMed |
| | Frontal operculum | HOCSA | FOperc |
| | Frontal orbital cortex | HOCSA | FOrbit |
| | Frontal pole | HOCSA | FPole |
| | Middle frontal gyrus | HOCSA | FMid |
| | Superior frontal gyrus | HOCSA | FSup |
| | Anterior cingulate cortex | HOCSA | CingAnt |
| | Posterior cingulate cortex | HOCSA | CingPost |
| | Paracingulate cortex | HOCSA | ParaCing |
| Primary somatosensory cortex (SI) | Area 1 | JHA | 1 |
| | Area 2 | JHA | 2 |
| | Area 3a | JHA | 3a |
| | Area 3b | JHA | 3b |
| Secondary somatosensory cortex (SII) | Area OP1 | JHA | OP1 |
| | Area OP2 | JHA | OP2 |
| | Area OP3 | JHA | OP3 |
| | Area OP4 | JHA | OP4 |
| Insula | Dysgranular insula Id1 | JHA | Id1 |
| | Granular insula Ig1 | JHA | Ig1 |
| | Granular Insula Ig2 | JHA | Ig2 |
| Parietal lobe | Superior parietal area 5Ci | JHA | 5Ci |
| | Superior parietal area 5L | JHA | 5L |
| | Superior parietal area 5M | JHA | 5M |
| | Superior parietal area 7A | JHA | 7A |
| | Superior parietal area 7M | JHA | 7 M |
| | Superior parietal area 7PC | JHA | 7PC |
| | Superior parietal area 7P | JHA | 7P |
| | Intraparietal area hIP1 | JHA | hIP1 |
| | Intraparietal area hIP2 | JHA | hIP2 |
| | Intraparietal area hIP3 | JHA | hIP3 |
| Occipital lobe | Visual area hOc1, BA 17 | JHA | hOc1 |
| | Visual area hOc2, BA 18 | JHA | hOc2 |
| | Visual area hOc3A | JHA | hOc3A |
| | Visual area hOc3d | JHA | hOc3d |
| | Visual area hOc3v | JHA | hOc3v |
| | Visual area hOc4 | JHA | hOc4 |
| | Visual area hOc5 | JHA | hOc5 |
| | Lateral inferior occipital cortex | HOCSA | OLatInf |
| | Lateral superior occipital cortex | HOCSA | OLatSup |
| | Lingual gyrus | HOCSA | Ling |
| | Occipital fusiform gyrus | HOCSA | OFusi |
| Temporal lobe | Auditory area TE1.0 | JHA | TE1.0 |
| | Auditory area TE1.1 | JHA | TE1.1 |
| | Auditory area TE1.2 | JHA | TE1.2 |
| | Auditory area TE3 | JHA | TE3 |
| | Inferior temporal gyrus, anterior part | HOCSA | TInfAnt |
| | Inferior temporal gyrus, posterior part | HOCSA | TInfPost |
| | Inferior temporal gyrus, temporooccipital part | HOCSA | TInfTempocc |
| | Middle temporal gyrus, anterior part | HOCSA | TMidAnt |
| | Middle temporal gyrus, posterior part | HOCSA | TMidPost |
| | Middle temporal gyrus, temporooccipital part | HOCSA | TMidTempocc |
| | Superior temporal gyrus, anterior part | HOCSA | TSupAnt |
| | Superior temporal gyrus, posterior part | HOCSA | TSupPost |
| | Temporal fusiform cortex, anterior part | HOCSA | TFusiAnt |
| | Temporal fusiform cortex, posterior part | HOCSA | TFusiPost |
| | Temporal occipital fusiform cortex | HOCSA | TOFusi |
| | Planum temporale | HOCSA | PT |
| | Temporal Pole | HOCSA | TPole |
| | Posterior parahippocampal gyrus | HOCSA | ParaHippoPost |

Areal naming as provided in the atlases and respective publications. JHA: Jülich histological atlas, HOCSA: Harvard–Oxford cortical structural atlas. Labelling of JHA areas according to publications: Amunts et al. (1999, 2000), Choi et al. (2006), Eickhoff et al. (2006b,c), Geyer (2004), Geyer et al. (1996, 1999, 2000), Grefkes et al. (2001), Kurth et al. (2010), Malikovic et al. (2007), Morosan et al. (2001), Rottschy et al. (2007), Scheperjans et al. (2008a,b).

implemented in the Düsseldorf–Jülich histological atlas (JHA; Zilles and Amunts, 2010) using the SPM Anatomy Toolbox (http://www.fz-juelich.de/inm/spm_anatomy_toolbox; Eickhoff et al., 2005). The rest of the cerebral cortex was subdivided in different targets, again based on the JHA where available. For those regions that have not yet been cytoarchitectonically defined, we used the macroscopic probabilistic Harvard–Oxford cortical structural atlas (HOCSA) as included in FSL (Oxford Centre for Functional Magnetic Resonance Imaging of the Brain, http://www.fmrib.ox.ac.uk/fsl/data/atlas-descriptions.html) for target definition. In total, 64 target areas were defined in each hemisphere (Table 1), for which locations are schematically depicted in Fig. 2.

Seeds and targets were defined separately for each hemisphere by using the centre of each region in a maximum probability map (MPM; Eickhoff et al., 2006a) included in the JHA and the HOCSA atlases. Centres were defined as the top 10% of the underlying probability that are also represented by the respective MPM. To perform diffusion-image analysis the ensuing area definitions had to be transformed from MNI standard space into the individual diffusion space (Eickhoff et al., 2010), being the reason why only the centre representation of the MPM has been chosen to avoid overlapping seed and target regions in individual diffusion spaces. Transformation fields were generated by normalising the mean b = 0 image from each subject to the MNI tissue probability maps (TPM) using a segmentation-based approach (Ashburner and Friston, 2005). By using the combination of a transformation from the MNI single subject template into the TPM space with the inverse transformation of the individual b = 0 image, we transformed seeds and targets from the template brain into the individual diffusion spaces. All diffusion-weighted images, including the b = 0 images, were spatially realigned. All 28 b = 0 images of each subject (7 b = 0 images of 4 scanning sessions) were then averaged to provide an anatomical reference for consecutive registration of all diffusion-weighted images to the individual mean b = 0 image which allowed for a consecutive application of the transformation procedure to all diffusion-weighted images. The representations of seeds and targets in individual diffusion space were then mapped on the grey–white matter interface with restriction to fractional anisotropy (FA) values of at least 0.25. This procedure was necessary to provide sufficient directional information for the tracking algorithm to proceed. Within the grey matter, directional information is poorly available due to low anisotropy. In particular, transforming the regions of interest (seeds and targets) onto the grey–white matter interface resulted in mean FA-values of around 0.4 within the transformed region of interest, thus providing sufficient directional information for consecutive tracking. The grey–white matter interface was gauged based on segmentation of the average of the 28 b = 0 images for each subject by means of unified segmentation (Ashburner and Friston, 2005) which provided a robust and reliable basis for defining the interface between the two tissue classes grey and white matter. By adding an FA threshold of 0.25 to the grey matter segment, it was possible to only identify those grey matter voxels that were located close to the grey matter and construct of the respective interface.

*Image analysis*

Data were preprocessed using SPM 5 (Wellcome Department of Imaging Neuroscience, London, UK, http://www.fil.ion.ucl.ac.uk) and FSL 4.1 (http://www.fmrib.ox.ac.uk/fsl). After correction for eddy currents and head motion, the four data sets (sessions) for each subject were averaged to improve signal-to-noise ratio. Data sets were additionally checked for motion artefacts or other acquisition-related quality compromises (ghosting, signal drop-outs etc). But due to a scanning protocol with focus on optimal acquisition of high quality data, only one data set had to be removed from further analysis, leaving 39 data sets which showed minimal motion and no other artefacts for consecutive analysis. Brain segmentation into three compartments (grey matter, white matter, cerebrospinal fluid (CSF)) was then performed on the averaged b = 0 images for each participant using the unified segmentation approach (Ashburner and Friston, 2005).

Diffusion probabilistic tractography was then performed using the Diffusion Toolbox FDT (version 4.0.4) implemented in FSL (Behrens et al., 2003a,b; Smith et al., 2004). Possible multiple fibre orientations in each voxel were estimated according to Behrens et al. (2007). The CSF-segment obtained from segmentation of the individual b = 0 images was used as exclusion mask for probabilistic tractography to avoid tracts passing through ventricles or sulci. The grey matter–white matter interface mask was used as stop mask for the tracking algorithm to stop after reaching a relevant target voxel. Otherwise, tracts might be prone to further proceed until they reach the CSF which would cause exclusion of this tract from further analysis.

Probabilistic tractography was carried out from each seed area using 100,000 samples for each seed voxel to improve signal-to-noise ratio and create a stable probability distribution. For each voxel in the brain, the number of samples (probabilistic tracts) passing through it was registered, together with the respective distance from the seed voxel along the tract. For visualisation purposes only, all individual tractography results were transformed into anatomical MNI space and then averaged across subjects.

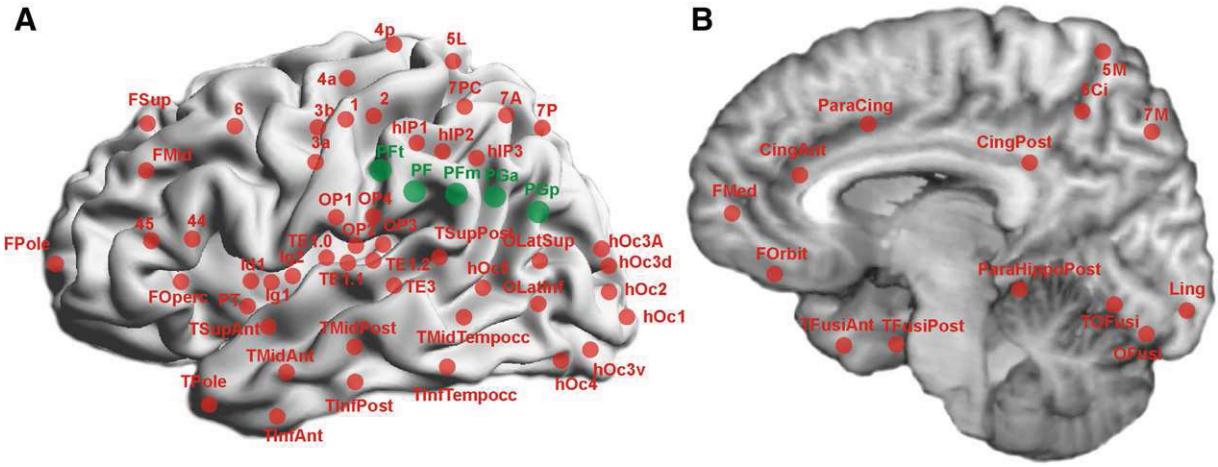


**Fig. 2.** Visualisation of seed (green) and target areas (red) on the (A) lateral 3D reconstructed and (B) medial surface view of the MNI single subject template. For labelling conventions of areas, cf. Table 1.

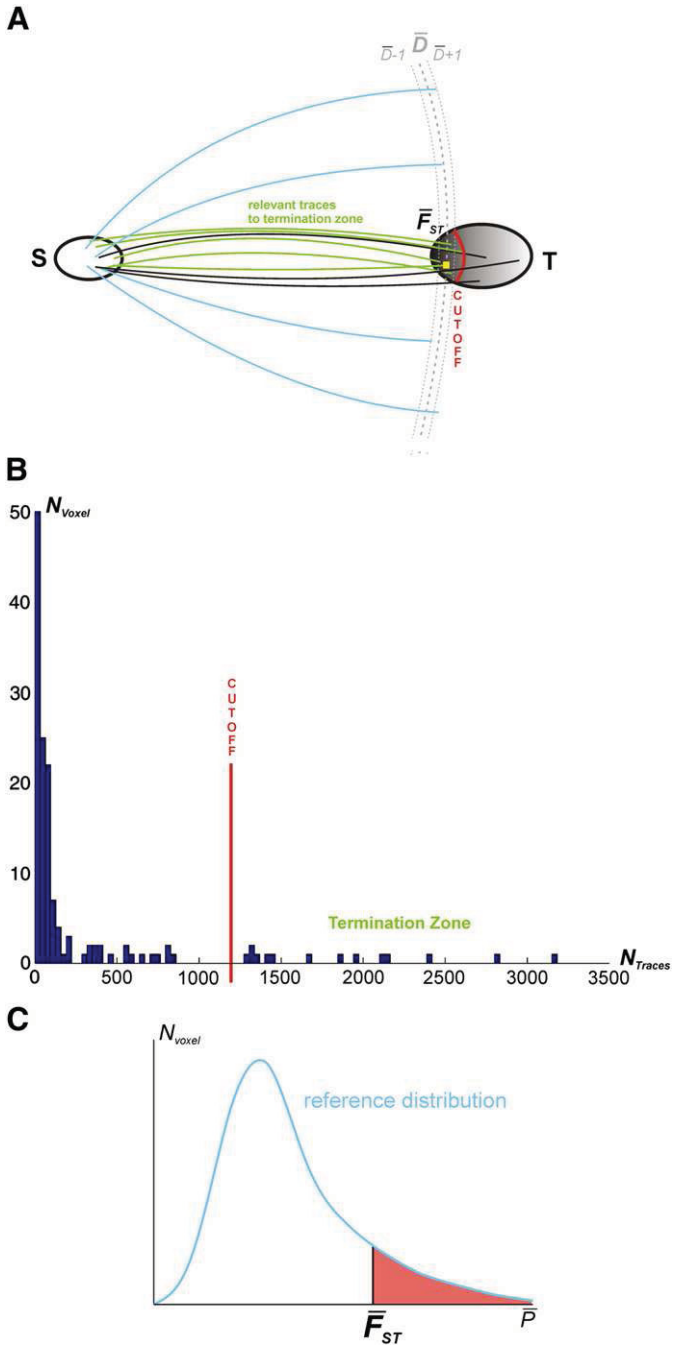


**Fig. 3.** (A) Schematic overview of the statistical approach used for identifying terminal zone of a particular seed-target connection (for details, see text). S: Seed, T: Target, $\overline{D}$: distance between seed and target voxels, exemplarily given for one highlighted voxel (yellow square in termination zone of target T), $\overline{D}+1, \overline{D}-1$: uncertainty of tract length around $\overline{D}$, $\overline{F}_{ST}$: defined mean frequency of traces between S and T. (B) Histogram showing an exemplary frequency distribution of traces running from a seed to one target with visualisation of the cutoff point for the identification of the termination zone. $N_{voxel}$ (y-axis): number of voxels in the target region which featured a particular trace-count as indicated by $N_{Traces}$ on the x-axis (following probabilistic tractography with 100,000 samples run from each seed voxel). (C) Reference distribution of traces derived from drawing a random sample of voxels at the same distance as the target voxels in the termination zone. $N_{voxel}$: number of voxels which showed a certain frequency of traces in the randomisation procedure to generate the reference distribution.

### *Statistical analysis*

Statistical analysis was performed using MATLAB (The MathWorks). To quantitatively compare the connection likelihood of the individual IPL areas with different targets in spite of the varying distances between them, we first recorded the number of traces (samples from probabilistic tractography) for all voxels within the entire mask of each target (Fig. 3A).

For the analysis of relevant traces, it has to be considered that cortical targets are irregularly shaped in three dimensional space due to the gyral and sulcal pattern of the respective region. Thus, the fibre tracts that can be assessed by DTI might terminate in only a small part of the target, i.e. that part of the target which is located closest to the seed. Moreover, the employed tractography analysis favours target voxels which are located close to the white matter as directional information is poor in more superficial grey matter due to low anisotropy values, even if DTI-based tractography is generally able to also reach voxels far within the grey matter.

Thus, most fibre tracts should predominantly reach the target in this kind of "termination zone", due to technical and biological constraints. To the contrary, the majority of voxels showed lower frequencies of traces since these voxels were only rarely hit by incoming traces when running the probabilistic tractography (left part of Fig. 3B). Analysis of tract counts was consequently restricted to this termination zone, excluding voxels within the target that only reflect stray connectivity (i.e. voxels which were rarely hit due to probabilistic phenomena), but may severely bias further analysis.

By restricting analysis to that termination zone, those voxels within each target mask which were reached most consistently in the probabilistic tractography were identified. It has to be emphasised that this was performed separately for each seed-target combination, i.e., a particular target was allowed to have distinct termination zones for the different seed areas.

When examining the distribution of trace frequencies for the different seed-target combinations, i.e. how many voxels were reached by which number of traces (trace density), two patterns became evident (Fig. 3B). In most instances, one or a few clusters of target voxels showed considerably higher trace density than all others, indicative of a distinct termination zone. Algorithmically, voxels forming this termination zone were identified using a stepwise threshold decrease. Initially, the 10 voxels with the highest trace density were considered. This minimum cluster-size was introduced to reduce the effect of outliers and potential technical artefacts. The threshold for inclusion was then successively lowered until the voxel to be included next showed a trace density less than half as high as the median trace density of the voxels already included. In cases where no such break could be identified, the procedure was stopped after inclusion of 5% of all target voxels.

The number of traces passing through the different voxels in the termination zone was averaged to yield the trace density $\overline{F}_{ST}$ representing the connectivity between the particular seed (S) and that target (T). When trying to compare these values across different seed-target combinations or when trying to interpret whether an observed $F_{ST}$ is indicative of an anatomical connection, one faces two problems. First, as 100,000 traces originated from each (individual) seed voxel, the number of traces will increase with the size of the seed volume. This holds true for any given number of samples. A reliable comparison between different seed-target connections would therefore be aggravated. Thus, a correction for this potentially Biasing factor 'seed size' is needed. Second, the number of traces is also highly dependent on the distance (along the tract) between the seed and the target. In particular, the further away a target is located from a particular seed, the lower the trace count that it will reach the target, as the number of potential "wrong turns" increases. Hence, low density values for a distant seed-target pair may actually reflect stronger connectivity than high values for a proximate pair. In fact, stray samples close to the seed result in higher trace counts than "true" connectivity at a more distant location.

In order to correct for these two potential biases (i.e. seed size and distance), we referenced the observed mean trace density $\overline{F}_{ST}$ against

a reference distribution reflecting the empirically expected trace density in the same distance to the respective seed. This would ameliorate the influence of both Biasing factors on further analysis, since the reference distribution will be drawn from voxels at the same distance from the same seed as the target. The distance between a seed and a target was defined as the physiological distance, i.e. following the natural way of the fibre tracts with all curves around sulci. Thus, the distance is no straight-line distance in 3D, but fitted to the anatomy. Thus, only voxels which were reached by at least one trace were included in any further analysis, yielding a more conservative approach as compared to including also those voxels with a trace count of zero. Actually, different voxels in the termination zone may be located in slightly different distances from the seed which was accommodated by recording the distances between each voxel in the termination zone and the seed. Subsequently, for each voxel of the termination zone, we identified all voxels within a whole brain grey–white matter interface mask that were located at the same distance from the seed as that target voxel. The trace densities of these voxels then provided a reference distribution for the number of probabilistic traces that may be expected in the same distance from the seed as that particular voxel of the termination zone. To account for potential rounding errors in distance $\overline{D}$ of each target voxel, the voxels for the reference distribution were drawn from a distance interval $+/-1$ voxel around the computed distance $\overline{D}$ (Fig. 3A).

To establish the reference distribution for the mean trace density $\overline{F}_{ST}$, we used a randomisation procedure. For each voxel in the termination zone, one trace density from the reference voxels as defined above was selected independently at random. This procedure thus yielded as many trace density values as were obtained from the termination zone that had the same distance from the seed. These random trace densities were then averaged to yield an estimate for the mean trace density of a random set of the same number of voxels in the same distance as the termination zone. As this mean trace density was computed from a voxel that were matched with those constituting the termination zone in terms of distance along the tracts, it reflects an at-chance trace density in the same range. This procedure of drawing the same number of samples and consecutive averaging of the trace counts observed for these (random but matched) voxels was repeated $10^6$ times yielding (due to the central limit theorem) a normal distribution for the mean trace density in the termination zone. In other words, we obtained a reference distribution of at-chance (mean) trace counts across an equally large number of voxels as contained in the seed, which were located in the same distance from the target. Depending on the distance from the seed, a differing number of reference voxels existed. At the relevant distances of up to about 120–130 steps from the seed, there were at least 3000 to 5000 reference voxels from which the samples for the reference distribution could be chosen (Suppl. Fig. S1).

The likelihood of observing $\overline{F}_{ST}$ by chance, given the distance of this target from the seed, was then expressed as the proportion of the realisations within the reference distribution that showed less or equal trace densities, being a quantitative description of this proportion (Fig. 3C). We thus evaluated the mean number of traces between seed and target (termination zone) against a reference distribution reflecting the by-chance distribution of mean trace counts in such set of voxels at the same distance from the seed. Note, that even though this assessment was based on a reference distribution, no inference was sought at this stage. Rather, these likelihoods were converted into standard Z-scores to allow statistical inference on their consistency across subjects in a second-level group analysis. A Z-score of 0 indicates that it is equally likely to find a higher or a lower mean trace density at that distance by chance. A positive Z-score points towards a termination zone that receives more traces than expected by chance in the same distance from the seed. In contrast, negative Z-scores would be found for targets that show a lower mean trace density than expected by chance in the same distance. It has to be noted that the probabilities obtained from comparison with the reference distribution do not reflect connection probabilities per se (how likely is the target connected) but rather the probabilities for excess of the expected trace number (how (un-) likely would one see the observed trace count at chance in the same distance). Importantly, the former probability would certainly decrease with increasing distance from the seed due to increasing uncertainty and "fanning out" of the tracts. The current approach does not attempt to correct for this phenomenon. Instead, it implements a reference distribution of how many trace counts could be expected by chance at a given distance and describes the observed effects relative to this reference.

Consistency of these findings across subjects was then tested for by means of one-sample T-tests performed separately for each seed-target combination ($p<0.001$; Bonferroni-corrected for multiple comparisons). Together with the individual Z-scores, this consistency test provides a measure for the likelihood of a given connection across subjects. Thus, the results of the present analysis will be referred to by calling them a connection which one should be more or less confident about.

Further statistical analysis was performed on the confidence measures (individual Z-scores) from each seed to every target area. Different target areas were grouped into anatomically and functionally defined groups to test for differences in anatomical connectivity from IPL seed areas to cortical regions involved in different functional systems. Repeated-measures ANOVAs of connection likelihood values were used to test for influences of the within-subject factors of "IPL seed" (PFt, PF, PFm, PGa, PGp), and "hemisphere" (left, right), as well as the interaction between them on connection likelihood. In particular, the main effect of the factor "IPL seed" assessed whether there was a significant difference between the five IPL seeds with respect to their connection likelihood to that group of targets. The main effect of factor "hemisphere" tested whether the connection likelihood between the five seeds and that assessed target differed between the two hemispheres. The interaction between both factors tested for differences in connection likelihood between left and right hemisphere that were conditioned upon the IPL seed considered.

### *Reference to macaque data*

In order to facilitate a comparison of the results of the present analysis with those from tracer studies in macaques, the relevant literature on connectivity of the inferior parietal lobule in macaque cortex has been reviewed and summarised in a figure (Fig. 10 of the Discussion) using the same layout as for the current results (Fig. 5). To this end, different labelling systems had to be combined and displayed on the schematic drawing of a typical macaque hemisphere in Fig. 10 adopted from Schmahmann and Pandya (2006), with minor changes according to Felleman and Van Essen (1991) and Luppino et al. (1993).

Results depicted in the figure and within the text of the Discussion were derived from the following publications on IPL connectivity of macaque cortex: Pandya and Seltzer (1982), Petrides and Pandya (1984), Cavada and Goldman-Rakic (1989a,b), Andersen et al. (1990), Neal et al. (1990a,b), Felleman and Van Essen (1991), Luppino et al. (1993), Lewis and Van Essen (2000), Matelli and Luppino (2001), Zhong and Rockland (2003), Gregoriou et al. (2006), Rozzi et al. (2006), Schmahmann and Pandya (2006), Petrides and Pandya (2009) as well as the CoCoMac database (http://www.cocomac.org; Stephan et al., 2001).

The parcellation scheme of the macaque IPL as referred to in the Discussion of the present manuscript was adopted from today's most widely used parcellation of Pandya and Seltzer (1982). This includes areas PF, PFG, PG, and Opt in rostro-caudal sequence, for which differential connection patterns have been shown by several groups. Since not all publications used this parcellation scheme, the results of

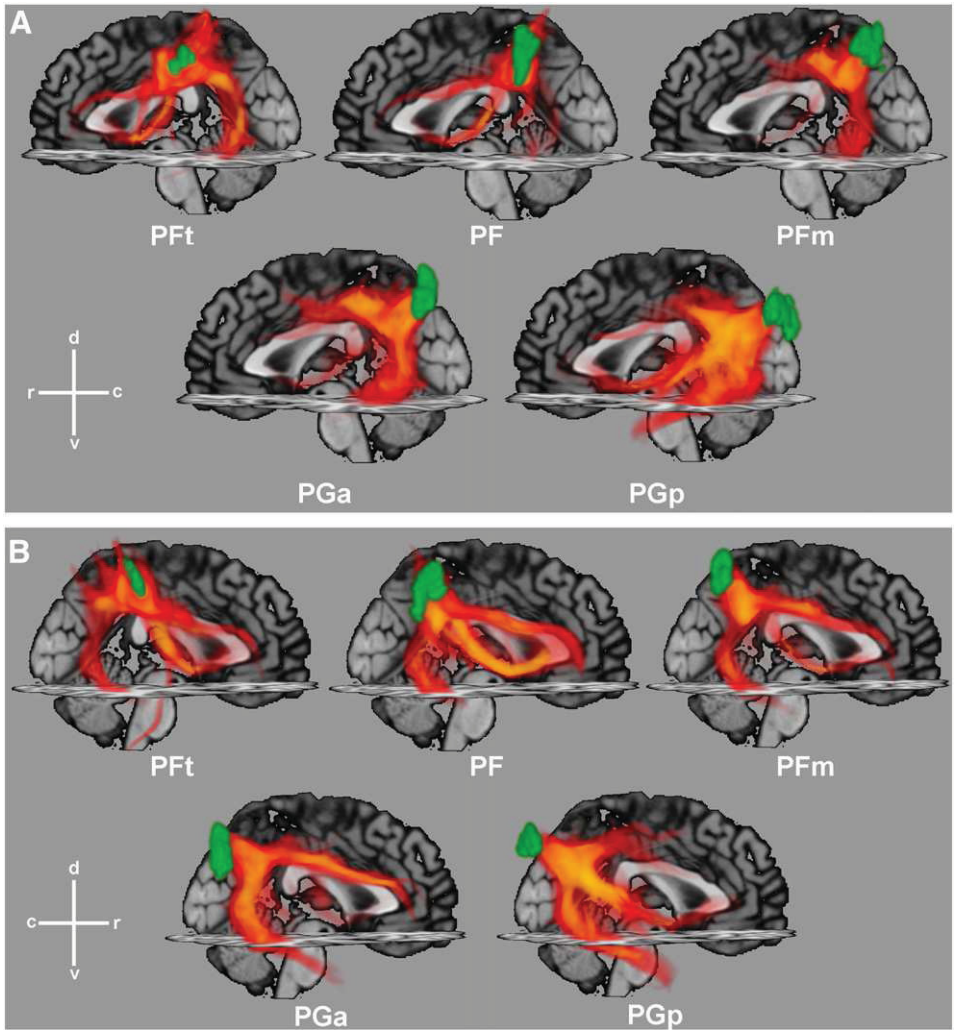


**Fig. 4.** Probabilistic tractography results for five IPL seed areas, ordered from top-left to bottom-right in a rostral sequence and overlaid with the respective cytoarchitectonic seed region (green), for (A) left and (B) right hemisphere. Probabilistic fibre tracts, projected back from individual diffusion spaces into anatomical MNI space, are displayed with regard of the uncertainty of tract traces (among others due to interindividual variability), as revealed by the probabilistic tracking algorithm. The density of traces is colour-coded from opaque yellow for low to transparent red for high uncertainties. Traces are projected onto the sagittal and transversal planes of the MNI single subject template for anatomical orientation. c caudal, d dorsal, r rostral, v ventral.

the respective publications had to be adapted accordingly. Whenever possible, this was based on the ORT algorithm in CoCoMac (Stephan et al., 2001), in other cases by consensus across the literature and among the investigators. Connections reported for area 7b (rostral IPL) were attributed in most cases to areas PF and PFG, whereas connections reported for area 7a (caudal IPL) were attributed to PG and Opt. If rostral or caudal subareas of 7b or 7a were explicitly distinguished and could be identified as either one of the four areas of Pandya and Seltzer, the reported connection was specifically attributed to the respective area.

## Results

### *Fibre tract pattern of IPL areas*

The courses of the (hemisphere-specific) fibre tract patterns for the individual IPL seed areas are visualised in Fig. 4. It should be noted that the probabilistic nature of the tractography as well as the inter-individual variability of fibre tract patterns contributes to substantial uncertainty of these group-averaged tracts.

Visual inspection of the tractography patterns indicates that homologous regions on either hemisphere show a largely similar course. The most conspicuous differences in fibre tract pattern can be observed between rostral (PFt, PF, PFm) and caudal (PGa, PGp) areas of the IPL. Tracts originating from rostral IPL areas tend to run mainly in direction of the inferior frontal, postcentral, and superior parietal regions. They predominantly follow the course of the superior longitudinal (SLF) and arcuate fascicles (AF). In contrast, tracts from caudal IPL areas preferentially follow fibre pathways in direction of lateral occipital and temporal areas, at this joining the inferior longitudinal fascicle via anterior parts of the SLF. Additionally, fibres from the latter region also reach the inferior frontal cortex by a more ventral pathway through the extreme capsule. Interestingly, this differentiation approximately matches the putative location of the border between Brodmann's areas 40 (rostral, corresponding topographically to the PF areas) and 39 (caudal, PG areas). It should be emphasised, however, that this change in the associated fibre tract patterns is not abrupt but rather shows a gradient when moving from rostral to caudal areas of the IPL with an accentuation at the transition between PFm and PGa.

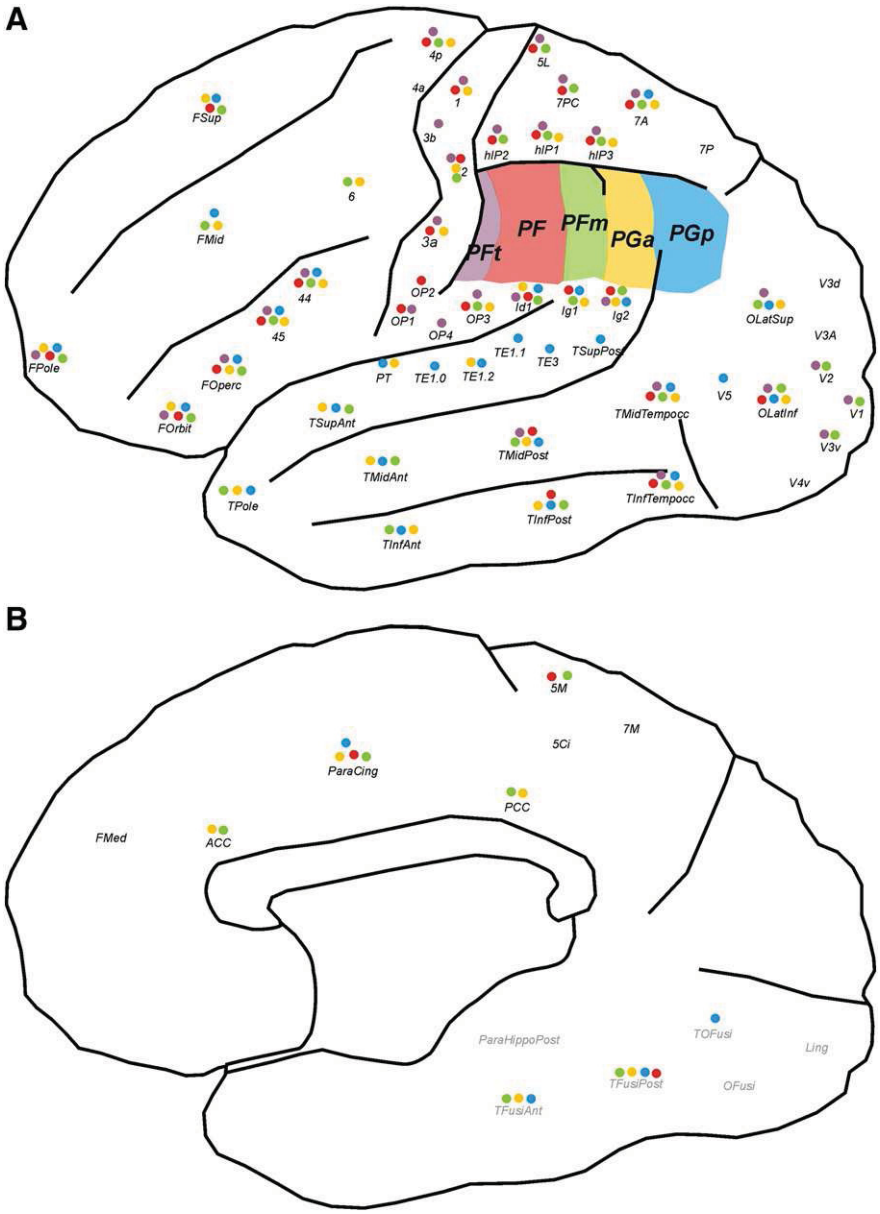


**Fig. 5.** Schematic drawings of (A) the lateral and (B) the mesial part of a human hemisphere, indicating those connections between the five IPL seed areas and cortical targets that were consistently (across subjects) found to be more likely than expected by chance for lateral (A) and mesial (B) target areas. IPL seed areas are marked in five different colours: PFt violet, PF red, PFm green, PGa yellow, PGp blue. Coloured dots beneath each target region indicate the presence of a connection to the respective seed region. For labelling conventions of areas, cf. Table 1.

This visualisation of the probabilistic fibre traces provides qualitative information about possible major pathways connecting the individual areas of the IPL to the rest of the brain, but requires a statistical analysis for quantification of the results.

### *Seed-target connections of IPL areas*

To quantify the respective connectivity patterns, mean trace density in the termination zone obtained from probabilistic tractography for each seed-target combination was assessed relative to the expected trace density at the same distance and statistically tested against its inter-individual variability, providing a measure for the connection likelihood for a given seed-target combination. The findings of these analyses are summarised in Fig. 5 which illustrates those connections of the individual IPL areas that were consistently expressed with higher connection likelihood than expected given their length ($p<0.001$ for the random-effects inference following Bonferroni-correction for multiple comparisons).

All areas showed consistent connections to inferior frontal (44, 45, frontal operculum, orbitofrontal cortex, frontal pole) and posterior insular regions. The visually apparent shift of predominant connectivity patterns from rostral to caudal IPL areas is also well supported by the statistical analysis. Rostral areas PFt and PF mainly showed consistent connections with targets located in the inferior frontal, somatosensory and superior parietal cortices while reaching only posterior parts of the temporal cortex. Intermediate areas of the IPL (PFm, PGa) likewise show reliable connections to the aforementioned targets, but additionally feature consistent fibre tracts to middle and superior frontal as well as anterior temporal regions. The most caudal area (PGp), finally, again connects with the inferior frontal cortex and, like PFm and PGa, to the entire temporal lobe. In contrast to the other areas, however, there is also significantly expressed connectivity to auditory and temporo-occipital areas.

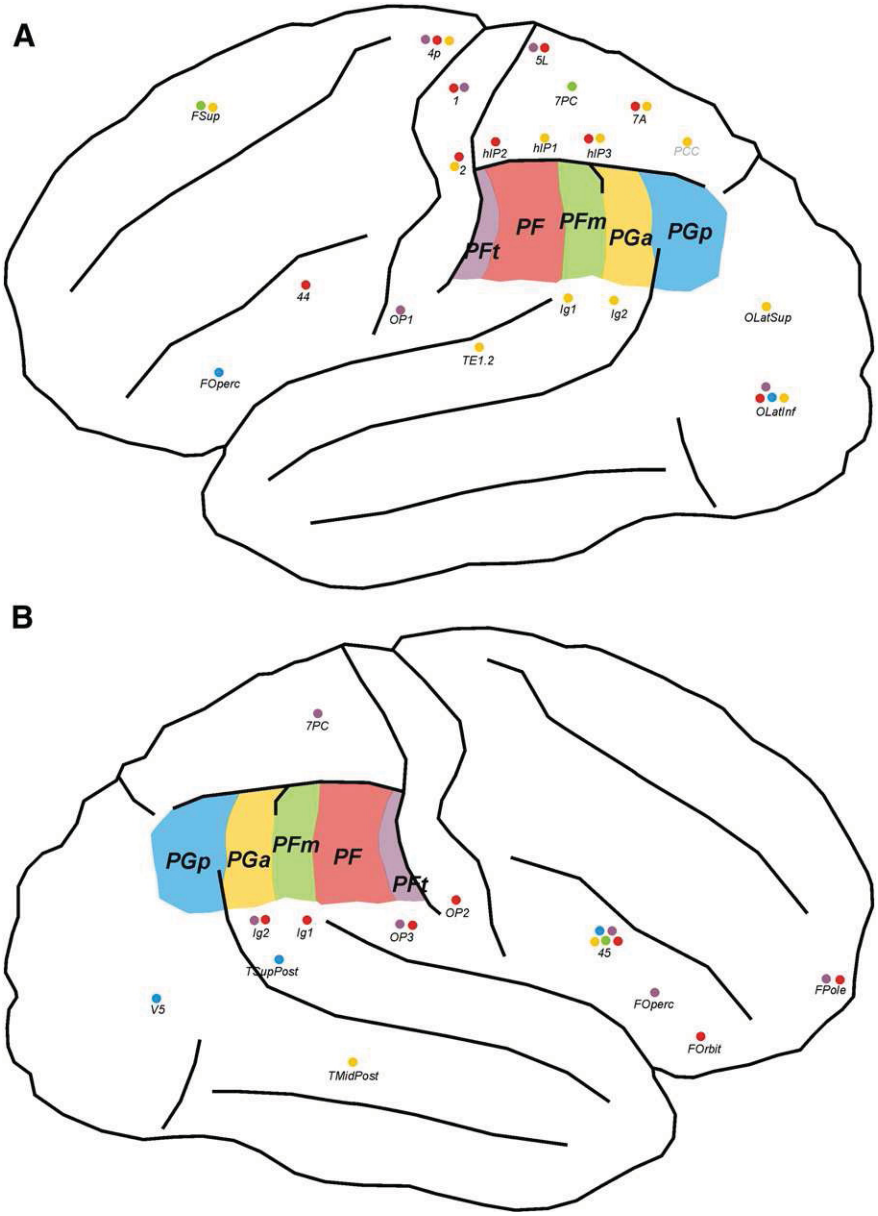


**Fig. 6.** Schematic drawings of a typical lateral view of a (A) left and (B) right human hemisphere, indicating those connections for which repeated-measures ANOVA revealed a significant left–right asymmetry effect. Only those connections are displayed which were consistently (across subjects) found to be more likely than expected by chance as visualised in Fig. 5. IPL seed areas are marked in five different colours: PFt violet, PF red, PFm green, PGa yellow, PGp blue. Coloured dots beneath each target region indicate the presence of a connection to the respective seed region. For labelling conventions of areas, cf. Table 1.

The visualisation of the fibre tract patterns (Fig. 4) already suggested inter-hemispheric asymmetries. Thus, the fibre tracts that showed consistently greater connection likelihood than expected by chance were further analysed by means of repeated-measures ANOVAs. Fig. 6 summarises the connections that were found to be more pronounced in either hemisphere following correction for multiple comparisons ($p<0.05$).

Rostral IPL areas PFt and PF showed more consistent connections with sensorimotor and superior parietal areas in the left hemisphere, whereas in the right hemisphere, more likely connections existed with secondary somatosensory, posterior insular and inferior opercular and orbito-frontal areas. Caudal IPL areas PGa and PGp had more consistent connections with intraparietal, superior parietal, posterior insular, lateral occipital and auditory areas in the left hemisphere, whereas more likely connections with posterior temporal, temporo-occipital, and inferior frontal areas existed within the right hemisphere. A complete list of the results of the ANOVA can be found in Supplementary Table S1.

While this binarisation into presence or absence of consistent evidence for a connecting fibre tract provides a useful overview over the connectivity of the human IPL, it may fail to reflect finer levels of the rostro-caudal gradients suggested by visual inspection. In order to reveal such gradients and provide more fine-graded information, the relative confidence for each connection has to be considered. Evidently, this analysis again has to accommodate distance-related effects. Connection likelihood of a particular seed-target combination was thus defined by averaging the Z-score (expressing above-chance connectivity) across subjects, reflecting the average chance that the observed trace density would be obtained in the same distance in our group of subjects. Summarising these mean Z-scores for each seed-

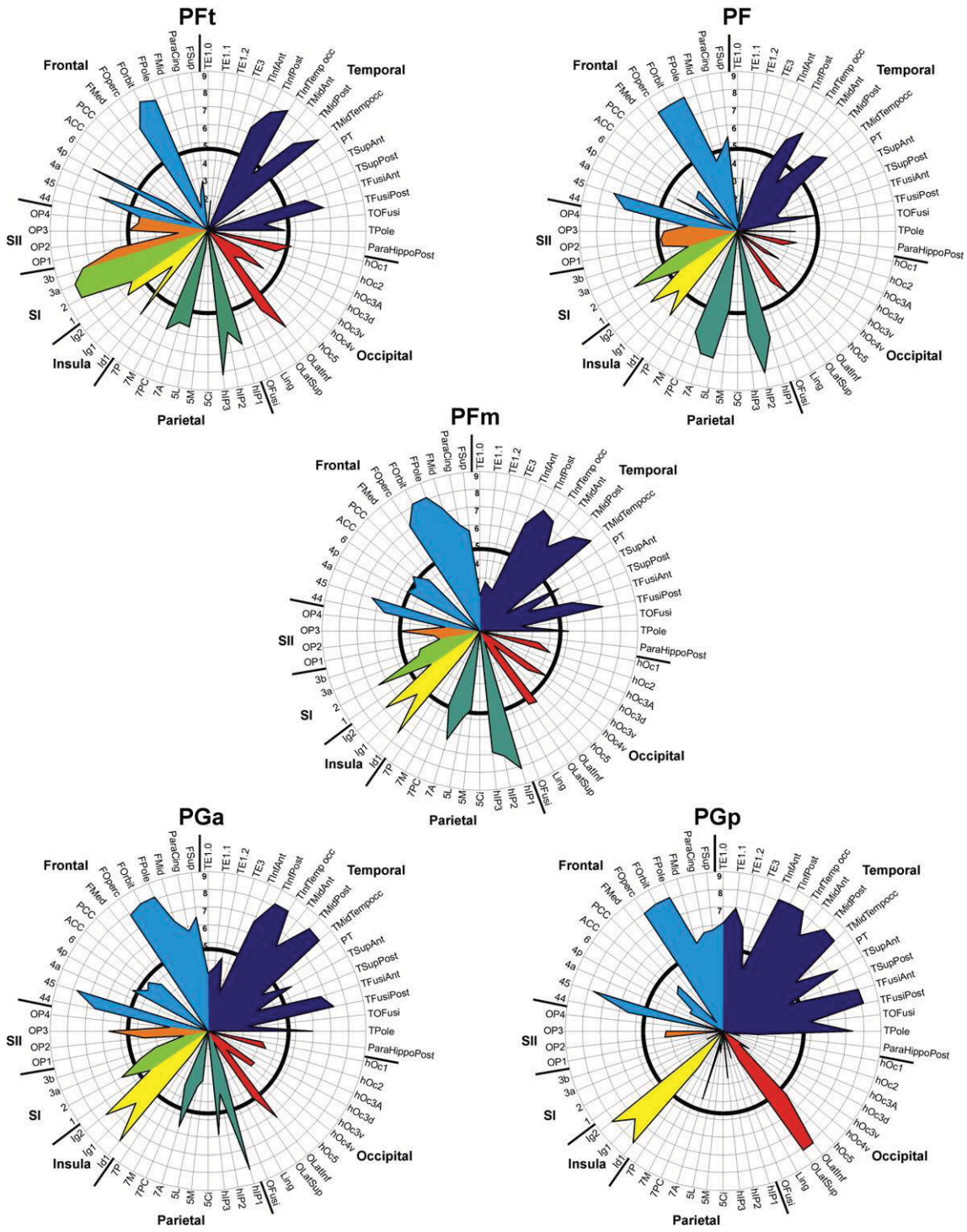


**Fig. 7.** Connectivity fingerprints for the left hemispheric seed regions. Results for consistency testing of fibre tract patterns (across subjects) for each seed-target combination are displayed as Z-scores, reflecting the chance that the observed trace density was higher (positive Z-scores) than expected according to the reference distribution. To clearly highlight the relevant connections (positive Z-scores) of the IPL seed areas, all non-positive (zero or negative) Z-scores (i.e. the chance that observed trace density was lower than or equally high as expected at the same distance) were set to zero. Labelling of areas as introduced in Table 1. Black circle within each polar plot marks a Z-score of 4.80, corresponding to a p-value of 0.001 (corrected for multiple comparisons), to indicate significance of each seed-target connection as a measure of consistency across subjects.

target connection in a polar plot provided a connectivity fingerprint for each assessed IPL area (cf. Passingham et al., 2002) in which higher values denote stronger evidence for above-chance connectivity.

Comparing the left- and right-hemispheric fingerprints for each seed region again indicated a comparable pattern of connectivity for both hemispheres. Fingerprints of the left hemisphere (Fig. 7) show more consistent connections to temporal areas for all IPL seed areas, probably reflecting the dominance of the arcuate fascicle in the left hemisphere. The shift of fibre tract pattern from rostral to caudal IPL areas is again confirmed by the more fine-grained information provided in the connectivity fingerprints. While most rostral area PFt showed predominant connections to superior parietal cortex and somatosensory regions (major weight of the fingerprint in lower left quadrant of the polar plot), most caudal area PGp featured strong

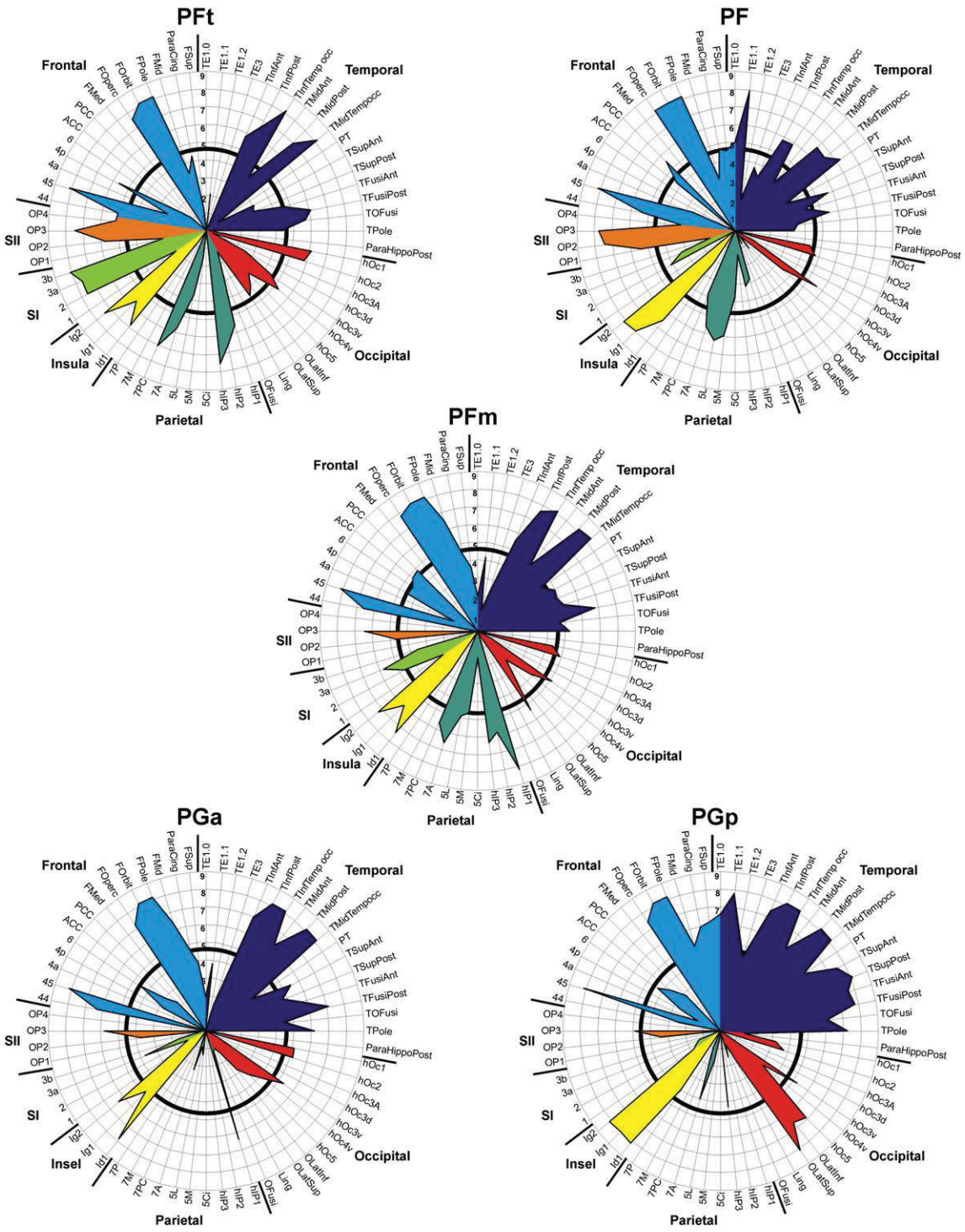


**Fig. 8.** Connectivity Fingerprints for each seed region in the right hemisphere. Results for consistency testing of fibre tract patterns (across subjects) for each seed-target combination are displayed as Z-scores, reflecting the chance that the observed trace density was higher (positive Z-scores) than expected based on the reference distribution. To clearly highlight the relevant connections (positive Z-scores) of the IPL seed areas, all non-positive (zero or negative) Z-scores (i.e. the chance that observed trace density was lower than or equally high as expected at the same distance) were set to zero. Labelling of areas as introduced in Table 1. Black circle within each polar plot marks a Z-score of 4.80, corresponding to a p-value of 0.001 (corrected for multiple comparisons), to indicate significance of each seed-target connection as a measure of consistency across subjects.

**Fig. 9.** Fibre tract strengths between IPL seed areas (x-axis) and anatomically and functionally relevant groups of targets for left (black bars) and right hemisphere (white bars). Individual fibre tract densities to all target areas, separated for left and right hemispheres, can be found in Supplementary Figs. S1–S4. Connection strengths are displayed as mean Z-scores across subjects (averaged across targets within each group), derived from the comparison for each seed-target connection with the reference distribution. Error bars denote standard error. For each plot, the statistics from the repeated-measures ANOVA are displayed beneath the heading of the plot. Grouping of target areas is indicated in Table 2. Fibre tract strengths between IPL seed areas (x-axis) and anatomically and functionally relevant groups of targets for left (black bars) and right hemisphere (white bars). Individual fibre tract densities to all target areas, separated for left and right hemispheres, can be found in Supplementary Figs. S1–S4. Connection strengths are displayed as mean Z-scores across subjects (averaged across targets within each group), derived from the comparison for each seed-target connection with the reference distribution. Error bars denote standard error. For each plot, the statistics from the repeated-measures ANOVA are displayed beneath the heading of the plot. Grouping of target areas is indicated in Table 2.

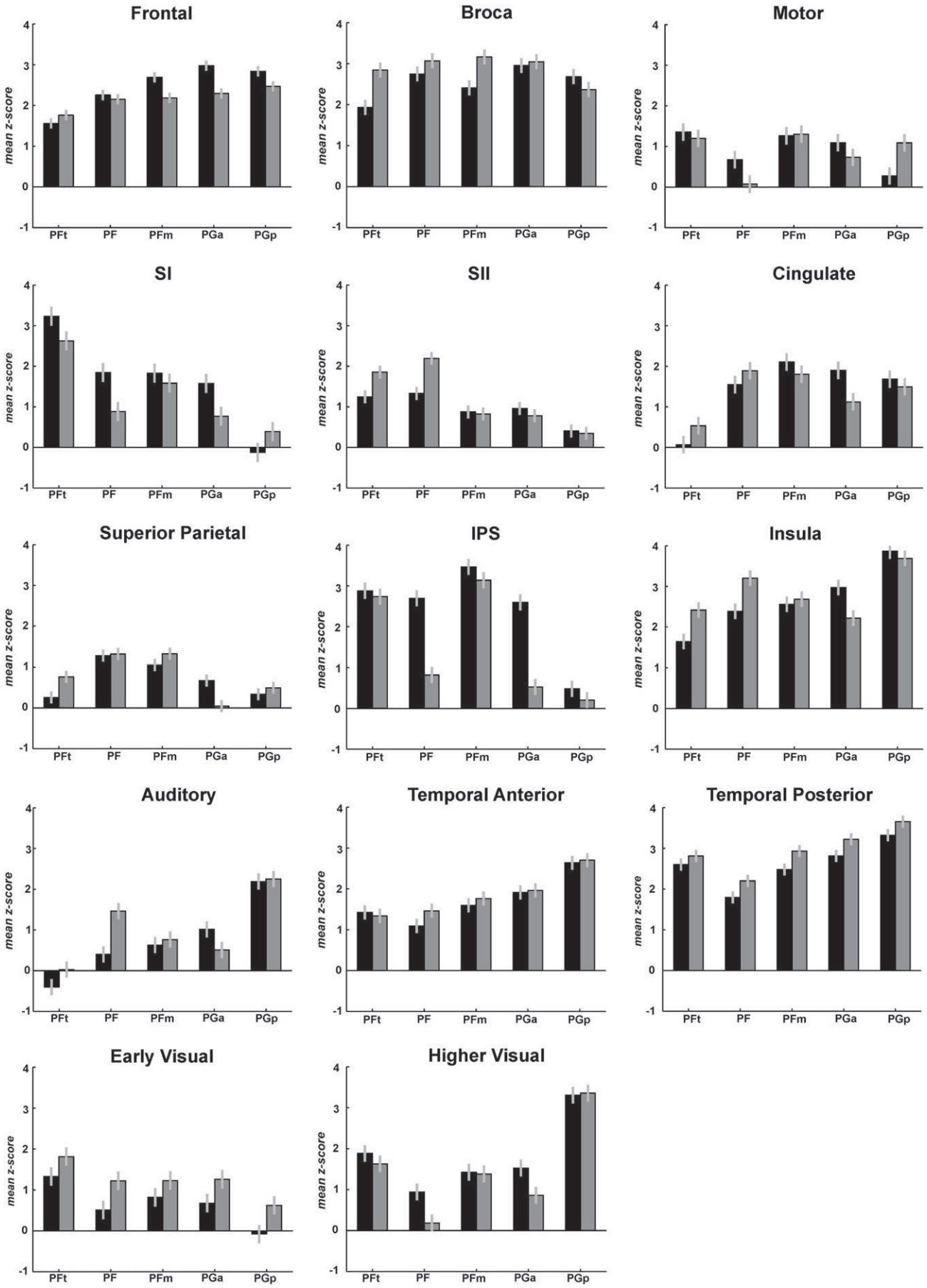
Frontal
Broca
Motor
SI
SII
Cingulate
Superior Parietal
IPS
Insula
Auditory
Temporal Anterior
Temporal Posterior
Early Visual
Higher Visual
mean z-score
PFt
PF
PFm
PGa
PGp

**Table 2**
Grouping of target areas in relation to anatomical and functional criteria.

| Group name | Included areas |
|---|---|
| Frontal | FMed, FMid, FOperc, FOrbit, FPole, FSup |
| Broca | 44, 45 |
| Motor | 4a, 4p, 6 |
| Primary somatosensory (SI) | 3a, 3b, 1, 2 |
| Secondary somatosensory (SII) | OP1, OP2, OP3, OP4 |
| Cingulate | ACC, PCC, ParaCing |
| Superior parietal | 5L, 5M, 5Ci, 7PC, 7A, 7M, 7P |
| Intraparietal sulcus (IPS) | hIP1, hIP2, hIP3 |
| Insula | Id1, Ig1, Ig2 |
| Auditory | TE1.0, TE1.1, TE1.2, TE3 |
| Temporal anterior | TSup Ant, TMidAnt, TInfAnt, TFusiAnt, TPole |
| Temporal posterior | TSupPost, TMidPost, TMidTempocc, TInfPost, TInfTempocc, TFusiPost, TOFusi |
| Early visual | V1, V2, V3A, V3d, V3v, V4v |
| Higher visual | V5, OLatSup, OLatInf |

Labelling of areas as introduced in Table 1.

**Table 3**
Statistics of connections between seeds and groups of targets.

| Group name | Main effect 'Seed' | Main effect 'Hemi' | Interaction 'Seed × Hemi' |
|---|---|---|---|
| Frontal | <0.001 | <0.001 | 0.004 |
| Broca | 0.003 | 0.002 | 0.005 |
| Motor | <0.001 | 0.700 | 0.013 |
| Primary somatosensory (SI) | <0.001 | 0.004 | 0.014 |
| Secondary somatosensory (SII) | <0.001 | 0.018 | 0.002 |
| Cingulate | <0.001 | 0.497 | 0.026 |
| Superior parietal | <0.001 | 0.444 | 0.002 |
| Intraparietal sulcus (IPS) | <0.001 | <0.001 | <0.001 |
| Insula | <0.001 | 0.192 | <0.001 |
| Auditory | <0.001 | 0.058 | 0.002 |
| Temporal anterior | <0.001 | 0.289 | 0.736 |
| Temporal posterior | <0.001 | <0.001 | 0.932 |
| Early visual | <0.001 | <0.001 | 0.951 |
| Higher visual | <0.001 | 0.010 | 0.178 |

Groups of areas as defined in Table 2. Values in the columns Main effect 'Seed', Main effect 'Hemi', and Interaction 'Seed × Hemi' denote the p-values of the repeated-measures ANOVA. Significant results for $p<0.001$ are marked in bold type. Hemi: Hemisphere.

connections to auditory and temporal areas (major weight of the fingerprint in upper right quadrant of polar plot; Figs. 7, 8). Between these two extremes, the connectivity fingerprints for areas PF, PFm, and PGa reflect a relatively continuous shift in connectivity patterns. In particular, the fingerprint of area PF, i.e., the area just caudal to PFt in rostral IPL, closely resembled that of the latter area. The fingerprint of area PFm in the centre of the IPL showed a balanced connectivity to the parietal-sensorimotor and the temporal group. The fingerprint of caudally adjacent area PGa already showed a preponderance of the upper right quadrant.

*Connections of IPL seed areas to anatomically- and functionally-defined target groups*

Entering the mean Z-scores across subjects into repeated-measures ANOVAs allowed for statistical confirmation of shift in predominant fibre tract patterns from rostral to caudal IPL seed areas (Fig. 9, Tables 2 and 3).

Targets were summarised into anatomically or functionally defined groups as follows. First, target areas within different anatomical brain regions were grouped together (frontal, parietal, occipital, temporal). Where meaningfully possible, groups were further subdivided with respect to functional systems (e.g. motor, primary and secondary somatosensory, early and higher visual, auditory) based on knowledge from neuroimaging, lesion data, and non-human primates. Such analysis for different groups of targets provided information about the involvement of the IPL seed areas in different functional systems. The connection likelihoods for each seed are displayed for each target individually in Supplementary Figs. S2–S5.

For all target groups, there was a significant main effect of factor "IPL seed" (Fig. 9), indicating that for each given target region connection likelihood was differentially expressed between the individual seed areas. This result thus statistically confirmed the above summary of the connectivity fingerprints (Figs. 7 and 8). While prefrontal areas showed a slight increase in connection likelihood from rostral to caudal IPL areas, Broca's region had highest fibre tract densities in the intermediate areas PF, PFm, and PGa, with lower connection likelihood to area PFt. Secondary (SII) and particularly primary (SI) somatosensory cortex, to the contrary, showed a pronounced decrease in fibre tract density from PFt to PGp (Fig. 9, first two rows). A similar, though less pronounced pattern was seen for the superior parietal cortex while the anterior intraparietal sulcus (Choi et al., 2006; Scheperjans et al., 2008a,b) featured an abrupt drop in connection likelihood from the anterior PF- to the posterior PG-areas.

The posterior insula (Kurth et al., 2010), in contrast, showed an increase in connection likelihood from rostral to caudal IPL seed areas. This pattern was even more pronounced for the auditory and temporal regions, which all showed a strong increase in fibre tract density from rostral to caudal IPL areas. In addition, it should be noted that the overall connection likelihood with the IPL is substantially higher for posterior temporal target areas as compared to the anterior temporal and auditory ones (Fig. 9, fourth row). Within the occipital lobe, two groups of areas could be differentiated: Early visual areas (V1–V4v) showed generally low connection likelihood with a slight decrease from rostral to caudal IPL areas whereas higher visual areas (on lateral occipital cortex up to V5) showed a pronounced increase in fibre tract density from rostral to caudal IPL areas (Fig. 9, last row).

## Discussion

The fibre tract patterns of five cytoarchitectonic areas on the lateral surface of the human inferior parietal lobule were assessed by means of probabilistic tractography. Connection likelihood was analysed by evaluating the number of traces reaching a particular target against those reaching other voxels in the same distance from the seed. Random-effects inference then delineated connections that were consistently (across subjects) expressed with higher than expected densities. Across IPL areas, most consistent connections existed with inferior frontal, posterior temporal and insular targets. Connectivity patterns, however, shifted gradually from rostral to caudal IPL areas. Whereas rostral areas featured most likely connections to somatosensory and superior parietal areas, more caudal areas were predominantly connected to the temporal lobe. Connectivity patterns of IPL areas favoured a left–right asymmetry with regard to different target areas of somatosensory, superior parietal (left hemisphere), and inferior frontal, orbito-frontal and temporal areas (right hemisphere).

*Methodological considerations*

Any kind of tractography study faces the problem of false positives or negatives due to limits in effective resolution, resulting in non-resolved crossing/kissing fibres. This can cause tractography traces to get absorbed into bigger fibre bundles like the superior longitudinal or arcuate fascicle (Ciccarelli et al., 2003; Klein et al., 2009). This problem is ameliorated by using probabilistic (instead of deterministic) tractography methods with crossing fibre models (Behrens et al., 2007). Moreover, tractography results are highly dependent on the distance between seed and target (Behrens et al., 2003a,b). This may already impair relative comparisons between individual results, the procedure currently most frequently used in tractography studies

(e.g. Behrens et al., 2003a; Rushworth et al., 2006; Uddin et al., 2010). More importantly, it makes inference about the relevance of a particular trace density for a given seed-target combination hardly possible. Thus, it is difficult to infer whether a particular observed trace-density is indeed indicative of a fibre connection between these two regions.

We aimed at addressing these two problems by the present algorithm by introducing a reference distribution of traces for each seed-target combination. The reference distribution was set depending on the distance between seed and target, thus accounting for the possible confounding factor "distance" within further analysis. Furthermore, this distribution provided a reference to evaluate each seed-target connection separately by testing if traces between seed and target were more consistently expressed (across subjects) than expected at the same distance from the seed. Thus, for each seed-target connection, we could evaluate if connection likelihood was consistently above chance.

Nevertheless, it still has to be emphasised that DTI does not provide information about anatomical connectivity sensu stricto, i.e. synaptic connectivity as revealed by invasive tracer studies in macaques, which will be discussed in the next section. Rather, this method assesses the presence and confidence about macroanatomical fibre bundles between seeds and targets.

By using probabilistic atlases for delineation of seed and target areas together with probabilistic tractograhpy, it was possible to stringently use probabilistic approaches throughout the current study. Like probabilistic tractography for fibre paths, probabilistic atlases accommodate inter-subject variability and hence allow inclusion of uncertainty estimates into the investigation. Combining two different probabilistic atlases of the human cerebral cortex (JHA

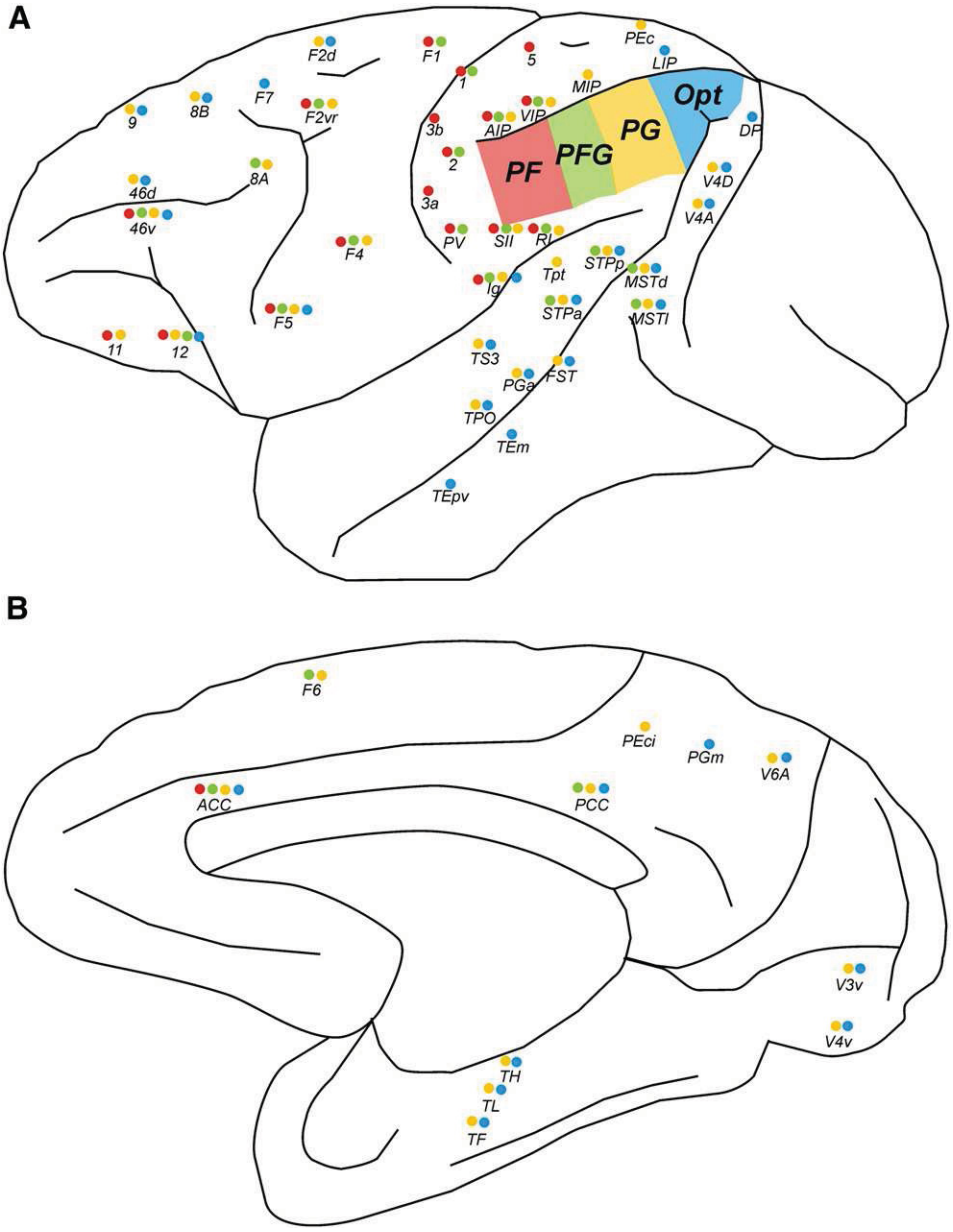


**Fig. 10.** Schematic drawings of (A) the lateral and (B) the mesial part of a macaque hemisphere, indicating those connections between the four lateral IPL areas and cortical targets that were found to be connected to either one the IPL areas. IPL areas are marked in four different colours: PF red, PFG green, PG yellow, Opt blue. Coloured dots beneath each target region indicate the presence of a connection to the respective seed region. Areas within the depth of a sulcus were placed along its rim to facilitate readability. Such depiction pertains to the following areas: areas Ig, and RI within the depth of the Sylvian fissure on the insular cortex; areas AIP, VIP, MIP, and LIP within the intraparietal sulcus; parts of areas 46v, and 46d within the depth of the principal sulcus; areas STPa, STPp, FST, MSTd, MSTl, TPO, TEm, and TEpv within the depth of the superior temporal sulcus. Connections depicted here were obtained from and named according to the relevant literature (cf. text) and by reference to the CoCoMac database (http://www.cocomac.org; Stephan et al., 2001).

and HCSA) allowed for whole brain coverage. Some regions, however, were covered in a more coarse fashion than others due to the current limitation of available atlases. For example, the middle and superior frontal gyrus were only covered by a single area each. Based on different parcellation schemes, it could be assumed that these two regions can at least be separated into areas 8, 9, and 46. As known from studies in macaques, these areas can be further subdivided, supporting the notion that a comparably fine-grained parcellation can be assumed for the human prefrontal cortex as well. Areas 46v, 46d, 8A, 8B, and 9 of the macaque prefrontal cortex show a differential connection pattern with the IPL areas (see discussion below). Thus, it can be assumed that such parcellation might yield a differential connectivity pattern also in humans. Our results may hence represent a first overview of the global connectivity patterns of inferior parietal areas rather than a fine-grained description of pre-frontal connections. By the time reliable information on a functionally relevant parcellation of the human prefrontal cortex will be available, future studies might add further insight into the patterns of anatomical connections between human prefrontal and inferior parietal areas.

It has to be further emphasised that our approach with definition of seed and target areas is different from the connectivity-based parcellation which aims at parcellation of a cortical region based on its connectivity pattern to every other voxel in the brain (Anwander et al., 2007; Behrens et al., 2003a; Eickhoff et al., 2011; Johansen-Berg et al., 2004) In these approaches, connectivity was assessed without a priori anatomical suppositions about potentially connected areas, thus allowing for an assumption-free investigation of brain connectivity. Our approach in turn is based on a priori knowledge on the location of cortical areas which limits the analysis to previously defined regions. Hua et al. (2009) described an approach which combined the ideas of both seed-target and connectivity-based parcellation approaches: First, they obtained overall probability distributions from all voxels inside the brain. In a second step, they drew regions of interest across the cortex. Each resulting trace of the first analysis was post-hoc assigned to one of the fibre tracts known to be connected with the respective region of interest which was passed by the tractography trace. Thus, Hua et al. (2009) also used a priori anatomical knowledge for definition of regions of interest. But in contrast to the approach of the present study, their regions of interest were not used as seed regions for tractography, but rather as targets through which existing tracts should go. Thus, they also identified those target regions which were reached by certain traces, but based on overall tract distributions within the brain. Conversely, we focused on traces which originated in different predefined seed regions.

### *Connectivity patterns of macaque IPL areas and homology considerations*

The overall pattern revealed by our results bears close resemblance to the axonal connection patterns found in tracer studies on macaques (Fig. 10), as both species showed a comparable rostro-caudal shift in preferential connectivity.

In macaques, rostral IPL areas mainly connected to (pre-) motor, inferior frontal, somatosensory, superior parietal and posterior temporal areas (Fig. 10). A similar pattern was found here for rostal human IPL areas PFt and PF, hinting at a possible homology between human areas PFt/PF and macaque areas PF/PFG, respectively. This is further supported by a recent tracing study (Petrides and Pandya, 2009) showing that macaque area PF is mainly connected to ventral premotor cortex (area 6v), whereas intermediate areas PFG and PG preferentially connected to areas 44 and 45. A similar pattern was found here for human IPL as rostral-most area PFt showed weaker connectivity to areas 44 and 45 than intermediate areas PF, PFm, and PGa (Fig. S2).

Caudal IPL areas in macaques showed connections to more dorsal parietal areas, the prefrontal cortex (in particular true for area PG) as well as numerous areas within the whole temporal lobe (in particular for Opt; Fig. 10). This pattern strongly resembled that of the two caudal-most areas of human IPL (areas PGa and PGp), suggesting a possible homology between human PGa/PGp and macaque PG/Opt, respectively.

Intermediate human IPL area PFm which does not have an obvious homologue in macaques showed characteristics of both rostral and caudal connection patterns. Interestingly, cytoarchitectonic features of this region also share characteristics of rostral and caudal IPL areas (Caspers et al., 2006). It may thus be speculated that this intermediate area in human IPL is a new evolutionary feature that may have derived from a more subtle subdivision of adjacent PFG or PG in the macaque IPL (Krubitzer, 2009). This view is further supported by recent evidence that especially central parts of the IPL may have evolved more pronouncedly in humans than other parts of the brain (Husain and Nachev, 2007; Rushworth et al., 2009; Simon et al., 2004).

Despite these congruencies, there are also notable differences in fibre tract patterns between human and macaque IPL, e.g. with respect to occipital connections. Whereas for macaques no connections between IPL and primary and secondary visual areas V1 and V2 were observed, the results of our present study suggest such fibre tracts in humans. Higher visual areas as V3 and V4 connect to caudal IPL areas in the macaque whereas in humans connections are also found with the more rostral IPL (e.g., for targets OLatSup, OLatInf). To provide a possible explanation for these differences, one has to consider several aspects.

It has been argued that the macaque visual system follows a rather strict hierarchy: While earlier visual areas such as V1 and V2 first project to higher extrastriate areas such as V3, V4, DP, and LIP, these areas in turn provide the relevant visually related connections with caudal IPL areas (Andersen et al., 1990). It might be assumed that a comparable hierarchical processing stream exists in humans, making the existence of any direct tract between early visual and IPL areas unlikely. This suspicion is strengthened by the notion that caudal rather than rostral IPL areas are primarily involved in visual processing (cf. Mountcastle et al., 1975; Hyvärinen, 1982 in macaques; e.g., Fink et al., 2001 in humans). On the other hand, however, a recent meta-analysis indicated that rostral IPL areas and higher visual areas are conjointly recruited by action observation (Caspers et al., 2010), matching the existence of mirror neurons in the rostral IPL of macaques (Rizzolatti, 2005). How such visual input reaches the rostral IPL, however, is still unclear. The present data suggest that connections from earlier visual areas may contribute to this functional interaction even though such connections have not yet been demonstrated in macaques. Such shortcuts may hold a particular relevance for the rapid, "on-line" processing of observed actions, in particular in the context of social interactions. The finding that not only mirror neurons, but also grasping neurons were found to be located within macaque area PFG (Rozzi et al., 2008) further supports this notion since grasping-related actions highly rely on visual input.

From a methodological perspective, however, one also has to consider the relative advantages and drawbacks of tracer studies (in macaques) and DTI. Whereas tracing methods reveal axonal connectivity and yield a high specificity, their sensitivity may be limited by the selection of injection sites and methods, incomplete tracer uptake or spread, unexpectedly slow transport (or to early sacrifice), the histological method used to detect the labelled brain sites and the (usual) lack of whole brain coverage (Köbbert et al., 2000; Stephan et al., 2001). In contrast, DTI is particularly prone to false positives due to limited resolution and limited specificity. This pertains in particular to the assimilation of traces into major fibre bundles that are a frequent source of false positive results. Independent of evolutionary differences, interpretation of the current finding thus faces the challenge that it is present in the more sensitive but distinctly less specific method but absent in the specific but somewhat less sensitive approach. In summary, we would thus cautiously suggest that

connections between visual areas and anterior IPL would be physiologically reasonable as a fast framework for action observation and may warrant further investigation by specifically targeted tracing experiments. Until such confirmation, however, the possibility of false positives in tractography has to be considered an at least equally likely scenario.

A similar argument pertains to the connections to the frontal pole found in the present study. For the macaque, it must remain tentative if such connections are indeed absent since review of the relevant literature (Petrides and Pandya, 1984; Cavada and Goldman-Rakic, 1989b; Andersen et al., 1990; Rozzi et al., 2006) together with information from the CoCoMac database did not provide final evidence about their presence or absence. Nevertheless, a recent study demonstrated nonexisting connections between IPL and anterior prefrontal regions in macaques (Petrides and Pandya, 2007). But it was also argued that in particular prefrontal cortex showed very strong expansion in the evolution from macaques to humans (Semendeferi et al., 2001). A comparable suggestion was raised for the IPL in humans as compared to macaques (Husain and Nachev, 2007; Simon et al., 2004), a concept which was particularly stressed for the central parts of IPL (see above; Rushworth et al., 2009). In a recent study, Mars et al. (2011) could show that the IPL, its central part in particular, was functionally connected with anterior prefrontal cortex whereas no such interaction was found in macaques. In the present study, we also found such connections between IPL areas and the frontal pole region which further supports these recent findings of resting-state functional connectivity and evolutionary considerations and provides evidence for a direct anatomical connection between these two cortical regions.

With regard to other prefrontal regions, the current study is certainly limited by the lack of reliable target regions. This limits the comparison to a juxtaposition of the connections of the 'superior frontal gyrus' target with a summary of results for macaque areas 8 and 9. Whereas all but the rostral-most IPL area were found to connect with the superior frontal gyrus, mainly caudal areas of the macaque IPL seemed to project to superior frontal areas 8B and 9. Likewise, for the middle frontal gyrus, the present human data mainly fit the macaque data of target areas 46d and 8A, but not area 46v. In both cases, we would resort to caution regarding evolutionary interpretations, since no reliable more fine-grained and functionally relevant parcellation of human prefrontal cortex is currently available. The issue of prefrontal connections of IPL areas thus warrants further investigation once such information becomes available in humans.

On a more general note, our results again highlight the difficulty of establishing inter-species differences in the concurrent presence of diverging methods and potential evolutionary changes. One approach to address this problem is to use the same method (DTI) in both species, as done in studies on the arcuate fasciculus (Rilling et al., 2008), prefrontal-cerebellar circuits (Ramnani et al., 2006), and prefrontal connections (Croxson et al., 2005). The studies show good agreement between human and macaque DTI data, but point to considerable inter-species differences in connectivity patterns even when using a comparable method. On the other hand, Dyrby et al. (2007) and Schmahmann et al. (2007) demonstrated that while many connections obtained from invasive tracing methods could also be replicated by means of DTI tractography in the same animal, others could not. Are thus all differences between humans and primates related to limitations of one (or both) technique? We would argue against this view, since evolutionary effects that result in the evident differences between macaque and man also warrant consideration. While humans share many aspects of cortical organisation with non-human primates, uniquely human features may not be neglected (Finlay et al., 2001; Kaas, 2006; Kaas and Preuss, 2003; Striedter, 2005). This may hold true particularly for the regions showing the most pronounced differences as discussed above, the prefrontal cortex (which is vastly expanded and presumably re-organised in humans, cf. Semendeferi et al., 2001) and the occipital lobe, which also has a considerable differential morphology in humans and macaques due to different importance of the visual system in these two species. While primary visual cortex (V1) in macaques occupies a major part of the lateral occipital cortex, the same region in humans is mainly located on the mesial surface within the calcarine sulcus. The same holds true for the extrastriate visual areas V2–V5 which in the macaque are located within the lunate sulcus and on the prelunate gyrus, bringing them close to the caudal end of the IPL (Kaas, 2006; Ungerleider and Haxby, 1994), whereas in humans these areas are located more caudo-ventrally (ventral visual stream) and caudo-dorsally (dorsal visual stream) (Amunts et al., 2000; Malikovic et al., 2007; Rottschy et al., 2007). Finally, differential connectivity pattern of comparable regions may also result from differential cortical structure and folding patterns as white matter tracts had to adapt to the gross morphological differences as well (Kaas, 2000).

Considering these potential pitfalls when comparing connectivity patterns of humans and macaques, it seems even more important to take a systems perspective and use a large number of target areas to establish connectivity profiles of several seed areas. Such an approach provides a complementary approach to the connectivity-based parcellation used by Mars et al. (2011). Using the present approach of predefined seed and target areas, we could show that connectivity of human IPL areas shifted gradually from rostral to caudal. We thus amended the findings of Mars et al. (2011) who demonstrated that a similar parcellation of the IPL as based on cytoarchitecture (Caspers et al., 2006, 2008) was possible by means of DTI. Within the present study, we could elucidate how these assumed differences manifested with regard to differential connections to numerous target areas. Furthermore, we could show, in spite of the discussed differences that a similar connection pattern as in macaques (Gregoriou et al., 2006; Rozzi et al., 2006) also existed in humans. This supported the notion of a differential involvement of IPL areas in functional cortical networks which was already assumed based on electrophysiological recordings from different parts of macaque IPL (Hyvärinen, 1982; Mountcastle et al., 1975; Seltzer and Pandya, 1984).

### *Relation to functional segregation*

The potential human mirror neuron system has received particular interest in the study of IPL functions (Rizzolatti and Craighero, 2004; Iacoboni, 2005; Keysers and Gazzola, 2009). In a recent meta-analysis, it was shown that particularly the rostral-most area PFt was strongly engaged in action observation and imitation (Caspers et al., 2010). In these tasks, PFt co-activated with a region in the caudal-most aspect of ventral premotor cortex (vPMC) (comparable to the macaque mirror neuron system; Rizzolatti, 2005). This view is supported by human DTI studies highlighting vPMC to rostral IPL connections (Rushworth et al., 2006; Tomassini et al., 2007) and a study by Kelly et al. (2010) on resting-state co-activation pattern of Broca's region, and more specifically by a recent macaque study of Petrides and Pandya (2009) showing differential connections from rostral IPL to different vPMC areas. PFt furthermore co-activated with SI, superior parietal and posterior temporal regions. The present study demonstrated that indeed rostral IPL areas showed consistent connections with Broca's region. But more importantly, area PFt also showed consistent anatomical connections with SI, superior and intraparietal, and posterior temporal areas. We would thus argue that these fibre tracts represent the structural scaffold for the previously described functional "mirror neuron" network (Caspers et al., 2010). This notion is further supported by the lateralization structure of the connections of rostral IPL: connections with sensorimotor regions were more consistently found in the left as compared to the right hemisphere in the present study. For the potential human mirror neuron network, it was argued that such higher motor functions would likely be assumed

to be supported by a bilateral network of brain areas (Iacoboni and Dapretto, 2006) which was supported by a recent meta-analysis (Caspers et al., 2010). But there have also been findings of a functional left-lateralization within this network (Rizzolatti and Arbib, 1998; Aziz-Zadeh et al., 2004). Based on the results of the present study, we would argue that the connections between rostral IPL and areas relevant within this potential mirror neuron network are more consistently expressed within the left hemisphere. It has to be noted that all our subjects were right-handed, thus introducing a potential bias towards the contralateral left hemisphere for any sensorimotor processing. It has furthermore to be stressed that mirror-related activity within IPL may also exhibit a right-lateralization, depending on the task demands (Biermann-Ruben et al., 2008). Such overriding of a potentially present general leftward-lateralization was in particular observed in the context of emotion-processing (Carr et al., 2003). Thus, it might be speculated that the predominance of left hemispheric anatomical connections as found in the present study only partially account for functional phenomena within the potential human mirror-neuron network. Findings of bilateral or right-lateralized activations within IPL might demonstrate that functional demands and the specific experimental context might be at least as important in determining functional recruitment as the structural basis of anatomical connections.

Within the language network, areas of the (left) caudal IPL, corresponding to Geschwind's area (Geschwind, 1970), have been related to semantic and phonological processing, especially during reading (Price, 2000; Vigneau et al., 2006). Presumably, the main fibre pathway connecting Broca's, Geschwind's, and Wernicke's area is the arcuate fasciculus (Catani et al., 2005; Parker et al., 2005; Frey et al., 2008; Saur et al., 2008). These studies also demonstrated an additional ventral fibre system via the external or extreme capsule. The present study showed that particularly PGa and PGp are connected to Broca's region via this ventral route.

Overall, all IPL areas showed quite consistent connections with Broca's region. This finding suggested that language-related functions might involve different parts of the IPL, specialised for different language-related aspects. With regard to the potential human mirror-neuron system within rostral IPL, these consistent connections to Broca's region might be regarded as evidence for the assumed relation between the mirror neurons and the development of language (Rizzolatti and Arbib, 1998). Within the IPL, more caudal areas might relate to reading aspects (Price, 2000), which would be supported by the current finding of additional visual input to these areas. Their connection to Broca's region and temporal though not auditory cortex furthermore point to an involvement in vocalisation (Catani et al., 2005; Saur et al., 2008). Moreover, PGp showed consistent connection patterns with auditory areas. It may thus represent the key IPL node for auditory language processing, a view supported by functional studies (Price, 2000; Saur et al., 2008). With respect to a hemispheric asymmetry of connectivity of these two caudal IPL areas, the present study revealed higher likelihood of connections to auditory, higher visual, and frontal opercular areas in the left hemisphere. It might be speculated how such connection pattern especially within the left hemisphere might relate to language functions. Geschwind (1965, 1970) not only highlighted the aspect of reading to be located within rostral parts of the angular gyrus, but furthermore stressed that this left IPL hub would integrate visual and auditory word forms to generate speech (Price, 2000). In functional studies, it became evident that some aspects of the semantic processing network were modality specific, thus having an auditory (auditory cortex) and a visual component (higher visual areas, inferior posterior temporal cortex). These earlier areas were found to be involved in either semantic or phonological processing (Vigneau et al., 2006). The predominant connections to both auditory and higher visual areas in the left hemisphere, as found in the present study, might support the notion that these areas integrate these different modalities for semantic or phonological processing, independent from input modality.

But the leftward asymmetry of connections of the caudal IPL areas also comprises connections to superior parietal and intraparietal areas. These latter areas have consistently been implicated in number magnitude processing. During more complex processing steps such as calculation, the left caudal IPL is strongly involved as well (Dehaene et al., 1998; Fias et al., 2003; Nieder, 2005; Ansari, 2008; Dehaene, 2009). With the predominance of left hemispheric connections to the intraparietal and superior parietal areas found in the present study, caudal IPL area PGa might reflect the relevant part of the angular gyrus which is involved in number processing. The respective underlying fibre tracts provide the anatomical basis for a close communication pathway between these areas, with a potential link to the language system with vocalisation of the numbers (see above).

Areas of right IPL are part of the ventral attention network as proposed by Corbetta and Shulman (2002, 2008). This network involves IPL, posterior temporal and inferior/middle frontal areas. Within the IPL, damage to areas close to the temporo-parietal junction (TPJ) is associated with the emergence of spatial neglect (Hillis, 2006). This would presumably match the location of areas PFm and PGa. In the present study, it could be shown that these areas featured consistent connections to posterior temporal and inferior frontal areas (like the other IPL areas), but particularly also to middle frontal cortex. Based on this fibre tract pattern which matches the co-activation pattern of respective functional studies (Corbetta and Shulman, 2002; Corbetta et al., 2008), it can be assumed that especially areas PFm and PGa play an important role in the ventral attention network, possibly in combination with caudal most area PGp. Further strong connections existed with lateral superior and intraparietal areas, providing a possible link to the dorsal part of the attention network (Corbetta and Shulman, 2002). Besides some remarks on a possible bilateral distribution of this network, especially the ventral attention network was most consistently found in the right hemisphere. Taking into account the right lateralization of consistent fibre tracts from these caudal IPL areas to posterior temporal, temporo-occipital and inferior frontal areas, the present study might provide the potential anatomical connectional basis of how the areas of the ventral attention network might interact. Based on the fibre connections found to be dominant in the right hemisphere, it seems reasonable to assume that information between posterior temporal and inferior frontal regions are transported via caudal IPL. The right hemisphere analogue of the arcuate fasciculus of the left hemisphere might provide the necessary pathways here.

The good agreement between anatomical fibre tract patterns of IPL areas and their possible functional roles provides strong evidence for their differential involvement in specific neural networks. The investigation of the functional and potentially context-specific relevance of these connections as revealed by effective connectivity analyses represents an important topic for future studies on connectivity of human IPL.

Supplementary materials related to this article can be found online at doi:10.1016/j.neuroimage.2011.06.027.

## Acknowledgments

This Human Brain Project/Neuroinformatics Research was funded by the National Institute of Biomedical Imaging and Bioengeneering, the National Institute of Neurological Disorders and Stroke and the National Institute of Mental Health (KZ). Further funding was granted by the Human Brain Project (R01-MH074457-01A1; SBE), the Initiative and Networking Fund of the Helmholtz Association within the Helmholtz Alliance on Systems Biology (Human Brain Model; KZ, SBE), and the Helmholtz Alliance for Mental Health in an Aging Society (HelMA; KZ).

## References


Amunts, K., Schleicher, A., Bürgel, U., Mohlberg, H., Uylings, H.B.M., Zilles, K., 1999. Broca's region revisited: cytoarchitecture and intersubject variability. J. Comp. Neurol. 412, 319–341.

Amunts, K., Malikovic, A., Mohlberg, H., Schormann, T., Zilles, K., 2000. Brodmann's areas 17 and 18 brought into stereotaxic space – where and how variable? Neuroimage 11, 66–84.

Andersen, R.A., Asanuma, C., Essick, G., Siegel, R.M., 1990. Corticocortical connections of anatomically and physiologically defined subdivisions within the inferior parietal lobule. J. Comp. Neurol. 296, 65–113.

Ansari, D., 2008. Effects of development and enculturation on number representation in the brain. Nat. Rev. Neurosci. 9, 278–291.

Anwander, A., Tittgemeyer, M., von Cramon, D.Y., Friederici, A.D., Knösche, T.R., 2007. Connectivity-based parcellation of Broca's area. Cereb. Cortex 17 (4), 816–825.

Ashburner, J., Friston, K.J., 2005. Unified segmentation. Neuroimage 26, 839–851.

Aziz-Zadeh, L., Iacoboni, M., Zaidel, E., Wilson, S., Mazziotta, J., 2004. Left hemisphere motor facilitation in response to manual action sounds. Eur. J. Neurosci. 19, 2609–2612.

Behrens, T.E., Johansen-Berg, H., Woolrich, M.W., Smith, S.M., Wheeler-Kingshott, C.A.M., Boulby, P.A., Barker, G.J., Sillery, E.L., Sheehan, K., Ciccarelli, O., Thompson, A.J., Brady, J.M., Matthews, P.M., 2003a. Non-invasive mapping of connections between human thalamus and cortex using diffusion imaging. Nat. Neurosci. 6 (7), 750–757.

Behrens, T.E., Woolrich, M.W., Jenkinson, M., Johansen-Berg, H., Nunes, R.G., Clare, S., Matthews, P.M., Brady, J.M., Smith, S.M., 2003b. Characterization and propagation of uncertainty in diffusion-weighted MR imaging. Magn. Reson. Med. 50, 1077–1088.

Behrens, T.E., Johansen-Berg, H., Jbabdi, S., Rushworth, M.F., Woolrich, M.W., 2007. Probabilistic diffusion tractography with multiple fibre orientations: What can we gain? Neuroimage 34 (1), 144–155.

Biermann-Ruben, K., Kessler, K., Jonas, M., Siebner, H.M., Bäumer, T., Münchau, A., Schnitzler, A., 2008. Right hemisphere contributions to imitation tasks. Eur. J. Neurosci. 27, 1843–1855.

Carr, L., Iacoboni, M., Dubeau, M.C., Mazziotta, J.C., Lenzi, G.L., 2003. Neural mechanisms of empathy in humans: a relay from neural systems for imitation to limbic areas. Proc. Natl. Acad. Sci. U. S. A. 100 (9), 5497–5502.

Caspers, S., Geyer, S., Schleicher, A., Mohlberg, H., Amunts, K., Zilles, K., 2006. The human inferior parietal cortex: cytoarchitectonic parcellation and interindividual variability. Neuroimage 33 (2), 430–448.

Caspers, S., Eickhoff, S.B., Geyer, S., Scheperjans, F., Mohlberg, H., Zilles, K., Amunts, K., 2008. The human inferior parietal lobule in stereotaxic space. Brain Struct. Funct. 212, 481–495.

Caspers, S., Zilles, K., Laird, A.R., Eickhoff, S.B., 2010. ALE meta-analysis of action observation and imitation in the human brain. Neuroimage 50, 1148–1167.

Catani, M., Jones, D.K., ffytche, D.H., 2005. Perisylvian language networks of the human brain. Ann. Neurol. 57, 8–16.

Cavada, C., Goldman-Rakic, P.S., 1989a. Posterior parietal cortex in rhesus monkey: I. Parcellation of areas based on distinctive limbic and sensory corticocortical connections. J. Comp. Neurol. 287, 393–421.

Cavada, C., Goldman-Rakic, P.S., 1989b. Posterior parietal cortex in rhesus monkey: II. Evidence of segregated corticocortical networks linking sensory and limbic areas with the frontal lobe. J. Comp. Neurol. 287, 422–445.

Choi, H.J., Zilles, K., Mohlberg, H., Schleicher, A., Fink, G.R., Armstrong, E., Amunts, K., 2006. Cytoarchitectonic identification and probabilistic mapping of two distinct areas within the anterior ventral bank of the human intraparietal sulcus. J. Comp. Neurol. 495 (1), 53–69.

Ciccarelli, O., Parker, G.J., Toosy, A.T., Wheeler-Kingshott, C.A., Barker, G.J., Boulby, P.A., Miller, D.H., Thompson, A.J., 2003. From diffusion tractography to quantitative white matter tract measures: a reproducibility study. Neuroimage 18 (2), 348–359.

Corbetta, M., Shulman, G.L., 2002. Control of goal-directed and stimulus-driven attention in the brain. Nat. Rev. Neurosci. 3 (3), 201–215.

Corbetta, M., Patel, G., Shulman, G.L., 2008. The reorienting system of the human brain: from environment to theory of mind. Neuron 58, 306–324.

Croxson, P.L., Johansen-Berg, H., Behrens, T.E.J., Robson, M.D., Pinsk, M.A., Gross, C.G., Richter, W., Richter, M.C., Kastner, S., Rushworth, M.F.S., 2005. Quantitative investigation of connections of the prefrontal cortex in the human and macaque using probabilistic diffusion tractography. J. Neurosci. 25 (39), 8854–8866.

Culham, J.C., Valyear, K.F., 2006. Human parietal cortex in action. Curr. Opin. Neurobiol. 16, 205–212.

Dehaene, S., 2009. Origins of mathematical intuition. The case of arithmetic. Ann. N. Y. Acad. Sci. 1156, 232–259.

Dehaene, S., Dehaene-Lambertz, G., Cohen, L., 1998. Abstract representations of numbers in the animal and human brain. Trends Neurosci. 21 (8), 355–361.

Dronkers, N.F., Wilkins, D.P., van Valin, R.D., Redfern, B.B., Jaeger, J.J., 2004. Lesion analysis of the brain areas involved in language comprehension. Cognition 92, 145–177.

Dyrby, T.B., Sogaard, L.V., Parker, G.J., Alexander, D.C., Lind, N.M., Baaré, W.F., Hay-Schmidt, A., Eriksen, N., Pakkenberg, B., Paulson, O.B., Jelsing, J., 2007. Validation of in vitro probabilistic tractography. Neuroimage 37 (4), 1267–1277.

Eickhoff, S.B., Stephan, K.E., Mohlberg, H., Grefkes, C., Fink, G.R., Amunts, K., Zilles, K., 2005. A new SPM toolbox for combining probabilistic cytoarchitectonic maps and functional imaging data. Neuroimage 25 (4), 1325–1335.

Eickhoff, S.B., Amunts, K., Mohlberg, H., Zilles, K., 2006a. The human parietal operculum. II. Stereotaxic maps and correlation with functional imaging results. Cereb. Cortex 16, 268–279.

Eickhoff, S.B., Heim, S., Zilles, K., Amunts, K., 2006b. Testing anatomically specified hypotheses in functional imaging studies using cytoarchitectonic maps. Neuroimage 32, 570–582.

Eickhoff, S.B., Schleicher, A., Zilles, K., Amunts, K., 2006c. The human parietal operculum. I. Cytoarchitectonic mapping of subdivisions. Cereb. Cortex 16, 254–267.

Eickhoff, S.B., Jbabdi, S., Caspers, S., Laird, A.R., Fox, P.T., Zilles, K., Behrens, T.E.J., 2010. Anatomical and functional connectivity of cytoarchitectonic areas within the human parietal operculum. J. Neurosci. 30 (18), 6409–6421.

Eickhoff, S.B., Bzdok, D., Laird, A.R., Roski, C., Caspers, S., Zilles, K., Fox, P.T., 2011. Co-activation patterns distinguish cortical modules, their connectivity and functional differentiation. NeuroImage 57, 938–949.

Felleman, D.J., Van Essen, D.C., 1991. Distributed hierarchical processing in the primate cerebral cortex. Cereb. Cortex 1, 1–47.

Fias, W., Lammertyn, J., Reynvoet, B., Dupont, P., Orban, G.A., 2003. Parietal representation of symbolic and nonsymbolic magnitude. J. Cogn. Neurosci. 15 (1), 47–56.

Fink, G.R., Marshall, J.C., Weiss, P.H., Zilles, K., 2001. The neural basis of vertical and horizontal line bisection judgements: an fMRI study of normal volunteers. Neuroimage 14, 59–67.

Finlay, B.L., Darlington, R.B., Nicastro, N., 2001. Developmental structure in brain evolution. Behav. Brain Sci. 24, 263–308.

Freund, H.J., 2003. Somatosensory and motor disturbances in patients with parietal lobe lesions. Adv. Neurol. 93, 179–193.

Frey, S., Campbell, J.S.W., Pike, G.B., Petrides, M., 2008. Dissociating the human language pathways with high angular resolution diffusion fiber tractography. J. Neurosci. 28 (45), 11435–11444.

Gernsbacher, M.A., Kaschak, M.P., 2003. Neuroimaging studies of language production and comprehension. Annu. Rev. Psychol. 54, 91–114.

Geschwind, N., 1965. Disconnection syndromes in animals and man. Brain 88, 237–294.

Geschwind, N., 1970. The organization of language and the brain. Science 170, 940–944.

Geyer, S., 2004. The microstructural border between the motor and the cognitive domain in the human cerebral cortex. Advances in anatomy, embryology, and cell biology, vol. 174. Springer, Berlin.

Geyer, S., Ledberg, A., Schleicher, A., Kinomura, S., Schormann, T., Bürgel, U., Klingberg, T., Larsson, J., Zilles, K., Roland, P.E., 1996. Two different areas within the primary motor cortex of man. Nature 382, 805–807.

Geyer, S., Schleicher, A., Zilles, K., 1999. Areas 3a, 3b, and 1 of human primary somatosensory cortex: 1. Microstructural organization and interindividual variability. Neuroimage 10, 63–83.

Geyer, S., Schormann, T., Mohlberg, H., Zilles, K., 2000. Areas 3a, 3b, and 1 of human primary somatosensory cortex. Part 2: spatial normalization to standard anatomical space. Neuroimage 11, 684–696.

Grefkes, C., Geyer, S., Schormann, T., Roland, P., Zilles, K., 2001. Human somatosensory area 2: observer-independent cytoarchitectonic mapping, interindividual variability, and population map. Neuroimage 14, 617–631.

Gregoriou, G.G., Borra, E., Matelli, M., Luppino, G., 2006. Architectonic organization of the inferior parietal convexity of the macaque monkey. J. Comp. Neurol. 496, 422–451.

Hillis, A.E., 2006. Neurobiology of unilateral spatial neglect. Neuroscientist 12, 153–163.

Hua, K., Oishi, K., Zhang, J., Wakana, S., Yoshioka, T., Zhang, W., Akhter, K.D., Li, X., Huang, H., Jiang, H., van Zijl, P., Mori, S., 2009. Mapping of functional areas in the human cortex based on connectivity through association fibres. Cereb. Cortex 19, 1889–1895.

Husain, M., Nachev, P., 2007. Space and the parietal cortex. Trends Cogn. Sci. 42, 766–773.

Hyvärinen, J., 1982. Posterior parietal lobe of the primate brain. Physiol. Rev. 62, 1060–1129.

Iacoboni, M., 2005. Neural mechanisms of imitation. Curr. Opin. Neurobiol. 15, 632–637.

Iacoboni, M., Dapretto, M., 2006. The mirror neuron system and the consequences of its dysfunction. Nat. Rev. Neurosci. 7, 942–951.

Jakobs, O., Wang, L.E., Dafotakis, M., Grefkes, C., Zilles, K., Eickhoff, S.B., 2009. Effects of timing and movement uncertainty implicate the temporo-parietal junction in the prediction of forthcoming motor actions. NeuroImage 47 (2), 667–677.

Johansen-Berg, H., Behrens, T.E., Robson, M.D., Drobnjak, I., Rushworth, M.F., Brady, J.M., Smith, S.M., Higham, D.J., Matthews, P.M., 2004. Changes in connectivity profiles define functionally distinct regions in human medial prefrontal cortex. Proc. Natl. Acad. Sci. U. S. A. 101 (36), 13335–13340.

Jones, D.K., Simmons, A., Williams, S.C., Horsfield, M.A., 1999. Non-invasive assessment of axonal fiber connectivity in the human brain via diffusion tensor MRI. Magn. Reson. Med. 42, 37–41.

Kaas, J.H., 2000. Why is brain size so important: design problems and solutions as neocortex gets bigger and smaller. Brain Mind 1, 7–23.

Kaas, J.H., 2006. Evolution of the neocortex. Curr. Biol. 16 (21), R910–R914.

Kaas, J.H., Preuss, T.M., 2003. Human brain evolution, In: Squire, L.R. (Ed.), Fundamental Neuroscience, 2nd ed. Elsevier, pp. 1147–1166.

Karnath, H.O., 2001. New insights into the functions of the superior temporal cortex. Nat. Rev. Neurosci. 2, 568–576.

Kelly, C., Uddin, L.Q., Shehzad, Z., Margulies, D.S., Castellanos, F.X., Milham, M.P., Petrides, M., 2010. Broca's region: linking human brain functional connectivity data and non-human primate tracing anatomy studies. Eur. J. Neurosci. 32 (3), 383–398.

Keysers, C., Gazzola, V., 2009. Expanding the mirror: vicarious activity for actions, emotions, and sensations. Curr. Opin. Neurobiol. 19, 666–671.

Klein, J.C., Behrens, T.E.J., Johansen-Berg, H., 2009. Connectivity fingerprinting of gray matter. In: Johansen-Berg, H., Behrens, T.E.J. (Eds.), Diffusion MRI — From Quantitative Measurement to In vivo Neuroanatomy. Academic Press, San Diego, pp. 377–402.

Köbbert, C., Apps, R., Bechmann, I., Lanciego, J.L., Mey, J., Thanos, S., 2000. Current concepts in neuroanatomical tracing. Prog. Neurobiol. 62, 327–351.

Krubitzer, L., 2009. In search of a unifying theory of complex brain evolution. Ann. N. Y. Acad. Sci. 1156, 44–67.

Kurth, F., Eickhoff, S.B., Schleicher, A., Hoemke, L., Zilles, K., Amunts, K., 2010. Cytoarchitecture and probabilistic maps of the human posterior insular cortex. Cereb. Cortex 20 (6), 1448–1461.
Lewis, J.W., Van Essen, D.C., 2000. Corticocortical connections of visual, sensorimotor, and multimodal processing areas in the parietal lobe of the macaque monkey. J. Comp. Neurol. 428, 112–137.
Luppino, G., Matelli, M., Camarda, R., Rizzolatti, G., 1993. Corticocortical connections of area F3 (SMA-proper) and area F6 (pre-SMA) in the macaque monkey. J. Comp. Neurol. 338, 114–140.
Makris, N., Kennedy, D.N., McInerney, S., Sorensen, A.G., Wang, R., Caviness Jr., V.S., Pandya, D.N., 2005. Segmentation of subcomponents within the superior longitudinal fascicle in humans: a quantitative, in vivo, DT-MRI study. Cereb. Cortex 15 (6), 854–869.
Malikovic, A., Amunts, K., Schleicher, A., Mohlberg, H., Eickhoff, S.B., Wilms, M., Palomero-Gallagher, N., Armstrong, E., Zilles, K., 2007. Cytoarchitectonic analysis of the human extrastriate cortex in the region of V5/MT+: a probabilistic, stereotaxic map of area hOc5. Cereb. Cortex 17 (3), 562–574.
Mars, R.B., Jbabdi, S., Sallet, J., O'Reilly, J.X., Croxson, P.L., Olivier, E., Noonan, M.P., Bergmann, C., Mitchell, A.S., Baxter, M.G., Behrens, T.E.J., Johansen-Berg, H., Tomassini, V., Miller, K.L., Rushworth, M.F.S., 2011. Diffusion-weighted imaging tractography-based parcellation of the human parietal cortex and comparison with human and macaque resting-state functional connectivity. J. Neurosci. 31 (11), 4087–4100.
Matelli, M., Luppino, G., 2001. Parietofrontal circuits for action and space perception in the macaque monkey. Neuroimage 14, S27–S32.
Morosan, P., Rademacher, J., Schleicher, A., Amunts, K., Schormann, T., Zilles, K., 2001. Human primary auditory cortex: cytoarchitectonic subdivisions and mapping into a spatial reference system. Neuroimage 13 (4), 684–701.
Mountcastle, V.B., Lynch, J.C., Georgopoulos, A., Sakata, H., Acuna, C., 1975. Posterior parietal association cortex of the monkey: command functions for operations within extrapersonal space. J. Neurophysiol. 38, 871–908.
Neal, J.W., Pearson, R.C.A., Powell, T.P.S., 1990a. The ipsilateral cortico-cortical connections of area 7b, PF, in the parietal and temporal lobes of the monkey. Brain Res. 524, 119–132.
Neal, J.W., Pearson, R.C.A., Powell, T.P.S., 1990b. The connections of area PG, 7a, with cortex in the parietal, occipital, and temporal lobes of the monkey. Brain Res. 532, 249–264.
Nieder, A., 2005. Counting on neurons: the neurobiology of numerical competence. Nat. Rev. Neurosci. 6, 177–190.
Pandya, D.N., Seltzer, B., 1982. Intrinsic connections and architectonics of posterior parietal cortex in the rhesus monkey. J. Comp. Neurol. 204, 196–210.
Parker, G.J.M., Luzzi, S., Alexander, D.C., Wheeler-Kingshott, C.A.M., Ciccarelli, O., Lambon Ralph, M.A., 2005. Lateralization of ventral and dorsal auditory-language pathways in the human brain. Neuroimage 24, 656–666.
Passingham, R.E., Stephan, K.E., Kötter, R., 2002. The anatomical basis of functional localization in the cortex. Nat. Rev. Neurosci. 3 (8), 606–616.
Petrides, M., Pandya, D.N., 1984. Projections to the frontal cortex from the posterior parietal region in the rhesus monkey. J. Comp. Neurol. 228, 105–116.
Petrides, M., Pandya, D.N., 2007. Efferent association pathways from the rostral prefrontal cortex in the macaque monkey. J. Neurosci. 27, 11573–11586.
Petrides, M., Pandya, D.N., 2009. Distinct parietal and temporal pathways to the homologues of Broca's area in the monkey. PLoS Biol. 7 (8), e1000170.
Price, C.J., 2000. The anatomy of language: contributions from functional neuroimaging. J. Anat. 197, 335–359.
Ramnani, N., Behrens, T.E., Johansen-Berg, H., Richter, M.C., Pinsk, M.A., Andersson, J.L., Rudebeck, P., Ciccarelli, O., Richter, W., Thompson, A.J., Gross, C.G., Robson, M.D., Kastner, S., Matthews, P.M., 2006. The evolution of prefrontal inputs to the cortico-pontine system: diffusion imaging evidence from macaque monkeys and humans. Cereb. Cortex 16 (6), 811–818.
Rilling, J.K., Glasser, M.F., Preuss, T.M., Ma, X., Zhao, T., Hu, X., Behrens, T.E.J., 2008. The evolution of the arcuate fasciculus revealed with comparative DTI. Nat. Neurosci. 11 (4), 426–428.
Rizzolatti, G., 2005. The mirror neuron system and its function in humans. Anat. Embryol. 210 (5–6), 419–421.
Rizzolatti, G., Arbib, M.A., 1998. Language within our grasp. Trends Neurosci. 21 (5), 188–194.
Rizzolatti, G., Craighero, L., 2004. The mirror-neuron system. Annu. Rev. Neurosci. 27, 169–192.
Rottschy, C., Eickhoff, S.B., Schleicher, A., Mohlberg, H., Kújovic, M., Zilles, K., Amunts, K., 2007. The ventral visual cortex in humans: cytoarchitectonic mapping of two extrastriate areas. Hum. Brain Mapp. 28 (10), 1045–1059.
Rozzi, S., Calzavara, R., Belmalih, A., Borra, E., Gregoriou, G.G., Matelli, M., Luppino, G., 2006. Cortical connections of the inferior parietal cortical convexity of the macaque monkey. Cereb. Cortex 16 (10), 1389–1417.
Rozzi, S., Ferrari, P.F., Bonini, L., Rizzolatti, G., Fogassi, L., 2008. Functional organization of inferior parietal lobule convexity in the macaque monkey: electrophysiological characterization of motor, sensory and mirror responses and their correlation with cytoarchitectonic areas. Eur. J. Neurosci. 28 (8), 1569–1588.
Rushworth, M.F.S., Behrens, T.E.J., Johansen-Berg, H., 2006. Connection patterns distinguish 3 regions of human parietal cortex. Cereb. Cortex 16, 1418–1430.
Rushworth, M.F.S., Boorman, E., Mars, R.B., 2009. Comparing brain connections in different species using diffusion weighted imaging. In: Johansen-Berg, H., Behrens, T.E.J. (Eds.), Diffusion MRI. : From Quantitative Measurement to In vivo Neuroanatomy. Academic Press, Amsterdam, pp. 445–460.
Saur, D., Kreher, B.W., Schnell, S., Kümmerer, D., Kellmeyer, P., Vry, M.S., Umarova, R., Musso, M., Glauche, V., Abel, S., Huber Rijntjes, M., Hennig, J., Weiller, C., 2008. Ventral and dorsal pathways for language. PNAS 105 (46), 18035–18040.
Scheperjans, F., Eickhoff, S.B., Hömke, L., Mohlberg, H., Hermann, K., Amunts, K., Zilles, K., 2008a. Probabilistic maps, morphometry, and variability of cytoarchitectonic areas in the human superior parietal cortex. Cereb. Cortex 18 (9), 2141–2157.
Scheperjans, F., Hermann, K., Eickhoff, S.B., Amunts, K., Schleicher, A., Zilles, K., 2008b. Observer-independent cytoarchitectonic mapping of the human superior parietal cortex. Cereb. Cortex 18 (4), 846–867.
Schmahmann, J.D., Pandya, D.N., 2006. Fiber Pathways of the Brain. Oxford University Press, Oxford.
Schmahmann, J.D., Pandya, D.N., Wang, R., Dai, G., D'Arceuil, H.E., de Crespigny, A.J., Wedeen, V.J., 2007. Association fibre pathways of the brain: parallel observations from diffusion spectrum imaging and autoradiography. Brain 130, 630–653.
Seltzer, B., Pandya, D.N., 1984. Further observations on parieto-temporal connections in the rhesus monkey. Exp. Brain Res. 55, 301–312.
Semendeferi, K., Armstrong, E., Schleicher, A., Zilles, K., Van Hoesen, G.W., 2001. Prefrontal cortex in humans and apes: a comparative study of area 10. Am. J. Phys. Anthropol. 114, 224–241.
Simon, O., Kherif, F., Flandin, G., Poline, J.B., Rivière, D., Mangin, J.F., Le Bihan, D., Dehaene, S., 2004. Automatized clustering and functional geometry of human parietofrontal networks for language, space, and number. Neuroimage 23, 1192–1202.
Smith, S.M., Jenkinson, M., Woolrich, M.W., Beckmann, C.F., Behrens, T.E.J., Johansen-Berg, H., Bannister, P.R., De Luca, M., Drobnjak, I., Flitney, D.E., Niazy, R., Saunders, J., Vickers, J., Zhang, Y., De Stefano, N., Brady, J.M., Matthews, P.M., 2004. Advances in functional and structural MR image analysis and implementation as FSL. Neuroimage 23 (1), 208–219.
Stephan, K.E., Kamper, L., Bozkurt, A., Burns, G.A.P.C., Young, M.P., Kötter, R., 2001. Advanced database methodology for the Collation of Connectivity data of the Macaque brain (CoCoMac). Philos. Trans. R. Soc. Lond. B 356, 1159–1186.
Striedter, G.F., 2005. Principles of Brain Evolution. Sinauer.
Tomassini, V., Jbabdi, S., Klein, J.C., Behrens, T.E.J., Pozzilli, C., Matthews, P.M., Rushworth, M.F.S., Johansen-Berg, H., 2007. Diffusion-weighted imaging tractography-based parcellation of the human lateral premotor cortex identifies dorsal and ventral subregions with anatomical and functional specializations. J. Neurosci. 27 (38), 10259–10269.
Uddin, L.Q., Supekar, K., Amin, H., Rykhlevskaia, E., Nguyen, D.A., Greicius, M.D., Menon, V., 2010. Dissociable connectivity within human angular gyrus and intraparietal sulcus: evidence from functional and structural connectivity. Cereb. Cortex 20 (11), 2636–2646.
Ungerleider, L.G., Haxby, J.V., 1994. 'What' and 'Where' in the human brain. Curr. Opin. Neurobiol. 4 (2), 157–165.
Vigneau, M., Beaucousin, V., Hervé, P.Y., Duffau, H., Crivello, F., Houdé, O., Mazoyer, B., Tzourio-Mazoyer, N., 2006. Meta-analyzing left hemisphere language areas: phonology, semantics, and sentence processing. Neuroimage 30, 1414–1432.
Zhong, Y.M., Rockland, K.S., 2003. Inferior parietal lobule projections to anterior inferotemporal cortex (area TE) in macaque monkey. Cereb. Cortex 13, 527–540.
Zilles, K., Amunts, K., 2010. Centenary of Brodmann's map — conception and fate. Nat. Rev. Neurosci. 11 (2), 1448–1461.

Behavioral/Systems/Cognitive

# Anatomical and Functional Connectivity of Cytoarchitectonic Areas within the Human Parietal Operculum

**Simon B. Eickhoff,**[1,2,3] **Saad Jbabdi,**[4] **Svenja Caspers,**[2,3] **Angela R. Laird,**[5] **Peter T. Fox,**[5] **Karl Zilles,**[2,3,6] **and Timothy E. J. Behrens**[4,7]

[1]Department of Psychiatry and Psychotherapy, Rheinisch-Westfälische Technische Hochschule Aachen University, D-52074 Aachen, Germany, [2]Institute of Neuroscience and Medicine (INM-2), Research Centre Jülich, D-52425 Jülich, Germany, [3]Jülich Aachen Research Alliance, Translational Brain Medicine, D-52425 Jülich, Germany, [4]Oxford Centre for Functional MRI of the Brain, University of Oxford, John Radcliffe Hospital, Oxford OX3 9D2, United Kingdom, [5]Research Imaging Center, University of Texas Health Science Institute, San Antonio, Texas 78229, [6]C. & O. Vogt Institute for Brain Research, University of Düsseldorf, D-40225 Düsseldorf, Germany, and [7]Department of Experimental Psychology, University of Oxford, Oxford OX1 3UD, United Kingdom

**In monkeys, the somatosensory cortex on the parietal operculum can be differentiated into several distinct cortical fields. Potential human homologues for these areas have already been defined by cytoarchitectonic mapping and functional imaging experiments. Differences between the two most widely studied areas [operculum parietale (OP) 1 and OP 4] within this region particularly pertain to their connection with either the perceptive parietal network or the frontal motor areas. In the present study, we investigated differences in anatomical connection patterns probed by probabilistic tractography on diffusion tensor imaging data. Functional connectivity was then mapped by coordinate-based meta-analysis of imaging studies. Comparison between these two aspects of connectivity showed a good congruency and hence converging evidence for an involvement of these areas in matching brain networks. There were, however, also several instances in which anatomical and functional connectivity diverged, underlining the independence of these measures and the need for multimodal characterization of brain connectivity. The connectivity analyses performed showed that the two largest areas within the human parietal operculum region display considerable differences in their connectivity to frontoparietal brain regions. In particular, relative to OP 1, area OP 4 is more closely integrated with areas responsible for basic sensorimotor processing and action control, while OP 1 is more closely connected to the parietal networks for higher order somatosensory processing. These results are largely congruent with data on nonhuman primates. Differences between anatomical and functional connectivity as well as between species, however, highlight the need for an integrative view on connectivity, including comparison and cross-validation of results from different approaches.**

## Introduction

The primate secondary somatosensory cortex is located on the parietal operculum (Kaas and Collins, 2003). Investigations in many species have provided converging evidence that it can be subdivided into several areas, featuring separate somatotopic maps differing from each other in cytoarchitecture and myeloarchitecture, response properties, and connectivity (Burton et al., 1995; Huffman et al., 1999; Krubitzer and Kaas, 1990; Krubitzer et al., 1995). The area immediately ventral to the anterior parietal somatosensory cortex [areas 3a, 3b, and 1 on the postcentral gyrus (PCG)] is termed the "parietal ventral area" (PV). It is followed caudally by area S2, located on the posterior part of the parietal operculum ventrally to the inferior parietal cortex (IPC). Together, PV and S2 are the most well characterized areas on the parietal operculum. While the term "SII region" is still widely prevalent in the functional neuroimaging literature, the lack of differentiation between the reference to the entire region and a particular area (now denoted S2 to clear up the confusion between SII region and "area SII") may cause unnecessary confusion when comparing findings from different experiments (Eickhoff, 2006c; Burton et al., 2008a, 2008b). We hence opted to avoid this term in the current study in favor of the purely anatomical description "parietal operculum," which comprises areas S2, PV, and the "ventral somatosensory area" (VS). The latter is located more medial than areas S2 and PV, shows poorer responsiveness to sensory stimuli, and crude somatotopic organization (Cusick et al., 1989; Krubitzer and Calford, 1992; Qi et al., 2002). More recently, it has been proposed that the latter region may actually consist of two separate rostral and caudal areas, VSr and VSc, respectively (Coq et al., 2004).

A homologous subdivision of the human parietal operculum was initially proposed based on a functional magnetic resonance imaging (fMRI) study providing evidence that the human pari-

Received Nov. 16, 2009; revised March 21, 2010; accepted March 26, 2010.

We acknowledge funding by the Human Brain Project/Neuroinformatics Research (National Institute of Biomedical Imaging and Bioengineering, National Institute of Neurological Disorders and Stroke, National Institute of Mental Health; to K.Z.), the Human Brain Project (R01-MH074457-01A1; to S.B.E.) and the Helmholz Initiative on Systems-Biology "The Human Brain Model" (to K.Z. and S.B.E.).

Correspondence should be addressed to Simon B. Eickhoff at the second address above. E-mail: S.Eickhoff@fz-juelich.de.

DOI:10.1523/JNEUROSCI.5664-09.2010

 0270-6474/10/306409-13$15.00/0

etal operculum may contain several somatotopically organized areas (Disbrow et al., 2000). Subsequently, a postmortem investigation of the parietal operculum revealed the existence of four distinct cytoarchitectonic areas in this region (Eickhoff et al., 2006a, 2006d), which were termed OP (operculum parietale) 1–4. Based on topography and somatotopic organization (Eickhoff et al., 2006c, 2007), OP 4 corresponds to primate area PV, while more caudally OP 1 constitutes the putative human homologue of area S2, and OP 3 is the most likely candidate for macaque area VS. OP 2 is not a somatosensory cortical field but is the homologue of the vestibular region PIVC (parietoinsular vestibular cortex) in nonhuman primates (Eickhoff et al., 2006e).

The functional roles of these human cortical regions are yet a matter of conjecture, as both S2 (OP 4) and PV (OP 1) are coactivated by a wide range of paradigms (Kell et al., 2005; Burton et al., 2008b; Jung et al., 2009). Tracer studies in nonhuman primates, however, have provided some evidence for differences in the connectivity pattern of these two areas (Qi et al., 2002; Disbrow et al., 2003; Kaas and Collins, 2003). Area S2 is regarded as a somatosensory "perceptive" area strongly interconnected with the inferior parietal cortex (Disbrow et al., 2003). In contrast, PV may sustain sensory-motor integration and, at least in new world monkeys such as marmosets, has denser connections with frontal motor and premotor cortices than S2 (Qi et al., 2002). Based on these observations, we here investigated the anatomical and functional connectivity of human areas OP 4 and OP 1.

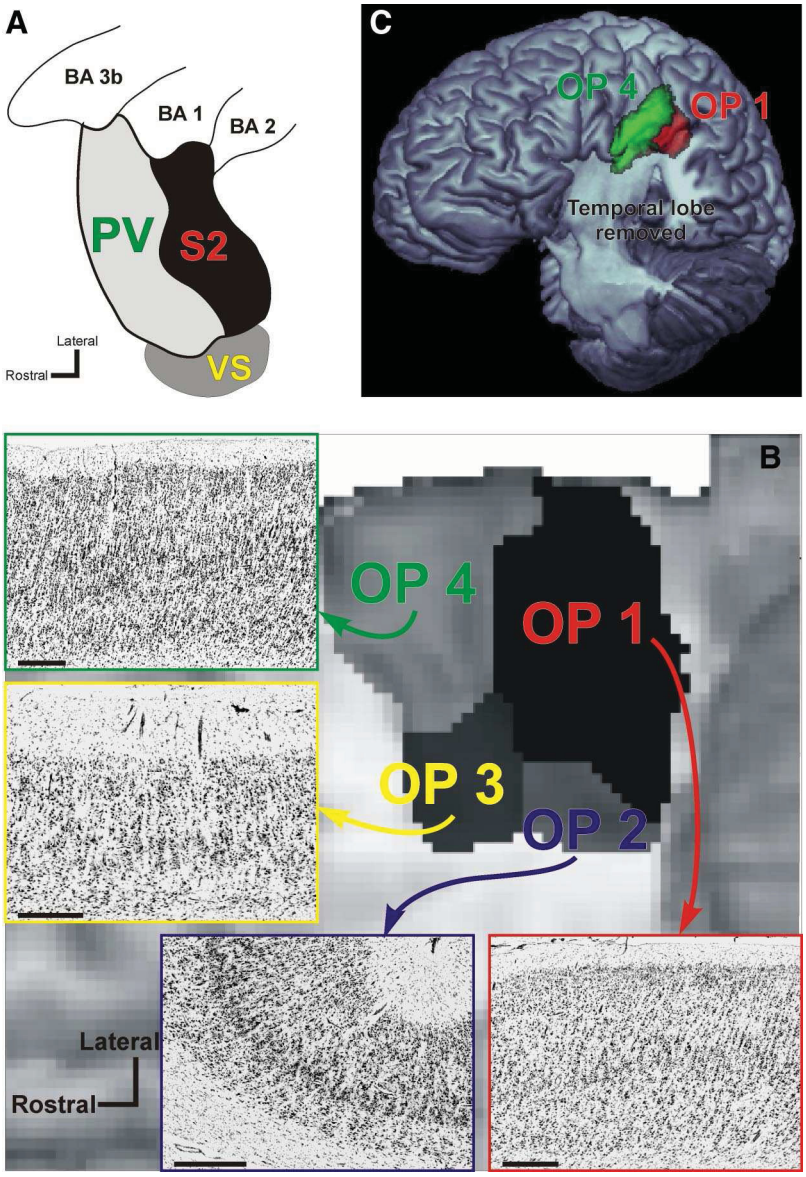


**Figure 1.** ***A***, Organization of cortical areas in the lateral sulcus of nonhuman primates [adopted and summarized from Disbrow et al. (2003) and Krubitzer et al. (1995)]. It should be noted that inconsistent evidence for further somatosensory areas in this region has been discussed and that a subdivision of VS into two separate areas, VSr (rostral) and VSc (caudal), has been proposed (Coq et al., 2004). ***B***, Anatomical organization of the human parietal operculum. Four distinct cytoarchitectonic areas (termed OP 1–4) have been delineated in this region using quantitative histological analysis. Following 3D reconstruction of the cytoarchitectonically analyzed postmortem brains and spatial normalization of these areas into the reference space of the MNI, probabilistic maps for the areas were computed and subsequently combined into an MPM. This anatomical MPM indicates the most likely area at each voxel of the reference space and is shown here in a ventral view on a surface rendering of the MNI single-subject template. The temporal lobes have been removed to obtain an unobstructed view onto the parietal operculum, where the different colors correspond to OP 1–4 as marked. Based on topography and somatotopic organization, OP 4 should correspond to primate area PV, OP 1 to area S2, and OP 3 to area VS. Finally, OP 2 is the homologue of the parietoinsular vestibular cortex in nonhuman primates. Bars in the histological images denote 1 mm. ***C***, Three-dimensional surface rendering of the MNI single-subject template after removal of the temporal lobe. The position of areas OP 1 and OP 4 as defined by their MPM representation is indicated on this view in red and green, respectively. In contrast to panel ***B***, which gives a view directly facing the parietal operculum, the tilted view used in this panel provides an overview on the extent of OP 1 and OP 4 on the free surface. Together with ***B***, it can be seen that OP 4 encroaches the free surface of the subcentral gyrus while covering about two-thirds of the mediolateral width of the parietal operculum. Area OP 1, on the other hand, barely reaches the free surface but covers about three-fourths of the mediolateral width of the parietal operculum.

## Materials and Methods

We investigated the frontoparietal connectivity of human areas OP 4 (S2) and OP 1 (PV) by using two independent approaches. Differences between OP 4 (S2) and OP 1 (PV) with respect to their anatomical connectivity to other frontoparietal regions were probed by probabilistic tractography on diffusion tensor imaging (DTI) data. Differences between OP 4 (S2) and OP 1 (PV) with respect to their functional connectivity with other frontoparietal regions were probed by coordinate-based meta-analysis of imaging studies.

### *Anatomical connectivity analysis by probabilistic tractography*

*Data acquisition.* Diffusion-weighted images were acquired in 17 healthy subjects (6 women and 11 men; mean ± SD age, 26.18 ± 4.81; range, 20–38) on a 1.5 T Siemens Sonata magnetic resonance scanner (maximum gradient strength of 40 mT/m). All subjects gave informed written consent into this study, which was approved by the Oxford Research Ethics Committee (Oxford, UK). Diffusion-weighted acquisitions were performed using echo planar imaging (voxel size: 2 × 2 × 2 mm, 60 isotropically distributed directions; $b$ value: 1000 s/mm$^2$). For each subject, three sets of diffusion-weighted data were obtained. Each set also contained five additional volumes with no diffusion weighting that were acquired distributed throughout the acquisition sequence.

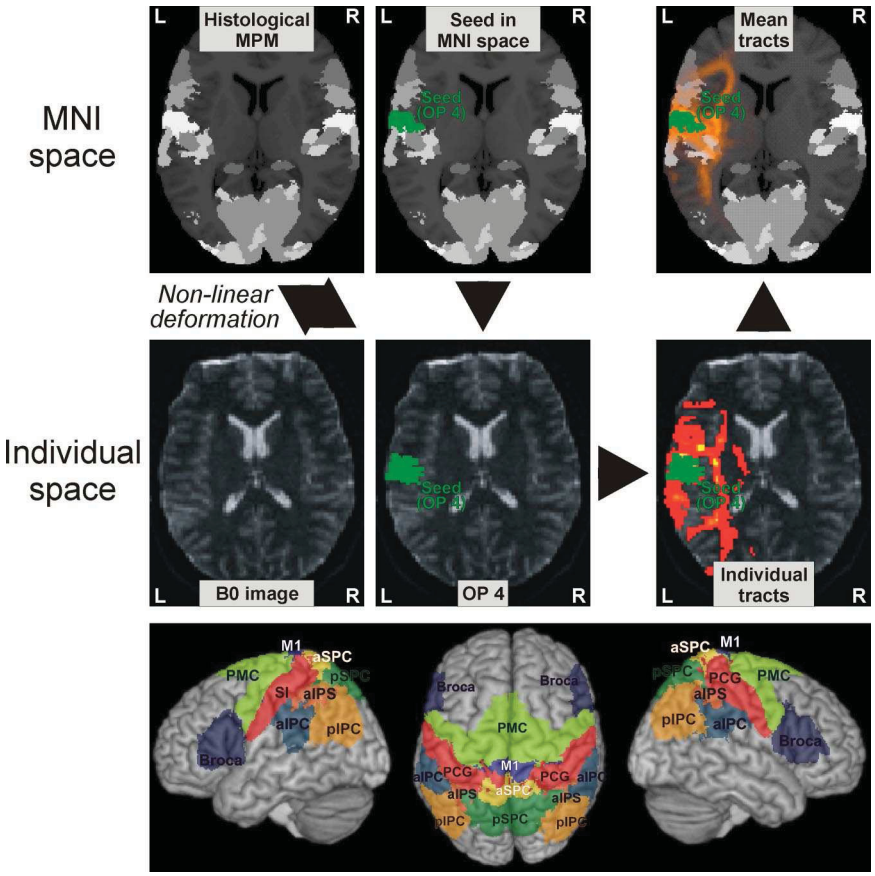


**Figure 2.** Top and middle panels, Seeds and targets were defined by representations of the respective cytoarchitectonic areas in an MPM of all histologically defined regions. This MPM is shown in the background of the figures in the top row. Different shades of gray denote the different cytoarchitectonic areas. For the sake of display clarity, however, these areas are not individually labeled in these figures. In the displayed example, the seed region was defined by the anatomical location of area OP 4, which is indicated in green. The volume of interest defining this seed, i.e., the location of area OP 4, is then transformed into single-subject diffusion space for probabilistic tractography. Quantitative analysis was then based on the sample count obtained from these analyses, i.e., the number of probabilistic traces originating from the seed (OP 1 or OP 4) reaching a particular target (cf. Table 1). For visualization, the ensuing tracts were also back-projected into the MNI space and averaged to represent the mean pathways. In the figures on the top and middle right, the color scale from red to yellow indicates the probability that the respective tract passes through the respective voxel as obtained from probabilistic tractography. MNI space refers to the reference space defined by the Montreal Neurological Institute for the definition of stereotaxic coordinates (Collins et al., 1994; Evans et al., 1992), which currently represents the most widely used standard for multisubject analysis of neuroimaging data. Bottom panel, Surface rendering of the target regions covering the frontal and parietal cortices displayed on a surface rendering of the MNI template. Each of these cytoarchitectonically defined targets is transformed into the single-subject diffusion space in the same manner as illustrated above for a seed region. An overview on the acronyms used to label the different regions as well as further information on these and their cytoarchitectonic correlates is given in Table 1.

Analysis of diffusion-weighted images was performed using the Functional MRI of the Brain Software Library (FSL) (www.fmrib.ox.ac.uk/fsl). First, all images were realigned to each other by affine registration to compensate for head scan movement and corrected for eddy currents (Smith et al., 2004). The data from the three acquisitions were subsequently averaged to improve the signal-to-noise ratio. We then calculated probability distributions on multiple fiber directions at each voxel in the diffusion data using a multiple fiber extension (Behrens et al., 2007) of a previously described diffusion modeling approach (Behrens et al., 2003a, 2003b). Here, the algorithm was limited to estimating two fiber orientations at each voxel based on the *b* value and number of gradient orientations in the diffusion data (Rushworth et al., 2006; Tomassini et al., 2007). That is, based on the diffusion-weighted images obtained from applying 60 gradient directions, the probability distributions of up to two independent fiber orientations were estimated at each voxel.

*Seed region definition.* Seed regions on the parietal operculum were defined by the anatomical locations of cytoarchitectonic areas OP 1 and OP 4, which are illustrated in Figure 1*B*. The borders of these areas were delineated by microscopic investigation and quantitative histological analysis in a sample of 10 human postmortem brains (Schleicher et al., 2005). These brains were subsequently reconstructed in three dimensions (3D) from digitized images of the histological sections, block-face images taken during the cutting of the brains, and T1 MRI scans obtained before histological processing. These individual brains were subsequently normalized into the reference space defined by the templates (Evans et al., 1992; Collins et al., 1994) provided by the Montreal Neurological Institute (MNI; Montreal, Canada), termed the MNI space. As the next step, a probabilistic cytoarchitectonic map was computed for each area, describing at every voxel of the reference space how likely this area was found at a particular position (Zilles et al., 2002). To generate a discrete parcellation of the cerebral cortex based on the probabilistic information contained in these (overlapping) maps, a summary map [maximum probability map (MPM)] was computed. This map identifies the most likely anatomical area at each voxel of the MNI single-subject template and hence provides a continuous, nonoverlapping map of the human brain (Eickhoff et al., 2005, 2006b). The MPM representations of areas OP 1 and OP 4 were then used as seeds for probabilistic tractography. That is, the regions of interest for which connectivity measures were computed correspond to the anatomical locations of OP 1 and OP 4 as defined by objective cytoarchitectonic analysis following normalization into a standard reference space.

Since, however, these definitions are only available in MNI space, whereas diffusion image analysis is performed in single-subject space, these MPM representations first had to be spatially transformed to match the individual subject's anatomy (Fig. 2). This mapping was achieved by computing transformation fields normalizing each subject's mean $b_0$ image and the MNI single-subject template, respectively, to the MNI tissue probability maps (TPMs) using a segmentation-based approach (Ashburner and Friston, 2005). For each subject, the transformation pointing from the MNI single-subject template to the TPMs was then combined with the inverse of the transformation from an individual $b_0$ image to the TPMs (mapping from the TPMs to the individual diffusion space). Hereby, the MPM-based seed regions could be transformed from the MNI single-subject template into the diffusion space of each individual subject despite the different image contrasts. Following probabilistic tractography (cf. below), the ensuing tracts were then back-projected into the MNI single-subject space using the same approach and averaged for visualization of white matter pathways connecting OP 1 and OP 4 with frontoparietal targets.

*Probabilistic tractography.* For each subject, probabilistic tractography was run from the seeds defined by the representations of areas OP 1 and OP 4 in the individual diffusion spaces, using the estimates of (multiple) fiber orientations in each voxel (Behrens et al., 2007). The approach draws a sample from each fiber orientation distribution at the current voxel and chooses the sample closest to the orientation of its previous step. The connection probability between a seed and another voxel in the brain is given by the number of traces arriving at the target site. The aim of this study was to elucidate differential connection patterns of areas

**Table 1. Target regions used for the analysis of anatomical connectivity of areas OP1 and OP4**

| Target region | Acronym | Cytoarchitectonic areas | References |
|---|---|---|---|
| Frontal | | | |
| Broca's region | Broca | Areas 44, 45 | Amunts et al., 1999, 2004 |
| Premotor cortex | PMC | Area 6 | Geyer, 2003 |
| Primary motor cortex | M1 | Areas 4a, 4p | Geyer et al., 1996 |
| Parietal | | | |
| Postcentral gyrus | PCG | Areas 3a, 3b, 1, 2 | Geyer et al., 1999, 2000; Grefkes et al., 2001 |
| Anterior intraparietal sulcus | aIPS | Areas hIP1, hIP2, hIP3 | Choi et al., 2006; Scheperjans et al., 2008a, 2008b |
| Anterior superior parietal cortex | aSPC | Areas 5Ci, 5L, 5M | Scheperjans et al., 2008a, 2008b |
| Posterior superior parietal cortex | pSPC | Areas 7A, 7M, 7P, 7PC | Scheperjans et al., 2008a, 2008b |
| Anterior inferior parietal cortex | aIPC | Areas PFt, PF, PFm | Caspers et al., 2006, 2008 |
| Posterior inferior parietal cortex | pIPC | Areas PGa, PGp | Caspers et al., 2006, 2008 |
| Thalamus | | | |
| Nuclei preferentially connecting to the somatosensory cortex | VPL/VPI | Ventroposterior lateral and inferior nuclei | Behrens et al., 2003a |
| Nuclei preferentially connecting to the premotor or primary motor cortex | VL/VA | Ventrolateral nuclei, ventral anterior nuclei | Behrens et al., 2003a |

OP 1 and OP 4. However, many of the strongest differences in connections expected from the macaque monkey (e.g., those toward Broca's region and the inferior parietal lobule) might also distinguish these regions solely in terms of their physical distance from their respective seeds. To ensure that our results could not be caused by any potential bias in tractography toward nearby connections, we corrected probability counts by the length of the pathway. This approach upweighted longer connections (Tomassini et al., 2007) and thus penalized short ones to exclude the possibility that physical distance alone could account for our results.

To evaluate differences in frontoparietal connectivity patterns of OP 1 and OP 4, target regions (outlined in Table 1 and illustrated in the bottom panel of Fig. 2) were created from the histological data using the same approach as that described for OP 1/OP 4. These targets cover the entire parietal lobe as well as the frontal motor and premotor areas, including Broca's region.

For each subject, we drew 5000 samples from the connectivity distribution (starting from the seed voxels in OP 1/OP 4) and computed the mean probability of connection for each seed–target combination. These values were then normalized on an individual basis by dividing by the total connection probability of each seed and then rescaled by multiplying with the mean total connection probability across all seeds and targets. Finally, connection densities were divided by the size of the target volumes of interest (VOIs), computed on an individual subject basis, and again rescaled by the mean size of all targets. These steps adjusted our data for the size of the seed and target regions.

Statistical analysis on these connection probabilities was performed using MATLAB (MathWorks). Repeated-measures ANOVAs of connection probability values were used to test for influence of within-subject factors of "opercular seed" (OP 1, OP 4),"target" (cf. Table 1), and "hemisphere" (left, right), as well as the interactions thereof.

The main effect of the factor "opercular seed" assessed whether there was a statistically significant difference between OP 1 and OP 4 with respect to the mean connection strength to all targets. The main effect of the factor "target" tested whether the 12 target regions differed from each other with respect to their anatomical connectivity with the parietal operculum (mean connectivity to OP 1 and OP 4). Finally, the interaction between "opercular seed" and "target" tested for differences in the frontoparietal connectivity of OP 1 and OP 4, i.e., whether the distribution of connection strengths to individual targets was different between OP 1 and OP 4. In this context, it is important to consider that in a two-way ANOVA the individual tests are not conditioned on each other; that is, the significance of, e.g., a particular main effect does not depend on the significance or insignificance of the other main effect or the interaction.

The level of significance was $p < 0.05$. If the effect of a factor or an interaction was significant, we used a subsequent pairwise multiple comparison procedure to isolate the levels of this factor that differed significantly from each other ( $p < 0.05$, corrected for multiple comparisons using Tukey's method) (Tukey, 1994).

### *Functional connectivity analysis by meta-analysis*

Functional connectivity analysis was performed by a meta-analysis of published functional imaging results. The concept behind mapping functional connectivity via meta-analysis originates from the notion that functional connectivity should represent the correlation of spatially removed neurophysiologic events, which implies that functionally connected regions should coactivate above chance in functional imaging studies.

This concept of meta-analytic connectivity modeling (MACM) was first used to investigate functional connectivity based on the frequency distributions of concurrent activation foci (Koski and Paus, 2000). Following the emergence of databases on functional neuroimaging results (Fox and Lancaster, 2002; Laird et al., 2009a), this approach was extended to provide voxelwise co-occurrence maps across the whole brain (Toro et al., 2008). The concept of MACM has then been integrated with the activation likelihood estimation (ALE) approach for quantitative meta-analysis (Turkeltaub et al., 2002) to yield functional connectivity maps of the human amygdala (Robinson et al., 2009). More recently, finally, the mapping of functional connectivity via coordinate-based meta-analysis has been validated by comparison to resting-state connectivity (Smith et al., 2009), showing very good concordance between both approaches.

Here, MACM was performed using the BrainMap database (www.brainmap.org), which contains a summary of the results for (at the time of analysis) ~6500 individual functional neuroimaging experiments. Given the high standardization of neuroimaging data reports and in particular the ubiquitous adherence to standard coordinate systems, the results reported in these studies can readily be compared to each other with respect to the location of significant activation. Using this broad pool of neuroimaging results, MACM can then be used to test for associations between activation probabilities of different areas. Importantly, this inference is performed independently of the applied paradigms or other experimental factors, but rather is solely based on the likelihood of observing activation in a target region [e.g., the premotor cortex (PMC)], given that activation is present within the seed area (e.g., OP 1 or OP 4). Results from such an analysis are therefore robust across many different experimental designs. Database-aided MACM that assesses the coactivation pattern of OP 1 and OP 4 as defined by their MPM representation across a large number of imaging studies should hence allow the delineation and comparison of their functional connectivity. However, functional connectivity per se only allows the delineation of interacting networks but not the causal influences therein. In practice, MACM was performed using the following approach. Studies causing activation within OP 1 or OP 4 were obtained through the BrainMap database. Criteria for retrieval were as follows: only fMRI and positron emission tomography studies in healthy subjects that reported functional mapping experiments containing a somatosensory or motor component were considered. Those investigating age, gender, disease, or drug effects were excluded. No further constraints (e.g., on acquisition and analysis details, experimental design, or stimulation procedures) were enforced. Hereby

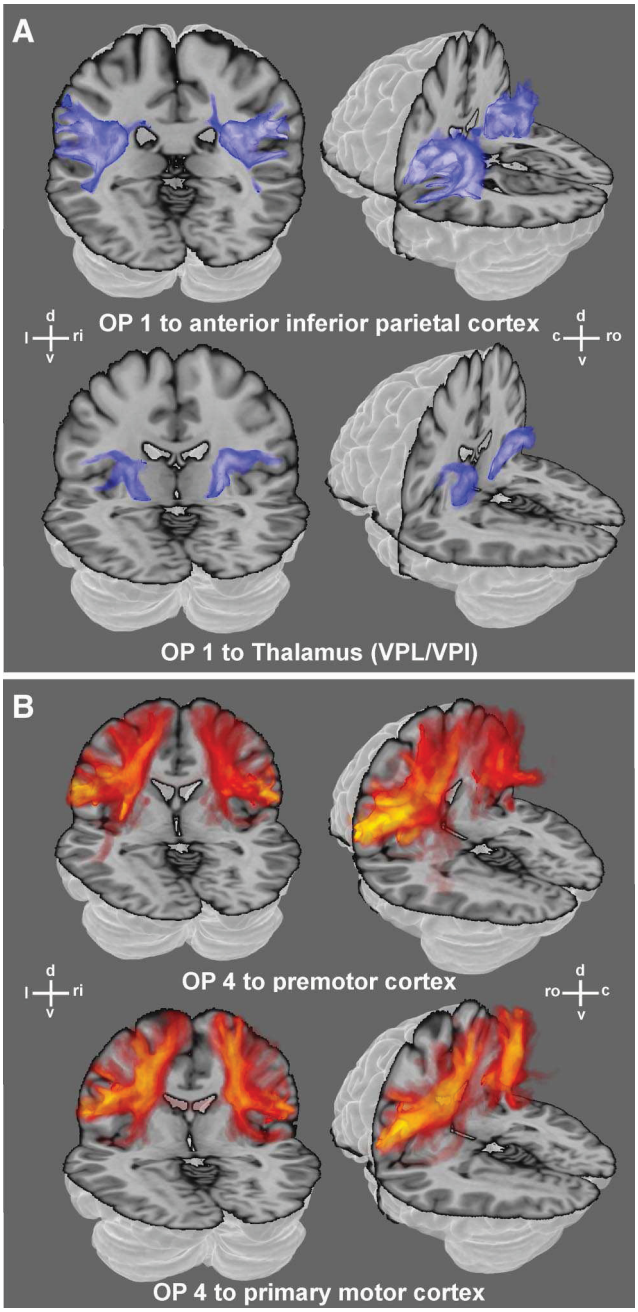


**Figure 3.** Examples of white matter fiber pathways as obtained from probabilistic tractography for OP 1 (***A***) and OP 4 (***B***) reconstructed in 3D. The data shown here illustrate the tracts connecting OP 1 and OP 4, respectively, with exemplary target regions (cf. Table 1) and hence reveal the pathways taken by the fiber tracts connecting the seeds and targets. The absolute strength of these connections, in turn, are summarized in Figure 4. All examples are displayed on the transparent MNI single-subject template. (d: dorsal, v: ventral, l: left, ri: right, ro: rostral, c: caudal). The color scales ranging from dark to light blue and from red to yellow, respectively, denote the probability that the particular tract runs through a given voxel. Light blue or yellow indicates those locations in the white matter where the respective pathways are very likely to be found. Dark blue or red, on the other hand, indicate less likely positions of the connecting fibers.

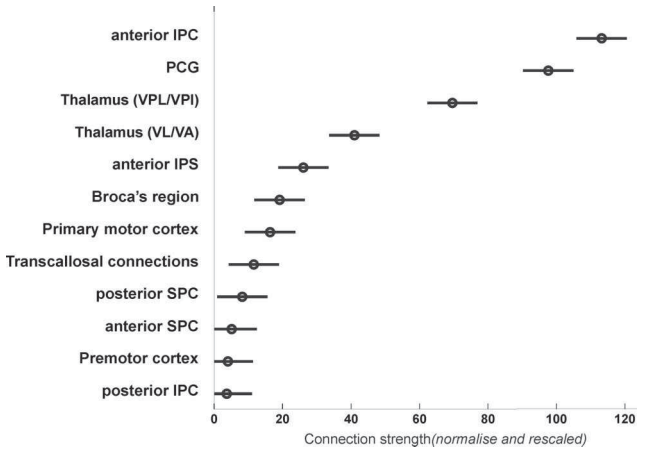


**Figure 4.** Mean connection strength (across subjects) between human parietal operculum (OP 1 and OP 4) and 12 different target regions assessed in the current study. Quantitative tractography was based on the sample count obtained when performing probabilistic tractography from the seed regions (OP 1 or OP 4) to the different targets (cf. Table 1) after these were transformed into the individual diffusion spaces of each subject. The connection probabilities obtained by this probabilistic tractography were normalized by dividing by the total connection probability of each seed and rescaled by multiplying by the mean total probability across all seeds and targets. Finally, connection densities were divided by the size of the target VOIs, computed on an individual basis, and again rescaled by the mean size of all targets to provide normalized connection strengths. The circles indicate the mean connection strength of each target with the entire parietal operculum, i.e., areas OP 1 and OP 4. The bars denote the 95% confidence intervals on these connection strengths.

we tried to avoid any bias in the data, but rather pool across as many different studies as possible.

Experiments that activate OP 1 or OP 4 were identified by comparing the foci reported for each of the ~1500 eligible experiments (functional mapping experiments available at the time of analysis that contained a somatosensory or motor component) in the BrainMap database to the cytoarchitectonic location of these cortical fields in the same reference space. The experiments used for the analysis of the functional connectivity of OP 1 (S2) were defined by the fact that (following correction for coordinates reported according to the Talairach reference space) they featured at least one focus of activation within the volume of cortex histologically delineated as OP 1, but no activation within the histologically delineated volume of OP 4. Hereby, the experiments that activated OP 1 or OP 4 were objectively identified. That is, activation within our seed areas was assessed observer independently by comparing the coordinates reported for all studies within the BrainMap database to the anatomical location of cytoarchitectonically defined OP 1 and OP 4 within the same reference space, independent of how this activation was termed in the original publication. Hereby, we avoided any influence of the fact that various labels have been used for activation in the region, e.g., SII, parietal operculum, Brodmann's area (BA) 43, BA 40, parietal cortex, or subcentral gyrus. Studies activating exclusively one of these two areas (either OP 1 or OP 4) were defined by at least one reported focus in the MPM representation of this area and the absence of any reported activation focus in the respective other area or, to increase specificity, a four voxel border zone between OP 1 and OP 4.

Given that OP 1 (S2) and OP 4 (PV) share a common border at which the face, hands, and feet are represented in either area, and acknowledging the fact that these two cortical fields are difficult to differentiate from each other functionally in nonhuman primates, the question evidently arises as to whether isolated activation in only one of these areas may be conceptually meaningful or most likely artificial. However, while S2 and PV tend to show concurrent activation in many experiments, there is already good evidence for differences in response properties between the various cortical fields on the parietal operculum of nonhuman primates (Robinson and Burton, 1980; Hsiao et al., 1993; Fitzgerald et al., 2004, 2006a, 2006b). Compared with electrophysiological experiments in monkeys, however, the range of tasks that may be assessed is considerably larger in human functional imaging experiments, including, in particular, experimental paradigms that investigate cognitive or affective influences on sensory-motor processing. It thus seems plausible that differences in response properties of opercular fields that have not yet been reported in monkeys may be unraveled in humans simply because the necessary paradigms are difficult to perform in animals. Moreover, differential response properties may manifest themselves as apparent shifts in somatotopic location in functional imaging data, in particular if differential

contrasts between two conditions are considered. In this case, homogenous activation of both cortical fields by one condition may offset, leaving only an isolated peak of activation well within the cortical field that was more responsive to the other condition. This phenomenon, to which neurophysiologic mechanisms at the neuronal level may also contribute, has been discussed in great detail in a recent study by Burton et al. (2008b). It is therefore very well conceivable that isolated activations within OP 1 or OP 4 are observed in human neuroimaging data despite their close proximity and the similarities in response characteristics.

It should be noted that the seeds representing OP 1 and OP 4, respectively, in the functional connectivity analysis were defined bilaterally. This approach was based on the observation that activation of the secondary somatosensory cortex is frequently bilateral, resulting in a much reduced and ultimately insufficient sample of studies reporting unilateral activation. These, however, would be required for a separate analysis of ipsilateral and contralateral connections.

*Meta-analysis algorithm.* For the coordinate-based meta-analysis of neuroimaging results, we used a revised version (Eickhoff et al., 2009b) of the ALE approach (Turkeltaub et al., 2002; Laird et al., 2005). The algorithm aims at identifying areas where the convergence of activations across different experiments is higher than expected under a spatially random association between them. The key idea behind ALE is to treat the reported foci not as single points but rather as centers for 3D Gaussian probability distributions. These distributions reflect the spatial uncertainty associated with each focus, i.e., each reported set of coordinates. The width of these uncertainty functions is determined by empirical estimates of the between-subject and between-template variances encountered in neuroimaging data (Eickhoff et al., 2009b). By weighting the former by the number of subjects on which the original experiment was based, this approach moreover accommodates the notion that larger sample sizes should provide more reliable approximations of a "true" effect and should therefore be modeled by tighter Gaussian distributions yielding more localizing power (Eickhoff et al., 2009b).

The probabilities of all foci reported in a given individual experiment were combined for each voxel, resulting in a modeled activation (MA) map. Taking the union of these MA maps across all experiments yielded an ALE score for each voxel describing the convergence of results at that particular location. To distinguish true convergence between studies from random convergence, i.e., noise, these ALE scores were subsequently compared with an empirical null distribution derived from a permutation procedure (Eickhoff et al., 2009b; Caspers et al., 2010). This null distribution reflects a random spatial association between experiments but regards the within-experiment distribution of foci as fixed. Hereby, a random effects inference is invoked, focusing inference on the above chance convergence between different experiments, not the clustering of foci within a particular experiment. Computationally, deriving this null hypothesis involved sampling a voxel at random from each of the MA maps and taking the union of these values in the same manner as that done for the (spatially contingent) voxels in the actual analysis. The true ALE scores were then tested against these ALE scores obtained under the null distribution, yielding a $p$ value for each ALE score based on the proportion of equal or higher random values. The resulting nonparametric $p$ values were then transformed into $z$-scores and thresholded at a cluster level-corrected threshold of $p < 0.05$ (Worsley et al., 1996).

*Analysis of behavioral domain profiles.* Evidently, the question also arises as to what mental processes are supported by OP 1 (S2) and OP 4 (PV) and whether the functional roles of these two parietal opercular areas differ from each other. In BrainMap, metadata are included on the cognitive, perceptual, or motor process isolated by the statistical contrast. The domain of behavioral system is classified according to five main categories: cognition, action, perception, emotion, and interoception (a complete list of the behavioral domains (BDs) in BrainMap can be accessed at http://brainmap.org/scribe/; experiments on pharmacology were excluded a priori from all analyses). We analyzed the BD metadata associated with the experiments reporting activation in OP 1 and OP 4, respectively, to determine the frequency of domain "hits" relative to its distribution across the whole brain (i.e., the entire database). In contrast to the more constrained functional connectivity analysis outlined above, this analysis was performed on the entire BrainMap database (no filter for experiments holding somatosensory or motor components). and experiments could be counted toward both regions to assemble a fully functional characterization. For each anatomical region, a $\chi^2$ test was performed to evaluate the regional distribution as compared with the overall database distribution (Laird et al., 2009b). If the region's distribution was significantly different, a binomial test was performed to determine which individual domains were over- or under-represented. Differences between the BD profiles of OP 1 and OP 4 were then assessed using the same approach as that for testing against a single region's profile against the database.

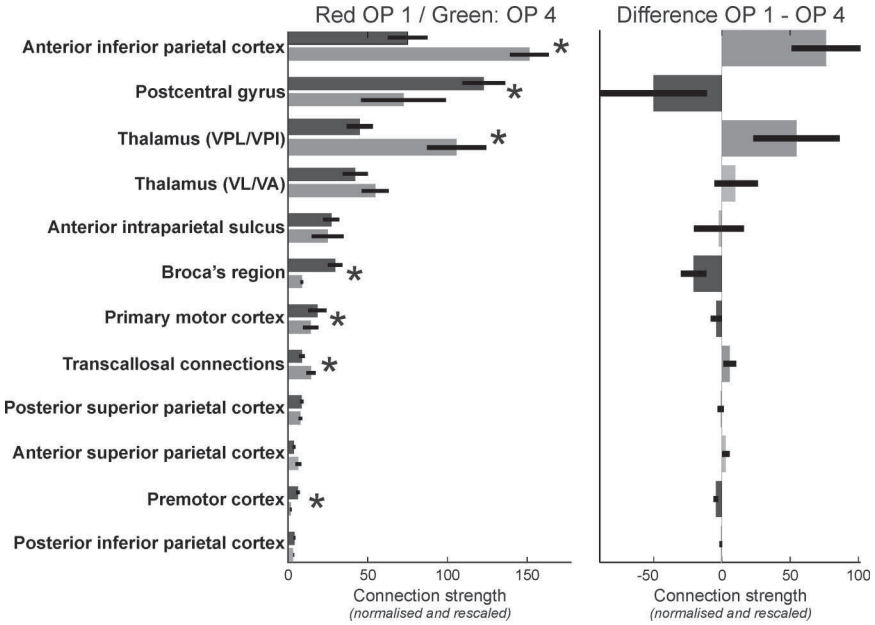


**Figure 5.** The statistical analysis of the anatomical connectivity data revealed a significant interaction between "seed" and "target" ($F = 7.83$; $p < 0.001$), indicating a difference in the patterns of frontoparietal connectivity between OP 1 and OP 4. Here, the anatomical connectivity of OP 1 and OP 4 to the different target regions is analyzed, resolving this "seed" × "target" interaction. In the left panel, the normalized connection strengths to all targets are displayed for both areas. The dark gray bars indicate the anatomical connectivity of OP 1, the medium gray bars indicate that of OP 4, and the error bars denote the SE. The right panel shows the difference between OP 1 and OP 4 connectivity. Significant ( $p < 0.05$, corrected) differences between these two seeds with respect to the anatomical connectivity to a particular target are indicated by gray scale bars (dark gray bars indicate a significantly higher connectivity of OP 1 to this target, and medium gray bars indicate a significantly higher connectivity of OP 4) and asterisks. Light gray bars denote targets for which no significant difference in the anatomical connectivity with OP 1 and OP 4, respectively, were found.

## Results

### Anatomical connectivity

*Identification of white matter connections between histologically defined areas*

Examples of the white matter tracts connecting the investigated areas of the parietal operculum to other regions of the frontal and parietal cortex are shown as group averages of the obtained tractography results (after normalization of the delineated tracts) in Figure 3. For each of the investigated areas, fiber tracts have been chosen that were significantly more connected to the respective area as compared with the other area (see below).

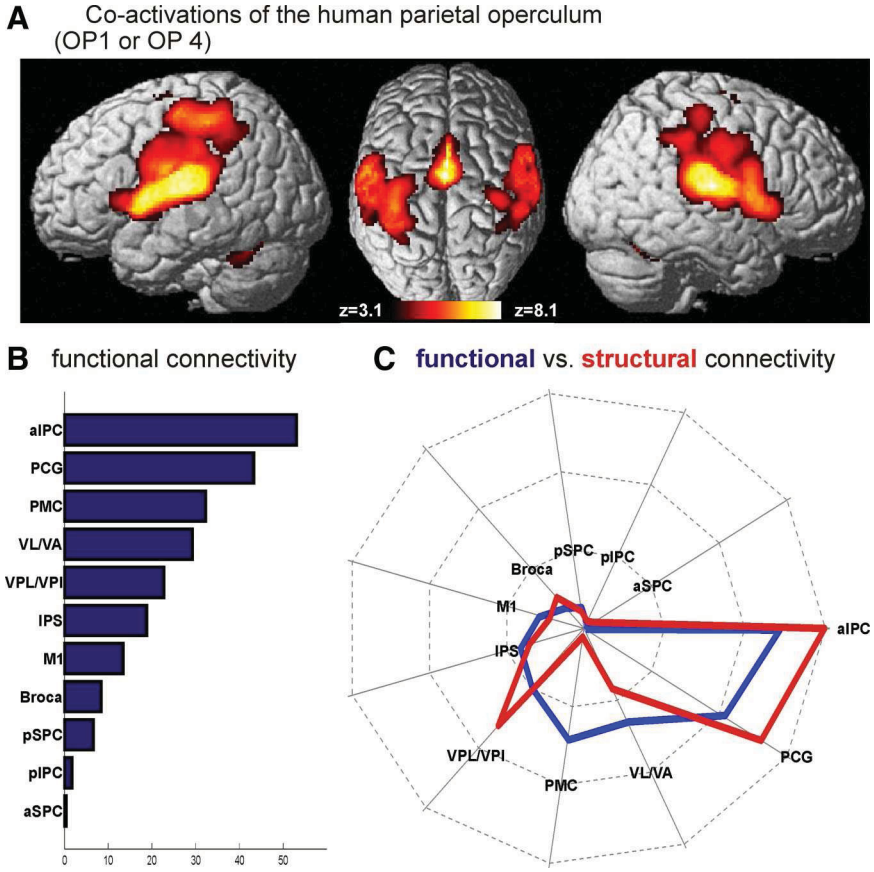


**Figure 6.** ***A***, Functional connectivity of the human parietal operculum as delineated by the significant ( $p < 0.05$, corrected) coactivation pattern obtained in a meta-analysis of 245 neuroimaging studies activating either OP 1 or OP 4. The color denotes the significance of the respective results. That is, while the presence of color indicates voxels that are significantly coactivated with the seed region, the particular color indicates the strength of this effect (*z*-score of the statistical analysis). ***B***, Strength of functional connectivity between the human parietal operculum and the different anatomically defined targets assessed in this study (compare Fig. 4) as defined by the volume fraction of the targets' MPM representations that were significantly coactivated with OP 1 or OP 4. The labels in this graph confirm to the acronyms summarized for reference in Table 1. ***C***, Comparison of the functional and anatomical connectivity of the human parietal operculum, i.e., OP 1 and OP 4 combined. The data used for this diagram correspond to the results shown in Figures 4 and 6*B*. However, to allow a direct comparison, the connection strengths displayed in Figures 4 and 6*B* were rescaled to unit total connectivity, accounting for the different scaling of the data obtained from the analysis of functional and anatomical connectivity. Again, labels in this graph confirm to the acronyms explained in Table 1.

It can be noted that all fiber tracts obtained through probabilistic tractography passed through the white matter following the respective major fiber pathways and showed little variance in their course to the respective targets. OP 1 showed significantly stronger connections to anterior IPC and ventral posterior lateral nucleus/ventral posterior inferior nucleus (VPL/VPI), whereas OP 4 was significantly more strongly connected to the premotor and primary motor cortex. Most notably, although these targets neighbored each other very closely, the respective connections could be separated by means of probabilistic tractography.

*Statistical analysis of connection strengths by repeated-measures ANOVA*

Assessing the normalized connection probabilities by means of repeated-measures ANOVA revealed a significant main effect of the factor "target" ($F = 41.77$; $p < 0.001$), indicating that the 12 assessed target regions differed from each other with respect to their anatomical connectivity with the parietal operculum (Fig. 4). Moreover, we found a significant interaction between "opercular seed" and "target" ($F = 7.66$; $p < 0.001$), reflecting differences in the frontoparietal connectivity of OP 1 and OP 4. There was, however, no significant main effect of "opercular seed," revealing that the mean connection strength of the connections to all targets does not differ significantly between OP 1 and OP 4. That is, although there is no difference between OP 1 and OP 4 with respect to the mean connection strength to all targets (absence of a significant main effect of "opercular seed"), the distribution of connection strengths to individual targets was different between OP 1 and OP 4 (significant interaction between "opercular seed" and "target"). Importantly, there was also no significant interaction with "hemisphere" ($F = 0.79$; $p = 0.65$), indicating the absence of a hemispheric asymmetry in anatomical connectivity.

*Anatomical connectivity of the parietal operculum (main effect across OP 1/OP 4)*

To resolve the significant main effect of "target," indicating that the different targets vary in their mean connection strength to OP 1 and OP 4, a direct comparison between the different targets ( $p < 0.05$, corrected by Tukey's method) was performed. This analysis compared the different levels of the factor "target" (i.e., the different target regions) with each other to assess which pairs differ in their mean value (i.e., connection strength of the particular area averaged across both seeds, OP 1 and OP 4). Statistical testing revealed (Fig. 4) that anterior IPC was significantly stronger connected to OP 1 and OP 4 than any other target. The differences in connectivity with OP 1/OP 4 between the PCG and all other regions showing a lower connection density were also significant. There was no significant difference in connectivity with OP 1/OP 4 between VPL/VPI and ventral lateral nucleus/ventral anterior nucleus (VL/VA). The connection probability from OP 1/OP 4 toward VPL/VPI was significantly different from that toward all other areas showing a lower connectivity (Fig. 4). The same was true for VL/VA, with the exception of the connectivity to the anterior IPS. The latter area showed significantly higher connection densities than posterior IPC, premotor cortex, and both superior parietal regions. Finally, connectivity of OP 1 and OP 4 to Broca's area was significantly higher than that to the posterior IPC and the premotor cortex, respectively.

*Differences in frontoparietal connectivity between OP 1 and OP 4*

Follow-up comparison on the strengths of the anatomical connectivity toward the different targets between OP 1 and OP 4 revealed that the "seed × target" interaction observed in the ANOVA was based on the following significant differences (Fig. 5). The two regions that were most closely connected to OP 1 and OP 4, the anterior IPC and the PCG, showed a different preference with respect to their connection. While the anterior IPC features significantly higher connection probabilities with OP 1 as compared with OP 4, the PCG is significantly more densely connected to area OP 4 than to OP 1. Besides the stronger connectivity to the anterior IPC, area OP 1 also showed significantly

higher probabilities for anatomical connections with VPL/VPI and a significantly higher number of transcallosal connections as compared with OP 4. In contrast, area OP 4 showed significantly higher probabilities for connections with Broca's region, the primary motor cortex, and the premotor cortex than area OP 1. Finally, there was no significant difference between both seed areas with respect to their connectivity to the superior parietal cortex, the anterior IPS, the posterior IPC, and VL/VA.

In summary, OP 4 was significantly more densely connected to frontal as well as primary sensory-motor areas, while OP 1 featured higher probabilities for parietal, thalamic, and interhemispheric connections.

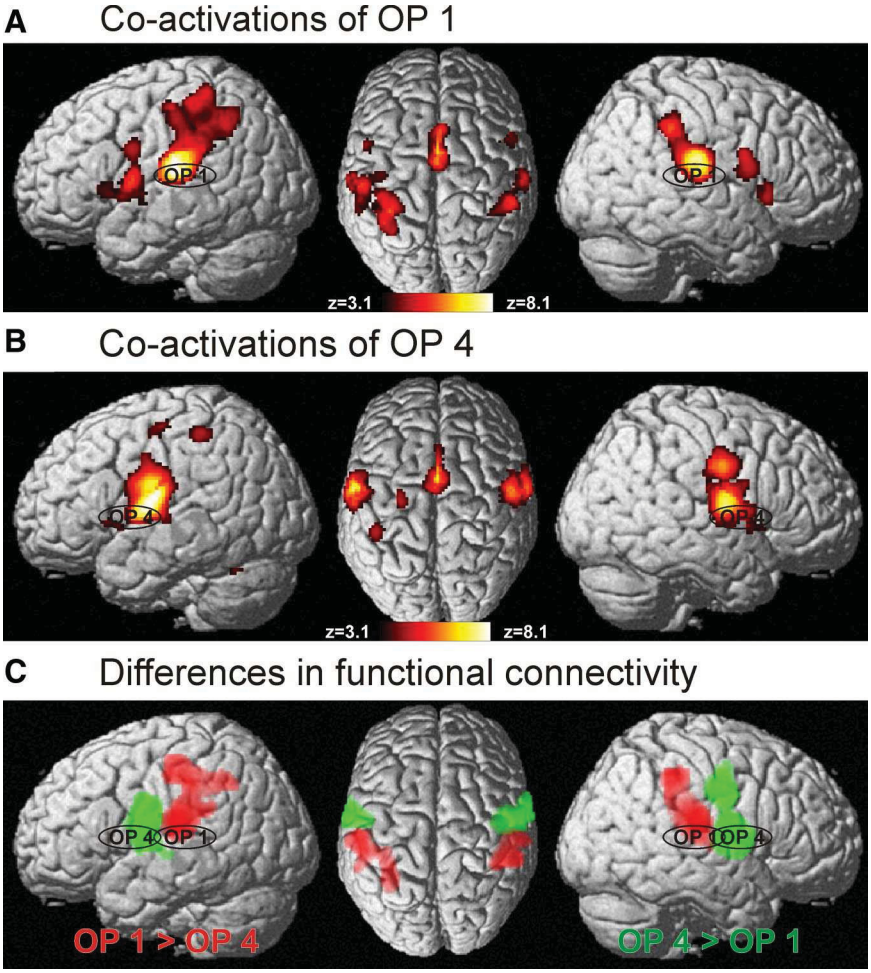


**Figure 7.** ***A***, Functional connectivity of area OP 1 as delineated by the significant coactivation pattern obtained in a meta-analysis of the 80 studies activating only this area. As in Figure 6, the color scale ranging from deep red to white-yellow indicates the strength of the effects (*z*-score of the statistical analysis; all indicated voxels were significantly coactivated at $p < 0.05$, cluster level corrected). ***B***, Functional connectivity of area OP 4 as delineated by the significant coactivation pattern obtained in a meta-analysis of the 61 studies activating only this area. Again, the color scale indicates the statistical effect size. ***C***, Regions showing significant difference in functional connectivity between areas OP 1 and OP 4. Red indicates those voxels that were significantly more often coactivated with OP 1 as compared with OP 4; voxels shown in green denote those regions that showed significantly higher probabilities of coactivating with OP 4 than with OP 1. All data shown at $p < 0.05$, corrected.

## Functional connectivity

Searching the BrainMap database, we found 245 functional neuroimaging experiments activating either OP 1 or OP 4. Of these, 80 experiments exclusively activated OP 1 (but featured no focus in OP 4 or the border zone), and another 61 reported activation only in OP 4.

### *Functional connectivity of the parietal operculum (main effect across OP 1/OP 4)*

The functional connectivity of the human parietal operculum was revealed by significant coactivations in all those studies that activated either of the two areas as shown in Figure 6*A*. As expected, coactivations and hence functional connectivity to OP 1 and OP 4 were found in a widely distributed frontoparietal network. Comparison of significant coactivation with the same target VOIs as those used for the DTI analysis (Table 1) yielded the following results (Fig. 6*B*). Functional connectivity was most prevalent in anterior IPC (53.1% of the voxels in this target VOI showing significant functional connectivity), followed by the PCG (43.3% of this target VOI showing significant functional connectivity), the premotor cortex (32.3%), and VL/VA (29.4%). The VPL/VPI (22.5%), the anterior IPS (18.8%), and the primary motor cortex (13.4%) showed intermediate functional connectivity, while Broca's region (8.4%) and in particular posterior superior parietal cortex (SPC) (6.6%), posterior IPC (1.7%), and anterior SPC (0.4%) showed little coactivation with our seed regions (OP 1/OP 4). Comparing this distribution of functional connectivity with the respective anatomical connectivity strengths, both similarities and differences become evident. (Fig. 6*C*). In particular, it can be noted that the regions featuring the strongest anatomical connections (anterior IPC, PCG) with the seed region on the parietal operculum defined by cytoarchitectonic areas OP 1 and OP 4 also show the highest functional connectivity. In contrast, both anatomical and functional connectivity with regions like anterior and posterior SPC and posterior IPC are congruently low. Notable exceptions, however, can be found with respect to the connectivity of OP1 and OP 4 with the premotor cortex and VL/VA. Here, functional connectivity is much stronger as compared with the density of anatomical connections.

### *Differences in frontoparietal functional connectivity between OP 1 and OP 4*

To assess the functional connectivity of OP 1 and OP 4, separate meta-analyses were performed including only those studies that specifically activated the respective area. The resulting coactivation maps (Fig. 7*A*,*B*) show patterns of functional connectivity that, albeit sharing some similarities, are distinctly different from each other. In particular, it can be noted, that OP 1 activations are primarily associated with activity of the anterior IPC, extending into the IPS. Regions coactivating with OP 4, on the other hand, were found anterior to those and consisted of the inferior frontal and pericentral somatosensory and motor cortices. Concurrent coactivation, finally, was in particular found bilaterally in the thalamus (with a focus on VL/VA known to project also strongly to the premotor and primary motor cortices), in the region of the supplementary motor cortex on the mesial wall of the frontal lobe and inferior frontal gyri on both hemispheres.

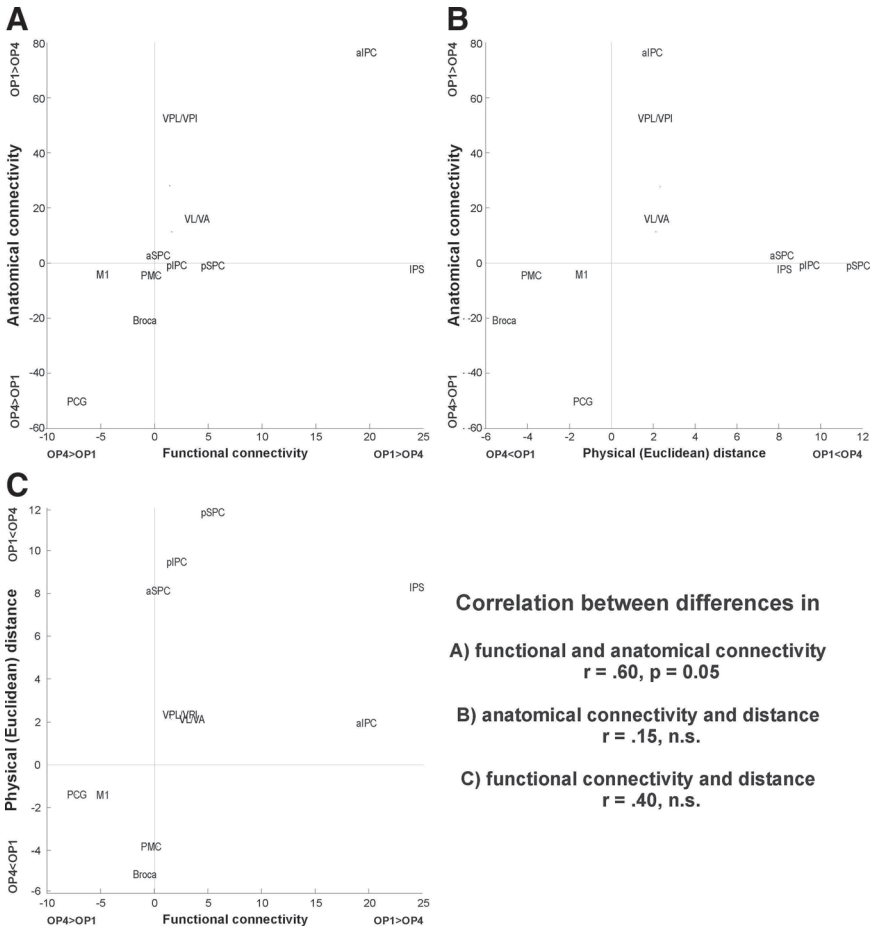


**Figure 8.** ***A***, Comparison of the differences between OP 1 and OP 4 in terms of their anatomical (as assessed by probabilistic tractography) and functional (as assessed by meta-analysis of neuroimaging data) connectivity to the assessed frontoparietal targets. Each target is represented by a data point indicated by the position of its acronym on a two-dimensional coordinate grid. The *x*-coordinate of this point indicates the difference in functional connectivity (quantified by coactivated volume fraction) between this target and OP 1 on one hand and OP 4 on the other. Precisely, the *x*-value of target acronym's position is equivalent to the strength of functional connectivity between this target and OP 1 minus the strength of functional connectivity between this target and OP 4. The *y*-coordinate indicates the difference in anatomical connectivity (quantified by normalized connection strength). That is, the *y*-value of target acronym's position is equivalent to the strength of anatomical connectivity from OP 1 and this target minus the strength of anatomical connectivity from OP 4 and this target. It may be argued that one or both of these measures may be confounded by the physical distance between seed and target. Hence, differences in anatomical and functional connectivity were also plotted against the difference between OP 1 and OP 4 in their physical distance (quantified by the mean Euclidean distance across seed voxels to the nearest target voxel) to the respective target. ***B*** and ***C***, The comparison between anatomical connectivity and physical (Euclidean) distance is shown in ***B***, and the comparison between functional connectivity and physical distance is shown in ***C***. It can be seen that differences between OP 1 and OP 4 in terms of functional and anatomical connectivity are significantly correlated to each other but not to physical distances to the targets.

To identify differences in functional connectivity between OP 1 and OP 4, we then contrasted the two functional connectivity maps (Laird et al., 2005), hereby delineating those voxels that showed significantly ( $p < 0.05$ corrected) higher probability of coactivation with OP 1 and OP 4, respectively (Fig. 7*C*). Significant differences were found in the parietal operculum, which is a trivial finding as the two cohorts of experiments being compared were defined by the presence of activations in OP 1 and OP 4, respectively. However, we also found several other regions showing significant differences in functional connectivity with OP 1 and OP 4, respectively. In particular, activation in OP 1 was significantly stronger associated with coactivations in anterior IPC, where 45.5% of all voxels showing significantly higher functional connectivity with OP 1 were located. Moreover, 35.2% of the significantly different voxels were localized in anterior IPS, and 18.5% were allocated to the PCG. Regions showing significantly higher functional connectivity with OP 4, in turn, were the PCG (where 68.8% of the voxels showing significantly higher connectivity to OP 4 were located), primary motor cortex (18.9%), and premotor cortex (10.3%).

### Comparison between anatomical and functional connectivity

These differences in functional connectivity of OP 1 and OP 4 to other frontoparietal areas relate well to the above-mentioned differences in anatomical connectivity between these two areas (Fig. 8). It can be noted that those target regions that have a stronger anatomical connectivity to OP 1 as compared with OP 4, e.g., the anterior IPC or the thalamus, also tend to have a higher functional connectivity with that region. In contrast, regions like M1 or Broca's area, which are more closely connected to OP 4 than to OP 1, also feature more frequent coactivations with OP 4. Finally, those regions that show little difference in anatomical connectivity coactivate at about the same amount with both areas. Consequently, there is a significant ( $p = 0.05$, $r = 0.60$) correlation between both measures of connectivity.

Besides these congruencies, however, there also exist few notable exceptions. For example, whereas there is little difference in anatomical connectivity to IPS between OP 1 and OP 4, OP 1 features a considerably stronger functional connectivity to this region. Likewise, whereas VPL/VPI are anatomically much more strongly connected to OP 1 as compared with OP 4, the corresponding difference in functional connectivity is considerably smaller.

To exclude a potential influence of the distance between different areas, we assessed how these differences in anatomical and functional connectivity relate to differences in the proximity, i.e., physical distance, between OP 1 and OP 4, respectively, and the different targets. As shown in Figure 8, differences in physical distance are not correlated to differences in anatomical or functional connectivity.

### Analysis of behavioral domain profiles

Assessing the BD meta-data associated with all experiments in the BrainMap database that featured at least one focus of activation in OP 1 and OP 4, respectively, indicated that the BD profiles of both cortical fields were significantly different from the overall distribution in the BrainMap database (Fig. 9). In particular, "action" was significantly over-represented in both parietal opercular regions. That is, a higher proportion of experiments that feature activation in OP 1/OP 4 relate to action as expected from the overall proportion of "action" experiments in the BrainMap database. "Emotion" and "cognition," in contrast, were underrepresented in both assessed cortical fields, whereas there was no

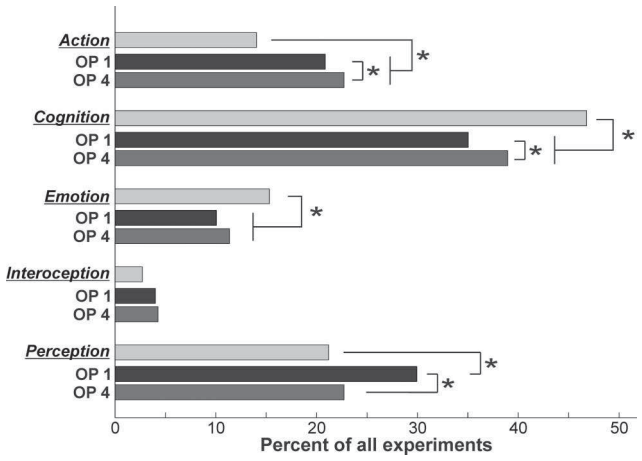


**Figure 9.** Behavioral domain profiles for all those experiments that feature at least one activation in OP 1 and OP 4, respectively. BrainMap counts (light gray histograms) represent the proportion of experiments in BrainMap that relate to the particular BD category. Dark gray and medium gray histograms represent the proportion of experiments featuring an activation in OP 1 and OP 4, respectively, that belong to the particular BD. All histograms were significantly different from each other with respect to overall shape. Asterisks denote significant ( $p < 0.05$) differences in the individual comparisons.

significant difference between OP 1 or OP 4 and the entire database with respect to experiments relating to interoception. Finally, only in OP 1, but not in OP 4, the "perception" BD was significantly over-represented.

There was also a significant difference in the BD profiles of experiments featuring activation in OP 1 and OP 4, respectively. This effect related to a higher proportion of "action" and "cognition" experiments found among those that activate OP 4. Among those experiments that activate OP 1, however, the proportion of those related to "perception" and in particular "somesthesis" was significantly higher than in OP 4.

## Discussion

In the present study, anatomical and functional connectivity of human parietal opercular areas OP 1 and OP 4 were investigated by probabilistic tractography and coordinate-based meta-analysis. Anatomical and functional connectivity of these two areas, considered together, was closest with the anterior IPC, PCG, and the thalamus. Particularly the PMC, however, showed stronger functional than anatomical connectivity to the parietal operculum. Probabilistic tractography and coactivation mapping revealed largely congruent differences (across methods) between OP 1 and OP 4 connectivity. OP 1 is closer connected to anterior IPC, the IPS, VPL/VPI, and the opposite hemisphere. OP 4, in turn, has closer anatomical and functional connections to the PCG and M1 as well as premotor and inferior frontal cortices.

### Comparison to connectivity in nonhuman primates

Macaque areas S2 and PV have dense reciprocal connections to the PCG (particularly areas 3b and 1) and inferior parietal area 7b (Disbrow et al., 2003), while marmosets feature a similar yet less specific pattern of connectivity (Krubitzer and Kaas, 1990; Qi et al., 2002). We here confirm the close connectivity of S2 (OP 1) and PV (OP 4) to the PCG and the inferior parietal cortex in humans. The dissociation reported here between S2 (connected to inferior parietal cortex) and PV (connected to the PCG) has not been found in any other primate species.

Area OP 4 (PV) featured significantly higher connectivity to the PMC and Broca's region than OP 1. Our data hence match observations of axonal connectivity between PMC and PV but not S2 in macaques (Disbrow et al., 2003). In marmosets, PMC connectivity of area S2 was reported but weaker than that of area PV (Stepniewska et al., 2006) While Disbrow et al. (2003) found no evidence for M1 connectivity of S2 or PV in macaques, an earlier study reported strong connectivity of a seed region comprising both areas with PMC and M1 (Cipolloni and Pandya, 1999). In marmosets, connections between M1 and PV (but not S2) have also been demonstrated (Qi et al., 2002). The human data fit this somewhat inconsistent picture by showing significantly stronger connectivity of OP 4 (PV) to all frontal targets, although the dissociation between anatomical and functional connectivity to the PMC and open questions about homologies warrant further investigation.

In macaques (Friedman and Murray, 1986; Disbrow et al., 2002, 2003) and marmosets (Krubitzer and Kaas, 1990; Qi et al., 2002), S2 and PV receive their main thalamic input from the ventroposterior inferior nucleus (VPI), while PV was reported to receive input from nuclei associated with the motor system (e.g., VL). Within the limits of resolution achievable by *in vivo* imaging methods, the current analysis confirms these findings in humans.

### Criteria for cortical areas

A sensory cortical area should be defined by the following criteria (Kaas, 1983; Orban et al., 2004): (1) a distinct histology, as shown for S2/PV in marmosets (Krubitzer and Kaas, 1990) and macaques (Krubitzer et al., 1995), as well as for OP 1 (S2)/OP 4 (PV) in humans (Eickhoff et al., 2006c); (2) a distinct pattern of connectivity, as demonstrated for S2/PV in marmosets (Krubitzer and Kaas, 1990; Qi et al., 2002) and macaques (Burton et al., 1995; Disbrow et al., 2002, 2003) and reported here for OP 1/OP 4 in humans; (3) the presence of a somatotopic map, as demonstrated for S2 (OP 1)/PV (OP 4) in marmosets (Krubitzer and Kaas, 1990; Qi et al., 2002), macaques (Krubitzer et al., 1995; Disbrow et al., 2003), and humans (Eickhoff et al., 2007); (4) distinct functional properties. Up to now, data on the functional differentiation between S2 (OP 1) and PV (OP 4) are limited but growing in nonhuman primates (Fitzgerald et al., 2004, 2006b) and man (Burton et al., 2008a, 2008b) as discussed below.

### Potential functional roles for OP 1/S2 and OP 4/PV

OP 4 is densely connected to the PCG and the frontal cortex and may consequently play a role in sensory-motor integration processes, such as incorporating sensory feedback into motor actions (Rizzolatti and Wolpert, 2005; Halsband and Lange, 2006). Knowledge of performed movements is also crucial in tactile object recognition and manipulation. Both roles have previously been ascribed to the parietal operculum (Inoue et al., 2002; Wasaka et al., 2005). Based on the current results, we suggest that they may be sustained particularly by OP 4. This interpretation is supported by studies showing that activity in OP 4 but not OP 1 is modulated by increased attention during tactile object discrimination (Young et al., 2004), and that activation to active discrimination tasks activated a more anterior focus than a passive somatosensory control task (Ledberg et al., 1995). In a series of studies, Fitzgerald and colleagues described several functionally distinct fields on the parietal operculum of macaque monkeys (Fitzgerald et al., 2004, 2006a, 2006b). They noted that neurons in fields proposed to match PV may relate to motor functions, as these showed responses similar to the hand manipulation neurons in the superior parietal cortex (Kalaska et al., 1983). Moreover, processing of proprioceptive input and integration of information across multiple digits favored the hypothesis that PV

may extract structural components of actively touched objects, which could then spatially guide further manipulation (Burton et al., 1997, 1999).

In contrast, strong connectivity of OP 1 with anterior parietal cortex, VPL/VPI, and the contralateral hemisphere may predispose it to perform more integrative aspects of somatosensory processing. Hence, OP 1 may represent the anatomical substrate of the various more complex functions reported to involve the parietal operculum, such as tactile working memory, stimulus discrimination (particularly frequency), and perceptual learning (Romo et al., 2002; Torquati et al., 2002; Pleger et al., 2003; Burton et al., 2008a, 2008b). Matching this view, neurons showing attention and stimulus discrimination have been described in the posterior parietal operculum (area S2) of macaque monkeys (Robinson and Burton, 1980; Hsiao et al., 1993). It is not yet precisely known how these functions (attention and stimulus discrimination) are implemented neuronally. Evidence from single-cell recordings, however, suggests that differences between parietal opercular fields with respect to modulations of synchrony, receptive field layout, and neuronal tuning may underlie their functional differentiation (Steinmetz et al., 2000; Fitzgerald et al., 2006a). Finally, OP 1 may also hold an important role in bimanual processing. In an fMRI/MEG study, Disbrow et al. (2001) demonstrated that S2/PV receives bilateral input, but extensive contralateral processing occurs before interhemispheric transfer. We propose that particularly the later ipsilateral component might be attributed to OP 1, given the higher amount of transcallosal connections in this area. This would match the observation that unilateral stimulation activation on the anterior parietal operculum (presumably OP 4) is followed by ipsilateral posterior activation (presumably OP 1) with a latency of ~30 ms (Mima et al., 1997).

Assessing the behavioral domain profiles of experiments featuring activation in OP 1 (S2) and OP 4 (PV), respectively, were well in accordance with the differentiation suggested by the differences in anatomical and functional connectivity, as well as the hypothesis from nonhuman primate data. This analysis of functional processes isolated by the statistical contrasts that activated the two parietal opercular areas confirmed that OP 1 (S2) was indeed more likely activated by somatosensory perceptive tasks, whereas OP 4 was more associated with action, i.e., motor-related experiments.

### Discrepancies between connectivity measures

Despite the close congruency between anatomical and functional connectivity (Figs. 6*C*, 8), several divergences were noted. These discrepancies may have resulted from various sources of measurement error and noise in the data that may differ systematically or unsystematically between both approaches. Examples for such methodological issues would be discrepancies in the effective spatial resolution of the data, differences in assessed sample, influences of the choices about the used models for diffusion tractography or functional connectivity analyses (as various methods exist for either approach), differences in potential confounds affecting the two very different approaches, or potentially dissimilar characteristics of unsystematic noise.

However, it should be noted that there are also major conceptual differences between functional and anatomical connectivity, as these assess different properties of brain networks. That is, there are several theoretical reasons, discussed below, why these two approaches may not provide completely congruent results even if there is no systematic or unsystematic error due to methodological or technical issues.

Coactivation of two regions may not be mediated by direct anatomical connections but via additional structures, e.g., relaying information from VL/VA or the premotor cortex to OP 4. Relay processes, however, could also be transmitted through cascades of several intermediates or via cortical-subcortical loops (Grefkes et al., 2008b; Eickhoff et al., 2009a).

A third area could induce correlated activation in regions not anatomically connected. That is, functional connectivity may be driven by an external source inducing concurrent activity in both areas, e.g., stimulus-driven activity in early sensory areas that is forwarded to parietal opercular areas for perceptual analysis and, in parallel, to premotor cortex for response preparation.

A very weak anatomical connection between two regions may still hold a high functional significance (Friston, 2002; Grefkes et al., 2008a), e.g., if one area's activity depends on a "go-signal" from another region. Functional connectivity is hence strongly influenced not only by the strength of an anatomical connection but also by the information conveyed through it.

None of these mechanisms inducing functional coupling would be reflected in anatomical connectivity measured by DTI. A deeper understanding of brain connectivity and the ensuing networks should thus rely on a combination of different but complementary approaches.

## References

Amunts K, Schleicher A, Burgel U, Mohlberg H, Uylings HB, Zilles K (1999) Broca's region revisited: cytoarchitecture and intersubject variability. J Comp Neurol 412:319–341.

Amunts K, Weiss PH, Mohlberg H, Pieperhoff P, Eickhoff S, Gurd JM, Marshall JC, Shah NJ, Fink GR, Zilles K (2004) Analysis of neural mechanisms underlying verbal fluency in cytoarchitectonically defined stereotaxic space—the roles of Brodmann areas 44 and 45. Neuroimage 22:42–56.

Ashburner J, Friston KJ (2005) Unified segmentation. Neuroimage 26:839–851.

Behrens TE, Johansen-Berg H, Woolrich MW, Smith SM, Wheeler-Kingshott CA, Boulby PA, Barker GJ, Sillery EL, Sheehan K, Ciccarelli O, Thompson AJ, Brady JM, Matthews PM (2003a) Non-invasive mapping of connections between human thalamus and cortex using diffusion imaging. Nat Neurosci 6:750–757.

Behrens TE, Woolrich MW, Jenkinson M, Johansen-Berg H, Nunes RG, Clare S, Matthews PM, Brady JM, Smith SM (2003b) Characterization and propagation of uncertainty in diffusion-weighted MR imaging. Magn Reson Med 50:1077–1088.

Behrens TE, Berg HJ, Jbabdi S, Rushworth MF, Woolrich MW (2007) Probabilistic diffusion tractography with multiple fibre orientations: what can we gain? Neuroimage 34:144–155.

Burton H, Fabri M, Alloway K (1995) Cortical areas within the lateral sulcus connected to cutaneous representations in areas 3b and 1: a revised interpretation of the second somatosensory area in macaque monkeys. J Comp Neurol 355:539–562.

Burton H, MacLeod AM, Videen TO, Raichle ME (1997) Multiple foci in parietal and frontal cortex activated by rubbing embossed grating patterns across fingerpads: a positron emission tomography study in humans. Cereb Cortex 7:3–17.

Burton H, Abend NS, MacLeod AM, Sinclair RJ, Snyder AZ, Raichle ME (1999) Tactile attention tasks enhance activation in somatosensory regions of parietal cortex: a positron emission tomography study. Cereb Cortex 9:662–674.

Burton H, Sinclair RJ, McLaren DG (2008a) Cortical network for vibrotactile attention: a fMRI study. Hum Brain Mapp 29:207–221.

Burton H, Sinclair RJ, Wingert JR, Dierker DL (2008b) Multiple parietal operculum subdivisions in humans: tactile activation maps. Somatosens Mot Res 25:149–162.

Caspers S, Geyer S, Schleicher A, Mohlberg H, Amunts K, Zilles K (2006) The human inferior parietal cortex: cytoarchitectonic parcellation and interindividual variability. 33:430–448.

Caspers S, Eickhoff SB, Geyer S, Scheperjans F, Mohlberg H, Zilles K, Amunts

K (2008) The human inferior parietal lobule in stereotaxic space. Brain Struct Funct 212:481–495.
Caspers S, Zilles K, Laird AR, Eickhoff SB (2010) ALE meta-analysis of action observation and imitation in the human brain. Neuroimage 50: 1148–1167.
Choi HJ, Zilles K, Mohlberg H, Schleicher A, Fink GR, Armstrong E, Amunts K (2006) Cytoarchitectonic identification and probabilistic mapping of two distinct areas within the anterior ventral bank of the human intraparietal sulcus. J Comp Neurol 495:53–69.
Cipolloni PB, Pandya DN (1999) Cortical connections of the frontoparietal opercular areas in the rhesus monkey. J Comp Neurol 403:431–458.
Collins DL, Neelin P, Peters TM, Evans AC (1994) Automatic 3D intersubject registration of MR volumetric data in standardized Talairach space. J Comput Assist Tomogr 18:192–205.
Coq JO, Qi H, Collins CE, Kaas JH (2004) Anatomical and functional organization of somatosensory areas of the lateral fissure of the New World titi monkey (Callicebus moloch). J Comp Neurol 476:363–387.
Cusick CG, Wall JT, Felleman DJ, Kaas JH (1989) Somatotopic organization of the lateral sulcus of owl monkeys: area 3b, S-II, and a ventral somatosensory area. J Comp Neurol 282:169–190.
Disbrow E, Roberts T, Krubitzer L (2000) Somatotopic organization of cortical fields in the lateral sulcus of Homo sapiens: evidence for SII and PV. J Comp Neurol 418:1–21.
Disbrow E, Roberts T, Poeppel D, Krubitzer L (2001) Evidence for interhemispheric processing of inputs from the hands in human S2 and PV. J Neurophysiol 85:2236–2244.
Disbrow E, Litinas E, Recanzone GH, Slutsky D, Krubitzer L (2002) Thalamocortical connections of the parietal ventral area (PV) and the second somatosensory area (S2) in macaque monkeys. Thalamus Relat Syst 1:289–302.
Disbrow E, Litinas E, Recanzone GH, Padberg J, Krubitzer L (2003) Cortical connections of the second somatosensory area and the parietal ventral area in macaque monkeys. J Comp Neurol 462:382–399.
Eickhoff SB, Stephan KE, Mohlberg H, Grefkes C, Fink GR, Amunts K, Zilles K (2005) A new SPM toolbox for combining probabilistic cytoarchitectonic maps and functional imaging data. Neuroimage 25:1325–1335.
Eickhoff SB, Amunts K, Mohlberg H, Zilles K (2006a) The human parietal operculum. II. Stereotaxic maps and correlation with functional imaging results. Cereb Cortex 16:268–279.
Eickhoff SB, Heim S, Zilles K, Amunts K (2006b) Testing anatomically specified hypotheses in functional imaging using cytoarchitectonic maps. Neuroimage 32:570–582.
Eickhoff SB, Lotze M, Wietke B, Amunts K, Enck P, Zilles K (2006c) Segregation of visceral and somatosensory afferents: an fMRI and cytoarchitectonic mapping study. Neuroimage 31:1004–1014.
Eickhoff SB, Schleicher A, Zilles K, Amunts K (2006d) The human parietal operculum. I. Cytoarchitectonic mapping of subdivisions. Cereb Cortex 16:254–267.
Eickhoff SB, Weiss PH, Amunts K, Fink GR, Zilles K (2006e) Identifying human parietal-insular vestibular cortex using fMRI and cytoarchitectonic mapping. Hum Brain Mapp 27:611–621.
Eickhoff SB, Grefkes C, Zilles K, Fink GR (2007) The somatotopic organization of cytoarchitectonic areas on the human parietal operculum. Cereb Cortex 17:1800–1811.
Eickhoff SB, Heim S, Zilles K, Amunts K (2009a) A systems perspective on the effective connectivity of overt speech production. Philos Transact A Math Phys Eng Sci 367:2399–2421.
Eickhoff SB, Laird AR, Grefkes C, Wang LE, Zilles K, Fox PT (2009b) Coordinate-based activation likelihood estimation meta-analysis of neuroimaging data: a random-effects approach based on empirical estimates of spatial uncertainty. Hum Brain Mapp 30:2907–2926.
Evans AC, Marrett S, Neelin P, Collins L, Worsley K, Dai W, Milot S, Meyer E, Bub D (1992) Anatomical mapping of functional activation in stereotactic coordinate space. Neuroimage 1:43–53.
Fitzgerald PJ, Lane JW, Thakur PH, Hsiao SS (2004) Receptive field properties of the macaque second somatosensory cortex: evidence for multiple functional representations. J Neurosci 24:11193–11204.
Fitzgerald PJ, Lane JW, Thakur PH, Hsiao SS (2006a) Receptive field properties of the macaque second somatosensory cortex: representation of orientation on different finger pads. J Neurosci 26:6473–6484.
Fitzgerald PJ, Lane JW, Thakur PH, Hsiao SS (2006b) Receptive field (RF) properties of the macaque second somatosensory cortex: RF size, shape, and somatotopic organization. J Neurosci 26:6485–6495.
Fox PT, Lancaster JL (2002) Opinion: Mapping context and content: the BrainMap model. Nat Rev Neurosci 3:319–321.
Friedman DP, Murray EA (1986) Thalamic connectivity of the second somatosensory area and neighboring somatosensory fields of the lateral sulcus of the macaque. J Comp Neurol 252:348–373.
Friston K (2002) Functional integration and inference in the brain. Prog Neurobiol 68:113–143.
Geyer S (2003) The microstructural border between the motor and the cognitive domain in the human cerebral cortex. Wien: Springer.
Geyer S, Ledberg A, Schleicher A, Kinomura S, Schormann T, Burgel U, Klingberg T, Larsson J, Zilles K, Roland PE (1996) Two different areas within the primary motor cortex of man. Nature 382:805–807.
Geyer S, Schleicher A, Zilles K (1999) Areas 3a, 3b, and 1 of human primary somatosensory cortex. 1. Microstructural organization and interindividual variability. Neuroimage 10:63–83.
Geyer S, Schormann T, Mohlberg H, Zilles K (2000) Areas 3a, 3b, and 1 of human primary somatosensory cortex. Part 2. Spatial normalization to standard anatomical space. Neuroimage 11:684–696.
Grefkes C, Geyer S, Schormann T, Roland P, Zilles K (2001) Human somatosensory area 2: observer-independent cytoarchitectonic mapping, interindividual variability, and population map. Neuroimage 14:617–631.
Grefkes C, Eickhoff SB, Nowak DA, Dafotakis M, Fink GR (2008a) Dynamic intra- and interhemispheric interactions during unilateral and bilateral hand movements assessed with fMRI and DCM. Neuroimage 41:1382–1394.
Grefkes C, Nowak DA, Eickhoff SB, Dafotakis M, Kust J, Karbe H, Fink GR (2008b) Cortical connectivity after subcortical stroke assessed with functional magnetic resonance imaging. Ann Neurol 63:236–246.
Halsband U, Lange RK (2006) Motor learning in man: a review of functional and clinical studies. J Physiol Paris 99:414–424.
Hsiao SS, O'Shaughnessy DM, Johnson KO (1993) Effects of selective attention on spatial form processing in monkey primary and secondary somatosensory cortex. J Neurophysiol 70:444–447.
Huffman KJ, Nelson J, Clarey J, Krubitzer L (1999) Organization of somatosensory cortex in three species of marsupials, *Dasyurus hallucatus*, *Dactylopsila trivirgata*, and *Monodelphis domestica*: neural correlates of morphological specializations. J Comp Neurol 403:5–32.
Inoue K, Yamashita T, Harada T, Nakamura S (2002) Role of human SII cortices in sensorimotor integration. Clin Neurophysiol 113:1573–1578.
Jung P, Baumgärtner U, Stoeter P, Treede RD (2009) Structural and functional asymmetry in the human parietal opercular cortex. J Neurophysiol 101:3246–3257.
Kaas JH (1983) What, if anything, is SI? Organization of first somatosensory area of cortex. Physiol Rev 63:206–231.
Kaas JH, Collins CE (2003) The organization of somatosensory cortex in anthropoid primates. Adv Neurol 93:57–67.
Kalaska JF, Caminiti R, Georgopoulos AP (1983) Cortical mechanisms related to the direction of two-dimensional arm movements: relations in parietal area 5 and comparison with motor cortex. Exp Brain Res 51:247–260.
Kell CA, von Kriegstein K, Rösler A, Kleinschmidt A, Laufs H (2005) The sensory cortical representation of the human penis: revisiting somatotopy in the male homunculus. J Neurosci 25:5984–5987.
Koski L, Paus T (2000) Functional connectivity of the anterior cingulate cortex within the human frontal lobe: a brain-mapping meta-analysis. Exp Brain Res 133:55–65.
Krubitzer LA, Calford MB (1992) Five topographically organized fields in the somatosensory cortex of the flying fox: microelectrode maps, myeloarchitecture, and cortical modules. J Comp Neurol 317:1–30.
Krubitzer LA, Kaas JH (1990) The organization and connections of somatosensory cortex in marmosets. J Neurosci 10:952–974.
Krubitzer L, Clarey J, Tweedale R, Elston G, Calford M (1995) A redefinition of somatosensory areas in the lateral sulcus of macaque monkeys. J Neurosci 15:3821–3839.
Laird AR, Fox PM, Price CJ, Glahn DC, Uecker AM, Lancaster JL, Turkeltaub PE, Kochunov P, Fox PT (2005) ALE meta-analysis: controlling the false discovery rate and performing statistical contrasts. Hum Brain Mapp 25:155–164.
Laird AR, Eickhoff SB, Kurth F, Fox PM, Uecker AM, Turner JA, Robinson JL,

Lancaster JL, Fox PT (2009a) ALE meta-analysis workflows via the brainmap database: progress towards a probabilistic functional brain atlas. Front Neuroinformatics 3:23.

Laird AR, Eickhoff SB, Li K, Robin DA, Glahn DC, Fox PT (2009b) Investigating the functional heterogeneity of the default mode network using coordinate-based meta-analytic modeling. J Neurosci 29:14496–14505.

Ledberg A, O'Sullivan BT, Kinomura S, Roland PE (1995) Somatosensory activations of the parietal operculum of man: a PET study. Eur J Neurosci 7:1934–1941.

Mima T, Ikeda A, Nagamine T, Yazawa S, Kunieda T, Mikuni N, Taki W, Kimura J, Shibasaki H (1997) Human second somatosensory area: subdural and magnetoencephalographic recording of somatosensory evoked responses. J Neurol Neurosurg Psychiatry 63:501–505.

Orban GA, Van ED, Vanduffel W (2004) Comparative mapping of higher visual areas in monkeys and humans. Trends Cogn Sci 8:315–324.

Pleger B, Foerster AF, Ragert P, Dinse HR, Schwenkreis P, Malin JP, Nicolas V, Tegenthoff M (2003) Functional imaging of perceptual learning in human primary and secondary somatosensory cortex. Neuron 40:643–653.

Qi HX, Lyon DC, Kaas JH (2002) Cortical and thalamic connections of the parietal ventral somatosensory area in marmoset monkeys (Callithrix jacchus). J Comp Neurol 443:168–182.

Rizzolatti G, Wolpert DM (2005) Motor systems. Curr Opin Neurobiol 15:623–625.

Robinson CJ, Burton H (1980) Somatic submodality distribution within the second somatosensory (SII), 7b, retroinsular, postauditory, and granular insular cortical areas of M. fascicularis. J Comp Neurol 192:93–108.

Robinson JL, Laird AR, Glahn DC, Lovallo WR, Fox PT (2009) Metaanalytic connectivity modeling: delineating the functional connectivity of the human amygdala. Hum Brain Mapp 31:173–184.

Romo R, Hernandez A, Zainos A, Lemus L, Brody CD (2002) Neuronal correlates of decision-making in secondary somatosensory cortex. Nat Neurosci 5:1217–1225.

Rushworth MF, Behrens TE, Johansen-Berg H (2006) Connection patterns distinguish 3 regions of human parietal cortex. Cereb Cortex 16:1418–1430.

Scheperjans F, Hermann K, Eickhoff SB, Amunts K, Schleicher A, Zilles K (2008a) Observer-independent cytoarchitectonic mapping of the human superior parietal cortex. Cereb Cortex 18:846–867.

Scheperjans F, Eickhoff SB, Homke L, Mohlberg H, Hermann K, Amunts K, Zilles K (2008b) Probabilistic maps, morphometry, and variability of cytoarchitectonic areas in the human superior parietal cortex. Cereb Cortex 18:2141–2157.

Schleicher A, Palomero-Gallagher N, Morosan P, Eickhoff SB, Kowalski T, de Vos K, Amunts K, Zilles K (2005) Quantitative architectectural analysis: a new approach to cortical mapping. Anat Embryol (Berl) 210:373–386.

Smith SM, Jenkinson M, Woolrich MW, Beckmann CF, Behrens TE, Johansen-Berg H, Bannister PR, De LM, Drobnjak I, Flitney DE, Niazy RK, Saunders J, Vickers J, Zhang Y, De SN, Brady JM, Matthews PM (2004) Advances in functional and structural MR image analysis and implementation as FSL. Neuroimage 23 [Suppl 1]:S208–S219.

Smith SM, Fox PT, Miller KL, Glahn DC, Fox PM, Mackay CE, Filippini N, Watkins KE, Toro R, Laird AR, Beckmann CF (2009) Correspondence of the brain's functional architecture during activation and rest. Proc Natl Acad Sci U S A 106:13040–13045.

Steinmetz PN, Roy A, Fitzgerald PJ, Hsiao SS, Johnson KO, Niebur E (2000) Attention modulates synchronized neuronal firing in primate somatosensory cortex. Nature 404:187–190.

Stepniewska I, Preuss T, Kaas JH (2006) Ipsilateral cortical connections of dorsal and ventral premotor areas in new world owl monkeys. J Comp Neurol 495:691–708.

Tomassini V, Jbabdi S, Klein JC, Behrens TE, Pozzilli C, Matthews PM, Rushworth MF, Johansen-Berg H (2007) Diffusion-weighted imaging tractography-based parcellation of the human lateral premotor cortex identifies dorsal and ventral subregions with anatomical and functional specializations. J Neurosci 27:10259–10269.

Toro R, Fox PT, Paus T (2008) Functional coactivation map of the human brain. Cereb Cortex 18:2553–2559.

Torquati K, Pizzella V, Della PS, Franciotti R, Babiloni C, Rossini PM, Romani GL (2002) Comparison between SI and SII responses as a function of stimulus intensity. Neuroreport 13:813–819.

Tukey JW (1994) The problem of multiple comparisons. In: The collected works of John W., vol. III Tukey (Braun HI, ed), pp. 1–300. New York: Chapman & Hall.

Turkeltaub PE, Eden GF, Jones KM, Zeffiro TA (2002) Meta-analysis of the functional neuroanatomy of single-word reading: method and validation. Neuroimage 16:765–780.

Wasaka T, Nakata H, Akatsuka K, Kida T, Inui K, Kakigi R (2005) Differential modulation in human primary and secondary somatosensory cortices during the preparatory period of self-initiated finger movement. Eur J Neurosci 22:1239–1247.

Worsley KJ, Marrett S, Neelin P, Vandal AC, Friston KJ, Evans AC (1996) A unified statistical approach for determining significant signals in images of cerebral activation. Hum Brain Mapp 4:58–74.

Young JP, Herath P, Eickhoff S, Choi J, Grefkes C, Zilles K, Roland PE (2004) Somatotopy and attentional modulation of the human parietal and opercular regions. J Neurosci 24:5391–5399.

Zilles K, Schleicher A, Palomero-Gallagher N, Amunts K (2002) Quantitative analysis of cyto- and receptor architecture of the human brain. In: Brain mapping, the methods (Mazziotta J, Toga A, eds), pp 573–602. San Diego: Academic.

Cerebral Cortex Advance Access published February 28, 2012

Cerebral Cortex
doi:10.1093/cercor/bhs048

# Organization of the Human Inferior Parietal Lobule Based on Receptor Architectonics

Svenja Caspers[1], Axel Schleicher[2], Mareike Bacha-Trams[1,3], Nicola Palomero-Gallagher[1], Katrin Amunts[1,4,5] and Karl Zilles[1,2,4]

[1]Institute of Neuroscience and Medicine (INM-1, INM-2), Research Centre Jülich, 52425 Jülich, Germany, [2]C. and O. Vogt Institute for Brain Research, Heinrich-Heine-University Düsseldorf, 40001 Düsseldorf, Germany, [3]Max-Planck-Institute for Human Cognitive and Brain Sciences, 04103 Leipzig, Germany, [4]JARA-BRAIN, Jülich-Aachen Research Alliance, 52425 Jülich, Germany and [5]Department of Psychiatry, Psychotherapy, and Psychosomatics, RWTH Aachen University, 52072 Aachen, Germany

Address correspondence to Dr Svenja Caspers, Institut für Neurowissenschaften und Medizin, INM-2, Forschungszentrum Jülich, 52425 Jülich, Germany. Email: s.caspers@fz-juelich.de.

**Human inferior parietal lobule (IPL) plays a key role in various cognitive functions. Its functional diversity, including attention, language, and action processing, is reflected by its structural segregation into 7 cytoarchitectonically distinct areas, each with characteristic connectivity patterns. We hypothesized that commonalities of the cytoarchitectonic, connectional, and functional diversity of the IPL should be reflected by a correlated transmitter receptor–based organization. Since the function of a cortical area requires a well-tuned receptor balance, the densities of 15 different receptors were measured in each IPL area. A hierarchical cluster analysis of the receptor balance revealed a tripartite segregation of the IPL into a rostral, middle, and caudal group. Comparison with other cortical areas showed strong similarities with Broca's region for all 3 groups, with the superior parietal cortex for the middle, and with extrastriate visual areas for the caudal group. Notably, caudalmost area PGp has a receptor fingerprint very similar to that of ventral extrastriate visual cortex. We therefore propose a new organizational model of the human IPL, consisting of 3 clusters, which corresponds to its known cytoarchitectonic, connectional, and functional diversity at the molecular level. This might reflect a general organizational principle of human IPL, beyond specific functional domains.**

**Keywords:** architecture, cerebral cortex, inferior parietal lobe, structural segregation, transmitter receptors

## Introduction

The human inferior parietal lobule (IPL) comprises the supramarginal gyrus rostrally and the angular gyrus caudally. Brodmann (1909) subdivided the human IPL into 2 cytoarchitectonical areas: BA 40 rostrally and BA 39 caudally. Electrophysiological studies in macaques and functional neuroimaging in humans suggest, however, a functionally much more heterogeneous IPL than Brodmann's map suggests. The cytoarchitectonic analysis of von Economo and Koskinas (1925) hinted at a more detailed parcellation. They defined several subtypes within the 2 main IPL areas (termed PF and PG) but could not establish them as unique.

In monkeys, rostral IPL is involved in sensorimotor integration and contains mirror neurons (Fogassi et al. 2005), whereas caudal IPL was found to participate in spatial attention, visuomotor, and auditory processes (Mountcastle et al. 1975; Hyvärinen 1982; Pandya and Seltzer 1982; Seltzer and Pandya 1984; Rozzi et al. 2008). A comparable functional segregation was found in humans: Rostral human IPL seems to be involved in motor planning and action-related functions and is part of the human mirror neuron system (Iacoboni 2005; Rizzolatti 2005; Keysers and Gazzola 2009; Caspers et al. 2010). The left caudal IPL is active during language-related tasks with focus on semantic and phonological issues (Price 2000; Vigneau et al. 2006), while the right caudal IPL was found to be involved in spatial and nonspatial attention as well as motor preparation (Fink et al. 2001; Corbetta et al. 2008).

This functional segregation found a structural correlation in recent observations. In monkeys, 4 areas were identified on the lateral surface of the IPL and 2 areas on the caudal part of the parietal operculum within the Sylvian fissure (Pandya and Seltzer 1982; Gregoriou et al. 2006). In humans, a similar parcellation could be established. Seven cytoarchitectonically distinct areas were recently described, 5 of which are located on the lateral surface, whereas the remaining 2 areas are located on the caudal parietal operculum (Caspers et al. 2006, 2008) (Fig. 1).

The functional and architectonical diversity of the IPL are also reflected by differential connectivity patterns of the areas. The fiber tracts between the IPL and other cortical areas change from rostral to caudal, as demonstrated in a recent diffusion tensor imaging study (Caspers, Eickhoff, et al. 2011): Whereas rostral IPL areas show strong connections with inferior frontal, motor, premotor, and somatosensory areas, caudal IPL areas are more strongly connected with posterior parietal, higher visual, and temporal areas. Areas in the middle of the IPL are connected with the targets of both rostral and caudal IPL areas. A comparable differential connectivity pattern was found by means of connectivity-based parcellation of the IPL (Mars et al. 2011). This pattern strikingly resembles that found in tracer studies in macaques (Cavada and Goldman-Rakic 1989a, 1989b; Andersen et al. 1990; Rozzi et al. 2006). Thus, the structural, functional, and connectivity data favor the concept of a highly segregated brain region.

Mapping the regional and laminar distribution patterns of different receptors in the cerebral cortex proved to be a powerful tool for detecting functionally meaningful cortical parcellations (Zilles and Palomero-Gallagher 2001; Zilles, Palomero-Gallagher, et al. 2002; Zilles, Schleicher, et al. 2002; Zilles and Amunts 2009). Not only primary motor, premotor, and primary somatosensory cortices (Geyer et al. 1997, 1998) but also higher order areas such as Broca's region (Amunts et al. 2010), the striate and extrastriate visual cortex (Eickhoff et al. 2007, 2008) as well as the superior parietal lobule (Scheperjans, Grefkes, et al. 2005; Scheperjans, Palomero-Gallagher, et al. 2005), the cingulate cortex (Palomero-Gallagher et al. 2009), and the superior temporal gyrus (Morosan et al. 2005) have been subdivided into distinct receptor-architectonical entities. Moreover, it has been demonstrated that cortical areas with similar receptor expression patterns are nodes in the same functionally distinct neural network (Zilles, Palomero-Gallagher, et al. 2002; Zilles and Amunts 2009).

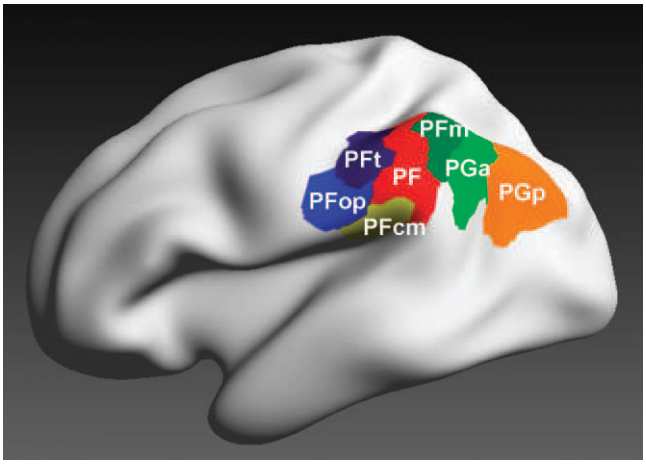


**Figure 1.** 3D reconstructed maximum probability maps of the 7 cytoarchitectonically defined IPL areas PFt, PFop, PF, PFm, PFcm, PGa, and PGp (Caspers et al. 2006, 2008) on the inflated lateral surface view of the Montreal Neurological Institute single subject template.

We therefore used quantitative in vitro autoradiography for multireceptor mapping in the human IPL to understand the molecular basis underlying its structural and functional heterogeneity. We studied the densities of multiple receptor binding sites and the regionally specific balances between them in each of the 7 cytoarchitectonic areas of the IPL (Caspers et al. 2006, 2008). Their regional receptor distribution patterns were then compared with those of cortical areas outside the IPL to gain further insight into the receptor-based organization of the cerebral cortex, similarities and dissimilarities of receptor expression patterns between distinct functional systems, and the putative relationships of the different IPL areas with various functional systems.

## Material and Methods

### *Postmortem Tissue Extraction and Preparation*

Nine human postmortem hemispheres (6 right and 3 left) were obtained from body donors without any known history of neurological or psychiatric disorders, according to legal requirements. Brains were removed from the skull within 24 h post-mortem (Table 1).

Each hemisphere was cut into 5 or 6 coronal slabs of about 25–30 mm thickness each. After shock freezing of the tissue at −50 °C for 10 min in liquid isopentane to avoid freezing artifacts within the cortex, the slabs were stored at −70 °C. Subsequently, each slab was cut into serial coronal sections (20 μm thickness) at −20 °C, using a large-scale cryostat microtome. The sections were thaw mounted onto glass slides prior to further processing (Fig. 2*A*,*B*).

### *Autoradiographic Labeling of Receptors*

For quantitative autoradiographic multireceptor analysis of the human IPL, alternating sections were 1) incubated with a tritiated receptor ligand, 2) incubated with a tritiated ligand and a nonradioactive displacing compound to measure the nonspecific binding of the receptor, or 3) stained for cell bodies using a modified silver stain (Merker 1983). Thus, a group of sections at the same sectioning level provided information about the receptor distribution of different receptors as well as the corresponding cytoarchitecture.

In total, distribution of 15 different receptors from 6 classical neurotransmitter systems was investigated in the present study: glutamatergic (α-amino-3-hydroxy-5-methyl-4-isoxazolepropionic acid [AMPA], kainate, *N*-methyl-D-aspartate [NMDA]), γ-aminobutyric acid (GABA)ergic ($GABA_A$-, $GABA_B$-, $GABA_A$-associated benzodiazepine-binding sites), cholinergic (nicotinic, muscarinic $M_1$, $M_2$, $M_3$), adrenergic ($\alpha_1$, $\alpha_2$), serotoninergic ($5\text{-}HT_{1A}$, $5\text{-}HT_2$), and dopaminergic ($D_1$). Supplementary Table S1 provides an overview of the binding protocols for all receptors studied. For all receptors and cases, nonspecific binding was less than 5% of the total binding. Thus, the total binding of each receptor could be accepted as an estimate of the specific binding.

**Table 1**
Data of postmortem brains used for receptor analysis of the IPL

| Brain no. | Hemisphere | Sex | Age (years) | Cause of death | Postmortem delay (h) |
|---|---|---|---|---|---|
| 1 | Left | Female | 77 | Coronary heart disease | 10 |
| 2 | Right | Male | 72 | Cardiac arrest | 8 |
| 3 | Left/right | Female | 77 | Pulmonary edema | 18 |
| 4 | Left/right | Male | 78 | Multiorganic failure | 12 |
| 5 | Left/right | Female | 75 | Bronchial cancer | 16 |
| 6 | Right | Male | 79 | Sudden cardiac death, chronic cardiac insufficiency | 12 |

After incubation with the tritiated ligands, the sections were coexposed with plastic scales of known concentrations of radioactivity to films sensitive to β-radiation (Hyperfilm, Amersham or Kodak BioMax MR films) for 8–18 weeks, depending on the receptor (Supplementary Table S1). The resulting autoradiographs (Fig. 2*C*) represent the regional and laminar distribution of receptor-binding sites. The gray value distribution within the autoradiographs was nonlinearly correlated with the local concentration of the radioactivity. The known radioactivity of the coexposed plastic standards was calibrated to brain homogenates with known protein concentration to allow transformation of gray values of the autoradiographs into total binding (femtomole per milligram protein), displayed within linearized images (Fig. 2*D*). For a more comfortable visualization of the local receptor distribution within the sections, the linearized images were contrast enhanced, smoothed, and pseudocolor coded in a spectral sequence (Fig. 2*E*). After digitization of the films, receptor concentrations were measured as described previously (Zilles, Palomero-Gallagher, et al. 2002; Zilles, Schleicher, et al. 2002; Zilles et al. 2004; Schleicher et al. 2009).

### *Quantitative Receptor Analysis of the IPL*

For the analysis of receptor densities in different cortical areas, regions of interest (ROIs) were defined, using the cell body–stained sections adjacent to each group of autoradiographs. ROIs covered the whole cortical width. Seven IPL areas (PFt, PFop, PF, PFm, PFcm, PGa, and PGp) were identified based on cytoarchitectonic criteria as published (Caspers et al. 2006). To assure that the 7 cytoarchitectonically defined IPL areas were identified in a similar way by their receptor distribution pattern and for consecutive analysis of laminar receptor distributions, borders between the IPL areas and surrounding cortical regions were delineated within all receptor autoradiographs. For delineation of these borders, a multivariate statistical algorithm–based approach was used (Schleicher et al. 2005, 2009). This algorithm uses laminar information of the gray-level index distribution within each section. Feature vectors described the shape of each profile and thus reflected the underlying laminar receptor architecture. Using the Mahalanobis distance as distance measure, adjacent blocks of profiles could be compared by means of Hotelling's $T^2$-test for significant differences in Mahalanobis distance (Bonferroni-corrected for multiple comparisons). Delineation of areas was possible since profiles from different cortical areas differed considerably in shape, which results in larger distances between them (Zilles et al. 2004; Schleicher et al. 2009). This procedure was repeatedly carried out for blocks of profiles (ranging from 10 to 24 profiles per block) to improve signal-to-noise ratio (Figs 3 and 4).

After delineation of the IPL areas, respective ROIs were defined (3 per area per hemisphere) for subsequent averaging where receptor densities of the 15 different receptors were measured (Zilles, Palomero-Gallagher, et al. 2002; Zilles, Schleicher, et al. 2002; Schleicher et al. 2009), using MATLAB 7.7 (The MathWorks Inc.). For each of the 7 IPL areas, receptor density values were averaged over the 9 hemispheres, providing a mean value for each receptor in each area.

The receptor balance of each area was visualized as receptor fingerprint. The mean receptor densities (averaged over all cortical

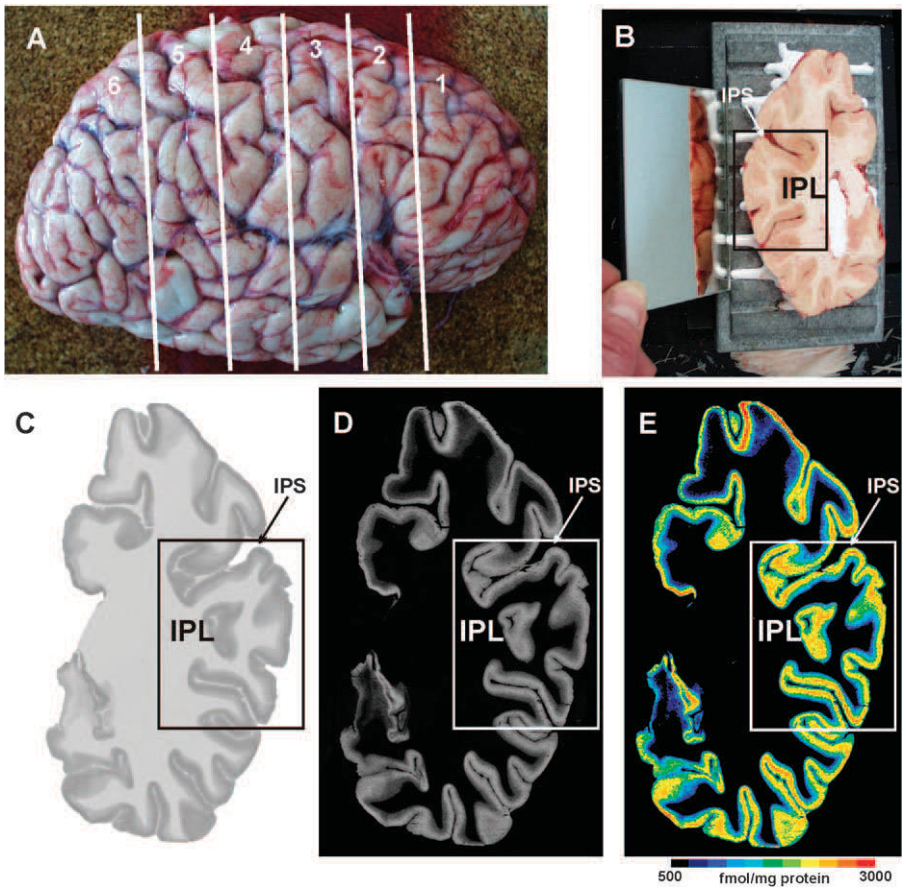


**Figure 2.** Quantitative in vitro receptor autoradiography. (*A*) Right human hemisphere prior to sectioning into 6 slabs (white lines) for further processing. (*B*) Blockface of a frozen slab on the cryotome with the labeled ROI in the present study (IPL). The mirror on the left side provides a lateral view of the tissue slab. (*C*) Autoradiograph of the $GABA_B$ receptor of the same slab, ROI marked by a box. (*D*) Scaled autoradiograph (same as in *C*) with gray values reflecting the receptor concentrations, calculated from coexposed plastic scales of known radioactivity concentrations. (*E*) Pseudocolor-coded autoradiograph (same as in *C*). The colors indicate receptor concentrations, from black for low to red for high concentrations (for concentrations in femtomole per milligram protein, see color bar). IPS: intraparietal sulcus.

layers) for each receptor type (averaged over hemispheres) were registered in a polar plot, which represent the characteristic receptor fingerprint of each area. These fingerprints could consecutively be compared with regard to their size and shape by using a unified scaling for each receptor for all areas (Zilles, Palomero-Gallagher, et al. 2002; Zilles, Schleicher, et al. 2002). This allows a direct comparison of different cortical areas to reveal similarities and differences in their receptor distribution pattern.

For comparison with other cortical areas, additional ROIs were defined based on published cytoarchitectonic and macroanatomical criteria. Cortical areas were chosen to optimally categorize the IPL areas in relation to other cortical areas. Therefore, ROIs within primary as well as higher order association cortices were defined: primary motor cortex (M1; Geyer et al. 1996); primary somatosensory areas 3b and 1 (S1_3b, S1_1; Geyer et al. 1999, 2000); primary and secondary visual cortex (V1, V2; Amunts et al. 2000); ventral extrastriate visual cortex lateral to V1 and V2 (mainly V3v, V4v; Rottschy et al. 2007); primary and secondary auditory cortex (A1, A2; Morosan et al. 2001); Broca's area (area 44; Amunts et al. 1999, 2010); and posterior superior parietal lobule (area 7A; Scheperjans, Hermann, et al. 2008; Scheperjans, Eickhoff, et al. 2008). ROIs within Broca's area and the superior parietal lobule were chosen representatively. It was shown that both these regions could be parcellated into several subdivisions based on their receptor architecture. But the architecture within these subdivisions was very similar to each other, especially as compared with other cortical areas (Scheperjans, Grefkes, et al. 2005; Scheperjans, Palomero-Gallagher, et al. 2005; Amunts et al. 2010). Thus, including more subdivisions within the present analysis would not add substantial new information for a basic functional classification of the IPL areas.

### *Statistical Analysis*

The mean density values of all 15 receptors studied were combined into a feature vector for each area. Since absolute receptor concentrations differed considerably between receptor types, all values were $z$-transformed across areas prior to any further analysis. The transformation enabled analyses where all receptors had equal weight. Similarities and differences between receptor distribution patterns of areas were analyzed by means of a hierarchical cluster analysis (MATLAB 7.7, Statistics Toolbox, The MathWorks Inc.), using Euclidean distances in combination with the Ward linkage method. Euclidean distances between feature vectors became smaller the more similar the areas were.

In addition, areal feature vectors were further analyzed by means of a multidimensional scaling (MDS; Systat 12) to detect similar and dissimilar groups of areas. MDS resulted in a 2D display of the 15-dimensional receptor feature vectors. To identify those receptors, which accounted most for separation into different clusters, a multivariate canonical discriminant analysis was performed (Systat 12).

All these analyses were carried out on the mean receptor densities of all IPL areas. The hierarchical cluster analysis was also conducted for the comparison of IPL with other cortical areas.

## Results

### *Receptor Mapping of IPL Areas*

The measurement of the receptor density of each area from the cortical surface to the cortex/white matter border demonstrates the quantitative laminar-specific distribution of the receptors.

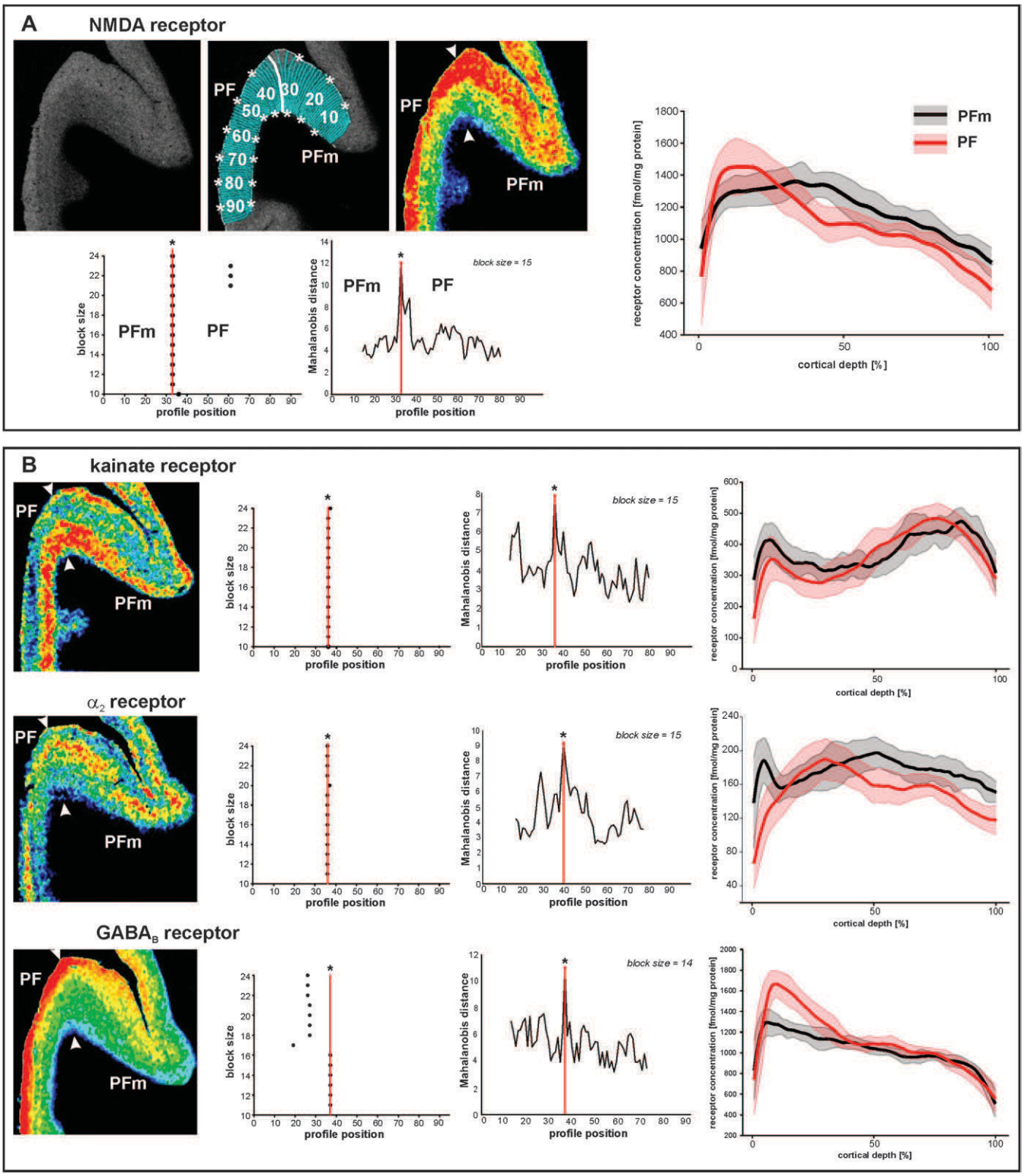


**Figure 3.** Parcellation of IPL based on receptor distribution patterns. (*A*) Part of a receptor autoradiograph (NMDA receptor) of the IPL (border region between areas PF and PFm as shown in Figure 5*A* for whole IPL). The autoradiograph of the cortical ribbon (upper left) was covered by traverses running perpendicular to the cortical layers (upper middle) and pseudocolor coded for visualization purposes only (upper right). Results of the algorithmic parcellation are shown below: the left graph shows the significant maxima of varying block sizes (ranging from 10 to 24); it indicates a consistently occurring border between 2 cortical areas at profile location 33. Right next to it, a line plot shows the Mahalanobis distances between neighboring blocks of profiles; it confirms the location of the maximal distance, and thus, the maximal dissimilarity between adjacent profiles at profile location 33, which defines an architectural border. The border is also labeled in the autoradiographs above. The graph on the right side of (*A*) shows the laminar distribution (with standard deviations) of the NMDA receptor throughout the cortical width (0% at the transition from the pial surface to layer I; 100% at the transition from layer VI to the white matter) in areas PF and PFm. The profiles differ between both areas. (*B*) Parcellation of the same part of the cortex by 3 other receptors (kainate, $\alpha_2$, and $GABA_B$). Figures and graphs of (*B*) show the results of the mapping procedure comparable to (*A*).

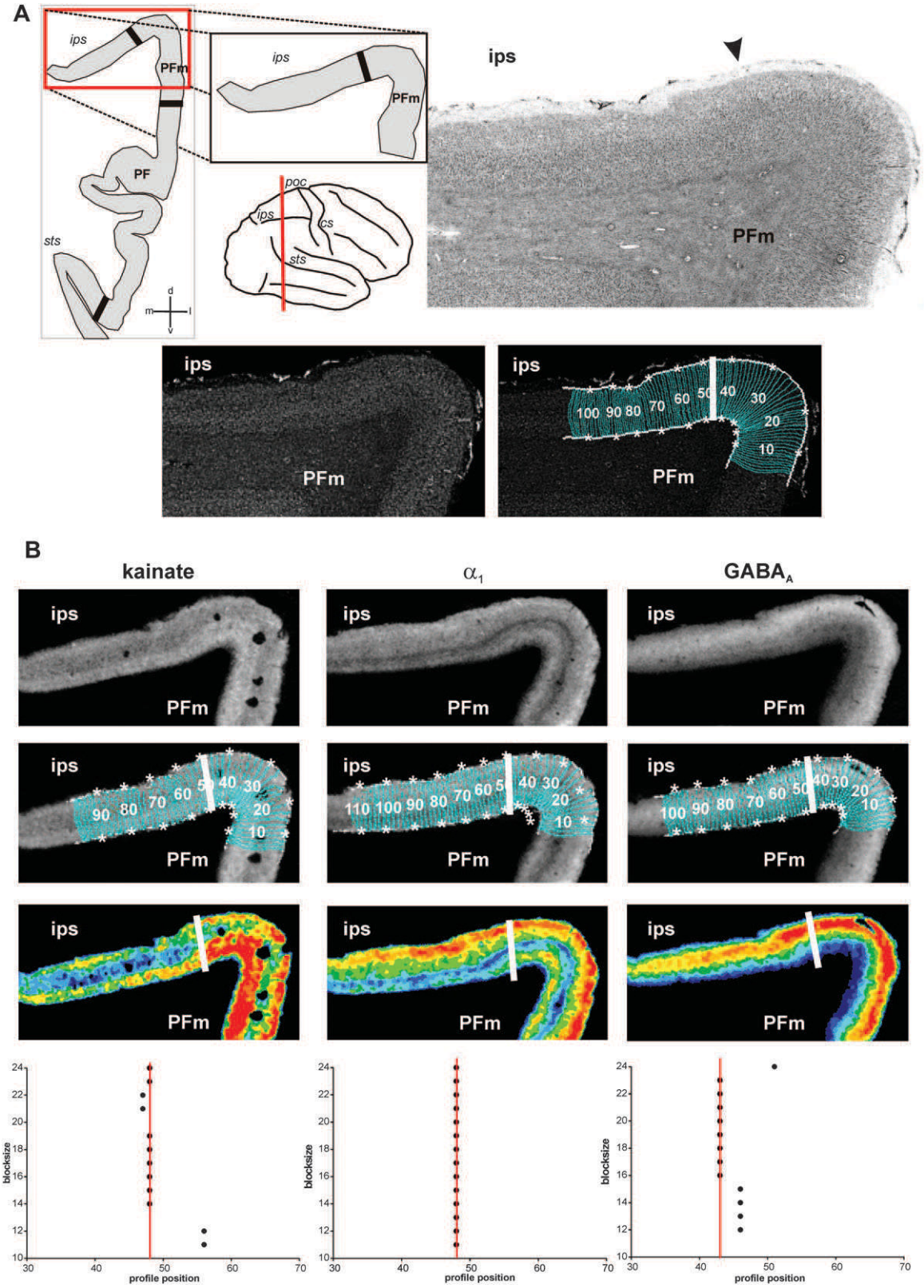


**Figure 4.** Algorithm-based detection of areal borders in receptor and corresponding cytoarchitectonic sections. (*A*) Cytoarchitectonic border between area PFm and areas within the intraparietal sulcus (IPS), sectioning level (red line), and schematic drawing of the IPL within this section with all detected borders (black thick lines) depicted on the left. Corresponding gray level index image and traverses covering the cortical ribbon beneath with detected border indicated by a white bold line at profile position no. 47. (*B*) Same border on corresponding sections of kainate, $GABA_A$, and $\alpha_1$ receptors. For each receptor, the linearized autoradiograph, superimposed with traverses covering the ROI, and pseudocolor coded for visualization purposes. Position of the border indicated by white bold lines and in the graphs at the bottom at the respective profile position (same type of graphs as in Fig. 3). Area PFm differs from intraparietal areas by means of higher concentrations of kainate in middle and lower layers, higher concentrations of $\alpha_1$ in infragranular layers and of $GABA_A$ in supragranular layers. Note the close resemblance of the position of the border in cyto- and receptor sections. cs: central sulcus, ips: intraparietal sulcus, poc: postcentral sulcus, sts: superior temporal sulcus.

The differences between the density profiles were used for the statistically testable and observer-independent definition of areal borders (for details, see Fig. 3 and Schleicher et al. 2005). As an example for the multireceptor mapping of the IPL, the receptor-architectonically defined border for different receptor types between areas PF and PFm is shown in Figure 3.

The receptor-based parcellation approach (Zilles, Palomero-Gallagher, et al. 2002; Zilles, Schleicher, et al. 2002; Morosan et al. 2005; Zilles and Amunts 2009) led to the identification of the same 7 IPL areas as previously identified by cytoarchitectonic criteria (Caspers et al. 2006, 2008): areas PFt, PFop, PF, PFm, PFcm, PGa, and PGp. The precise match between receptor and cytoarchitectonic mapping can be demonstrated by comparing receptor architectonic with corresponding (neighboring) cytoarchitectonic sections of the same brain (Fig. 4).

Differences in laminar patterns largely contribute (in addition to differences in the absolute concentration within the cortex) to the regional segregation of the IPL into 7 receptor-architectonic areas. The border regions between neighboring IPL areas are shown in Figures 5 and 6.

It has already been noted that not all receptors show each border (Zilles, Palomero-Gallagher, et al. 2002; Zilles, Schleicher, et al. 2002) and that borders are not equally clear pronounced by all receptor types. However, if a border has been detected by several or all receptor types, it has the same spatial position (Figs 3–6). Differences between the rostral-most IPL areas PFop, PFt, and PF were most prominently indicated by the kainate, NMDA, $GABA_A$, and $\alpha_1$ receptors. Here, PF showed higher concentrations for the kainate, NMDA, and $\alpha_1$ receptors and lower concentrations for the $GABA_A$ receptor as compared with PFt and PFop (Fig. 5).

Figure 6 displays the border regions between the more caudal IPL areas. Area PFm could be distinguished from area PF most clearly by the NMDA and $GABA_B$ receptors, whereby PFm

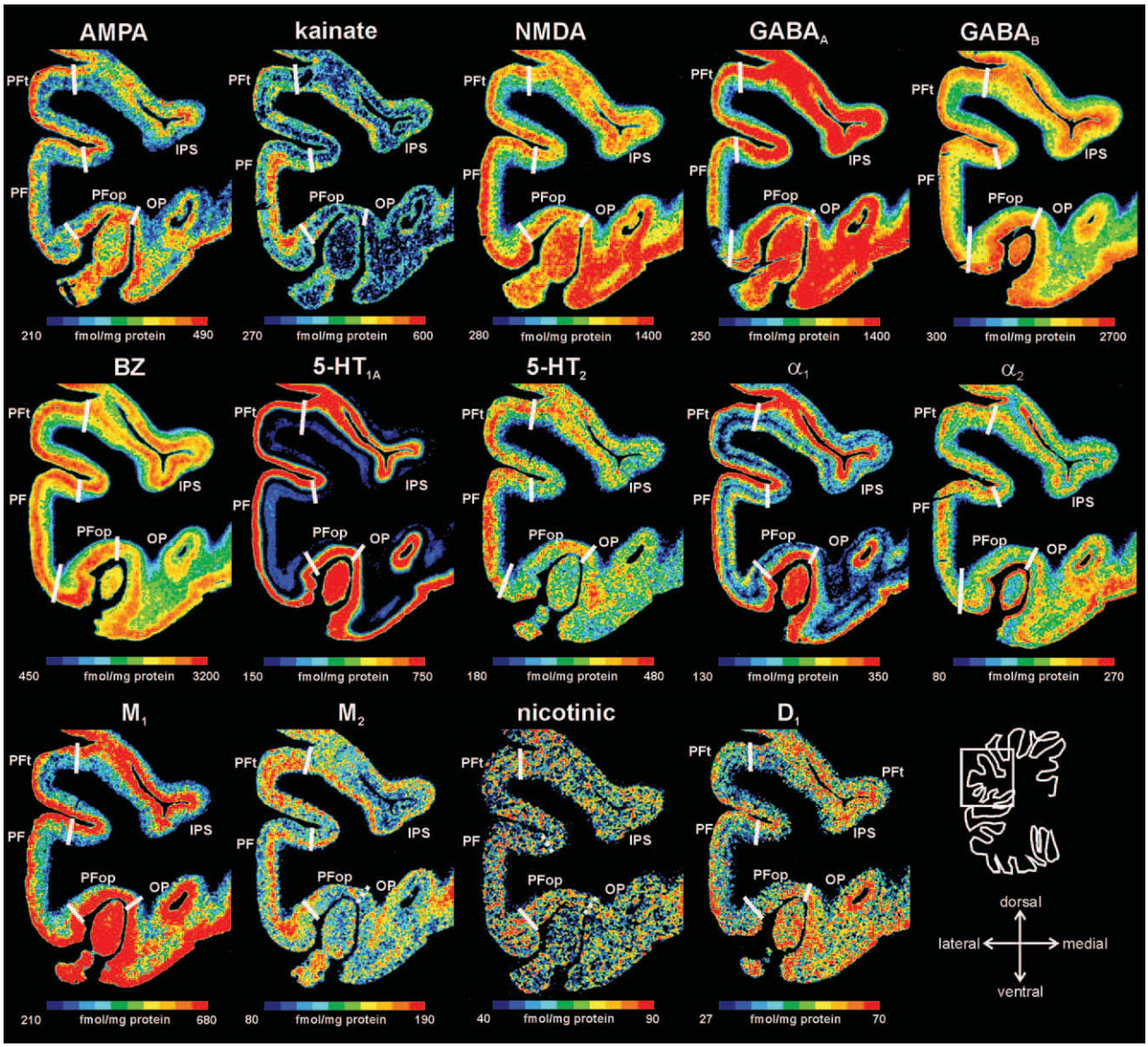


**Figure 5.** Receptor distribution patterns in areas PF, PFop, and PFt illustrated for 14 of the 15 receptors studied. Pseudocolor-coded autoradiographs show the borders between the IPL areas (white lines). The color bar beneath each autoradiograph indicates receptor concentrations by the different colors, from black for low to red for high concentrations (in femtomole per milligram protein). Note that the scaling is different for each receptor.

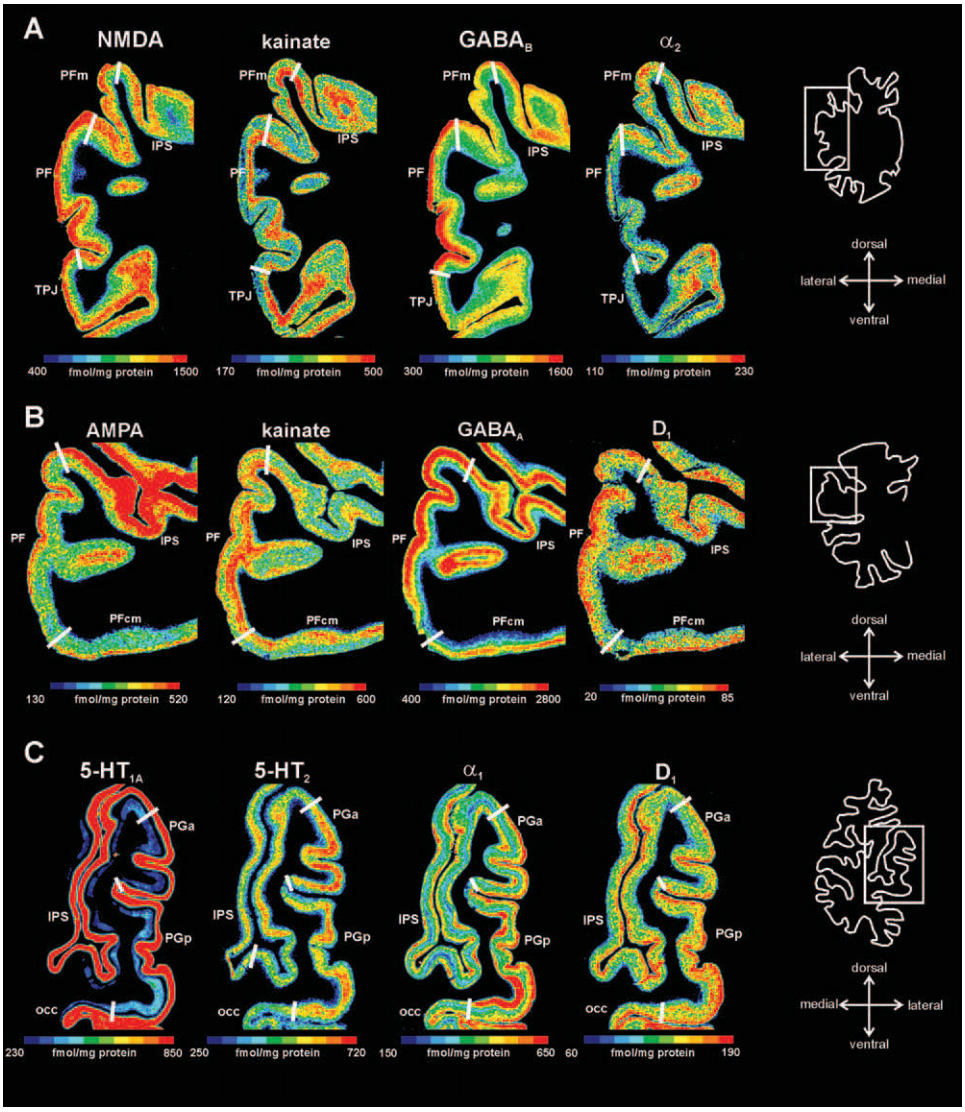


**Figure 6.** Receptor distribution patterns of areas PF, PFm, PFcm, PGa, and PGp for those receptors, which showed most prominent differences between the areas. (*A*) Delineation of areas PF and PFm (same level as in Fig. 3). (*B*) Delineation of areas PF and PFcm. (*C*) Delineation of areas PGa and PGp. For other conventions, see Figure 4.

had lower concentrations in the supragranular layers than area PF. Conversely, area PFm showed higher concentrations of kainate and $\alpha_2$ receptors in the supragranular layers than area PF (Fig. 6*A*).

Area PFcm most prominently differed from area PF with regard to the AMPA, kainate, $GABA_A$, and the $D_1$ receptors, whereby PFcm showed considerably lower concentrations than PF (Fig. 6*B*).

Caudal-most areas PGa and PGp were best delineated by the 5-$HT_{1A}$, 5-$HT_2$, $\alpha_1$, and $D_1$ receptors. PGp showed higher concentrations of 5-$HT_{1A}$ and $\alpha_1$ receptors in the infragranular layers and of the $D_1$ receptor in the supragranular layers than PGa. Concentrations of 5-$HT_2$ receptors were higher in supragranular layers of PGa as compared with PGp (Fig. 6*C*).

### *Quantitative Analysis of Mean Receptor Densities*

#### *Receptor Fingerprints of the IPL Areas*

The receptor densities of each IPL area and each receptor type are displayed in Table 2. Highest mean densities (averaged over all cortical layers) are found for the NMDA, $GABA_A$, $GABA_B$, and benzodiazepine-binding sites, lowest densities are reached by the $D_1$, nicotinic, and $M_2$ receptors. Maximal or minimal receptor densities of each receptor type are found in different areas of the IPL. Thus, each area has a specific balance between the different receptor types.

The area-specific balances between the 15 receptors can be visualized as "receptor fingerprints" (Fig. 7). Comparing the shapes of the fingerprints revealed a rostrocaudal gradient: The fingerprints based on absolute receptor concentrations (Fig. 7*A*) showed higher concentrations of the benzodiazepine binding sites in the rostral (Fig. 7, upper part) as compared with more caudal IPL areas (Fig. 7, lower part). Fingerprints based on normalized receptor concentrations (Fig. 7*B*) additionally showed lower AMPA, $GABA_A$, $\alpha_2$, and $D_1$ receptor concentrations and higher kainate, 5-$HT_{1A}$, and 5-$HT_2$ receptor concentrations in the rostral as compared with the caudal IPL areas. Caudal-most area PGp is characterized by high concentrations of the $M_2$ receptor, whereas area PGa shows exceptionally high concentrations of the nicotinic receptor.

**Table 2**
Mean receptor densities (averaged over all cortical layers) in femtomole per milligram protein (±SD) of IPL areas

| Receptor | IPL areas | | | | | | |
|---|---|---|---|---|---|---|---|
| | PFop | PFt | PFcm | PF | PFm | PGa | PGp |
| AMPA | 358.09 ± 62.73 | 363,65 ± 51.11 | 324.84 ± 65.24 | 424.66 ± 65.09 | 398.26 ± 48,09 | 437.99 ± 64.62 | 464.30 ± 85.84 |
| Kainate | 457.37 ± 77.49 | 541.48 ± 91.61 | 521,42 ± 131.47 | 659.84 ± 92.94 | 596.46 ± 97.96 | 587.77 ± 122.92 | 487.41 ± 104.19 |
| NMDA | 1142.85 ± 84.49 | 1077.73 ± 107.60 | 1114.54 ± 129.36 | 1158.25 ± 97.03 | 1240.96 ± 79.20 | 1223.37 ± 73.86 | 1116.08 ± 124.75 |
| $GABA_A$ | 1588.22 ± 131.31 | 1675.23 ± 126.70 | 1460.58 ± 164.06 | 1508.03 ± 124.92 | 1539.34 ± 102.92 | 1939.48 ± 157.07 | 1832.05 ± 244.97 |
| $GABA_B$ | 2195.31 ± 213.24 | 2285.14 ± 152.90 | 2033.04 ± 280.58 | 2192.64 ± 208.12 | 2200.67 ± 260.67 | 2664.09 ± 121.44 | 2297.44 ± 248.66 |
| BZ | 2828.36 ± 250.41 | 2797.80 ± 280.24 | 2845.69 ± 410.11 | 2716.50 ± 281.80 | 2489.03 ± 344.75 | 2445.60 ± 293.86 | 2378.00 ± 331.18 |
| $5\text{-}HT_{1A}$ | 439.85 ± 73.24 | 405.46 ± 60.78 | 414.99 ± 103.43 | 361.44 ± 49.54 | 335.93 ± 47.62 | 313.00 ± 46.05 | 328.45 ± 65.46 |
| $5\text{-}HT_2$ | 433.94 ± 41.13 | 434.17 ± 48.31 | 434.28 ± 53.21 | 441.92 ± 49.34 | 424.76 ± 59.87 | 412.24 ± 70.71 | 382.79 ± 59.43 |
| $M_1$ | 535.57 ± 73.88 | 470.10 ± 61.39 | 497.67 ± 92.89 | 459.90 ± 69.93 | 489.62 ± 80.42 | 456.47 ± 67.90 | 452.02 ± 61.00 |
| $M_2$ | 159.29 ± 14.33 | 161.32 ± 12.12 | 138.68 ± 19.31 | 170.53 ± 25.40 | 173.50 ± 26.22 | 158.87 ± 29.98 | 201.75 ± 48.54 |
| $M_3$ | 902.58 ± 220.18 | 850.92 ± 178.10 | 660.20 ± 143.45 | 821.06 ± 105.22 | 775.76 ± 107.59 | 736.76 ± 96.82 | 741.39 ± 131.85 |
| nic | 44.93 ± 10.09 | 48.10 ± 8.83 | 38.29 ± 8.85 | 58.91 ± 13.44 | 60.39 ± 11.46 | 68.50 ± 11.51 | 46.07 ± 11.59 |
| $\alpha_1$ | 362.04 ± 36.82 | 365.44 ± 34.94 | 335.63 ± 36.52 | 372.21 ± 57.03 | 393.38 ± 49.38 | 343.41 ± 50.17 | 356.91 ± 40.37 |
| $\alpha_2$ | 304.26 ± 80.51 | 335.93 ± 88.95 | 297.52 ± 95.33 | 370.43 ± 118.34 | 303.08 ± 84.95 | 343.25 ± 86.58 | 327.10 ± 64.74 |
| $D_1$ | 89.11 ± 10.07 | 81.54 ± 11.86 | 86.46 ± 12.34 | 100.46 ± 15.63 | 105.61 ± 16.27 | 132.44 ± 18.00 | 105.14 ± 16.55 |

Note: Fifteen different receptors were measured in 9 hemispheres. SD: standard deviation.

### *Molecular Organization of the IPL*

For a comprehensive analysis of similarities between the receptor fingerprints of the different IPL areas, we performed a hierarchical cluster analysis (Fig. 8*A*). Three groups with similar receptor distributions within each group were identified: a rostroventral group with areas PFt, PFop, and PFcm; a middle group of areas PF and PFm; and a caudal group consisting of areas PGa and PGp. Furthermore, it became apparent that the PG areas were more similar to each other as compared with the rest of the IPL. This result reflects a clear architectural distinction between rostral and caudal IPL.

A consecutive canonical discriminant analysis with 2 discriminating dimensions (*x*- and *y*-axes in Fig. 8*B*) revealed a most pronounced distinction between the clusters within the first dimension (*x*-axis; 72% explained variance), complemented by the distinction within the second dimension (*y*-axis; 28% explained variance). Ranking the coefficients of the canonical discriminant analysis revealed those receptors, which contributed most to the distinction between the clusters in both dimensions. The kainate and $5\text{-}HT_2$ receptors contributed most to the distinction in both dimensions (absolute values of the coefficients: kainate: 2.22 [score 1] and 1.91 [score 2]; $5\text{-}HT_2$: 2.84 [score 1] and 1.58 [score 2]). The $M_1$ and $\alpha_2$ receptors provided additional criteria for this segregation within the first dimension (absolute values of coefficients: $M_1$: 1.10; $\alpha_2$: 1.05), whereas the $GABA_A$, nicotinic, and $D_1$ receptors were responsible for distinction between the clusters within the second dimension (absolute values of coefficients: $GABA_A$: 1.02; nicotinic: 1.10; $D_1$: 1.18).

MDS analysis (Fig. 8*C*) of the receptor densities highlights an inhomogeneity within the caudal cluster of areas PGa and PGp: the receptor organization of PGp seems to be more different (higher distance) from all the other IPL areas. This dissimilarity was not revealed by our previous cytoarchitectonic analysis of the IPL (Caspers et al. 2006, 2008). Based on the present results, area PGp might be reclassified as not being a typical parietal cortex. It might provide a transition to adjoining visual cortex, which can be underpinned by comparison with the receptor architecture of other cortical areas (see next paragraph).

### *Comparison with Other Cortical Areas*

We compared the IPL fingerprints with those of primary, secondary, and higher order sensory areas and the motor cortex to study the functional aspect of the receptor-based IPL segregation (Fig. 9).

Using a hierarchical cluster analysis, the fingerprints of the primary and secondary auditory and visual as well as primary somatosensory and motor cortices differed considerably from the cluster containing the IPL areas. The 7 IPL areas formed the same rostral, middle, and caudal subclusters as already found in the first cluster analysis of the IPL areas alone (Fig. 8*A*–*C*). The middle and caudal clusters of IPL areas are more similar to area 44 of Broca's area than the rostral cluster comprising PFcm, PFop, and PFt. The fingerprints of the centrally positioned areas PF and PFm are similar to the fingerprint of the superior parietal lobule. The caudally positioned areas PGa and PGp are similar to the higher ventral extrastriate area hOC3v (V3v), particularly for area PGp.

This result suggests again a potential role of area PGp as a higher visual area, linking occipital and parietal cortex.

## Discussion

Functional performance of a cortical area depends on a well-tuned and area-specific balance between numerous receptor types (Barnes and Sharp 1999; Goldman-Rakic et al. 2000; Gibbs and Summers 2002; Bergson et al. 2003; Bredt and Nicoll 2003; Friedman et al. 2004). Based on the similarities in receptor fingerprints of the 7 IPL areas, we propose a new organizational model of the IPL (Fig. 8*D*), comprising a rostroventral (areas PFt, PFop, and PFcm), an intermediate (areas PF and PFm), and a caudal group (areas PGa and PGp). The molecular structure of caudal-most IPL area PGp argues for a reclassification of this area as transition area between parietal and visual areas.

### *The 3-Region Model of Human IPL*

It has been shown repeatedly that receptor distributions are not only related to functional network properties of cortical areas (Barnes and Sharp 1999; Goldman-Rakic et al. 2000; Gibbs and Summers 2002; Bergson et al. 2003; Bredt and Nicoll 2003; Friedman et al. 2004) but also to their connectivity pattern (Rakic et al. 1988). The 3-region model of human IPL as revealed by multireceptor distribution could thus provide the molecular basis for the structural, functional, and connectivity components within a common organizational framework.

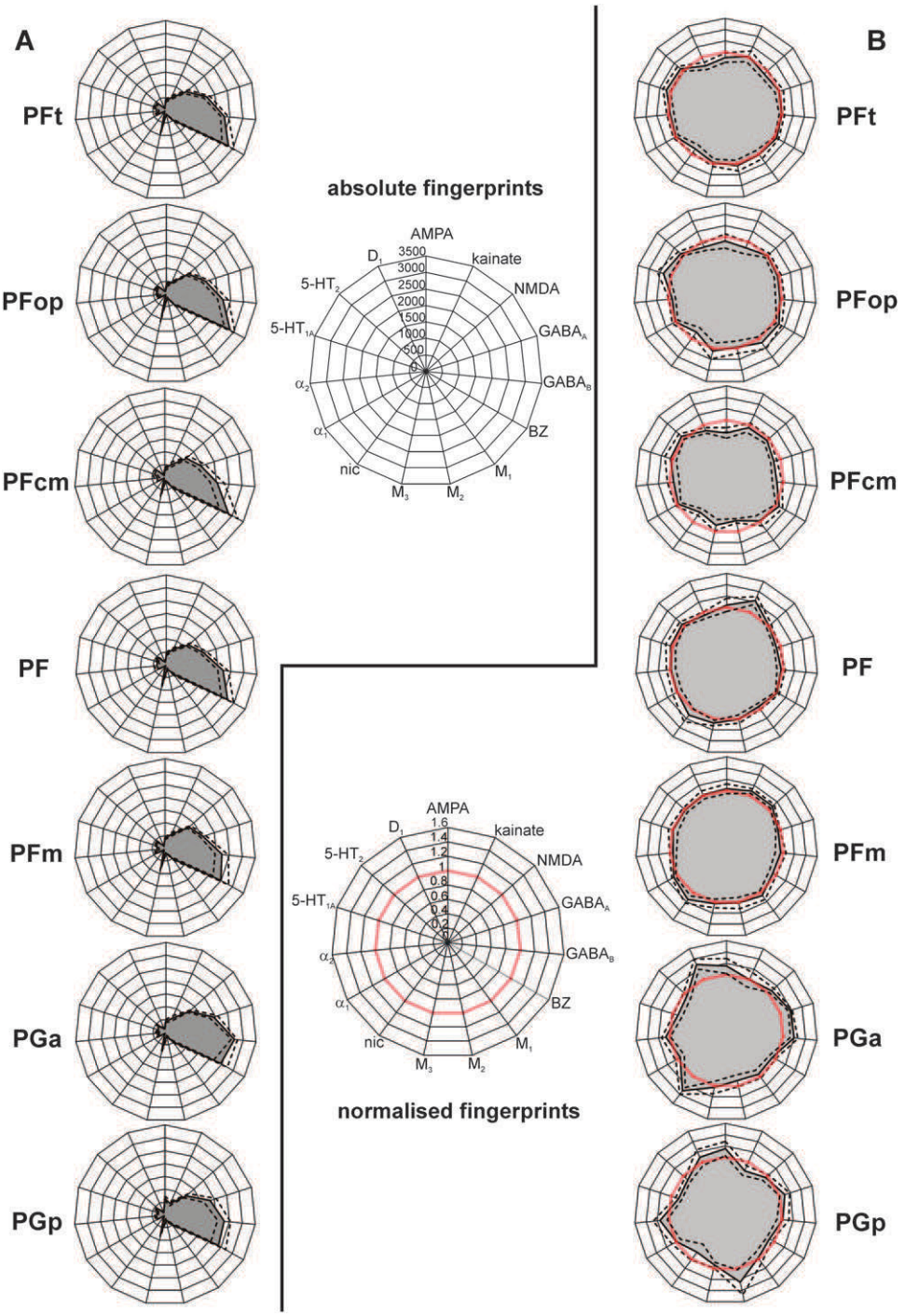


**Figure 7.** Receptor fingerprints of the 7 IPL areas PFt, PFop, PF, PFm, PFcm, PGa, and PGp. (*A*) Polar plots (scaling 0–3500 femtomole per milligram protein) showing the mean (averaged over all cortical layers) absolute receptor concentrations of all 15 receptors (with standard error of the mean as dotted lines) of each area. (*B*) Polar plots (scaling 0–1.6) showing the normalized receptor concentration of all 15 receptors (with standard error of the mean as dotted lines). Normalization of the receptor concentrations was calculated based on each receptor's mean over the whole IPL. Red thick line indicates the 100% line (labeled 1) where the receptor concentration of an area was equal to the mean receptor concentration averaged over the whole IPL. Note the difference in size and shape between the fingerprints of the different areas.

*Fiber Tracts*

The fiber tracts of the IPL show pronounced differences between rostral, middle, and caudal IPL. The rostral IPL is most likely connected with ventral premotor cortex and the caudal IPL with temporal areas (Croxson et al. 2005; Rushworth et al. 2006; Tomassini et al. 2007). This finding was supported by resting-state functional connectivity and structural connectivity–based parcellation analyses (Mars et al. 2011), which demonstrated a subdivision of right human IPL into 5 clusters, largely matching the cytoarchitectonic subdivision (Caspers et al. 2006, 2008). Caspers, Eickhoff, et al. (2011) demonstrated in a probabilistic fiber tracking study that rostral IPL areas had connections with inferior and middle frontal, premotor, primary motor, and somatosensory areas, whereas the connections of the more

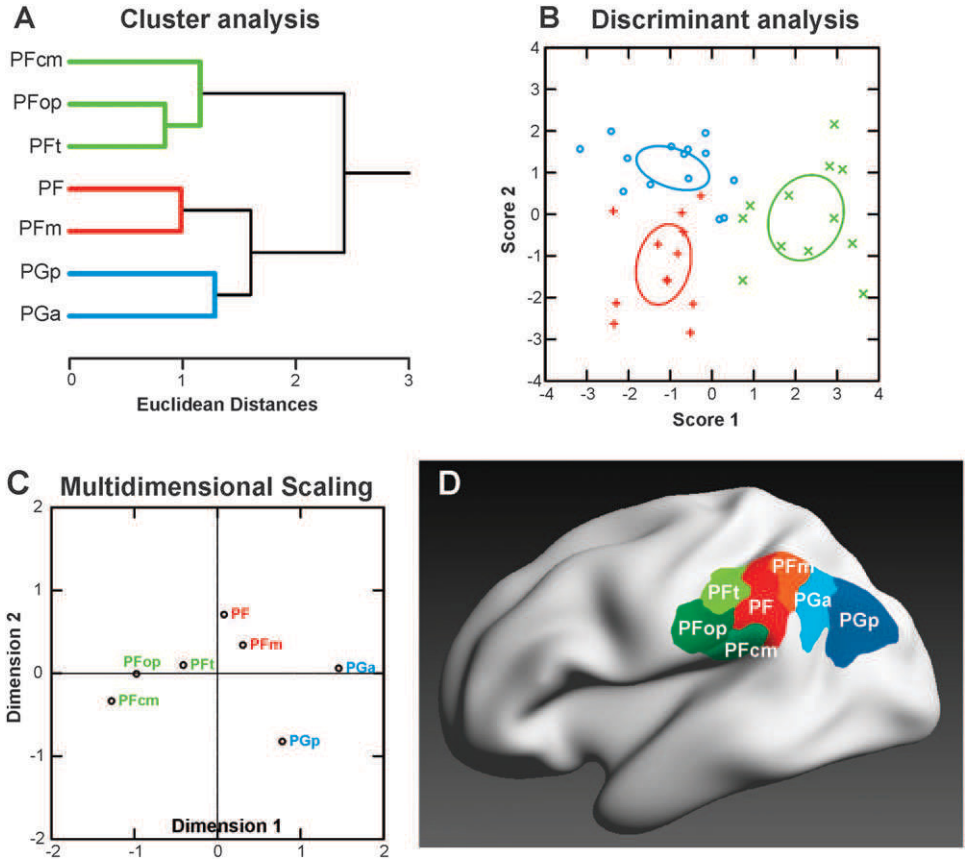


**Figure 8.** Segregation of IPL areas based on multiple receptor densities averaged over all cortical layers. (*A*) Hierarchical cluster analysis reveals 3 receptor-architectonically distinct clusters: a rostral cluster with areas PFop, PFt, PFcm (green), an intermediate cluster with areas PF and PFm (red), and a caudal cluster with areas PGa and PGp (blue). (*B*) Canonical discriminant analysis of all available receptor data in IPL. For each of the 3 clusters, the *n* data points ($n$ = number of areas in that cluster × number of hemispheres, some points are missing due to missing values for some receptor types) are indicated by different symbols. Ellipses provide the 90% confidence interval of the centroids. Same color coding as in (*A*). (*C*) MDS analysis visualizes the differences between the 3 clusters. Same color coding as in (*A*). (*D*) Visualization of the resulting 3 clusters within the IPL, using the same depiction of the cytoarchitectonically defined IPL areas (Caspers et al. 2006, 2008) as in Figure 1. Color coding of the areas corresponding to the receptor-based cluster segregation: rostral cluster (areas PFt, PFop, and PFcm): shades of green; middle cluster (areas PF and PFm): shades of red; caudal cluster (areas PGa and PGp): shades of blue.

central and caudal IPL areas shifted to target regions in superior parietal, extrastriate visual, and temporal cortices. The middle areas shared connection patterns of both rostral and caudal areas with prominent connections to frontal, superior parietal, and intraparietal areas. The differences in connection patterns between rostral, middle (sharing connection patterns of rostral and caudal IPL areas), and caudal IPL areas thus favored the view of a tripartition of the cortex in the IPL.

*Functions*

Shalom and Poeppel (2008) proposed such a tripartition for the involvement of the IPL in language tasks. The IPL was assumed to provide the analysis part within the larger language framework comprising frontal, parietal, and temporal cortices. Different functional aspects of language are processed in each of the 3 partitions of these regions. In the IPL, the rostral partition processes sounds and single phonemes, that is, the basic components of language; middle IPL areas provide the syntax, that is, the rule which needs to be applied to assemble the basic components; caudal IPL areas finally determine the semantic content of words or sentences and thus refer to the meaning of information.

The receptor balance of the middle and caudal IPL areas strongly resembled that of Broca's region, whereas the fingerprints of the rostral cluster were less similar. A relationship of middle and caudal IPL areas with the core of Broca's region was also found in a recent study on fiber tracts of the IPL areas (Caspers, Eickhoff, et al. 2011) where middle and caudal IPL areas were most likely connected with Broca's region. This connectivity study and our receptor patterns fit well the model proposed by Shalom and Poeppel (2008) suggesting different and comparable hierarchical levels of language processing within the frontal and inferior parietal lobe: rostral IPL was supposed to share functional properties with ventral premotor cortex, caudally adjacent to the Broca region (area 44), whereas middle and caudal IPL areas strongly interact with Broca's region to fulfill the "rule application function" and "analysis of meaning function." Receptor-architectonic, functional, and connectivity data thus provide evidence for a 3-region model within the language domains of the frontal and parietal lobes. Thus, the 3-region model of the IPL suggests a new organizational principle in this brain region.

Functional neuroimaging studies of the IPL using other than language-related tasks further support the proposal of a tripartite organization. Rostral human IPL areas were found to be involved in reaching and grasping tasks (Peeters et al. 2009). The very rostral part was found to be activated during observation of tool use and interpreted as being uniquely human.

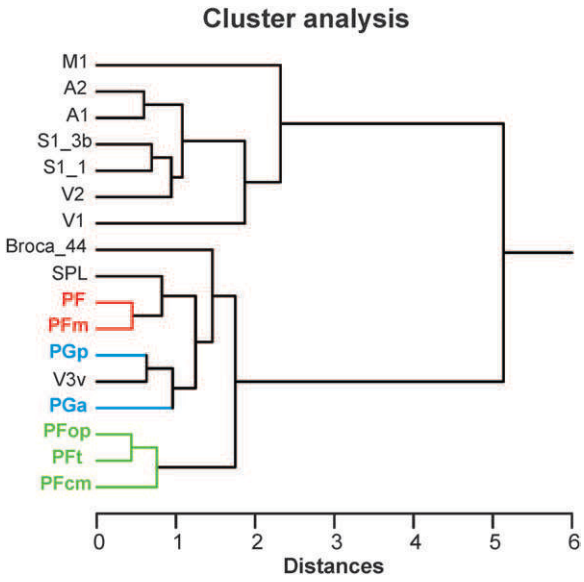


**Figure 9.** Receptor distributions of IPL areas compared with those of other cortical areas. The hierarchical cluster analysis that shows the same tripartition of the IPL areas as shown in Figure 8 but additionally reveals similarities of the intermediate cluster (areas PF and PFm, red) with superior parietal areas (SPLs) and of the caudal cluster (areas PGa and PGp, blue) with extrastriate visual areas. The IPL areas are most similar to each other and similar to higher order areas (Broca_44, SPL, and V3v) but are most dissimilar to primary and secondary areas (A1/A2, M1, S1, and V1/V2). Note the close resemblance of area PGp with extrastriate visual area V3v. A1/A2: primary/secondary auditory cortex, Broca_44: area 44 of Broca's region, M1: primary motor cortex, S1_3b: area 3b of primary somatosensory cortex, S1_1: area 1 of primary somatosensory cortex, SPL: superior parietal lobule, V1/V2: primary/secondary visual cortex, V3v: ventral extrastriate visual cortex.

Recent meta-analyses demonstrated that rostral IPL area PFt participates in the action observation and imitation network (Molenberghs et al. 2009; Van Overwalle and Baetens 2009; Caspers et al. 2010). Data from studies in macaques also point to the relevance of rostral-most IPL together with ventral premotor area 6 for the mirror neuron system (Rizzolatti 2005; Petrides and Pandya 2009). This fits the interaction within the language network (Shalom and Poeppel 2008) as described above. The middle IPL areas PF and PFm are activated by nonspatial attention tasks, especially when reevaluating conflicting choice options (Vossel et al. 2006; Boorman et al. 2009; Mevorach et al. 2009; Caspers, Heim, et al. 2011) as well as spatial attention and reorienting tasks (Rushworth et al. 2001; Corbetta et al. 2008). Together with intraparietal areas, middle IPL contributes to rule change during visually guided attention (Corbetta and Shulman 2002). Caudal areas PGa and PGp were most prominently implicated in language-related processing with special focus on semantic and phonological processing, partially found in both hemispheres (Price 2000; Hickok and Poeppel 2004; Marangolo et al. 2006; Vigneau et al. 2006). These areas have also consistently been found during moral decision making, being particularly concerned with egocentric and allocentric perspective taking (for review: Raine and Yang 2006).

The involvement of the IPL within different functional domains could thus be summarized as follows: Rostral IPL deals with tool, action, or sound. Middle IPL areas provide rules for word differentiation as well as visually guided attention and nonspatial attention processes. Caudal IPL is involved in decoding the meaning of words, scenes, or personal morally relevant interactions. Thus, the same IPL areas are involved in different tasks, which should have a functional commonality representing the role of the IPL areas on a more abstract level. It already seems plausible to assume that the hierarchical 3-region model of language functions in the IPL is a starting point for searching analogous commonalities in other functional domains.

The present study provides evidence for a general 3-region model of the IPL on a molecular basis regarding the receptor balance of different neurotransmitter systems. The relevance of the receptor balance of an area for its involvement in different functional networks has been repeatedly stressed (Barnes and Sharp 1999; Goldman-Rakic et al. 2000; Gibbs and Summers 2002; Bergson et al. 2003; Bredt and Nicoll 2003; Friedman et al. 2004). It can thus be assumed that not the distribution pattern of a single receptor, but the interplay between different receptors of different neurotransmitter systems as displayed in the receptor fingerprints of each IPL area (Fig. 7) might set the molecular basis for the role, which is played by 3 different parts of the IPL across various functional domains.

### *The Role of Area PGp*

The present findings additionally provide new insights into the potential role of area PGp. Its receptor distribution was different from the other IPL areas and showed most pronounced similarities with higher extrastriate visual areas, particularly V3v. This is further promoted by connectivity analyses, which showed consistent connections between PGp and extrastriate visual areas (Caspers, Eickhoff, et al. 2011). It might thus be hypothesized that area PGp might serve as linking hub between occipital and parietal cortex for transformation of visual input to visual associations.

The cytoarchitectonic analysis of the IPL areas (Caspers et al. 2006) did not show a comparable difference. The cytoarchitecture of area PGp resembled that of the other IPL areas. It could be clearly demarcated from areas of the occipital cortex where the layers are dominated by large pyramidal cells as described by von Economo and Koskinas (1925). Area PGp is, therefore, clearly different from this "occipital type" of cortical architecture at the cytoarchitectonical level.

The probabilistic fiber tracking with area PGp as seed region shows connections to extrastriate visual areas (Caspers, Eickhoff, et al. 2011). The same situation was demonstrated in macaques for area Opt (Cavada and Goldman-Rakic 1989a, 1989b; Andersen et al. 1990; Rozzi et al. 2006), which favored the view that visual input to the IPL arrives via this caudal-most area.

The visual system has classically been subdivided into a ventral and dorsal visual stream, processing either "what" or "where" information, respectively (Ungerleider and Mishkin 1982; Ungerleider and Haxby 1994). The role of the dorsal visual stream within this framework was nevertheless not fully elucidated, fostering the notion of not only processing "where" but "how" information (Goodale and Milner 1992; Milner and Goodale 1995; Kravitz et al. 2011). It was furthermore suggested that the 2 systems are not fully separated from each other but rather interact to fulfill the task of providing the information on how an action should be executed (Pisella et al. 2006; Kravitz et al. 2011). The interaction is supposed to involve a ventrodorsal pathway, which involves caudal IPL. This region interacts with medially located areas of the superior parietal lobule, the posterior cingulate and retrosplenial cortex, and the parahippocampal gyrus. It might provide information about peripersonal

space with regard to egocentric or allocentric perspectives (Pisella et al. 2006; Rushworth et al. 2006; Kravitz et al. 2011). This corresponds to the findings of activation within caudal IPL during moral decision making where additional activation clusters were found in posterior cingulate cortex in addition to ventral and medial prefrontal cortex (Raine and Yang 2006). Here, the simultaneous activation of caudal IPL with posterior cingulate cortex was especially found during personal versus impersonal and utilitarian versus nonutilitarian moral judgments (Greene et al. 2004). Both these decisions involve allocentric versus egocentric perspectives to come to the respective moral judgment.

The results of the present study support the idea of area PGp serving as higher visual processing hub within the IPL. The similarity between the receptor balances of area PGp with that of ventral extrastriate visual area hOC3v (V3v) supports the idea that area PGp is key region in the ventrodorsal visual stream (Pisella et al. 2006), since it receives input from an area of that visual stream.

## Conclusions and Outlook

Based on the regionally specific multireceptor balances (receptor fingerprints), a 3-region model of human IPL is proposed (Fig. 8*D*). A hierarchical cluster analysis of the receptor fingerprints between the IPL areas and visual-, motor-, auditory-, and language-related cortical areas shows the highest similarity of all IPL areas with area 44 of Broca's region, of the areas in the middle of IPL with the superior parietal cortex, and for the most caudal areas with the extrastriate visual cortex. Notably, PGp has a receptor fingerprint very similar to that of ventral extrastriate area hOC3v (V3v). Since receptor fingerprints covary with the cytoarchitecture, function, and connectivity of each IPL area, the present study provides a molecular perspective of the organizational principles behind the regional and functional segregation of the IPL.

As a link to the function of an area, the receptor-based delineation of cortical areas poses an additional question: Do the receptor density patterns always follow the cytoarchitectonic boundaries? In our study, we independently mapped receptor profiles of each receptor and defined receptor-based borders within the respective sections. Additionally, we measured the cytoarchitectonic profiles of the same brain within alternate cell body–stained sections. The borders of both approaches did precisely coincide. It has to be noted that not all receptors showed every border of the IPL or other cortical areas (Zilles, Palomero-Gallagher, et al. 2002; Amunts et al. 2010). Vice versa, some receptors might show additional borders, which would hint at further subdivisions of cortical areas on a molecular level. Taking an independent mapping approach for all receptors will allow providing complete brain maps for each receptor in future studies, each revealing an individual view on the molecular architecture of the cortex.

## Supplementary Material

Supplementary material can be found at: http://www.cercor.oxfordjournals.org/

## Funding

This project was supported by grants of the Initiative and Networking Fund of the Helmholtz Association within the Helmholtz Alliance on Systems Biology (Human Brain Model to K.Z.); the Helmholtz Alliance for Mental Health in an Aging Society (HelMA to K.A. and K.Z.); and the German Ministry for Education and Research (01GW0771 and 01GW0623 to K.A.). The funders had no role in study design, data collection and analysis, decision to publish, or preparation of the manuscript.

## Notes

*Conflict of Interest*: None declared.

## References

Amunts K, Lenzen M, Friederici AD, Schleicher A, Morosan P, Palomero-Gallagher N, Zilles K. 2010. Broca's region: novel organizational principles and multiple receptor mapping. PLoS Biol. 8(9):e1000489.

Amunts K, Malikovic A, Mohlberg H, Schormann T, Zilles K. 2000. Brodmann's areas 17 and 18 brought into stereotaxic space—where and how variable? Neuroimage. 11:66–84.

Amunts K, Schleicher A, Bürgel U, Mohlberg H, Uylings HBM, Zilles K. 1999. Broca's region revisited: cytoarchitecture and intersubject variability. J Comp Neurol. 412:319–341.

Andersen RA, Asanuma C, Essick G, Siegel RM. 1990. Corticocortical connections of anatomically and physiologically defined subdivisions within the inferior parietal lobule. J Comp Neurol. 296:65–113.

Barnes NM, Sharp T. 1999. A review of central 5-HT receptors and their function. Neuropharmacology. 38(8):1083–1152.

Bergson C, Levenson R, Goldman-Rakic PS, Lidow MS. 2003. Dopamine receptor-interacting proteins: the Ca(2+) connection in dopamine signalling. Trends Pharmacol Sci. 24:486–492.

Boorman ED, Behrens TE, Woolrich MW, Rushworth MF. 2009. How green is the grass on the other side? Frontopolar cortex and the evidence in favor of alternative courses of action. Neuron. 62(5):733–743.

Bredt DS, Nicoll RA. 2003. AMPA receptor trafficking at excitatory synapses. Neuron. 40:361–379.

Brodmann K. 1909. Vergleichende Lokalisationslehre der Großhirnrinde. Leipzig (Germany): Barth.

Caspers S, Eickhoff SB, Geyer S, Scheperjans F, Mohlberg H, Zilles K, Amunts K. 2008. The human inferior parietal lobule in stereotaxic space. Brain Struct Funct. 212:481–495.

Caspers S, Eickhoff SB, Rick T, von Kapri A, Kuhlen T, Huang R, Shah NJ, Zilles K. 2011. Probabilistic fibre tract analysis of cytoarchitectonically defined human inferior parietal lobule areas reveals similarities to macaques. Neuroimage. 58(2):362–380.

Caspers S, Geyer S, Schleicher A, Mohlberg H, Amunts K, Zilles K. 2006. The human inferior parietal cortex: cytoarchitectonic parcellation and interindividual variability. Neuroimage. 33(2):430–448.

Caspers S, Heim S, Lucas MG, Stephan E, Fischer L, Amunts K, Zilles K. 2011. Moral concepts set decision strategies to abstract values. PLoS One. 6(4):e18451.

Caspers S, Zilles K, Laird AR, Eickhoff SB. 2010. ALE meta-analysis of action observation and imitation in the human brain. Neuroimage. 50:1148–1167.

Cavada C, Goldman-Rakic PS. 1989a. Posterior parietal cortex in rhesus monkey: I. Parcellation of areas based on distinctive limbic and sensory corticocortical connections. J Comp Neurol. 287:393–421.

Cavada C, Goldman-Rakic PS. 1989b. Posterior parietal cortex in rhesus monkey: II. Evidence of segregated corticocortical networks linking sensory and limbic areas with the frontal lobe. J Comp Neurol. 287:422–445.

Corbetta M, Patel G, Shulman GL. 2008. The reorienting system of the human brain: from environment to theory of mind. Neuron. 58:306–324.

Corbetta M, Shulman GL. 2002. Control of goal-directed and stimulus-driven attention in the brain. Nat Rev Neurosci. 3(3):201–215.

Croxson PL, Johansen-Berg H, Behrens TE, Robson MD, Pinsk MA, Gross CG, Richter W, Richter MC, Kastner S, Rushworth. 2005. Quantitative investigation of connections of the prefrontal cortex in the human and macaque using probabilistic diffusion tractography. J Neurosci. 25:8854–8866.

Eickhoff SB, Rottschy C, Kujovic M, Palomero-Gallagher N, Zilles K. 2008. Organizational principles of human visual cortex revealed by receptor mapping. Cereb Cortex. 18(11):2637–2645.
Eickhoff SB, Rottschy C, Zilles K. 2007. Laminar distribution and co-distribution of neurotransmitter receptors in early human visual cortex. Brain Struct Funct. 212:255–267.
Fink GR, Marshall JC, Weiss PH, Zilles K. 2001. The neural basis of vertical and horizontal line bisection judgements: an fMRI study of normal volunteers. Neuroimage. 14:59–67.
Fogassi L, Ferrari PF, Gesierich B, Rozzi S, Chersi F, Rizzolatti G. 2005. Parietal lobe: from action organization to intention understanding. Science. 308:662–667.
Friedman JI, Stewart DG, Gorman JM. 2004. Potential noradrenergic targets for cognitive enhancement in schizophrenia. CNS Spectr. 9:350–355.
Geyer S, Ledberg A, Schleicher A, Kinomura S, Schormann T, Bürgel U, Klingberg T, Larsson J, Zilles K, Roland PE. 1996. Two different areas within the primary motor cortex of man. Nature. 382:805–807.
Geyer S, Matelli M, Luppino G, Schleicher A, Jansen Y, Palomero-Gallagher N, Zilles K. 1998. Receptor autoradiographic mapping of the mesial motor and premotor cortex of the macaque monkey. J Comp Neurol. 397:231–250.
Geyer S, Schleicher A, Zilles K. 1997. The somatosensory cortex of human: cytoarchitecture and regional distributions of receptor-binding sites. Neuroimage. 6:27–45.
Geyer S, Schleicher A, Zilles K. 1999. Areas 3a, 3b, and 1 of human primary somatosensory cortex: 1. Microstructural organization and interindividual variability. Neuroimage. 10(1):63–83.
Geyer S, Schormann T, Mohlberg H, Zilles K. 2000. Areas 3a, 3b, and 1 of human primary somatosensory cortex. Part 2: spatial normalization to standard anatomical space. Neuroimage. 11:684–696.
Gibbs ME, Summers RJ. 2002. Role of adrenoceptor subtypes in memory consolidation. Prog Neurobiol. 67(5):345–391.
Goldman-Rakic PS, Muly EC III, Williams GV. 2000. D(1) receptors in prefrontal cells and circuits. Brain Res Brain Res Rev. 31:295–301.
Goodale MA, Milner AD. 1992. Separate visual pathways for perception and action. Trends Neurosci. 15:20–25.
Greene JD, Nystrom LE, Engell AD, Darley JM, Cohen JD. 2004. The neural bases of cognitive conflict and control in moral judgment. Neuron. 44:389–400.
Gregoriou GG, Borra E, Matelli M, Luppino G. 2006. Architectonic organization of the inferior parietal convexity of the macaque monkey. J Comp Neurol. 496:422–451.
Hickok G, Poeppel D. 2004. Dorsal and ventral streams: a framework for understanding aspects of the functional anatomy of language. Cognition. 92:67–99.
Hyvärinen J. 1982. Posterior parietal lobe of the primate brain. Physiol Rev. 62:1060–1129.
Iacoboni M. 2005. Neural mechanisms of imitation. Curr Opin Neurobiol. 15:632–637.
Keysers C, Gazzola V. 2009. Expanding the mirror: vicarious activity for actions, emotions, and sensations. Curr Opin Neurobiol. 19:666–671.
Kravitz DJ, Kadharbatcha SS, Baker CI, Mishkin M. 2011. A new neural framework for visuospatial processing. Nat Rev Neurosci. 12:217–230.
Marangolo P, Piras F, Galati G, Burani C. 2006. Functional anatomy of derivational morphology. Cortex. 42:1093–1106.
Mars RB, Jbabdi S, Sallet J, O'Reilly JX, Croxson PL, Olivier E, Noonan MP, Bergmann C, Mitchell AS, Baxter MG, et al. 2011. Diffusion-weighted imaging tractography-based parcellation of the human parietal cortex and comparison with human and macaque resting-state functional connectivity. J Neurosci. 31(11):4087–4100.
Merker B. 1983. Silver staining of cell bodies by means of physical development. J Neurosci Methods. 9:235–241.
Mevorach C, Humphreys GW, Shalev L. 2009. Reflexive and preparatory selection and suppression of salient information in the right and left posterior parietal cortex. J Cogn Neurosci. 21:1204–1214.
Milner AD, Goodale MA. 1995. The visual brain in action. Oxford: Oxford University Press.
Molenberghs P, Cunnington R, Mattingley JB. 2009. Is the mirror neuron system involved in imitation? A short review and meta-analysis. Neurosci Biobehav Rev. 33(7):975–980.
Morosan P, Rademacher J, Schleicher A, Amunts K, Schormann T, Zilles K. 2001. Human primary auditory cortex: cytoarchitectonic subdivisions and mapping into a spatial reference system. Neuroimage. 13:684–701.
Morosan P, Schleicher A, Amunts K, Zilles K. 2005. Multimodal architectonic mapping of human superior temporal gyrus. Anat Embryol (Berl). 210(5–6):401–406.
Mountcastle VB, Lynch JC, Georgopoulos A, Sakata H, Acuna C. 1975. Posterior parietal association cortex of the monkey: command functions for operations within extrapersonal space. J Neurophysiol. 38:871–908.
Palomero-Gallagher N, Vogt BA, Schleicher A, Mayberg HS, Zilles K. 2009. Receptor architecture of human cingulate cortex: evaluation of the four-region neurobiological model. Hum Brain Mapp. 30(8):2336–2355.
Pandya DN, Seltzer B. 1982. Intrinsic connections and architectonics of posterior parietal cortex in the rhesus monkey. J Comp Neurol. 204:196–210.
Peeters R, Simone L, Nelissen K, Fabbri-Destro M, Vanduffel W, Rizzolatti G, Orban GA. 2009. The representation of tool use in humans and monkeys: common and uniquely human features. J Neurosci. 29(37):11523–11539.
Petrides M, Pandya DN. 2009. Distinct parietal and temporal pathways to the homologues of Broca's area in the monkey. PLoS Biol. 7(8):e1000170.
Pisella L, Binkofski F, Lasek K, Toni I, Rossetti Y. 2006. No double-dissociation between optic ataxia and visual agnosia: multiple sub-streams for multiple visuo-manual integrations. Neuropsychologia. 44:2734–2748.
Price CJ. 2000. The anatomy of language: contributions from functional neuroimaging. J Anat. 197:335–359.
Raine A, Yang Y. 2006. Neural foundations to moral reasoning and antisocial behaviour. Soc Cogn Affect Neurosci. 1:203–213.
Rakic P, Goldman-Rakic PS, Gallager D. 1988. Quantitative autoradiography of major neurotransmitter receptors in the monkey striate and extrastriate cortex. J Neurosci. 8:3670–3690.
Rizzolatti G. 2005. The mirror neuron system and its function in humans. Anat Embryol (Berl). 210:419–421.
Rottschy C, Eickhoff SB, Schleicher A, Mohlberg H, Kujovic M, Zilles K, Amunts K. 2007. Ventral visual cortex in humans: cytoarchitectonic mapping of two extrastriate areas. Hum Brain Mapp. 28:1045–1059.
Rozzi S, Calzavara R, Belmalih A, Borra E, Gregoriou GG, Matelli M, Luppino G. 2006. Cortical connections of the inferior parietal convexity of the macaque monkey. Cereb Cortex. 16(10):1389–1417.
Rozzi S, Ferrari PF, Bonini L, Rizzolatti G, Fogassi L. 2008. Functional organization of inferior parietal lobule convexity in the macaque monkey: electrophysiological characterization of motor, sensory and mirror responses and their correlation with cytoarchitectonic areas. Eur J Neurosci. 28(8):1569–1588.
Rushworth MF, Behrens TE, Johansen-Berg H. 2006. Connection patterns distinguish 3 regions of human parietal cortex. Cereb Cortex. 16:1418–1430.
Rushworth MF, Paus T, Sipila PK. 2001. Attention systems and the organization of the human parietal cortex. J Neurosci. 21:5262–5271.
Scheperjans F, Eickhoff SB, Hömke L, Mohlberg H, Hermann K, Amunts K, Zilles K. 2008. Probabilistic maps, morphometry, and variability of cytoarchitectonic areas in the human superior parietal cortex. Cereb Cortex. 18(9):2141–2157.
Scheperjans F, Grefkes C, Palomero-Gallagher N, Schleicher A, Zilles K. 2005. Subdivisions of human parietal area 5 revealed by quantitative receptor autoradiography: a parietal region between motor, somatosensory, and cingulated cortical areas. Neuroimage. 25:975–992.
Scheperjans F, Hermann K, Eickhoff SB, Amunts K, Schleicher A, Zilles K. 2008. Observer-independent cytoarchitectonic mapping of the human superior parietal cortex. Cereb Cortex. 18(4):846–867.
Scheperjans F, Palomero-Gallagher N, Grefkes C, Schleicher A, Zilles K. 2005. Transmitter receptors reveal segregation of cortical areas in

the human superior parietal cortex: relations to visual and somatosensory regions. Neuroimage. 28:362–379.
Schleicher A, Morosan P, Amunts K, Zilles K. 2009. Quantitative architectural analysis: a new approach to cortical mapping. J Autism Dev Disord. 39(11):1568–1581.
Schleicher A, Palomero-Gallagher N, Morosan P, Eickhoff SB, Kowalski T, Amunts K, Zilles K. 2005. Quantitative architectural analysis: a new approach to cortical mapping. Anat Embryol (Berl). 210(5):373–386.
Seltzer B, Pandya DN. 1984. Further observations on parieto-temporal connections in the rhesus monkey. Exp Brain Res. 55:301–312.
Shalom DB, Poeppel D. 2008. Functional anatomic models of language: assembling the pieces. Neuroscientist. 14(1):119–127.
Tomassini V, Jbabdi S, Klein JC, Behrens TE, Pozzilli C, Matthews PM, Rushworth MFS, Johansen-Berg H. 2007. Diffusion-weighted imaging tractography-based parcellation of the human lateral premotor cortex identifies dorsal and ventral subregions with anatomical and functional specializations. J Neurosci. 27:10259–10269.
Ungerleider LG, Haxby JV. 1994. 'What' and 'where' in the human brain. Curr Opin Neurobiol. 4(2):157–165.
Ungerleider LG, Mishkin M. 1982. Two cortical visual systems. In: Ingle DJ, Goodale MA, Mansfield RJW, editors. Analysis of visual behaviour. Cambridge (MA): MIT Press. p. 549–586.
Van Overwalle F, Baetens K. 2009. Understanding other's actions and goals by mirror and mentalizing systems: a meta-analysis. Neuroimage. 48(3):564–584.
Vigneau M, Beaucousin V, Hervé PY, Duffau H, Crivello F, Houdé O, Mazoyer B, Tzourio-Mazoyer N. 2006. Meta-analyzing left hemisphere language areas: phonology, semantics, and sentence processing. Neuroimage. 30:1414–1432.
von Economo K, Koskinas G. 1925. Die Cytoarchitektonik der Hirnrinde des erwachsenen Menschen. Wien (Austria): Springer.
Vossel S, Thiel CM, Fink GR. 2006. Cue validity modulates the neural correlates of covert endogenous orienting of attention in parietal and frontal cortex. Neuroimage. 32:1257–1264.
Zilles K, Amunts K. 2009. Receptor mapping: architecture of the human cerebral cortex. Curr Opin Neurol. 22(4):331–339.
Zilles K, Palomero-Gallagher N. 2001. Cyto-, myelo-, and receptor architectonics of the human parietal cortex. Neuroimage. 14:S8–S20.
Zilles K, Palomero-Gallagher N, Grefkes C, Scheperjans F, Boy C, Amunts K, Schleicher A. 2002. Architectonics of the human cerebral cortex and transmitter receptor fingerprints: reconciling functional neuroanatomy and neurochemistry. Eur Neuropsychopharmacol. 12:587–599.
Zilles K, Palomero-Gallagher N, Schleicher A. 2004. Transmitter receptors and functional anatomy of the cerebral cortex. J Anat. 205:417–432.
Zilles K, Schleicher A, Palomero-Gallgher N, Amunts K. 2002. Quantitative analysis of cyto- and receptor architecture of the human brain. In: Toga A, Mazziotta J, editors. Brain mapping: the methods. 2nd ed. San Diego (CA): Academic Press. p. 573–602.

NeuroImage 50 (2010) 1148–1167

Contents lists available at ScienceDirect

NeuroImage

journal homepage: www.elsevier.com/locate/ynimg

# ALE meta-analysis of action observation and imitation in the human brain

Svenja Caspers [a,b,*], Karl Zilles [a,b,c], Angela R. Laird [d], Simon B. Eickhoff [a,b,e]

[a] Institute of Neuroscience and Medicine (INM-2), Research Centre Jülich, 52425 Jülich, Germany
[b] JARA-BRAIN, Jülich-Aachen Research Alliance, 52425 Jülich, Germany
[c] C. and O. Vogt Institute for Brain Research, Heinrich-Heine-University Düsseldorf, 40001 Düsseldorf, Germany
[d] Research Imaging Institute, University of Texas Health Science Center, San Antonio, TX, USA
[e] Department of Psychiatry and Psychotherapy, RWTH Aachen University, 52074 Aachen, Germany

ARTICLE INFO

*Article history:*
Received 5 November 2009
Revised 23 December 2009
Accepted 24 December 2009
Available online 4 January 2010

*Keywords:*
Action observation
Imitation
Inferior parietal
Meta-analysis
Mirror neurons

ABSTRACT

Over the last decade, many neuroimaging studies have assessed the human brain networks underlying action observation and imitation using a variety of tasks and paradigms. Nevertheless, questions concerning which areas consistently contribute to these networks irrespective of the particular experimental design and how such processing may be lateralized remain unresolved. The current study aimed at identifying cortical areas consistently involved in action observation and imitation by combining activation likelihood estimation (ALE) meta-analysis with probabilistic cytoarchitectonic maps. Meta-analysis of 139 functional magnetic resonance and positron emission tomography experiments revealed a bilateral network for both action observation and imitation. Additional subanalyses for different effectors within each network revealed highly comparable activation patterns to the overall analyses on observation and imitation, respectively, indicating an independence of these findings from potential confounds. Conjunction analysis of action observation and imitation meta-analyses revealed a bilateral network within frontal premotor, parietal, and temporo-occipital cortex. The most consistently rostral inferior parietal area was PFt, providing evidence for a possible homology of this region to macaque area PF. The observation and imitation networks differed particularly with respect to the involvement of Broca's area: whereas both networks involved a caudo-dorsal part of BA 44, activation during observation was most consistent in a more rostro-dorsal location, i.e., dorsal BA 45, while activation during imitation was most consistent in a more ventro-caudal aspect, i.e., caudal BA 44. The present meta-analysis thus summarizes and amends previous descriptions of the human brain networks related to action observation and imitation.



## Introduction

The neural bases of action observation and action imitation in the human brain have been a longstanding interest of neuroscientific research. Increasing attention was focused on these functions and their neuronal correlates when “mirror neurons” were identified in the macaque brain using single-cell recordings (Gallese et al., 1996; Fogassi et al., 2005). These neurons are active not only when performing an action but also when observing another subject performing the same action (Gallese et al., 1996). This discovery in the macaque brain raised the question of whether a comparable system also exists in humans (e.g., Rizzolatti et al., 2001). However, since single-cell recordings are rarely feasible in humans, a direct demonstration of mirror properties for individual human neurons has not yet been provided. Consequently, evidence for possible “mirror” areas in humans is predominantly based on the results of functional neuroimaging experiments. Over the last decade, several studies using functional magnetic resonance imaging (fMRI) and positron emission tomography (PET) have investigated different aspects of action processing in the human brain (e.g., Buccino et al., 2004b; Iacoboni et al., 1999) that are conceptually related to “mirror” properties, in particular action observation and imitation.

Investigation into the human action observation network directly relates to the properties of mirror neurons as defined in nonhuman primates. It is assumed that observing actions enables the mirror neuron system to understand the actions themselves as well as the underlying intentions (e.g., Fabbri-Destro and Rizzolatti 2008; Rizzolatti 2005; Rizzolatti and Fabbri-Destro 2008). By understanding the action with one's own motor system, it is possible to infer on the intentions behind a motor act (e.g., Prinz 2006; Schütz-Bosbach and Prinz, 2007), a mechanism that already has been proposed long before the discovery of mirror neurons (e.g., Viviani and Terzuolo, 1973). Such ability is then seen as a crucial step towards the development of complex interpersonal and social interactions as witnessed in humans but also other primates (Iacoboni 2009; Rizzolatti and Fabbri-Destro, 2008).

* Corresponding author. Institut für Neurowissenschaften und Medizin, INM-2, Forschungszentrum Jülich, 52425 Jülich, Germany. Fax: +49 2461 612990.
*E-mail address:* s.caspers@fz-juelich.de (S. Caspers).

1053-8119/$ – see front matter © 2009 Elsevier Inc. All rights reserved.
doi:10.1016/j.neuroimage.2009.12.112

Understanding an action and its intention might also provide an important link between the sole observation of an action and its subsequent imitation by directly copying the observed action (e.g., Fabbri-Destro and Rizzolatti, 2008; Rizzolatti and Craighero, 2004; Rumiati et al., 2005). Furthermore, imitation offers a potential mechanism for learning from the early stages of life. The motor system can learn how specific actions are carried out by imitating them (e.g., Bandura and Wood, 1989; Brass and Heyes, 2005; Iacoboni, 2005), a mechanism that has long been discovered much earlier in human neonates (Meltzoff and Moore, 1977). Furthermore, just like action understanding, imitation processes play an important role during social interactions: people also tend to imitate behaviours of their social partners (either consciously or subconsciously) to adapt to a given social situation (e.g., Bargh et al., 1996; Iacoboni, 2009; Niedenthal et al., 1985; Schilbach et al., 2008a).

Therefore, assessment of the neural substrates of both action observation and action imitation is not only important for understanding action-related processes but also holds further implications for cognitive and social neuroscience. In spite of the considerable number of neuroimaging studies on these action-related topics, the organisation of the respective networks in the human brain and their anatomical correlates are still disputed (Dinstein et al., 2008; Iacoboni, 2005, 2009; Keysers and Gazzola, 2009). One controversial aspect is the role of Broca's region in action- related processes (Brass and Heyes, 2005; Molenberghs et al., 2009; Molnar-Szakacs et al., 2005; Vogt et al., 2007). Another is the hemispheric dominance of such functions, as arguments have been made for a leading role of either hemisphere as well as for a bilateral distribution (e.g., Iacoboni and Dapretto, 2006). Finally, since observation and imitation are closely related, the question of whether they are sustained by the same neuronal networks or engage different brain areas is still disputed (e.g., Heyes, 2001; Brass and Heyes, 2005; Turella et al., 2009a,b).

One reason for the diverging evidence on the involvement of different brain regions in these networks is the heterogeneity of the experimental approaches, such as paradigms and effectors (e.g., hand/fingers, face, feet), that have been used to delineate the neural correlates of these functions. To identify those areas in the human brain that are consistently implicated in action processing, the results of these different studies should be synopsized in a quantitative, unbiased fashion. Previous summaries of published studies on action observation or imitation have consisted of qualitative reviews of the reported activation sites (e.g., Brass and Heyes, 2005; Fabbri-Destro and Rizzolatti, 2008; Iacoboni, 2005, 2009; Rizzolatti et al., 2001). However, a promising new approach for identifying the neural substrates of action observation and imitation in humans is the use of coordinate-based meta-analysis. These analyses aim at revealing areas that are consistently activated in a particular class of paradigms (Laird et al., 2005a, 2009; Eickhoff et al., 2009).

The aim of the present study was to provide a quantitative meta-analysis of the current neuroimaging literature to delineate consistently activated cortical regions associated with action observation and imitation. In a first step, the neural correlates of these processes were analysed separately. Additional subanalyses that assessed the effects of potential confounds, such as effectors or instructions, were carried out to evaluate the consistency of the findings. Conjunction and contrast analyses were performed to reveal divergent and convergent areas for action observation and imitation. Using probabilistic cytoarchitectonic maps of cortical areas, activations identified in each analysis were specifically allotted to the most probable brain area.

## Material and methods

### *Data used for the meta-analysis*

Functional imaging studies included in the meta-analysis were obtained from the BrainMap database (www.brainmap.org; Fox and Lancaster, 2002, Laird et al., 2005b) and a PubMed literature search (www.pubmed.org, search strings: “mirror neurons”, “imitation”, and “action observation”) on functional magnetic resonance imaging (fMRI) and positron emission tomography (PET) experiments. The literature cited in the obtained papers was also assessed to identify additional neuroimaging studies dealing with action observation or imitation processing. Only studies that reported results of whole-brain group analyses as coordinates in a standard reference space (Talairach/Tournoux, MNI) were analysed, while single-subject reports were excluded. Based on these criteria, 87 articles (reporting 83 fMRI and 4 PET studies) were designated as suitable for meta-analysis. Together, these studies included data from 1289 subjects and reported 139 experiments with 1932 activation foci (Table 1).

The reported tasks were subsumed into two main categories: “action observation” and “action imitation”: 104 experiments reported action observation tasks (1061 subjects, 1390 activation foci), and 35 reported imitation tasks (459 subjects, 542 activation foci). Action observation comprised those experiments in which subjects were instructed to observe the action performed by others without performing their own motor act. In this first analysis, the general action observation brain network was assessed. There are, however, several possible confounds that may influence the analysis across the whole sample of observation and imitation experiments, like effectors, instructions or the involvement of an object. To explore the effects of these potential confounds, we subdivided the studies into several subgroups. These were then analysed separately to reveal the neural correlates of different forms of action observation and compared among each other by contrast and conjunction analyses: observation of hand actions (‘right hand’ (37 experiments), ‘left hand’ (2 experiments), ‘both hands’, or ‘hand not specified’ (23 experiments)), observation of right hand actions, observation of face actions, observation of non-hand actions (either ‘face’, ‘body’, or ‘leg/foot’), observation of object-related hand actions, and observation of non-object-related hand actions. A further analysis was performed within those areas which were found to be consistently active for observation of hand actions: observation of hand actions with instruction ‘passively observe’, and observation of hand actions with instruction ‘observe to imitate’ (Table 2).

Action imitation comprised all those tasks in which subjects were asked to imitate actions performed by a visual model as exactly as possible. As for the action observation category, general effects associated with action imitation were analyzed first. Then, subgroups of the imitation studies were analysed separately for imitation of hand actions (either ‘right hand’ (15 experiments), ‘left hand’ (2 experiments), ‘both hands’, or ‘hand not specified’ (11 experiments)), imitation of right hand actions, and imitation of non-object-related hand actions (Table 2). A subgroup of studies on imitation of object-related hand actions could not been analysed due to an insufficient sample size.

Differences in coordinate spaces (MNI vs. Talairach space) were accounted for by transforming coordinates reported in Talairach space into MNI coordinates using a linear transformation (Lancaster et al., 2007).

### *Meta-analysis algorithm*

Meta-analysis was carried out using the revised version (Eickhoff et al., 2009) of the activation likelihood estimation (ALE) approach for coordinate-based meta-analysis of neuroimaging results (Turkeltaub et al., 2002; Laird et al., 2005a,b). The algorithm aims at identifying areas showing a convergence of activations across different experiments, and determining if the clustering is higher than expected under the null distribution of a random spatial association between the results obtained in the experiments. The key idea behind ALE is to treat the reported foci not as single points, but rather as centers for 3D Gaussian probability distributions capturing the spatial uncertainty

**Table 1**
Overview of the 87 studies included in the meta-analysis on action observation and imitation.

| Publication | Subjects | Mode | Experiment (rep. foci) | Effector (o/no) | Instruction | Contrast | Stimulus |
|---|---|---|---|---|---|---|---|
| Adamovich et al., 2009 | 13 | fMRI | OBS (24) | Hand (o) | Observe to imitate | Task>rest | Hand manipulating objects |
| | | | IMI (14) | Hand (o) | Imitate as observed | Task>rest | Hand manipulating objects |
| Agnew and Wise, 2008 | 20 | fMRI | OBS (5) | Right hand (no) | Passively observe | OBS motion>OBS static | Hand static or moving |
| | | | OBS (11) | Right hand (no) | Passively observe | OBS motion>EXE motion | Hand static or moving |
| Aziz-Zadeh et al., 2006a | 12 | fMRI | IMI (25) | Right hand (o) | Imitate as observed | Task>rest | Finger movement |
| | | | IMI (30) | Left hand (o) | Imitate as observed | Task>rest | Finger movement |
| Aziz-Zadeh et al., 2006b | 12 | fMRI | OBS (9) | Hand/foot/face (o) | Passively observe | Task>rest | Combination of lower three |
| | | | OBS (4) | Foot (o) | Passively observe | Task>rest | Foot pressing on objects |
| | | | OBS (4) | Hand (o) | Passively observe | Task>rest | Hand reaching/grasping objects |
| | | | OBS (6) | Face (o) | Passively observe | Task>rest | Mouth biting fruits |
| Baumgaertner et al., 2007 | 19 | fMRI | OBS (2) | Right hand (o) | Passively observe | OBS action>OBS nonaction | Hand manipulating objects |
| Bidet-Caulet et al., 2005 | 10 | fMRI | OBS (15) | Body (no) | Listen to action sound | Task>rest | Hearing human footsteps |
| Blakemore et al., 2005 | 12 | fMRI | OBS (11) | Hand (o) | Rate intensity of touch | OBS touch>OBS object | Touch to human neck or face |
| Buccino et al., 2001 | 12 | fMRI | OBS (9) | Face (o) | Passively observe | OBS motion>OBS static | Mouth biting fruits |
| | | | OBS (6) | Hand (o) | Passively observe | OBS motion>OBS static | Hand reaching/grasping objects |
| | | | OBS (4) | Foot (o) | Passively observe | OBS motion>OBS static | Foot pressing on objects |
| | | | OBS (5) | Face (no) | Passively observe | OBS motion>OBS static | Mouth chewing |
| | | | OBS (2) | Hand (no) | Passively observe | OBS motion>OBS static | Hand mimicking object actions |
| | | | OBS (2) | Foot (no) | Passively observe | OBS motion>OBS static | Foot mimicking object actions |
| Buccino et al., 2004a | 12 | fMRI | OBS (10) | Left hand (o) | Observe to imitate | Task>rest | Left hand playing guitar chords |
| | | | OBS (17) | Left hand (o) | Passively observe | Task>rest | Left hand playing guitar chords |
| | | | IMI (13) | Left hand (o) | Imitate as observed | Task>rest | Left hand playing guitar chords |
| Calvert and Campbell, 2003 | 8 | fMRI | OBS (27) | Face (no) | Read lips | OBS motion>OBS static | Mouth moving |
| Calvo-Merino et al., 2005 | 20 | fMRI | OBS (23) | Body (no) | Rate tiring capacity | Task>rest | Ballet/capoeira movements |
| Calvo-Merino et al., 2006 | 24 | fMRI | OBS (20) | Body (no) | Rate symmetry | Gender-specific> gender-common motion | Ballet movements |
| Carr et al., 2003 | 11 | fMRI | IMI (32) | Face (no) | Imitate as observed | Task>rest | Emotional faces |
| | | | OBS (22) | Face (no) | Passively observe | Task>rest | Emotional faces |
| Chaminade et al., 2002 | 10 | PET | IMI (6) | Hand (o) | Imitate as observed | IMI>EXE | Hand manipulating Lego blocks |
| Chaminade et al., 2005 | 12 | fMRI | IMI (20) | Hand (no) | Imitate as observed | IMI>EXE | Hand/foot moving |
| Cheng et al., 2007 | 20 | fMRI | OBS (15) | Right hand (o) | Passively observe | OBS motion>OBS scramble | Hand reaching/grasping objects |
| Chong et al., 2008 | 16 | fMRI | OBS (14) | Hand (o) | Discriminate grip type | OBS motion>OBS figure | Hand reaching/grasping objects |
| Costantini et al., 2005 | 13 | fMRI | OBS (8) | Right hand (no) | Passively observe | OBS motion>OBS object | Moving finger/object, possible |
| | | | OBS (16) | Right hand (no) | Passively observe | OBS motion>OBS object | Moving finger/object, impossible |
| Cross et al., 2006 | 10 | fMRI | OBS (23) | Body (no) | Passively observe | Task>rest | Dance movements |
| Cross et al., 2009 | 17 | fMRI | OBS (12) | Body (no) | Passively observe | OBS familiar>OBS untrained | Dance movements |
| Cunnington et al., 2006 | 14 | fMRI | OBS (10) | Right hand (no) | Observe to imitate | OBS>EXE | Finger gestures |
| Decety et al., 2002 | 18 | PET | IMI (17) | Hand (o) | Imitate as observed | IMI>EXE | Hand manipulating objects |
| Dinstein et al., 2007 | 13 | fMRI | IMI (6) | Right hand (no) | Imitate as observed | Task>rest | Finger gestures |
| | | | OBS (6) | Right hand (no) | Passively observe | Task>rest | Finger gestures |
| Engel et al., 2008 | 18 | fMRI | OBS (20) | Hand (no) | Passively observe | OBS motion>OBS static | Hand movements |
| Filimon et al., 2007 | 16 | fMRI | OBS (14) | Right hand (o) | Passively observe | OBS motion>OBS object | Hand reaching objects |
| Frey and Gerry, 2006 | 19 | fMRI | OBS (6) | Hand (o) | Observe to imitate | Task>rest | Hand constructing objects |
| Galati et al., 2008 | 11 | fMRI | OBS (26) | Body (no) | Listen to action sound | Task>rest | Hearing action sounds with primer |
| Gazzola et al., 2006 | 16 | fMRI | OBS (8) | Hand (o) | Listen to action sound | Sound action>environment | Hand action sounds |
| | | | OBS (20) | Face (o) | Listen to action sound | Sound action>environment | Mouth action sounds |
| Gazzola et al., 2007 | 16 | fMRI | OBS (22) | Right hand (o) | Passively observe | OBS motion>OBS static | Human/robotic hand reaching/grasping objects |
| German et al., 2004 | 16 | fMRI | OBS (18) | Hand (o) | Rate completeness | OBS pretend>OBS real | Everyday actions |
| Grèzes et al., 2003 | 12 | fMRI | IMI (8) | Hand (o) | Imitate as observed | Task>rest | Hand reaching/grasping objects |
| | | | IMI (7) | Hand (no) | Imitate as observed | Task>rest | Hand movements |
| Grèzes et al., 2004 | 6 | fMRI | OBS (5) | Body (o) | Rate expectation | OBS self>OBS other | Carrying boxes of different weight |
| Grosbras and Paus, 2006 | 20 | fMRI | OBS (24) | Hand (o) | Passively observe | OBS neutral>OBS control | Hand reaching/grasping objects |
| | | | OBS (32) | Hand (o) | Passively observe | OBS angry>OBS control | Hand reaching/grasping objects |
| | | | OBS (28) | Face (no) | Passively observe | OBS neutral>OBS control | Moving faces |
| | | | OBS (25) | Face (no) | Passively observe | OBS angry>OBS control | Emotional faces |
| Hamzei et al., 2003 | 6 | fMRI | OBS (3) | Right hand (o) | Passively observe | OBS motion>OBS static | Hand reaching/grasping objects |
| Haslinger et al., 2005 | 12 | fMRI | OBS (26) | Right hand (o) | Passively observe | OBS motion>OBS static | Playing piano/moving hand |
| | | | OBS (26) | Left hand (o) | Passively observe | OBS motion>OBS static | Playing piano/moving hand |
| Hermsdörfer et al., 2001 | 7 | fMRI | OBS (6) | Right hand (no) | Decide same/different | OBS motion>OBS control | Hand gestures |
| | | | OBS (8) | Right hand (no) | Decide same/different | OBS motion>OBS control | Finger gestures |
| Iacoboni et al., 1999 | 12 | fMRI | IMI (3) | Right hand (no) | Imitate as observed | IMI>EXE | Finger movements |
| Iacoboni et al., 2001 | 12 | fMRI | IMI (1) | Right hand (no) | Imitate as observed | IMI>EXE | Finger movements |
| Iacoboni et al., 2004 | 13 | fMRI | OBS (16) | Body (no) | Passively observe | OBS interaction>OBS single | Everyday actions |
| Iacoboni et al., 2005 | 23 | fMRI | OBS (36) | Right hand (o) | Passively observe | OBS motion>OBS object | Hand reaching/grasping objects |
| Iseki et al., 2008 | 16 | fMRI | OBS (11) | Body (no) | Passively observe | OBS motion>OBS scramble | Stepping movements |
| | | | OBS (10) | Body (no) | Passively observe | OBS motion>OBS scramble | Stepping movements |
| Jackson et al., 2006 | 16 | fMRI | IMI (16) | Hand/foot (no) | Imitate as observed | IMI>OBS | Hand/foot movements |
| Johnson-Frey et al., 2003 | 18 | fMRI | OBS (9) | Right hand (o) | Recognize duplicate | OBS motion>OBS touch | Hand touching/grasping objects |

**Table 1** (*continued*)

| Publication | Subjects | Mode | Experiment (rep. foci) | Effector (o/no) | Instruction | Contrast | Stimulus |
|---|---|---|---|---|---|---|---|
| Jonas et al., 2007 | 19 | fMRI | OBS (3) | Right hand (no) | Recognize oddball | Task>rest | Finger movements |
| | | | IMI (5) | Right hand (no) | Imitate as observed | Task>rest | Finger movements |
| Keysers et al., 2004 | 14 | fMRI | OBS (5) | Foot (o) | Passively observe | OBS touch>OBS object | Touch to human leg with objects |
| Koski et al., 2002 | 14 | fMRI | IMI (15) | Hand (no) | Imitate as observed | IMI with goal>without goal | Finger movements with goals |
| Koski et al., 2003 | 8 | fMRI | IMI (26) | Hand (no) | Imitate as observed | IMI>EXE | Mirrored finger movements |
| Leslie et al., 2004 | 15 | fMRI | IMI (23) | Face (no) | Imitate as observed | Task>rest | Emotional faces |
| | | | OBS (16) | Face (no) | Passively observe | Task>rest | Emotional faces |
| Lewis et al., 2005 | 20 | fMRI | OBS (9) | Hand (o) | Listen to action sound | Sound tool>sound animal | Tool action/animal sounds |
| Lotze et al., 2006 | 20 | fMRI | OBS (7) | Right hand (o) | Passively observe | OBS body-referred action>OBS isolated action | Everyday actions |
| | | | OBS (16) | Right hand (no) | Imagine being addressed | OBS emotional action>OBS isolated action | Emotional gestures towards observer |
| Lui et al., 2008 | 16 | fMRI | OBS (7) | Hand (no) | Passively observe | OBS motion>imagine motion | Finger gestures |
| Makuuchi 2005 | 9 | fMRI | IMI (2) | Right hand (no) | Imitate as observed | IMI>EXE | Finger gestures |
| Makuuchi et al., 2005 | 22 | fMRI | IMI (23) | Left hand (no) | Imitate as observed | IMI>EXE | Finger gestures |
| Manthey et al., 2003 | 12 | fMRI | OBS (23) | Hand (o) | Passively observe | OBS meaningful action>OBS meaningless action | Hand manipulating objects |
| Meister and Iacoboni, 2007 | 14 | fMRI | OBS (25) | Right hand (o) | Count no. of fingers | Task>rest | Hand manipulating objects |
| Molnar-Szakacs et al., 2005 | 58 | fMRI | OBS (5) | Hand (no) | Passively observe | Task>rest | Finger movements |
| | | | IMI (4) | Hand (no) | Imitate as observed | Task>rest | Finger movements |
| Molnar-Szakacs et al., 2006 | 12 | fMRI | OBS (72) | Right hand (o) | Passively observe | Task>rest | Hand manipulating objects |
| Menz et al., 2009 | 15 | fMRI | OBS (5) | Right hand (o) | Observe to imitate | Task>rest | Hand manipulating objects |
| | | | IMI (15) | Right hand (o) | Imitate as observed | Task>rest | Hand manipulating objects |
| Montgomery et al., 2007 | 14 | fMRI | OBS (16) | Right hand (no) | Observe to imitate | Task>rest | Finger gestures |
| | | | IMI (18) | Right hand (no) | Imitate as observed | Task>rest | Finger gestures |
| | | | OBS (16) | Right hand (o) | Observe to imitate | Task>rest | Finger gestures |
| | | | IMI (18) | Right hand (o) | Imitate as observed | Task>rest | Finger gestures |
| Montgomery and Haxby, 2008 | 12 | fMRI | OBS (16) | Face (no) | Observe to imitate | Task>rest | Emotional faces |
| | | | IMI (18) | Face (no) | Imitate as observed | Task>rest | Emotional faces |
| | | | OBS (11) | Right hand (no) | Observe to imitate | Task>rest | Finger gestures |
| | | | IMI (16) | Right hand (no) | Imitate as observed | Task>rest | Finger gestures |
| Morris et al., 2008 | 8 | fMRI | OBS (7) | Body (no) | Passively observe | OBS motion>OBS object | Everyday actions |
| Mouras et al., 2008 | 10 | fMRI | OBS (14) | Body (no) | Passively observe | Task>rest | Sexual intercourse |
| Mühlau et al., 2005 | 12 | fMRI | IMI (24) | Hand (no) | imitate as observed | IMI variable>IMI stereotype | Hand/finger gestures |
| Pierno et al., 2006 | 14 | fMRI | OBS (9) | Right hand (o) | Passively observe | OBS motion>OBS static | Hand reaching/grasping objects |
| Pierno et al., 2009 | 15 | fMRI | OBS (4) | Right hand (no) | Passively observe | OBS motion>OBS static | Hand pointing to objects |
| | | | OBS (8) | Right hand (o) | Passively observe | OBS motion>OBS static | Hand reaching/grasping objects |
| Rocca et al., 2008a | 14 | fMRI | OBS (6) | Right hand (no) | Passively observe | OBS>EXE | Finger movements |
| Rocca et al., 2008b | 11 | fMRI | OBS (12) | Right hand (no) | Passively observe | OBS>EXE | Finger movements |
| | | | OBS (11) | Left hand (no) | Passively observe | OBS>EXE | Finger movements |
| Rumiati et al., 2005 | 10 | PET | IMI (9) | Hand (no) | Imitate as observed | IMI>OBS | Meaningful/meaningless hand movements |
| Sakreida et al., 2005 | 19 | fMRI | OBS (10) | Hand/foot/face (no) | Passively observe | OBS distal>OBS proximal | Hand/foot/mouth movements |
| | | | OBS (11) | Hand/foot/face (no) | Passively observe | OBS proximal>OBS distal | Hand/foot/mouth movements |
| | | | OBS (14) | Body (no) | Passively observe | OBS axial>OBS distal + proximal | Axial rotation of body |
| Schaefer et al., 2009 | 10 | fMRI | OBS (4) | Right hand (o) | Passively observe | OBS touch>OBS non-touch | Hand being touched by brush |
| Schubotz and von Cramon, 2008 | 18 | fMRI | OBS (14) | Hand (o) | Passively observe | Task>rest | Hand writing and pretending to |
| Schulte-Rüther et al., 2007 | 26 | fMRI | OBS (12) | Face (no) | Focus on emotion | OBS emotion>OBS person | Emotional faces |
| Shmuelof and Zohary, 2005 | 11 | fMRI | OBS (13) | Hand (o) | Passively observe | OBS hand + contralat. object>OBS contralat. hand + object | Hand reaching/grasping objects |
| Tai et al., 2004 | 7 | PET | OBS (3) | Hand (o) | Passively observe | OBS motion>OBS static | Human hand grasping object |
| | | | OBS (2) | Hand (o) | Passively observe | OBS motion>OBS static | Non-human hand grasping object |
| Tanaka et al., 2001 | 9 | fMRI | IMI (12) | Right hand (no) | Imitate as observed | Task>rest | Finger movements |
| | | | IMI (8) | Right hand (no) | Imitate as observed | Task>rest | Finger gestures |
| Tanaka and Inui, 2002 | 12 | fMRI | IMI (6) | Right hand (no) | Imitate as observed | IMI>OBS | Finger gestures |
| Tettamanti et al., 2005 | 17 | fMRI | OBS (5) | Face (o) | Listen to action sound | Sentence face>abstract | Action-related sentences |
| | | | OBS (8) | Hand (o) | Listen to action sound | Sentence hand>abstract | Action-related sentences |
| | | | OBS (5) | Foot (o) | Listen to action sound | Sentence foot>abstract | Action-related sentences |
| Turella et al., 2009a | 17 | fMRI | OBS (16) | Right hand (no) | Passively observe | OBS motion>OBS static | Hand reaching/grasping objects |
| Uddin et al., 2005 | 10 | fMRI | OBS (5) | Face (no) | Decide self/different | OBS self>OBS other | Faces of self and familiar person |
| van der Gaag et al., 2007 | 17 | fMRI | IMI (57) | Face (no) | Imitate as observed | Task>rest | Emotional faces |
| | | | OBS (29) | Face (no) | Passively observe | Task>rest | Emotional faces |
| | | | OBS (35) | Face (no) | Decide same/different | Task>rest | Emotional faces |
| | | | OBS (26) | Face (no) | Observe to imitate | Task>rest | Emotional faces |
| Villarreal et al., 2008 | 17 | fMRI | OBS (24) | Hand (o) | Rate type of motion | Task>rest | Hand manipulating objects |
| | | | OBS (29) | Hand (no) | Rate type of motion | Task>rest | Finger gestures |

(*continued on next page*)

**Table 1** (*continued*)

| Publication | Subjects | Mode | Experiment (rep. foci) | Effector (o/no) | Instruction | Contrast | Stimulus |
|---|---|---|---|---|---|---|---|
| Vogt et al., 2007 | 32 | fMRI | OBS (13) | Left hand (o) | Observe to imitate | OBS practised action>OBS non-practised action | Left hand playing guitar chords |
| | | | IMI (5) | Left hand (o) | Imitate as observed | IMI practised action>IMI non-practised action | Left hand playing guitar chords |
| Wheaton et al., 2004 | 12 | fMRI | OBS (5) | Face (no) | Passively observe | OBS motion>OBS static | Mouth movements |
| | | | OBS (5) | Right hand (no) | Passively observe | OBS motion>OBS static | Right hand movements |
| | | | OBS (14) | Foot (no) | Passively observe | OBS motion>OBS static | Leg movements |
| Willems et al., 2007 | 16 | fMRI | OBS (3) | Right hand (no) | Rate match | OBS gesture mismatch>OBS correct match | Spoken and sign language |
| Williams et al., 2006 | 16 | fMRI | IMI (6) | Right hand (no) | Imitate as observed | Task>rest | Finger movements |
| Williams et al., 2007 | 12 | fMRI | IMI (34) | Right hand (no) | Imitate as observed | IMI>EXE | Finger movements |
| Zentgraf et al., 2005 | 10 | fMRI | OBS (12) | Body (no) | Observe to imagine | Task>rest | Gymnastic movements |
| | | | OBS (9) | Body (no) | Observe to evaluate | Task>rest | Gymnastic movements |

The column "Mode" refers to the type of data acquisition used in the respective study (fMRI, PET). The column "Experiment" reports the meta-analysis category with which each experiment of the respective study was labelled. The count of reported foci is added in brackets. The column "Effector" reports the effector used during action observation or imitation as reported in the respective study, with "hand" meaning either "both hands" or "a non-specified hand". The involvement of an object during the observed or imitated action is added in brackets (o object, no non-object).
OBS: action observation, IMI: action imitation, EXE: action execution without visual model (in contrast to imitation).

associated with each focus. The width of these uncertainty functions was determined based on empirical data on the between-subject and between-template variance, which represent the main components of this uncertainty. Importantly, the applied algorithm weights the between-subject variance by the number of examined subjects per study, accommodating the notion that larger sample sizes should provide more reliable approximations of the 'true' activation effect and should therefore be modelled by 'smaller' Gaussian distributions (Eickhoff et al., 2009).

The probabilities of all activation foci in a given experiment were combined for each voxel, resulting in a modelled activation map (MA map). Taking the union across these MA maps yields voxel-wise ALE scores describing the convergence of results at each particular location. Since neurophysiologically, activation should predominantly be localized within the grey matter, all analyses were restricted to those voxels where a probability of at least 10% for grey matter could be assumed based on the ICBM tissue probability maps (Evans et al., 1994).

To distinguish 'true' convergence between studies from random convergence, i.e., noise, the ALE scores were compared to an empirical null distribution derived from a permutation procedure. This null distribution reflects a random spatial association between experiments, while regarding the within-experiment distribution of foci as fixed. Thus, a random-effects inference is invoked, focussing inference on the above-chance convergence between different experiments, not the clustering of foci within a particular experiment. Computationally, deriving this null hypothesis involved sampling a voxel at random from each of the MA maps and taking the union of these values. The ALE score obtained under this assumption of spatial independence was recorded and the permutation procedure iterated $10^{11}$ times to obtain a sufficient sample of the ALE null distribution. The 'true' ALE scores were tested against the ALE scores obtained under the null distribution and thresholded at a cluster-level corrected threshold of $p<0.05$ for each separate meta-analysis performed.

Conjunction analysis was carried out to determine the intersection between the meta-analyses on observation and imitation. Results are reported for a corrected $p$-value of $<0.05$. Contrast analyses were calculated by means of ALE subtraction analysis, accounting for potential differences in sample size. To increase the specificity of the results, the analysis of differences was restricted to those voxels that showed an effect in main action observation or imitation meta-analyses. The reported contrasts were also thresholded at a corrected $p$-value of $<0.05$.

The resulting areas were anatomically labeled by reference to probabilistic cytoarchitectonic maps of the human brain using the SPM Anatomy Toolbox (Eickhoff et al., 2005, 2007). Using a Maximum Probability Map (MPM), activations were assigned to the most probable histological area at their respective locations. Previous studies have provided details about the cytoarchitecture, intersubject variability, and borders of the areas implicated in the current analysis that can be found in the following publications, such as Broca's region (BA 44, BA 45: Amunts et al., 1999), inferior parietal areas (PFop, PFt, PFcm, PF: Caspers et al., 2006, 2008), primary motor cortex (4a; Geyer et al., 1996), premotor cortex (BA 6; Geyer, 2004), primary somatosensory areas (BA 2: Grefkes et al., 2001; BA 1: Geyer et al., 1999, 2000), secondary somatosensory area OP1 (Eickhoff et al., 2006a,b), visual area V5 (Malikovic et al., 2007), superior parietal area 7A, intraparietal area hIP3 (Scheperjans et al., 2008a,b), and intraparietal area hIP1 (Choi et al., 2006).

**Table 2**
Details of analyses and subanalyses carried out in the present meta-analysis.

| | | Experiments | Subjects | Activation foci |
|---|---|---|---|---|
| Observation | | 104 | 1061 | 1390 |
| | of hand actions | 62 | 804 | 823 |
| | –with instruction 'passively observe' | 38 | 459 | 516 |
| | –with instruction 'observe to imitate' | 8 | 131 | 111 |
| | of right hand actions | 37 | 477 | 475 |
| | of non-hand actions | 32 | 364 | 508 |
| | of face actions | 17 | 188 | 291 |
| | of object-related hand actions | 37 | 516 | 587 |
| | of non-object-related hand actions | 25 | 318 | 236 |
| Imitation | | 35 | 459 | 542 |
| | of hand actions | 30 | 405 | 396 |
| | of right hand actions | 15 | 211 | 193 |
| | of non-object-related hand actions | 19 | 320 | 245 |

## Results

### *Individual meta-analyses of action observation and imitation networks*

#### *Action observation network*

Brain regions showing consistent activation across the 104 action observation experiments were observed symmetrically across both hemispheres in frontal areas BA 44/45, lateral dorsal premotor cortex (dPMC, BA 6), supplementary motor area (SMA, BA 6), rostral inferior parietal lobule (IPL, area PFt), primary somatosensory cortex (SI, BA 1/2), superior parietal (SPL, area 7A), intraparietal cortex (IPS, area hIP3), posterior middle temporal gyrus (pMTG) at the transition to

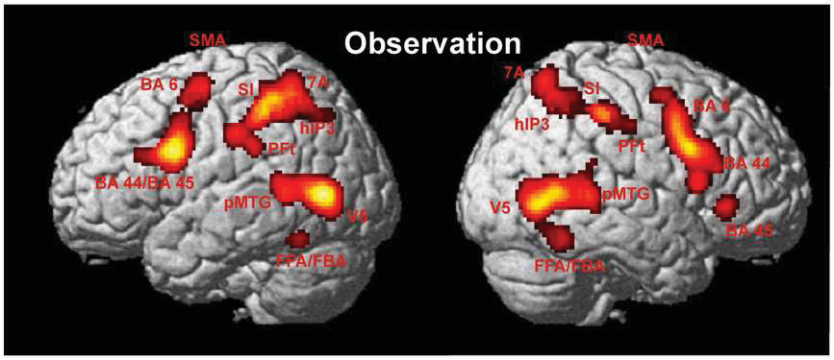


**Fig. 1.** Significant meta-analysis results for action observation, summarized over all effectors. All results are displayed on the left and right lateral surface view of the MNI single subject template. pMTG posterior middle temporal gyrus, SMA supplementary motor area (hidden within the interhemispheric fissure); BA 44, 45: Broca's area (Amunts et al., 1999); BA 6: lateral premotor cortex (Geyer 2004); SI: primary somatosensory cortex (BA 2, Grefkes et al., 2001); 7A: superior parietal area (Scheperjans et al., 2008a,b); PFt: inferior parietal area (Caspers et al., 2006, 2008); hIP3: intraparietal area (Scheperjans et al., 2008a,b); V5: extrastriate visual area (Malikovic et al., 2007).

visual area V5, and fusiform face area/fusiform body area (FFA/FBA; Fig. 1). Coordinates of the activation maxima of the meta-analysis on action observation are given in Table 3.

**Table 3**
Peaks of activation for the two categories "action observation", and "action imitation."

| Macroanatomical location | Cytoarchitectonic location | MNI coordinates | | |
|---|---|---|---|---|
| | | *x* | *y* | *z* |
| *Action observation* | | | | |
| L IFG / PrG | BA 44 / BA 45 / vent-lat BA 6 | −50 | 9 | 30 |
| L lat dPMC | dors-lat BA 6 | −26 | −4 | 56 |
| L med PMC (SMA) | med BA 6 | −2 | 18 | 50 |
| L SI / IPS / SPL | BA 2 / hIP3 / 7A | −34 | −44 | 52 |
| L IPL | PFt / PFop | −60 | −24 | 36 |
| L STS / pMTG | | −54 | −50 | 8 |
| L lat occipital | V5 | −46 | −72 | 2 |
| L fusiform (FFA/FBA) | | −44 | −56 | −18 |
| R IFG | BA 44 | 52 | 12 | 26 |
| R IFG | BA 45 | 56 | 30 | −2 |
| R lat dPMC / MFG | dors-lat BA 6 | 34 | −2 | 54 |
| R med PMC (SMA) | med BA 6 | 4 | 12 | 58 |
| R SI | BA 1 / 2 | 60 | −20 | 40 |
| R IPL | PFt | 44 | −34 | 44 |
| R SPL | 7A | 22 | −62 | 64 |
| R IPS | hIP3 | 30 | −54 | 48 |
| R STS / pMTG | | 56 | −40 | 4 |
| R lat occipital | V5 | 52 | −64 | 0 |
| R fusiform (FFA/FBA) | | 44 | −54 | −18 |
| *Action imitation* | | | | |
| L IFG / PrG | BA 44 / vent-lat BA 6 | −60 | 12 | 14 |
| L lat dPMC | dors-lat BA 6 | −36 | −14 | 62 |
| L med PMC (SMA) | med BA 6 | −1 | 12 | 52 |
| L SI / IPS | BA 2 / hIP3 | −38 | −40 | 50 |
| L STS / pMTG | | −54 | −50 | 10 |
| L lat occipital | V5 | −52 | −70 | 6 |
| R IFG | BA 44 / 45 | 58 | 16 | 10 |
| R lat dPMC / MFG | dors-lat BA 6 / MFG | 42 | 4 | 56 |
| R med PMC (SMA) | med BA 6 | 14 | 6 | 66 |
| R anterior insula | | 42 | 4 | 1 |
| R SI / IPL | BA 2 / PFt | 52 | −36 | 52 |
| R SII / IPL | OP1 / PFcm | 60 | −26 | 20 |
| R lat occipital | V5 | 54 | −64 | 4 |
| R fusiform (FFA/FBA) | | 44 | −54 | −22 |

All peaks are assigned to the most probable brain areas as revealed by the SPM Anatomy Toolbox (Eickhoff et al., 2005, 2007).
FFA/FBA: fusiform face area/fusiform body area, IFG: inferior frontal gyrus, IPL: inferior parietal lobule, IPS: intraparietal sulcus, MFG: middle frontal gyrus, PMC: premotor cortex, pMTG: posterior middle temporal gyrus, PrG: precentral gyrus, SI: primary somatosensory cortex, SII: secondary somatosensory cortex, SMA: supplementary motor cortex, SPL: superior parietal lobule, STS: superior temporal sulcus, dors-lat: dorso-lateral, med: medial, lat: lateral, vent-lat: ventro-lateral.
For further naming details, see Materials and Methods and Results sections.

To assess the effects of potentially confounding factors, additional subanalyses for different effectors and instructions were carried out, revealing a comparable brain network to that of the general analysis across all experiments. Brain areas consistently active during the observation of hand actions include: frontal BA 44, dPMC (BA 6), IPL area PFt, SPL area 7A, IPS area hIP3, SI cortex (BA 2), and pMTG at the transition to visual area V5 bilaterally. BA 45 was only found to be consistently active in the right hemisphere. In contrast to the analysis based on all action observation experiments, activation of FFA/FBA was not found in the observation of hand actions alone (Fig. 2A and Table 4).

When only including right hand actions in the analysis, the same areas were consistently found to be activated across studies (Fig. 2B and Table 4). That is, while the smaller number of studies resulted in lower statistical power and hence smaller clusters of convergence, results were replicated when testing across all action observation, observation on hand actions, and observation of right hand actions.

In contrast to hand-related actions, the analysis of observation of non-hand actions (e.g., involving the face or the whole body) showed consistent activations within frontal and temporo-occipital areas bilaterally, including BA 44, PMC and SMA (BA 6), pMTG and V5. FFA/FBA was only active in the right hemisphere, whereas the only consistent parietal activation, which was located within the IPS (hIP3), was found in the left hemisphere (Fig. 2C and Table 4). The same activation pattern was found for the analysis of observation limited to face actions, except for SMA which did not show consistent activation (Fig. 2D and Table 4).

Contrasting observation of hand and non-hand actions revealed a higher consistency of activations within BA 44 for non-hand actions. In contrast, a higher convergence of reported activations evoked by the observation of hand actions was found in the PMC (BA 6), SI (BA 2), the IPL (area PFt), and the pMTG at the border to V5 (Fig. 2E).

A further subanalysis assessed the effects of different instructions that were given to the subjects in the various action observation tasks. The observation of hand actions with the instruction to 'passively observe' recruited a comparable network as the main analysis on action observation, consisting of lateral premotor, IPL, SPL, and IPS cortex, SI, and pMTG (Fig. 3A). In contrast, observation of hand actions with the instruction 'observe to imitate' mainly led to consistent activations in lateral premotor and posterior temporal and extrastriate visual cortex, without consistent activation of parietal areas (Fig. 3B).

Contrast analysis between different instructions provided to subjects revealed more consistent activation within IPL (area PFt) bilaterally as well as in left BA 44, SI, and intraparietal sulcus (area hIP3) for the instruction 'passively observe' whereas the instruction 'observe to imitate' revealed no stronger association in any region (Fig. 3C and Table 4). However, we note that the subanalysis on

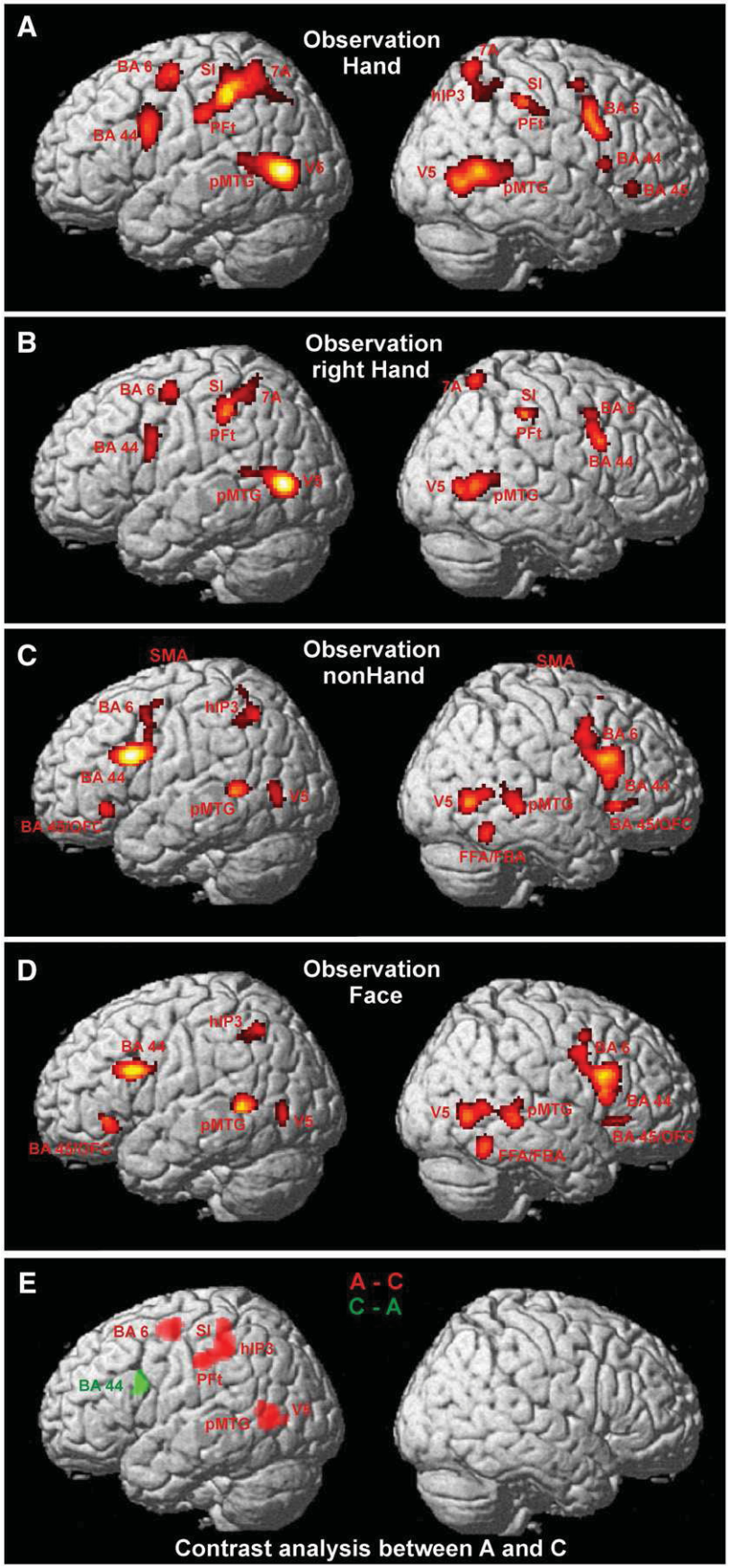


**Fig. 2.** Significant meta-analysis results for (A) observation of hand actions, (B) observation of right hand actions, (C) observation of non-hand actions, (D) observation of face actions, and (E) contrast analysis between observation of hand actions and observation of non-hand actions (colour-coding of respective contrasts within the figure). For other conventions, see Fig. 1.

**Table 4**
Peaks of activation for the subanalyses within the observation sample.

| Macroanatomical location | Cytoarchitectonic location | MNI coordinates | | |
|---|---|---|---|---|
| | | *x* | *y* | *z* |
| *Observation hand* | | | | |
| L IFG / PrG | BA 44 / vent-lat BA 6 | −50 | 6 | 30 |
| L lat dPMC | dors-lat BA 6 | −26 | −4 | 56 |
| L SI / IPS | BA 2 / hIP3 | −36 | −42 | 36 |
| L IPL | PFt | −58 | −24 | 36 |
| L STS / pMTG | | −56 | −48 | 10 |
| L lat occipital | V5 | −46 | −70 | 4 |
| R IFG / PrG | BA 44 / vent-lat BA 6 | 52 | 8 | 36 |
| R IFG | BA 45 | 56 | 30 | −4 |
| R lat dPMC / MFG | dors-lat BA 6 / MFG | 36 | 0 | 54 |
| R SI | BA 2 | 42 | −34 | 46 |
| R IPL | PFt | 60 | −26 | 42 |
| R SPL | 7A | 22 | −62 | 64 |
| R STS / pMTG | | 52 | −60 | 4 |
| R lat occipital | V5 | 50 | −66 | 0 |
| *Observation right hand* | | | | |
| L IFG / PrG | BA 44 / vent-lat BA 6 | −51 | 5 | 29 |
| L lat dPMC / MFG | dors-lat BA 6 / MFG | −26 | −4 | 54 |
| L IPL / SI | PFt / BA 2 | −44 | −36 | 42 |
| L SI / SPL | BA 1 / 2 / 7A | −32 | −48 | 56 |
| L STS / pMTG | | −56 | −50 | 12 |
| L lat occipital | V5 | −46 | −70 | 4 |
| R IFG / PrG | BA 44 / vent-lat BA 6 | −54 | 8 | 36 |
| R IPL / SI | PFt / BA 2 | 49 | −32 | 47 |
| R SPL | 7A | 22 | −62 | 64 |
| R lat occipital / pMTG | V5 / pMTG | 52 | −72 | 4 |
| *Observation non-hand* | | | | |
| L IFG / PrG | BA 44 / BA 45 / vent-lat BA 6 | −49 | 11 | 31 |
| L IFG / OFC | BA 45 / OFC | −44 | 28 | −6 |
| L med PMC (SMA) | med BA 6 | 4 | 10 | 58 |
| L SPL / IPS | 7A / hIP3 | −32 | −54 | 51 |
| L pMTG / STS | | −52 | −48 | 6 |
| L lat occipital / pMTG | V5 / pMTG | −48 | −70 | 6 |
| R IFG / PrG | BA 44 / BA 45 / vent-lat BA 6 | 53 | 13 | 29 |
| R IFG / OFC | BA 45 / OFC | 46 | 20 | 2 |
| R med PMC (SMA) | med BA 6 | −4 | 10 | 58 |
| R pMTG / STS | | 56 | −38 | 0 |
| R lat occipital / pMTG | V5 / pMTG | 54 | −64 | 0 |
| R fusiform (FFA/FBA) | | 46 | −54 | −18 |
| *Observation face* | | | | |
| L IFG / PrG | BA 44 / BA 45 / vent-lat BA 6 | −48 | 15 | 27 |
| L IFG / OFC | BA 45 / OFC | −44 | 28 | −6 |
| L med PMC (SMA) | med BA 6 | | | |
| L SPL / IPS | 7A / hIP3 | −32 | −56 | 48 |
| L pMTG / STS | | −52 | −48 | 6 |
| L lat occipital / pMTG | V5 / pMTG | −49 | −71 | 2 |
| R IFG / PrG | BA 44 / BA 45 / vent-lat BA 6 | 53 | 13 | 27 |
| R IFG / OFC | BA 45 / OFC | 50 | 24 | −1 |
| R med PMC (SMA) | med BA 6 | | | |
| R pMTG / STS | | 56 | −38 | 0 |
| R lat occipital / pMTG | V5 / pMTG | 54 | −64 | 0 |
| R fusiform (FFA/FBA) | | 46 | −54 | −18 |
| *Observation hand passively observe* | | | | |
| L IFG / PrG | BA 44 / vent-lat BA 6 | −51 | 6 | 31 |
| L lat dPMC / MFG | dors-lat BA 6 / MFG | −26 | −4 | 54 |
| L SI / IPL | BA 2 / PFt | −52 | −28 | 40 |
| L lat occipital | V5 | −46 | −70 | 4 |
| R IFG / PrG | BA 44 / vent-lat BA 6 | 52 | 9 | 36 |
| R SI / IPL | BA 2 / PFt | 42 | −32 | 44 |
| R SPL | 7A | 22 | −62 | 64 |
| R pMTG | | 52 | −58 | 4 |
| R lat occipital | V5 | 44 | −70 | 2 |
| *Observation hand observe to imitate* | | | | |
| L IFG / PrG | BA 44 / vent-lat BA 6 | −51 | 8 | 39 |
| L lat dPMC | dors-lat BA 6 | −34 | −14 | 60 |
| L M1 | 4a | −40 | −28 | 58 |
| L pMTG | | −55 | −51 | 12 |
| L lat occipital / pMTG | V5 / pMTG | −52 | −70 | 6 |
| R IFG | BA 44 | 58 | 14 | 10 |
| R anterior insula | | 42 | 5 | −1 |
| R SPL | 7A | 9 | −63 | 64 |
| R pMTG | | 52 | −48 | 8 |
| R lat occipital / pMTG | V5 / pMTG | 54 | −72 | 2 |
| *Observation hand object* | | | | |
| L IFG / PrG | BA 44 / vent-lat BA 6 | −51 | 7 | 30 |
| L lat dPMC / MFG | dors-lat BA 6 / MFG | −26 | −4 | 56 |
| L SI / IPS | BA 2 / hIP3 | −36 | −42 | 52 |
| L IPL | PFt | −58 | −24 | 36 |
| L lat occipital / pMTG | V5 / pMTG | −46 | −70 | 4 |
| R IFG / PrG | BA 44 / vent-lat BA 6 | 54 | 9 | 34 |
| R SI / IPL | BA 2 / PFt | 42 | −34 | 46 |
| R SPL | 7A | 22 | −62 | 64 |
| R pMTG | | 52 | −60 | 4 |
| R lat occipital | V5 | 44 | −72 | 4 |
| *Observation hand non-object* | | | | |
| L SI / IPS | BA 2 / hIP1 | −37 | −46 | 50 |
| L IPL | PF | −54 | −36 | 46 |
| L pMTG | | −56 | −50 | 6 |
| L lat occipital / pMTG | V5 / pMTG | −50 | −64 | 6 |
| R IFG / PrG | BA 44 / vent-lat BA 6 | 51 | 8 | 37 |
| R pMTG | | 54 | −40 | 8 |
| R lat occipital / pMTG | V5 / pMTG | 50 | −68 | 2 |

All peaks are assigned to the most probable brain areas as revealed by the SPM Anatomy Toolbox (Eickhoff et al., 2005, 2007). For naming conventions, see Table 3.

observation with instruction 'observe to imitate' was based on only 8 experiments. The meta-analysis algorithm accommodates for such differences in sample size. But with such large differences as found here, a potential confounding effect due to sample size cannot fully be excluded. Thus, it cannot be ruled out that a lack of consistent activation within parietal cortex might have resulted from the small number of studies. Further subdividing the studies according to the other instructions only yielded very low numbers of studies for different categories, thus not providing enough data for further subanalyses.

Dividing the experiments on hand action observations into those that presented object-related actions and those that did not revealed a further differentiation within the observation network. The observation of object-related hand actions was more consistently associated with activations in BA 44, lateral PMC (BA 6), IPL area PFt, SPL area 7A, the pMTG and V5 bilaterally, as well as with activations in SI (BA 2) and the anterior IPS (area hIP3) on the right hemisphere (Fig. 4A and Table 4). In contrast, observation of non-object-related hand actions was mainly associated with activations in the temporo-occipital areas (Fig. 4B and Table 4).

Contrast analysis between observation of object- and non-object-related actions revealed a stronger association of activation with object-related actions within left BA 44, lateral PMC (BA 6), and inferior parietal area PFt, and in right superior parietal area 7A and temporo-occipital cortex (Fig. 4C).

*Action imitation network*

Action imitation tasks also most consistently evoked activation in an extended bilateral network comprising frontal BA 44, the PMC (BA 6) and adjacent superior frontal gyrus (SFG), the SMA (BA 6), SI (area 2), IPL (area PFt), and visual area V5. The pMTG was found to be consistently activated only in the left hemisphere, whereas ventral IPL area PFcm at the border to the secondary somatosensory cortex (SII) area OP1, the FFA/FBA, and the frontal aspect of the insular cortex

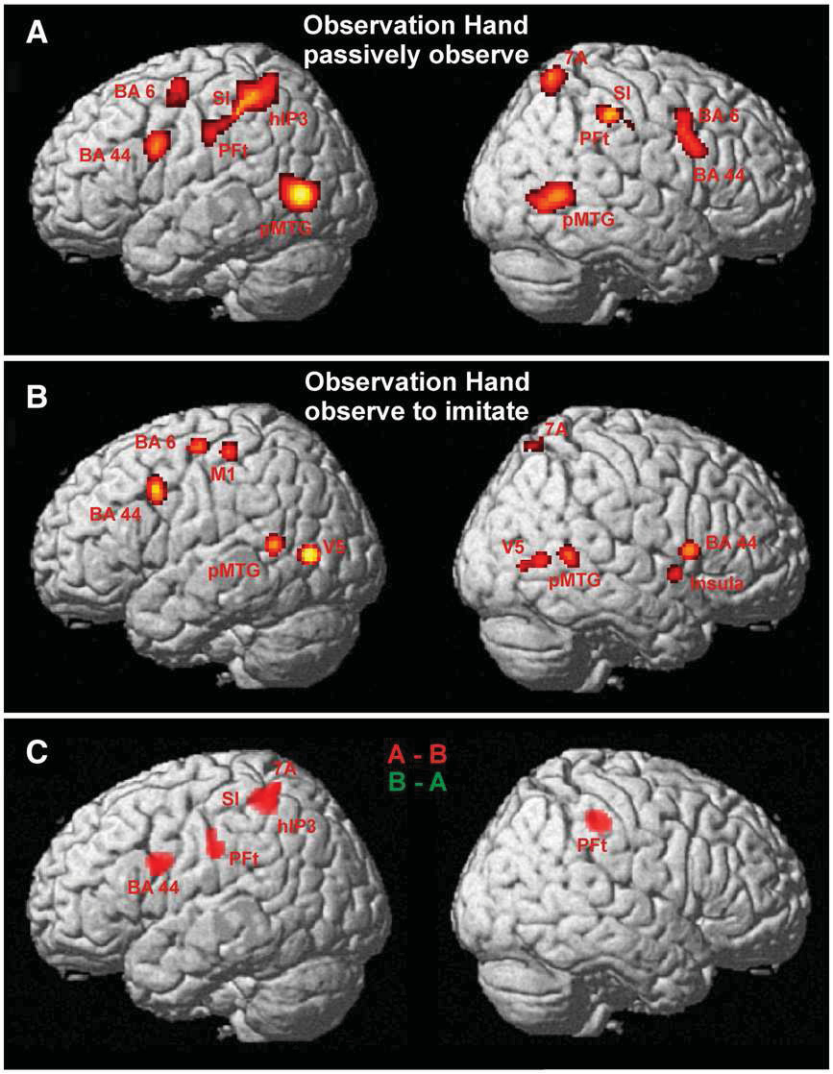


**Fig. 3.** Significant meta-analysis results for (A) observation of hand actions with instruction 'passively observe,' (B) observation of hand actions with instruction 'observe to imitate,' and (C) contrast analysis between both categories (colour-coding of respective contrasts within the figure). For other conventions, see Fig. 1.

were only consistently activated in the right hemisphere (Fig. 5). Coordinates of the activation maxima for the main meta-analysis on action imitation are given in Table 3.

Additional subanalyses were carried out on the imitation of hand actions, right hand actions, and non-object-related hand actions. Imitation of hand actions and right hand actions both revealed patterns of activation that were highly comparable to action imitation across all experiments. A major difference was only found with respect to imitation of right hand actions: here, the pMTG was not only consistently activated in the left, but also in the right hemisphere (Figs. 6A, B and Table 5).

Imitation of non-object-related actions, however, only evoked consistent activation of the motor and lateral premotor areas, like BA 44, BA 6, and adjacent SFG (Fig. 6C and Table 5), but not in temporo-occipital areas.

### *Conjunction and contrast analyses*

#### *Conjunction analysis*

To identify brain regions that are consistently activated by action observation as well as action imitation tasks, a conjunction analysis of the two meta-analyses reported above was performed.

Common significant activations were found bilaterally in frontal BA 44, lateral PMC (BA 6), the SMA (BA 6), rostral IPL (areas PFop and PFt), SI (BA 2), and visual area V5. Moreover, the left hemispheric pMTG was also found in both networks whereas activation of the right FFA/FBA was commonly found in the right hemisphere (Fig. 7A and Table 6).

#### *Contrast analysis*

To assess which areas were more consistently associated with action observation or imitation, an ALE subtraction was performed on those voxels where either of the two analyses showed a significant activation to determine the relative divergence of these tasks. In comparison with imitation tasks, action observation tasks were more associated with activations in a rostro-dorsal part of BA 44, lateral PMC, the pMTG and V5 bilaterally as well as with activation in left IPL areas PFt/PFop and in right SPL area 7A (Fig. 7B and Table 7).

In contrast, activations in action imitation experiments were more consistently found in a caudo-ventral part of left BA 44 (at the border to caudally adjacent BA 6) bilaterally, and in the SI (BA 2), the adjacent IPL (area PFt), and the FFA/FBA within the right hemisphere (Fig. 7B and Table 7).

Comparable results could be found when performing separate conjunction and contrast analyses for the subsamples on effectors, involvement of an object, and instructions that have been reported in the previous sections. Small differences were only found with respect to the size of the activation clusters whereas the location remained stable.

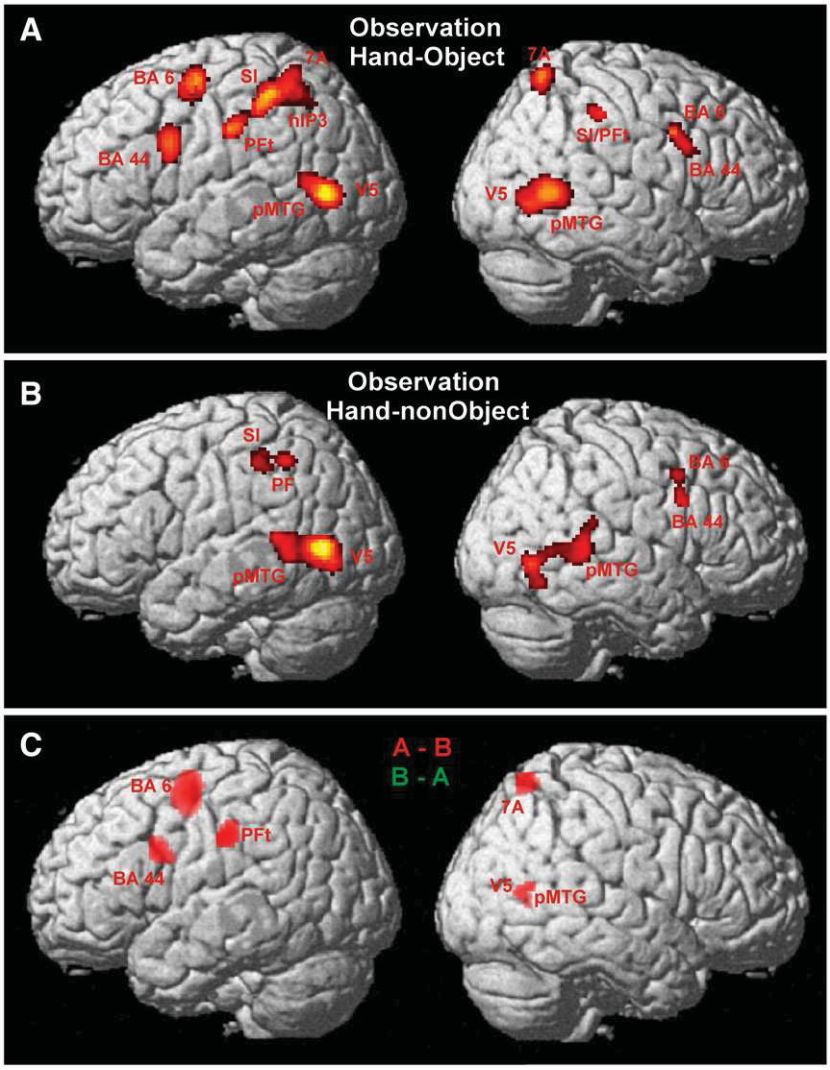


**Fig. 4.** Significant meta-analysis results for (A) observation of object-related hand actions, (B) observation of non-object-related hand actions, and (C) contrast analysis between both categories (colour-coding of respective contrasts within the figure). For other conventions, see Fig. 1.

## Discussion

The present study assessed the action observation and imitation networks in the human brain in a meta-analysis of 139 fMRI and PET experiments. Both action observation and imitation experiments were consistently associated with activation in a largely bilateral network of premotor, primary somatosensory, inferior parietal, and intraparietal as well as temporo-occipital areas. Further analysis revealed that this activation pattern is largely independent from possible confounds, such as effectors. However, activation in Broca's area (BA 44, BA 45) differed between the observation and the imitation of an action: while activation due to observation was more consistent in a rostro-dorsal aspect (BA 45), activation due to imitation consistently recruited the caudo-ventral part (BA 44). Another notable difference pertained to the posterior middle temporal cortex: While action observation involved this cortical

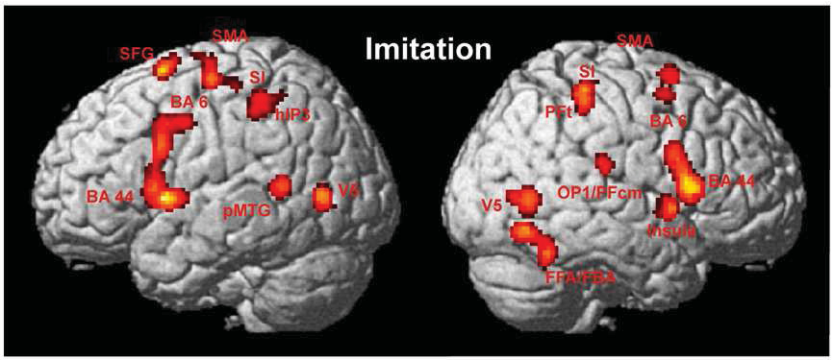


**Fig. 5.** Significant meta-analysis results for action imitation. MI: primary motor cortex (areas 4a, 4p; Geyer et al., 1996). For other conventions, see Fig. 1.

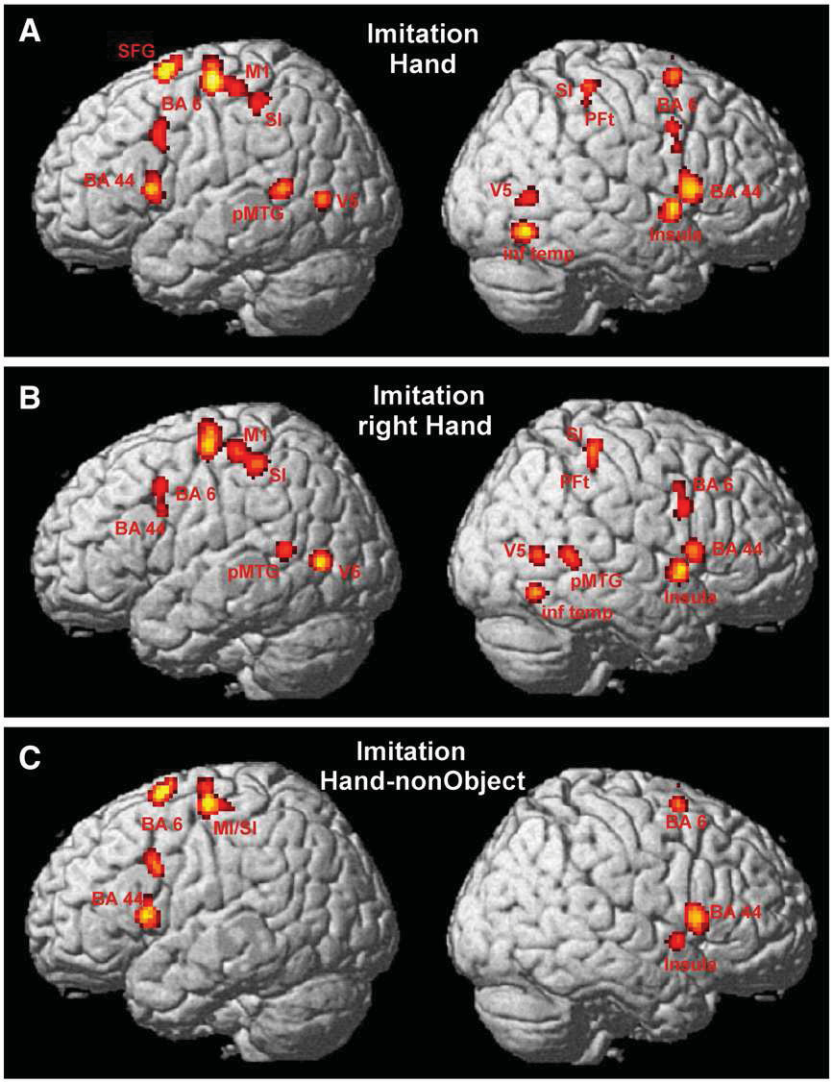


**Fig. 6.** Significant meta-analysis results for (A) imitation of hand actions, and (B) imitation of right hand actions, and (C) imitation of non-object-related hand actions. For other conventions, see Fig. 1.

region bilaterally, imitation tasks only involved the left pMTG. In the context of imitation, activation in right pMTG was only found for imitation of right hand actions.

*Methodological considerations*

The results of any given neuroimaging experiment are influenced by various study-specific idiosyncrasies, including the experimental design, implementation of the paradigm, task requirements, included subjects and the analysis of the data. Hence, the results of any particular experiment can rarely yield generalisable inference on the cortical substrates of a particular cognitive process. One way to overcome these drawbacks is to integrate the results from several neuroimaging studies by means of quantitative meta-analyses (Eickhoff et al., 2009; Laird et al., 2009; Turkeltaub et al., 2002). Hereby, inference is directed towards identifying those regions where previous experiments showed converging evidence for activation. Significant results in a meta-analysis are achieved if convergence across studies occurs more likely than expected by chance, even though this does not require all or even the majority of the studies to activate at that particular location. Using the revised version of the ALE meta-analysis algorithm (Eickhoff et al., 2009) provided objective modelling of spatial uncertainty relative to sample sizes within different studies and testing for convergence across different experiments. Therefore, possible drawbacks of former coordinate-based meta-analysis approaches (Laird et al., 2005a,b; Turkeltaub et al., 2002) were avoided. Nevertheless, differences in sample size between different meta-analyses (e.g., on action observation and action imitation) may influence the obtained results, in particular with respect to the size of the significant clusters. Furthermore, it has to be noted that meta-analyses on the basis of ALE algorithms only reveal a consistency of activations across studies. Information about strength of a resulting activation cluster is not considered, as these are reported inconsistently and by incompatible measures in the original publications (e.g., percent signal change vs. contrast estimates vs. *Z*-scores). Consequently, a task which evokes stronger activation in any particular experiment than another may result in less significant and/or extended activation on meta-analyses, if the convergence between studies is less pronounced.

Also, coordinate-based meta-analyses only use reported peak activations for the analysis, thus discarding a large amount of spatial information from the original statistical parametric images. To address this problem, image-based meta-analyses have been proposed, which use the full statistic images of the experiments (e.g., Schilbach et al., 2008b). While such approaches use more information from the original data, their applicability is quite limited since they require comparable contrast images and error estimates for every

**Table 5**
Peaks of activation for the subanalyses within the imitation sample.

| Macroanatomical location | Cytoarchitectonic location | MNI coordinates | | |
|---|---|---|---|---|
| | | *x* | *y* | *z* |
| *Imitation hand* | | | | |
| L IFG / PrG | BA 44 / vent-lat BA 6 | −52 | 10 | 38 |
| L IFG | BA 44 | −54 | 14 | 8 |
| L lat dPMC | dors-lat BA 6 | −36 | −14 | 62 |
| L M1 | 4a | −40 | −28 | 58 |
| L SFG | | −16 | 8 | 66 |
| L SI | BA 2 | −36 | −38 | 52 |
| L STS / pMTG | | −54 | −50 | 10 |
| L lat occipital / pMTG | V5 / pMTG | −52 | −68 | 6 |
| R IFG / PrG | BA 44 / vent-lat BA 6 | 56 | 7 | 38 |
| R IFG | BA 44 / 45 | 58 | 15 | 11 |
| R lat dPMC / SFG | dors-lat BA 6 / SFG | 16 | 6 | 64 |
| R anterior insula | | 44 | 6 | 0 |
| R SI | BA 1 / 2 | 48 | −34 | 60 |
| R IPL | PF / PFt | 54 | −36 | 52 |
| R lat occipital / pMTG | V5 / pMTG | 54 | −64 | 6 |
| R inf temporal | | 44 | −66 | −10 |
| *Imitation right hand* | | | | |
| L IFG / PrG | BA 44 / vent-lat BA 6 | 56 | 8 | 34 |
| L lat dPMC | dors-lat BA 6 | −34 | −14 | 62 |
| L M1 | 4a | −40 | −28 | 58 |
| L SI | BA 2 | −36 | −38 | 54 |
| L pMTG | | −54 | −52 | 10 |
| L lat occipital / pMTG | V5 / pMTG | −52 | −70 | 6 |
| R IFG | BA 44 | 58 | 14 | 8 |
| R SI | BA 1 / 2 | 46 | −36 | 58 |
| R IPL | PF / PFt | 54 | −36 | 52 |
| R anterior insula | | 44 | 6 | −2 |
| R pMTG | | 52 | −48 | 6 |
| R lat occipital / pMTG | V5 / pMTG | 54 | −62 | 6 |
| R inf temporal | | −44 | −64 | −11 |
| *Imitation hand non-object* | | | | |
| L IFG / PrG | BA 44 / vent-lat BA 6 | −53 | 10 | 35 |
| L IFG | BA 44 /45 | −54 | 14 | 8 |
| L lat dPMC / M1 | dors-lat BA 6 / 4a | −40 | −16 | 62 |
| L lat dPMC / SFG | dors-lat BA 6 / SFG | −18 | 6 | 68 |
| R IFG | BA 44 / 45 | 60 | 16 | 8 |
| R lat dPMC / SFG | dors-lat BA 6 / SFG | 16 | 6 | 64 |
| R anterior insula | | 42 | 6 | −2 |

All peaks are assigned to the most probable brain areas as revealed by the SPM Anatomy Toolbox (Eickhoff et al., 2005, 2007). M1 primary motor cortex, for other naming conventions, see Table 3.

included study. That is, image-based analyses may use more data from each individual experiment but the number of experiments that can be included is generally greatly reduced. However, a recent comparison of image- and coordinate-based meta-analyses (Salimi-Khorshidi et al., 2009) revealed good agreement between meta-analyses based on full statistical contrast images and reduced 3D coordinates. Given this evaluation and the difficulties of obtaining full image data from a sufficient amount of published experiments, it seems that coordinate-based approaches such as ALE represent the most practical tool for meta-analyses on neuroimaging data.

An important caveat for the interpretation of meta-analyses is the potential presence of confounding factors in the assessed experiments. Meta-analyses pool across many studies to identify convergent findings while disregarding experiment-specific variability in design and analysis. However, the averaging effects of meta-analyses that allow for the influence of confounding factors to be ignored only pertain to unsystematic study variations. If, however, an additional cognitive process is present in a significant number of the included experiments, the ensuing activations may confound the meta-analysis. In this case, activation in a certain area would not be attributable to the process of interest but to processes that were concurrently present in the included experiments. For example, it has been argued that activation of Broca's area during imitation tasks could result from covert speech (e.g., Brass and Heyes, 2005). Assuming that vocalisation is present in the majority of the imitation experiments, vocalisation-related activity will be indistinguishable from an imitation-related one. This scenario, however, also raises the fundamental question, whether two processes that co-occur consistently in neuroimaging experiments should actually be distinguished from each other. That is, covered vocalisation and the corresponding activation of BA 44 may be an intrinsic part of action imitation rather than a confound that must be excluded. Evidence for such a genuine role of BA 44 in imitation processes, for example, is provided by recent transcranial magnetic stimulation (TMS) and lesion studies, which showed that lesions (artificial or pathological) in BA 44 led to imitation failure (Fazio et al., 2009; Heiser et al., 2003).

### *Areas involved in both networks*

Overall, the current meta-analysis revealed a network for the observation and imitation of actions that expands both hemispheres and reaches far beyond the 'classical' mirror neuron areas within ventral premotor and inferior parietal cortex. This view of an "expanded MNS" involving similar areas as revealed by the current meta-analysis, has recently been assumed based on human imaging studies (Fabbri-Destro and Rizzolatti, 2008; Iacoboni, 2009) and with respect to possible homologies to the macaque mirror neuron system (Keysers and Gazzola, 2009). The present meta-analysis could provide further evidence to this discussion regarding the involvement of these networks in processing of observed and imitated actions. The results showed that areas other than the 'classical' mirror neuron areas vPMC and rostral IPL were consistently activated across studies, i.e., dPMC, SMA, pMTG, and V5.

Among the commonly activated areas are BA 44 and the rostral IPL/anterior IPS (areas PFt/hIP3). These two regions are thought to be the human homologues of macaque ventral premotor area F5 and rostral inferior parietal areas PFG and PF, i.e., those areas where mirror neurons were discovered using invasive recordings (e.g., Fogassi et al., 2005; Gallese et al., 1996; Rozzi et al., 2008). Activation of these regions by action observation tasks is not surprising, since "activation during action observation" is one of the key properties defining a mirror neuron (e.g., Rizzolatti, 2005). Thus, if BA 44 and the rostral IPL are indeed the homologues of the mirror neuron areas in other primates, they should be activated by action observation tasks. Activation during action imitation, however, is not a typical mirror neuron characteristic. Rather, it has been stressed that monkeys are not able to imitate in a comparable way as humans (e.g., Iacoboni, 2009; Rizzolatti, 2005). In human neuroimaging studies on imitation paradigms, however, robust activation of BA 44 and the rostral IPL have been reported (e.g., Hamilton and Grafton, 2008; Iacoboni, 2009; Iacoboni and Dapretto, 2006; Rizzolatti et al., 2001) and are confirmed in the current meta-analysis. A straightforward explanation for these findings could be provided by the experimental setup of most action imitation experiments. Typically these involve concurrent execution of an observed action, i.e., both properties that define mirror neurons. It has, however, also been argued that potential mirror neurons in the human brain may have an independent relevance for imitation tasks, even though they don't hold the same function in non-human primates (e.g., Brass and Heyes, 2005; Culham and Valyear, 2006; Heyes, 2001). This view is largely based on conceptualising mirror properties as a matching between sensory input and motor acts (e.g., Kilner et al., 2007; Jakobs et al., 2009) and stressing the importance of such a mechanism for action observation, execution, and crucially also imitation (e.g., Fabbri-Destro and Rizzolatti, 2008). Rizzolatti (2005) moreover stressed the possibility that in particular the caudal aspect of BA 44 may represent the putative homologue of macaque area F5. Our meta-analysis confirms and extends this view in a quantitative analysis over a large number of individual experiments. Since imitation and observation recruited the very caudal aspect of BA 44

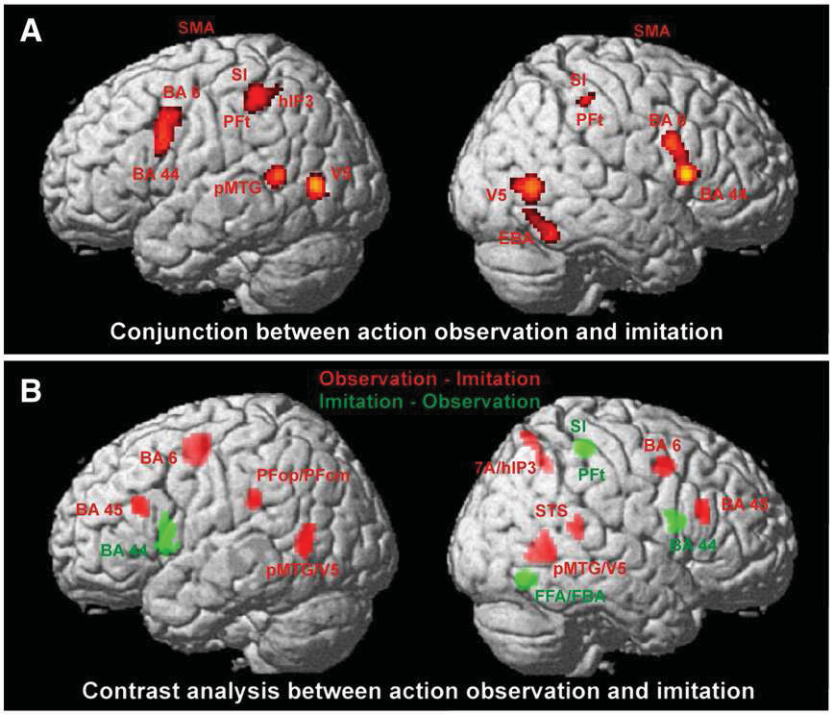


**Fig. 7.** Significant results for (A) the conjunction and (B) the contrast analysis between the main categories action observation and action imitation (colour-coding of respective contrasts within the figure). For other conventions, see Fig. 1.

at the border to BA 6, the same region was activated during imitation as thought to be a human mirror region (Rizzolatti, 2005). With respect to the parietal cortex, the current meta-analysis could provide new evidence for the discussion of potential homologies between humans and monkeys by showing that human area PFt seems to be most consistently involved in processes that have been ascribed to area PF of the macaque.

Importantly, the location of the convergent activation within Broca's area (BA 44, BA 45) differed between action observation and action imitation tasks. Only the caudo-dorsal part of BA 44 was involved in both networks, whereas a higher consistency of activation for imitation was found in a more caudo-ventral aspect of BA 44. In turn, more consistent activation by observation tasks was found in the rostro-dorsal aspect of Broca's region (BA 45). This dissociation has already been noted in previous experiments and was interpreted as deriving from the requirements of forward modelling processes during imitation (e.g., Molnar-Szakacs et al., 2005; Morin and Grèzes, 2008, Brass and Heyes, 2005; Vogt et al., 2007). Furthermore, an explicit model for this differentiation within Broca's region was introduced by Koechlin et al. (2003) and Koechlin and Jubault (2006): Within this model, Broca's region is most likely involved in context specific recognition of stimuli. Further differentiation regarding the amount of cognitive control results in a bipartition: Activation within BA 44 was seen as being responsible for the initiation and termination of simple actions whereas activation in BA 45 was more likely ascribed to the supraordinate aspect of the action (Koechlin and Jubault, 2006). Following this model and the works by Molnar-Szakacs et al. (2005) and Vogt et al. (2007), the differentiation within Broca's region found in the present meta-analysis could be interpreted as follows. Actions shown during the observation experiments were generally more complex, whereas actions in the imitation experiments were kept simpler. This difference is owed to feasibility constraints in the scanner for imitation but not for observation studies. Thus, the

**Table 6**
Peak activations for the conjunction between "action observation" and "action imitation."

| Macroanatomical location | Cytoarchitectonic location | Anatomical MNI coordinates | | |
|---|---|---|---|---|
| | | *x* | *y* | *z* |
| L IFG / PrG | BA 44 / vent-lat BA 6 | −56 | 8 | 28 |
| L vPMC | vent-lat BA 6 | −54 | 6 | 40 |
| L SMA | med BA 6 | −1 | 16 | 52 |
| L SI / IPS | BA 2 / hIP3 | −38 | −40 | 50 |
| L STS / pMTG | | −54 | −50 | 10 |
| L lat occipital | V5 | −52 | −70 | 6 |
| R IFG | BA 44 | 58 | 16 | 10 |
| R SMA | med BA 6 | 4 | 12 | 56 |
| R IPL | PFt | 51 | −36 | 50 |
| R SPL | 7A / 7PC | 30 | −62 | 63 |
| R fusiform (FFA/FBA) | | 44 | −54 | −20 |
| R lat occipital | V5 | 54 | −64 | 4 |

All peaks are assigned to the most probable brain areas as revealed by the SPM Anatomy Toolbox (Eickhoff et al., 2005, 2007). For naming details, see Table 3.

**Table 7**
Peak activations for contrast analysis.

| Macroanatomical location | Cytoarchitectonic location | MNI coordinates | | |
|---|---|---|---|---|
| | | *x* | *y* | *z* |
| *Imitation>observation* | | | | |
| L IFG | BA 44 | −56 | 12 | 9 |
| R IFG | BA 44 | 58 | 10 | 20 |
| R SI / IPL | BA 2 / PFt | 50 | −36 | 54 |
| R inf. temporal | | 42 | −66 | −12 |
| *Observation>imitation* | | | | |
| L IFG | BA 45 | −52 | 28 | 22 |
| L lat dPMC / SFG | dors-lat BA 6 / SFG | −20 | −6 | 52 |
| L IPL | PFop / PFcm | −50 | −34 | 24 |
| L pMTG | | −46 | −60 | 6 |
| R IFG | BA 45 | 54 | 28 | 22 |
| R lat PMC / PrG | lat BA 6 | 48 | 4 | 46 |
| R SPL / IPS | 7A / hIP3 | 28 | −60 | 54 |
| R STS | | 54 | −40 | 16 |
| R pMTG / lat occipital | pMTG / V5 | 47 | −57 | 4 |

All peaks are assigned to the most probable brain areas as revealed by the SPM Anatomy Toolbox (Eickhoff et al., 2005, 2007). For naming details, see Table 3.

dominance of the rostro-caudal part of Broca's region (BA 45) during action observation might result from the processing of more complex movements. As such, there is a high need for integrating and assessing the context of the whole action. This is less the case for the more simple actions used during the imitation experiments. These, however, pose higher needs for control and forward modelling provided by caudal BA 44.

The supplementary motor area (SMA) was also consistently found to be active during action observation as well as action imitation tasks. Whereas action-related activations in BA 44 were linked to, e.g., motor sequence learning, motor imagery, and action preparation (e.g., Binkofski et al., 1999; Johnson-Frey et al., 2003; Krams et al., 1998; Mecklinger et al., 2002) or recognition of abstract motor behaviour and associative motor learning (e.g., Binkofski et al., 2000; Hazeltine et al., 1997; Seitz and Roland, 1992), one function of SMA was seen in temporally sequencing different parts of a complex movement (e.g., Tanji, 1994; Mita et al., 2009). Tankus et al. (2009) ascribed SMA activation to the encoding of speed and direction of a movement. Furthermore, it has been shown that lesions in SMA lead to deficits in sequencing actions (Gentilucci et al., 2000). Following these previous studies, the association of SMA activation with observation and imitation tasks can be interpreted as reflecting the temporal sequencing of the action. After disassembling a complex action into different executable parts, the individual parts have to be put into a temporal sequence to imitate the observed action correctly. For observation alone, this step might as well be necessary to capture all parts of the observed action for subsequent understanding of the action as a whole. This is supported by the notion that the activation within SMA during observation was mainly driven by the observation of non-hand actions which included whole body movements which are much more complex than simple finger and hand movements. To further enlighten the role of the SMA in temporal sequencing, the observation experiments have been subdivided into those with video (i.e., moving) and those with static stimuli, assuming that static stimuli would not require the involvement of the SMA. Both subanalyses revealed a comparable network as the overall observation analysis, with a higher consistency of activations for the video subsample. But since the sample sizes were largely unequal (79 video, 15 static), a potential bias toward the video sample could not fully be excluded. Furthermore, the static sample also involved complex actions which required a disassembly of the actions into different executable parts. Therefore, the need for temporal sequencing, and thus, the involvement of the SMA in this subsample could not completely be ruled out by conceptual reasons, either.

Furthermore, the posterior middle temporal gyrus/superior temporal sulcus (pMTG/STS), anterior and dorsal to V5, was consistently involved in action observation and imitation. This region is known to be involved in the processing of biological motion (e.g., Buccino et al., 2001; Puce and Perrett, 2003; Morris et al., 2008). Since the majority of all action observation and imitation experiments included in the present meta-analysis featured the display of video clips showing natural human movements, the activation of the pMTG/STS is well explained by this role.

Extrastriate visual area V5 has been involved within both networks revealed by the present meta-analysis. Activations in V5 have been reported in previous studies due to recognition and early processing of visually presented motion stimuli (e.g., Seymour et al., 2009; Thompson et al., 2009; Vaina et al., 2001). In the context of action observation and imitation, the involvement of area V5 could be explained in line with these previous reports, serving as an encoder of the dynamic aspect of the movement.

A part of the fusiform gyrus was also involved in both networks, most probably the fusiform face area / fusiform body area (FFA/FBA). The name of this region refers to the involvement of FFA and FBA in recognition of faces and bodies. (e.g., Downing et al., 2006; Kitada et al., 2009). In the current meta-analysis, activation in FFA/FBA was primarily found during observation of face actions and, more generally, non-hand actions, which also involved, e.g., the whole body. No activation in this region was found for the observation of hand actions. The same holds true for the imitation sample: Whereas the total analysis which also contained imitation of face actions revealed activation in FFA/FBA, the analysis of imitation of hand actions did not reveal such an activation (there, the activation is located more rostro-dorsally). Thus, in both networks, FFA/FBA most likely serves as an encoder of facial and body stimuli. Furthermore, both networks only involved right FFA/FBA which is also in line with recent studies on the lateralization of visual perception areas, arguing in favour of a specialization of hemispheres with respect to different levels of processing which results in a specialization of the right hemisphere for tasks where spatial metrics and conjoining features play an essential role, like in the recognition of faces and bodies (e.g., Willems et al., 2009; Umiltá et al., 1985; for review: Dien, 2009).

Both action observation and imitation were also robustly associated with activations of the primary somatosensory cortex (SI). While an involvement of sensorimotor cortices during action observation has been demonstrated in a recent study explicitly dealing with this issue (Gazzola and Keysers, 2009), other studies provide evidence that somatosensory cortical regions also respond to the sight of touch (Blakemore et al., 2005; Carlsson et al., 2000; Keysers et al., 2004). But still, the neurobiology of this phenomenon remains elusive. Given that primary or unimodal sensory cortices such as SI are driven by modality-specific thalamic input, these activations should be attributable to top-down modulation from associative areas. One interpretation for SI activation during action observation is that this region may act as a simulator of "what it could feel like to act as seen." This idea of SI as providing a proprioceptive and tactile matching of seen actions has recently been advanced (Gazzola and Keysers, 2009; Keysers and Gazzola, 2009), saying that an action needs to be mapped onto one's own sensorimotor system to fully understand the motor components of the observed action. It could be speculated that this simulatory processes in SI might be coordinated by the ventral premotor cortex (BA 44 and adjacent BA 6) which has been assumed to be responsible for forward modelling processes, especially during imitation experiments (Molnar-Szakacs et al., 2005).

### *Neural correlates of action observation*

The action observation network, as delineated by the present meta-analysis of 104 functional neuroimaging experiments, spanned both hemispheres in a largely symmetrical manner, consisting of frontal, parietal, and posterior temporal areas as assumed previously (e.g., Culham and Valyear, 2006; Fadiga et al., 2005; Lui et al., 2008; Rizzolatti and Craighero, 2004). The involvement of frontal premotor, parietal, and extrastriate visual areas within this network was also further supported by transcranial magnetic stimulation (TMS) studies. It has been shown that transient inactivation ("virtual lesions") over these areas may result in an impaired action observation ability (for review, e.g., Fadiga and Craighero, 2004), e.g., for the discrimination of biomechanically possible actions (Candidi et al., 2008) or for the correct rearrangement of a sequence of actions (Gangitano et al., 2008).

A main question of our analysis regarding the organization of this network relates to the effect of possible confounds such as effectors, use of an object, or instructions given to the subject.

Different locations of the activations when observing actions performed by different effectors raised the question of a possible somatotopic organization within the involved areas. Buccino et al. (2004b) reported a somatotopy within the fronto-parietal part of the observation network, with observation of mouth movements activating most ventral parts (BA 44 and rostral IPL, respectively), observation of foot actions more dorsal parts, and observation of hand actions in between. With focus on the lateral premotor cortex,

similar findings were reported by Sakreida et al. (2005) as well as Wheaton et al. (2004). Besides these findings on visual action processing, Gazzola et al. (2006) found a comparable somatotopical arrangement of activations in the premotor cortex for the processing of action sounds, indicating a topic arrangement of concepts rather than sensory representations. In contrast, a recent meta-analysis on action observation by Morin and Grèzes (2008) did not find a clear somatotopical arrangement of activations within the lateral premotor cortex. By comparing MNI coordinates and counting the number of hits in the macroanatomically defined lateral premotor cortex and BA 44 for different effectors, they found association of activations within BA 44 slightly more often for observation of whole body and leg movements than for observation of mouth or finger movements. In contrast, the meta-analysis by Van Overwalle and Baetens (2009) did report a somatotopic arrangement comparable to that found by Buccino et al. (2004b) and confirmed in the present, more extended analysis.

Our meta-analysis on action observation revealed a bilateral network with pronounced involvement of the lateral premotor and parietal cortex, which was confirmed to be largely independent of the effector by subanalyses on observation of hand actions, right hand actions, and non-hand actions. Contrasting observation of hand and non-hand actions, however, revealed a notable difference with regard to possible somatotopy: whereas observation of non-hand (i.e., whole body, face, and leg) actions were more associated with activation in BA 44, observation of hand actions was more consistently associated with activations in a more dorsal part of premotor cortex (BA 6). For the parietal lobe, our meta-analysis did not provide such a possible somatotopical arrangement: whereas observation of hand actions was consistently associated with activations within parietal cortex, the observation of non-hand actions was not. The difference to the results of Morin and Grèzes (2008) might be caused by the difference in sample size, which was considerably larger in our study, or the applied method. Nevertheless, it must be pointed out that meta-analyses may not be ideally suited to investigate somatotopy since pooling of data from very different studies could diminish or even delete such effects (Morin and Grèzes, 2008), especially when somatotopic organization is not very pronounced, as in the parietal cortex (e.g., Buccino et al., 2004b; Rizzolatti and Arbib, 1998).

Another potential influencing factor for the organization of the action observation brain network is the involvement of an object within the observed action. Separating the experiments on observation of hand actions into object-related and non-object-related ones revealed a major difference: whereas activation within the temporo-occipital cortex (pMTG, V5) was consistently found within both subanalyses, activation within the fronto-parietal part of the observation network was mainly driven by observation of object-related actions.

It has been proposed that activation in these regions reflects visually guided feedback control of an action (e.g., Shmuelof and Zohary, 2007). This hypothesis, however, was mainly inferred from imitation or grasping studies. The involvement of the SPL and adjacent IPS in somatosensory and visuomotor integration, reaching movements in particular, as well as object recognition has frequently been demonstrated in neuroimaging studies (e.g., Battaglia-Mayer and Caminiti, 2002; Grèzes and Decety, 2001; Hahn et al., 2006; Pellijeff et al., 2006; Rizzolatti and Matelli, 2003, Buccino et al., 2001). Moreover, it is also supported by lesion studies of patients suffering from optic ataxia, a syndrome with deficits in the online control of visually guided actions (e.g., Glover 2003). It was assumed that these superior and adjacent intraparietal areas form a human parietal reach region (e.g., Connolly et al., 2003), referring to the comparable region in macaques (for review, e.g., Grefkes and Fink, 2005). Other authors, however, reported the parietal cortex active also for the observation of non-object-related actions (e.g., Montgomery et al., 2007). These discrepant findings indicate that there apparently is no strict and exclusive neurophysiological distinction between object and non-object-related actions. Rather, the type of the observed movement and/or its spatio-temporal properties may drive neurons in some grasp-related areas.

For the lateral premotor cortex additional strong association with actions aiming at a certain target have been found. This was also interpreted as providing additional information to the visuomotor integration process required for object-related actions (for review, e.g., Hoshi and Tanji, 2007). This correlation was supported by a recent meta-analysis on the involvement of the premotor cortex in different types of action observation (Morin and Grèzes, 2008), which revealed a less consistent activation within premotor areas during non-object-related actions. Buccino et al. (2004b), however, reported that observation of object- as well as non-object-related actions activates lateral premotor areas to a comparable degree.

The data of our meta-analysis on 104 individual experiments also provide evidence that activation in the fronto-parietal part of the action observation network may not only be related to the observation of an action per se but also particularly involved in the (implicit) processing of object features and their integration within the observed motor act. For the parietal part of the network, this is in line with the concept of a human parietal reach region. For the frontal part, a stronger association with object- and goal-directed actions was assumed when considering one of these areas as a possible human homologue of macaque area F5 since macaque mirror neurons more strongly responded to such actions as compared to non-goal- and non-object-related actions (e.g., Morin and Grèzes, 2008). Our meta-analysis results support this notion, providing a further aspect for future research on such possible homologies between humans and macaques (Morin and Grèzes 2008; Nelissen et al., 2006).

For this frontal part of the network, another notable involvement was found: this part of the cortex, together with the temporo-occipital visual areas, was constantly involved when passively observing a movement, but also when intending to imitate the observed movement. Furthermore, the primary motor cortex was consistently activated during active observation. In an early study, Grèzes et al. (1999) studied a possible differentiation between active and passive observation. They also found increasing activity within premotor cortex and on the precentral gyrus (presumably primary motor cortex), but also in inferior and superior parietal cortices, which was interpreted as reflecting the information processes needed for subsequent action. The results of the present meta-analysis did not show any involvement of the parietal cortex. But the samples of active and passive observation experiments considerably differed in sample size. Thus, even with the meta-analysis algorithm covering for such differences, such larger difference could still have introduced potential bias to the present analysis. This could have led to detection failure of parietal activations during active observation since only 8 experiments could have been involved in this analysis. Thus, the present meta-analysis provides first hints that especially primary and premotor areas might consistently be involved in active observation, whereas involvement of the parietal cortex could not finally be resolved.

Another consistently activated region during action observation was the dorso-lateral premotor cortex (dPMC; BA 6). Activation of this region was also found consistently in imitation experiments, but the exact location differed between the observation and imitation sample, leading to no common activation being detected in the conjunction analysis.

Summarizing previous reports, recent reviews suggested that the dPMC is involved in learning appropriate motor responses based on arbitrary cues (Chouinard and Paus, 2006), and thus, motor planning and preparation (Hoshi and Tanji, 2004). Furthermore, it was proposed that the dPMC integrates different pieces of sensorimotor information to formulate the appropriate motor program (Hoshi and Tanji, 2007). Given this current knowledge on the dPMC, we would

assume that within the action observation and action imitation networks, the dPMC might provide the composition of the appropriate motor program during movement preparation. Such a step should be required during action observation particularly to understand the observed action (e.g., Grafton and Hamilton, 2007), and certainly, for the realization of the observed action by imitation.

*Neural correlates of action imitation*

The action imitation network as revealed by the present meta-analysis recruited frontal, parietal, and temporo-occipital areas as previously assumed in qualitative reviews (e.g., Brass and Heyes, 2005; Heyes, 2001; Iacoboni, 2005, 2009; Turella et al., 2009a,b).

One issue of controversial discussion is a possible lateralization within activations of the action imitation network since previous studies have provided conflicting evidence on this issue. Since imitation is one form of higher-order motor processing, it could be assumed that it recruits a bilateral brain network rather than showing a hemispheric lateralisation (e.g., Iacoboni and Dapretto, 2006). Support for this assumption is provided by functional (e.g., Aziz-Zadeh et al., 2006a; Molnar-Szakacs et al., 2005) and virtual lesion studies (e.g., Aziz-Zadeh et al., 2002; Heiser et al., 2003), arguing in favour of a bilateral organization of an imitation network, in particular for frontal premotor areas.

Predominant right hemispheric activations during imitation have also been reported, e.g., within right occipito-temporal junction (Binkofski et al., 2000; Iacoboni et al., 1999, 2001), even disregarding the used hand (Aziz-Zadeh et al., 2006a), or in temporal and frontal areas for right hand movements (Biermann-Ruben et al., 2008) as well as imitation of emotional faces Carr et al., 2003).

Other studies, however, reported a dominance of left hemispheric areas during imitation tasks, which was interpreted in reference to the lateralisation of language functions (e.g., Aziz-Zadeh et al., 2004; Rizzolatti and Arbib, 1998; Iacoboni et al., 2005). Moreover, Goldenberg and Karnath (2006) argued in favour of a left-lateralisation of imitation-related processes based on lesion studies.

The quantitative results of the present meta-analysis argue in favour of a bilateral activation pattern for action imitation. Most of the included imitation experiments involved the imitation of hand movements with either the right or an unspecified hand (29 out of 35). Since action imitation contains a major component of motor execution, it could have been assumed that this imbalance would result in a dominance of left hemispheric activations, for frontal motor areas in particular. Instead, activations within these areas were evenly found in both hemispheres. Our data are thus in line with the idea of imitation being a higher-order motor process supported by a bilateral network as assumed by Iacoboni and Dapretto (2006).

Within this context, one idiosyncrasy of the imitation network could be noted: only the subanalysis 'imitation of right hand actions' revealed consistent activation within the right pMTG while imitation in general and imitation of hand actions did not. The importance of the right pMTG/STS for imitation processes was first pointed to by Iacoboni et al. (2001), based on an imitation study on right hand actions. In this study, activation of the pMTG for imitation was even stronger than the pure observation of the respective action.

Furthermore, it has to be noted that imitation studies included in the present meta-analysis involved online ($n=24$) as well as delayed imitation experiments ($n=11$). Comparison of these two subsets revealed largely comparable brain networks between both subsamples and compared to the imitation analysis including all experiments. Moreover, direct comparison revealed a higher consistency of activations for delayed as compared to simultaneous imitation in all of the activated brain areas. This could most likely be interpreted as resulting from a higher difficulty of the delayed imitation paradigms, thus a higher cognitive demand, as compared to the online imitation paradigms (e.g., Buccino et al., 2004a). A comparable effect is known for the imagery of action where strong activations can be found in premotor and visual areas in particular, in the absence of a visual model. The imagination of an action also requires a higher cognitive demand, thus resulting in stronger activations (e.g., Creem-Regehr and Lee, 2005; David et al., 2006; Grafton et al., 1996; Johnson-Frey et al., 2005). Thus, further investigation seems required to detect possibly subtle differences between on- and off-line performances of imitative behaviour.

*Reference to recent meta-analyses*

Two recent smaller meta-analyses (Molenberghs et al., 2009; Van Overwalle and Baetens, 2009) also reported a largely bilateral activation pattern for imitation tasks. Both these meta-analyses, however, used a region of interest (ROI)-based approach and assessed only activations which fell within predefined regions of the lateral premotor and parietal (Molenberghs et al., 2009) and posterior temporal cortex (Van Overwalle and Baetens, 2009). The definition of these ROIs was based either on estimates of the location of anatomical areas using the Talairach atlas (Molenberghs et al., 2009) or on manually delineated ones based on previous knowledge from the literature (Van Overwalle and Baetens, 2009) which could have confounded the results. Since the delineation of cortical areas should only reliably be possible by means of cytoarchitectonic investigation (not by means of macroanatomical anatomy; Amunts et al., 2007; Zilles et al., 2002), the areal definition within these previous studies might potentially introduce bias towards a misinterpretation of areal boundaries. Our meta-analysis used a different approach, assessing the action imitation network as a whole, without any a priori assumptions or focus on ROIs.

Since, in general, our findings on the action imitation network are well in line with those of previous meta-analyses as discussed above, the present meta-analysis could confirm and amend the findings of previous smaller analyses using an unbiased quantitative algorithm to synthesise results from a larger sample of primary studies.

One major difference to the analysis of Molenberghs et al. (2009) relates to the involvement of BA 44 within the action imitation network which is controversially discussed in the literature (e.g., Brass and Heyes 2005; Iacoboni 2005). The difference between our and Molenberghs' result might on the one hand be due to a methodological difference. Since we used the revised version of the ALE algorithm (Eickhoff et al., 2009), potential drawbacks of previous approaches which were used by Molenberghs et al., could be avoided. On the other hand, activation within BA 44 might have failed reaching significance in their analysis, especially considering the fact that the respective activation is located at the very caudal part of BA 44 (as stated above). This fact might have resulted in a failure of detection in an ROI-based approach as performed by Molenberghs. Furthermore, we were able to include a larger amount of imitation experiments within our analysis. For the ROI within BA 44 in Molenberghs' analysis, an even smaller amount of activations was found since several studies did not seem to report respective activation foci within their predefined ROI. This small number of activation foci provides difficulties for the interpretation of their negative result for BA 44. The larger sample of studies within our analysis increased the power of the ALE analysis. By objectively analysing reported activations without any preallocation to a certain ROI, our analysis was able to find activation within BA 44, with a major focus in its most caudal aspect. This provides further evidence for the role of BA 44 in imitation as stated in the section about the areas involved in both networks.

## Conclusions

In the present quantitative meta-analysis of neuroimaging data, we identified the cortical regions that are consistently implicated in the human observation and imitation networks. Hereby, the findings

of 139 individual experiments could, for the first time, objectively be generalized in an unbiased fashion.

It was shown that action observation and imitation are sustained by a bilateral network spanning fusiform, posterior temporal, parietal, and premotor areas including BA 44. These activation patterns are largely independent from possible confounds, such as effector, involvement of an object, or instructions given to the subjects. There was, however, evidence for a somatotopical organization of activations within the lateral premotor cortex (cf., Buccino et al., 2001) as well as for a stronger association of fronto-parietal areas with observation of object- as compared to non-object-related actions. Moreover, we found a three-way differentiation within Broca's region. The caudo-dorsal part of BA 44 is involved in both action observation and imitation; a more rostro-dorsal aspect within BA 45 was more consistently activated by observation tasks and a more caudo-ventral part of BA 44 was primarily involved in the imitation network.

Thus, the current meta-analysis on action observation and imitation provides objective evidence for common neural correlates of these networks across different experiments. Furthermore, evidence on putative homologies between humans and macaques was provided by the observation that human inferior area PFt showed most consistent activation across all analyses carried out in the present meta-analysis and hence seems to match the functional properties of primate area PF.

## Acknowledgments

This Human Brain Project/Neuroinformatics Research was funded by the National Institute of Biomedical Imaging and Bioengineering, the National Institute of Neurological Disorders and Stroke and the National Institute of Mental Health. Further funding was granted by the Human Brain Project (R01-MH074457-01A1; S.B.E., A.R.L.), the Initiative and Networking Fund of the Helmholtz Association within the Helmholtz Alliance on Systems Biology (Human Brain Model; K.Z., S.B.E.), and the Helmholtz Alliance for Mental Health in an Aging Society (HelMA; K.Z.).

## References

Adamovich, S.V., August, K., Merians, A., Tunik, E., 2009. A virtual reality-based system integrated with fMRI to study neural mechanisms of action observation–execution: a proof of concept study. Restor. Neurol. Neurosci. 27, 209–223.

Agnew, Z., Wise, R.J.S., 2008. Separate areas for mirror responses and agency within the parietal operculum. J. Neurosci. 28 (47), 12268–12273.

Amunts, K., Schleicher, A., Bürgel, U., Mohlberg, H., Uylings, H.B.M., Zilles, K., 1999. Broca's region revisited: cytoarchitecture and intersubject variability. J. Comp. Neurol. 41 (2), 319–341.

Amunts, K., Schleicher, A., Zilles, K., 2007. Cytoarchitecture of the cerebral cortex—more than localization. NeuroImage 37 (4), 1061–1065.

Aziz-Zadeh, L., Maeda, F., Zaidel, E., Mazziotta, J., Iacoboni, M., 2002. Lateralization in motor facilitation during action observation: a TMS study. Exp. Brain Res. 144, 127–131.

Aziz-Zadeh, L., Iacoboni, M., Zaidel, E., Wilson, S., Mazziotta, J., 2004. Left hemisphere motor facilitation in response to manual action sounds. Eur. J. Neurosci. 19, 2609–2612.

Aziz-Zadeh, L., Koski, L., Zaidel, E., Mazziotta, J., Iacoboni, M., 2006a. Lateralization of the human mirror neuron system. J. Neurosci. 26 (11), 2964–2970.

Aziz-Zadeh, L., Wilson, S.M., Rizzolatti, G., Iacoboni, M., 2006b. Congruent embodied representations for visually presented actions and linguistic phrases describing actions. Curr. Biol. 16, 1818–1823.

Bandura, A., Wood, R., 1989. Human agency in social cognitive theory. Am. Psychol. 44 (9), 1175–1184.

Bargh, J.A., Chen, M., Burrows, L., 1996. Automaticity of social behaviour: direct effects of trait construct and stereotype-activation on action. J. Pers. Soc. Psychol. 71 (2), 230–244.

Battaglia-Mayer, A., Caminiti, R., 2002. Optic ataxia as a result of the breakdown of the global tuning fields of parietal neurones. Brain 125, 225–237.

Baumgaertner, A., Buccino, G., Lange, R., McNamara, A., Binkofski, F., 2007. Eur. J. Neurosci. 25, 881–889.

Bidet-Caulet, A., Voisin, J., Bertrand, O., Fonlupt, P., 2005. Listening to a walking human activates the temporal biological motion area. NeuroImage 28, 132–139.

Biermann-Ruben, K., Kessler, K., Jonas, M., Siebner, H.R., Bäumer, T., Münchau, A., Schnitzler, A., 2008. Right hemisphere contributions to imitation tasks. Eur. J. Neurosci. 27, 1843–1855.

Binkofski, F., Buccino, G., Stephan, K.M., Rizzolatti, G., Seitz, R.J., Freund, H.J., 1999. A parieto-premotor network for object manipulation: evidence from neuroimaging. Exp. Brain Res. 128, 210–213.

Binkofski, F., Amunts, K., Stephan, K.M., Posse, S., Schormann, T., Freund, H.J., Zilles, K., Seitz, R.J., 2000. Broca's region subserves imagery of motion: a combined cytoarchitectonic and fMRI study. Hum. Brain Mapp. 11, 273–285.

Blakemore, S.J., Bristow, D., Bird, G., Frith, C., Ward, J., 2005. Somatosensory activations during the observation of touch and a case of vision–touch synaesthesia. Brain 128, 1571–1583.

Brass, M., Heyes, C., 2005. Imitation: is cognitive neuroscience solving the correspondence problem? Trends Cogn. Sci. 9 (10), 489–495.

Buccino, G., Binkofski, F., Fink, G.R., Fadiga, L., Fogassi, L., Gallese, V., Seitz, R.J., Zilles, K., Rizzolatti, G., Freund, H.J., 2001. Action observation activates premotor and parietal areas in a somatotopic manner: an fMRI study. Eur. J. Neurosci. 13, 400–404.

Buccino, G., Vogt, S., Ritzl, A., Fink, G.R., Zilles, K., Freund, H.J., Rizzolatti, G., 2004a. Neural circuits underlying imitation learning of hand actions: an event-related fMRI study. Neuron 42, 323–334.

Buccino, G., Binkofski, F., Riggio, L., 2004b. The mirror neuron system and action recognition. Brain Lang. 89, 370–376.

Calvert, G.A., Campbell, R., 2003. Reading speech from still and moving faces: the neural substrates of visible speech. J. Cogn. Neurosci. 15 (1), 57–70.

Calvo-Merino, B., Glaser, D.E., Grèzes, J., Passingham, R.E., Haggard, P., 2005. Action observation and acquired motor skills: an fMRI study with expert dancers. Cereb. Cortex 15, 1243–1249.

Calvo-Merino, B., Grèzes, J., Glaser, D.E., Passingham, R.E., Haggard, P., 2006. Seeing or doing? Influence of visual and motor familiarity in action observation. Curr. Biol. 16, 1905–1910.

Candidi, M., Urgesi, C., Ionta, S., Aglioti, S., 2008. Virtual lesion of ventral premotor cortex impairs visual perception of biomechanically possible but not impossible actions. Soc. Neurosci. 3, 388–400.

Carlsson, K., Petrovic, P., Skare, S., Petersson, K.M., Ingvar, M., 2000. Tickling expectations: neural processing in anticipation of a sensory stimulus. J. Cogn. Neurosci. 12, 691–703.

Carr, L., Iacoboni, M., Dubeau, M.C., Mazziotta, J.C., Lenzi, G.L., 2003. Neural mechanisms of empathy in humans: a relay from neural systems for imitation to limbic areas. Proc. Natl. Acad. Sci. U.S.A. 100 (9), 5497–5502.

Caspers, S., Geyer, S., Schleicher, A., Mohlberg, H., Amunts, K., Zilles, K., 2006. The human inferior parietal lobule: cytoarchitectonic parcellation and interindividual variability. NeuroImage 33 (2), 430–448.

Caspers, S., Eickhoff, S.B., Geyer, S., Scheperjans, F., Mohlberg, H., Zilles, K., Amunts, K., 2008. The human inferior parietal lobule in stereotaxic space. Brain Struct. Funct. 212 (6), 481–495.

Chaminade, T., Meltzoff, A.N., Decety, J., 2002. Does the end justify the means? A PET exploration of the mechanisms involved in human imitation. NeuroImage 15, 318–328.

Chaminade, T., Meltzoff, A.N., Decety, J., 2005. An fMRI study of imitation: action representation and body schema. Neuropsychologia 43, 115–127.

Cheng, Y., Meltzoff, A.N., Decety, J., 2007. Motivation modulates the activity of the human mirror-neuron system. Cereb. Cortex 17, 1979–1986.

Choi, H.J., Zilles, K., Mohlberg, H., Schleicher, A., Fink, G.R., Armstrong, E., Amunts, K., 2006. Cytoarchitectonic identification and probabilistic mapping of two distinct areas within the anterior ventral bank of the human intraparietal sulcus. J. Comp. Neurol. 495 (1), 53–69.

Chong, T.T., Williams, M.A., Cunnington, R., Mattingley, J.B., 2008. Selective attention modulates inferior frontal gyrus activity during action observation. NeuroImage 40, 298–307.

Chouinard, P.A., Paus, T., 2006. The primary motor and premotor areas of the human cerebral cortex. Neuroscientist 12 (2), 143–152.

Connolly, J.D., Andersen, R.A., Goodale, M.A., 2003. FMRI evidence for a 'parietal reach region' in the human brain. Exp. Brain Res. 153, 140–145.

Costantini, M., Galati, G., Ferretti, A., Caulo, M., Tartaro, A., Romani, G.L., Aglioti, S.M., 2005. Neural systems underlying observation of humanly impossible movements: an fMRI study. Cereb. Cortex 15, 1761–1767.

Creem-Regehr, S.H., Lee, J.N., 2005. Neural representations of graspable objects: are tools special? Cogn. Brain Res. 22, 457–469.

Cross, E.S., Hamilton, A.F., Grafton, S.T., 2006. Building a motor simulation de novo: observation of dance by dancers. NeuroImage 31, 1257–1267.

Cross, E.S., Kraemer, D.J.M., Hamilton, A.F., Kelley, W.M., Grafton, S.T., 2009. Sensitivity of the action observation network to physical and observational learning. Cereb. Cortex 19 (2), 315–326.

Culham, J.C., Valyear, K.F., 2006. Human parietal cortex in action. Curr. Opin. Neurobiol. 16, 205–212.

Cunnington, R., Windischberger, C., Robinson, S., Moser, E., 2006. The selection of intended actions and the observation of others' actions: a time-resolved fMRI study. NeuroImage 29, 1294–1302.

David, N., Bewernick, B.H., Cohen, M.X., Newen, A., Lux, S., Fink, G.R., Shah, N.J., Vogeley, K., 2006. Neural representations of self versus other: visual–spatial perspective taking and agency in a virtual ball-tossing game. J. Cogn. Neurosci. 18 (6), 898–910.

Decety, J., Chaminade, T., Grèzes, J., Meltzoff, A.N., 2002. A PET exploration of the neural mechanisms involved in reciprocal imitation. NeuroImage 15, 265–272.

Dien, J., 2009. A tale of two recognition systems: implications of the fusiform face area and visual word form area for lateralized object recognition models. Neuropsychologia 47 (1), 1–16.

Dinstein, I., Hasson, U., Rubin, N., Heeger, D.J., 2007. Brain areas selective for both observed and executed movements. J. Neurophysiol. 98, 1415–1427.

Dinstein, I., Thomas, C., Behrmann, M., Heeger, D.J., 2008. A mirror up to nature. Curr. Biol. 18 (1), R13–R18 Erratum in: Curr. Biol. 18 (3), 233.
Downing, P.E., Peelen, M.V., Wiggett, A.J., Tew, B.D., 2006. The role of the extrastriate body area in action perception. Soc. Neurosci. 1 (1), 52–62.
Eickhoff, S.B., Stephan, K.E., Mohlberg, H., Grefkes, C., Fink, G.R., Amunts, K., Zilles, K., 2005. A new SPM toolbox for combining probabilistic cytoarchitectonic maps and functional imaging data. NeuroImage 25, 1325–1335.
Eickhoff, S.B., Schleicher, A., Zilles, K., Amunts, K., 2006a. The human parietal operculum. I. Cytoarchitectonic mapping of subdivisions. Cereb. Cortex 16 (2), 254–267.
Eickhoff, S.B., Amunts, K., Mohlberg, H., Zilles, K., 2006b. The human parietal operculum. II. Stereotaxic maps and correlation with functional imaging results. Cereb. Cortex 16 (2), 268–279.
Eickhoff, S.B., Paus, T., Caspers, S., Grosbras, M.H., Evans, A.C., Zilles, K., Amunts, K., 2007. Assignment of functional activations to probabilistic cytoarchitectonic areas revisited. NeuroImage 36 (3), 511–521.
Eickhoff, S.B., Laird, A.R., Grefkes, C., Wang, L.E., Zilles, K., Fox, P.T., 2009. Coordinate-based ALE meta-analysis of neuroimaging data: a random-effects approach based on empirical estimates of spatial uncertainty. Hum. Brain Mapp. 30 (9), 2907–2926.
Engel, A., Burke, M., Fiehler, K., Bien, S., Rösler, F., 2008. How moving objects become animated: the human mirror neuron system assimilates non-biological movement patterns. Soc. Neurosci. 3 (3-4), 368–387.
Evans, A.C., Kamber, M., Collins, D.L., MacDonald, D., 1994. An fMRI based probabilistic atlas of neuroanatomy. In: Shorvon, S, Fish, D, Andermann, F, Bydder, GM (Eds.), Magnetic Resonance Scanning and Epilepsy, pp. 263–274.
Fabbri-Destro, M., Rizzolatti, G., 2008. Mirror neurons and mirror systems in monkeys and humans. Physiology 23, 171–179.
Fadiga, L., Craighero, L., 2004. Electrophysiology of action representation. J. Clin. Neurophysiol. 21 (3), 157–169.
Fadiga, L., Craighero, L., Olivier, E., 2005. Human motor cortex excitability during the perception of others' action. Curr. Opin. Neurobiol. 15, 213–218.
Fazio, P., Cantagallo, A., Craighero, L., D'Ausilio, A., Roy, A.C., Pozzo, T., Calzolari, F., Granieri, E., Fadiga, L., 2009. Encoding of human action in Broca's area. Brain 132, 1980–1988.
Filimon, F., Nelson, J.D., Hagler, D.J., Sereno, M.I., 2007. Human cortical representations for reaching: mirror neurons for execution, observation, and imagery. NeuroImage 37, 1315–1328.
Fogassi, L., Ferrari, P.F., Gesierich, B., Rozzi, S., Chersi, F., Rizzolatti, G., 2005. Parietal lobe: from action organization to intention understanding. Science 308, 662–667.
Fox, P.T., Lancaster, J.L., 2002. Opinion: mapping context and content: the BrainMap model. Nat. Rev., Neurosci. 3 (4), 319–321.
Frey, S.H., Gerry, V.E., 2006. Modulation of neural activity during observational learning of actions and their sequential orders. J. Neurosci. 26 (51), 13194–13201.
Galati, G., Committeri, G., Spitoni, G., Aprile, T., Di Russo, F., Pitzalis, S., Pizzamiglio, L., 2008. A selective representation of the meaning of actions in the auditory mirror system. NeuroImage 40, 1274–1286.
Gallese, V., Fadiga, L., Fogassi, L., Rizzolatti, G., 1996. Action recognition in the premotor cortex. Brain 119, 593–609.
Gangitano, M., Mottaghy, F.M., Pascual-Leone, A., 2008. Release of premotor activity after repetitive transcranial magnetic stimulation of prefrontal cortex. Soc. Neurosci. 3, 289–302.
Gazzola, V., Keysers, C., 2009. The observation and execution of actions share motor and somatosensory voxels in all tested subjects: single-subject analyses of unsmoothed fMRI data. Cereb. Cortex 19 (6), 1239–1255.
Gazzola, V., Aziz-Zadeh, L., Keysers, C., 2006. Empathy and the somatotopic auditory mirror system in humans. Curr. Biol. 16, 1824–1829.
Gazzola, V., Rizzolatti, G., Wicker, B., Keysers, C., 2007. The anthropomorphic brain: the mirror neuron system responds to human and robotic actions. NeuroImage 35, 1674–1684.
Gentilucci, M., Bertolani, L., Benuzzi, F., Negrotti, A., Pavesi, G., Gangitano, M., 2000. Impaired control of an action after supplementary motor area lesion: a case study. Neuropsychologia 38, 1398–1404.
German, T.P., Niehaus, J.L., Roarty, M.P., Giesbrecht, B., Miller, M.B., 2004. Neural correlates of detecting pretense: automatic engagement of the intentional stance under covert conditions. J. Cogn. Neurosci. 16 (10), 1805–1817.
Geyer, S., 2004. The microstructural border between the motor and the cognitive domain in the human cerebral cortex. Advances in Anatomy Embryology and Cell Biology, vol. 174. Springer, Berlin.
Geyer, S., Ledberg, A., Schleicher, A., Kinomura, S., Schormann, T., Bürgel, U., Klingberg, T., Larsson, J., Zilles, K., Roland, P.E., 1996. Two different areas within the primary motor cortex of man. Nature 382 (6594), 805–807.
Geyer, S., Schleicher, A., Zilles, K., 1999. Areas 3a, 3b, and 1 of human primary somatosensory cortex: 1. Microstructural organization and interindividual variability. NeuroImage 10, 63–83.
Geyer, S., Schormann, T., Mohlberg, H., Zilles, K., 2000. Areas 3a, 3b, and 1 of human primary somatosensory cortex: Part 2. Spatial normalization to standard anatomical space. NeuroImage 11, 684–696.
Glover, S., 2003. Optic ataxia as a deficit specific to the on-line control of actions. Neurosci. Biobehav. Rev. 27 (5), 447–456.
Goldenberg, G., Karnath, H.O., 2006. The neural basis of imitation is body part specific. J. Neurosci. 26, 1133–1137.
Grafton, S.T., Hamilton, A.F., 2007. Evidence for a distributed hierarchy of action representation in the brain. Hum. Movement Sci. 590–616.
Grafton, S.T., Arbib, M.A., Fadiga, L., Rizzolatti, G., 1996. Localization of grasp representations in humans by PET: 2. Observation compared with imagination. Exp. Brain Res. 112, 103–111.
Grefkes, C., Fink, G.R., 2005. The functional organization of the intraparietal sulcus in humans and monkeys. J. Anat. 207 (1), 3–17.
Grefkes, C., Geyer, S., Schormann, T., Roland, P., Zilles, K., 2001. Human somatosensory area 2: observer-independent cytoarchitectonic mapping, interindividual variability, and population map. NeuroImage 14, 617–631.
Grèzes, J., Decety, J., 2001. Functional anatomy of execution, mental simulation, observation, and verb generation of actions: a meta-analysis. Hum. Brain Mapp. 12, 1–19.
Grèzes, J., Costes, N., Decety, J., 1999. The effects of learning and intention on the neural network involved in the perception of meaningless actions. Brain 122, 1875–1887.
Grèzes, J., Armony, J.L., Rowe, J., Passingham, R.E., 2003. Activations related to "mirror" and "canonical" neurones in the human brain: an fMRI study. NeuroImage 18, 928–937.
Grèzes, J., Frith, C.D., Passingham, R.E., 2004. Inferring false beliefs from the actions of oneself and others: an fMRI study. NeuroImage 21, 744–750.
Grosbras, M.H., Paus, T., 2006. Brain networks involved in viewing angry hands or faces. Cereb. Cortex 16, 1087–1096.
Hahn, B., Ross, T.J., Stein, E.A., 2006. Neuroanatomical dissociation between bottom-up and top-down processes of visuospatial selective attention. NeuroImage 32, 842–853.
Hamilton, A.F., Grafton, S.T., 2008. Action outcomes are represented in human inferior frontoparietal cortex. Cereb. Cortex 18, 1160–1168.
Hamzei, F., Rijntjes, M., Dettmers, C., Glauche, V., Weiller, C., Büchel, C., 2003. The human action recognition system and its relationship to Broca's area: an fMRI study. NeuroImage 19, 637–644.
Haslinger, B., Erhard, P., Altenmüller, E., Schroeder, U., Boecker, H., Ceballos-Baumann, A.O., 2005. Transmodal sensorimotor networks during action observation in professional pianists. J. Cogn. Neurosci. 17 (2), 282–293.
Hazeltine, E., Grafton, S.T., Ivry, D., 1997. Attention and stimulus characteristics determine the locus of motor-sequence encoding. A PET study. Brain 120, 123–140.
Heiser, M., Iacoboni, M., Madea, F., Marcus, J., Mazziotta, J.C., 2003. The essential role of Broca's area in imitation. Eur. J. Neurosci. 17 (5), 1123–1128.
Hermsdörfer, J., Goldenberg, G., Wachsmuth, C., Conrad, B., Ceballos-Baumann, A.O., Bartenstein, P., Schwaiger, M., Boecker, H., 2001. Cortical correlates of gesture processing: clues to the cerebral mechanisms underlying apraxia during the imitation of meaningless gestures. NeuroImage 14, 149–161.
Heyes, C., 2001. Causes and consequences of imitation. Trends Cogn. Sci. 5 (6), 253–261.
Hoshi, E., Tanji, J., 2004. Functional specialization in dorsal and ventral premotor areas. Prog. Brain Res. 143, 507–511.
Hoshi, E., Tanji, J., 2007. Distinctions between dorsal and ventral premotor areas: anatomical connectivity and functional properties. Curr. Opin. Neurobiol. 17 (2), 234–242.
Iacoboni, M., 2005. Neural mechanisms of imitation. Curr. Opin. Neurobiol. 15, 632–637.
Iacoboni, M., 2009. Imitation, empathy, and mirror neurons. Annu. Rev. Psychol. 60, 653–670.
Iacoboni, M., Dapretto, M., 2006. The mirror neuron system and the consequences of its dysfunction. Nat. Rev., Neurosci. 7, 942–951.
Iacoboni, M., Woods, R.P., Brass, M., Bekkering, H., Mazziotta, J.C., Rizzolatti, G., 1999. Cortical mechanisms of human imitation. Science 286, 2526–2528.
Iacoboni, M., Koski, L.M., Brass, M., Bekkering, H., Woods, R.P., Dubeau, M.C., Mazziotta, J.C., Rizzolatti, G., 2001. Reafferent copies of imitated actions in the right superior temporal cortex. Proc. Natl. Acad. Sci. U.S.A. 98 (24), 13995–13999.
Iacoboni, M., Lieberman, M.D., Knowlton, B.J., Molnar-Szakacs, I., Moritz, M., Throop, C.J., Fiske, A.P., 2004. Watching social interactions produces dorsomedial prefrontal and medial parietal BOLD fMRI signal increases compared to a resting baseline. NeuroImage 21, 1167–1173.
Iacoboni, M., Molnar-Szakacs, I., Gallese, V., Buccino, G., Mazziotta, J.C., Rizzolatti, G., 2005. Grasping the intentions of others with one's own mirror neuron system. PLoS Biol. 3 (3), e79.
Iseki, K., Hanakawa, T., Shinozaki, J., Nankaku, M., Fukuyama, H., 2008. Neural mechanisms involved in mental imagery and observation of gait. NeuroImage 41 (3), 1021–1031.
Jackson, P.L., Meltzoff, A.N., Decety, J., 2006. Neural circuits involved in imitation and perspective-taking. NeuroImage 31, 429–439.
Jakobs, O., Wang, L.E., Dafotakis, M., Grefkes, C., Zilles, K., Eickhoff, S.B., 2009. Effects of timing and movement uncertainty implicate the temporo-parietal junction in the prediction of forthcoming motor actions. NeuroImage 47 (2), 667–677.
Johnson-Frey, S.H., Maloof, F.R., Newman-Norlund, R., Farrer, C., Inati, S., Grafton, S.T., 2003. Actions or hand–object interactions? Human inferior frontal cortex and action observation. Neuron 39, 1053–1058.
Johnson-Frey, S.H., Newman-Norlund, R., Grafton S.T., 2005. A distributed left hemisphere network active during planning of everyday tool use skills. Cereb. Cortex 15, 681-695.
Jonas, M., Siebner, H.R., Biermann-Ruben, K., Kessler, K., Bäumer, T., Büchel, C., Schnitzler, A., Münchau, A., 2007. Do simple intransitive finger movements consistently activate frontoparietal mirror neuron areas in humans? NeuroImage 36, T44–T53.
Kitada, R., Johnsrude, I.S., Kochiyama, T., Lederman, S.J., 2009. Functional specialization and convergence in the occipito-temporal cortex supporting haptic and visual identification of human faces and body parts: an fMRI study. J. Cogn. Neurosci. 21 (10), 2027–2045.
Keysers, C., Gazzola, V., 2009. Expanding the mirror: vicarious activity for actions, emotions, and sensations. Curr. Opin. Neurobiol. 19, 666–671.
Keysers, C., Wicker, B., Gazzola, V., Anton, J.L., Fogassi, L., Gallese, V., 2004. A touching sight: SII/PV activation during the observation and experience of touch. Neuron 42, 335–346.
Kilner, J.M., Friston, K.J., Frith, C.D., 2007. Predictive coding: an account of the mirror neuron system. Cogn. Process 8 (3), 159–166.

Koechlin, E., Jubault, T., 2006. Broca's area and hierarchical organization of human behavior. Neuron 50, 963–974.
Koechlin, E., Ody, C., Kouneiher, F., 2003. The architecture of cognitive control in the human prefrontal cortex. Science 302, 1181–1185.
Koski, L., Wohlschläger, A., Bekkering, H., Woods, R.P., Dubeau, M.C., Mazziotta, J.C., Iacoboni, M., 2002. Modulation of motor and premotor activity during imitation of target-directed actions. Cereb. Cortex 12, 847–855.
Koski, L., Iacoboni, M., Dubeau, M.C., Woods, R.P., Mazziotta, J.C., 2003. Modulation of cortical activity during different imitative behaviors. J. Neurophysiol. 89, 460–471.
Krams, M., Rushworth, M.F., Deiber, M.P., Frackowiak, R.S., Passingham, R.E., 1998. The preparation, execution and suppression of copied movements in the human brain. Exp. Brain Res. 120, 386–398.
Laird, A.R., Fox, P.M., Price, C.J., Glahn, D.C., Uecker, A.M., Lancaster, J.L., Turkeltaub, P. E., Kochunov, P., Fox, P.T., 2005a. ALE meta-analysis: controlling the false discovery rate and performing statistical contrasts. Hum. Brain Mapp. 25 (1), 155–164.
Laird, A.R., Lancaster, J.L., Fox, P.T., 2005b. BrainMap: the social evolution of a human brain mapping database. Neuroinformatics 3 (1), 65–78.
Laird, A.R., Eickhoff, S.B., Kurth, F., Fox, P.M., Uecker, A.M., Turner, J.A., Robinson, J.L., Lancaster, J.L., Fox, P.T., 2009. ALE meta-analysis workflows via the BrainMap database: progress towards a probabilistic functional brain atlas. Front. Neuroinformatics 3, 23.
Lancaster, J.L., Tordesillas-Gutiérrez, D., Martinez, M., Salinas, F., Evans, A., Zilles, K., Mazziotta, J.C., Fox, P.T., 2007. Bias between MNI and Talairach coordinates analyzed using the ICBM-152 brain template. Hum. Brain Mapp. 28 (11), 1194–1205.
Leslie, K.R., Johnson-Frey, S.H., Grafton, S.T., 2004. Functional imaging of face and hand imitation: towards a motor theory of empathy. NeuroImage 21, 601–607.
Lewis, J.W., Brefczynski, J.A., Phinney, R.E., Janik, J.J., DeYoe, E.A., 2005. Distinct cortical pathways for processing tool versus animal sounds. J. Neurosci. 25 (21), 5148–5158.
Lotze, M., Heymans, U., Birbaumer, N., Veit, R., Erb, M., Flor, H., Halsband, U., 2006. Differential cerebral activation during observation of expressive gestures and motor acts. Neuropsychologia 44, 1787–1795.
Lui, F., Buccino, G., Duzzi, D., Benuzzi, F., Crisi, G., Baraldi, P., Nichelli, P., Porro, C.A., Rizzolatti, G., 2008. Neural substrates for observing and imagining non-object-directed actions. Soc. Neurosci. 3, 261–275.
Makuuchi, M., 2005. Is Broca's area crucial for imitation? Cereb. Cortex 15, 563–570.
Makuuchi, M., Kaminaga, T., Sugishita, M., 2005. Brain activation during ideomotor praxis: imitation and movements executed by verbal command. J. Neurol. Neurosurg. Psychiatry 76, 25–33.
Malikovic, A., Amunts, K., Schleicher, A., Mohlberg, H., Eickhoff, S.B., Wilms, M., Palomero-Gallagher, N., Armstrong, E., Zilles, K., 2007. Cytoarchitectonic analysis of the human extrastriate cortex in the region of V5/MT+: a probabilistic map of area hOc5. Cereb. Cortex 17 (3), 562–574.
Manthey, S., Schubotz, R.I., von Cramon, D.Y., 2003. Premotor cortex in observing erroneous action: an fMRI study. Cogn. Brain Res. 15, 296–307.
Mecklinger, A., Gruenewald, C., Besson, M., Magine, M.N., von Cramon, D.Y., 2002. Separable neuronal circuits for manipulable and non-manipulable objects in working memory. Cereb. Cortex 12, 1115–1123.
Meister, I.G., Iacoboni, M., 2007. No language-specific activation during linguistic processing of observed actions. PLoS One e891, 9.
Meltzoff, A.N., Moore, M.K., 1977. Imitation of facial and manual gestures by human neonates. Science 198 (4312), 75–78.
Menz, M.M., McNamara, A., Klemen, J., Binkofski, F., 2009. Dissociating networks of imitation. Hum. Brain Mapp 30 (10), 3339–3350.
Mita, A., Mushiake, H., Shima, K., Matsuzaka, Y., Tanji, J., 2009. Interval time coding of neurons in the presupplementary and supplementary motor areas. Nat. Neurosci. 12 (4), 502–507.
Molenberghs, P., Cunnington, R., Mattingley, J.B., 2009. Is the mirror neuron system involved in imitation? A short review and meta-analysis. Neurosci. Biobehav. Rev. 33 (7), 975–980.
Molnar-Szakacs, I., Iacoboni, M., Koski, L., Mazziotta, J.C., 2005. Functional segregation within pars opercularis of the inferior frontal gyrus: evidence from fMRI studies of imitation and action observation. Cereb. Cortex 15, 986–994.
Molnar-Szakacs, I., Kaplan, J., Greenfield, P.M., Iacoboni, M., 2006. Observing complex action sequences: the role of the fronto-parietal mirror neuron system. NeuroImage 33, 923–935.
Montgomery, K.J., Haxby, J.V., 2008. Mirror neuron system differentially activated by facial expressions and social hand gestures: a functional magnetic resonance imaging study. J. Cogn. Neurosci. 20 (10), 1866–1877.
Montgomery, K.J., Isenberg, N., Haxby, J.V., 2007. Communicative hand gestures and object-directed hand movements activated the mirror neuron system. SCAN 2, 114–122.
Morin, O., Grèzes, J., 2008. What is "mirror" in the premotor cortex? A review. Neurophysiol. Clin. 38 (3), 189–195.
Morris, J.P., Pelphrey, K.A., McCarthy, G., 2008. Perceived causality influences brain activity evoked by biological motion. Soc. Neurosci. 3 (1), 16–25.
Mouras, H., Stoléru, S., Moulier, V., Pélégrini-Issac, M., Rouxel, R., Grandjean, B., Glutron, D., Bittoun, J., 2008. Activation of mirror-neuron system by erotic video clips predicts degree of induced erection: an fMRI study. NeuroImage 42, 1142–1150.
Mühlau, M., Hermsdörfer, J., Goldenberg, G., Wohlschläger, A.M., Castrop, F., Stahl, R., Röttinger, M., Erhard, P., Haslinger, B., Ceballos-Baumann, A.O., Conrad, B., Boecker, H., 2005. Left inferior parietal dominance in gesture imitation: an fMRI study. Neuropsychologia 43, 1086–1098.
Nelissen, K., Luppino, G., Vanduffel, W., Rizzolatti, R., Orban, G.A., 2006. Observing others: multiple representations in the frontal lobe. Science 310, 332–336.
Niedenthal, P.M., Cantor, N., Kihlstrom, J.F., 1985. Prototype matching: a strategy for social decision making. J. Pers. Soc. Psychol. 48 (3), 575–584.
Pellijeff, A., Bonilha, L., Morgan, P.S., McKenzie, K., Jackson, S.R., 2006. Parietal updating of limb posture: an event-related fMRI study. Neuropsychologia 44, 2685–2690.
Pierno, A.C., Becchio, C., Wall, M.B., Smith, A.T., Turella, L., Castiello, U., 2006. When gaze turns into grasp. J. Cogn. Neurosci. 18 (12), 2130–2137.
Pierno, A.C., Tubaldi, F., Turella, L., Grossi, P., Barachino, L., Gallo, P., Castiello, U., 2009. Neurofunctional modulation of brain regions by the observation of pointing and grasping actions. Cereb. Cortex 19 (2), 367–374.
Prinz, W., 2006. What re-enactment earns us. Cortex 42 (4), 515–517.
Puce, A., Perrett, D., 2003. Electrophysiology and brain imaging of biological motion. Philos. Trans. R. Soc. Lond. B Biol. Sci. 358, 435–445.
Rizzolatti, G., 2005. The mirror neuron system and its function in humans. Anat. Embryol. 210, 419–421.
Rizzolatti, G., Arbib, M.A., 1998. Language within our grasp. Trends Neurosci. 21 (5), 188–194.
Rizzolatti, G., Craighero, L., 2004. The mirror-neuron system. Ann. Rev. Neurosci. 27, 169–192.
Rizzolatti, G., Fabbri-Destro, M., 2008. The mirror system and its role in social cognition. Curr. Opin. Neurobiol. 18, 179–184.
Rizzolatti, G., Matelli, M., 2003. Two different streams form the dorsal visual system: anatomy and functions. Exp. Brain Res. 153, 146–157.
Rizzolatti, G., Fogassi, L., Gallese, V., 2001. Neurophysiological mechanisms underlying the understanding and imitation of action. Nat. Rev., Neurosci. 2, 661–670.
Rocca, M.A., Tortorella, P., Ceccarelli, A., Falini, A., Tango, D., Scotti, G., Comi, G., Filippi, M., 2008a. The "mirror-neuron system" in MS: a 3 tesla fMRI study. Neurology 70, 255–262.
Rocca, M.A., Falini, A., Comi, G., Scotti, G., Filippi, M., 2008b. The mirror-neuron system and handedness: a "right" world? Hum. Brain Mapp. 29, 1243–1254.
Rozzi, S., Ferrari, P.F., Bonini, L., Rizzolatti, G., Fogassi, L., 2008. Functional organization of inferior parietal lobule convexity in the macaque monkey: electrophysiological characterization of motor, sensory and mirror responses and their correlation with cytoarchitectonic areas. Eur. J. Neurosci. 28 (8), 1569–1588.
Rumiati, R.I., Weiss, P.H., Tessari, A., Assmus, A., Zilles, K., Herzog, H., Fink, G.R., 2005. Common and differential neural mechanisms supporting imitation of meaningful and meaningless actions. J. Cogn. Neurosci. 17 (9), 1420–1431.
Sakreida, K., Schubotz, R.I., Wolfensteller, U., von Cramon, D.Y., 2005. Motion class dependency on observers' motor areas revealed by functional magnetic resonance imaging. J. Neurosci. 25 (6), 1335–1342.
Salimi-Khorshidi, G., Smith, S.M., Keltner, J.R., Wager, T.D., Nichols, T.E., 2009. Meta-analysis of neuroimaging data: a comparison of image-based and coordinate-based pooling of studies. NeuroImage 45 (3), 810–823.
Schaefer, M., Xu, B., Flor, H., Cohen, L.G., 2009. Effects of different viewing perspectives on somatosensory activations during observation of touch. Hum. Brain Mapp. 30, 2722–2730.
Scheperjans, F., Eickhoff, S.B., Hömke, L., Mohlberg, H., Hermann, K., Amunts, K., Zilles, K., 2008b. Probabilistic maps, morphometry, and variability of cytoarchitectonic areas in the human superior parietal cortex. Cereb. Cortex 18 (9), 2141–2157.
Scheperjans, F., Hermann, K., Eickhoff, S.B., Amunts, K., Schleicher, A., Zilles, K., 2008a. Observer-independent cytoarchitectonic mapping of the human superior parietal cortex. Cereb. Cortex 18 (4), 846–867.
Schilbach, L., Eickhoff, S.B., Mojzisch, A., Vogeley, K., 2008a. What's in a smile? Neural correlates of facial embodiment during social interaction. Soc. Neurosci. 3 (1), 37–50.
Schilbach, L, Eickhoff, S.B., Rotarska-Jagiela, A., Fink, G.R., Vogeley, K., 2008b. Minds at rest? Social cognition as the default mode of cognizing and its putative relationship to the "default system" of the brain. Conscious Cogn. 17 (2), 457–467.
Schubotz, R.I., von Cramon, D.Y., 2008. The case of pretense: observing actions and inferring goals. J. Cogn. Neurosci. 21 (4), 642–653.
Schütz-Bosbach, S., Prinz, W., 2007. Perceptual resonance: action-induced modulation of perception. Trends Cogn. Sci. 11 (8), 349–355.
Schulte-Rüther, M., Markowitsch, H.J., Fink, G.R., Piefke, M., 2007. Mirror neuron and theory of mind mechanisms involved in face-to-face interactions: a functional magnetic resonance imaging approach to empathy. J. Cogn. Neurosci. 19 (8), 1354–1372.
Seitz, R.J., Roland, P.E., 1992. Learning of sequential finger movements in man: a combined kinematic and positron emission tomography stuy. Eur. J. Neurosci. 4, 154–165.
Seymour, K., Clifford, C.W., Logothetis, N.K., Bartels, A., 2009. The coding of color, motion, and their conjunction in the human visual cortex. Curr. Biol. 19 (3), 177–183.
Shmuelof, L., Zohary, E., 2005. Dissociation between ventral and dorsal fMRI activation during object and action recognition. Neuron 47, 457–470.
Shmuelof, L., Zohary, E., 2007. Watching others' actions: mirror representation in the parietal cortex. Neuroscientist 13 (6), 667–672.
Tai, Y.F., Scherfler, C., Brooks, D.J., Sawamoto, N., Castiello, U., 2004. The human premotor cortex is 'mirror' only for biological actions. Curr. Biol. 14, 117–120.
Tanaka, S., Inui, T., 2002. Cortical involvement for action imitation of hand/arm postures versus finger configurations: an fMRI study. NeuroReport 13 (13), 1599–1602.
Tanaka, S., Inui, T., Iwaki, S., Konishi, J., Nakai, T., 2001. Neural substrates involved in imitating finger configurations: an fMRI study. NeuroReport 12 (6), 1171–1174.
Tanji, J., 1994. The supplementary motor area in the cerebral cortex. Neurosci. Res. 19 (3), 251–268.
Tankus, A., Yeshurun, Y., Flash, T., Fried, I., 2009. Encoding of speed and direction of movement in the human supplementary motor area. J. Neurosurg. 110 (6), 1304–1316.
Tettamanti, M., Buccino, G., Saccuman, M.C., Gallese, V., Danna, M., Scifo, P., Fazio, F., Rizzolatti, G., Cappa, S.F., Perani, D., 2005. Listening to action-related sentences activates fronto-parietal motor circuits. J. Cogn. Neurosci. 17 (2), 273–281.

Thompson, B., Aaen-Stockdale, C., Koski, L., Hess, R.F., 2009. A double dissociation between striate and extrastriate visual cortex for pattern motion perception revealed using rTMS. Hum Brain Mapp. 30 (10), 3115–3126.
Turella, L., Erb, M., Grodd, W., Castiello, U., 2009a. Visual features of an observed agent do not modulate human activity during action observation. NeuroImage 46, 844–853.
Turella, L., Pierno, A.C., Tubaldi, F., Castiello, U., 2009b. Mirror neurons in humans: consisting or confounding evidence? Brain Lang. 108, 10–21.
Turkeltaub, P.E., Eden, G.F., Jones, K.M., Zeffiro, T.A., 2002. Meta-analysis of the functional neuroanatomy of single-word reading: method and validation. NeuroImage 16 (3.1), 680–765.
Uddin, L.Q., Kaplan, J.T., Molnar-Szakacs, I., Zaidel, E., Iacoboni, M., 2005. Self-face recognition activates a fronto-parietal "mirror" network in the right hemisphere: an event-related fMRI study. NeuroImage 25, 926–935.
Umiltá, C., Rizzolatti, G., Anzola, G.P., Luppino, G., Porro, C., 1985. Evidence of interhemispheric transmission in laterality effects. Neuropsychologia 23 (2), 203–213.
Vaina, L.M., Solomon, J., Chowdhury, S., Sihna, P., Belliveau, J.W., 2001. Functional neuroanatomy of biological motion perception in humans. Proc. Natl. Acad. Sci. U.S.A. 98, 11659–11661.
van der Gaag, C., Minderaa, R.B., Keysers, C., 2007. Facial expressions: what the mirror neuron system can and cannot tell us. Soc. Neurosci. 2 (3-4), 179–222.
Van Overwalle, F., Baetens, K., 2009. Understanding other's actions and goals by mirror and mentalizing systems: a meta-analysis. NeuroImage 48 (3), 564-584.
Villarreal, M., Fridman, E.A., Amengual, A., Falasco, G., Gerscovich, E.R., Ulloa, E.R., Leiguarda, R.C., 2008. The neural substrate of gesture recognition. Neuropsychologia 46, 2371–2382.
Viviani, P., Terzuolo, C.A., 1973. Modeling of a simple motor task in man: intentional arrest of an ongoing movement. Kybernetik 14 (1), 35–62.
Vogt, S., Buccino, G., Wohlschläger, A.M., Canessa, N., Shah, N.J., Zilles, K., Eickhoff, S.B., Freund, H.J., Rizzolatti, G., Fink, G.R., 2007. Prefrontal involvement in imitation learning of hand actions: effects of practice and expertise. NeuroImage 37, 1371–1383.
Wheaton, K.J., Thompson, J.C., Syngeniotis, A., Abbott, D.F., Puce, A., 2004. Viewing the motion of human body parts activates different regions of premotor, temporal, and parietal cortex. NeuroImage 22, 277–288.
Willems, R.M., Özyürek, A., Hagoort, P., 2007. When language meets action: the neural integration of gesture and speech. Cereb. Cortex 17, 2322–2333.
Willems, R.M., Peelen, M.V., Hagoort, P., 2009. Cerebral lateralization of face-selective and body-selective visual areas depends on handedness. Cereb. Cortex doi:10.1093/cercor/bhp234.
Williams, J.H.G., Waiter, G.D., Gilchrist, A., Perrett, D.I., Murray, A.D., Whiten, A., 2006. Neural mechanisms of imitation and 'mirror neuron' functioning in autistic spectrum disorder. Neuropsychologia 44, 610–621.
Williams, J.H.G., Whiten, A., Waiter, G.D., Pechey, S., Perrett, D.I., 2007. Cortical and subcortical mechanisms at the core of imitation. Soc. Neurosci. 2 (1), 66–78.
Zentgraf, K., Stark, R., Reiser, M., Künzell, S., Schienle, A., Kirsch, P., Walter, B., Vaitl, D., Munzert, J., 2005. Differential activation of pre-SMA and SMA proper during action observation: effects of instructions. NeuroImage 26, 662–672.
Zilles, K., Schleicher, A., Palomero-Gallagher, N., Amunts, K., 2002. Quantitative analysis of cyto- and receptorarchitecture of the human brain, In: Toga, A.W., Mazziotta, J.C. (Eds.), Brain Mapping: The Methods, 2nd ed. Academic Press, New York, pp. 573–602.

OPEN ACCESS Freely available online

PLoS one

# Moral Concepts Set Decision Strategies to Abstract Values

**Svenja Caspers[1]*, Stefan Heim[1,2,3,4], Marc G. Lucas[5,6], Egon Stephan[5], Lorenz Fischer[7], Katrin Amunts[1,2,3], Karl Zilles[1,2,8]**

**1** Institute of Neuroscience and Medicine (INM-1, INM-2), Research Centre Jülich, Jülich, Germany, **2** JARA-BRAIN, Jülich-Aachen Research Alliance, Jülich, Germany, **3** Department of Psychiatry, Psychotherapy, and Psychosomatics, RWTH Aachen University, Aachen, Germany, **4** Section Neurological Cognition Research, Department of Neurology, RWTH Aachen University, Aachen, Germany, **5** INEKO, Department Psychology, University of Cologne, Cologne, Germany, **6** Department of Business Studies – Leadership and Organization, FernUniversität Hagen, Hagen, Germany, **7** Institute of Economic and Social Psychology, University of Cologne, Cologne, Germany, **8** C. and O. Vogt Institute for Brain Research, Heinrich-Heine-University Düsseldorf, Düsseldorf, Germany

## Abstract

Persons have different value preferences. Neuroimaging studies where value-based decisions in actual conflict situations were investigated suggest an important role of prefrontal and cingulate brain regions. General preferences, however, reflect a superordinate moral concept independent of actual situations as proposed in psychological and socioeconomic research. Here, the specific brain response would be influenced by abstract value systems and moral concepts. The neurobiological mechanisms underlying such responses are largely unknown. Using functional magnetic resonance imaging (fMRI) with a forced-choice paradigm on word pairs representing abstract values, we show that the brain handles such decisions depending on the person's superordinate moral concept. Persons with a predominant collectivistic (altruistic) value system applied a "balancing and weighing" strategy, recruiting brain regions of rostral inferior and intraparietal, and midcingulate and frontal cortex. Conversely, subjects with mainly individualistic (egocentric) value preferences applied a "fight-and-flight" strategy by recruiting the left amygdala. Finally, if subjects experience a value conflict when rejecting an alternative congruent to their own predominant value preference, comparable brain regions are activated as found in actual moral dilemma situations, i.e., midcingulate and dorsolateral prefrontal cortex. Our results demonstrate that superordinate moral concepts influence the strategy and the neural mechanisms in decision processes, independent of actual situations, showing that decisions are based on general neural principles. These findings provide a novel perspective to future sociological and economic research as well as to the analysis of social relations by focusing on abstract value systems as triggers of specific brain responses.

**Citation:** Caspers S, Heim S, Lucas MG, Stephan E, Fischer L, et al. (2011) Moral Concepts Set Decision Strategies to Abstract Values. PLoS ONE 6(4): e18451. doi:10.1371/journal.pone.0018451

**Editor:** Tianzi Jiang, Institute of Automation, Chinese Academy of Sciences, China

**Received** December 6, 2010; **Accepted** March 1, 2011; **Published** April 1, 2011



**Funding:** This work was supported by the Initiative and Networking Fund of the Helmholtz Association within the Helmholtz Alliance on Systems Biology (Human Brain Model; KZ), the Helmholtz Alliance for Mental Health in an Aging Society (HelMA; KZ, KA), and a grant of the German Federal Ministry of Education and Research ('Bundesministerium für Bildung und Forschung', BMBF; No: 01GW0613; KA). The funders had no role in study design, data collection and analysis, decision to publish, or preparation of the manuscript.

**Competing Interests:** The authors have declared that no competing interests exist.

* E-mail: s.caspers@fz-juelich.de

## Introduction

Research on value systems is of interest in disciplines such as psychology, sociology, socioeconomics, and related fields. Abstract values represent persons' concepts serving as a general framework for any evaluation preceding decisions and actions [1–3]. Based on the pioneering work of Piaget [4] and Kohlberg [5] on value research in its present form, two lines of value theories emerged: Value typologies provide different dimensions on which values are based [2–3,6–7], without any hierarchical ranking. One of the most robust dimensions is 'individualism' vs. 'collectivism' [6–8]. Individualists are understood as persons, who prefer an egocentric strategy by exerting their own strengths and abilities for personal success, whereas collectivists rely on an altruistic strategy, relationships to other people, and ranking obligations and duties higher than their personal needs. Hierarchical theories rank values according to their importance for the individual or to the complexity of the values [1,5,9]. As a synopsis of these two opposing positions, a third line emerged which integrates typological and hierarchical concepts. It states that different hierarchies of values exist in parallel, between which subjects shift depending on their social and professional situation [10–11].

Independent of a particular value theory, it is widely accepted that values and personal ideals influence a person's mindset and behaviour. Neuroscience touched this topic by investigating the neural correlates of moral judgement and morality [12–14], primarily assessing decision processes in actual dilemma situations. These studies assessed how people decide between two options in a morally challenging situation. Here, brain areas within the frontal and cingulate cortex were found to be involved. The abstract value system of the person, however, was not investigated. Instead, the persons' value system was assessed indirectly, using actual situations in which a normal person would weigh the possible alternatives with respect to the competing moral values. But moral judgement in general should involve a broader range of values as stated in different value theories [1–9], and should be relevant not

only to moral dilemma, but also to most decisions in every day life [1,15]. Thus, it might be expected that principles of decision making found in actual moral dilemma situations only show one aspect of a moral general decision principle in humans which is based on each person's value concept.

Thus, assessing such an influence of an abstract value system on human behaviour should address the neural processing of concepts independent from an actual situation [12]. Dealing with abstract values might involve comparable brain areas as recruited in moral judgement tasks, such as the dorsolateral prefrontal, medial frontal, and anterior to midcingulate cortex. But it remains elusive how activation in these brain regions might be modulated depending on different moral concepts in different persons.

In a functional magnetic resonance imaging (fMRI) study on word pairs representing abstract values, we assessed the question how a person's mindset and thus, his or her way of decision making is influenced by the person's predominant value profile. We could indeed reveal differential neural strategies in different persons.

## Results and Discussion

### Behavioural analysis

We performed functional magnetic resonance imaging (fMRI) in 38 healthy subjects (21 male, 17 female). Stimuli were visually presented words representing abstract values at different levels of complexity (Fig. 1, Table 1), based on the integrating value theories [10–11].

Each word was assigned to one of two types of values, 'individualistic' (e.g., 'power', 'autonomy') and 'collectivistic' (e.g., 'tradition', 'community'), each of which encompassed three levels of increasing complexity. The hierarchy of complexity started with a first level of values relevant to family and self, followed by a second level with reference to the peer-group of a person, and reached the third level with values related to mankind (Fig. 1, Table 1). Stimuli were presented as pairs of words from different or the same levels and types, giving a total of 540 trials. Subjects were instructed to spontaneously select the most appealing word in each word pair by button press (forced-choice situation).

Subjects responded in nearly 100% of the trials (mean of missed trials: 6 out of 540). The profile of choices was analysed for each subject to test whether persons could generally be differentiated into groups with differing value preferences. Using a two-step cluster-analysis, subjects were assigned to two groups, one with preference of 'individualistic' values (IND; $n = 14$ subjects; 10 male), and the other with preference of 'collectivistic' values (COL; $n = 24$ subjects; 11 male). In a 2 (value orientation of group) x 2 (value orientation of stimulus) ANOVA, groups differed significantly (all $P<0.001$) in their choices for first and third level words of the collectivistic type, and first and second level words of the individualistic type (Fig. 1). Groups did not differ with regard to their age and IQ (Table 2), neither overall or with sex as covariate. Since a correlation between personal ideals and personality structure was discussed controversially in different value theories [1–11], all subjects were tested on a five-dimensional personality scale (NEO-FFI). Individualists and collectivists only differed significantly in the dimension 'Conscientiousness', with collectivists scoring higher on this dimension (Table 2).

The groups as revealed by the two-step cluster analysis represent a distinction in accordance with the value theories, showing a subdivision of subjects on the typological dimension 'individualism vs. collectivism'. Thus, based on the value theories, one would expect reaction times to differ between the stimuli. In his value study, Graves [11] showed that subjects would react faster to stimulus words in accordance with their own mindset than to words which do not belong to their own mindset. Thus, we analysed the reaction times (RTs) of the subjects by dividing the respective trials into those where subjects chose a word according to their own overall value profile, and those where subjects chose a word not representing their overall value profile. RTs were scaled for each subject individually by the mean RT across all trials since RTs differed considerably between subjects. Scaled RTs then entered an ANOVA to test whether RTs differed significantly for the above mentioned choice types. ANOVA was significant at $P<0.0001$ ($F_{1,48} = 45.46$) for factor 'choice type'. Figure 2 shows the respective boxplots for both choice types, and highlights the fact that RTs for choices not in accordance with the person's overall value profile are significantly longer than those for own words. Thus, subjects indeed acted as predicted by the value theory [11] since decisions against their overall value profile took longer.

It has to be noted that a subdivision of subjects based on the typology dimension 'individualism vs. collectivism' was the only statistically testable distinction. Further subdivisions with regard to the different levels of complexity (i.e., the hierarchical element of the value theories) could not be reliably established. Therefore, the following analyses of group fMRI data are based on this result of the two-step cluster analysis, i.e. a subdivision of participants into individualists and collectivists. Such a subdivision of subjects is in line with our presumptions of the integrating value theories. This prerequisite provides the relevant basis for the interpretation of the neurobiological correlates.

### Differences in brain activation between individualists and collectivists

How is this behavioural differentiation of value preferences represented in the brain? Based on the behavioural characteristics of collectivists and individualists as provided by the value theories [1–11] it could be hypothesized that collectivists would weigh the given opportunities, also taking their possible repercussion to other people into account, whereas individualists might be more self-centred when making their choice, only bearing in mind the repercussion of their decision on themselves.

The fMRI data of all subjects were analysed for a main effect of factor 'group' to identify overall differences in brain activity between individualists and collectivists. Both groups recruited the brain network for reading [16–17] (Broca's area [areas 44, 45], posterior inferior temporal gyrus, and occipito-temporal transition on the fusiform gyrus).

But the general processing strategies on all decisions (either congruent, i.e. collectivists chose collectivistic values and individualists chose individualistic values, or incongruent, i.e. collectivists chose individualistic values and vice versa) differed between groups (Fig. 3): Collectivists showed significantly stronger activation (main effect COL > IND) within left rostral inferior parietal cortex (IPL, area PFt [18–19]) and intraparietal sulcus (IPS, areas hIP1, hIP2 [20]), the right midcingulate cortex (area 24; MCC [21]) at the border to the medial superior frontal gyrus (mSFG), and the right middle frontal gyrus (MFG). Conversely, individualists showed a significantly stronger activation (main effect IND > COL) in the superficial part of the left amygdala (area SF [22]).

Whereas collectivists recruited a network of cortical brain areas, individualists showed stronger activation of a subcortical structure. Such differential recruitment of cortical vs. subcortical structures points to fundamentally different strategies of individualists and collectivists when facing decisions. This is even more important when considering that these structures belong to different systems,

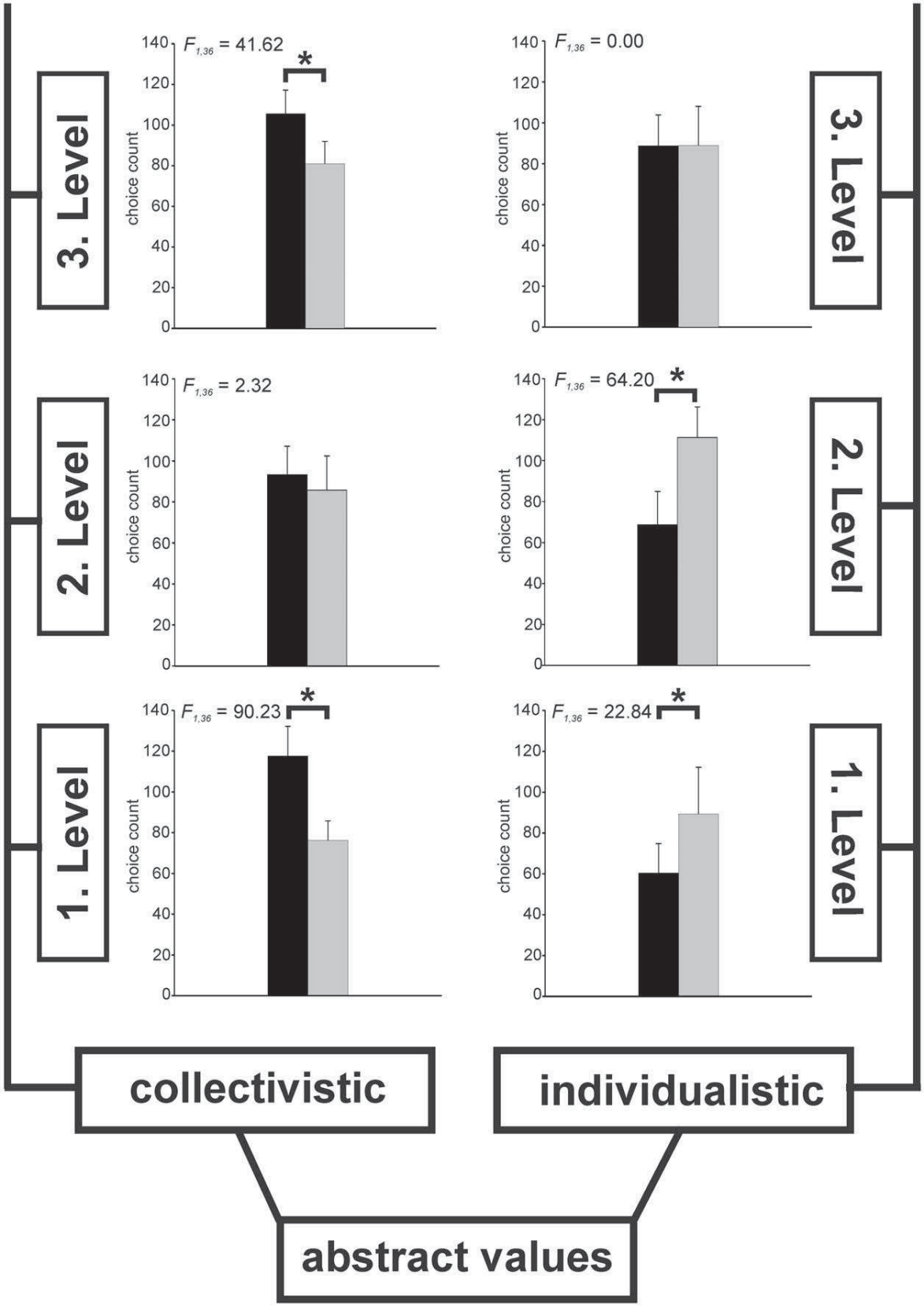
3. Level
2. Level
1. Level
choice count
$F_{1,36}$ = 41.62
$F_{1,36}$ = 0.00
$F_{1,36}$ = 2.32
$F_{1,36}$ = 64.20
$F_{1,36}$ = 90.23
$F_{1,36}$ = 22.84
*
collectivistic
individualistic
abstract values

**Figure 1. Categories of values as obtained from the value theories.** Bar graphs show for each of the six categories the mean count of choices made by the subjects in the MR scanner, averaged over the two groups (Individualists: grey bars, Collectivists: black bars) derived from the two-step cluster-analysis. Error bars provide the standard deviation. Significant differences between groups are indicated by asterisks (ANOVA for interaction between factor 'group' and 'value orientation of stimulus', $P<0.001$, $df = 1$, individual $F$-values within figure).
doi:10.1371/journal.pone.0018451.g001

i.e. the amygdala to the limbic system (for the individualists) and frontal and parietal areas to association cortices (for the collectivists). The following paragraphs should elucidate on the basis of the existing literature how these neurobiological correlates might reflect differential ways of thinking for persons with different moral concepts as hypothesized based on the value theories.

Collectivists recruited three different cortical brain regions during their decisions. Characterizing the different contributing areas of the network would provide a cue on how these areas might be used in collectivists to reach a decision. If there exists a neurobiological correlate for the value-theory driven hypothesis that collectivists would weigh the given alternatives, especially with regard to an acceptable outcome for others, one would expect at least two different requirements to be fulfilled: (i) ability to weigh alternatives with regard to their outcome (such as detection of potential failures or bad options), and (ii) appreciation of others with judgement about their needs. The possibility to fulfil these requirements should therefore be provided by areas of the recruited cortical brain network.

One area recruited by the collectivists was the left IPL/IPS region, which has been implicated in non-spatial stimulus selection. According to Mevorach et al. [25], during stimulus selection, the left IPL/IPS provides a top-down control of extrastriate visual areas to regulate the processing of non-salient stimuli, thus enabling the subject to ignore salient aspects and choose non-salient stimuli [26]. The effect does not seem to reflect task difficulty, since no increased activation in left IPL/IPS was found when the task was simply made more difficult without a corresponding change in saliency [27–28]. Based on these former studies, the recruitment of the left IPL/IPS by the collectivistic group could be interpreted as enabling the person, for each word pair, to reject the possibly at first most salient word. Instead, collectivists were also able to appreciate the less salient word and choose it. It has to be noted that, in the present study, such a

**Table 1.** Stimulus words used for the fMRI paradigm (six categories, six words each).

| **collectivistic** | **1. level** | **2. level** | **3. level** |
|---|---|---|---|
| | (context of family) | (context of peer group) | (context of mankind) |
| | 'Zusammengehörigkeit' | 'Sicherheit' | 'Menschlichkeit' |
| | *togetherness* | *safety* | *Humanity* |
| | 'Geborgenheit' | 'Sorgfalt' | 'Harmonie' |
| | *protection* | *diligence* | *harmony* |
| | 'Familie' | 'Loyalität' | 'Gemeinschaft' |
| | *family* | *loyalty* | *community* |
| | 'Tradition' | 'Verantwortung' | 'Teamfähigkeit' |
| | *tradition* | *responsibility* | *teamwork* |
| | 'Zusammenhalt' | 'Gerechtigkeit' | 'Konvention' |
| | *solidarity* | *fairness* | *convention* |
| | 'Beständigkeit' | 'Maßstäbe' | 'Geselligkeit' |
| | *constancy* | *standards* | *sociability* |
| **individualistic** | **1. level** | **2. level** | **3. level** |
| | (context of self) | (context of peer group) | (context of mankind) |
| | 'Spaß' | 'Erfolg' | 'Flexibilität' |
| | *fun* | *success* | *flexibility* |
| | 'Kreativität' | 'Selbständigkeit' | 'Wertschätzung' |
| | *creativity* | *autonomy* | *esteem* |
| | 'Macht' | 'Kompetenz' | 'Unabhängigkeit' |
| | *power* | *competence* | *independence* |
| | 'Status' | 'Leistung' | 'Nachsicht' |
| | *status* | *performance* | *indulgence* |
| | 'Respekt' | 'Risikobereitschaft' | 'Hingabe' |
| | *respect* | *risk-taking* | *commitment* |
| | 'Herausforderung' | 'Zielstrebigkeit' | 'Selbstentfaltung' |
| | *challenge* | *determination* | *self-development* |

The stimulus words in the table are given as the original German word (in single quotation marks) and as the English translation beneath (in italics). Words and their ordering are based on the open systems theory of values [10–11] and related theories [1–9].
doi:10.1371/journal.pone.0018451.t001

**Table 2.** Characteristics of groups COL and IND with regard to age, sex, and personality structure.

| | Group IND | Group COL | *P-Values* | *F-Values* |
|---|---|---|---|---|
| **Age and IQ (standardized data, $\mu = 100$, $\sigma = 15$)** | | | | |
| N males | 10 | 11 | | |
| N females | 4 | 13 | | |
| age ± SD | 35.60±12.93 | 37.91±13.82 | *0.34* | $F_{1,35} = 0.96$ |
| age male ± SD | 36.55±12.72 | 43.10±13.60 | *0.25* | $F_{2,35} = 1.44$ |
| age female ± SD | 33.00±15.12 | 33.92±13.11 | | |
| IQ ± SD | 124.33±9.88 | 120.35±10.55 | *0.23* | $F_{1,35} = 1.51$ |
| IQ male ± SD | 125.40±9.84 | 118.20±13.25 | *0.48* | $F_{2,35} = 0.76$ |
| IQ female ± SD | 122.25±11.15 | 122.00±8.09 | | |
| **Personality structure (standardized data, range 0–4)** | | | | |
| Dimension 'Neuroticism' | 1.60±0.66 | 1.53±0.65 | *0.76* | |
| Dimension 'Extraversion' | 2.36±0.42 | 2.34±0.53 | *0.89* | |
| Dimension 'Openness' | 2.60±0.54 | 2.31±0.50 | *0.10* | |
| Dimension 'Agreeableness' | 2.49±0.41 | 2.76±0.47 | *0.08* | |
| Dimension 'Conscientiousness' | 2.71±0.49 | 3.01±0.38 | *0.04* * | $F_{1,36} = 4.65$, Wilks' $\lambda = 0.87$ |

All data are given as mean ± standard deviation (SD). Scores on the intelligence quotient (IQ) were derived from the culture-free test CFT-20 [83], scores on the five personality dimensions were derived from the NEO-FFI [84]. Testing for statistical significance was performed using a MANCOVA (age, IQ), and discriminant analysis (NEO-FFI). Significant results are indicated by an asterisk.

doi:10.1371/journal.pone.0018451.t002

saliency effect could be observed on abstract value words, not objects as in former studies [25–28]. This might provide further hints that this effect is a more general principle which only was assumed so far [26].

The MCC was linked to error detection and response selection [29–30], aiming at avoidance of a bad outcome [31]. Thus, behaviour will be reorganized to promote actions which can effectively avoid future harm. This theory of MCC function was originally based on pain and distress studies [32–33], but later also established for other kinds of cognitive processing with the need for avoiding a bad outcome [34–35]. In meta-analyses, it was furthermore stressed that especially this part of the cingulate cortex forms the cognitive division, being activated in cognitively demanding tasks. This could involve motor-response selection tasks, tasks with divided attention or with competing streams of information [36–37]. Especially for the intersection between MCC and mSFG, as found in the present study, the concept of counterfactual thinking has lately been proposed [38]. This concept enables the person to ask what would have happened if the decision had been the other way round. The involvement of the mSFG particularly refers to counterfactual reasoning about action versus inaction. Here, the mSFG serves as an internal action monitor, which also includes the suppression of a prepotent action or monitoring the outcome of a self-selected action [38–41]. Thus, the activation of the present study could likely be interpreted as serving as a "response monitor" for the selection process required when choosing between two abstract values. But the mSFG activation could furthermore play a role in the social context of the decision process. It was reported that mSFG was involved in forming judgements about other people, especially concerning the reputation a person has in view of another [42–44]. Being only activated in the collectivists, they seem to use this cortical region to carefully weigh their possibilities to reach the best possible solution with the best outcome for them and for others, also taking care of their reputation.

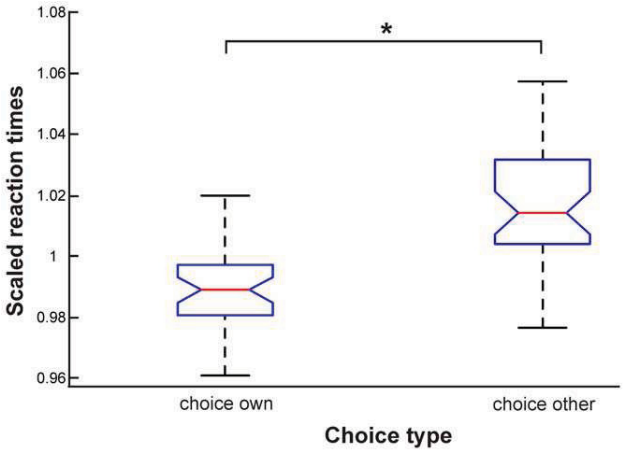


**Figure 2. Results of the statistical analysis of scaled reaction times of different trial types.** Box plots show mean scaled reaction times with percentiles for the two choice types choice for a word in accordance with one's own value profile (choice own), and choice for a word not in accordance with the own value profile (choice other). ANOVA ($P<0.0001$) revealed a significant effect of factor 'choice type' as marked by the asterisk.

doi:10.1371/journal.pone.0018451.g002

The MFG was found to be active during self-other differentiation processes, enabling the subject to ascribe a mental state to another person in relation to one's own [45]. As part of the dorsolateral prefrontal cortex (BA 46 and 9), this region seems to be involved in social reasoning. It was shown that the MFG plays a role in the evaluation of the fairness and permissibility of behaviour as demonstrated by fMRI and transcranial magnetic stimulation neuroeconomical studies [46–48]. This involvement in socially relevant decisions was further supported by studies in which social norms were violated, pointing to a respective evaluative function of the right MFG in particular [48–50]. In

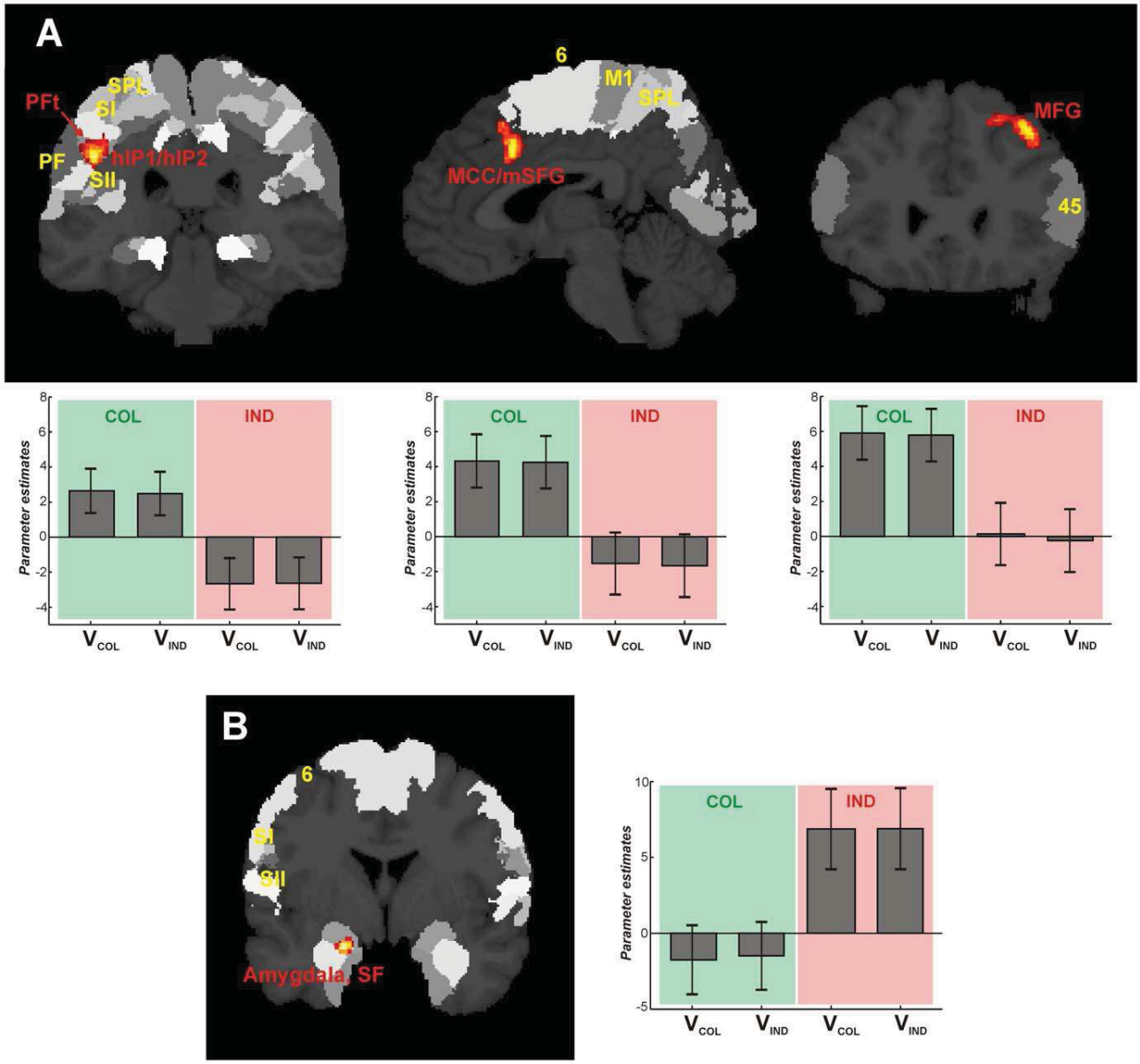


**Figure 3. Significant brain activations for the main effects of factor 'group'.** (A) Main effect COL > IND: Coronal and sagittal sections of the MNI single subject template, showing significant activation ($p<0.05$ cluster-level corrected, extent threshold $k=200$ voxels), labelled in red) within left rostral inferior parietal lobule (PFt) [18–19] and intraparietal sulcus (hIP1, hIP2) [20], cluster size: 833 voxels, $T_{210}=4.45$, peak MNI coordinates: $x=-46$, $y=-32$, $z=33$); right middle cingulate cortex (MCC, BA24) [21] at the border to medial superior frontal gyrus (mSFG), cluster size: 285 voxels, $T_{210}=4.16$, peak MNI coordinates: $x=3$, $y=16$, $z=33$; right middle frontal gyrus (MFG), cluster size: 577 voxels, $T_{210}=4.16$, peak MNI coordinates: $x=39$, $y=26$, $z=42$. (B) Main effect IND > COL: Coronal section of the MNI single subject template, showing significant activation ($p_{uncorr.}<0.001$, extent threshold $k=10$, labelled in red) within the superficial part of the left amygdala (SF [22]), cluster size: 61 voxels, $T_{210}=4.02$, peak MNI coordinates: $x=-20$, $y=-2$, $z=-21$. For reading convenience, surrounding areas of the Jülich-Düsseldorf cytoarchitectonic atlas [23] as displayed by the SPM anatomy toolbox [24] are labelled in yellow whereas areas found to be active in the present study are labelled in red. Yellow labelled area codes are as follows: hIP1/hIP2: areas of anterior intraparietal sulcus, M1: primary motor cortex, area PF: area of rostral inferior parietal lobule, SI: primary somatosensory cortex, SII: secondary somatosensory cortex, SPL: superior parietal lobule, area 6: premotor cortex. Bar plots beneath (for A) and beside (for B) each section show the parameter estimates (i.e. the strength of the BOLD-effect for each condition as measured during fMRI, revealing if and to what degree the each condition contributed to the observed activation) at peak MNI coordinates for collectivists (COL; green), and individualists (IND; red) when choosing either individualistic ($V_{IND}$) or collectivistic values ($V_{COL}$). Error bars provide the standard error.
doi:10.1371/journal.pone.0018451.g003

moral dilemma situations, this region is also involved, assumed to provide the normative evaluation when different moral goals conflict with each other [51]. Thus, the involvement of the MFG in the present study could be interpreted as being the "social monitor", comparable to the "response monitor" of the MCC/mSFG region, in a situation where collectivists had to decide between different abstract moral values. Especially the fairness and social permissibility aspect might be essential for the collectivists, deduced from their orientation towards other people. Even when deciding in an abstract fashion, collectivists seemed to try to find

the fairest solution when making their choice between two abstract values. Therefore, again the present study points to a more general principle of socially relevant decision-making, irrespective of an actual situation.

Interpreting the possible role of this cortical brain network recruited by the collectivists during the decision process, their strategy might likely be called a 'balancing and weighing strategy'. This was hypothesized based on the behavioural characteristics of the collectivists. The recruited brain areas contribute different aspects of this strategy, since they enable the collectivists to weigh both alternatives and try to detect possible errors or any social unfairness in their decision, aiming at finding the optimal choice for everyone. Together, these areas form a cortical brain network which is recruited by the collectivist to apply their orientation towards other people with an altruistic attitude to decision processes, underpinning our theory-driven hypothesis of how a neurobiological correlate of a collectivistic moral concept might be organized to reach a decision.

For individualists, on the contrary, a different strategy would be hypothesized based on their behavioural characteristics. According to the value theories, individualists would most likely focus the outcome of their decision to their personal advantage or benefit. The potential neurobiological correlate of such a strategy was at least completely different from the one of the collectivistic strategy, i.e. the involvement of a subcortical limbic structure in contrast to a network of cortical association regions.

The only activation found to be more active in the individualists than the collectivists was the superficial part SF of the left amygdala. The amygdala was implicated in processing of stimuli which are either arousing or emotional. Here, the emotional valence could have been either positive or negative [52–56]. Spoken in a more general fashion, the amygdala seems to process the relevance of a stimulus in a personal situation. Ascribing this role to the amygdala might point to possible differential response mechanisms of the amygdala in different people, depending on their interpretation of the situation [55–56]. The preponderance of amygdala activation in only one of two groups of people in the present study, i.e. the individualists, supports this theory. It shows that a person's mindset and general value orientation might be one factor which influences their point of view and consecutively, the response characteristic of the amygdala. The specific activation of only the superficial part SF of the amygdala further supports the current interpretation of the amygdala providing the social information within the decision process of the present study. This SF region was found to be important for continuous evaluation of socially relevant situations [57–58]. Having found activation only in the left amygdala seems to further support the so far proposed interpretation: In two meta-analyes the left amygdala was found to be not only involved in pure negative emotion processing, but furthermore in a sustained evaluation process of the emotional valence and arousal of the stimulus [59–60].

Thus, the strategy of the individualists might be interpreted as a 'fight-and-flight'-strategy. They did not try to weigh each decision in each possible way as the collectivists did, but aimed at detecting the social relevance, and consecutively, the possible menace of the decision with regard to their own social status. Behaviourally, this is in accordance with the individualists' orientation to egocentric values. Based on the value theories, it was assumed that individualists would focus on their personal outcome when facing a decision. The neurobiological correlate of such a strategy found in the present study supports this notion, but also reveals the fundamental difference to the strategy of the collectivists: individualists seemed to be more emotionally engaged in a decision process, entering a different level of processing than collectivists.

It has to be stressed that these differential strategies were found in decisions on *abstract* moral values, irrespective of an *actual* situation, in contrast to the referenced literature. Thus, moral concepts and general value orientations provide principle brain mechanisms for the subject of how to approach a decision. Here, brain regions beyond the known cingulate and prefrontal regions which are recruited during actual moral conflict situations [12–15] were involved.

Taken together, these findings could support the notion of two main components existing within the complex of 'morality': moral reasoning (cognition) and moral feelings (emotion), which are supported by different networks of cortical (cognition) and subcortical (emotion) areas [61–63]. Together with studies on antisocial and psychopathic behaviour it was argued that either one or the other system might be impaired in antisocial individuals, mainly preventing them from having a feeling for morality (emotion component) [61]. Comparable to that dichotomy, we could hypothesize that the two components of morality, i.e. emotion vs. cognition, are generally demanded differently, depending on the predominant moral concept of a person. Whereas collectivists seem to concentrate on moral reasoning aspects when solving a decision, individualists are more involved with the moral emotion aspect. It can be assumed that in principle, all people have access to both components of moral decision making. But depending on their current moral concept, the one or the other component outweighs the other. The idea of the integrating value theories [10–11] that every person is in principle equipped with either moral concept, switching between the different manifestations depending on their social and professional situation, provides the theoretical background for such an interpretation. Thus, our results provide a new aspect to the discussion about the possible dichotomy of moral judgement, showing that even in healthy, psychosocially normal persons, one or the other component (cognition or emotion) might be dominant.

In context of psychopathic behaviour and possible impairments in the neural circuits of morality, it was argued that antisocial behaviour is to occur first, and then causes a switch in moral thinking, not vice versa. This was explained as a need to adjust moral thinking to repeated (antisocial) activities to reduce cognitive dissonance [64–66]. With respect to healthy, psychosocially normal persons, a comparable causal system could be assumed: If the moral concept of a person shifts depending on his or her social or professional situation [10–11], the predominance of one or the other component of moral judgement might shift sequentially to adjust the decision processes to every day life. On the contrary, it seems unlikely that a shift in the decision making system would precede a shift of the overall moral concept. But for this problem, our results provide only first hints for one of the two possibilities, leaving a further investigation for future studies.

To our knowledge, this is the first study which experimentally investigates neurobiological correlates of how a person's mindset might influence the way of decision making. With our design, we were able to find behavioural data which distinguished subjects based on their overall value profile which provided the basis for consecutive analysis of possible neurobiological correlates. The interpretation of these findings must remain tentative. But based on the insights gained from the present study, showing that subjects can be grouped with regard to their overall value concept, and that neurobiological correlates could be identified for such a distinction, modelling of the second part of psychological value research, i.e. the different levels of increasing complexity could be a challenge for future studies.

## Conflict processing in individualists and collectivists

This difference in processing strategies between individualists and collectivists when facing abstract value decisions lead to the question if these decisions on abstract values also bear a conflict potential which might involve comparable brain areas as found in actual moral dilemma situations. Such conflicts might then be experienced and processed differently in persons with different moral concepts. We tested this hypothesis by taking the non-chosen words in each trial as a possible conflict reason. Thus, the fMRI data of both groups were re-analysed, sorting the trials into non-chosen individualistic and collectivistic words, assuming that the volunteers might have experienced a conflict when they did not choose in accordance with their overall value profile.

A first hint to such conflict situations was provided by the subjects' reports when debriefing them after scanning. Subjects reported that in most trials they easily chose one of the two presented words. But there were also trials in which both words were equally wrong for them, causing the subjects to feel that their choice would be equally bad. Furthermore, there were trials in which both words were equally good, which caused subjects to have a problem with choosing one of them. Finally, there were trials in which subjects experienced that they did not chose in line with the rest of their decisions, a fact which made them feel angry.

To test if this assumption also has a behavioural basis derived from the data during the experiment, we analysed the reaction times (RT) to different stimuli, taking the RTs as an indicator for potential conflict [1–11]. Thus, RTs were grouped according to the sorting of the trials, providing four different groups of RTs: 1. both words belonged to the overall value profile of the subject (positive conflict); 2. neither of the words belonged to the overall value profile of the subject (negative conflict); 3. only one word belonged to the value profile of the subject, and the participant chose in accordance with the own value profile (no conflict – positive decision); 4. only one word belonged to the value profile of the subject, but the participant did not choose in accordance with the own value profile (no conflict – negative decision). Based on the value theories it could be hypothesized that trials of group 1 and 4 would cause a potential conflict, because they resulted in not having chosen a word of one's own value profile.

To statistically test this hypothesis, RTs for each trial type were first scaled for each subject individually by the mean RT of each subject because averaged RTs differed considerably between subjects. Scaled RTs entered an ANOVA to test if RTs of the four trial types differed significantly from each other across subjects. The ANOVA was significant at $P<0.0001$ ($F_{3,148}=21.23$) for a main effect of the factor 'trial type'. Thus, consecutive multiple comparison testing was applied to identify those pairs of trial types for which RTs differed from each other. These tests revealed that RTs of trial types 1 and 4 were significantly longer than those of trial types 2 and 3. This shows that the decision process for trials 1 and 4 took longer than for trials 2 and 3. Together with the reports of the subjects after scanning, this result is a further hint that decisions were experienced differently depending on the trial type, with greater potential for conflict when a word of one own's value profile was not chosen. Statistical results are summarized in Figure 4.

Based on these behavioural peculiarities, we re-analysed the respective brain data to investigate if such behavioural differences have a correlate in brain activity, referring to the different trial types as different potential conflicts which subjects experienced.

In this analysis, the brain network for reading was found again. Additionally, a significant interaction effect was found in two brain regions: left dorsolateral prefrontal cortex (DLPFC) at the border region between BA46 and BA10, and right medial superior frontal gyrus (mSFG, maximum 1) at the transition to the midcingulate cortex (area 24, MCC, maximum 2) [21] (Fig. 5).

Activation within these brain regions was driven by those trials in which subjects rejected their predominant value, i.e. collectivists rejected collectivistic and individualists rejected individualistic values (Fig. 5A). Thus, these brain regions were significantly involved when subjects experienced a conflict. Refusing a congruent value was possible either when two 'wrong' values constituted a trial (DILEMMA condition), or when one word of each value type was presented but subjects made a 'wrong' decision, i.e. not congruent with their dominant value profile (WORSE-CHOICE condition). Thus, a consecutive region of interest (ROI) analysis was carried out to identify the condition which perplexed subjects the most (Fig. 5B): While individualists recruited mSFG only during the WORSE-CHOICE condition, collectivists used this brain region equally in both conditions. A mirror-inverted activation pattern was found in MCC. Within DLPFC, activation did not differ between groups, but was generally higher for the WORSE-CHOICE than for the DILEMMA condition.

Having not chosen in accordance with the own value concept thus indeed caused a conflict and involved comparable brain areas as found in moral dilemma situations [12–15]. Here, the DLPFC was ascribed the role of a rule keeper, providing general rules for persons' behaviour in decision processes [67]. This region may interact with other frontal regions [68], such as the mSFG/MCC. Both collectivists and individualists recruited the DLPFC equally strong, with a slight preponderance during the WORSE-CHOICE condition, which might reflect an equally high need for general rules in a decision process. But in individualists, the processing of this conflict was mainly supported by recruitment of the mSFG, showing that the conflict was caused by the counterfactual thinking which reveals that it would have been possible to choose a congruent value in accordance with the own value profile. Taking the social relevance of the mSFG into account as well [42–45], this preponderant activation of the mSFG in individualists might again show that they try to do what is best for themselves but perhaps mainly because they want to be seen in a good light by others (i.e. reputation). The WORSE-CHOICE condition might provide a situation in which the individualists fear a loss of their reputation because they chose contrary to their 'normal' choices. Collectivists, on the other hand, additionally activated the MCC, trying to detect if there was an error in the decision. This again matches their behavioural characteristics of orientation towards other people.

Thus, the conflict analysis supports the notion of different strategies for individualists and collectivists when facing value-based decisions.

## Conclusion and outlook

The present study demonstrates that persons with different value preferences apply different neural strategies when facing a decision. These neurobiological correlates reflect hypotheses derived from behavioural characteristics of persons with different moral concepts. As shown for decisions independent of an actual situation, the current analysis provides a general basis for the understanding of decision processes in the brain. Brain areas beyond those activated in actual moral dilemma situations were found to be involved. It remains for future studies to elucidate if neural correlates can also be established for other typological or hierarchical characteristics of values, beyond those found here for the value typology 'individualism vs. collectivism'. Since value theories have also been applied to economics, leadership, and organizational research [69–70], including cultural differences [6], understanding of the neurobiological basics of value processing in

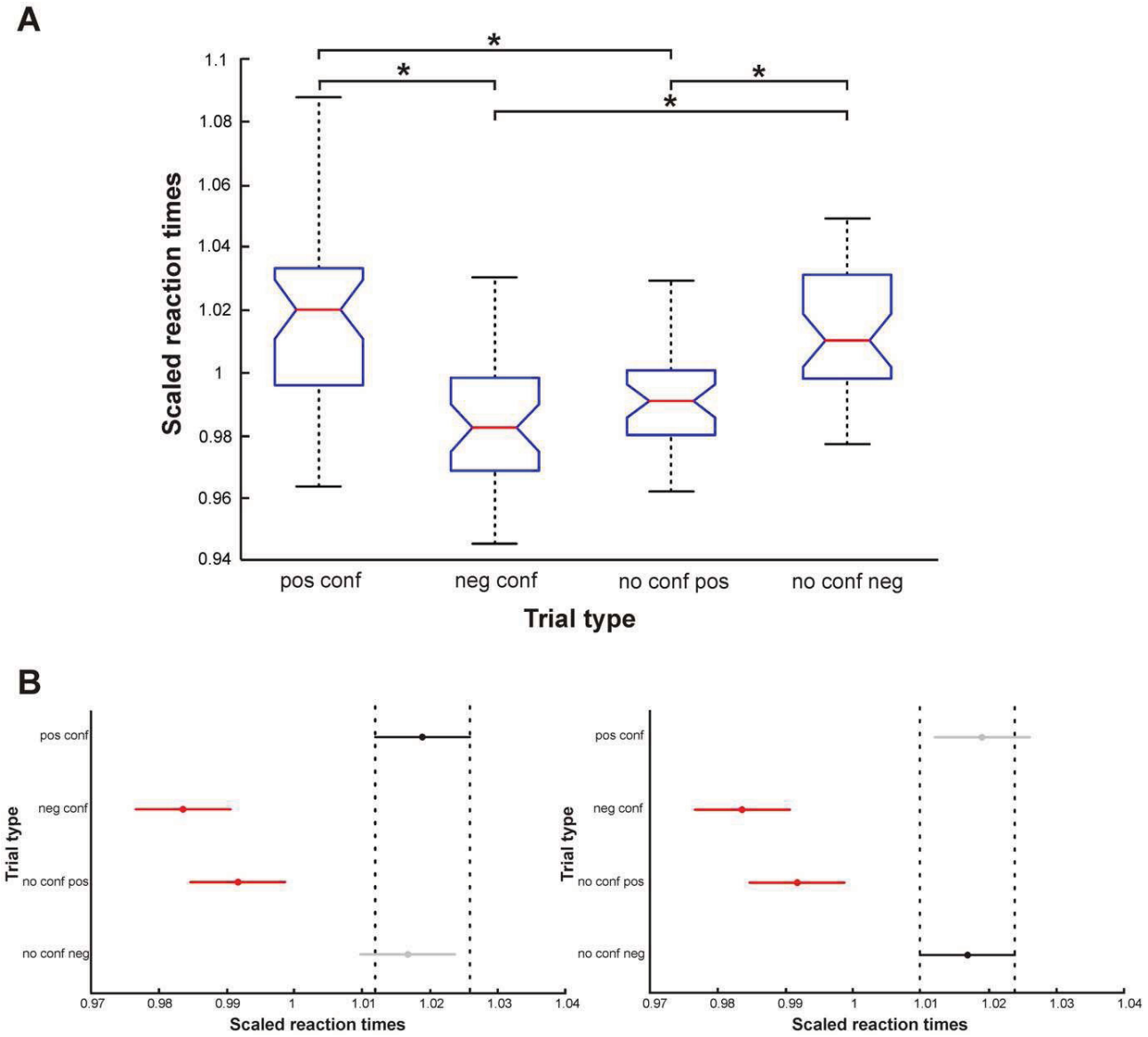


**Figure 4. Results of the statistical analysis of scaled reaction times of different trial types.** (A) Box plots showing mean scaled reaction times with percentiles for the four trial types positive conflict (pos conf), negative conflict (neg conf), no conflict – positive decision (no conf pos), and no conflict – negative decision (no conf neg). ANOVA ($P<0.0001$) revealed a significant effect of factor 'trial type'. Asterisks mark those pairwise comparisons which proved to be significant during consecutive multiple comparison testing. (B) Dot plots showing for trial type 'pos conf' (left panel, black bar) and 'no conf neg' (right panel, black bar) that their reaction times were significantly different from trials 'neg conf' and 'no conf pos' (red bars), but not from each other (grey bar). Bars mark the standard error of each estimated mean scaled reaction time (marked as dots).
doi:10.1371/journal.pone.0018451.g004

persons with different value preferences is likely to have a profound impact on future research in these areas.

## Materials and Methods

### Ethics Statement

The experimental setup of the study was approved by the local Ethics Committee of the RWTH Aachen University, Germany. Written informed consent was obtained from all participants.

### Participants

38 healthy volunteers participated in the experiment (21 males, mean age ± SD = 39.67±13.25, range 22 – 61; 17 female, mean age ± SD = 33.71±13.11, range 19 – 59). All participants were native German speakers and had normal or corrected-to-normal vision. Subjects had no known history of neurological or psychiatric disorders. One male subject was excluded from the brain data analysis due to failure of pre-processing of the data, thus only being considered for the behavioural analysis.

### Experimental design, stimuli, and stimulus presentation

Each participant performed a functional magnetic resonance imaging (fMRI) forced-choice paradigm on words with value-based meanings. These words were generated based on psychological theories and general concepts of human basic values [1–11]. Following these classification of values, two main sections of values

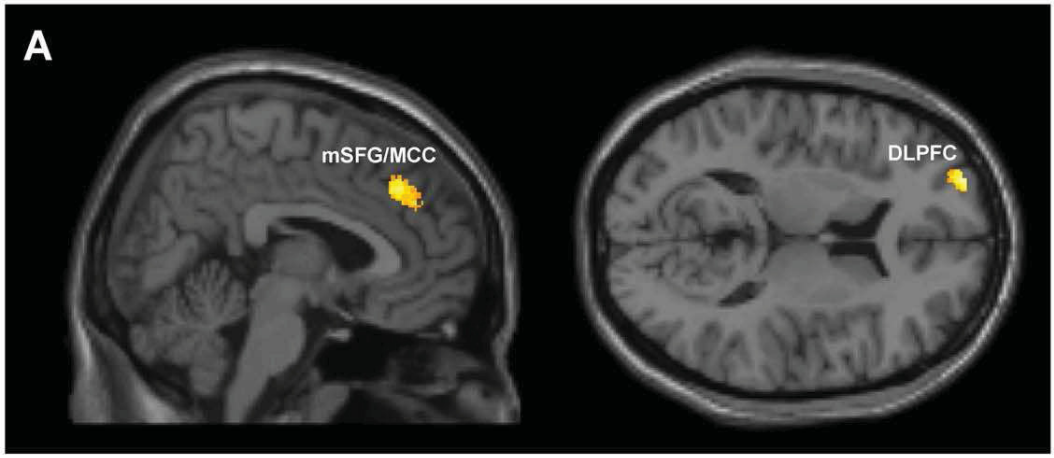


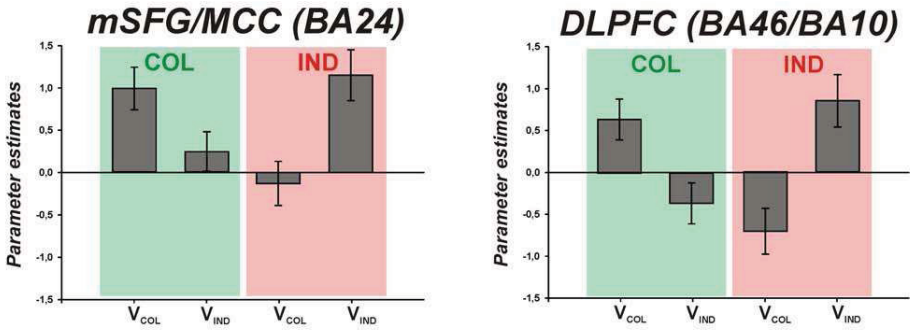





## B ROI-based analysis

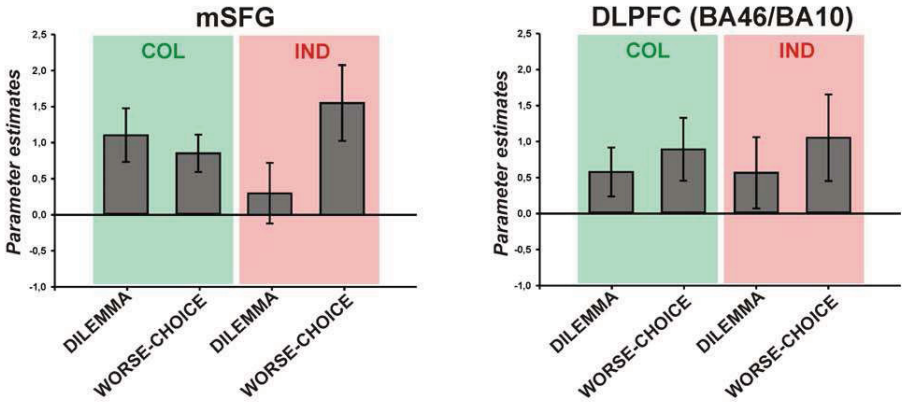





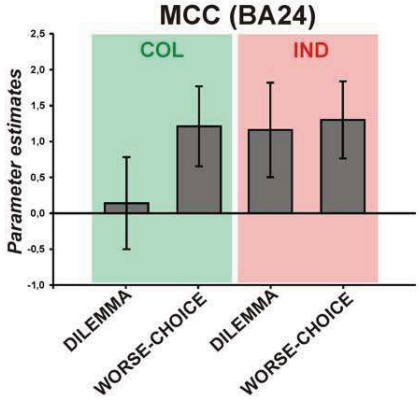

**Figure 5. Significant brain activation and consecutive ROI-based analysis for non-selected words.** (A) Sagittal and horizontal section of the MNI single subject template, showing significant activation ($p_{uncorr}<0.001$, extent threshold $k=150$) within the dorsolateral prefrontal cortex at the border to the frontal pole region (DLPFC (BA46/BA10), cluster size: 168 voxels, MNI coordinates of peak activity: $x=-27$, $y=56$, $z=15$), and the medial superior frontal gyrus (mSFG, cluster size: 315 voxels, maximum 1, MNI coordinates of peak activity: $x=6$, $y=35$, $z=36$) at the border to the middle cingulate cortex (MCC (BA24 [19]), maximum 2, MNI coordinates of peak activity: $x=2$, $y=45$, $z=30$). Bar plots beneath the sections show the parameter estimates (i.e. the strength of the BOLD-effect for each condition as measured during fMRI, revealing if and to what degree the each condition contributed to the observed activation) as in Fig. 2. (B) ROI-based analysis in the same brain regions as in A, beneath the respective section of A. The MCC/mSFG cluster was separated for this analysis by applying a significance threshold of $p_{uncorr}<0.0005$ to the statistical map of A, allowing for a separate extraction of parameter estimates at each maximum individually. Each graph shows the parameter estimates of activations for the two incongruent conditions (DILEMMA, WORSE-CHOICE). Error bars provide the standard error.
doi:10.1371/journal.pone.0018451.g005

could be differentiated: individualistic (i.e. self-centred) and collectivistic (i.e. group-oriented) values. Within these two sections a further differentiation of values is possible with respect to their relation to other individuals, providing an ordering of values referring to increasing complexity: at a first level, the most basic values appear, encompassing only the individual itself and significant others; at the second level, values in relation to peer groups, like colleagues, friends etc., are based; at the third level, values with relation to every other person are grouped. This hierarchical ordering system of values and value development in humans is based on early psychological theories of e.g. Piaget [4], Maslow [9] or Kohlberg [5]. In total, six value categories were used within the current experiment.

For each of the six word categories, six different words were generated based on words provided in value theories [1–11]. Since German language is case sensitive concerning nouns (capital initial letters) and verbs or adjectives (small initial letters), it was assured that only nouns were chosen as stimulus words for the paradigm. Verb- or adjective-derived nouns were excluded in order to control for syntactic word category. In order to generate accurate German words with different value meanings, translations of words from these earlier studies [1–11] were checked for the most selective synonym using the German Duden glossary of synonyms [71]. This procedure was necessary since direct translation of words from the original publications was not always suitable due to ambivalent meaning in German language. Translations were double-checked for accuracy and appropriateness by speech and language therapists of the Neurolinguistics Department of the RWTH Aachen University. The stimulus words for all categories can be found in Table 1.

Before entering the scanner, participants were instructed on the general design of the task, i.e. participants just knew they would see a set of word pairs, being presented in a rapid sequence. They were instructed to spontaneously choose the word of each word pair which appealed most to them, independent of any actual situation. The participants did not see the words before the start of the experiment in the MR scanner. Explanation about the intention of the study or the content of the stimulus words was not provided to assure impartiality of the participants when performing the task in the MR scanner. To assure that subjects understood the general principle of how to choose words, they were provided with examples from fields other than value concepts, e.g.: "You see the words 'vanilla flavour' and 'chocolate flavour': Which word appeals most to you, independent of any given situation?" or "You see the words 'red' and 'green': Which word appeals most to you, independent of any given situation?" Selection of words was indicated by button presses, using the left index finger for the left word on the screen and the right index finger for the right word on the screen.

After scanning, subjects were debriefed of the experiment to ensure that the task was carried out as intended. Therefore, subjects were asked (in accordance to former studies of value research [1–11]) to provide a general appraisal of how they experienced the different choice situations.

Word pairs were presented as written strings in Helvetica font at 48 pts, with one word on the left and one word on the right side of the screen, equally distant from the centre of the screen. Each word from each category was combined with each word from every other category, providing a total of 540 word pairs as stimuli. Each word appeared 30 times, 50% of the trials on the left and 50% on the right side of the screen. This was assured not only for the overall appearance of the word across different categories, but also for the combination of the word with six words from one other category. This change in position was implemented in order to avoid habituation effects or possible preferences of the subjects for one side of the screen.

Stimuli were back-projected onto a screen placed on the back wall of the scanner room, seen by the subjects via a small angled mirror suspended from the top of the head coil. Stimulus presentation was controlled by a computer placed in the control room using Presentation software (Neurobehavioral Systems, Albany, CA, USA).

The study employed a modified event-related design. Stimuli were presented in randomized order, with a different randomisation for each participant. The total duration of the experiment was about 22 minutes. Each trial, i.e. presentation of each word pair, lasted 1.3 seconds, followed by a blank screen for 1 second, providing an inter-stimulus interval of 2.3 seconds. The combination of the total trial duration (2.3 s) and the fMRI repetition time (2.5 s; cf next paragraph) resulted in distributed sampling serving as a temporal jitter [72–73]. The distributed sampling procedure was chosen instead of a jitter by implementation of a variable time period between each trial onset to ensure equally short trial durations for each and every trial. Such rapid presentation of stimuli was chosen to reliably detect the relevant effect of how values are processed in the brain. According to the value theories [1–11], a short presentation of stimulus words is essential to gain an unbiased view of a person's mindset. Otherwise, a potential bias might be introduced if subjects are given too much time to rethink their answer. A further advantage was the increased number of stimuli for each value category presented in a reasonable total time frame, which increases statistical power [74–75].

## Functional and anatomical magnetic resonance imaging data acquisition

The functional magnetic resonance imaging (fMRI) experiment was carried out on a 3T Siemens Tim-TRIO scanner (Erlangen, Germany). A standard birdcage head coil was used with foam paddings to reduce head motion. Functional data were recorded from the whole brain, using a gradient-echo echoplanar imaging (EPI) sequence for blood-oxygen-level-dependent (BOLD) contrast with the following parameters: echo time (TE) = 30 ms, flip angle = 90°, repetition time (TR) = 2.5 s, 41 axial slices, slice thickness: 3 mm, slice distance 10%, field of view (FoV) = $200\times200$ mm$^2$ with an in-plane resolution of 3 mm×3 mm.

After the experimental EPI runs, a high-resolution T1-weighted anatomical image was obtained for later normalisation of the EPI data into MNI space using a 3D-MPRAGE sequence (176 axial

slices, TR = 2.25 s; TE = 3.03 ms, FoV = 256×256 $mm^2$, flip angle = 9°, final voxel resolution: 1 mm×1 mm×1 mm).

### Image analysis

Data were processed using MATLAB 7 (The Mathworks Inc., Natick, USA) and the SPM 5 software package (Wellcome Department of Imaging Neuroscience, London, UK, http://www.fil.ion.ucl.ac.uk). Pre-processing of each data set included the standard procedures of realignment, normalisation to the MNI single subject template [76] and spatial smoothing with an 8 mm FWHM Gaussian kernel. The anatomical images served as reference for the transformation to the MNI reference brain, co-registering all functional EPI images to the corresponding anatomical data set, using the unified segmentation approach [77].

For the statistical analysis at the single subject level, trials were assigned to the six word categories individually for each subject, using the subject's decision on each word pair as the categorizing variable (individual selection of trials from each subject's Presentation log-files, providing six trial categories). Failure to choose a word within the time frame of the inter-stimulus interval of 2.3 seconds was counted as a missed trial. The respective trials were excluded from further analysis. The whole study and analysis applied a modified event-related design to optimally model the relevant time periods of such cognitive experiment [78]. Having single events (presentation of each pair of stimulus words as trials), the durations of each trial were set as very short blocks according to the reaction time of the subjects. I.e. the end of each trial was set individually for each trial at the time of the button press, giving variable trial durations. Variable durations for each trial were used in order to model the relevant time period of the BOLD signal during stimulus attainment, cognitive processing of the stimulus, and decision most accurately. Variable trial durations did not enter any further analyses beyond first-level single subject analyses, neither as additional parameters nor as regressors or covariates.

Thus, the relevant block functions resembled such block functions which are known from blocked designs. In the present study, each "block" is in fact a mini-block with duration of several hundred milliseconds (i.e. the reaction time in the individual trial), with steep increase of the slope at stimulus onset, remaining on the activity plateau for the short period until button press (reaction time), and final return to baseline. The duration of the plateau phase was variable, depending on the reaction time to each stimulus. The respective block functions for each category were then convolved with a canonical hemodynamic response function (HRF) with its first derivative to allow for a more flexible and thus optimised fit to the experimental data. According to the Linearity Theory for event-related designs with stimulus-onset asynchrony of around 1 second [79–80], overlapping HRFs from consecutive trials (due to rapid sequence of events) could be separated from each other assuming additive effects for the emergent total HRF. For each participant, the contrasts of each category vs. the implicit resting baseline as implemented in SPM were calculated. This implicit resting baseline consisted of all blank-screen intervals between the stimuli. When reaction times were longer than the stimulus presentation time, thus overlapping with the blank-screen period, only the rest of the blank-screen period after the button press was considered for the implicit resting baseline.

For the group analysis, the individual contrast images of all six categories were entered into a repeated-measures ANOVA as a second-level random effects analysis. A factorial design was implemented with factors "subject", "group" (from the behavioural analysis, either "individualistic" or "collectivistic"), and "trial category". Coordinates are reported in standard MNI stereotaxic coordinates as implemented in SPM 5 [81].

### Statistical analysis of neuropsychological and behavioural data

Neuropsychological and behavioural data were analysed using SPSS 15 for Windows (SPSS Inc., Chicago, IL, USA).

Behavioural data of subjects' performance during the fMRI experiment were tested to identify sub-groups of the participants related to their value preferences, conducting a two-step cluster-analysis which provides the optimum number of clusters in a given data set (see also [82]). Six variables were entered into the analysis, one for each category of value words. Manifestations of the variables were the count of choices for each participant for each value category, i.e. how often a subject chose a word from the respective value category. The analysis was run allowing for a maximum of 15 clusters, log-likelihood distance estimation, Akaike's information criterion as clustering criterion, no noise-handling for outlier treatment, initial distance change threshold of 0, a maximum of eight branches per leaf node, and a maximum of three depth levels. All variables were standardised during the clustering procedure. A Bonferroni-correction for multiple comparisons was applied. Discriminant analyses were carried out with step-wise inclusion of variables (inclusion criterion of $p \leq 0.05$, exclusion criterion of $p \geq 0.10$), priors set to equal, and calculation of Wilk's lambda. The correct assignment of participants to one group was tested with the cross-validated statistics, giving a re-classification rate of 100% for both groups.

Outside the scanner, additional neuropsychological data were obtained from each participant. Individual IQ testing was administered using the short form (part 1) of the culture-free intelligence test CFT-20 [83]. Personality traits were assessed using the multidimensional personality inventory NEO-FFI of Costa and McCrae [84], which assesses five robust dimensions of personality (Table 2). These data were used to characterize the resulting groups of the two-step cluster analysis. IQ and NEO-FFI data of subjects were entered into a MANCOVA (for IQ together with age) and a discriminant analysis (NEO-FFI), respectively.

## Acknowledgments

The authors thank Muna van Ermingen-Marbach from the Department of Psychiatry, Psychotherapy and Psychosomatics of the RWTH Aachen University for her help with creation of the stimulus material, and Nicola Palomero-Gallagher for language-editing and proof-reading the final version of the manuscript.

## Author Contributions

Conceived and designed the experiments: SC SH MGL. Performed the experiments: SC SH. Analyzed the data: SC SH MGL ES LF KA KZ. Contributed reagents/materials/analysis tools: KA KZ. Wrote the paper: SC SH KZ. Advised on interpretation of data with respect to value theories and their meaning for psychological and business research: ES LF. Advised on neuroscientific aspects of study design and interpretation of the results: KA KZ.

## References

1. Rokeach M (1973) The nature of human values. New York: Free Press.
2. Schwartz SH, Bilsky W (1987) Toward a universal psychological structure of human values. J Pers Soc Psychol 53: 550–562.
3. Schwartz SH (1992) Universals in the content and structure of values: Theoretical advances and empirical tests in 20 countries. In: Zanna M, ed. Advances in experimental social psychology, vol 25. New York: Academic Press. pp 1–65.

4. Piaget J (1976) Das moralische Urteil beim Kind, ed. 2 Frankfurt: Suhrkamp (Original publication (1932): Le jugement moral chez l'enfant).
5. Kohlberg L (1969) State and sequence: The cognitive-developmental approach to socialization. In: Goslin DA, ed. Handbook of socialization theory and research. Chicgao: Rand McNally. pp 347–480.
6. Hofstede G (1980) Culture's consequences: International differences in work-related values. Beverly Hills, Los Angeles: Sage.
7. Stackman RW, Pinder CC, Connor PE (2000) Values lost: Redirecting research on values in the workplace. In: Askanasy N, Wilderom CPM, Peterson MF, eds. Handbook of organizational culture and climate. Thousand Oaks: Sage. pp 37–45.
8. Kluckhohn F, Strodtbeck F (1961) Variations in value orientations. Westport: Greenwood.
9. Maslow AH (1962) Toward a psychology of being. Princeton: Van Nostrand.
10. Loevinger J (1970) Measuring ego development. San Francisco: Jossey-Bass.
11. Graves CW (1970) Levels of existence: an open system theory of values. J Hum Psychol 10: 131–155.
12. Moll J, de Oliviera-Souza R, Zahn R (2008) The neural basis of moral cognition: sentiments, concepts, and values. Ann N Y Acad Sci 1124: 161–180.
13. Funk CM, Gazzaniga MS (2009) The functional brain architecture of human morality. Curr Opin Neurobiol 19: 678–681.
14. Shenhav A, Greene JD (2010) Moral judgements recruit domain-general valuation mechanisms to integrate representations of probability and magnitude. Neuron 67(4): 667–677.
15. Sommer M, Rothmayr C, Döhnel K, Meinhardt J, Schwerdtner J, et al. (2010) How should I decide? The neural correlates of everyday moral reasoning. Neuropsychologia 48(7): 2018–2026.
16. Schlaggar BL, McCandliss BD (2007) Development of neural systems for reading. Annu Rev Neurosci 30: 475–503.
17. Richardson FM, Price CJ (2009) Structural MRI studies of language function in the undamaged brain. Brain Struct Funct 213: 511–523.
18. Caspers S, Geyer S, Schleicher A, Mohlberg H, Amunts K, et al. (2006) The human inferior parietal cortex: cytoarchitectonic parcellation and interindividual variability. NeuroImage 33: 430–448.
19. Caspers S, Eickhoff SB, Geyer S, Scheperjans S, Mohlberg H, et al. (2008) The human inferior parietal lobule in stereotaxic space. Brain Struct Funct 212: 481–495.
20. Choi HJ, Zilles K, Mohlberg H, Schleicher A, Fink GR, et al. (2006) Cytoarchitectonic identification and probabilistic mapping of two distinct areas within the anterior ventral bank of the human intraparietal sulcus. J Comp Neurol 495: 53–69.
21. Palomero-Gallagher N, Vogt BA, Schleicher A, Mayberg HS, Zilles K (2009) Receptor architecture of human cingulate cortex: evaluation of the four-region neurobiological model. Hum Brain Mapp 30: 2336–2355.
22. Amunts K, Kedo O, Kindler M, Pieperhoff P, Mohlberg H, et al. (2005) Cytoarchitectonic mapping of the human amygdala, hippocampal region and entorhinal cortex: intersubject variability and probability maps. Anat Embryol 210: 343–352.
23. Zilles K, Amunts K (2010) Centenary of Brodmann's map – conception and fate. Nat Rev Neurosci 11: 139–145.
24. Eickhoff SB, Stephan KE, Mohlberg H, Grefkes C, Fink GR, et al. (2005) A new SPM toolbox for combining probabilistic cytoarchitectonic maps and functional imaging data. NeuroImage 25: 1325–1335.
25. Mevorach C, Humphreys GW, Shalev L (2006) Opposite biases in salience-based selection for the left and right posterior parietal cortex. Nat Neurosci 9: 740–742.
26. Riddoch MJ, Chechlacz M, Mevorach C, Mavritsaki E, Allen H, et al. (2010) The neural mechanisms of visual selection: the view from neuropsychology. Ann N Y Acad Sci 1191: 156–181.
27. Mevorach C, Humphreys GW, Shalev L (2009) Reflexive and preparatory selection and suppression of salient information in the right and left posterior parietal cortex. J Cogn Neurosci 21: 1204–1214.
28. Mevorach C, Humphreys GW, Shalev L (2006) Effects of saliency, not global dominance, in patients with left parietal damage. Neuropsychologia 44: 307–319.
29. Corbetta M, Miezin FM, Dobmeyer S, Shulman GL, Petersen SE (1991) Selective and divided attention during visual discrimination of shape, color, and speed: functional anatomy by positron emission tomography. J Neurosci 11: 2383–2402.
30. Paus T (2001) Primate anterior cingulate cortex: where motor control, drive and cognition interface. Nat Rev Neurosci 2(6): 417–424.
31. Vogt BA, Vogt L (2003) Cytology of human dorsal midcingulate and supplementary motor cortices. J Chem Neuroanat 26: 301–309.
32. Derbyshire SWG (2000) Exploring the pain "neuromatrix". Curr Rev Pain 4: 467–477.
33. Peyron R, Laurent B, Garcia-Larrea L (2000) Functional imaging of brain responses to pain. A review and meta-analysis. Neurophysiol Clin 30: 263–288.
34. Faymonville ME, Laureys S, Degueldré C, Del Fiore G, Luxen A, et al. (2000) Neural mechanisms of antinociceptive effects of hypnosis. Anesthesiology 92: 1257–1267.
35. Bush G, Vogt BA, Holmes J, Dale AM, Greve D (2002) Dorsal anterior cingulate cortex: a role in reward-based decision making. Proc Natl Acad Sci U S A 99: 523–528.
36. Picard N, Strick PL (1996) Motor areas of the medial wall: a review of their location and functional activation. Cereb Cortex 6: 342–353.
37. Bush G, Luu P, Posner MI (2000) Cognitive and emotional influences in anterior cingulate cortex. Trends Cogn Sci 4(6): 215–222.
38. Barbey AK, Krueger F, Grafman J (2009) Structured event complexes in the medial prefrontal cortex support counterfactual representations for future planning. Philos Trans R Soc Lond B Biol Sci 364: 1291–1300.
39. Barch DM, Braver TS, Akbudak E, Conturo T, Ollinger J, et al. (2001) Anterior cingulate cortex and response conflict: effects of response modality and processing domain. Cereb Cortex 11: 837–848.
40. Botvinick MM, Cohen JD, Carter CS (2004) Conflict monitoring and anterior cingulate cortex: an update. Trends Cogn Sci 8: 539–546.
41. Walton ME, Devlin JT, Rushworth MF (2004) Interactions between decision making and performance monitoring within prefrontal cortex. Nat Neurosci 7: 1259–1265.
42. Amodio DM, Frith CD (2006) Meeting of minds: the medial frontal cortex and social cognition. Nat Rev Neurosci 7: 268–277.
43. Mitchell JP, Neil Macrae C, Banaji MR (2005) Forming impressions of people versus inanimate objects: social-cognitive processing in the medial prefrontal cortex. NeuroImage 26: 251–257.
44. Zink CF, Tong Y, Chen Q, Bassett DS, Stein JL, et al. (2008) Know your place: Neural processing of social hierarchy in humans. Neuron 58: 273–283.
45. Platek SM, Keenan JP, Gallup GG Jr, Mohamed FB (2004) Where am I? The neurological correlates of self and other. Cogn Brain Res 19: 114–122.
46. Sanfey AG, Rilling JK, Aronson JA, Nystrom LE, Cohen JD (2003) The neural basis of economic decision-making in the Ultimatum Game. Science 300(5626): 1755–1758.
47. Knoch D, Pascual-Leone A, Meyer K, Treyer V, Fehr E (2006) Diminishing reciprocal fairness by disrupting the right prefrontal cortex. Science 314(5800): 829–832.
48. Barbey AK, Krueger F, Grafman J (2009) An evolutionarily adaptive neural architecture for social reasoning. Trends Neurosci 32(12): 603–610.
49. Buckholtz JW, Asplund CL, Dux PE, Zald DH, Gore JC, et al. (2008) The neural correlates of third-party punishment. Neuron 60(5): 930–940.
50. Spitzer M, Fischbacher U, Herrnberger B, Grön G, Fehr E (2007) The neural signature of social norm compliance. Neuron 56 (1): 185–196.
51. Greene JD, Nystrom LE, Engell AD, Darley JM, Cohen JD (2004) The neural bases of cognitive conflict and control in moral judgement. Neuron 44 (2): 389–400.
52. Winston JS, Gottfried JA, Kilner JM, Dolan RM (2005) Integrated neural representations of odor intensity and affective valence in human amygdala. J Neurosci 25: 8903–8907.
53. Hamann SB, Ely TD, Hoffman JM, Kilts CD (2002) Ecstasy and agony: activation of the human amygdala in positive and negative emtion. Psychol Sci 13: 135–141.
54. Costafreda SG, Brammer MJ, David AS, Fu CHY (2008) Predictors of amygdala activation during the processing of emotional stimuli: A meta-analysis of 385 PET and fMRI studies. Brain Res Rev 58: 57–70.
55. Adolphs R (2003) Is the human amygdala specialized for processing social information? Ann N Y Acad Sci 985: 326–340.
56. Adolphs R (2010) What does the amygdala contribute to social cognition? Ann N Y Acad Sci 1191: 42–61.
57. Goossens L, Kukolja J, Onur OA, Fink GR, Maier W, et al. (2009) Selective processing of social stimuli in the superficial amygdala. Hum Brain Mapp 30: 3332–3338.
58. Hurlemann R, Rehme AK, Diessel M, Kukolja J, Maier W, et al. (2008) Segregating intra-amygdalar response to dynamic facial emotion with cytoarchitectonic maximum probability maps. J Neurosci Meth 172: 13–20.
59. Baas D, Aleman A, Kahn RS (2004) Lateralization of amygdala activation: a systematic review of functional neuroimaging studies. Brain Res Rev 45: 96–103.
60. Fusar-Poli P, Placentino A, Carletti F, Allen P, Landi P, et al. (2009) Laterality effect on emotional faces processing: ALE meta-analysis of evidence. Neurosci Lett 452: 262–267.
61. Raine A, Yang Y (2006) Neural foundations to moral reasoning and antisocial behaviour. Soc Cogn Affect Neurosci 1 (3): 203–213.
62. Greene JD, Nystrom LE, Engell AD, Darley JM, Cohen JD (2004) The neural bases of cognitive conflict and control in moral judgement. Neuron 44: 389–400.
63. Harenski CL, Hamann S (2006) Neural correlates of regulating negative emotions related to moral violations. NeuroImage 30: 313–324.
64. Berthoz S, Grezes J, Armony JL, Passingham RE, Dolan RJ (2006) Affective response to one's own moral violations. NeuroImage 31: 945–950.
65. Moll J, Oliviera-Souza R, Eslinger PJ, Bramati IE, Mourao-Miranda J, et al. (2002) The neural correlates of moral sensitivity: a functional magnetic resonance imaging investigation of basic and moral emotions. J Neurosci 22 (7): 2730–2736.
66. Blair RJR (1995) A cognitive developmental approach to morality – investigating the psychopath. Cognition 57: 1–29.
67. Koechlin E, Basso G, Pietrini P, Panzer S, Grafman J (1999) The role of the anterior prefrontal cortex in human cognition. Nature 399: 148–151.
68. Sakai K, Passingham RE (2003) Prefrontal interactions reflect future task operations. Nat Neurosci 6: 75–81.
69. Aycan Z, Kanungo RN, Mendonca M, Yu K, Deller J, et al. (2000) Impact of culture on human resource management practices: A 10 country comparison. Appl Psychol 49: 192–221.

70. Chatman JA, Polzer JT, Barsade SG, Neale MA (1998) Being different yet feeling similar: The influence of demographic composition and organizational culture on work processes and outcomes. Admin Sci Quart 43: 749–780.
71. Bibliographisches Institut AG (2009) Duden – Das Wörterbuch der Synonyme. Mannheim: Dudenverlag.
72. Price CJ, Veltman DJ, Ashburner J, Josephs O, Friston KJ (1999) The critical relationship between the timing of stimulus presentation and data acquisition in blocked designs with fMRI. NeuroImage 10: 36–44.
73. Heim S, Eickhoff SB, Opitz B, Friederici AD (2006) BA 44 in Broca's area supports syntactic gender decisions in language production. Neuroreport 17 (11): 1097–1101.
74. Friston KJ, Holmes A, Price CJ, Buchel C, Worsley KJ (1999) Multisubject fMRI studies and conjunction analyses. NeuroImage 10: 385–396.
75. Buckner RL, Goodman J, Burock M, Rotte M, Koutstaal W, et al. (1998) Functional-anatomical correlates of object priming in humans revealed by rapid presentation event-related fMRI. Neuron 20: 285–296.
76. Holmes CJ, Hoge R, Collins L, Woods R, Toga AW, et al. (1998) Enhancement of MR images using registration for signal averaging. J Comput Assist Tomogr 22: 324–333.
77. Ashburner J, Friston KJ (2005) Unified segmentation. NeuroImage 26: 839–851.
78. Amaro E, Jr., Barker GJ (2006) Study design in fMRI: basic principles. Brain Cogn 60 (3): 220–232.
79. Friston KJ, Josephs O, Rees G, Turner R (1998) Non-linear event-related responses in fMRI. Mag Res Med 39: 41–52.
80. Burock MA, Buckner RL, Woldorff MG, Rosen BR, Dale AM (1998) Randomized event-related experimental designs allow for extremely rapid presentation rates using functional MRI. Neuroreport 9: 3735–3739.
81. Evans AC, Marrett S, Neelin P, Collins L, Worsley K, et al. (1992) Anatomical mapping of functional activation in stereotaxic coordinate space. NeuroImage 1: 43–53.
82. Heim S, Tschierse J, Amunts K, Wilms M, Vossel S, et al. (2008) Cognitive subtypes of dyslexia. Acta Neurobiol Exp (Wars) 68 (1): 73–82.
83. Weiß RH (1998) Test for Basic Intelligence, Scale 2 (German: Grundintelligenz Skala 2. CFT-20). Göttingen: Hogrefe.
84. Borkenau P, Ostendorf F (1993) NEO-Five-Factorial-Inventory of Costa and McCrae (German: NEO-Fünf-Faktoren-Inventar nach Costa und McCrae). Göttingen: Hogrefe.

NeuroImage 60 (2012) 2389–2398

Contents lists available at SciVerse ScienceDirect

NeuroImage

journal homepage: www.elsevier.com/locate/ynimg

# Across-study and within-subject functional connectivity of a right temporo-parietal junction subregion involved in stimulus–context integration

Oliver Jakobs [a,b,c], Robert Langner [a,c,f], Svenja Caspers [c], Christian Roski [c], Edna C. Cieslik [c], Karl Zilles [b,c,d], Angela R. Laird [e], Peter T. Fox [e], Simon B. Eickhoff [a,c,d,f,*]

[a] Department of Psychiatry, Psychotherapy and Psychosomatics, Medical School, RWTH Aachen University, Aachen, Germany
[b] C & O. Vogt Institute of Brain Research, Heinrich Heine University, Düsseldorf, Germany
[c] Institute of Neuroscience and Medicine (INM-1, INM-2), Research Centre Jülich, Jülich, Germany
[d] Jülich–Aachen Research Alliance (JARA-Brain), Germany
[e] University of Texas Health Science Center at San Antonio, San Antonio, TX, USA
[f] Institute of Clinical Neuroscience and Medical Psychology, Heinrich Heine University, Düsseldorf, Germany

ARTICLE INFO

*Article history:*
Accepted 15 February 2012
Available online 23 Febuary 2012

*Keywords:*
fMRI
Resting state
Meta-analysis
Connectivity modeling
Right temporo-parietal junction

ABSTRACT

Bidirectional integration between sensory stimuli and contextual framing is fundamental to action control. Stimuli may entail context-dependent actions, while temporal or spatial characteristics of a stimulus train may establish a contextual framework for upcoming stimuli. Here we aimed at identifying core areas for stimulus–context integration and delineated their functional connectivity (FC) using meta-analytic connectivity modeling (MACM) and analysis of resting-state networks.

In a multi-study conjunction, consistently increased activity under higher demands on stimulus–context integration was predominantly found in the right temporo-parietal junction (TPJ), which represented the largest cluster of overlap and was thus used as the seed for the FC analyses. The conjunction between task-dependent (MACM) and task-free (resting state) FC of the right TPJ revealed a shared network comprising bilaterally inferior parietal and frontal cortices, anterior insula, premotor cortex, putamen and cerebellum, i.e., a 'ventral' action/attention network. Stronger task-dependent (vs. task-free) connectivity was observed with the pre-SMA, dorsal premotor cortex, intraparietal sulcus, basal ganglia and primary sensori motor cortex, while stronger resting-state (vs. task-dependent) connectivity was found with the dorsolateral prefrontal and medial parietal cortex.

Our data provide strong evidence that the right TPJ may represent a key region for the integration of sensory stimuli and contextual frames in action control. Task-dependent associations with regions related to stimulus processing and motor responses indicate that the right TPJ may integrate 'collaterals' of sensory processing and apply (ensuing) contextual frames, most likely via modulation of preparatory loops. Given the pattern of resting-state connectivity, internal states and goal representations may provide the substrates for the contextual integration within the TPJ in the absence of a specific task.



## Introduction

Sensorimotor control is an integral part of our daily life and the essential prerequisite to interact with one's environment, i.e. the internal and external milieu. Thus, the convergence and integration of both intero- and exteroceptive stimuli in the human brain is fundamental to allow for a comprehensive environmental picture (Berlucchi and Aglioti, 2010). In most functional neuroimaging experiments the selection of the adequate behavioral response is based on only a limited number of stimuli, i.e. the brain has to evaluate which stimuli are crucial to meet the task (Bays et al., 2010). This subset of bottom-up (sensory) input is subsequently weighted against top-down information such as contextual rules and goals. Fundamentally, top-down signals represent feedback from 'higher' (usually multimodal) brain regions to unimodal sensory or motor areas. Anatomically, such top-down feedback is implemented by diffuse connectivity into (primarily) dendritic terminals in cortical layers II–III, whereas bottom-up (feed-forward) connections primarily terminate in layer IV of a more circumscribed patch of the cortex. The result of this complex procedure consists of highly integrated data and constitutes the basis upon which the respective movements are planned. In the following, the term 'contextual integration' is used to denote the top-down modulation of sensorimotor processing by context-specific a-priori information. Context is here defined as any information affecting actions that is not provided by the given response stimulus itself but by the environment, ranging from explicit

* Corresponding author at: Institute for Neuroscience and Medicine, Research Center Jülich, Leo-Brandt Str. 5, D-52425 Jülich, Germany. Fax: +49 2461 61 2820.
*E-mail address:* S.Eickhoff@fz-juelich.de (S.B. Eickhoff).

1053-8119/$ – see front matter © 2012 Elsevier Inc. All rights reserved.
doi:10.1016/j.neuroimage.2012.02.037

instructions about stimulus–response mappings to implicit expectations extracted from regularities in the stimulation sequence. The first aim of our study was to identify regions that are consistently (i.e. across different studies) activated by context-dependent sensorimotor control.

So far, we have only considered task-induced integration processes. However, the human brain is assumed to operate along a continuum between task-related performance and 'mental rest', i.e. 'unconstrained' cognition (Schilbach et al., 2008). This presumption is in line with several studies (Fox and Raichle, 2007; Smith et al., 2009) demonstrating that 'physiological rest' does not equate 'mental rest'. Rather, it has been hypothesized (Schilbach et al., 2008) that the absence of an externally structured task entails a re-allocation of resources toward internally oriented, i.e. 'conceptual' (Binder et al., 1999), operations resulting in 'mind-wandering' (cf. Smallwood and Schooler, 2006). Thus, the second aim of our study was to assess the functional connectivity (FC) of the above-mentioned areas in both task-dependent and task-independent mental states. The third aim was to test for commonalities and differences in the FC pattern of these two fundamental states of brain function.

To date, a large number of functional neuroimaging studies have adopted task-based experimental designs to investigate the neural correlates of stimulus–response associations in humans (Egner, 2007) and non-human primates (Connolly et al., 2009). Despite the differences in experimental designs, several studies have provided consistent evidence for an implementation of these processes in a bilateral fronto-parietal network. In line with data from single-cell recordings in non-human primates (Gottlieb and Snyder, 2010), the inferior parietal lobe (IPL) and adjacent intraparietal sulcus are conceptualized to evaluate and integrate incoming sensory input from different modalities. In this context, Spence and Driver (2004) claimed that the posterior parietal cortex plays a critical role in mediating the integration of spatial aspects of multimodal stimuli (e.g. visual, auditory or tactile) and their transformation into action-based representations. This is well in line with the presumption of IPL/IPS acting as a heteromodal integrative 'hub' committed to multisensory processing (Gottlieb, 2007; Toni et al., 2002). Such multimodal integration processes, however, may not be restricted to the posterior parietal cortex. Rather, there is evidence that multi-modal integration is also supported by regions within the (pre-)frontal and temporal cortex (Calvert et al., 2004; Driver and Noesselt, 2008). In particular, contextual information from the (pre-)frontal cortex enriches these integrative processes and permits a bidirectional coupling between stimulus and contextual framework (Koechlin and Jubault, 2006). Moreover, the function of (pre-)frontal areas in the system of sensorimotor control also comprises the exertion of 'executive control' on the (pre-)motor system (Koechlin and Summerfield, 2007). In particular, these regions were found to be involved in rule-based adjustment of motor plans, movement timing and action monitoring. Finally, the (pre-)motor areas are thought to select, initiate and execute the adequate motor program based on highly integrated information from parietal and (pre-)frontal cortex (Picard and Strick, 1996; Rizzolatti et al., 1998). Sensorimotor control thus depends on the integration of cognitive aspects with the monitoring of the internal and external milieu and the selection of appropriate responses based on these information.

In this context, the question arises as to which regions are consistently activated during the implementation of sensorimotor control, i.e. the association of a given stimulus with an arbitrary (instructed) response. Three recently published functional neuroimaging studies (Cieslik et al., 2010; Eickhoff et al., 2011; Jakobs et al., 2009) applied variations of a manual two-choice reaction-time task with graduated levels of difficulty in stimulus–response mapping. Testing for neural effects of increasing demands on stimulus–response association in each study revealed a similar bilateral, though right-hemispherically dominant, fronto-parietal network. In order to statistically validate this prima facie evidence, i.e. to detect regions featuring a significant overlap across the abovementioned studies, we applied an image-based meta-analysis (IBMA) technique to investigate the multi-study conjunction of results. In this context, regions consistently activated across studies are assumed to implement higher-order processes in the cascade of stimulus–response association.

However, even the common evidence provided by three studies might still reflect design-specific effects to a degree that precludes broad generalizations about this fundamental network. Thus, in the second part of the current study, we used meta-analytic connectivity modeling (MACM) to delineate the FC pattern of higher-order sensorimotor regions (i.e. consistently activated clusters observed in the IBMA) in the presence of an externally structured task. The basic idea behind this approach is to assess which brain regions are co-activated above chance with particular seed regions in functional neuroimaging experiments. Here, we used the BrainMap database (Laird et al., 2009; www.brainmap.org) to identify co-activations with our seed regions (i.e. the results of the above-mentioned IBMA) across all studies listed in this database and subsequently performed an ALE (activation likelihood estimation) meta-analysis on these studies (Eickhoff et al., 2009; Laird et al., 2009).

As mentioned above, regions participating in stimulus–context integration are also engaged in task-free brain states. Thus, it may be speculated that a shared procedure is based upon a subset of regions, which are activated irrespective of the current mental state. To test this hypothesis, we investigated 'resting-state' FC using functional imaging data from 100 healthy volunteers. The time-series of each seed region was cross-correlated with the time-series of all other gray-matter voxels in the brain. Consistent functional coupling across mental states (i.e. overlap of regions co-activated across studies with our seed and regions with significant intrinsic connectivity to our seed) would indicate that the seed and target regions participate in very much the same networks during task-dependent stimulus–context integration and task-free, unstructured processing. In contrast, divergent results would delineate networks that depend on the mental state and thus allow for a differentiation of internally and externally driven FC networks (Eickhoff and Grefkes, 2011).

## Material and methods

### *Image-based meta-analysis*

We performed an IBMA by multi-study conjunction over three recently published fMRI studies (Cieslik et al., 2010; Eickhoff et al., 2011; Jakobs et al., 2009). Regions consistently activated by higher demands on sensorimotor integration were identified by first computing the respective contrasts in each study, thresholded at $p<0.05$ (cluster-level FWE-corrected; cluster-forming threshold at voxel-level $p<0.001$; Worsley et al., 1996). In particular, the minimal number of voxels required to meet the threshold criterion ranged from 305 to 315 voxels [voxel size 1.5 $mm^3$ isotropic; Jakobs et al., 2009: 308 voxels; Cieslik et al., 2010: 305 voxels; Eickhoff et al., 2011: 315 voxels]. Hence, the comparability across studies was ensured by enclosing similar numbers of subjects and applying the same preprocessing algorithms. Regions consistently engaged (across studies) by increasing demands for stimulus–context integration in sensorimotor control were then identified by means of conjunction analysis. Subsequently, all findings were anatomically localized using version 1.5 of the SPM Anatomy toolbox (www.fz-juelich.de/ime/spm_anatomy_toolbox, Eickhoff et al., 2005, 2006c, 2007).

Each of the three included studies applied a manual reaction-time task requiring participants to respond as fast and correctly as possible to visually presented stimuli by pressing a button with either their left or right index finger.

In the first study (Cieslik et al., 2010), 24 participants were instructed to react to lateralized stimuli (red dots) briefly presented

(200 ms) in a randomized order. Before each task block, participants were instructed to respond with either the corresponding (spatially congruent response) or the contralateral (spatially incongruent response) index finger. Activation related to increased integration demands was then assessed by contrasting incongruent with congruent trials independently of the stimulus- or response-side.

In the second study (Jakobs et al., 2009), 26 participants responded to centrally presented visual stimuli (arrows), which were either pointing uniformly to one side or in a randomized order to either side (random hands condition; 50% chance for each side) with the corresponding index finger. Increasing demands on stimulus–context integration were delineated by contrasting random hands with unilateral conditions.

In the third study (Eickhoff et al., 2011), left- or right-pointing arrows were centrally presented to 20 participants. This time, however, arrow direction was non-uniformly distributed, with 80% pointing to one side. This laterality bias was randomly varied between blocks of trials. Moreover, in some blocks this bias was covertly reversed in the middle of the block. Increased integration demands were assessed by testing for activity that was parametrically related to the acquisition and adaptation of response biases in line with the probabilistic structure of the stimuli.

The respective contrasts reflecting increased demands for stimulus–context integration in sensorimotor control were thresholded at a cluster-level FWE-corrected $p<0.05$. The ensuing activation maps were then subjected to a conjunction analysis, i.e. we performed the conjunction against the (conservative) conjunction null hypothesis using the minimum statistic (Nichols et al., 2005). In practice, this was implemented by first applying a voxel-level cluster-forming threshold to all three analyses. Subsequently, each of the three excursion sets was filtered for cluster extent to threshold at cluster-level FWE-corrected $p<0.05$ (cluster-forming threshold at voxel-level $p<0.001$, i.e., $T>3.09$). Finally, we computed the intersection between the three thresholded and filtered SPM{T}-maps. This procedure exactly conforms to the conjunction-null minimum statistic, as the intersection only becomes non-zero (and hence significant) if each of the three individual analyses was significant. This IBMA provided four regions of overlapping activation. The right TPJ showed a cluster size of 104 voxels. Additionally, we observed three smaller clusters (right IPS, bilateral dPMC) with an average cluster size just over 20 voxels. Given this dramatic difference in cluster extent, we decided to exclude these considerably smaller regions and focus our analysis on the predominant finding, which survived conservative thresholding. Hence, the only region of spatially extended overlap between significant activation in all three individual analyses (i.e. the right TPJ) represented the seed for the subsequent connectivity modeling.

*Task-based FC: meta-analytic connectivity modeling*

FC of the seed(s) during the performance of structured tasks was defined by delineating the co-activation pattern of the seed based on the activations reported in published functional imaging results. The concept behind this approach is predicated on the notion that FC is reflected in the correlation of activity in spatially distinct brain regions. That is, regions that are functionally connected should co-activate above chance in functional neuroimaging studies and vice versa. In this context, it should be noted that there are major conceptual differences between anatomical, functional and effective connectivity: (1) Anatomical connectivity denotes the presence of fiber connections linking two areas in the brain, i.e. the existence of a structural connection between their neurons. In contrast, (2) FC is correlative in nature, i.e. solely based on the likelihood of observing activation in a target region, given that activation is present within the seed area. In MACM, as performed in the current study, the unit of observation is not a specific point in an acquired time series but a particular neuroimaging experiment. MACM thus extends the scale on which FC is evaluated beyond data points in a time series (single study) to a whole set of neuroimaging experiments (MACM across studies). Here, FC is expressed as coherent activation across experiments and should delineate networks that are conjointly recruited by a broad range of tasks. Finally, (3) effective connectivity is defined as the causal influence one area exerts over another and may be tested with approaches such as dynamic causal modeling or structural equation modeling.

Here, analysis of task-based FC was performed by MACM using the BrainMap database (Laird et al., 2009, www.brainmap.org). This database contained, at the time of analysis, the location of reported activation foci and associated meta-data of approximately 10,000 neuroimaging experiments. Of these, only fMRI studies that reported functional mapping data from healthy participants were considered. Studies investigating age, gender, disease, or drug effects were excluded. No further constraints (e.g., on acquisition or analysis details, experimental design, or stimulation procedures) were applied. Comparability with respect to the location of significant activation was ensured given the high standardization in the publication of neuroimaging data, i.e. the ubiquitous adherence to standard coordinate systems, such that all experiments contained in the database refer to activation coordinates within the same standard space. Using this broad pool of neuroimaging results, MACM can then be used to test for associations between activation probabilities of different areas. Importantly, this inference is performed independently of the paradigms used or other experimental factors but rather is solely based on the likelihood of observing activation in a target region given that activation is present within the seed area. This completely data-driven approach thus avoids selection biases that may result from adhering to current cognitive ontologies, which might not always overlap with the organizational modes of brain function.

In practice, MACM was performed in two steps: First, we identified all experiments in the BrainMap database that featured at least one focus of activation within the volume of the respective seed region (i.e. the cluster obtained from the IBMA). Second, quantitative meta-analysis (see below) was employed to test for the across-study convergence of the activity foci reported in these experiments. As all experiments entering this analysis were selected by the fact that they feature activation in the seed, highest convergence will be observed in the seed region. Significant convergence of other activity foci, however, indicates consistent co-activation, i.e., task-based FC with the seed. Thus, it has to be noted that the FC pattern as observed in the MACM analysis is not specific to a distinct task or paradigm but rather reflects regional coupling that is present across a broad range of different tasks and paradigms.

For the meta-analysis in the second step, the revised version of the activation likelihood estimation (ALE) approach was used (Eickhoff et al., 2009; Laird et al., 2009). This algorithm aims at identifying areas where the convergence of activations across different experiments is higher than expected under conditions of random spatial associations between them. The key idea behind ALE is to treat reported activation foci not as points but centers of 3-D Gaussian probability distributions reflecting the associated spatial uncertainty. For each experiment included, the probability distributions of all reported foci are combined into a modeled activation (MA) map (Turkeltaub et al., 2012). Taking the union across these MA maps for all experiments yielded voxel-wise ALE scores describing the convergence of results at each particular location of the brain. To distinguish 'true' convergence across studies from random convergence (i.e. noise), ALE scores are compared to an empirical null distribution reflecting a random spatial association between experiments (Eickhoff et al., 2011). Hereby, a random-effects inference is invoked, focusing on the above-chance convergence between studies, not the clustering of foci within a particular study. The p-value of an observed ALE score is given by the proportion of equal or higher values obtained

under the null distribution. The ALE maps, reflecting the across-study convergence of co-activations with the seed region, were thresholded at cluster level–corrected $p<0.05$ (cluster-forming threshold: $p<0.001$ at voxel level) and converted to Z-scores for visualization.

*Task-independent connectivity: resting-state correlations*

Resting-state fMRI images were acquired in 100 healthy volunteers (50 females, mean age 45.2 years) without any record of neurological or psychiatric disorders. All participants gave written informed consent to the study protocol, which had been approved by the local ethics committee of the University of Bonn. Before the imaging session, participants were instructed to keep their eyes closed and just let their mind wander without thinking of anything in particular but not to fall asleep (which was confirmed in post-scan debriefing). For each participant, 300 resting-state EPI images were acquired using blood-oxygen-level-dependent (BOLD) contrast [gradient-echo EPI pulse sequence, TR = 2.2 s, TE = 30 ms, flip angle = 90°, in-plane resolution = 3.1×3.1 $mm^2$, 36 axial slices (3.1 mm thickness) covering the entire brain].

The first four scans served as dummy images allowing for magnetic field saturation and were discarded prior to further processing using SPM8 (www.fil.ion.ucl.ac.uk/spm). The EPI images were first corrected for head movements by affine registration using a two-pass procedure in which the images were first aligned to the initial volumes and subsequently to the mean of all volumes after the first pass. The mean EPI image for each participant was then spatially normalized to the MNI single-subject template (Holmes et al., 1998) using the 'unified segmentation' approach (Ashburner and Friston, 2005), and the ensuing deformation was applied to the individual EPI volumes. Finally, images were smoothed by a 5-mm FWHM Gaussian kernel to improve signal-to-noise ratio and compensate for residual anatomical variations.

The time-series data of each voxel were processed as follows (cf. Fox et al., 2009; Weissenbacher et al., 2009): In order to reduce spurious correlations, variance that could be explained by the following nuisance variables was removed: (i) The six motion parameters derived from the image realignment; (ii) the first derivative of the realignment parameters; (iii) mean gray matter, white matter and CSF signal per time-point as obtained by averaging across voxels attributed to the respective tissue class in the SPM 8 segmentation; and (iv) coherent signal changes across the whole brain as reflected by the first five components of a principal component analysis (PCA) decomposition of the whole-brain time-series. All of these nuisance variables entered the model as first-order and – except for the PCA components – also as second-order terms. We note that the above approach, in particular the removal of variance related to the most dominant signal components, may remove some signal of interest but should increase specificity of the ensuing results (Bellec et al., 2006; Fox and Raichle, 2007). Data was then band-pass filtered preserving frequencies between 0.01 and 0.08 Hz, since meaningful resting-state correlations will predominantly be found in t frequency range, given that the BOLD response acts as a low-pass filter (Biswal et al., 1995; Fox and Raichle, 2007; Greicius et al., 2003).

As for the MACM analysis, seed regions of interest were provided by the clusters obtained from the IBMA. Time-courses were extracted for all voxels within the particular cluster that were located in the gray matter of the individual participant as indicated by a segmentation of the individual EPI image (Ashburner and Friston, 2005). Of the 104 voxels in the right TPJ cluster, the number of voxels more likely representing gray matter than any other tissue class was on average (across subjects) 90.7 (SD = 10.6; range: 71–104). The time course of the seed region was then expressed as the first eigenvariate of the individual voxels. Linear (Pearson) correlation coefficients between the time series of the seed regions (clusters obtained from the IBMA) and all other gray-matter voxels in the brain were computed to quantify resting-state FC. These voxel-wise correlation coefficients were then transformed into Fisher's Z-scores and tested for consistency by a one-sample *T*-test across subjects. The results of this random-effects analysis were then thresholded at a cluster level–corrected threshold of $p<0.05$ (cluster–forming threshold: $p<0.001$ at voxel-level).

*Conjunction and differences between MACM and resting-state FC*

In order to delineate areas showing task-dependent and task-independent FC with the seed region(s) obtained from the IBMA, we performed a conjunction analysis between the MACM and resting-state analyses using the strict minimum statistic (Nichols et al., 2005). That is, for each seed region, we identified those voxels that showed significant FC with this seed in the analysis of interactions in the task-dependent as well as in the analysis of interactions in the task-independent state. In practice such consistent connectivity was delineated by computing the intersection of the (cluster-level FWE-corrected) connectivity maps from the two analyses detailed above.

Comparison between task-dependent and task-independent FC was performed by computing the voxel-wise contrast between the Z-scores obtained from the MACM and resting-state analyses. Difference Z-scores were deemed significant if they corresponded to $p<0.001$. Finally, results from the difference analysis were masked with the respective main effect, that is, voxels showing stronger connectivity in MACM vs. resting-state analyses were only retained if they indeed showed a significant task-driven connectivity with the seed (as revealed by the MACM analysis).

## Results

*Image-based meta-analysis*

In each of the three included studies, increased demands on sensorimotor control recruited a widespread bilateral though right-dominant fronto-parietal network (Figs. 1A–C). The IBMA then indicated four regions of overlapping activation. Among these, a cluster in the right TPJ represented the most extensive region of overlap with a cluster size of 104 voxels. Additionally, we observed three considerably smaller clusters (right IPS, bilateral dPMC) with an average cluster size just over 20 voxels. Given this clear difference in cluster extent, we decided to focus the subsequent connectivity analyses on the predominant cluster found in the right TPJ (Fig. 1D). Thus, the right TPJ (area PFm, Caspers et al., 2006, 2008; MNI peak coordinates: 58/−46/27 [cluster-size: 104 voxels/351 $mm^3$], see Supplementary Fig. S1) was used as the sole seed region for the analysis of task-depended and task-independent FC via MACM and resting-state correlations.

*FC analysis by coordinate-based meta-analysis (MACM)*

In addition to the 'shared' network as described below, task-dependent FC (Fig. 2B1), as revealed by MACM, involved the bilateral pre-supplementary motor area (pre-SMA, area 6, Geyer, 2004), ventral and dorsal premotor cortex (vPMC/dMPC, area 6, Geyer, 2004), and the thalamus. Furthermore, left-hemispheric putamen, (vPMC), M1 (area 4p; Geyer et al., 1996), and S1 (areas 3b, 3a, 2; Geyer et al., 1999, 2000; Grefkes et al., 2001) as well as right-hemispheric pallidum and caudate nucleus revealed significant co-activation. Co-activations were also found in the region of the right areas 44/45 (Amunts et al., 1999) and bilateral anterior intraparietal sulcus (hIP2; Choi et al., 2006) extending into the superior (area 7PC, Scheperjans et al., 2008a,b) and inferior (area PFcm, Caspers et al., 2006, 2008) parietal lobe. When assessing the paradigm classes of

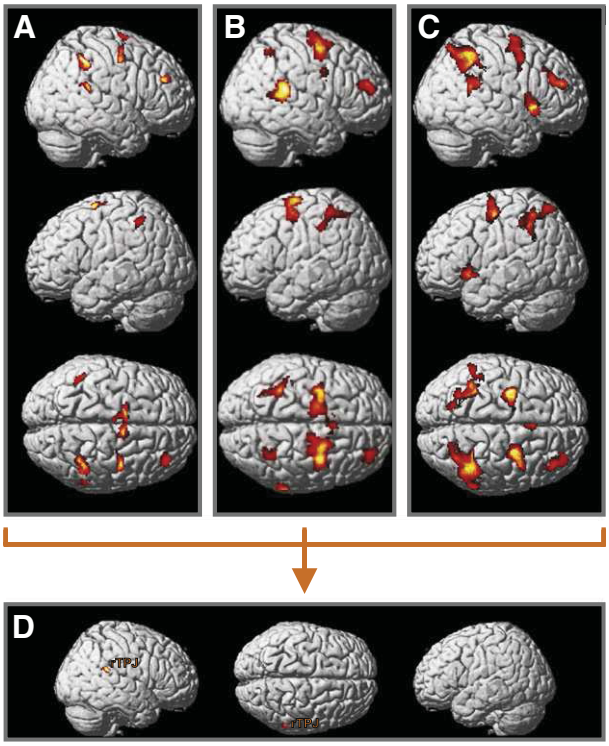


**Fig. 1.** In three recently published neuroimaging studies (A: Eickhoff et al., 2011, B: Jakobs et al., 2009, C: Cieslik et al., 2010), we applied variations of a manual two-choice reaction time task to investigate neural correlates of increasing demands on sensorimotor top-down control. In each of these studies, we observed activation of a similar bilateral, though right-hemispheric dominant fronto-parietal network. Significant activations are projected onto rendered surfaces of the MNI single-subject template brain. The subsequent image-based meta-analysis revealed a single focus of convergent activation in the right temporo-parietal junction (D) which was thus used as the seed region for the analysis of functional connectivity.

those experiments that featured activation in the right TPJ seed and hence contributed to the MACM analysis, we observed that several different kinds of paradigms/tasks were associated with right TPJ activation (see Supplementary Fig. S2). A strong predominance of any particular kind of task, however, was not found, with strong contributions of somatosensory, visual, cognitive, and motor tasks.

*FC analysis of resting-state imaging data*

In the resting state (Fig. 2B2), reflecting rTPJ connectivity in the absence of a structured task, we observed, in addition to the shared network described below, significant correlations with the dorsolateral prefrontal cortex (DLPFC), insula (Id1, Kurth et al., 2010b), middle cingulate cortex (Palomero-Gallagher et al., 2008, 2009) and inferior/superior parietal lobe. Additional left-hemispheric correlation was found with the operculum (OP1, OP4; Eickhoff et al., 2006a,b), cerebellum (lobule VII, crus I & II; Diedrichsen et al., 2009), dPMC, precuneus, and temporal pole, whereas additional right-hemispheric correlation occurred with area 45 (Amunts et al., 1999) and inferior temporal gyrus.

*Conjunction across MACM and resting-state FC analyses*

The conjunction (Fig. 2C) across both individual FC analyses (Figs. 2B1 & B2) revealed a shared network comprising bilaterally the inferior parietal cortex (areas PF, PFm) extending into the TPJ, inferior frontal area 44, the anterior dorsal insula and the SMA (area 6, Geyer, 2004). Right-hemispheric activation was observed in the dPMC and middle cingulate cortex, the posterior DLPFC (cf. Rottschy et al., 2012), the middle temporal gyrus, putamen and OP 4. Activation restricted to the left hemisphere was only found in the cerebellum (lobule VI). In summary, in both task-dependent and task-free states, the right TPJ entertains close FC with a bilateral, though right-dominant network resembling the 'ventral action-control/attention network' as described by Corbetta and Shulman (2002).

*Difference between MACM and resting-state FC analyses*

Fig. 2A1 illustrates the pattern of FC that was specific for the task-dependent state as revealed by the contrast of 'MACM > resting state connectivity' (see also Supplementary Table S1). We observed significantly stronger task-dependent FC of the right TPJ with the medial premotor cortex (SMA/pre-SMA), bilateral area 44, dPMC, intraparietal sulcus/superior parietal lobe (7A, 7PC, hIP3), and thalamus as well as left-hemispheric regions of more pronounced connectivity with vPMC, putamen, insula lobe, and cerebellum (lobule VI). In the right hemisphere, V5 (hOC5, Malikovic et al., 2007) featured stronger task-dependent than task-independent FC with the right TPJ.

The reversed contrast ('resting state > MACM connectivity', Fig. 2A2) revealed areas featuring stronger FC with the seed in the task-free resting state (see also Supplementary Table S1). Such a pattern was significantly seen bilaterally in the medial superior parietal lobe (5 Ci, 7A, 5 M, Scheperjans et al., 2005), dorsolateral prefrontal cortex, and anterior/middle cingulate cortex.

## Discussion

We demonstrated that across three studies, increased demand on stimulus–context integration in sensorimotor control was consistently associated with increased activation of the right TPJ (Fig. 1D, see also Fig. S1). Subsequently, whole-brain functional connectivity of this region was delineated via meta-analytic connectivity modeling (task-dependent FC) and analysis of resting-state images from 100 healthy volunteers (task-independent FC).

Convergent functional coupling across approaches, i.e. independent of the presence or absence of an externally structured task, was observed in a shared network with right-hemispheric dominance. Herein, the inferior parietal cortex, area 44, anterior dorsal insula, and SMA (Fig. 2C) were found bilaterally. Dorsal premotor cortex, middle temporal gyrus, middle cingulate cortex, putamen, and parietal opercular area OP4 of the right hemisphere as well as the left-hemispheric cerebellum featured unilateral convergent functional coupling with the right TPJ.

Stronger task-independent FC with the seed ('resting state > MACM connectivity', Fig. 2A2, Table S1) was observed bilaterally in the medial superior parietal lobe (precuneus) and adjacent posterior cingulate cortex, dorsolateral prefrontal cortex, and anterior/middle cingulate cortex.

The reversed contrast, i.e. FC specific for the task-dependent state ('MACM connectivity > resting state', Fig. 2A1, Table S1), revealed significantly stronger coupling of the right TPJ with bilateral premotor regions (SMA/pre-SMA, dPMC), area 44, superior parietal cortex, and thalamus. In addition, we observed differential co-activation with left-hemispheric vPMC, insula, putamen, and cerebellum (lobule VI) as well as with V5 (hOC5) in the right hemisphere.

*Concepts of functional connectivity*

FC is defined as the 'temporal coincidence of spatially distant neuro-physiological events' and may be assessed with cross-correlation of, e.g., spiking patterns or field potentials in neurophysiological experiments (Schlögl and Supp, 2006). Currently, however, most FC analyses are based on (resting-state) fMRI. In their seminal study, Biswal et al. (1995) cross-correlated the time courses of resting-state fMRI signals from different brain regions, noting that FC may be inferred from significant correlation in the signal fluctuations

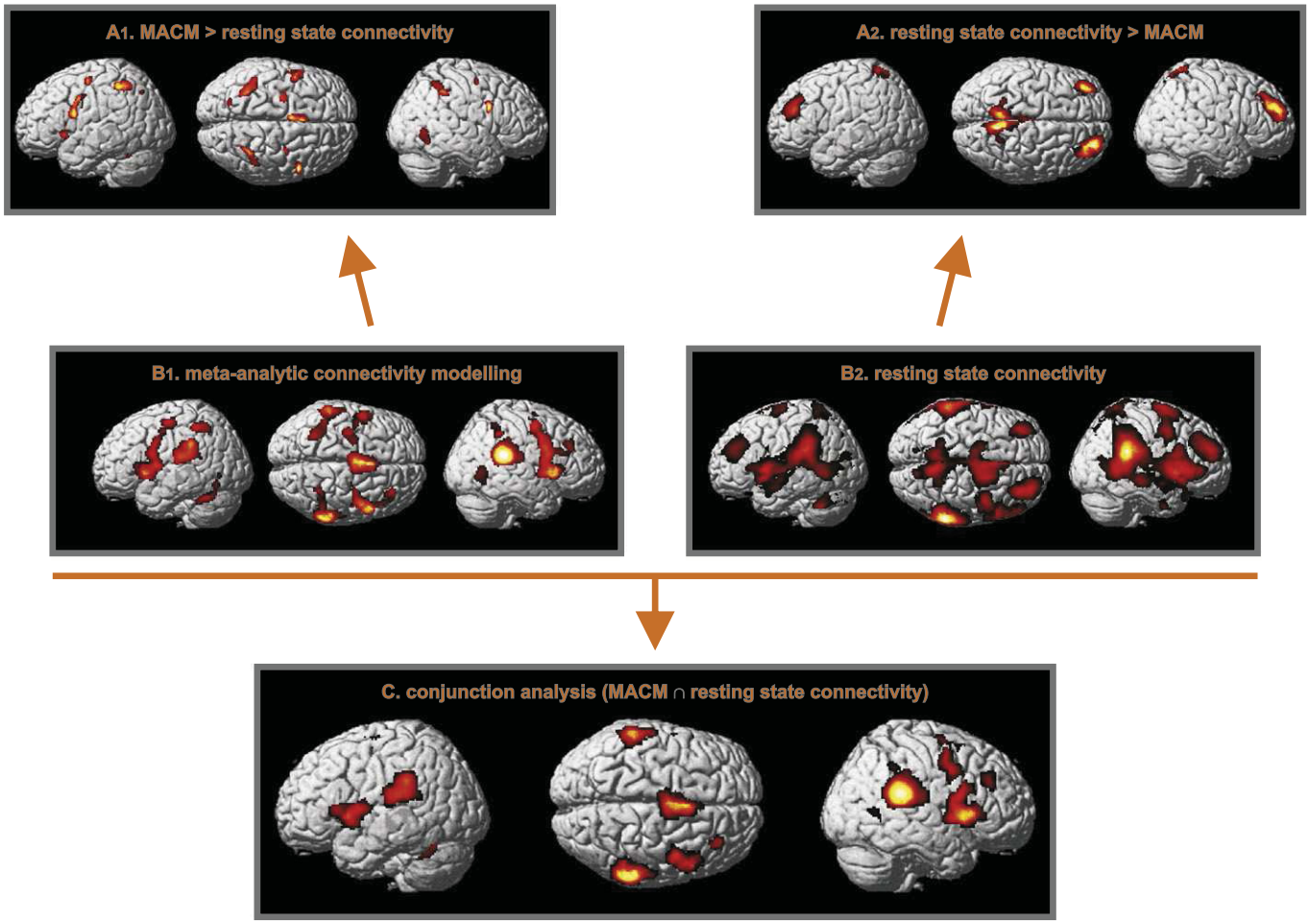


**Fig. 2.** The conjunction analysis (C) across task-dependent connectivity (MACM, B1) and that obtained for the task-free state (B2) revealed a shared network comprising bilateral inferior parietal cortex, area 44, insula, and supplementary motor area (SMA), right premotor and middle cingulate cortex, middle temporal gyrus, putamen, and OP4 as well as the left cerebellum. In both task-driven and task-free states, the right TPJ thus entertains close functional connectivity with a bilateral though right-dominant 'ventral' action-control/attention network (Corbetta and Shulman, 2002). Functional connectivity specific for the task-dependent mental state (A1) additionally involved bilateral (pre-)SMA, dorsal premotor cortex, area 44, intraparietal sulcus, and thalamus, left basal ganglia and vPMC as well as right V5. Conversely, in the resting-state analysis (A2), reflecting TPJ connectivity in the absence of a structured task, we observed selectively increased connectivity with bilateral dorsolateral prefrontal cortex, medial superior parietal cortex (precuneus), and anterior/middle cingulate cortex.

across distant brain regions. Here, we assessed correlation (across scans, i.e., time) between the BOLD-signal time course of the right TPJ and time courses of all other locations in the brain. Using this approach, we aimed at identifying regions that are significantly (functionally) coupled with the seed region in the task-independent state.

Large-scale databases such as BrainMap (Laird et al., 2009, www.brainmap.org) and algorithms for meta-analytic connectivity modeling (MACM; Laird et al., 2009; Eickhoff et al., 2009) constitute the basis for comprehensive task-based FC analyses: MACM is based on the idea of assessing which brain regions co-activate above chance with the seed across a large range of functional tasks. In contrast to the more traditional definition of FC as coherent fluctuations across time, in MACM, the unit of observation is the neuroimaging experiment. The strength of MACM is the delineation of networks that are conjointly recruited across a broad range of tasks, reflecting robust patterns of coordinated activity in response to an externally structured task.

These two approaches hence provide complementary methods of investigating FC: Task-independent FC was assessed by correlating resting-state fMRI time-series, while task-dependent FC was revealed by investigating significant co-activations of the seed region across different neuroimaging experiments (Eickhoff and Grefkes, 2011). Together, these allow a comprehensive assessment of the FC of the right TPJ across fundamentally different mental states.

*Right TPJ in and beyond stimulus–context integration*

In the present study, we defined the location of a seed region in the right TPJ based on a multi-study conjunction of experiments on stimulus–context integration and then assessed its co-activation patterns across a wide range of tasks as well as resting-state BOLD signal correlations. Therefore, the FC analyses did not pertain specifically to stimulus–context integration but rather provided an across-task and a no-task assessment of the interactions of the seed (Eickhoff and Grefkes, 2011). That is, our results reflect general interactions of the seed region, not those specific to stimulus–context integration. Nevertheless, the approach taken to identify the seed has important implications for the interpretation of our connectivity data, as a rather broadly defined macroanatomical region like the TPJ may contain several different functional modules. That is, different areas within a region like the TPJ may hold different functions and hence potentially also connectivity patterns. In fact, when considering the current literature on the TPJ, it may be noted that this region is not only implicated in action control and stimulus–context integration but also in several other tasks, some of which seem to hold psychological similarities (e.g. stimulus-driven attention, visual search; Corbetta and Shulman, 2002; Mavritsaki et al., 2010; Menon et al., 2001), while others appear completely unrelated (e.g. social cognition, mentalizing, perspective taking; Decety and Lamm, 2007; David et al., 2008;

Vogeley et al., 2001). There is thus good evidence for a functional heterogeneity within the TPJ. Given this very likely differentiation, we would argue that the tasks used to define a seed should have an important influence on the subsequent connectivity analyses even though these consider across-task and no-task interactions. To illustrate this point, it may be assumed that a seed in the right TPJ defined by a conjunction across social-cognition tasks would have had a different location within this region and most likely also a different pattern of MACM and resting-state connectivity. While our approach hence does not definitively associate a brain region and its connectivity to a particular cognitive function such as stimulus–context integration, the functional context established by the definition of the seed nevertheless provides its precise allocation to a (functional) module and hence an important constraint to the interpretation of the observed connectivity patterns. This holds in particular for regions that are as broadly defined and functionally heterogeneous as the TPJ.

*Right TPJ and the concept of predictive coding*

The performed multi-study conjunction indicated that the right TPJ (area PFm) as the most extensive region of overlap between three neuroimaging contrasts probing increased demands for sensorimotor control and stimulus–response integration. Previous studies point to a key role of this region also in other 'higher cognitive functions', such as attention (Corbetta and Shulman, 2002) or visuomotor integration (Mooshagian et al., 2008). This raises the question as to how these operations can be integrated in a comprehensive theoretical construct.

Predictive coding (Rao and Ballard, 1999; Summerfield and Mangels, 2006; Kilner et al., 2007a) is a hypothesis on the fundamental nature of neuronal information processing. Within this model the brain is conceptualized as a Bayesian machine, i.e. perception is based upon generative models enabling probabilistic inference on sensory inputs and the underlying causes. This is enabled by a hierarchical organization of brain regions with reciprocal connections between them. The prediction error, i.e. the difference between sensory input and internal prediction, is computed at each level and passed to higher levels via forward connections. Its size reflects the accuracy of the predictions and potential necessity for adjustment. Feedback connections pass predictions back to the lower level. The objective of these computations is the (unconscious and highly automated) minimization of the environmental entropy (i.e. average uncertainty) to optimize predictions about incoming information. So far, evidence for predictive coding has mainly been discussed in the context of sensory paradigms (Behrens et al., 2007; Summerfield and Mangels, 2006). However, observations of faster reaction times and reduced error rates for predominant relative to deviant cues have raised the notion of predictive motor coding. Mechanistically, predictions about prospective sensory input should entail the a priori preparation of an adequate motor program. If an upcoming stimulus matches the prediction, the prepared motor program simply has to be released, instead of being chosen de novo from the motor repertoire, resulting in more efficient reactions.

As each of the three studies used to define the seed region presented lateralized visual stimuli and required lateralized responses, it may be argued that the observed effects may be attributable to increased attention and spatial (re-)orientation (Corbetta and Shulman, 2002; Thiel et al., 2004). In particular, stimuli appeared more frequently in the unexpected (and hence unattended; Shulman et al., 2009) location in 'high-demand' conditions. This is well in line with a study of Downar et al. (2000) observing an involvement of (predominantly) the right TPJ in multimodal change detection, i.e. detection of 'salient' stimuli. We would argue that these interpretations (re-orientation or attentional demands) may be reconciled with predictive coding concepts. Under this theoretical framework, stimulus-driven re-orienting may be understood as the upstream effects of high prediction errors, which trigger a reactive orientation toward the site of the unpredicted stimulus. In a Bayesian system of sensory inference, attention may thus be conceptualized as inference on the precision of predictions (Feldman and Friston, 2010). If a prediction error is high, attentional re-orientation is instantiated.

Lesions of (especially) the right (Vallar et al., 1993) TPJ have been conjectured to clinically manifest themselves as a lack of awareness of space on the contralesional side of the body, i.e., neglect (Mavritsaki et al., 2010). In accordance with the theoretical framework outlined above, a unilateral deficit in evaluating upstreaming stimuli may result in persistent 'attention' to only one (i.e. the ipsilesional) side of the environment. However, Karnath et al. (2001) emphasized that 'the superior temporal cortex rather than the IPL or TPO junction is the substrate of spatial neglect in both monkeys and humans' (p. 952). Thus, the putative involvement of (r)TPJ lesions in neglect is still a matter of debate.

In summary, based on the assumption that probabilistic inference is an integral part of sensory processing and motor preparation, the concept of predictive coding may provide a theoretical framework for the computational processes underlying stimulus–response integration for sensorimotor control. Based on the current multi-study conjunction we would argue that the right TPJ might be a key structure for implementing attentional (re-)orientation by inference on prediction errors within this framework.

*Core network of consistent functional connectivity*

The term 'core network' denotes regions featuring convergent functional coupling with the right TPJ in the task-driven and endogenously controlled state (Fig. 2C). Its nodes are thus part of very much the same networks as the seed irrespective of the current mental state. In this context, it has to be noted that close resemblance between 'resting-state networks' and those jointly engaged in task-based studies has been reported and hence the notion of 'rest' in the absence of a specific task has evolved into a concept of an unconstrained sampling of different brain networks with preponderance for introspective aspects (Raichle et al., 2001; Schilbach et al., 2008; Smith et al., 2009).

The human insula (most notably the anterior dorsal portion) activates in a broad range of tasks across diverse functional domains, such as emotion processing, interoception, (working) memory and attention (Craig, 2009; Kurth et al., 2010a). Thus, the insula is regarded as integration area, mediating dynamic information flow between large-scale brain networks (Dosenbach et al., 2006; Menon and Uddin, 2010) as well as providing a link between the processing of external information and monitoring the internal milieu (Craig, 2009). In the current study, consistent co-activation of the anterior dorsal insula may therefore originate from its function as an integrative hub controlling the flow of information and implementing task-sets, i.e., high-level priors.

Several neuroimaging studies provide evidence for a role of the inferior parietal cortex (IPL) in the multi-modal integration of stimuli (Renier et al., 2009) as well as movement planning and execution (Iacoboni, 2006). The FC with the (right) TPJ reflects the dense anatomical connectivity between these (Lewis and Van Essen, 2000). Most likely, the IPL might implement the planning, selection and preparation of movement routines that is controlled by the predictions (and associated errors) provided by the right TPJ.

It should be noted that this 'core network' (right TPJ, anterior insula, IPL) resembles the so-called 'ventral attention network' (Corbetta and Shulman, 2002), typically activated during the detection of salient and behaviorally relevant stimuli, i.e. stimulus-driven reorienting, and acting as a 'circuit breaker' for ongoing processes in the dorsal attention network (Corbetta et al., 2008). The close similarity between the 'core network' and the 'ventral attention network'

thus fits well with the Bayesian framework of stimulus-driven reorienting as outlined above. In line with the FC data provided by Fox et al. (2006) we would thus argue for an important role of the TPJ within the ventral attention network, potentially reflecting a computational core in a predictive coding system.

*Stronger couplings in the task-dependent state*

In a system of Bayesian inference, minimization of prediction errors requires the supply with bottom-up (sensory) information. In this context, bilateral activation of the thalamus may be reconciled with its putative function as 'input gate' routing upstreaming information to sensorimotor and association cortices (Johansen-Berg et al., 2005) with collaterals to the TPJ as a predictive integrator. This interpretation may particularly hold for the right hemisphere where activation in the thalamus was observed in those parts that were shown to connect to the temporal cortex (including the TPJ) (Behrens et al., 2003). On the left hemisphere, in contrast, predominant activation in regions projecting to the prefrontal cortex (probably mediodorsal nucleus) may reflect the role of the thalamus as a cortico-cortical integration hub (Cappe et al., 2009), such as the possible involvement of the mediodorsal thalamus in sending prospective motor information to the DLPFC (Watanabe and Funahashi, 2012).

Regions of the posterior parietal cortex, in particular the superior parietal lobe and intraparietal sulcus (SPL/IPS), are involved in stimulus–context integration and stimulus–response matching (Wolfensteller and von Cramon, 2010). Thus, functional coupling with these regions may indicate pre-processing of incoming information by these, i.e. 'outsourcing' of lower-level integration processes. In other words, there may be parallel processing of the stimuli themselves (in the SPL/IPS) and their match with current predictive codes (in the right TPJ), allowing inference on both stimuli and predictions. Formally, this would entail a functional hierarchy between the SPL/IPS and the higher-level right TPJ.

Subsequently, the frontal areas may utilize this prediction to adjust behavioral plans and goals (Koechlin and Summerfield, 2007), linking predictive coding on sensory information with predictive motor coding. In the current study, bilateral co-activation of area 44 may indicate this region as an important node for the 'action' stream, which is consistent with previous evidence implicating this region in behavioral planning and executive top-down influences on premotor areas (Koechlin and Jubault, 2006). The coupling between the right TPJ and area 44 may hence correspond to an alignment between predictions and the preparation of adequate behavioral responses. Such response patterns may be pre-selected and hence prepared in the likewise co-activated premotor areas, i.e., the dPMC and the pre-SMA. While FC analyses may not reveal the directionality of interactions, based on previous evidence we would propose the following relationship between these regions: Whereas area 44 provides the link between the sensory and motor domain, the pre-SMA may subsequently control the implementation of motor preparation in the dPMC. This view would be in line with observations that the pre-SMA is involved in executive motor control, e.g., modifications of movement plans by inhibition or switching of responses (Picard and Strick, 1996). In contrast, the dPMC features close interactions with the motor output system (Chouinard and Paus, 2006; Dum and Strick, 2005) and therefore is a putative recipient of the generated motor plans. In the proposed model, the dPMC would thus constitute the lowest stage of the motor stream, implementing the actual preparation of motor responses.

In summary, we thus propose that the task-based FC data, in synopsis with previous evidence from humans and non-human primates, may indicate interaction of the right TPJ with a 'sensory stream' of predictive coding consisting of the thalamus as the sensory gateway and the SPL/IPS for stimulus processing on one hand as well as with a 'motor stream' comprising area 44, pre-SMA and dPMC, itself potentially organized in a hierarchical fashion reflecting a progression from more abstract motor plans to the preparation of a particular action (i.e. the specification of free parameters in motor commands, such as direction, extent and force of a given movement).

*Stronger couplings in the task-independent state*

Patterns of neural activation in the absence of an externally structured task reflect the brain's 'physiological baseline' (Gusnard and Raichle, 2001) but may not be equated with 'mental rest' due to the high spatio-temporal structuring of ongoing activity that seems to reflect task-relevant networks (cf. Fox and Raichle, 2007; Smith et al., 2009). Rather than being at rest, the brain should thus be in a state of unconstrained cognition (Schilbach et al., 2008), i.e. implementing a broad variety of (predominantly internally oriented) operations. In the current study, we observed increased connectivity of the right TPJ in this task-independent (compared to stimulus-driven) brain state with a bilateral network comprising the anterior cingulate and dorsolateral prefrontal cortices as well as the precuneus and adjacent posterior cingulate cortex (PrC/PPC).

Interestingly, medial parietal and cingulate cortices were reported to show highest levels of glucose consumption in the endogenously controlled state (Gusnard and Raichle, 2001) and de-activate upon commencement of structured tasks (Schilbach et al., 2008), supporting the notion of a 'default-mode network'. Nevertheless, activity within these regions is not restricted to the 'physiological baseline'. Rather, they have been observed in a broad range of internally directed cognitive tasks including episodic memory and first-person perspective taking (Vogeley et al., 2001) as well as the processing of self-relevant information and intentions, including intentions to act (cf. Cavanna and Trimble, 2006). It may hence be assumed that in the mode of unconstrained cognition these midline regions may gather and integrate information about past self-referential events. Hereby, they could provide personal experience as an important backdrop for mental operations in the absence of externally structured tasks or sensory information. In contrast, the (anterior) dorsolateral prefrontal cortex has been conceptualized as a key node for the generation and representation of internal goal and task-set representation, i.e., overarching plans (Koechlin and Summerfield, 2007). Though speculative, we would thus propose that the right TPJ may provide the computational link between autobiographic memories (past; PrC/PPC), self-reference (present; anterior cingulate cortex and goal-representations (future; DLPFC) by evaluating predictive codes. In a Bayesian framework, this would thus represent the basis of forming predictions about future long-term goals based on previous experience. How does this relate to the apparent role of the right TPJ during stimulus-driven tasks, namely optimizing short-term representations of the sensory environment for motor preparation? We would conclude that by interaction with domain-specific brain regions, the right TPJ and anterior insula forming the 'core network' may implement the governance of predictive coding across a wide range of mental states, irrespective of the domain (perceptual, motor or cognitive) and time course (short-term or long-term).

Supplementary materials related to this article can be found online at doi:10.1016/j.neuroimage.2012.02.037.

## Acknowledgments

This work was partly funded by the Human Brain Project (R01-MH074457; A.R.L., S.B.E., P.T.F), the Initiative and Networking Fund of the Helmholtz Association within the Helmholtz Alliance on Systems Biology (Human Brain Model; K.Z., S.B.E.) and the DFG (IRTG 1328, S.B.E.).

## References


Amunts, K., Schleicher, A., Bürgel, U., Mohlberg, H., Uylings, H.B., Zilles, K., 1999. Broca's region revisited: cytoarchitecture and intersubject variability. J. Comp. Neurol. 412 (2), 319–341.

Ashburner, J., Friston, K.J., 2005. Unified segmentation. Neuroimage 26 (3), 839–851.

Bays, P.M., Singh-Curry, V., Gorgoraptis, N., Driver, J., Husain, M., 2010. Integration of goal- and stimulus-related visual signals revealed by damage to human parietal cortex. J. Neurosci. 30 (17), 5968–5978.

Behrens, T.E., Johansen-Berg, H., Wollrich, M.W., Smith, S.M., Wheeler-Kingshott, C.A., Boulby, P.A., Barker, G.J., Sillery, E.L., Sheehan, K., Ciccarelli, O., Thompson, A.J., Brady, J.M., Matthews, P.M., 2003. Non-invasive mapping of connections between human thalamus and cortex using diffusion imaging. Nat. Neurosci. 6 (7), 750–757.

Behrens, T.E., Woolrich, M.W., Walton, M.E., Rushworth, M.F., 2007. Learning the value of information in an uncertain world. Nat. Neurosci. 10 (9), 1214–1221.

Bellec, P., Perlbarg, V., Jbabdi, S., Pélégrini-Issac, M., Anton, J.L., Doyon, J., Benali, H., 2006. Identification of large-scale networks in the brain using fMRI. Neuroimage 29 (4), 1231–1243.

Berlucchi, G., Aglioti, S.M., 2010. The body in the brain revisited. Exp. Brain Res. 200 (1), 25–35.

Binder, J.R., Frost, J.A., Hammeke, T.A., Bellgowan, P.S., Rao, S.M., Cox, R.W., 1999. Conceptual processing during the conscious resting state. A functional MRI study. J. Cogn. Neurosci. 11 (1), 80–95.

Biswal, B., Yetkin, F.Z., Haughton, V.M., Hyde, J.S., 1995. Functional connectivity in the motor cortex of resting human brain using echo-planar MRI. Magn. Reson. Med. 34 (4), 537–541.

Calvert, G., Spence, C., Stein, B.E., 2004. Handbook of Multisensory Processes. MIT press.

Cappe, C., Rouiller, E.M., Barone, P., 2009. Multisensory anatomical pathways. Hear. Res. 258 (1–2), 28–36.

Caspers, S., Geyer, S., Schleicher, A., Mohlberg, H., Amunts, K., Zilles, K., 2006. The human inferior parietal cortex: cytoarchitectonic parcellation and interindividual variability. Neuroimage 33 (2), 430–448.

Caspers, S., Eickhoff, S.B., Geyer, S., Scheperjans, F., Mohlberg, H., Zilles, K., Amunts, K., 2008. The human inferior parietal lobule in stereotaxic space. Brain Struct. Funct. 212 (6), 481–495.

Cavanna, A.E., Trimble, M.R., 2006. The precuneus: a review of its functional anatomy and behavioural correlates. Brain 129 (Pt 3), 564–583.

Choi, H.J., Zilles, K., Mohlberg, H., Schleicher, A., Fink, G.R., Armstrong, E., Amunts, K., 2006. Cytoarchitectonic identification and probabilistic mapping of two distinct areas within the anterior ventral bank of the human intraparietal sulcus. J. Comp. Neurol. 495 (1), 53–69.

Chouinard, P.A., Paus, T., 2006. The primary motor and premotor areas of the human cerebral cortex. Neuroscientist 12 (2), 143–152.

Cieslik, E.C., Zilles, K., Kurth, F., Eickhoff, S.B., 2010. Dissociating bottom-up and top-down processes in a manual stimulus–response compatibility task. J. Neurophysiol. 104 (3), 1472–1483.

Connolly, P.M., Bennur, S., Gold, J.I., 2009. Correlates of perceptual learning in an oculomotor decision variable. J. Neurosci. 29 (7), 2136–2150.

Corbetta, M., Shulman, G.L., 2002. Control of goal-directed and stimulus-driven attention in the brain. Nat. Rev. Neurosci. 3 (3), 201–215.

Corbetta, M., Patel, G., Shulman, G.L., 2008. The reorienting system of the human brain: from environment to theory of mind. Neuron 58 (3), 306–324.

Craig, A.D., 2009. How do you feel–now? The anterior insula and human awareness. Nat. Rev. Neurosci. 10 (1), 59–70.

David, N., Aumann, C., Santos, N.S., Bewemick, B.H., Eickhoff, S.B., Newen, A., Shah, N.J., Fink, G.R., Vogeley, K., 2008. Differential involvement of the posterior temporal cortex in mentalizing but not perspective taking. Soc. Cogn. Affect. Neurosci. 3 (3), 279–289.

Decety, J., Lamm, C., 2007. The role of the right temporoparietal junction in social interaction: how low-level computational processes contribute to meta-cognition. Neuroscientist 13 (6), 580–593.

Diedrichsen, J., Balsters, J.H., Flavell, J., Cussans, E., Ramnani, N., 2009. A probabilistic MR atlas of the human cerebellum. Neuroimage 46 (1), 39–46.

Dosenbach, N.U., Visscher, K.M., Palmer, E.D., Miezin, F.M., Wenger, K.K., Kang, H.C., Burgund, E.D., Grimes, A.L., Schlaggar, B.L., Petersen, S.E., 2006. A core system for the implementation of task sets. Neuron 50 (5), 799–812.

Downar, J., Crawley, A.P., Mikulis, D.J., Davis, K.D., 2000. A multimodal cortical network for the detection of changes in the sensory environment. Nat. Neurosci. 3 (3), 277–283.

Driver, J., Noesselt, T., 2008. Multisensory interplay reveals crossmodal influences on 'sensory-specific' brain regions, neural responses, and judgments. Neuron 57 (1), 11–23.

Dum, R.P., Strick, P.L., 2005. Frontal lobe inputs to the digit representations of the motor areas on the lateral surface of the hemisphere. J. Neurosci. 25 (6), 1375–1386.

Egner, T., 2007. Congruency sequence effects and cognitive control. Cogn. Affect. Behav. Neurosci. 7 (4), 380–390.

Eickhoff, S.B., Grefkes, C., 2011. Approaches for the integrated analysis of structure, function and connectivity of the human brain. Clin. EEG Neurosci. 42 (2), 107–121.

Eickhoff, S.B., Stephan, K.E., Mohlberg, H., Grefkes, C., Fink, G.R., Amunts, K., Zilles, K., 2005. A new SPM toolbox for combining probabilistic cytoarchitectonic maps and functional imaging data. Neuroimage 25 (4), 1325–1335.

Eickhoff, S.B., Schleicher, A., Zilles, K., Amunts, K., 2006a. The human parietal operculum. I. Cytoarchitectonic mapping of subdivisions. Cereb. Cortex 16 (2), 254–267.

Eickhoff, S.B., Amunts, K., Mohlberg, H., Zilles, K., 2006b. The human parietal operculum. II. Stereotaxic maps and correlation with functional imaging results. Cereb. Cortex 16 (2), 268–279.

Eickhoff, S.B., Heim, S., Zilles, K., Amunts, K., 2006c. Testing anatomically specified hypotheses in functional imaging using cytoarchitectonic maps. Neuroimage 32 (2), 570–582.

Eickhoff, S.B., Paus, T., Caspers, S., Grosbras, M.H., Evans, A.C., Zilles, K., Amunts, K., 2007. Assignment of functional activations to probabilistic cytoarchitectonic areas revisited. Neuroimage 36 (3), 511–521.

Eickhoff, S.B., Laird, A.R., Grefkes, C., Wang, L.E., Zilles, K., Fox, P.T., 2009. Coordinate-based activation likelihood estimation meta-analysis of neuroimaging data: a random-effects approach based on empirical estimates of spatial uncertainty. Hum. Brain Mapp. 30 (9), 2907–2926.

Eickhoff, S.B., Pomjanski, W., Jakobs, O., Zilles, K., Langner, R., 2011. Neural correlates of developing and adapting behavioral biases in speeded choice reactions—an FMRI study on predictive motor coding. Cereb. Cortex 21 (5), 1178–1191.

Feldman, H., Friston, K.J., 2010. Attention, uncertainty, and free-energy. Front. Hum. Neurosci. 4, 215.

Fox, M.D., Raichle, M.E., 2007. Spontaneous fluctuations in brain activity observed with functional magnetic resonance imaging. Nat. Rev. Neurosci. 8 (9), 700–711.

Fox, M.D., Corbetta, M., Snyder, A.Z., Vincent, J.L., Raichle, M.E., 2006. Spontaneous neuronal activity distinguishes human dorsal and ventral attention systems. Proc. Natl. Acad. Sci. U. S. A. 103 (26), 10046–10051.

Fox, M.D., Zhang, D., Snyder, A.Z., Raichle, M.E., 2009. The global signal and observed anticorrelated resting state brain networks. J. Neurophysiol. 101 (6), 3270–3283.

Geyer, S., 2004. The microstructural border between the motor and the cognitive domain in the human cerebral cortex. Adv. Anat. Embryol. Cell Biol. 174, 1–89 (I-VIII).

Geyer, S., Ledberg, A., Schleicher, A., Kinomura, S., Schormann, T., Bürgel, U., Klingberg, T., Larsson, J., Zilles, K., Roland, P.E., 1996. Two different areas within the primary motor cortex of man. Nature 382 (6594), 805–807.

Geyer, S., Schleicher, A., Zilles, K., 1999. Areas 3a, 3b, and 1 of human primary somatosensory cortex. Neuroimage 10 (1), 63–83.

Geyer, S., Schormann, T., Mohlberg, H., Zilles, K., 2000. Areas 3a, 3b, and 1 of human primary somatosensory cortex. Part 2. Spatial normalization to standard anatomical space. Neuroimage 11 (6 Pt 1), 684–696.

Gottlieb, J., 2007. From thought to action: the parietal cortex as a bridge between perception, action, and cognition. Neuron 53 (1), 9–16.

Gottlieb, J., Snyder, L.H., 2010. Spatial and non-spatial functions of the parietal cortex. Curr. Opin. Neurobiol. 20 (6), 731–740.

Grefkes, C., Geyer, S., Schormann, T., Roland, P., Zilles, K., 2001. Human somatosensory area 2: observer-independent cytoarchitectonic mapping, interindividual variability, and population map. Neuroimage 14 (3), 617–631.

Greicius, M.D., Krasnow, B., Reiss, A.L., Menon, V., 2003. Functional connectivity in the resting brain: a network analysis of the default mode hypothesis. Proc. Natl. Acad. Sci. U. S. A. 100 (1), 253–258.

Gusnard, D.A., Raichle, M.E., 2001. Searching for a baseline: functional imaging and the resting human brain. Nat. Rev. Neurosci. 2 (10), 685–694.

Holmes, C.J., Hoge, R., Collins, L., Woods, R., Toga, A.W., Evans, A.C., 1998. Enhancement of MR images using registration for signal averaging. J. Comput. Assist. Tomogr. 22 (2), 324–333 Mar-Apr.

Iacoboni, M., 2006. Visuo-motor integration and control in the human posterior parietal cortex: evidence from TMS and fMRI. Neuropsychologia 44 (13), 2691–2699.

Jakobs, O., Wang, L.E., Dafotakis, M., Grefkes, C., Zilles, K., Eickhoff, S.B., 2009. Effects of timing and movement uncertainty implicate the temporo-parietal junction in the prediction of forthcoming motor actions. Neuroimage 47 (2), 667–677.

Johansen-Berg, H., Behrens, T.E., Sillery, E., Ciccarelli, O., Thompson, A.J., Smith, S.M., Matthews, P.M., 2005. Functional-anatomical validation and individual variation of diffusion tractography-based segmentation of the human thalamus. Cereb. Cortex 15 (1), 31–39.

Karnath, H.O., Ferber, S., Himmelbach, M., 2001. Spatial awareness is a function of the temporal not the posterior parietal lobe. Nature 411 (6840), 950–953.

Kilner, J.M., Friston, K.J., Frith, C.D., 2007. The mirror-neuron system: a Bayesian perspective. Neuroreport 18 (6), 619–623.

Koechlin, E., Jubault, T., 2006. Broca's area and the hierarchical organization of human behavior. Neuron 50 (6), 963–974.

Koechlin, E., Summerfield, C., 2007. An information theoretical approach to prefrontal executive function. Trends Cogn. Sci. 11 (6), 229–235.

Kurth, F., Zilles, K., Fox, P.T., Laird, A.R., Eickhoff, S.B., 2010a. A link between the systems: functional differentiation and integration within the human insula revealed by meta-analysis. Brain Struct. Funct. 214 (5–6), 519–534.

Kurth, F., Eickhoff, S.B., Schleicher, A., Hoemke, L., Zilles, K., Amunts, K., 2010b. Cytoarchitecture and probabilistic maps of the human posterior insular cortex. Cereb. Cortex 20 (6), 1448–1461.

Laird, A.R., Eickhoff, S.B., Kurth, F., Fox, P.M., Uecker, A.M., Turner, J.A., Robinson, J.L., Lancaster, J.L., Fox, P.T., 2009. ALE meta-analysis workflows via the brainmap database: progress towards a probabilistic functional brain atlas. Front. Neuroinformatics 3, 23.

Lewis, J.W., Van Essen, D.C., 2000. Corticocortical connections of visual, sensorimotor, and multimodal processing areas in the parietal lobe of the macaque monkey. J. Comp. Neurol. 428 (1), 112–137.

Malikovic, A., Amunts, K., Schleicher, A., Mohlberg, H., Eickhoff, S.B., Wilms, M., Palomero-Gallagher, N., Armstrong, E., Zilles, K., 2007. Cytoarchitectonic analysis of the human extrastriate cortex in the region of V5/MT+: a probabilistic, stereotaxic map of area hOc5. Cereb. Cortex 17 (3), 562–574.

Mavritsaki, E., Allen, H.A., Humphreys, G.W., 2010. Decomposing the neural mechanisms of visual search through model-based analysis of fMRI: top-down excitation,

active ignoring and the use of saliency by the right TPJ. Neuroimage 52 (3), 934–946.
Menon, V., Uddin, L.Q., 2010. Saliency, switching, attention and control: a network model of insula function. Brain Struct. Funct. 214 (5–6), 655–667.
Menon, V., Adleman, N.E., White, C.D., Glover, G.H., Reiss, A.L., 2001. Error-related brain activation during a Go/NoGo response inhibition task. Hum. Brain Mapp. 12 (3), 131–143.
Mooshagian, E., Kaplan, J., Zaidel, E., Iacoboni, M., 2008. Fast visuomotor processing of redundant targets: the role of the right temporo-parietal junction. PLoS One 3 (6), e2348.
Nichols, T., Brett, M., Andersson, J., Wager, T., Poline, J.B., 2005. Valid conjunction inference with the minimum statistic. Neuroimage 25 (3), 653–660.
Palomero-Gallagher, N., Mohlberg, H., Zilles, K., Vogt, B., 2008. Cytology and receptor architecture of human anterior cingulate cortex. J. Comp. Neurol. 508 (6), 906–926.
Palomero-Gallagher, N., Vogt, B.A., Schleicher, A., Mayberg, H.S., Zilles, K., 2009. Receptor architecture of human cingulate cortex: evaluation of the four-region neurobiological model. Hum. Brain Mapp. 30 (8), 2336–2355.
Picard, N., Strick, P.L., 1996. Motor areas of the medial wall: a review of their location and functional activation. Cereb. Cortex 6 (3), 342–353 (May-Jun).
Raichle, M.E., MacLeod, A.M., Snyder, A.Z., Powers, W.J., Gusnard, D.A., Shulman, G.L., 2001. A default mode of brain function. Proc. Natl. Acad. Sci. U. S. A. 98 (2), 676–682.
Rao, R.P., Ballard, D.H., 1999. Predictive coding in the visual cortex: a functional interpretation of some extra-classical receptive-field effects. Nat. Neurosci. 2 (1), 79–87.
Renier, L.A., Anurova, I., De Volder, A.G., Carlson, S., VanMeter, J., Rauschecker, J.P., 2009. Multisensory integration of sounds and vibrotactile stimuli in processing streams for “what” and “where”. J. Neurosci. 29 (35), 10950–10960.
Rizzolatti, G., Luppino, G., Matelli, M., 1998. The organization of the cortical motor system: new concepts. Electroencephalogr. Clin. Neurophysiol. 106 (4), 283–296.
Rottschy, C., Langner, R., Dogan, I., Reetz, K., Laird, A.R., Schulz, J.B., Fox, P.T., Eickhoff, S.B., 2012. Modelling neural correlates of working memory: A coordinate-based meta-analysis. NeuroImage 60 (1), 830–846.
Scheperjans, F., Grefkes, C., Palomero-Gallagher, N., Schleicher, A., Zilles, K., 2005. Subdivisions of human parietal area 5 revealed by quantitative receptor autoradiography: a parietal region between motor, somatosensory, and cingulate cortical areas. Neuroimage 25 (3), 975–992.
Scheperjans, F., Hermann, K., Eickhoff, S.B., Amunts, K., Schleicher, A., Zilles, K., 2008a. Observer-independent cytoarchitectonic mapping of the human superior parietal cortex. Cereb. Cortex 18 (4), 846–867.
Scheperjans, F., Eickhoff, S.B., Hömke, L., Mohlberg, H., Hermann, K., Amunts, K., Zilles, K., 2008b. Probabilistic maps, morphometry, and variability of cytoarchitectonic areas in the human superior parietal cortex. Cereb. Cortex 18 (9), 2141–2157.
Schilbach, L., Eickhoff, S.B., Rotarska-Jagiela, A., Fink, G.R., Vogeley, K., 2008. Minds at rest? Social cognition as the default mode of cognizing and its putative relationship to the “default system” of the brain. Conscious. Cogn. 17 (2), 457–467.
Schlögl, A., Supp, G., 2006. Analyzing event-related EEG data with multivariate autoregressive parameters. Prog. Brain Res. 159, 135–147.
Shulman, G.L., Astafiev, S.V., Franke, D., Pope, D.L., Snyder, A.Z., McAvoy, M.P., Corbetta, M., 2009. Interaction of stimulus-driven reorienting and expectation in ventral and dorsal frontoparietal and basal ganglia-cortical networks. J. Neurosci. 29 (14), 4392–4407.
Smallwood, J., Schooler, J.W., 2006. The restless mind. Psychol. Bull. 132 (6), 946–958.
Smith, S.M., Fox, P.T., Miller, K.L., Glahn, D.C., Fox, P.M., Mackay, C.E., Filippini, N., Watkins, K.E., Toro, R., Laird, A.R., Beckmann, C.F., 2009. Correspondence of the brain's functional architecture during activation and rest. Proc. Natl. Acad. Sci. U. S. A. 106 (31), 13040–13045.
Spence, C., Driver, J., 2004. Crossmodal Space and Crossmodal Attention. Oxford University Press.
Summerfield, C., Mangels, J.A., 2006. Dissociable neural mechanisms for encoding predictable and unpredictable events. J. Cogn. Neurosci. 18 (7), 1120–1132.
Thiel, C.M., Zilles, K., Fink, G.R., 2004. Cerebral correlates of alerting, orienting and reorienting of visuospatial attention: an event-related fMRI study. Neuroimage 21 (1), 318–328.
Toni, I., Shah, N.J., Fink, G.R., Thoenissen, D., Passingham, R.E., Zilles, K., 2002. Multiple movement representations in the human brain: an event-related fMRI study. J. Cogn. Neurosci. 14 (5), 769–784.
Turkeltaub, P.E., Eickhoff, S.B., Laird, A.R., Fox, M., Wiener, M., Fox, P., 2012. Minimizing within-experiment and within-group effects in Activation Likelihood Estimation meta-analysis. Hum Brain Mapp. 33 (1), 1–13.
Vallar, G., Antonucci, G., Guariglia, C., Pizzamiglio, L., 1993. Deficits of position sense, unilateral neglect and optokinetic stimulation. Neuropsychologia 31 (11), 1191–1200.
Vogeley, K., Bussfeld, P., Newen, A., Herrmann, S., Happé, F., Falkai, P., Maier, W., Shah, N.J., Fink, G.R., Zilles, K., 2001. Mind reading: neural mechanisms of theory of mind and self-perspective. Neuroimage 14 (1 Pt 1), 170–181.
Watanabe, Y., Funahashi, S., 2012. Thalamic mediodorsal nucleus and working memory. Neurosci Biobehav Rev. 36 (1), 134–142.
Weissenbacher, A., Kasess, C., Gerstl, F., Lanzenberger, R., Moser, E., Windischberger, C., 2009. Correlations and anticorrelations in resting-state functional connectivity MRI: a quantitative comparison of preprocessing strategies. Neuroimage 47 (4), 1408–1416.
Wolfensteller, U., von Cramon, D.Y., 2010. Bending the rules: strategic behavioral differences are reflected in the brain. J. Cogn. Neurosci. 22 (2), 278–291.
Worsley, K.J., Marrett, S., Neelin, P., Vandal, A.C., Friston, K.J., Evans, A.C., 1996. A unified statistical approach for determining significant signals in images of cerebral activation. Hum. Brain Mapp. 4 (1), 58–73.

Cerebral Cortex December 2009;19:2930-2945
doi:10.1093/cercor/bhp063
Advance Access publication April 30, 2009

# Functional Heterogeneity of Inferior Parietal Cortex during Mathematical Cognition Assessed with Cytoarchitectonic Probability Maps

S. S. Wu[1], T. T. Chang[1,2], A. Majid[1], S. Caspers[3], S. B. Eickhoff[3] and V. Menon[1,4,5]

[1]Department of Psychiatry and Behavioral Sciences, Stanford University School of Medicine, Stanford, CA 94305, [2]Institute of Neuroscience, National Yang-Ming University, Taipei 112, Taiwan, [3]Research Centre Jülich, Institute of Neurosciences and Biophysics-Medicine, 52425 Jülich, Germany, [4]Program in Neuroscience and [5]Symbolic Systems Program, Stanford University School of Medicine, Stanford, CA 94305

S. S. Wu and T. T. Chang contributed equally to the study

**Although the inferior parietal cortex (IPC) has been consistently implicated in mathematical cognition, the functional roles of its subdivisions are poorly understood. We address this problem using probabilistic cytoarchitectonic maps of IPC subdivisions intraparietal sulcus (IPS), angular gyrus (AG), and supramarginal gyrus. We quantified IPC responses relative to task difficulty and individual differences in task proficiency during mental arithmetic (MA) tasks performed with Arabic (MA-A) and Roman (MA-R) numerals. The 2 tasks showed similar levels of activation in 3 distinct IPS areas, hIP1, hIP2, and hIP3, suggesting their obligatory role in MA. Both AG areas, PGa and PGp, were strongly deactivated in both tasks, with stronger deactivations in posterior area PGp. Compared with the more difficult MA-R task, the MA-A task showed greater responses in both AG areas, but this effect was driven by less deactivation in the MA-A task. AG deactivations showed prominent overlap with lateral parietal nodes of the default mode network, suggesting a nonspecific role in MA. In both tasks, greater bilateral AG deactivation was associated with poorer performance. Our findings suggest a close link between IPC structure and function and they provide new evidence for behaviorally salient functional heterogeneity within the IPC during mathematical cognition.**

**Keywords:** angular gyrus, automaticity, intraparietal sulcus, mental arithmetic, supramarginal gyrus

## Introduction

The neural basis of mathematical cognition has been intensely studied in recent years given its importance as a skill we use nearly every day. Brain imaging studies have consistently identified a distributed set of brain regions that includes, most prominently, the ventral visual areas, including the lingual and fusiform gyri, inferior parietal cortex (IPC), and the ventrolateral prefrontal cortex (PFC; Burbaud et al. 1995; Dehaene et al. 1999; Delazer et al. 2006; Menon, Rivera, White, Eliez, et al. 2000; Menon, Rivera, White, Glover, et al. 2000; Menon et al. 2002; Rickard et al. 2000; Zago et al. 2001). Within this distributed network, the IPC is thought to play a critical role in representing and manipulating quantitative information, whereas other brain regions, such as the ventrolateral and dorsolateral PFC, are engaged in supportive functions such as working memory, sequencing, controlled retrieval, and decision making (Rueckert et al. 1996; Dehaene et al. 1999; Kazui et al. 2000; Menon, Rivera, White, Glover, et al. 2000; Gruber et al. 2001; Delazer et al. 2003; Zago et al. 2008). The IPC comprises multiple heteromodal regions that play an important role in semantic, phonological, and visuospatial representation of numerical information (Caspers et al. 2008). IPC regions along the banks of the intraparietal sulcus (IPS) as well as the adjoining angular gyrus (AG) and supramarginal gyrus (SMG) have all been implicated in tasks involving mathematical problem solving. Little is known, however, about the differential contributions of these regions, an issue that has been particularly confounded by lack of knowledge about the precise anatomical boundaries of the IPC.

Current efforts in understanding the role of the IPC in mathematical cognition have focused on the IPS because of its role in basic number identification and number comparison tasks (Cohen et al. 2000; Duffau et al. 2002; Delazer et al. 2003; Cohen Kadosh et al. 2007; Piazza et al. 2007). To a lesser extent, the left AG has drawn interest, based on its purported role in rapid, verbally mediated fact retrieval. In a meta-analysis of their data, Dehaene et al. (2003) suggested that the number manipulation in the IPS is supplemented by the left AG when verbal manipulation of numbers is needed and that attention to visuospatial representations on the mental number line is supported by the bilateral posterior superior parietal lobule. Less attention has been paid to the SMG, a brain region important for phonological rehearsal and working memory functions that are evoked during mathematical problem-solving tasks.

Several brain imaging studies have investigated the role of the left and right IPC in mental arithmetic (MA) operations such as single- and double-digit addition, subtraction, and multiplication (Roland and Friberg 1985; Burbaud et al. 1995; Dehaene and Cohen 1997; Menon, Rivera, White, Eliez, et al. 2000; Gruber et al. 2001; Simon et al. 2002). IPC responses during the solution of more abstract and complex mathematical problems, such as calculus integrals, have also been investigated (Krueger et al. 2008). In both cases, the specific contribution of various subdivisions of the IPC in mathematical problem solving is still unclear. Findings to date have been contradictory with respect to task-related dissociations in the IPC during computationally demanding tasks compared with more automated tasks. Whereas some brain imaging studies have reported greater bilateral activation in the IPS during more computationally demanding MA tasks, others have reported greater responses in the left AG during more automated MA tasks (Grabner et al. 2007; Ischebeck et al. 2007). Importantly, at least one study has reported relative decreases, or deactivation, in the left and right AG and the SMG during a simple well-automated multiplication task, compared with a magnitude judgment task (Rickard et al. 2000). To our knowledge, the study by Rickard and colleagues was the first and only study that reported deactivation in both the left and right AG and SMG during MA. Interestingly, this study noted deactivation in every one of their participants, but the precise localization of this deactivation was ambiguously stated to be in a bilateral area centered between the SMG and the AG. Besides the lack of precise localization of IPC responses,

another central issue here is that task-related differences can arise from greater activation in the more automated task or greater deactivation during the more computationally demanding task. We address both these issues here at length. Recent studies have highlighted prominent and consistent deactivations of IPC regions in and around the AG across a broad range of cognitive tasks (Greicius et al. 2003; Mechelli et al. 2003; Humphries et al. 2007; Schulman et al. 2003; Harrison et al. 2008; Sweet et al. 2008). Moreover, there is growing evidence to suggest that the level of deactivation decreases with increasing task difficulty (Greicius et al. 2003; Schulman et al. 2003). These deactivations have received less attention in the domain of MA problem solving, and several researchers have, on the contrary, highlighted the engagement, rather than disengagement of the AG in more automated fact retrieval. To address this issue, we systematically investigated both activation and deactivation in specific subdivisions of the IPC as a function of task difficulty.

A major reason for the contradictory findings in the literature has been the poor demarcation of the boundaries of regions that constitute the IPC. There are 2 fundamental problems here; first, the boundaries between the IPS and rest of the IPC are unknown. Second, demarcation of the AG from the SMG is ambiguous as far as macroanatomical features are concerned. Brodmann (1909) differentiated the IPC into 2 areas: the SMG (BA 40) on the rostral aspects of the IPC and AG (BA 39) on the caudal aspects of the IPC. According to Brodmann, the SMG and the AG are demarcated by the Jensen sulcus, but using this sulcus as a border between BA 40 and BA 39 is problematic because of its highly irregular and variable form. Even more problematic is the issue of demarcating the AG and the SMG from the IPS. Other more recently developed parcellation schemes (Tzourio-Mazoyer et al. 2002; Desikan et al. 2006) commonly used in brain imaging studies also suffer from similar deficiencies. Importantly, no existing methods offer a scheme to parcellate the IPS. The dorsal and ventral aspects of the IPS are often arbitrarily ascribed to the IPC or the superior parietal lobule. For example, some studies have treated the ventral bank of the IPS as a part of the AG, whereas others have referred to it as the IPS (Menon, Rivera, White, Glover, et al. 2000; Ischebeck et al. 2006). Thus, the boundaries segregating the IPS from the AG and the SMG are ill specified, leading to misrepresentation of observed functional brain responses in these regions.

The recent availability of probabilistic cytoarchitectonic maps has the potential to inform and significantly enhance our understanding of the functional architecture of the IPC in mathematical cognition. Cytoarchitectonic maps obtained from postmortem brains suggest that the human IPC has a more finely grained parcellation than previously suggested by the classical Brodmann map. These maps provide objective a priori regions of interest (ROI) that can be used to test anatomically specific hypotheses about the localization of functional activations (Caspers et al. 2008). Recent studies have suggested that the borders of the IPS, SMG, and the AG cannot be reliably detected using macroanatomic or gross anatomical features on magnetic resonance images (MRIs) (Caspers et al. 2008). Detailed analysis of cell types suggests that the IPS can be subdivided into at least 3 regions, as shown in Figure 1. The human intraparietal area 2 (hIP2) occupies the anterior, lateral bank of the human IPS, and area hIP1 is located immediately posterior and medial to hIP2 (Choi et al. 2006). These regions correspond roughly to the monkey anterior intraparietal area, whereas area hIP3 that occupies the posterior human IPS corresponds approximately to monkey ventral intraparietal area (Scheperjans, Eickhoff, et al. 2008; Scheperjans, Hermann, et al. 2008). Ventral to these IPS regions are 2 areas that cover the AG and 5 that cover the SMG (Caspers et al. 2006). The AG consists of the anterior and posterior areas PGa and PGp, respectively, encompassing the caudal aspects of the IPC. In contrast, 3 larger, more dorsal regions— PFm, PF, PFt— and 2 smaller ventral regions— PFcm and PFop— encompass the rostral segments of the IPC along the rostral to caudal axis. Posteriorly, region PFm of the SMG borders the AG region PGa (Caspers et al. 2006, 2008). To account for variability in size and extent of these areas across individuals, cytoarchitectonic probabilistic maps have been calculated for each area in stereotaxic space (Caspers et al. 2008; Scheperjans, Eickhoff, et al. 2008). These probabilistic maps provide a robust anatomical reference for more accurately characterizing structure–function relations in the human IPC during mathematical problem solving.

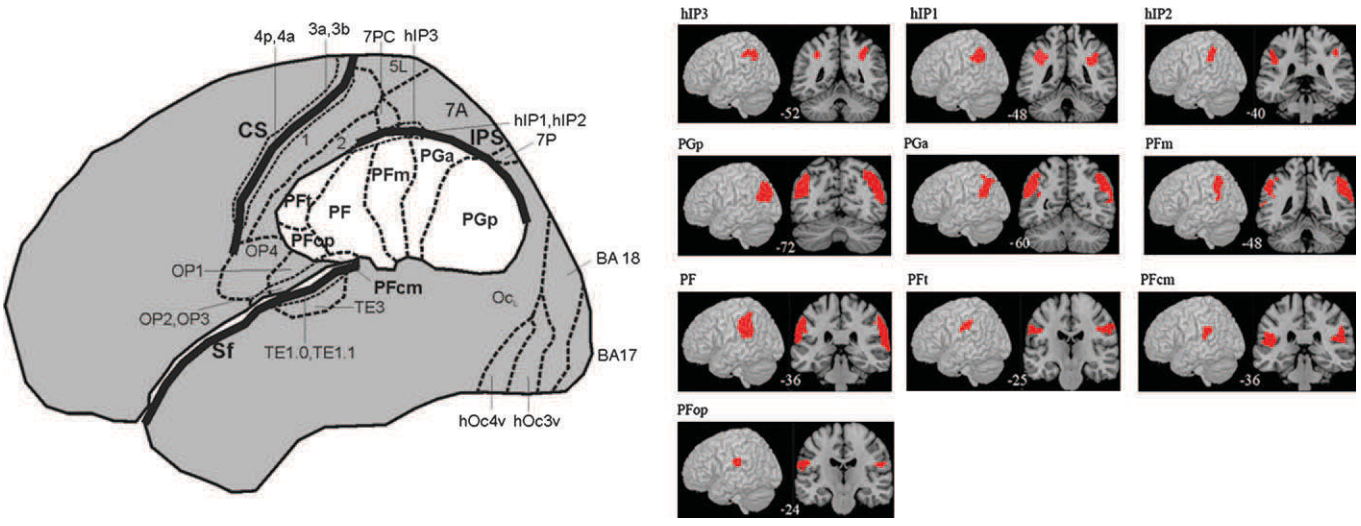


**Figure 1.** Cytoarchitectonic maps of the IPC. Cytoarchitectonic maps of 3 IPS—hIP3, hIP1, and hIP2, 2 AG—PGp and PGa, and 5 SMG—PFm, PF, PFt, PFcm, and PFop areas of the IPC used in the study, ordered along a posterior to anterior gradient (Caspers et al. 2006; Choi et al. 2006; Scheperjans, Hermann, et al. 2008). Surface renderings and coronal sections are shown with the numbers at the bottom of each panel indicating the location of the slices (*y*-axis in MNI coordinates).

In the present study, we compared brain responses to simple MA tasks involving familiar and well-rehearsed Arabic numerals to similar MA tasks performed with less familiar Roman numerals. Previous brain imaging studies of mathematical cognition have focused primarily on MA operations that are well rehearsed and automated in adults. An important question regarding the function of specific IPC regions relates to how they respond to different levels of task automaticity and individual differences in task proficiency. To address this question, we examined IPC responses during both automated and nonautomated MA tasks. We use the notion of automaticity here in the same sense as Logan (1988). In this view, automated processes are more dependent on memory-based solutions and retrieval, whereas nonautomated processes rely on algorithmic computations. It is currently not known exactly how IPS, AG, and SMG responses change with task automaticity, an issue we address here using cytoarchitectonically distinct maps of the IPC.

Behavioral studies have provided compelling evidence that changing the surface format of numerals is an effective way to alter the automaticity of mathematical information processing (Perry 1952; McCarthy and Dillon 1973; Gonzalez and Kolers 1982; Campbell and Fugelsang 2001; Hiscock et al. 2001; Venkatraman et al. 2006; Ansari 2007). For example, Campbell and Fugelsang (2001) found that participants were slower and less accurate at assessing 1-digit math problems that were presented in written English format (e.g. three + four = eight) than in a number format (e.g. 3 + 4 = 8). They proposed that the decrease in performance arose from the more complex written format using less efficient strategies and that participants relied more on explicit calculation than direct retrieval-based strategies (Schunn et al. 1997). Several studies have also compared processing of familiar Arabic numerals with the less familiar Roman numerals (Perry 1952; McCarthy and Dillon 1973; Gonzalez and Kolers 1982). These studies have consistently found that mental addition with Roman numerals takes significantly longer than with Arabic numerals. In a paced serial addition task, participants had significantly higher accuracy and shorter reaction times (RTs) when the stimuli were presented in Arabic, compared with Roman, format (Hiscock et al. 2001). Taken together, these studies suggest that automaticity of mathematical information processing can be manipulated in a controlled manner by merely altering the surface format of the numerals.

We used arithmetic verification tasks similar to those used in previous studies (Menon, Rivera, White, Eliez, et al. 2000; Menon, Rivera, White, Glover, et al. 2000), except that the participants performed 2 versions of the task—MA with Arabic (MA-A task) and MA with Roman numerals (MA-R task). Although the format of the Arabic and Roman equations (e.g. 2 + 3 − 1 = 4 and II + III − I = IV) was similar, the Roman numeral condition relied less on efficient and automatic memory retrieval than the Arabic numeral equations (Campbell and Fugelsang 2001; Hiscock et al. 2001). We used 3-operand, rather than 2-operand, equations in order to keep the tasks relatively simple while simultaneously providing sufficient variability in performance to facilitate examination of the relation between accuracy and brain response in the IPC (Menon, Rivera, White, Glover, et al. 2000). Lassaline and Logan (1993) have argued that transfer of memory-based automaticity is narrow because learning tends to be item specific. This suggests that participants typically cannot directly retrieve facts from memory when presented with MA problems in the Roman format. A key difference between the 2 tasks is that the MA-R requires more controlled and effortful retrieval, whereas the MA-A task involves more direct and effortless retrieval.

In summary, the main aims of our study were to 1) investigate the differential involvement of the IPS, AG, and SMG during MA using cytoarchitectonically defined subdivisions of the IPC, 2) examine activation and deactivation of the IPS, AG, and SMG as a function of task automaticity, 3) compare differential responses of the IPC and the PFC in relation to task automaticity, and 4) investigate the neural basis of individual differences in MA performance as a function of task automaticity. We predicted that participants would perform the MA-A task more accurately and faster than the MA-R task, reflecting the higher task automaticity with familiar mathematical symbols. In conjunction with these behavioral differences, we hypothesized that 1) the IPS would show activation in both tasks, with lesser activation during the more automated MA-A task, 2) the AG would show deactivation in both tasks, with greater deactivation in the MA-R task, 3) deactivations in the AG would overlap strongly with the default mode network (DMN), a set of brain regions that typically show domain general reductions in brain responses during difficult cognitive tasks (Greicius et al. 2003), 4) a dissociation between IPS and PFC responses would be observed, with the PFC showing greater between-task differences than the IPS, and 5) individual differences in MA task performance would be differentially related to activation in the IPS and deactivation in the AG.

## Materials and Methods

### *Participants*

Eighteen healthy adult participants (7 males and 11 females; ages 18–31.5, mean 22.28 years ± 3.95) participated in the study after giving written informed consent. All protocols were approved by the human participants Institutional Review Board at the Stanford University School of Medicine. All participants were volunteers and were treated in accordance with the APA "Ethical Principles of Psychologists and Code of Conduct."

### *fMRI Experiments*

This study consisted of 2 identical MA experiments, one using Arabic numerals and the other using Roman numerals. Arabic and Roman problems were presented in separate blocks in order to prevent subjects from switching across stimulus types and changing task strategy between conditions. The order of experiments was randomized across participants.

#### *MA with Arabic numerals (MA-A)*

Participants were presented with 16 alternating experimental and control epochs, each lasting 32 s. Each experimental (Calculation) epoch consisted of eight 3-operand equations of the form $a + b - c = d$ (e.g. 5 + 4 − 2 = 7); only single-digit numerals from 1 to 9 were used. Each equation was presented for 3.5 s followed by a blank screen for 0.5 s. Participants were instructed to respond by pressing one of 2 keys, based on whether they thought the equation was correct (e.g. 4 + 5 − 2 = 7) or incorrect (e.g. 4 + 5 − 2 = 8). Half of the equations presented were correct, and the other half incorrect; the order of correct and incorrect equations was randomized. Each control (Identification) epoch consisted of eight 7-symbol strings (e.g. 4 @ 3 & 2 # 5). Each string was presented for 3.5 s followed by a blank screen for 0.5 s. Participants were instructed to respond by pressing one of 2 keys, based on whether they thought the string contained the numeral 5. Half of the strings presented contained the numeral 5, the other half did not; the order of presentation of these strings was randomized.

#### *MA with Roman Numerals (MA-R)*

This experiment was identical to the MA-A task, except that the equations consisted of Roman numerals (e.g. VI + II − I = VII). During the control epochs, participants were asked to determine whether the string contained the Roman numeral V (e.g. IX @ VI & I % V).

### *Stimulus presentation*

The task was programmed using PsyScope (Cohen et al. 1993) on a Macintosh (Cupertino, CA) computer. Scan and task onsets were synchronized using a TTL pulse delivered to the scanner timing microprocessor board from a "CMU Button Box" microprocessor (http://poppy.psy.cmu.edu/psyscope) connected to the Macintosh. Stimuli were presented visually at the center of a screen using a custom-built magnet-compatible projection system (Resonance Technology, CA). An external timer maintained an accuracy of stimulus presentation to 1 ms.

### *Behavioral Data Analysis*

RT and the number of correct responses for experimental and control epochs were computed. RT was analyzed using analysis of variance (ANOVA) with 2 repeated measures: numeral type (Roman vs. Arabic) and task condition (Calculation vs. Identification).

### *fMRI Data Acquisition*

Images were acquired on a 3T GE Signa scanner using a standard GE whole head coil (software Lx 8.3). Head movement was minimized during scanning by a comfortable custom-built restraint. A total of 28 axial slices (4.5 mm thickness, 0.5 mm skip) parallel to the AC-PC line and covering the whole brain were imaged with a temporal resolution of 2 s using a T2*-weighted gradient echo spiral pulse sequence (Glover and Lai 1998) with the following parameters: TR = 2000 ms, TE = 30 ms, flip angle = 70°, 1 interleave. The field of view was 20 cm, and the matrix size was 64 × 64, providing an in-plane spatial resolution of 3.125 mm. To reduce blurring and signal loss arising from field inhomogeneities, an automated high-order shimming method based on spiral acquisitions was used before acquiring functional MRI scans (Kim et al. 2002). A high-resolution T1-weighted spoiled grass gradient recalled inversion recovery 3D MRI sequence was acquired to facilitate anatomical localization of functional activity. The following parameters were used: TI = 300 ms, TR = 8 ms; TE = 3.6 ms; flip angle = 15°; 22 cm field of view; 124 slices in coronal plane; 256 × 192 matrix; 2 NEX, acquired resolution = 1.5 × 0.9 × 1.1 mm. Structural and functional images were acquired in the same scan session.

### *fMRI Data Analysis*

The first 5 volumes were not analyzed to allow for signal equilibration effects. Images were reconstructed, by inverse Fourier transform, for each of the time points into 64 × 64 × 28 image matrices (voxel size 3.125 × 3.125 × 4.5 mm). A linear shim correction was applied separately for each slice during reconstruction using a magnetic field map acquired automatically by the pulse sequence at the beginning of the scan (Glover and Lai 1998). Functional MRI data were preprocessed using SPM5 (http://www.fil.ion.ucl.ac.uk/spm). Images were realigned to correct for motion, corrected for errors in slice timing, spatially transformed to standard stereotaxic space (based on the Montreal Neurologic Institute coordinate system), resampled every 2 mm using sinc interpolation and smoothed with a 4-mm full-width half-maximum Gaussian kernel to decrease spatial noise prior to statistical analysis.

Statistical analysis was performed on individual and group data using the general linear model and the theory of Gaussian random fields as implemented in SPM5 (http://www.fil.ion.ucl.ac.uk/spm/software/spm5/). Individual subject analyses were first performed by modeling task-related and task-unrelated confounds. Low-frequency noise was removed with a high-pass filter (0.5 cycles/min) applied to the fMRI time series at each voxel. A temporal smoothing function (Gaussian kernel corresponding to half-width of 4 s) was applied to the fMRI time series to enhance the temporal signal-to-noise ratio. Regressors were modeled with a boxcar function corresponding to the epochs during which each condition was presented and convolved with a hemodynamic response function. We then defined the effects of interest for each participant with the relevant contrasts of the parameter estimates. Group analysis was performed using a random effects model that incorporated a 2-stage hierarchical procedure (Holmes and Friston 1998). For the first-level analysis, contrast images for each participant and each effect of interest were generated as described above. For the second-level analysis, these contrast images were analyzed using a general linear model to determine voxel-wise group *t*-statistics. One contrast image was generated per participant, for each effect of interest. Two-tailed *t*-tests were used to determine group-level activation for each effect. Finally, the *t*-statistics were normalized transformed to *Z* scores, and significant clusters of activation were determined using the joint expected probability distribution of height and extent of *Z* scores (Poline et al. 1997), with height ($Z > 2.33$; $P < 0.01$) and extent thresholds ($P < 0.01$).

The following between-task comparisons were then performed at the group level using paired *t*-tests: 1) MA-A: Arabic Calculation – Arabic Identification; (2) MA-R: Roman Calculation – Roman Identification; and the following between-numeral comparisons: (3) MA-A – MA-R: (Arabic Calculation – Arabic Identification) – (Roman Calculation – Roman Identification); (4) MA-R – MA-A: (Roman Calculation – Roman Identification) – (Arabic Calculation – Arabic Identification). In the latter 2 comparisons, which involve double subtractions, additional analyses were conducted to distinguish between differences arising from calculation task-related increases in activation, as opposed to identification task-related decreases in activation (or "deactivation"). For each significant cluster that was detected in these comparisons (i.e. comparisons 3 and 4), mean *t*-scores were first computed for the MA-A (comparison 1) and MA-R (comparison 2) tasks. Clusters in comparisons 3 and 4 were then categorized as arising from deactivation if 1) the mean *t*-score (averaged across all participants) was significantly negative in comparisons 2 and 1, respectively; and 2) the mean *t*-score was not significantly different from 0 in comparisons 1 and 2, respectively. A parallel analysis was conducted using percent signal change between the Calculation and Identification conditions. The results in each case were similar to those obtained using *t*-scores, so only the latter is reported here.

Regression analysis was used to examine the relation between MA experimental task accuracy and activation in the MA-A and MA-R tasks. Voxel-wise *t*-statistics maps were generated and significant clusters of activation were determined using a voxel-wise statistical height threshold of ($Z > 2.33$; $P < 0.01$), with corrections for multiple spatial comparisons at the cluster level ($P < 0.05$). Both the magnitude and the sign of the activations were examined in order to ascertain whether the observed brain–behavior relations were related to task-related activation or deactivation. Activation foci were superimposed on high-resolution T1-weighted images and their locations were interpreted using known neuroanatomical landmarks (Mai et al. 2007).

### *IPC ROI*

ROI were based on the cytoarchitectonically distinct maps of 3 IPS (hIP3, hIP1, and hIP2), 2 AG (PGp and PGa), and 5 SMG (PFm, PF, PFt, PFcm, and PFop) regions, as described above (Fig. 1). In the order listed, these ROI run successively along the caudal to rostral axis of the IPC. Detailed information about the anatomical boundaries of these maps has been published elsewhere (Caspers et al. 2006; Choi et al. 2006; Scheperjans, Hermann, et al. 2008). Probability maps of each of these ROIs were evaluated using the SPM Anatomy Toolbox (Eickhoff et al. 2005).

The Anatomy Toolbox allowed us to characterize and label functional activations in relation to the probabilistic ROI. The spatial distribution of regional activations was characterized by 3 metrics— the percentage of an activation cluster that was in a specific ROI, the percentage of a specific ROI that belonged to an activated cluster, and probability that a peak in the cluster was assigned to an ROI (Eickhoff et al. 2005, 2007). Because of the spatial overlap in the 7 probabilistic IPC ROI, we used maximum probability maps, which yield nonoverlapping ROIs, to uniquely characterize the magnitude of regional responses. This approach yields regions that 1) reflect most adequately the underlying anatomy and 2) show a high degree of sensitivity in statistical analysis of functional activations (Eickhoff et al. 2007).

## Results

### *Behavior*

Accuracy and RTs for the MA-R and MA-A calculation and identification trials are summarized in Figure 2. For RT, ANOVAs revealed a significant 2-way interaction between condition

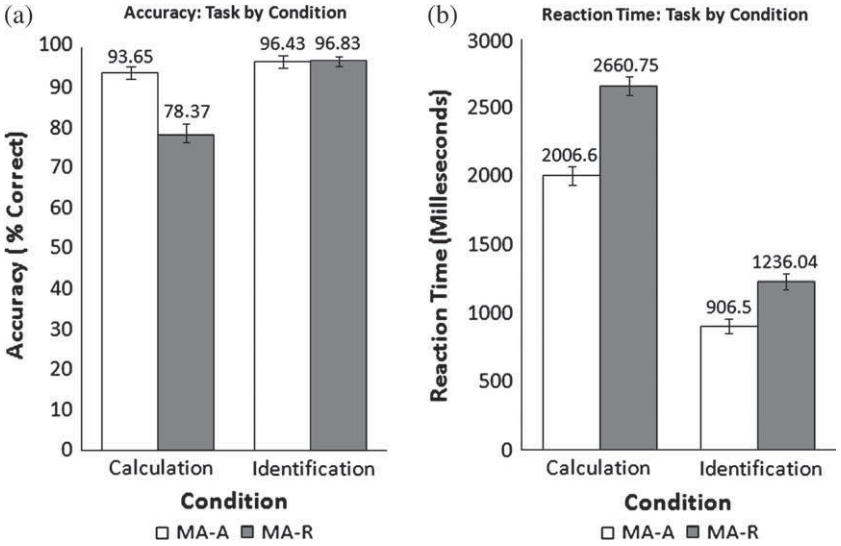


**Figure 2.** Accuracy and RT during the MA-A and MA-R tasks. (*a*) Accuracy and (*b*) RT during Calculation and Identification conditions in the MA-A and MA-R tasks. Accuracy was significantly lower, and RTs were significantly greater, during the calculation condition of the MA-R task. A significant task by condition interaction was observed for both accuracy and RT. Mean and standard error are shown.

(Calculation and Identification) and task (MA-A and MA-R); $F(1,17) = 13.582$, $P < 0.005$, partial $\eta^2 = 0.444$. RTs in both MA-A and MA-R conditions were significantly higher in Calculation than Identification conditions ($F(1,17) = 481.423$, $P < 0.001$, partial $\eta^2 = 0.966$). The mean RT for both conditions within the MA-A task were lower than the mean RT for MA-R ($F(1,17) = 126.885$, $P < 0.001$, partial $\eta^2 = 0.882$).

For accuracy, an ANOVA revealed a significant 2-way interaction between condition and task ($F(1,17) = 33.437$, $P < 0.000$, partial $\eta^2 = 0.663$). Average accuracy in both MA-A and MA-R tasks were significantly higher in Identification than Calculation ($F(1,17) = 42.918$, $P < 0.001$, partial $\eta^2 = 0.716$). The average accuracy for both conditions within the MA-A task was significantly greater than the average accuracy of the conditions in MA-R ($F(1,17) = 20.631$, $P < 0.001$, partial $\eta^2 = 0.548$).

### *IPC Activation during the MA-A and MA-R Tasks*

*MA-A (Arabic Calculation versus Number Identification)*
We detected significant activation (Calculation > Identification) as well as deactivation (Identification > Calculation) within the IPC, as shown in Figure 3a and Table 1. Note that deactivation here refers to greater activation during the low-level control (Identification) condition (see Discussion and Supplementary Fig. S3 for a consideration of deactivation with respect to a resting baseline). All 3 IPS areas (hIP1, hIP2, and hIP3) showed strong activation during the MA-A task, whereas the 2 AG areas (PGa and PGp) showed strong deactivation (Fig. 4). In contrast, the 5 SMG areas showed minimal activation. We then examined the spatial profile of activation using probabilistic labeling of IPC responses (Fig. 5*a*). The analysis showed that posterior IPS area hIP3 had the strongest and most spatially extensive activation, followed by area hIP1. In contrast, about 50% of PGp was deactivated, followed by 30% of PGa. The deactivations also extended anteriorly to cover 14% of SMG area PFm (Table 2).

*MA-R (Roman Calculation versus Number Identification)*
We detected significant activation as well as deactivation within the IPC, as shown in Figures 3b and 4b. As with the MA-A task, all 3 IPS ROI showed strong activation during the MA-A task, whereas the 2 AG ROI showed strong deactivation (Fig. 4*b*). Again, the SMG ROI showed minimal activation. Table 2 shows the spatial distribution of activations and deactivations in each of the IPC ROI. The relative pattern of activation and deactivation in these ROI is almost identical to that in the MA-A task, except that the deactivations were stronger and more spatially extensive in regions PGp and PGa of the AG (Table 2, Fig. 4*b*).

### *Activation Outside the IPC during the MA-A and MA-R Tasks*

*MA-A (Arabic Calculation versus Number Identification)*
Significant activation was also observed in the left inferior PFC (BA 44, 47) and anterior insula (BA 48), left superior parietal lobule and midoccipital gyrus (BA 7, 19), and right midoccipital gyrus (BA 7, 40), right inferior temporal cortex (BA 37), the fusiform gyrus (BA 19), and cerebellum (vermis, bilateral crus 1 and 2, lobules VI, VIII, and right lobule 7b), as shown in Figure 3a (Schmahmann et al. 1999). Extensive deactivation was also observed in the right middle temporal gyrus and bilaterally in the superior frontal gyrus (Fig. 3*a*). A detailed listing of the brain areas that showed activations and deactivations is shown in Table 1.

*MA-R (Roman Calculation versus Number Identification)*
Outside the IPC, significant activation was observed in the right inferior and midoccipital gyri (BA 18, 19), the right inferior temporal gyrus (BA 37), the right insula and adjoining orbitofrontal cortex (BA 47/12), and cerebellum (vermis, bilateral crus 1 and 2, lobules IV, V, VI, and VIII). Extensive deactivation was also observed in the right superior and middle temporal gyri and in the left superior frontal gyrus (Fig. 3*b*, Table 1).

### *IPC Activation Differences between the MA-A and MA-R Tasks*

*MA-A – MA-R*
We examined brain regions that showed greater activation in the MA-A, compared with the MA-R, condition. As shown in Figure 6,

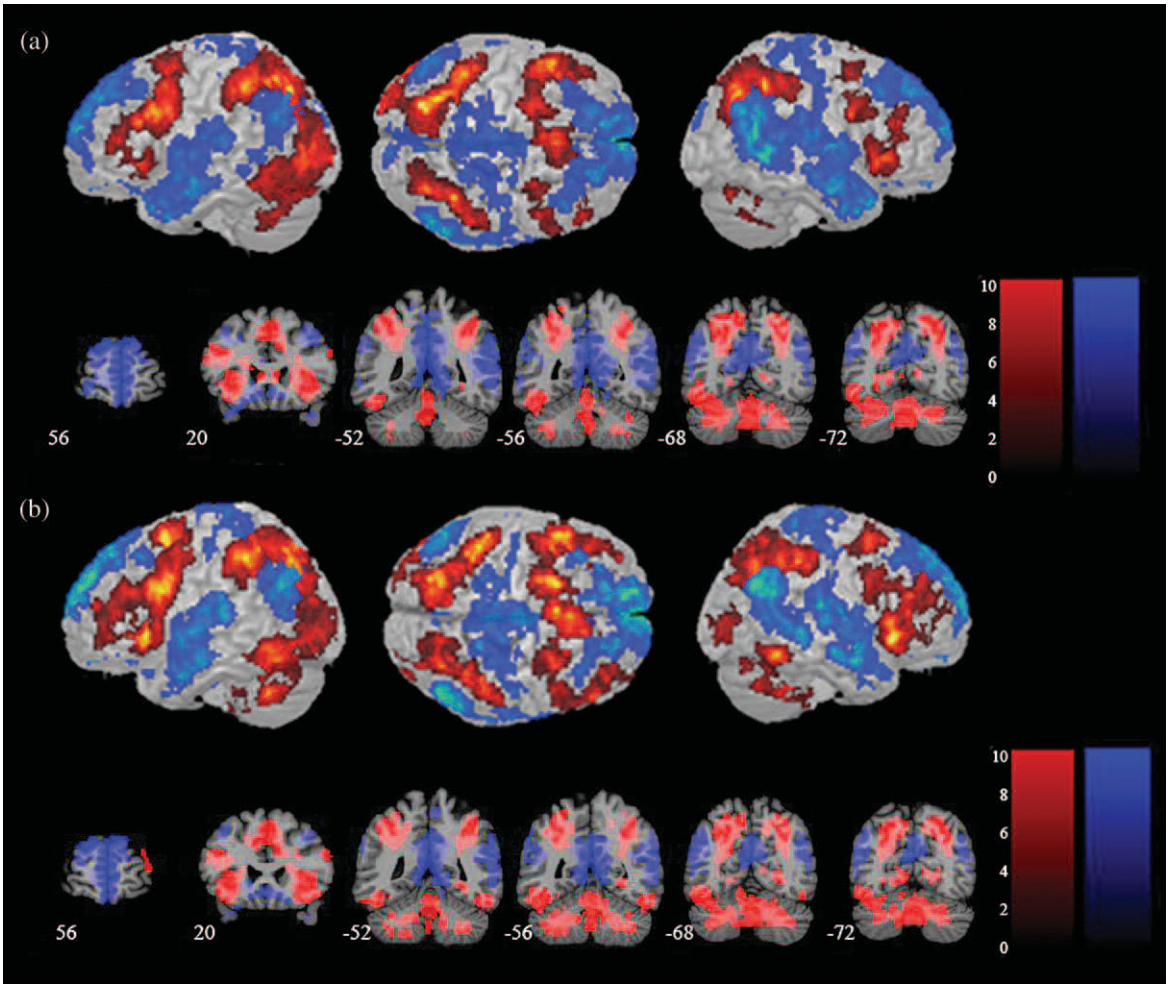


**Figure 3.** Brain activation and deactivation during the MA-A and MA-R calculation tasks. (*a*) Surface rendering and coronal sections of brain regions that showed significant activation (Calculation > Identification) and deactivation (Identification > Calculation) in the MA-A calculation task. Activations are shown in red and deactivations are shown in blue. (*b*) Activations and deactivations in the MA-R calculation task. Each cluster was significant after correction for height ($p < 0.01$) and spatial extent ($p < 0.01$).

**Table 1**
Brain regions that showed significantly greater activation and deactivation during the MA-A and MA-R calculation, compared with number identification, tasks

| Comparison | Brain region | BA | Corrected *P* value | No. of voxels | Peak *Z* score | Peak MNI coordinates (mm) | | |
|---|---|---|---|---|---|---|---|---|
| | | | | | | *x* | *y* | *z* |
| MA-A | | | | | | | | |
| Calculation — Identification | | | | | | | | |
| | L inferior frontal gyrus, L insula | 44, 47, 48 | <0.001 | 12 210 | 5.12 | −52 | 14 | 30 |
| | L superior parietal lobule L middle occipital gyrus | 7, 19 | <0.001 | 10 206 | 6.03 | −22 | −70 | 42 |
| | R inferior parietal lobule R middle occipital gyrus | 40, 7 | <0.001 | 2458 | 5.32 | 34 | −52 | 44 |
| Identification — Calculation | | | | | | | | |
| | L/R medial superior frontal gyrus | 10, 30 | <0.001 | 15 247 | 6.19 | −2 | 54 | 8 |
| | R middle temporal gyrus, R/L precuneus | 37, 21, 23 | <0.001 | 20 467 | 5.90 | 56 | −58 | 12 |
| | L angular gyrus | 39 | <0.001 | 1244 | 4.61 | −46 | −72 | 42 |
| | | MA-R | | | | | | |
| Calculation — Identification | | | | | | | | |
| | R inferior parietal lobule, R middle occipital gyrus | 40, 7 | <0.001 | 2734 | 4.99 | 36 | −50 | 42 |
| | R inferior temporal gyrus | 37 | <0.01 | 361 | 5.18 | 54 | −54 | −18 |
| | R cerebellum (vermis 8, crus 2) | 47 | <0.001 | 28 755 | 6.03 | 2 | −64 | −30 |
| | R inferior/middle occipital gyrus | 18, 19 | <0.01 | 321 | 3.71 | 36 | −88 | 4 |
| Identification — Calculation | | | | | | | | |
| | L superior frontal gyrus, R middle cingulate, R precuneus | 9, 23 | <0.001 | 28 183 | 5.68 | −14 | 52 | 34 |
| | L angular gyrus | 39 | <0.001 | 1223 | 5.07 | −54 | −66 | 28 |
| | R middle occipital gyrus, R superior/middle temporal gyrus | 39, 22 | <0.001 | 1813 | 5.38 | 48 | −70 | 28 |

Note: For each significant cluster, region of activation, significance level, number of activated voxels, maximum *Z* score, and location of peak in MNI coordinates are shown. Each cluster was significant after correction for height ($p < 0.01$) and spatial extent ($p < 0.01$). BA, Brodmann area.

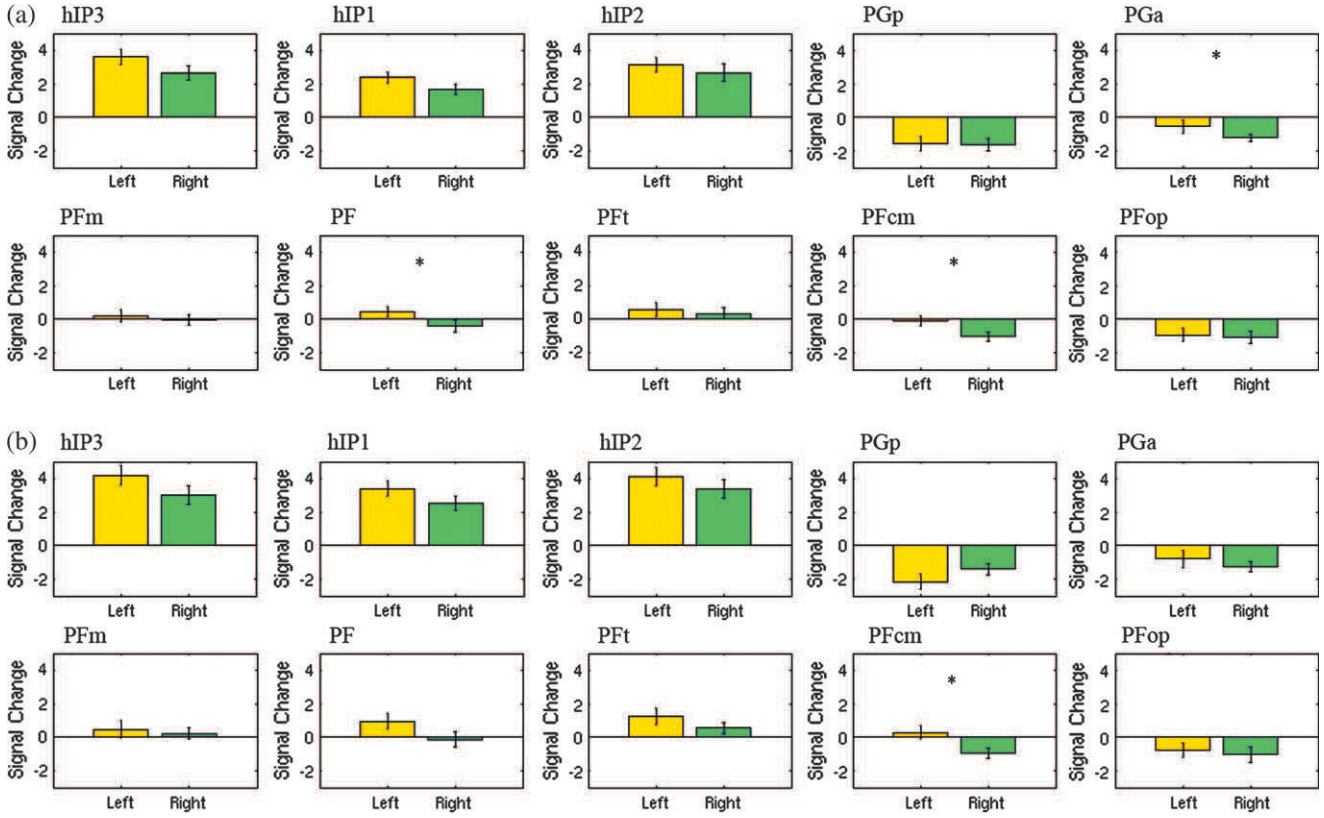


**Figure 4.** Relative strength of activation and deactivation in each cytoarchitectonically defined IPC region during the MA-A and MA-R calculation tasks. (*a*) Activation and deactivation in each cytoarchitectonically defined IPC ROI during the MA-A task. All 3 IPS areas (hIP3, hIP1, and hIP2) were activated, whereas AG regions (PGp and PGa) were deactivated. SMG regions (PFm, PF, PFt, PFcm, and PFop) showed minimal activation. Hemispheric differences were observed in AG region PGa, and SMG regions PF and PFcm. (*b*) A similar pattern of activation and deactivation was observed during the MA-R task. In this case, hemispheric differences were observed only in the SMG region PFcm. *indicates regions that showed significant hemispheric differences, $p < 0.05$ after FDR correction for multiple comparisons. Mean and standard error are shown.

a direct comparison between the 2 tasks revealed statistically significant differences in the left IPC and the adjoining temporoparietal cortex. More detailed analysis of the spatial distribution of the responses revealed that the differences were primarily localized to the AG – PGa and PGp together accounted for 73% of the activation and only 1.8% of the activation extended into SMG region PFm (Table 4). ROI analyses were conducted to further examine both the direction and magnitude of responses within the IPC cluster, in order to examine whether between-task differences above arose from *increases* during MA-A, or from *decreases* during the MA-R task (deactivation). This analysis revealed that activation in the AG cluster arose from greater deactivation during the MA-R condition (Fig. 6).

*MA-R – MA-A*

We then examined whether any brain regions showed greater activation in the MA-R, compared with the MA-A, tasks. No differences were observed in any of the IPC regions, even at a liberal threshold of $P < 0.05$, uncorrected.

### *Activation Differences Outside the IPC between the MA-A and MA-R Tasks*

*MA-A – MA-R*

Compared with the MA-R task, the MA-A task showed greater responses bilaterally in the medial aspects of the superior frontal gyrus (BA 10). Further analysis revealed that in this cluster, between-task differences arose from greater deactivation during the MA-R task (Table 3).

*MA-R – MA-A*

Compared with the MA-A task, the MA-R showed greater responses in 6 clusters within the PFC and the cerebellum (Fig. 7 and Table 3). PFC regions that showed differences included the left inferior frontal gyrus with adjoining anterior insula (BA 44, 48), left inferior and middle frontal gyrus (BA 47, 11), left middle and superior frontal gyri (BA 9, 8), and right inferior frontal gyrus and adjoining anterior insular (BA 47, 48) and the bilateral presupplementary motor area (pre-SMA; BA 6). Cerebellar regions that showed differences included the left cerebellum lobule VIII and vermis 8.

We then examined whether the activation clusters noted in the *MA-R – MA-A* comparison above arose from task-related decreases during MA-A, or from task-related increases during MA-R (deactivation). This analysis showed that activation in all the 6 clusters arose from greater *activation* in the MA-R task (Fig. 7).

### *Relation of AG Deactivation to the DMN*

The DMN (Greicius et al. 2003) consists of 2 bilateral nodes in the IPC as well as the medial PFC and posteromedial cortex (Greicius et al. 2003). These regions are typically deactivated during cognitive tasks in a domain general manner, and furthermore, the magnitude of deactivation normally increases in proportion to

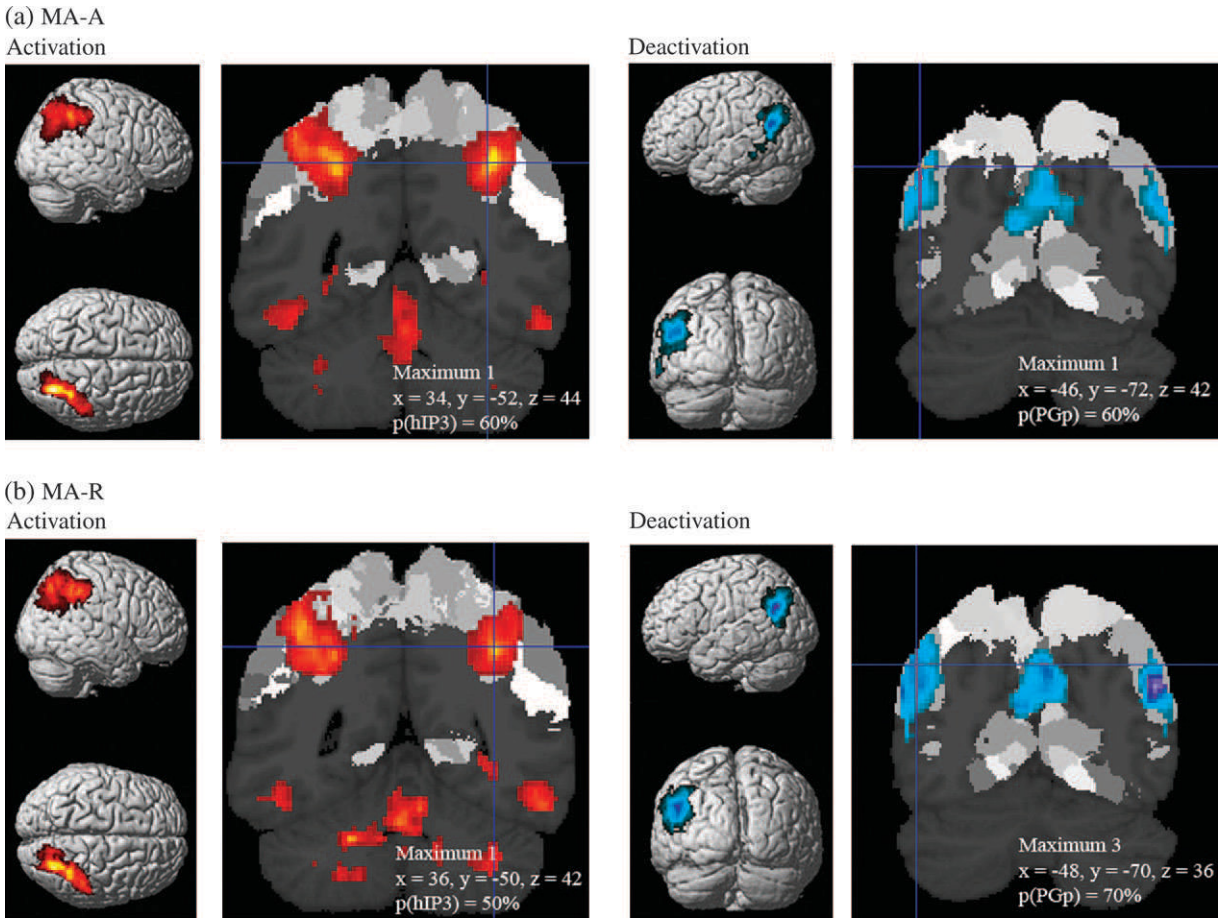


**Figure 5.** Activation and deactivation in cytoarchitectonically defined IPC regions during the MA-A and MA-R calculation tasks. (*a*) Activations (Calculation > Identification) and deactivations (Calculation < Identification) during the MA-A task, overlaid on cytoarchitectonic probability maps of the IPC. Task-related activations had the highest probability of being localized to the posterior-most IPS region hIP3, whereas deactivations had the highest probability of being localized to posterior-most AG region PGp. (*b*) A similar profile was observed in the MA-R task, except that deactivations were more extensive and stronger within AG regions PGp and PGa. Each cluster was significant after correction for height ($p < 0.01$) and spatial extent ($p < 0.01$). Table 2 provides additional details of localization of activation and deactivation foci.

**Table 2**
Probabilistic labeling of IPC regions that showed significant activation and deactivation during the MA-A and MA-R calculation, compared with number identification, tasks

| Comparison | Assigned region | % of region activated | % of cluster in region | Probability of peak in assigned region (%) | Peak MNI coordinates (mm) | | |
|---|---|---|---|---|---|---|---|
| | | | | | *x* | *y* | *z* |
| MA-A | | | | | | | |
| Calculation — Identification | R IPS (hIP3) | 91.6 | 11.1 | 60 | 34 | −52 | 44 |
| | R IPS (hIP1) | 62.1 | 5.8 | 20 | 44 | −48 | 44 |
| Identification — Calculation | L AG (PGp) | 49.2 | 42.9 | 60 | −46 | −72 | 42 |
| | L AG (PGa) | 30.4 | 20.1 | | | | |
| | L SMG (PFm) | 13.6 | 5.5 | | | | |
| | L SMG (PF) | 1.6 | 1.2 | | | | |
| MA-R | | | | | | | |
| Calculation — Identification | R IPS (hIP3) | 89.1 | 9.7 | 50 | 36 | −50 | 42 |
| | R IPS (hIP1) | 80.3 | 6.7 | | | | |
| Identification — Calculation | L AG (PGp) | 54.1 | 48.0 | 70 | −48 | −70 | 36 |
| | L AG (PGa) | 33.6 | 22.6 | | | | |
| | L SMG (PFm) | 9.8 | 4.0 | | | | |
| | L SMG (PF) | 0.8 | 0.7 | | | | |

Note: IPC regions that showed significantly greater activation (Calculation > Identification) during the MA-A, compared with the MA-R, task (Identification > Calculation). For each significant cluster, the probabilistic region, percentage of activation in the region, percentage of cluster that was in the region, peak MNI coordinate, and the probability of the peak being in the region are shown. Each cluster was significant after correction for height ($p < 0.01$) and extent ($p < 0.01$). Cytoarchitectonically defined probability maps were used to interpret the locations of the cluster and peaks within subdivisions of the IPS, AG, and SMG.

cognitive load. We first examined whether deactivations observed in the IPC during the 2 tasks overlapped with the DMN. We observed strong deactivation in the right AG area PGp in both tasks and more extensive bilateral overlap in the MA-R task (Supplementary Fig. S1). We then examined whether the left AG region that showed greater deactivation in the MA-R, compared with the

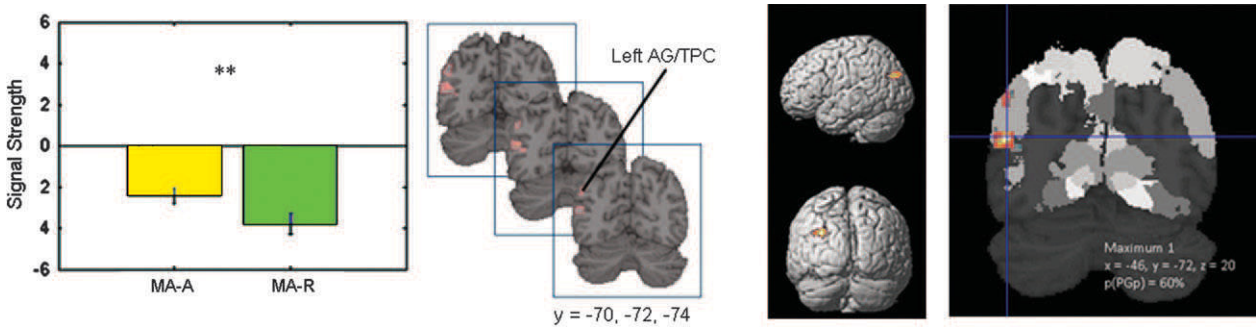


**Figure 6.** Probabilistic labeling of IPC regions that showed significant differences in activation between the MA-A and MA-R calculation tasks. (Left) Task-related differences arose from activation, rather than deactivation, with the MA-R showing greater negative activations than the MA-A task. These differences were localized to the left AG and the posterior temporo-parietal cortex (TPC). **indicates that differences between the MA-A and MA-R task were significant at $P < 0.01$. (Right) Probabilistic labeling of IPC responses showing that deactivations had the highest probability of being localized to posterior-most angular gyrus region PGp. Each cluster was significant after correction for height ($p < 0.01$) and spatial extent ($p < 0.01$). Table 4 provides additional details of localization of task-related differences.

**Table 3**
Brain regions that showed significant differences between the MA-A and MA-R calculation tasks

| Comparison | Brain region | BA | Corrected *P* value | No. of voxels | Peak *Z* Score | Peak MNI coordinates (mm) | | |
|---|---|---|---|---|---|---|---|---|
| | | | | | | *x* | *y* | *z* |
| MA-A – MA-R | | | | | | | | |
| | L angular gyrus L temporoparietal cortex | 39, 19 | <0.001 | 373 | 3.87 | −46 | −72 | 20 |
| | L/R superior frontal gyrus | 10 | <0.01 | 238 | 3.32 | −4 | 56 | 24 |
| MA-R - MA-A | | | | | | | | |
| | L inferior frontal gyrus, L anterior Insula | 44, 48 | <0.001 | 544 | 4.28 | −54 | 10 | 8 |
| | L inferior/middle frontal gyrus | 47, 11 | <0.01 | 331 | 3.59 | −26 | 32 | −4 |
| | L middle/superior frontal gyrus | 9, 8 | <0.01 | 278 | 4.56 | −22 | 8 | 58 |
| | L/R presupplementary motor area | 6 | <0.01 | 286 | 3.44 | −2 | 6 | 60 |
| | R inferior frontal gyrus R anterior insula | 47, 48 | <0.01 | 227 | 4.19 | 38 | 20 | −6 |
| | L cerebellum (lobule VIII/vermis 8) | | <0.001 | 947 | 4.54 | −24 | −58 | −42 |

Note: Brain regions that showed significantly greater activations in the MA-A, compared with the MA-R task and the MA-R, compared with the MA-A task. For each cluster, region of activation, significance level, number of activated voxels, maximum *Z* score, and location of peak in MNI coordinates are shown. Each cluster was significant after correction for height ($p < 0.01$) and spatial extent ($p < 0.01$).

**Table 4**
Probabilistic labeling of IPC regions that showed greater responses during the MA-A, compared with the MA-R, calculation task

| Comparison | Assigned region | % of region activated | % of cluster in region | Probability of peak in assigned region (%) | Peak MNI coordinates (mm) | | |
|---|---|---|---|---|---|---|---|
| | | | | | *x* | *y* | *z* |
| MA-A – MA-R | | | | | | | |
| | L AG (PGp) | 17.5 | 50.8 | 60 | −46 | −72 | 20 |
| | L AG (PGa) | 10.0 | 22.0 | 30 | −60 | −60 | 22 |
| | L SMG (PFm) | 1.3 | 1.8 | | | | |

Note: IPC regions that showed significantly greater activations during the MA-A compared with MA-R task. Each cluster was significant after correction for height ($p < 0.01$) and spatial extent ($p < 0.01$). Other details as in Table 2. The MA-R task did not show significantly greater activations in any IPC region.

MA-A, task overlapped anatomically with DMN. As shown in Supplementary Figure S2, there was significant overlap between AG regions deactivated during these tasks and the DMN.

### *Relation between Performance and Brain Activation during the MA-A Task*

We next examined the relationship between brain response and accuracy during the MA-A task. We found that accuracy during the MA-A task was associated with responses in the left ($r = 0.69$, $P < 0.01$) and right ($r = 0.74$, $P < 0.01$) IPC. Probabilistic labeling showed that both left and right IPC clusters overlapped most strongly with the posterior AG area PGp (Table 5 and Fig. 8). Furthermore, poorer accuracy was predominantly associated with deactivation in the AG region PGp (Fig. 8). No such relations were observed between brain activation and RT.

### *Relation between Performance and Brain Activation during the MA-R Task*

Accuracy during the MA-R task was associated with reduced deactivation in the left ($r = 0.578$, $P < 0.05$) and right IPC ($r = 0.718$, $P < 0.01$). As shown in Figure 8 and Table 5, the clusters were localized to AG area PGa in the left hemisphere, extending anteriorly to SMG area PFm and dorsally to IPS region hIP1. The profile was somewhat different in the right hemisphere, with the cluster being localized more posteriorly to AG area PGp and the superior parietal lobule. No such relations were observed between brain activation and RT.

## Discussion

Our findings provide new insights into the functional organization of the IPC during mathematical cognition. The newly developed cytoarchitectonically distinct maps of the IPC allowed us to localize brain responses to each task condition with an anatomical precision that was not possible heretofore. In particular, the demarcation of the IPS from the AG and the SMG allowed us to examine the extent, level, and distribution of brain responses in a reliable manner. This in turn allowed us to examine the effects of task automaticity in relation to individual subject differences in performance with a high level

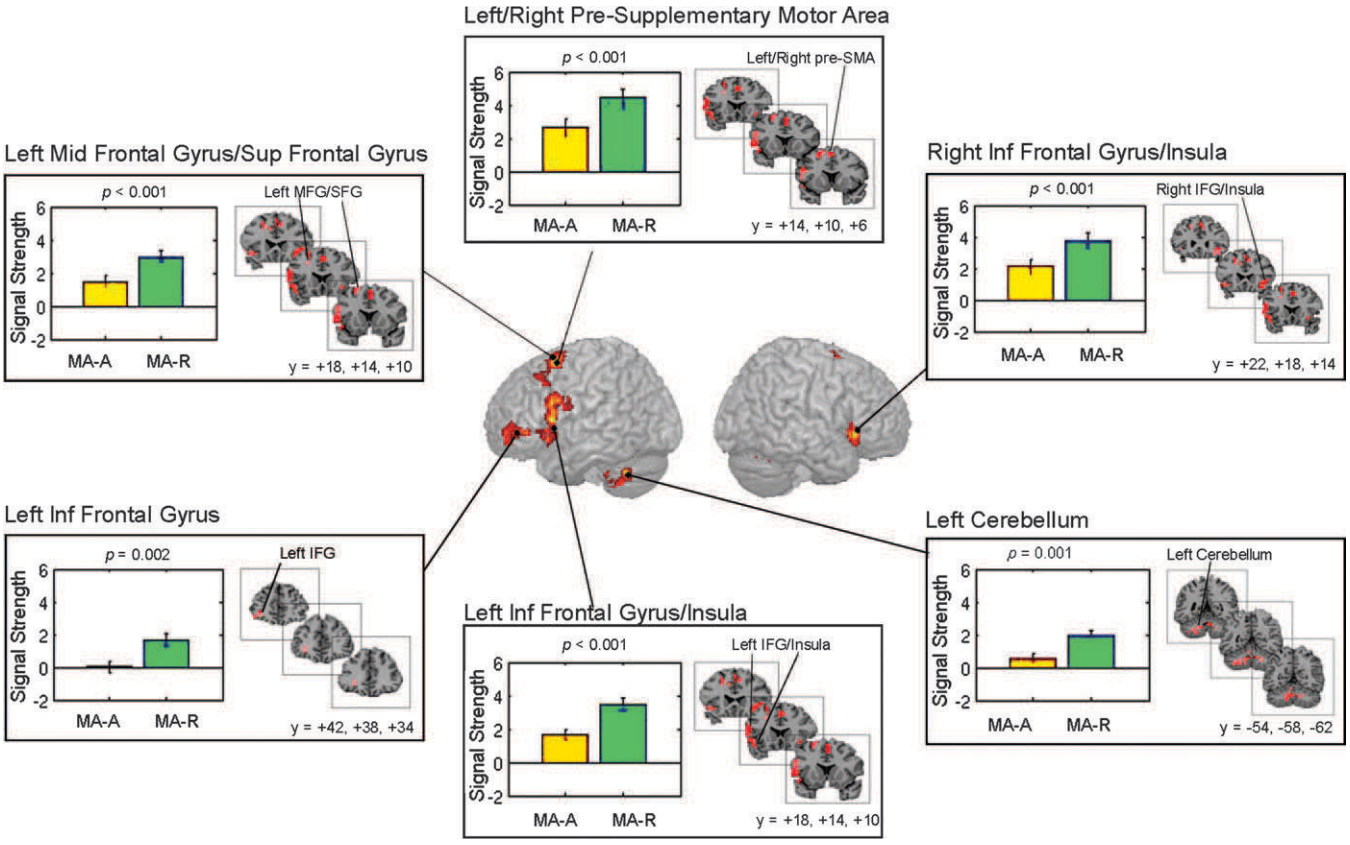


**Figure 7.** Brain regions that showed significant differences in activation between the MA-R and MA-A calculation tasks. Six brain regions, all outside the IPC, showed significantly greater activation in the MA-R, compared with the MA-A, task: 1) left inferior frontal cortex and adjoining anterior insula (IFC; BA 44, 48), 2) left inferior frontal gyrus (BA 47), 3) middle and superior frontal gyri (BA 9, 8), 4) right inferior frontal cortex and adjoining insular cortex (BA 47, 48), 5) bilateral presupplementary motor area (pre-SMA; BA 6), and 6) left cerebellum (lobule VIII). In each of these regions, both the MA-R and the MA-A tasks showed positive activations (Calculation > Identification), and task-related differences arose from greater positive activations in the MA-R task. Each cluster was significant after correction for height ($p < 0.01$) and spatial extent ($p < 0.01$). Table 3 provides additional details of localization of activation foci.

of precision and consistency. Our results point to important functional heterogeneities in the IPC, and they suggest that task automaticity modulates neural responses in the IPS, AG, and SMG differently. Our findings emphasize that the contributions of the IPC to mathematical cognition are not unitary. We discuss the implications of our findings for understanding the neural basis of mathematical cognition below.

### *Behavioral Differences*

As predicted, we found that participants are less accurate and slower at processing the less familiar Roman numerals (Gonzalez and Kolers 1982; Hiscock et al. 2001). Accuracy and RTs were significantly different during the Calculation and Identification conditions in the MA-A and MA-R tasks. These results suggest that participants were equally adept at recognizing the 2 types of numerals, but were significantly slower in performing MA with Roman numerals. These results indicate that the MA-A task is performed in a significantly more automated manner than the MA-R task, consistent with the view that automatized processes are often marked by significant "speed-up" in response times due to more efficient memory retrieval (Logan 1988). Because the decision-making aspects of the MA-A and MA-R tasks did not differ, differences in RT likely reflect the effortful, directed, retrieval required during the MA-R task. RT differences in the identification condition suggest that Arabic numerals were recognized more efficiently than Roman numerals. Taken together with brain imaging results, the behavioral findings support the observation that cognitive operations are not independent of the symbols that initiate them (Gonzalez and Kolers 1982).

### *Differential IPC and PFC Responses in Relation to Task Automaticity*

Before discussing regional differences within the IPC, we first focus on overall global differences in brain response in relation to task automaticity. Although there was extensive overlap in the IPC and PFC regions activated during the MA-A and MA-R tasks, activations in these regions could be dissociated: there was significantly greater activation of the PFC during the MA-R, compared with the MA-A, task, whereas there was greater "activation" of the IPC during the MA-A, compared with the MA-R, task. These results suggest that the IPC and PFC contribute differently to automated versus nonautomated MA tasks. Notably, activations of the right anterior insula in the PFC and the lobule VIII and vermis 8 regions of the cerebellum were observed only in the MA-R task.

During the MA-R task, greater activation was observed bilaterally in the ventrolateral PFC as well as the pre-SMA and the cerebellum. However, left hemisphere responses were stronger and more extensive and overlapped with language and syntactic processing regions in BA 44 and 47. These differences may arise from the need to transform numerals in the Roman

**Table 5**
Probabilistic labeling of IPC regions where activation or deactivation was significantly correlated with accuracy during the MA-A and MA-R calculation tasks

| Comparison | Assigned region | % of region activated | % of cluster in region | Probability of peak in assigned region (%) | Peak MNI coordinates (mm) | | |
|---|---|---|---|---|---|---|---|
| | | | | | *x* | *y* | *z* |
| MA-A | | | | | | | |
| | L AG (PGp) | 6.2 | 28.4 | 60 | −40 | −80 | 28 |
| | R AG (PGp) | 20.1 | 56.5 | 80 | 42 | −72 | 38 |
| MA-R | | | | | | | |
| | L AG (PGa) | 22.5 | 48.2 | 20 | −40 | −62 | 38 |
| | L SMG (PFm) | 4.7 | 6.1 | 20 | −44 | −60 | 30 |
| | L IPS (hIP1) | 3.4 | 4.1 | | | | |
| | L AG (PGp) | 1.3 | 3.7 | 60 | −46 | −66 | 42 |
| | R AG (PGp) | 18.3 | 44.0 | 60% | 40 | −78 | 28 |

Note: IPC regions that showed significant correlations between activation and performance accuracy during the MA-A and MA-R tasks. Each cluster was significant after correction for height ($p < 0.01$) and spatial extent ($p < 0.05$). Other details as in Table 2.

format into phonological representations that facilitate fact retrieval and calculation. Lexical processing, translation of symbols, and the articulatory rehearsal needed prior to fact retrieval are also known to engage a frontocerebellar loop (Desmond et al. 1997; Fiez and Raichle 1997; Chen and Desmond 2005; Hayter et al. 2007), consistent with our finding of coactivation of the ventrolateral PFC and cerebellar lobule VIII. Interestingly, there were no differences in the mid-dorsolateral PFC, a finding that may reflect greater demands on retrieval and maintenance rather than active manipulation of numerical quantity in working memory (D'Esposito et al. 2000; Curtis and D'Esposito 2003; Derrfuss et al. 2004; Blumenfeld and Ranganath 2006). Importantly, our ventrolateral PFC foci overlap with prefrontal regions that have been implicated in effortful retrieval during a complex series of mental calculations (Anderson and Qin 2008).

Additionally, the MA-R task elicited greater responses in pre-SMA, a region that has been implicated in sequential planning of information in working memory. This may reflect preparation for motor output that accompanies multistage numerical computations during the more complex 3-operand condition. This region also showed greater responses in a previous study where we examined differences between processing of 3- and 2-operand MA trials (Menon, Rivera, White, Glover, et al. 2000). In that study, the increase in pre-SMA activation reflected the longer duration (about 850 ms) of the motor preparatory activity in a 3-operand, compared with a 2-operand, condition. Electrophysiological recordings have consistently implicated the SMA and pre-SMA during motor preparation (Tanji and Mushiake 1996) and delay-related fMRI responses have been reported during working memory tasks (Petit et al. 1998).

### *Dissociating IPS, AG and SMG Contributions to MA*

During both the MA-A and MA-R tasks, the IPS showed increased activation during the Calculation compared with the Identification conditions (Figs 4 and 5). Increases were observed in the hIP3, hIP1, and hIP2, encompassing the posterior, middle, and anterior IPS segments shown in Figure 1. Activations were highest in the posterior-most area hIP3. In contrast, both the posterior AG area PGp and the anterior AG area PGa showed deactivation in both tasks, with stronger and more extensive deactivation in area PGp. Deactivation here refers to greater responses in the control number identification task compared with the calculation task. The MA-A task did not show activation above the control condition in either AG region, contrary to its predicted role in automated fact retrieval. Signal changes in the SMG were modest and nonsignificant in both tasks.

We then examined differences in activation of the IPS, AG, and the SMG between the automated and nonautomated tasks. We observed differences in the AG but not in the IPS or the SMG. It is particularly noteworthy that between-task differences arose from differences in *deactivation* rather than differences in *activation* (Figs 4 and 5). In the left AG, the MA-R task showed greater deactivation than the MA-A task, whereas the right AG showed equal levels of deactivation. Other regions of the IPC, including the left and right IPS areas hIP3, hIP1, and hIP2, showed similar levels of activation in both tasks; these IPC regions were not modulated by task automaticity.

One potential issue in interpreting these findings is that it leaves unclear whether the deactivations observed in our study may have arisen from greater activation of the AG during the number identification condition. In order to address this issue, we analyzed a different fMRI dataset, acquired in a separate group of 21 adult participants, with both number identification and passive fixation "rest" baseline conditions. We found no deactivations in the AG when we compared number identification to rest; in contrast, as expected, we observed significant activation in the left IPS, in the left and right striate, extrastriate, lingual, and fusiform gyri, and the left sensorimotor cortex (Supplementary Fig. S3). This analysis strongly suggest that the within-task deactivations and between-task differences in deactivation reported here arise from differences in deactivation during the MA Calculation task as opposed to activations during the Identification task.

Our findings help to clarify the functional distinction between key IPC regions that have been implicated in mathematical cognition. Delazer et al. (2003) suggested that with MA training, there is a shift from the bilateral IPS to the left AG, especially as individuals begin to rely less on computation and more heavily on retrieval. It is, however, not clear whether these changes are related to differences in activation or deactivation. Between-task comparisons indicated a positive difference in AG activation during the more automated task, compared with the less automated task, reflecting greater deactivation in the MA-R than in the MA-A task. In view of these findings, it is possible that the "shift" to the AG observed in the Delazer et al. study may have been due to decreased deactivation when the task became more automated after training. This notion was confirmed by the results of a subsequent study (Ischebeck et al. 2006), in which the AG showed less negative responses after training on multiplication problems. Similarly, Grabner et al. (2007) observed AG deactivation during mental calculation in individuals with poor mathematical abilities. However, to date, no study of mathematical cognition to our knowledge has examined whether task-related differences in specific IPS and AG regions arise primarily from activation or from deactivation, thus leaving unclear the precise functions subserved by the IPC. Importantly, many existing studies leave open the possibility that some of the IPC responses may reflect suppression from increased task difficulty rather than processing specificity for MA, an issue we address more directly in our study. Taken together, these findings highlight the need for careful analysis of the magnitude and sign of changes in activation in each specific MA task, particularly with respect to the AG but also to a lesser extent with the SMG whose various subdivisions showed a complex profile of

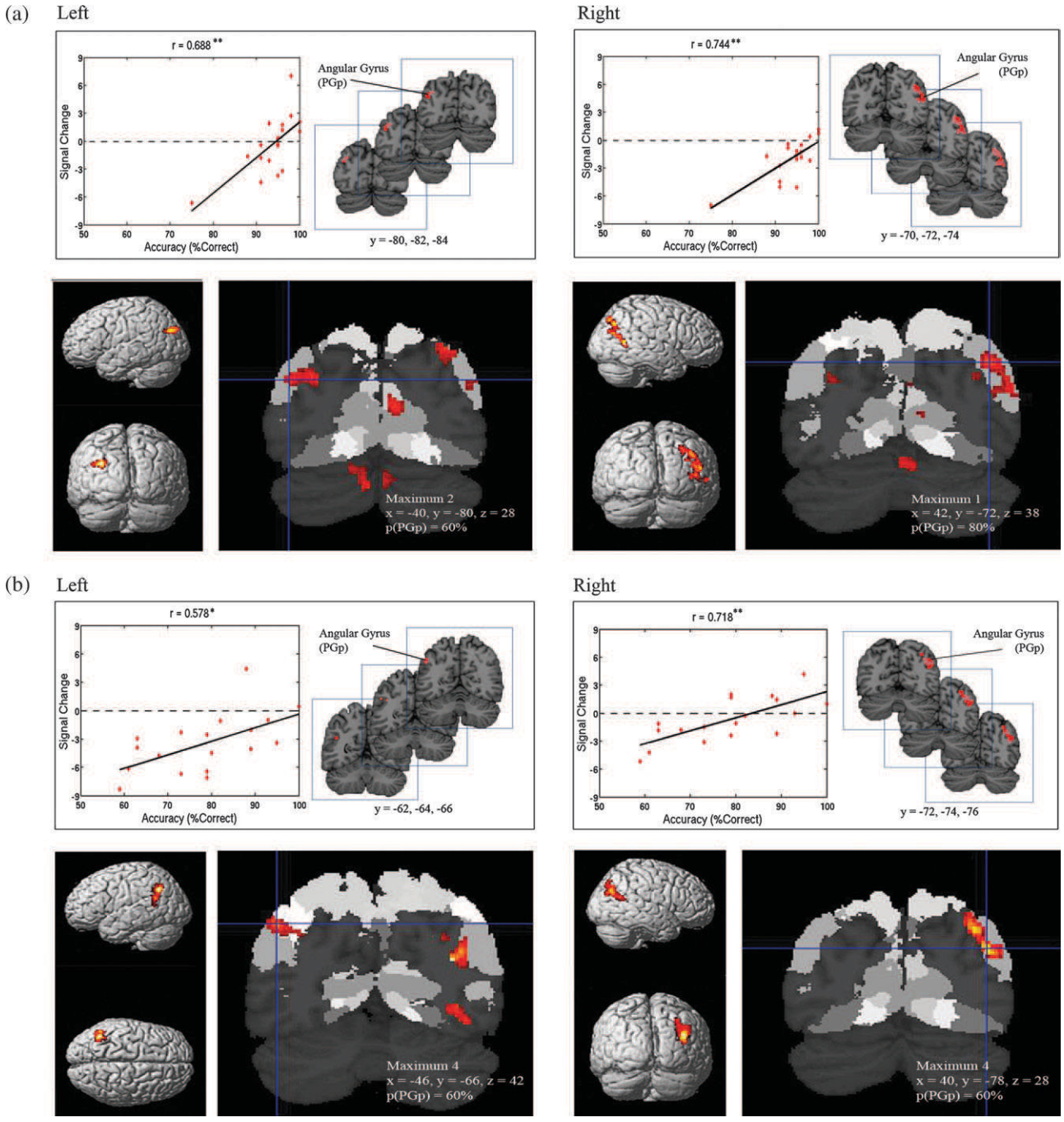


**Figure 8.** Probabilistic labeling of IPC regions where brain responses were significantly correlated with accuracy on the MA-A and MA-R calculation tasks. (*a*) During the MA-A task, accuracy was significantly correlated with brain responses in the left and right posterior AG area PGp. The dashed line demarcates activation from deactivation and helps illustrate that performance was primarily related to deactivation, rather than activation. Furthermore, greater deactivation in focal clusters within the PGp was associated with poorer performance. As noted in the text, the outlier did not affect the statistical significance of these findings. The bottom panels show probabilistic labeling of responses overlaid on cytoarchitectonic maps of the IPC. (*b*) A similar pattern was observed in the MA-R task, except that responses were stronger in area PGp and accuracy was correlated with responses in the anterior AG region PGa (see Table 5). Each cluster was significant after correction for height ($p < 0.01$) and spatial extent ($p < 0.01$).

low-level activation and deactivation. Most importantly, these findings point to functionally heterogeneous responses in cytoarchitectonically distinct areas of the IPC.

### *Obligatory Involvement of IPS in Automated and Nonautomated MA*

All 3 segments of the IPS showed positive task-related activations during both the MA-R and MA-A tasks, but these activations did not differ between the 2 tasks. This suggests that the IPS is fully recruited in each condition, in contrast to the AG and the IFC. The invariant and obligatory nature of activation in the IPS further confirms its critical role in mathematical problem solving. The middle IPS area hIP1 overlaps with the horizontal IPS (hIPS), a region thought to be important for representing and manipulating quantity (Ansari 2008). This IPS region was activated strongly in both

the MA-A and the MA-R tasks, even though the stimuli were visually well balanced in the MA and number identification tasks. However, no differences were observed between the MA-A and MA-R tasks. This suggests that although the hIPS region is sensitive to MA operations, it is not differentially modulated by task automaticity when basic number processing is controlled for. The same basic pattern was observed in each IPS region, even though the posterior-most area hIP3 had the strongest activation among the 3 subdivisions. All 3 IPS areas, hIP3, hIP1, and hIP2, therefore, appear to play an obligatory role in MA tasks, irrespective of the level of automaticity.

### *Task-Dependent AG Deactivation and Its Relation to the DMN*

Our findings are inconsistent with simplistic notions of the left AG as being primarily involved in verbally mediated fact retrieval (Dehaene et al. 2003; Delazer et al. 2003). Although retrieval was more automated in the MA-A, very little positive activation was observed in this region in either task. Both the Rickard et al.'s (2000) study that involved simple 2-operand multiplication and our study, which involves 3-operand calculation, showed deactivation in the AG. Part of the reason for the divergence of these findings from studies such as those reviewed by Dehaene et al. (2003) is that sufficient attention has not been paid to deactivation when multiple task conditions were compared. For instance, the left AG was reported to show increased activation for multiplication relative to subtraction (Chochon et al. 1999; Lee 2000), for multiplication and division relative to a letter substitution control (Gruber et al. 2001), and for exact calculation than approximation (Dehaene et al. 1999). It is likely that these activations may have arisen from greater deactivation in the more difficult task. Our findings suggest that it is crucial to assess the precise, quantitative, profile of responses if we are to understand the nature of cognitive and brain mechanisms responsible for memory retrieval and algorithmic computation. It should also be noted that it was not just the left AG that showed significant deactivation in our study. The right AG also showed significant deactivation, but deactivation related differences between the MA-A and the MA-R tasks were more significant on the left than the right.

The AG regions that showed task-related deactivation differences in our study overlapped with IPC regions that have previously identified as being part of the DMN (Supplementary Fig. S1). More detailed analyses conducted to examine extent of the overlap showed that the parts of the AG that overlapped with the DMN were significantly more deactivated during the MA-R task than during the MA-A task. Other parts of the AG, which did not overlap with the DMN, showed positive activations in both the MA-A and MA-R tasks, but these activations did not differ between tasks (Supplementary Fig. S2).

AG areas outside of the DMN, most notably in the lateral temporal lobes, were also deactivated, but these deactivations did not differ between the MA-A and MA-R tasks. The DMN, and therefore the AG regions that overlap with it, are typically suppressed when the executive control network is recruited during demanding cognitive tasks (Seeley et al. 2007; Sridharan et al. 2008). In agreement with this observation, greater deactivation in the AG region was accompanied by greater activation in the bilateral PFC regions during the MA-R task. Our findings are also consistent with previous observations that suppression of the DMN increases with task difficulty (Schulman et al. 2003; Greicius and Menon 2004). The lateral IPC has been shown to be deactivated across a broad range of cognitive tasks, but its precise anatomical localization has not been adequately clarified. Whether these deactivations are primarily in the AG proper, rather than in more dorsal or rostral regions bordering the IPS and the SMG, has been unclear. Our analysis using the cytoarchitectonic maps described above strongly suggests that these deactivations are localized to the AG. One view of the deactivations observed in the IPC is that it helps to divert attentional resources to the PFC and more dorsal IPC regions for processing task-relevant visual information (Schulman et al. 2003; Greicius and Menon 2004; Todd et al. 2005). For example, Schulman et al. (2003) asked participants to search and detect stimulus targets embedded amongst nontarget stimuli and found that, whereas the IPS was activated both during search and target detection, the right AG was deactivated during search (Schulman et al. 2003). In addition, Todd et al. (2005) found that suppression of the AG increased with visual short-term memory load. These findings suggest that suppression of the right AG is necessary during demanding tasks, especially during tasks in which attention is voluntarily directed.

Importantly, the 2 other major nodes of the DMN— the posterior cingulate cortex and the ventromedial PFC—showed no differences between the tasks. These regions are also sensitive to task difficulty and typically are deactivated together during more difficult cognitive tasks (Schulman et al. 2003; Greicius and Menon 2004). Our findings therefore suggest that deactivation in the AG can be decoupled from most of the midline structures of the DMN. The reason for this functional dissociation is not entirely clear at this time, but our findings are consistent with the view that these nodes serve different cognitive and mental functions even though they are generally considered as operating within a "network". Based on tasks that upregulate the DMN, it appears that posterior cingulate cortex and the ventromedial PFC are more related to self-related and autobiographical information processing (Greicius et al. 2003), whereas the AG is sensitive to integration of long-range semantic information (Humphries et al. 2007).

### *Task-Dependent Left AG Deactivation and Its Relation to Verbal Processing*

How then are we to understand the role of the left AG in mathematical cognition? Although a role for the left AG in verbally mediated retrieval of MA facts has been suggested by several investigators, the nature of this involvement is unknown. In this context, recent findings in the literature on left AG involvement in verbal processing are quite revealing. The left AG shows deactivation to nonwords compared with a resting state baseline, with no difference observed between words and the resting state baseline (Mechelli et al. 2003; Rissman et al. 2003; Binder et al. 2005; Xiao et al. 2005). In an important study of the topic, Humphries et al. (2007) found that whereas the middle temporal gyrus and the inferior frontal gyrus showed greater activation during congruent, random, and pseudorandom sentences and word lists, the left AG showed activation only when semantic information had to be integrated over a 6–15 s time course. In all other conditions, the AG was either at baseline or significantly deactivated. Only very complex semantic processing elevates the AG above resting baseline, words, pseudowords, and even simple sentences suppress it. These findings led Humphries et al. (2007) to suggest that one important function of the AG is integration of

semantic information into an ongoing context. The incoming stimulus interrupts processing of the internal narrative, but the level of semantic input to the AG is impoverished during low-level semantic processing, resulting in a reduction in AG activity compared with a low-level task or even the resting state baseline. In other words, during low-level tasks, the AG is engaged in internally generated cognitive processes that are suspended during more complex cognitive tasks (Greicius et al. 2003; Greicius and Menon 2004). Whether similar effects might be at play during demanding multistep problem solving, for example, in tasks involving word problems (Thevenot and Oakhill 2005) and elaborate verbal processes in calculation (Ansari 2008), remains to be investigated with more appropriate experimental designs.

An alternate view of the AG function centers on its role at the interface of memory and attention. Studies of memory retrieval in patients with lesions to the IPC suggest weakened retrieval effects in the absence of cues and paucity in the semantic contents of the retrieval (Cabeza et al. 2008). Clearly, further studies are needed to test these hypotheses and examine the precise conditions in which semantic content of individual stimuli modulate responses in the left and the right AG. Critically, for us here, these notions of AG function point to a domain-general, rather than a domain-specific, role in mathematical cognition.

### *AG and IPS Relation to Individual Differences in Performance*

Analysis of brain–behavior relations provides further insights into the role of the IPS and AG in mathematical cognition. In the AG, deactivation was associated with reduced accuracy during both tasks. This effect was most strongly observed in the posterior AG area PGp in both hemispheres, although the effects were stronger in the right hemisphere. A similar pattern was observed in the MA-R task, except that responses were stronger in area PGp and accuracy was also correlated with responses in the anterior AG region PGa. These results converge on our findings of between-task differences in deactivation and further suggest that disengagement of the AG is necessary for accurate task performance. Our results are also consistent with the observation above that the AG is deactivated, or relatively suppressed, to a greater extent during performance of the less automated MA-R task. More importantly, these findings suggest that AG deactivation is related to individual differences in performance and the subjective difficulty of performing the MA tasks. These AG regions overlap with the DMN and provide new evidence that suppression of the lateral parietal lobe nodes, but not the midline structures of the DMN, such as the posterior cingulate cortex or the ventromedial PFC, is crucial for accurate MA task performance. In this regard, the observed brain–behavior relations differ in interesting ways from those in cognitive studies of other domains such as attention (Polli et al. 2005; Weissman et al. 2006).

Our findings are partly consistent with those of Grabner et al. (2007), who found that left AG responses during multiplication were correlated with measures of math competence acquired outside the scanner (Grabner et al. 2007). The AG cluster observed by Grabner and colleagues is in close proximity to the left PGa peak detected during the more demanding MA-R task. However, our findings of brain–behavior correlations were associated more with focal task-related deactivation, rather than activation. Furthermore, deactivations were observed in both hemispheres in our studies. There are 2 potential reasons for this discrepancy. One, our study used task-specific measures of performance, rather than general measures of math intelligence. Two, the use of just 2 fixation blocks, placed at the beginning and end of the task, may also have contributed to errors in estimating the profile of activation and deactivation during the multiplication task in the Grabner and colleagues' study. Taken together, however, these findings suggest that performance, task automaticity as well as general domain competence—factors related to subjective difficulty—all contribute to modulation of AG responses during mathematical information processing tasks.

Beyond the AG, activations in the left mid-IPS area hIP1 and the adjoining SMG area PFm were also correlated with accuracy, but only in the more difficult MA-R task. These results suggest that modulation of responses in specific IPC regions depends on task automaticity and performance and that IPC contributions to increased performance and efficiency are heterogeneous not only between the 2 lateral IPC regions but also within each hemisphere.

## Conclusions

Our study provides a unique understanding of the architecture of the IPC in mathematical cognition. More importantly, our findings also pinpoint the link between cytoarchitectonically defined regions of the IPC and the functionally heterogeneous contributions of the IPS and AG to mathematical cognition. The findings reported here point to close links between structure and function within the IPC and they provide new insights into the differential contributions of specific regions of the IPC in relation to automated and successful MA task performance. The functional heterogeneities we found are important for understanding the role of the IPS, AG, and the SMG of the IPC in mathematical cognition. Our study also suggest that failure to take into account the complex profile of activation and deactivation above baseline can lead to misleading conclusions about the role of the IPC in this domain. The systems neuroscience view advanced here suggests that the AG regions must be disengaged as part of a general cognitive mechanism involved during complex information processing tasks (Greicius and Menon 2004). In this context, we highlight further studies needed to investigate the precise cognitive operations subserved by both the activated and deactivated regions of the IPC and how they influence calculation, fact retrieval, learning, and development of domain proficiency.

## Supplementary Material

Supplementary material can be found at: http://www.cercor.oxfordjournals.org/


## Funding

National Institutes of Health (HD047520 and HD059205) and the National Science Foundation (BCS/DRL-0750340).

## Notes

We thank Sonia Crottaz-Herbette for assistance with data acquisition and Valorie Salimpoor for assistance with data analysis. *Conflict of Interest*: None declared.



Address correspondence to: V. Menon, PhD, Symbolic Systems Program, Program in Neuroscience and Department of Psychiatry and

Behavioral Sciences, 780 Welch Rd, Room 201, Stanford University School of Medicine, Stanford, CA 94305, USA. Email: menon@stanford.edu.

## References


Anderson JR, Qin Y. 2008. Using brain imaging to extract the structure of complex events at the rational time band. J Cogn Neurosci. 20: 1624–1636.

Ansari D. 2007. Does the parietal cortex distinguish between "10," "ten," and ten dots? Neuron. 53:165–167.

Ansari D. 2008. Effects of development and enculturation on number representation in the brain. Nat Rev Neurosci. 9:278–291.

Binder JR, Medler DA, Desai R, Conant LL, Liebenthal E. 2005. Some neurophysiological constraints on models of word naming. Neuroimage. 27:677–693.

Blumenfeld RS, Ranganath C. 2006. Dorsolateral prefrontal cortex promotes long-term memory formation through its role in working memory organization. J Neurosci. 26:916–925.

Brodmann K. 1909. Vergleichende Lokalisationslehre der Großhirnrinde. Leipzig: Barth.

Burbaud P, Degreze P, Lafon P, Franconi JM, Bouligand B, Bioulac B, Caille JM, Allard M. 1995. Lateralization of prefrontal activation during internal mental calculation: a functional magnetic resonance imaging study. J Neurophysiol. 74:2194–2200.

Cabeza R, Ciaramelli E, Olson IR, Moscovitch M. 2008. The parietal cortex and episodic memory: an attentional account. Nat Rev Neurosci. 9:613–625.

Campbell JI, Fugelsang J. 2001. Strategy choice for arithmetic verification: effects of numerical surface form. Cognition. 80:B21–B30.

Caspers S, Eickhoff SB, Geyer S, Scheperjans F, Mohlberg H, Zilles K, Amunts K. 2008. The human inferior parietal lobule in stereotaxic space. Brain Struct Funct. 212:481–495.

Caspers S, Geyer S, Schleicher A, Mohlberg H, Amunts K, Zilles K. 2006. The human inferior parietal cortex: cytoarchitectonic parcellation and interindividual variability. Neuroimage. 33:430–448.

Chen SH, Desmond JE. 2005. Temporal dynamics of cerebro-cerebellar network recruitment during a cognitive task. Neuropsychologia. 43:1227–1237.

Chochon F, Cohen L, van de Moortele PF, Dehaene S. 1999. Differential contributions of the left and right inferior parietal lobules to number processing. J Cogn Neurosci. 11:617–630.

Choi HJ, Zilles K, Mohlberg H, Schleicher A, Fink GR, Armstrong E, Amunts K. 2006. Cytoarchitectonic identification and probabilistic mapping of two distinct areas within the anterior ventral bank of the human. J Comp Neurol. 495:53–69.

Cohen JD, MacWhinney B, Flatt M, Provost J. 1993. PsyScope: a new graphic interactive environment for designing psychology experiments. Behav Res Methods Instrum Comput. 25:257–271.

Cohen Kadosh R, Cohen Kadosh K, Kaas A, Henik A, Goebel R. 2007. Notation-dependent and -independent representations of numbers in the parietal lobes. Neuron. 53:307–314.

Cohen L, Dehaene S, Chochon F, Lehericy S, Naccache L. 2000. Language and calculation within the parietal lobe: a combined cognitive, anatomical and fMRI study. Neuropsychologia. 38: 1426–1440.

Curtis CE, D'Esposito M. 2003. Persistent activity in the prefrontal cortex during working memory. Trends Cogn Sci. 7:415–423.

D'Esposito M, Postle BR, Rypma B. 2000. Prefrontal cortical contributions to working memory: evidence from event-related fMRI studies. Exp Brain Res. 133:3–11.

Dehaene S, Cohen L. 1997. Cerebral pathways for calculation: double dissociation between rote verbal and quantitative knowledge of arithmetic. Cortex. 33:219–250.

Dehaene S, Piazza M, Pinel P, Cohen L. 2003. Three parietal circuits for number processing. Cogn Neuropsychol. 20:487–506.

Dehaene S, Spelke E, Pinel P, Stanescu R, Tsivkin S. 1999. Sources of mathematical thinking: behavioral and brain-imaging evidence. Science. 284:970–974.

Delazer M, Domahs F, Bartha L, Brenneis C, Lochy A, Trieb T, Benke T. 2003. Learning complex arithmetic—an fMRI study. Brain Res Cogn Brain Res. 18:76–88.

Delazer M, Karner E, Zamarian L, Donnemiller E, Benke T. 2006. Number processing in posterior cortical atrophy—a neuropsychological case study. Neuropsychologia. 44:36–51.

Derrfuss J, Brass M, von Cramon DY. 2004. Cognitive control in the posterior frontolateral cortex: evidence from common activations in task coordination, interference control, and working memory. Neuroimage. 23:604–612.

Desikan RS, Segonne F, Fischl B, Quinn BT, Dickerson BC, Blacker D, Buckner RL, Dale AM, Maguire RP, Hyman BT, et al. 2006. An automated labeling system for subdividing the human cerebral cortex on MRI scans into gyral based regions of interest. Neuroimage. 31:968–980.

Desmond JE, Gabrieli JD, Wagner AD, Ginier BL, Glover GH. 1997. Lobular patterns of cerebellar activation in verbal working-memory and finger-tapping tasks as revealed by functional MRI. J Neurosci. 17:9675–9685.

Duffau H, Denvil D, Lopes M, Gasparini F, Cohen L, Capelle L, Van Effenterre R. 2002. Intraoperative mapping of the cortical areas involved in multiplication and subtraction: an electrostimulation study in a patient with a left parietal glioma. J Neurol Neurosurg Psychiatry. 73:733–738.

Eickhoff SB, Paus T, Caspers S, Grosbras MH, Evans AC, Zilles K, Amunts K. 2007. Assignment of functional activations to probabilistic cytoarchitectonic areas revisited. Neuroimage. 36:511–521.

Eickhoff SB, Stephan KE, Mohlberg H, Grefkes C, Fink GR, Amunts K, Zilles K. 2005. A new SPM toolbox for combining probabilistic cytoarchitectonic maps and functional imaging data. Neuroimage. 25:1325–1335.

Fiez JA, Raichle ME. 1997. Linguistic processing. Int Rev Neurobiol. 41:233–254.

Glover GH, Lai S. 1998. Self-navigated spiral fMRI: interleaved versus single-shot. Magn Reson Med. 39:361–368.

Gonzalez EG, Kolers PA. 1982. Mental manipulation of arithmetic symbols. J Exp Psychol Learn Mem Cogn. 8:308–319.

Grabner RH, Ansari D, Reishofer G, Stern E, Ebner F, Neuper C. 2007. Individual differences in mathematical competence predict parietal brain activation during mental calculation. Neuroimage. 38:346–356.

Greicius MD, Krasnow B, Reiss AL, Menon V. 2003. Functional connectivity in the resting brain: a network analysis of the default mode hypothesis. Proc Natl Acad Sci USA. 100:253–258.

Greicius MD, Menon V. 2004. Default-mode activity during a passive sensory task: uncoupled from deactivation but impacting activation. J Cogn Neurosci. 16:1484–1492.

Gruber O, Indefrey P, Steinmetz H, Kleinschmidt A. 2001. Dissociating neural correlates of cognitive components in mental calculation. Cereb Cortex. 11:350–359.

Harrison BJ, Pujol J, Lopez-Sola M, Hernandez-Ribas R, Deus J, Ortiz H, Soriano-Mas C, Yucel M, Pantelis C, Cardoner N. 2008. Consistency and functional specialization in the default mode brain network. Proc Natl Acad Sci USA. 105:9781–9786.

Hayter AL, Langdon DW, Ramnani N. 2007. Cerebellar contributions to working memory. Neuroimage. 36:943–954.

Hiscock M, Caroselli JS, Kimball LE, Panwar N. 2001. Performance on paced serial addition tasks indicates an associative network for calculation. J Clin Exp Neuropsychol. 23:306–316.

Holmes AP, Friston KJ. 1998. Generalisability, random effects & population inference. Neuroimage. 7:S754.

Humphries C, Binder JR, Medler DA, Liebenthal E. 2007. Time course of semantic processes during sentence comprehension: an fMRI study. Neuroimage. 36:924–932.

Ischebeck A, Zamarian L, Egger K, Schocke M, Delazer M. 2007. Imaging early practice effects in arithmetic. Neuroimage. 36:993–1003.

Ischebeck A, Zamarian L, Siedentopf C, Koppelstatter F, Benke T, Felber S, Delazer M. 2006. How specifically do we learn? Imaging the learning of multiplication and subtraction. Neuroimage. 30: 1365–1375.

Kazui H, Kitagaki H, Mori E. 2000. Cortical activation during retrieval of arithmetical facts and actual calculation: a functional magnetic resonance imaging study. Psychiatry Clin Neurosci. 54:479–485.

Kim DH, Adalsteinsson E, Glover GH, Spielman DM. 2002. Regularized higher-order in vivo shimming. Magn Reson Med. 48:715–722.

Krueger F, Spampinato MV, Pardini M, Pajevic S, Wood JN, Weiss GH, Landgraf S, Grafman J. 2008. Integral calculus problem solving: an fMRI investigation. Neuroreport. 19:1095–1099.
Lassaline ME, Logan GD. 1993. Memory-based automaticity in the discrimination of visual numerosity. J Exp Psychol Learn Mem Cogn. 19:561–581.
Lee KM. 2000. Cortical areas differentially involved in multiplication and subtraction: a functional magnetic resonance imaging study and correlation with a case of selective acalculia. Ann Neurol. 48:657–661.
Logan GD. 1988. Toward an instance theory of automatization. Psychol Rev. 95:492–527.
Mai JK, Paxinoss G, Voss T. 2007. Atlas of the human brain. San Diego (CA): Academic Press.
McCarthy SV, Dillon W. 1973. Visual serial search for arabic and roman numbers. Percept Mot Skills. 37:128–130.
Mechelli A, Gorno-Tempini ML, Price CJ. 2003. Neuroimaging studies of word and pseudoword reading: consistencies, inconsistencies, and limitations. J Cogn Neurosci. 15:260–271.
Menon V, Mackenzie K, Rivera SM, Reiss AL. 2002. Prefrontal cortex involvement in processing incorrect arithmetic equations: evidence from event-related fMRI. Hum Brain Mapp. 16:119–130.
Menon V, Rivera SM, White CD, Eliez S, Glover GH, Reiss AL. 2000. Functional optimization of arithmetic processing in perfect performers. Brain Res Cogn Brain Res. 9:343–345.
Menon V, Rivera SM, White CD, Glover GH, Reiss AL. 2000. Dissociating prefrontal and parietal cortex activation during arithmetic processing. Neuroimage. 12:357–365.
Perry DK. 1952. Speed and accuracy of reading arabic and roman numerals. J Appl Psychol. 36:346–347.
Petit L, Courtney SM, Ungerleider LG, Haxby JV. 1998. Sustained activity in the medial wall during working memory delays. J Neurosci. 18: 9429–9437.
Piazza M, Pinel P, Le Bihan D, Dehaene S. 2007. A magnitude code common to numerosities and number symbols in human intraparietal cortex. Neuron. 53:293–305.
Poline JB, Worsley KJ, Evans AC, Friston KJ. 1997. Combining spatial extent and peak intensity to test for activations in functional imaging. Neuroimage. 5:83–96.
Polli FE, Barton JJ, Cain MS, Thakkar KN, Rauch SL, Manoach DS. 2005. Rostral and dorsal anterior cingulate cortex make dissociable contributions during antisaccade error commission. Proc Natl Acad Sci USA. 102:15700–15705.
Ramnani N. 2006. The primate cortico-cerebellar system: anatomy and function. Nat Rev Neurosci. 7:511–522.
Rickard TC, Romero SG, Basso G, Wharton C, Flitman S, Grafman J. 2000. The calculating brain: an fMRI study. Neuropsychologia. 38:325–335.
Rissman J, Eliassen JC, Blumstein SE. 2003. An event-related FMRI investigation of implicit semantic priming. J Cogn Neurosci. 15: 1160–1175.
Roland PE, Friberg L. 1985. Localization of cortical areas activated by thinking. J Neurophysiol. 53:1219–1243.
Rueckert L, Lange N, Partiot A, Appollonio I, Litvan I, Le Bihan D, Grafman J. 1996. Visualizing cortical activation during mental calculation with functional MRI. Neuroimage. 3:97–103.
Scheperjans F, Eickhoff SB, Homke L, Mohlberg H, Hermann K, Amunts K, Zilles K. 2008. Probabilistic maps, morphometry, and variability of cytoarchitectonic areas in the human superior parietal cortex. Cereb Cortex. 18:2141–2157.
Scheperjans F, Hermann K, Eickhoff SB, Amunts K, Schleicher A, Zilles K. 2008. Observer-independent cytoarchitectonic mapping of the human superior parietal cortex. Cereb Cortex. 18:846–867.
Schmahmann JD, Doyon J, McDonald D, Holmes C, Lavoie K, Hurwitz AS, Kabani N, Toga A, Evans A, Petrides M. 1999. Three-dimensional MRI atlas of the human cerebellum in proportional stereotaxic space. Neuroimage. 10:233–260.
Schulman GL, McAvoy MP, Cowan MC, Astafiev SV, Tansy AP, d'Avossa G, Corbetta M. 2003. Quantitative analysis of attention and detection signals during visual search. J Neurophysiol. 90: 3384–3397.
Schunn CD, Reder LM, Nhouyvanisvong A, Richards DR, Stroffolino PJ. 1997. To calculate or not to calculate: a source activation confusion model of problem familiarity's role in strategy selection. J Exp Psychol Learn Mem Cogn. 23:3–29.
Seeley WW, Menon V, Schatzberg AF, Keller J, Glover GH, Kenna H, Reiss AL, Greicius MD. 2007. Dissociable intrinsic connectivity networks for salience processing and executive control. J Neurosci. 27:2349–2356.
Simon O, Mangin JF, Cohen L, Le Bihan D, Dehaene S. 2002. Topographical layout of hand, eye, calculation, and language-related areas in the human parietal lobe. Neuron. 33:475–487.
Sridharan D, Levitin DJ, Menon V. 2008. A critical role for the right fronto-insular cortex in switching between central-executive and default-mode networks. Proc Natl Acad Sci USA. 105:12569–12574.
Sweet LH, Paskavitz JF, Haley AP, Gunstad JJ, Mulligan RC, Nyalakanti PK, Cohen RA. 2008. Imaging phonological similarity effects on verbal working memory. Neuropsychologia. 46:1114–1123.
Tanji J, Mushiake H. 1996. Comparison of neuronal activity in the supplementary motor area and primary motor cortex. Brain Res Cogn Brain Res. 3:143–150.
Thevenot C, Oakhill J. 2005. The strategic use of alternative representations in arithmetic word problem solving. Q J Exp Psychol A. 58:1311–1323.
Todd JJ, Fougnie D, Marois R. 2005. Visual short-term memory load suppresses temporo-parietal junction activity and induces inattentional blindness. Psychol Sci. 16:965–972.
Tzourio-Mazoyer N, Landeau B, Papathanassiou D, Crivello F, Etard O, Delcroix N, Mazoyer B, Joliot M. 2002. Automated anatomical labeling of activations in SPM using a macroscopic anatomical parcellation of the MNI MRI single-subject brain. Neuroimage. 15: 273–289.
Venkatraman V, Siong SC, Chee MW, Ansari D. 2006. Effect of language switching on arithmetic: a bilingual FMRI study. J Cogn Neurosci. 18:64–74.
Weissman DH, Roberts KC, Visscher KM, Woldorff MG. 2006. The neural bases of momentary lapses in attention. Nat Neurosci. 9: 971–978.
Xiao Z, Zhang JX, Wang X, Wu R, Hu X, Weng X, Tan LH. 2005. Differential activity in left inferior frontal gyrus for pseudowords and real words: an event-related fMRI study on auditory lexical decision. Hum Brain Mapp. 25:212–221.
Zago L, Pesenti M, Mellet E, Crivello F, Mazoyer B, Tzourio-Mazoyer N. 2001. Neural correlates of simple and complex mental calculation. Neuroimage. 13:314–327.
Zago L, Petit L, Turbelin MR, Andersson F, Vigneau M, Tzourio-Mazoyer N. 2008. How verbal and spatial manipulation networks contribute to calculation: an fMRI study. Neuropsychologia. 46:2403–2414.